Development of Carbon–Carbon, Carbon–Nitrogen, and Carbon–Hydrogen Bond Functionalization Methodologies and Efforts Toward the Total Synthesis of Dragmacidin E

A DISSERTATION SUBMITED TO THE FACULTY OF THE UNIVERSITY OF MINNESOTA BY

Jason Thomas Brethorst

IN PARTIAL FULFILLMENT OF THE REQUIREMENTS FOR THE DEGREE OF DOCTOR OF PHILOSOPHY

Advisor: Christopher J. Douglas

August 2017

Acknowledgements

The completion of this dissertation would not have been possible without the help of so many people. I will not be able to name everyone and for that I apologize.

I would like to start by thanking my family. I have not always been the best son or brother, especially during my graduate studies, but I have received nothing but love and support from them nonetheless.

I would also like to thank Ashley Dreis, without whom I would not be where I am today. Your fervent challenging pushed me to new levels of understanding, particularly the understanding I have of myself.

I would like to thank my advisor, Chris Douglas. Your patience, understanding, and insight over the last six years has been greatly appreciated. You have been an excellent example for how one can stay dedicated to one's discipline while maintaining a life outside of that.

I would like to thank all of the Douglas group members, particularly Matt Eastwood, Grant Frost, and Sarah Wegwerth. You have helped create an intellectually stimulating and fun environment, and you are the reason I have enjoyed coming to work every day for the last six years.

I would also like to thank Professors Tom Hoye and Joe Topczewski. I have thoroughly enjoyed the chemistry discussions had during Synthesis Lunch, and I have learned a lot from them.

Finally, I would like to thank my thesis committee members: Steve Kass, Dan Harki, Tom Hoye, and Chris Douglas. I appreciate the time you have given up to help make this dissertation possible.

Dedication

This dissertation is dedicate to all curious minds, who seek understanding above all else.

"I have no special talents. I am only passionately curious."

– Albert Einstein

Abstract

Chapter 1: this chapter introduces the area of carbon–carbon sigma bond activation, as well as the contributions made to the field by the Douglas group. Efforts to develop a diastereoselective intramolecular alkene cyanoamidation methodology involving C–CN bond activation are described. The development of an intramolecular alkene aminocyanation methodology utilizing N–CN bond activation is also described.

Chapter 2: this chapter provides a brief summary of the development of metal-organic cooperative catalysis approaches to bond activation and functionalization methodologies, including prior work reported by the Douglas group on the intramolecular hydroacylation of alkenes. Efforts to develop chiral organic co-catalysts for these intramolecular alkene hydroacylation reactions are also described.

Chapter 3: this chapter introduces the dragmacidin family of natural products. A particular emphasis is placed on previously reported syntheses of dragmacidins D, E, and F, and how these synthetic efforts have contributed to the structural assignment of this family of natural products.

Chapter 4: this chapter depicts our efforts toward the total synthesis of dragmacidin E. A retrosynthetic analysis focused on utilizing the intramolecular alkene hydroacylation methodology developed by the Douglas group is described, as well as efforts to synthesize a suitable substrate for this key synthetic step.

Table of Contents

List of Abbreviations

(pin)	pinacolato
Ac	acetyl
acac	acetylacetonate
Ar	aryl
BDE	bond dissociation energy
Bn	benzyl
Boc	*tert*-butyloxycarbonyl
Bz	benzoyl
calcd	calculated
cat.	catalytic
CDI	carbonyl diimidazole
cod	1,5-cyclooctadiene
coe	cyclooctene
Cp	cyclopentadienyl
Cp*	1,2,3,4,5-pentamethylcyclopentadienyl
Cy	cyclohexyl
d.r.	diastereomeric ratio
DABCO	1,4-diazabicyclo[2.2.2]octane
dba	dibenzylideneacetone
DBFphos	4,6-bis(diphenylphosphino)dibenzofuran
DBU	1,8-diazabicyclo[5.4.0]undec-7-ene
DCE	1,2-dichloroethane
DCM	dichloromethane
DDQ	2,3-dichloro-5,6-dicyano-1,4-benzoquinone
DEAD	diethyl azodicarboxylate
DIBAL	diisobutyl aluminum hydride
DIPEA	diisopropylamine
DMAP	4-dimethylaminopyridine
DME	1,2-dimethoxyethane
DMF	dimethylformamide
DMPU	1,3-dimethyl-3,4,5,6-tetrahydro-2(1H)-pyrimidinone
DMSO	dimethylsulfoxide
DPEphos	bis[(2-diphenylphosphino)phenyl] ether
DPPA	diphenylphosphoryl azide
dppb	1,4-bis(diphenylphosphino)butane

dppe	1,2-bis(diphenylphosphino)ethane
dppf	1,1′-ferrocenediyl-bis(diphenylphosphine)
dppp	1,3-bis(diphenylphosphino)propane
ee	enantiomeric excess
ent	enantiomer
equiv.	equivalent
ESI	electrospray ionization
Et	ethyl
GC/MS	gas chromatography/mass spectrometry
HPLC	high pressure liquid chromatography
HRMS	high resolution mass spectrometry
HWE	Horner-Wadsworth-Emmons
hν	light
i-Pr	iso-propyl
IR	Infrared Spectroscopy
KIE	kinetic isotope effect
L	ligand
LDA	lithium diisopropylamide
Me	methyl
MEM	2-Methoxyethoxymethyl
MOCC	metal-organic cooperative catalysis
MONOPHOS	(3,5-dioxa-4-phosphacyclohepta[2,1-a:3,4-a']dinaphthalen-4yl)dimethylamine
MS	mass spectrometry
MTBE	methyl tertiary-butyl ether
NBS	*N*-bromosuccinimide
*n*Bu	normal butyl
NIS	*N*-iodosuccinimide
Nixantphos	4,6-Bis(diphenylphosphino)phenoxazine
NMO	N-Methylmorpholine N-oxide
NMR	nuclear magnetic resonance
Np	naphthyl
n-Pr	normal propyl
N-Selectride	sodium tri-sec-butylborohydride
Nuc	nucleophile
PDC	pyridinium dichromate
PEG	poly(ethylene glycol)
Ph	phenyl

PMB	para-methoxybenzyl
PMP	para-methoxyphenyl
PPG	poly(propylene glycol)
PPTS	pyridinium para-toluenesulfonate
PTFE	poly(tetrafluoroethylene)
Py	pyridyl
quant.	quantitative
Rf	retention factor
RT	room temperature
Rt	retention time
SEM	2-(trimethylsilyl)ethoxymethyl
SNAr	nucleophilic aromatic substitution
TBAF	tetrabutylammonium fluoride
TBDPS	tert-butyldiphenylsilyl
TBS	tert-butyldimethylsilyl
t-Bu	tertiary butyl
TEOC	2-trimethylsilylethoxycarbonyl
Tf	trifluoromethanesulfonate
TFA	trifluoroacetic acid
THF	tetrahydrofuran
TLC	thin layer chromatography
TMEDA	*N*,*N*,*N*',*N*'-tetramethylethylenediamine
TMS	trimethylsilyl
tol	tolyl
Tp	tris(pyrazolyl)borate
TPAP	tetrapropylammonium perruthenate
Ts	4-toluenesulfonyl
Xantphos	4,5-bis(diphenylphosphino)-9,9-dimethylxanthene
μwave	microwave irradiation

List of Tables

List of Figures

List of Schemes

.

CHAPTER 1: ORGANONITRILE BOND ACTIVATION AND FUNCTIONALIZATION

1.1. Introduction to C–C Bond Activation

Organic chemistry is often defined as the chemistry of carbon. Perhaps the most important feature of carbon is the strength of the highly covalent bonds it forms to itself and to hydrogen. These unreactive bonds provide the skeletal framework through which complex molecular structures can be built. The importance of carbon-carbon sigma bonds (henceforth abbreviated as 'C–C bonds') to molecular structure is reflected in the emphasis placed on their formation when chemists approach synthetic challenges. This emphasis on C–C bond formation has vaulted reactions such as the Diels-Alder, aldol, and Suzuki to prominence within the field of organic chemistry. It is therefore less intuitive to see how the cleavage of C–C bonds would be of significant use to synthetic organic chemists. However, if such a cleavage could be coupled to other C–C bond forming transformations, a great deal of structural complexity could be generated in a short amount of time. Such a novel strategy could open new doors into how chemists approach the synthesis of complex molecules, as C–C bonds could then also be viewed as a functional group.

Carbon–carbon sigma bond (C–C) activation is a contemporary area of research that aims to selectively cleave C–C bonds, often for the purpose of generating new C–C

bonds and increasing structural complexity.[1-9] While C–C bonds are routinely cleaved in the fossil fuel industry in a process known as hydrocarbon cracking,[10] this cleavage is by no means selective and the process drastically reduces molecular complexity. A key discovery that has led to the development of numerous areas of research, including C–C bond activation, was that transition metals are capable of oxidatively inserting into sigma bonds (Scheme 1.1).[11]

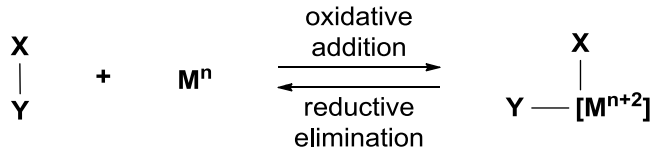

Scheme 1.1. Oxidative addition and reductive elimination of the generic X–Y covalent bond. M = transition metal, n = oxidation state.

The insertion process, i.e. oxidative addition, cleaves the original X–Y sigma bond and generates two new metal-ligand covalent bonds, X–M and Y–M,. resulting in an increased formal oxidation state of the metal center. The microscopic reverse of oxidative addition, i.e. reductive elimination, involves the re-formation of the X–Y sigma bond upon loss of two metal-ligand covalent bonds, X–M and Y–M, thereby decreasing the formal oxidation state of the metal center. It should be noted that in the field of C–C bond activation, the term "activation" generally refers to oxidative addition into a C–C bond. Further manipulation of the resulting organometallic intermediate is necessary for a transformative reaction to take place. The overall process is said to have effectively functionalized a C–C bond. Therefore, C–C bond activation is often used in conjunction with the term C–C bond functionalization.

Oxidative addition was initially demonstrated with moderately reactive small molecules, e.g. H_2, HCl, MeI,[11] but these initial reports prompted investigations into the possibility that a similar mechanistic process could be used for the activation of traditionally unreactive small molecules, e.g. alkanes and N_2. This possibility was further supported in the report by Kliman and Dubeck on the insertion of a Ni(II) species into the C–H bond of azobenzene in an intramolecular fashion to afford metallacycle **1.1** (Scheme 1.2).[12]

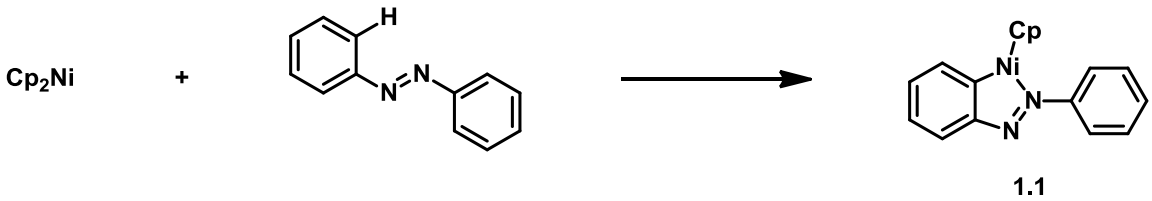

Scheme 1.2. Kliman and Dubeck's report on the insertion of Cp_2Ni into the C–H bond of azobenzene.

Kliman and Dubeck's discovery brought about an area of research focused on the activation and functionalization of C–H sigma bonds. Despite the fields of C–H and C–C bond activation being closely related, C–H activation has far exceeded C–C activation in research progress. C–C activation is less well-studied, which is largely due to the greater difficulty associated with the selective activation of C–C bonds. There are a number of fundamental reasons for this difficulty and they will be discussed in the following paragraphs.

A basic consideration is that a typical organic molecule has both C–C and C–H bonds with C–H bonds generally outnumbering C–C bonds. Organic molecules could then be viewed as having a greater concentration of C–H bonds than C–C bonds. Since a

reaction rate is the multiple of both a rate constant and a concentration, developing a reaction that selectively activates C–C bonds over C–H bonds is inherently challenging due to the typical constitution of organic molecules.

Steric factors are also important when comparing C–C and C–H activation. Due to the tetrahedral geometry adopted by sp^3-hybridized carbon, and the *cis*-addition that results from concerted oxidative addition, activation of a sp^3-hybridized C–C bond creates steric interactions that are far more severe than those that arise from insertion into a C–H bond (Scheme 1.3).

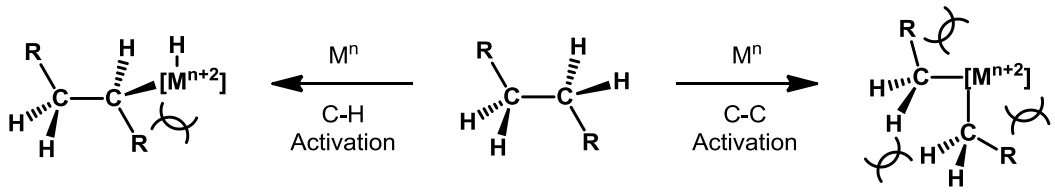

Scheme 1.3. Steric interactions resulting from insertion into C–H and C–C bonds. M = transition metal, n = oxidation state.

Orbital interactions must also be considered when comparing C–C and C–H bond activation. For a transition metal to undergo concerted oxidative addition into a C–C or C–H bond, the orbitals of the C–C or C–H bond must rotate off-axis in order to establish orbital overlap with the metal (Figure 1.1). The spherical nature of the hydrogen 1s orbital allows the C–H bond to maintain more orbital overlap during this off-axis rotation. Conversely, the directionality of the sp^3-hybridized orbitals in the C–C bond leads to more significant disruption of orbital overlap when off-axis rotation occurs, the consequence of which is a higher energetic barrier for oxidative addition into C–C bonds.

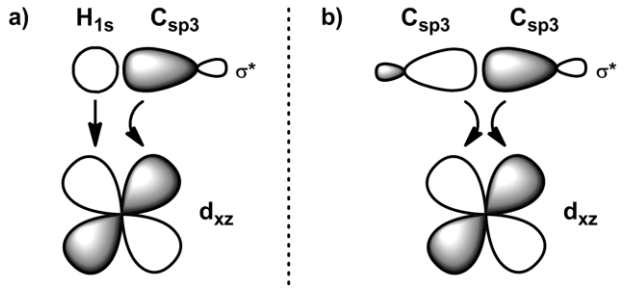

Figure 1.1. Orbital rotation required for a) C–H activation and b) C–C activation.

Finally, enthalpic factors also contribute to the difficulty associated with selectively enacting C–C bond activation over C–H bond activation (Scheme 1.4). Oxidative addition into C–H or C–C bonds by a transition metal (M) is generally uphill in energy in both cases. This is the result of two factors: 1) the strength of C–H and C–C bonds (bond dissociation energies of approx. 100 kcal/mol and 90 kcal/mol, respectively)[13]; and 2) the low bond dissociation energies (BDEs) of the two new bonds formed, e.g. H–M or C–M (BDEs of approx. 60 kcal/mol and 25 kcal/mol, respectively)[14]. However, the strength of the H–M bond makes oxidative addition into C–H bonds less enthalpically unfavorable than oxidative addition into C–C bonds. If the transition state for oxidative addition reflects these differences in H–M and C–M bond strengths, C–H activation should again be favored over C–C activation. It is worth mentioning here that the unfavorable energetics of bond activation, for both C–H and C–C bonds, is why bond activation must be coupled to other bond-forming manipulations to result in a favorable transformation.

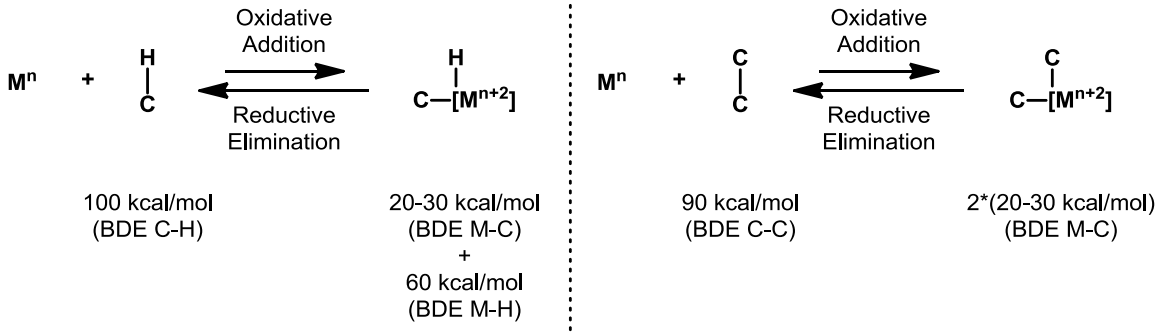

Scheme 1.4. Enthalpic challenges of C–H and C–C bond activation.

1.2. Strategies Utilized to Facilitate C–C Activation

The previous section demonstrated that C–C and C–H activation are both challenging processes due to kinetic and thermodynamic factors, with C–C activation being the more challenging of the two. An important consideration, however, is that the aforementioned enthaplic data is derived from general circumstances. For example, C_{aryl}–M bonds tend to be stronger than C_{alkyl}–M bonds,[14] and C_{acyl}–C bonds are typically weaker than other C–C bonds.[13] Exceptions like this are exploited to make the process of C–C activation not only feasible, but often favorable. Two basic strategies are usually employed: decreasing the stability of the starting material or increasing the stability of the organometallic intermediate. The following sections will cover the tactics chemists have developed to enact these strategies.

1.2.1 Relief of Ring Strain

There is a large amount of potential energy in strained ring systems.[15] Oxidative addition into a ring C–C bond can relieve some of this strain and provide the enthaplic driving force required to overcome the normally unfavorable process of C–C bond

activation. As such, this tactic is used to promote C–C bond activation via the strategy of decreasing the stability of the starting material.

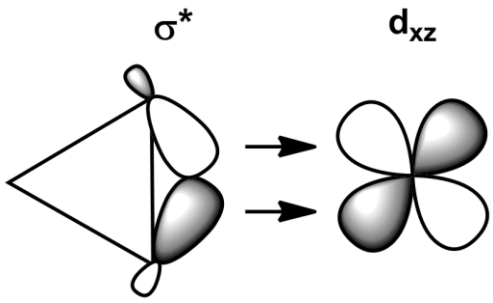

Figure 1.2. Cyclopropane "banana bonds" and orbital rotation required for C–C activation.

In addition to providing an enthaplic driving force, the unique disposition of the C–C orbitals in cyclopropane (sometimes referred to as “banana bonds”) can reduce the kinetic barrier for C–C activation. Since the C–C orbitals in cyclopropane are already twisted from the bonding axis due to ring strain,[16] the amount of rotation required to establish orbital overlap with the incoming metal is reduced (see Figure 1.2 above). As such, less orbital overlap in the C–C bond is lost in the transition state for C–C activation in cyclopropane which lowers the kinetic barrier.

The first example of C–C activation of a strained ring came from a report by Tipper in 1955.[17] In this report, Tipper attempted to synthesize platinum complex **1.2**, a cyclopropane analog of Zeises’ dimer (Scheme 1.5a). Tipper had concluded that platinum complex **1.2** was formed in the reaction of Pt(II) chloride with cyclopropane, however, a report by Chatt et al.[18] a few years later revealed the true significance of the work. In their report, Chatt et al.[18] demonstrated that the reaction of Pt(II) chloride with cyclopropane actually gave ring-opened platinacyclobutane **1.3**, which was thought to be

polymeric in nature. Ligation with pyridine gave the more well-defined platinacyclobutane **1.4**, which was able to be more thoroughly characterized and led to the discovery of the C–C activated nature of the product.

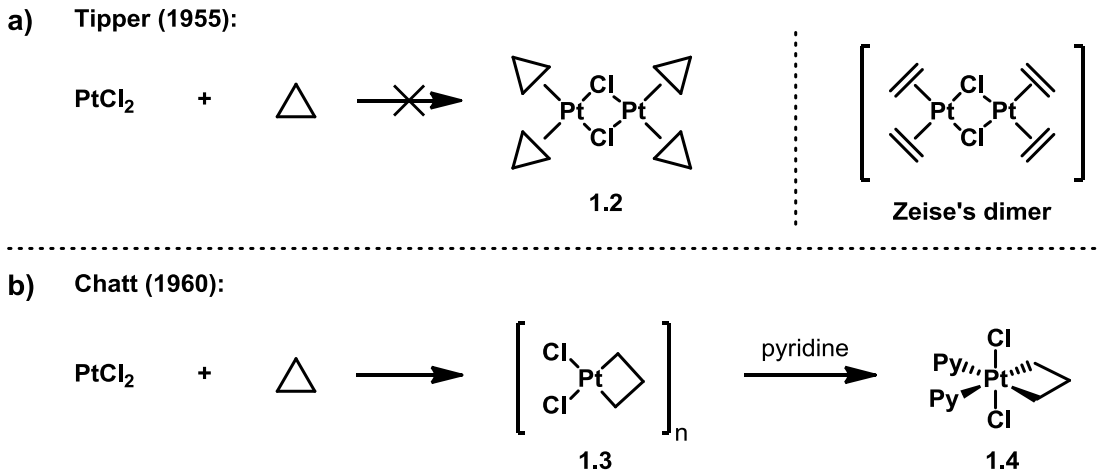

Scheme 1.5. a) Tipper's attempt to form a cyclopropane-ligated metal complex; and b) Chatt et al.'s discovery of the true structure of the product of the reaction.

Another important finding related to both C–C and C–H activation was reported by Bergman et al. in 1984.[19] They showed that even at low temperatures, rhodium(III) precatalyst **1.5** inserted into the C–H bond of cyclopropane after irradiation (Scheme 1.6). More importantly, they demonstrated that by simply allowing the C–H activated complex **1.6** to warm, rearrangement occurred to give rhodacyclobutane **1.7**. This indicated that in this system C–H activation was kinetically favored and C–C activation was thermodynamically favored.

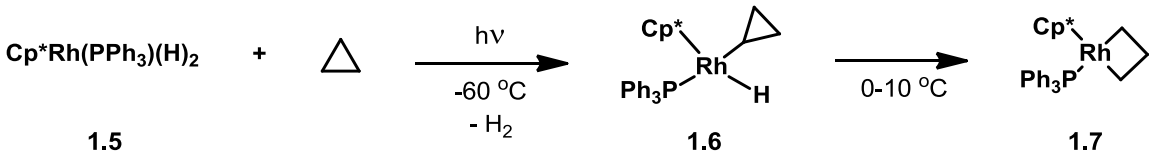

Scheme 1.6. Activation of both C–H and C–C bonds in cyclopropane using rhodium.

Since the early discoveries by Chatt[18] and Bergman[19], C–C bond activation of strained rings has received considerable attention.[1,2,4,20] A highlight in the field came about in 2007 when Murakami et al. demonstrated the utility of C–C bond activation when they reported the synthesis of the sesquiterpene natural product β-cuparenone (Scheme 1.7).[21] In this report, spiropentane **1.8** underwent rhodium catalyzed C–C activation under a carbon monoxide atmosphere to yield cyclopentanone **1.9**. The authors speculated that this occurs via C–C activation of spiropentane **1.8** to give rhodacyclobutane **1.10**, which was followed by 1,1-migratory insertion into a CO ligand to give rhodacyclopentanone **1.11**. beta-carbon elimination of rhodacyclopentanone **1.11** resulted in the release of ring strain and provided rhodacyclohexanone **1.12**. Reductive elimination from rhodacyclohexanone **1.12** and subsequent double-bond isomerization gave cyclopentanone **1.9**. The synthesis of cyclopentanone **1.9** via C–C activation of spiropentane **1.8** was followed by conjugate addition of a methyl nucleophile and provided racemic β–cuparenone in 62% yield over two steps.

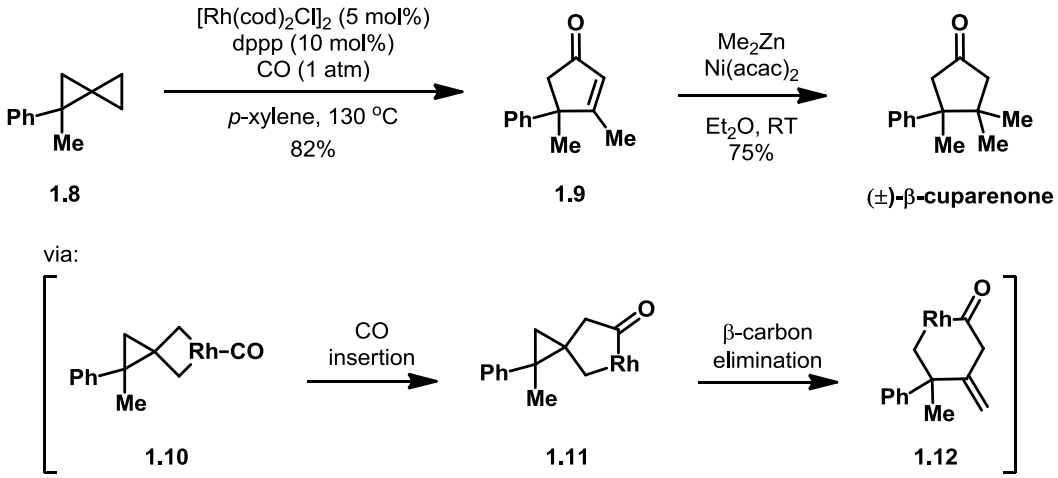

Scheme 1.7. Murakami's application of C–C activation of strained rings towards the synthesis of (±)-β-cuparenone.

1.2.2 Aromatic Stabilization

Aromaticity is a phenomenon that imparts unusual stability to molecules that possess this characteristic. Designing a substrate wherein C–C activation leads to an aromatic intermediate is another tactic used to overcome the enthalpic penalty that normally accompanies C–C bond activation. As such, this tactic aims to promote C–C bond activation via the strategy of increasing the stability of the organometallic intermediate.

An early illustrations of the aromatic stabilization tactic was a report[22] by Crabtree et. al. in which a cationic iridium(III) complex was used with *t*-butylethylene to convert 1,1-dimethylcyclopentane (**1.13**) to η^5-cyclopentadienyliridium complex **1.15** (Scheme 1.8). Cyclopentane **1.13** undergoes dehydrogenation via C–H activation, beta-hydride elimination, and hydrogenation of *t*-butylethylene to provide η^4-cyclopentadienyliridium complex **1.14**. Additional heating of η^4-cyclopentadienyliridium complex **1.14** led to the formation of C–C activation product **1.15**.

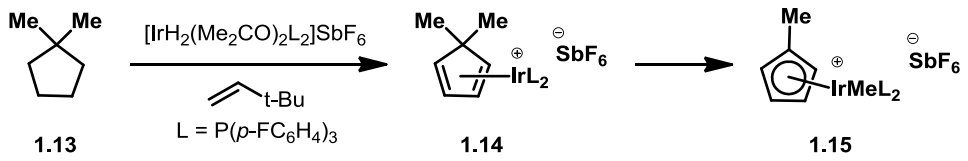

Scheme 1.8. Crabtree's utilization of aromatic stabilization to facilitate C–C activation.

Chaudret et. al. utilized aromatic stabilization in the synthesis of a variety of steroid analogues, such as phenol **1.16**, via C–C bond activation in the early 1990s (Scheme 1.9).[23,24] They not only demonstrated the applicability of C–C bond activation via aromatic stabilization, but that careful substrate design could also allow for selectivity. Despite the success of early examples, aromatic stabilization is the least commonly adopted strategy for C–C bond activation.

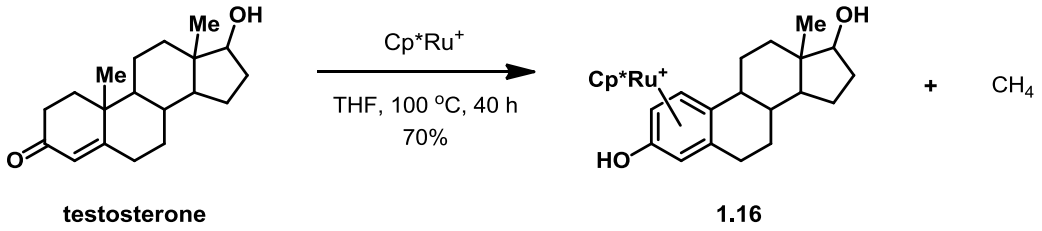

Scheme 1.9. Derivatization of testosterone via aromatic stabilization enabled bond activation.

1.2.3 Chelation Assistance

Chelation assistance aims to overcome both the kinetic and thermodynamic challenges of C–C activation by directing the transition metal towards the bond to be activated. This largely came about due to the observation of cyclometalation, a term used to describe the phenomenon wherein a transition metal undergoes intramolecular oxidative addition to form a cyclic structure and a C–M bond (Scheme 1.10).[25] Recall from Scheme 1.2 the insertion of Cp_2Ni into azobenzene reported[12] by Kliman and Dubeck. Here, insertion into the C–H bond by nickel presumably occurs after

coordination of the metal to one of the nitrogen atoms. Research into the phenomenon of cyclometalation revealed that 5-membered metallacycles were preferentially formed over 6-membered metallacycles due to greater stability.[26]

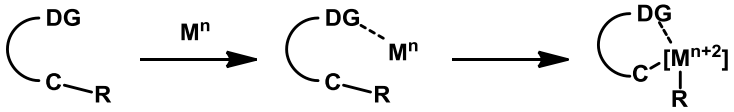

Scheme 1.10. Cyclometalation, an intramolecular bond activation process. M = transition metal, n = oxidation state, R = C/H, DG = directing group.

Strategic placement of a chelating functional group facilitates C–C activation in two ways: 1) ligation to the transition metal results in the continuous placement of the metal center near the bond to be activated. This effectively increases the local concentration of the metal and thereby speeds up the rate of C–C bond activation. 2) If a 5-membered metallacycle is formed upon oxidative addition into a C–C bond, the enthalpic penalty for C–C bond activation is offset to some degree by the increased stability of the metallacycle compared to a linear analogue. It could therefore be said that unlike the previous two tactics, which were primarily focused on the enthalpic challenges of C–C bond activation while secondarily addressing kinetic issues, chelation assistance addresses both kinetic and enthalpic issues simultaneously.

One of the first successful examples of chelation assistance for C–C bond activation was reported by Suggs and Jun in 1984.[27] Treatment of 8-quinolinyl ketone **1.17** with stoichiometric rhodium resulted in the formation of C–C bond activated intermediate **1.18** in just minutes at room temperature as the chlorine-bridged polymer (see Scheme 1.11 below). This was explicitly demonstrated via X-ray crystallography of

rhodium complex **1.19**, which formed readily by treating the chlorine-bridged polymer **1.18** with excess pyridine. It should be noted that in addition to having the benefit of chelation assistance, the C–C bond being activated in 8-quinolinyl ketone **1.17** is also weaker (BDE approx. 85 kcal/mol)[13] than a typical C–C bond (BDE approx. 90 kcal/mol)[13] due to the presence of the carbonyl moiety. It is also likely that rhodacycle **1.18** benefits from metal-to-ligand back-bonding, thereby increasing the strength of the C_{acyl}–M bond.

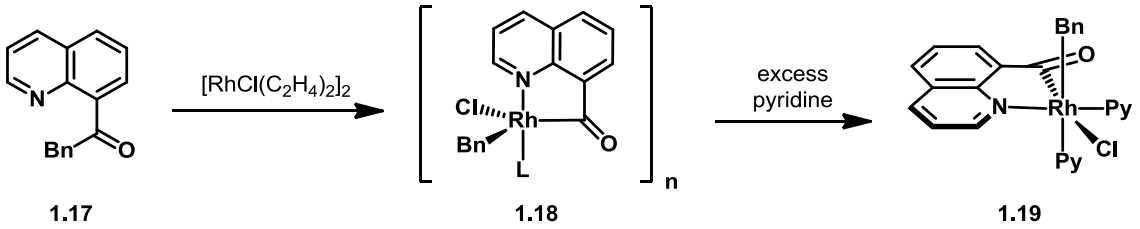

Scheme 1.11. Stoichiometric activation of C–C bonds in 8-quinolinyl ketones.

Suggs later demonstrated that this tactic could be accomplished with only a catalytic amount of the transition metal catalyst. In this report, 8-quinolinyl ketones **1.20**–**1.22** were all converted to 8-quinolinylethyl ketone **1.23** using ethylene and a catalytic amount of rhodium (Scheme 1.12).[28]

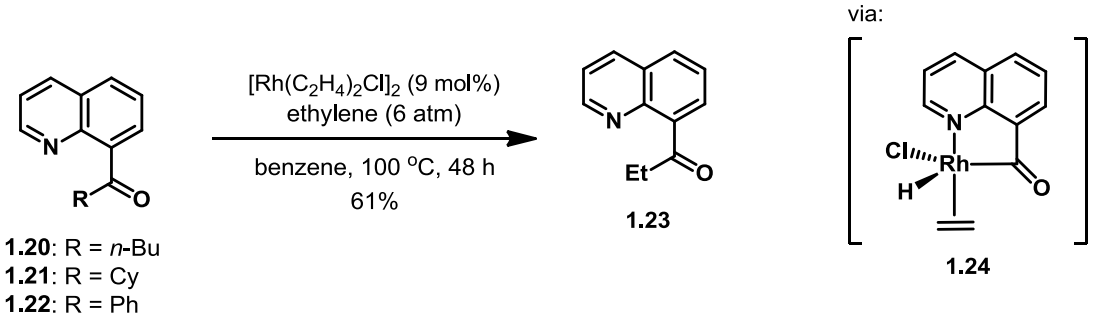

Scheme 1.12. Catalytic C–C bond activation and functionalization of 8-quinolinyl ketones.

Suggs and Jun suggested that this transformation occurred through a C–C bond activation intermediate similar to rhodacycle **1.18** (refer to Scheme 1.11 above). After C–C bond activation had occurred, migratory insertion of the alkyl group across metal-bound ethylene would allow for beta-hydride elimination to generate a new alkene (not shown) and, after ligand exchange with ethylene, rhodium-hydride **1.24**. Migratory insertion of hydride in rhodacycle **1.24**, followed by reductive elimination generated 8-quinolinylethyl ketone **1.23**. The authors note that alkenes besides ethylene were not efficient in the reaction. It is also worth noting that 8-quinolinylphenyl ketone **1.22** was successfully transformed into 8-quinolinylethyl ketone **1.23** despite the fact that no beta-hydrogens are available upon oxidative addition. Suggs and Jun ruled out the possibility of beta-elimination to form benzyne with deuterium-labeling studies (not shown). They suggest that in this case C–C bond activation is followed by migratory insertion into ethylene, which then provides the beta-hydrogens needed to enter their proposed catalytic cycle.

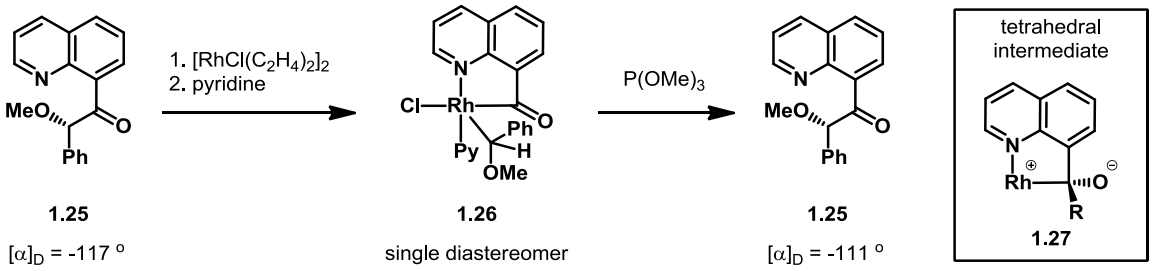

Scheme 1.13. Experimental evidence for a tetrahedral intermediate en route to C–C bond activation.

Suggs also reported the stereochemical consequences of C–C bond activation in 8-quinolinyl ketone **1.25** (Scheme 1.13).[29] In this report, C–C bond activation of the chiral carbon in 8-quinolinyl ketone **1.25**, after trapping with pyridine, resulted in the chiral-at-rhodium complex **1.26**. Phosphite-induced reductive elimination of rhodium complex **1.26** regenerated 8-quinolinyl ketone **1.25** with nearly the same enantiopurity. This result suggested to Suggs that both bond-breaking and bond-forming processes occurred with either a retention or inversion of configuration at the stereogenic carbon.

An interesting observation was that rhodium complex **1.26** was formed as a single diastereomer via NMR (see Scheme 1.13 above). However, heating rhodacycle **1.26** resulted in racemization at the rhodium center. Furthermore, the rate of racemization for rhodium was comparable to the rate of racemization for the stereogenic carbon. This led Suggs to propose tetrahedral intermediate **1.27** as an intermediate en route to C–C bond activation complex **1.26**. He noted that formation of tetrahedral intermediate **1.27**, followed by collapse and concomitant migration of the alkyl group to the metal would provide rhodacycle **1.26** in a mechanism similar to that of the Baeyer-Villiger reaction. Suggs also suggested that stereoinduction at rhodium then arose from collapse of tetrahedral intermediate **1.27**.

One of the first reports demonstrating the activation of a strong, unstrained C–C bond that was not driven by aromatization came from Milstein et al. in 1993.[30] In this seminal report PCP ligand **1.28** was used to direct a rhodium-hydride species towards the C_{methyl}–C_{aryl} bond (Scheme 1.14). It was envisioned that after C–C bond activation had

occurred, reductive elimination of methane might be used as a driving force for the reaction.

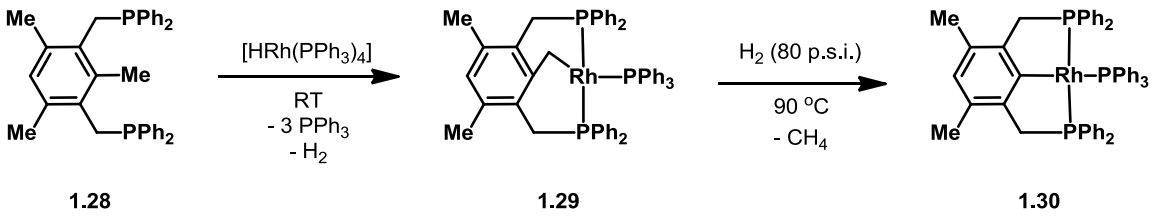

1.28 **1.29** **1.30**

Scheme 1.14. Milstein et al.'s use of PCP pincer ligands in the study of C–C and C–H activation chemistry.

At room temperature, however, C–H activation was favored resulting in alkyl rhodium complex **1.29** and loss of H_2. This is perhaps not surprising as the benzylic C–H bonds are far weaker (BDE = 88 kcal/mol) than the C_{methyl}-C_{aryl} bond (102 kcal/mol).[31]

Interestingly, heating alkyl rhodium complex **1.29** under a hydrogen atmosphere resulted in complete conversion to the product of C–C activation, aryl rhodium complex **1.30**. Milstein et al. suggested that this occurred via the activation of H_2 by alkyl rhodium complex **1.29**, which then undergoes reductive elimination to give the original PCP ligand **1.28** and thus establish C–H activation as a reversible process. However, when PCP ligand **1.28** undergoes C–C bond activation, the reductive elimination of methane was suggested to be irreversible and thus provided the driving force for the formation of aryl rhodium complex **1.30**.

Activation of C–CN bonds has also received considerable attention.[32] A generally-accepted mechanistic detail is that the metal is "directed" to the C–CN bond by the nitrile itself (see Scheme 1.15 below). Coordination of the nitrile to the metal in an η^2 fashion keeps the metal in close proximity to the C–CN bond, which increases the local

concentration of the metal and thus helps overcome the kinetic barrier. I would also speculate that the large amount of s character present in the sp-hybridized orbital of the nitrile carbon would also reduce the disruption of orbital overlap in the C–CN bond during the off-bonding-axis rotation that occurs upon oxidative addition, much like that of the 1s hydrogen orbital (refer back to Figure 1.1). Such an effect would also reduce the kinetic barrier for activation of C–CN bonds.

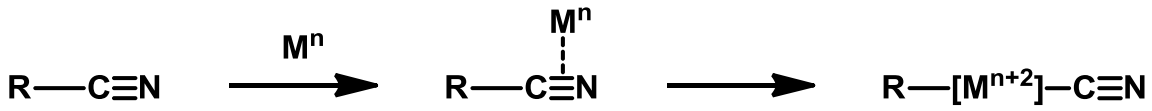

Scheme 1.15. Chelation mode of organonitriles facilitating C–C bond activation.

One of the first examples of C–CN bond activation was reported by Muetterties et al. in 1971.[33] Their report showed that trialkylphosphine ligands enabled Pt(0) insertion into the C–CN bond of benzonitrile to give *trans*-platinum complex **1.31** (Scheme 1.16).

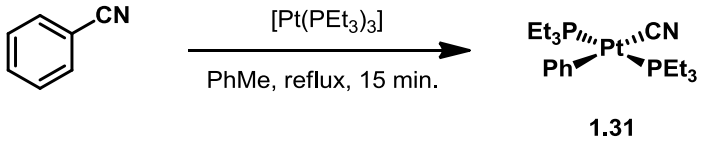

1.31

Scheme 1.16. Oxidative addition into the C–CN bond of benzonitrile.

One of the first reports to utilize this chemistry for increasing molecular complexity came from Nakao et al. in 2004.[34] Here the authors demonstrated that nickel, in combination with an electron-rich phosphine, was able to catalytically activate the C–CN bond of aryl nitriles **1.32** (Scheme 1.17). When this C–CN activation was coupled to migratory insertion across alkynes **1.33**, tetrasubstituted alkenes **1.34** were formed in moderate to good yield.

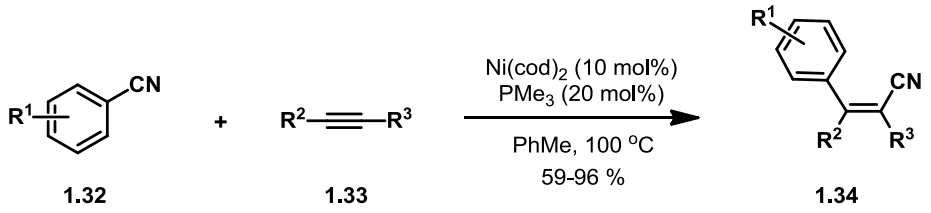

Scheme 1.17. Nakao's application of C–CN bond activation in the carbocyanation of alkynes.

An enantioselective transformation via C–CN bond activation was demonstrated by Takemoto et al. in 2008.[35] In this report, cyanoformamides **1.35** underwent C–CN bond activation which was coupled to intramolecular migratory insertion across an alkene to provide enantio-enriched oxindoles **1.36** (Scheme 1.18). This was achieved through the combination of palladium, chiral phosphoramidite ligand **1.37** and the Lewis base additive DMPU.

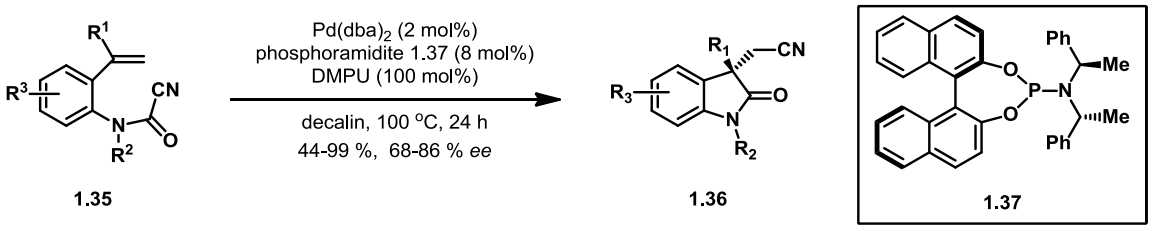

Scheme 1.18. Takemoto's enantioselective oxindole formation via C–CN bond activation.

1.3. Prior Work in the Douglas Group Involving Catalytic Bond Activation and Functionalization Methodologies

1.3.1 Bond Activation via 8-acylquinoline Directing Groups

The work done on C–C bond activation in the 1980s and 90s laid the foundation for the field. A common drawback to many of the aforementioned tactics developed during that time was that they were quite restricted in their scope and, more importantly, the reported examples often did not result in increased molecular complexity. A communication by the Douglas group in 2009 demonstrated how C–C bond activation

could be used to generate a significant amount of molecular complexity with a single transformation (Scheme 1.19).[36]

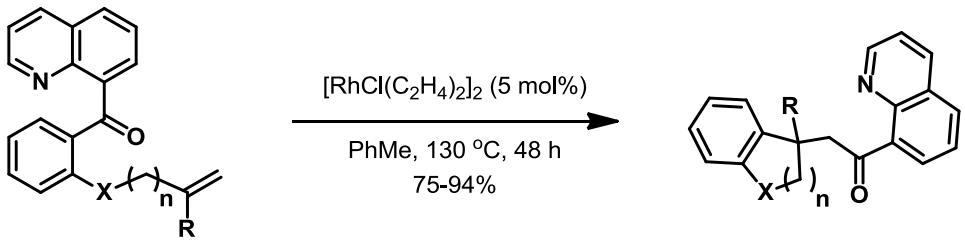

1.38
X = O, NMe, CH_2
n = 1,2
R = Me, Et, Ph

1.39

Scheme 1.19. Douglas' application of C–C activation leading to the construction of all-carbon quaternary stereocenters.

In this report, 8-quinolinylaryl ketones **1.31** underwent activation of the C_{aryl}–C_{acyl} bond followed by intramolecular migratory insertion and reductive elimination to give cyclized products **1.32**. These intramolecular alkene carboacylation reactions generated all-carbon quaternary stereocenters, thus demonstrating the power of C–C bond activation.

C–C bond functionalization using a quinoline directing group was extended to include an intermolecular variant. A 2009 report from Douglas et al. demonstrated that 8-quinolinylaryl ketone **1.40** could undergo either C–C or C–H bond activation, which was coupled to migratory insertion across norbornene (Scheme 1.20).[37]

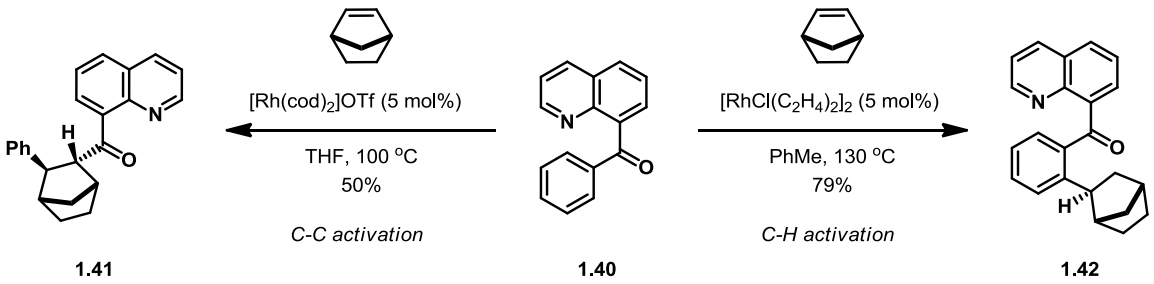

Scheme 1.20. Douglas et al.'s reported intermolecular C–C and C–H functionalization of quinolinyl ketone **1.40** with norbornene.

Surprisingly, a simple change of the solvent and precatalyst counterion resulted in the selection for either alkene carboacylation product **1.41** or alkene hydroacylation product **1.42**, arising from C–C or C–H activation of 8-quinolinylaryl ketone **1.40**, respectively. The *anti*- stereochemical relationship present in carboacylation product **1.41** was thought to arise by *in situ* epimerization of the α–carbonyl stereocenter.

Norbornene was chosen as the alkene coupling partner because it avoids competition between reductive elimination and beta–hydride elimination after migratory insertion has occurred. This is a consequence of the *syn*-addition that occurs during migratory insertion, and the need for a beta hydrogen to be *syn*-coplanar to the metal in order to undergo beta-elimination. Migratory insertion across norbornene is also more favorable than is typical with acyclic alkenes, as the loss of sp^2-hybridization that occurs during insertion relieves some of the ring strain present in the bicyclic system. It is worth noting that in Suggs' previous report[28] ethylene was the only alkene successfully coupled to C–C bond activation, despite attempts with other alkenes.

The success of 8-acylquinoline directing groups in the realm of C–C bond activation led to their extension into the area of C–O bond activation. In a 2011 report[38]

from Douglas et al., C_{acyl}–O bond activation of 8-quinolinyl esters **1.43** was accomplished with a cationic rhodium(I) catalyst (Scheme 1.21). This C–O bond activation was coupled to an intramolecular migratory insertion, which after reductive elimination afforded benzofurans **1.44**. This methodology generated a quaternary stereocenter and established a fully atom-economical transformation of an ester moiety.

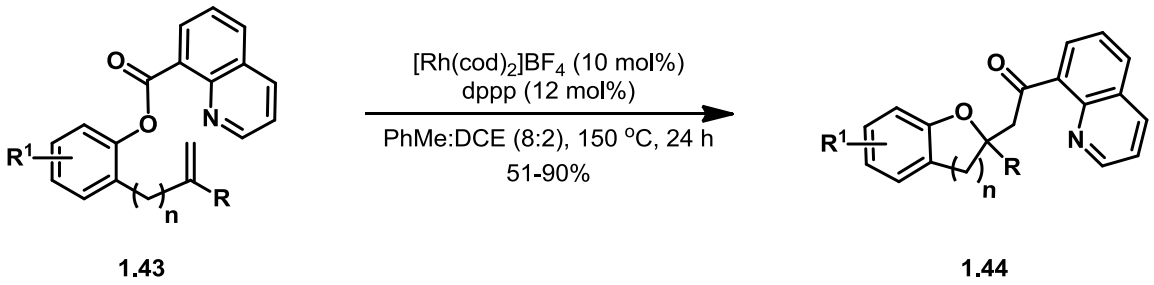

1.43 **1.44**

Scheme 1.21. Douglas et al.'s use of a quinoline directing group to effect intramolecular alkene oxyacylation via C–O bond activation.

1.3.2 Bond Activation and Functionalization of Organonitriles

The Douglas group has also explored C–C bond activation and functionalization reactions of organonitriles. As mentioned in section 1.2.3, nitriles can act as a directing group for methodologies seeking to utilize bond activation. Nitriles, however, are more versatile than most directing groups as they are also a commonly-employed functional group in-and-of themselves. The ability to effectively transform the directing group into a moiety of synthetic use is crucial for chelation-assisted bond activation methodologies to become a general synthetic strategy.

The first report of a C–CN bond activation and functionalization methodology from the Douglas group was in 2011. In this report cyanoformate esters **1.45** were converted to butenolides **1.46** via an intramolecular alkyne acylcyanation, followed by

double bond isomerization of the initial exocyclic alkene **1.48** (see Scheme 1.22 below).[39] A side products of these reactions was carbonate **1.47**, which was thought to arise from the reaction of free alcohol **1.49** and starting cyanoformate ester **1.45**. Alcohol **1.49** could be formed via decarbonylation after C–CN activation of the cyanoformate ester **1.45**. It was empirically discovered that the formation of carbonate **1.47** could be avoided through a combination of higher reaction temperatures and shorter reaction times.

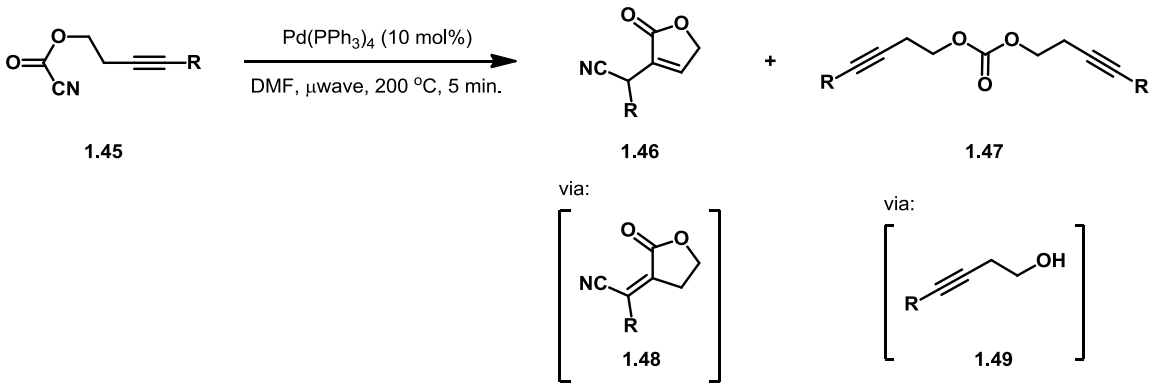

Scheme 1.22. Douglas et al.'s reported intramolecular cyanoesterification of alkynes.

Decarbonylation is a serious problem in the activation of C_{acyl}–CN bonds, as it generates a metal-carbonyl species that is deactivated towards oxidative addition due to the large amount of metal-to-ligand back-bonding into the carbonyl π* orbital. Decarbonylation becomes more problematic as the non-activated C_{acyl}–R bond weakens, becoming more prone to migration. The Douglas group demonstrated a way around the problem of decarbonylation through a formal intramolecular acylcyanation of alkenes via C–CN activation of α-iminonitriles **1.50** (Scheme 1.23).[40] Here the ketone was masked as the imine, which can be easily removed by hydrolysis after the reaction is complete. A

highlight of this methodology is that it generates an all-carbon quaternary stereocenter while allowing for further functionalization via manipulation of the nitrile.

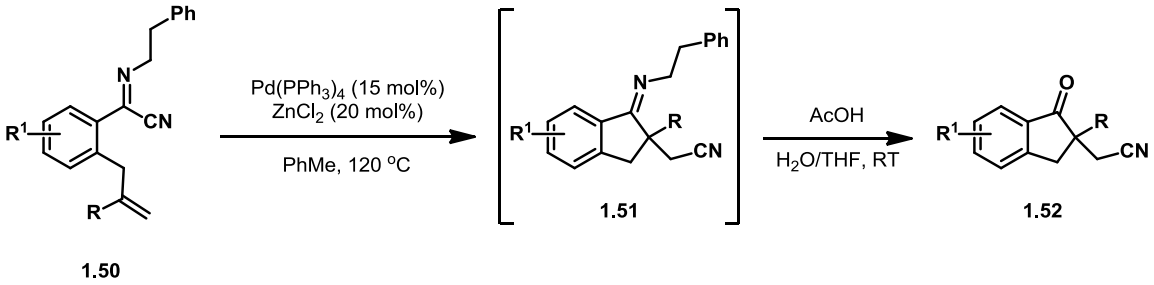

Scheme 1.23. Formal intramolecular acylcyanation of alkenes via α-iminonitriles.

Even before Takemoto's report[35] in 2008, the Douglas group has also explored the enantioselective cyanoamidation of alkenes as an application of C–CN activation. This led to a study of the mechanism through which these reactions occur, placing an emphasis on the source of enantioselectivity, the results of which have been recently reported (Scheme 1.24)[41] This study showed that the influence of solvent choice on enantioselectivity could be modeled well with the Abboud−Abraham−Kamlet−Taft (AATK) equation,[42] which is a more comprehensive assessment of solvent polarity compared to simple dielectric constants. Here, an inverse relationship between solvent polarizability (π*) and enantioselectivity was observed. It was also shown that the Lewis base additive DMPU, which was used in the report by Takemoto, had no effect on enantioselectivity and actually had an inhibitory effect on the rate of the reaction. The Lewis acid additive BPh_3, on the other hand, led to increased reaction rates but had a detrimental effect on enantioselectivity.

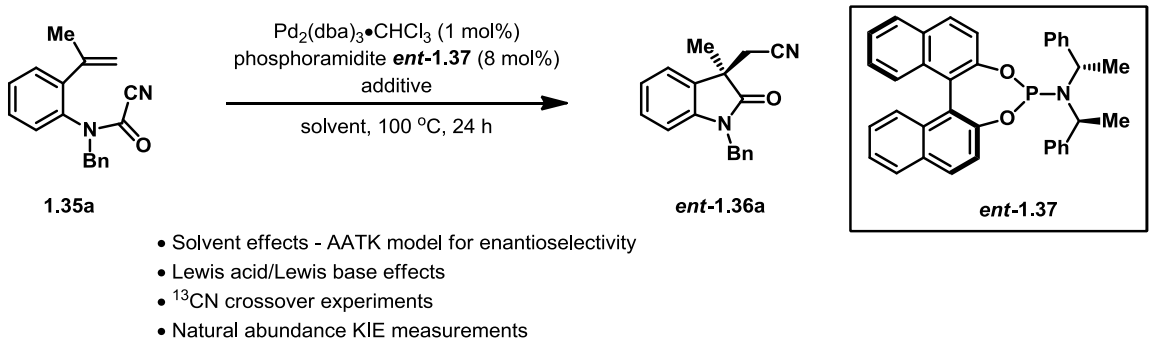

Scheme 1.24. Mechanistic studies on the intramolecular cyanoamidation of alkenes.

The use of ^{13}CN isotope labels allowed crossover studies to be performed. In the presence of the Lewis base DMPU and in the absence of other additives, full crossover of the ^{13}CN label was observed. This result suggested dissociation of the nitrile at some point in the reaction mechanism, which was thought to occur through ligand exchange once bound to palladium. In the presence of the Lewis acid BPh_3 crossover still occurred but to a much lesser degree. It was hypothesized that in the presence of Lewis acid cyanide dissociation from palladium is inhibited due to increased back-bonding of the metal. This results in neutral Pd(II) complex **1.53** as the species undergoing migratory insertion as the enantio-determining step of the reaction (Figure 1.3). Without Lewis acid, however, cyanide dissociation results in cationic Pd(II) complex **1.54** whereby the aryl groups present on the amine portion of the ligand can engage in secondary coordination to the metal. This secondary coordination stabilizes the metal cation and provides a more rigid structures through which enantio-induction would be more effective.

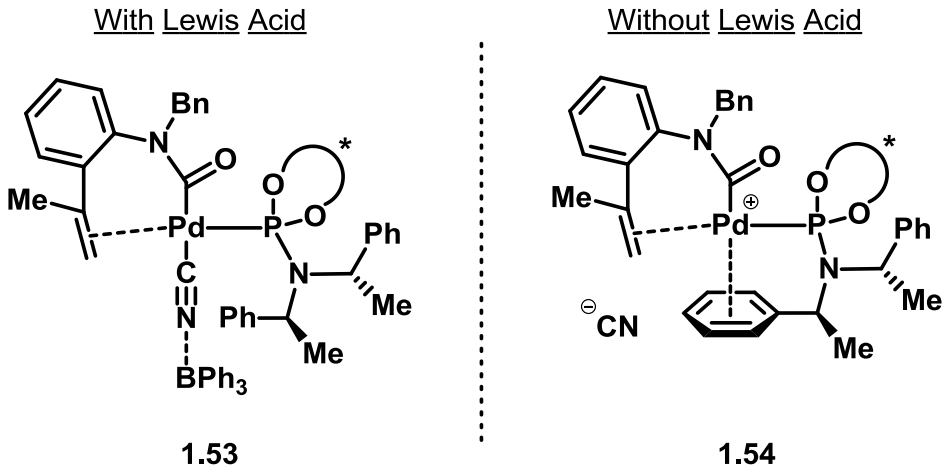

Figure 1.3. Proposed Pd(II) complexes en route to alkene cyanoamidation, with and without Lewis acid additives. * = chiral

1.4. Diastereoselective Intramolecular Alkene Cyanoamidation via the Activation and Functionalization of C–CN Bonds

The following section describes work that received contributions from Ashley Dreis, Sadie Otte, Matt Eastwood, Elizabeth Alonzi, myself, and Christopher Douglas. This work was recently reported in the European Journal of Organic Chemistry.[43]

1.4.1 Research Proposal

Reports for asymmetric intramolecular alkene cyanoamidation, from both the Takemoto[35] and Douglas[41] groups, have focused on variants of these C–C bond functionalization methodologies that rely on catalyst control to effect enantioselectivity. During efforts to optimize catalyst-controlled asymmetric alkene cyanoamidation methodologies, Ashley Dreis hypothesized that a substrate-controlled approach, utilizing a chiral auxiliary, might be a viable means of effecting asymmetric transformations. Takemoto's report on enantioselective intramolecular alkene cyanoamidation, as well as the mechanistic work reported by the Douglas group, often used a benzyl group to protect

the cyanoformamide nitrogen (Scheme 1.25a). It was hypothesized that the use of a chiral protecting group, in place of the previously-utilized benzyl group, could allow for diastereoselective intramolecular alkene cyanoamidations that take advantage of substrate control rather than relying on catalyst control (Scheme 1.25b). Furthermore, any inherent diastereoselectivity could potentially be enhanced with the appropriate choice of ligand.

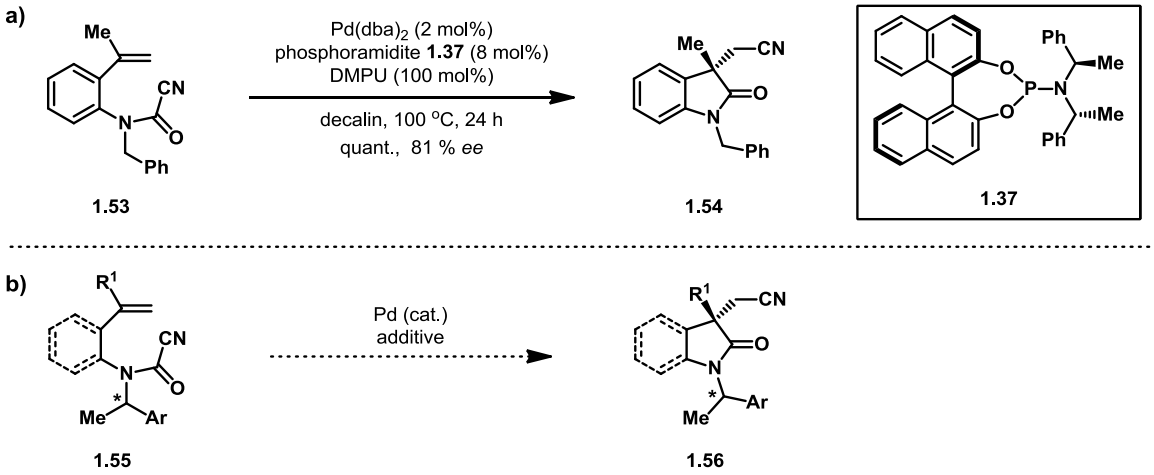

Scheme 1.25. a) enantioselective intramolecular alkene cyanoamidation with a benzyl-protected cyanoformamide and b) proposed diastereoselective intramolecular alkene cyanoamidation using a chiral protecting group.

1.4.2 Initial Screening Results

Aliphatic cyanoformamides **1.57** were targeted as the primary substrates for exploration into diastereoselective intramolecular alkene cyanoamidation methodologies (see scheme, Table 1.1 below). A synthetic route to these substrates (not shown), utilizing commercially-available chiral amines, was developed by Ashley Dreis, who also performed initial screening efforts.

Subjecting cyanoformamide **1.57a** (Ar = Ph, *R* configuration) to alkene cyanoamidation conditions with triphenylphosphine as ligand resulted in full conversion

to desired δ-lactam **1.58a** with a diastereomeric ratio of 3.8-to-1 (Table 1.1, entry 1). With this promising result in hand, other achiral phosphine ligands were screened for reactivity. Unfortunately, the use of P(*o*-tol)$_3$, PPh_2Me, and PCy_3 as ligands all led to a decrease in diastereoselectivity (entries 2-4). Use of the chiral phosphoramidite ***ent*-1.37** actually led to a diastereomeric ratio favoring what had previously been the minor diastereomer with achiral ligands (entry 5). Furthermore, phosphoramidite ***ent*-1.37** as ligand also resulted in a significant amount of undesired γ-lactam **1.59a**.

The formation of γ-lactam **1.59a** is hypothesized to occur via: 1) alkene isomerization; 2) C–CN activation and insertion into the isomerized alkene; and 3) beta-hydride elimination with subsequent elimination of HCN. The reversal of diastereoselectivity and decreased chemoselectivity observed with the use of phosphoramidite ***ent*-1.37** suggested that a mis-match between catalyst and substrate control may be operative, with catalyst control predominating in this case. To probe this, phosphoramidite **1.37** was tested as the ligand. Consistent with the mis-match hypothesis, phosphoramidite **1.37** resulted in significant enhancement of the d.r. relative to the use of achiral phosphine ligands (Table 1.1, entry 6).

Table 1.1. Initial screening of reactivity and diastereoselectivity for intramolecular alkene cyanoamidation utilizing a chiral protecting group.

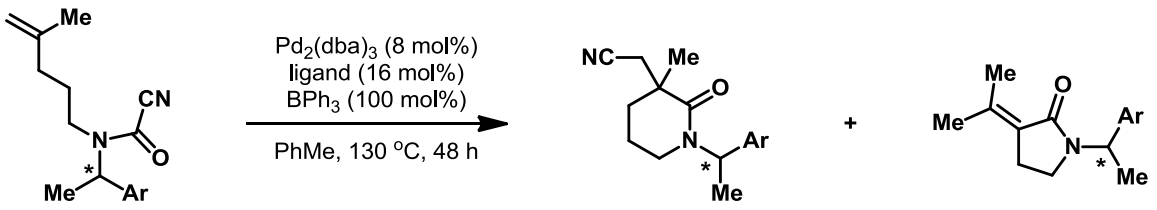

1.57a-c **1.58a-c** **1.59a-c**

Entry	Ar	Stereocenter (*) Configuration	Ligand	Consumption of **1.57**	Product Ratio (**1.58**: **1.59**)	d.r.
1	Ph	*R*	PPh_3	100 %	1:0	3.8:1
2	Ph	*R*	P(*o*-tol)$_3$	100 %	1:0	2.6:1
3	Ph	*R*	PPh_2Me	100 %	1:0	3.1:1
4	Ph	*R*	PCy_3	100 %	1:0	3.4:1
5	Ph	*R*	***ent*-1.37**	100 %	1.5:1	1:1.6
6	Ph	*R*	**1.37**	100 %	7.2:1	6.3:1
7	Ph	*S*	**1.60**	100 %	14.6:1	8.1:1
8	Ph	*S*	**1.61**	100 %	1:0	8.7:1
9	Np	*S*	PPh_3	100 %	1:0	4.1:1
10	Np	*S*	***ent*-1.37**	100 %	1.5:1	10.2:1
11	Np	*S*	**1.37**	100 %	2.3:1	2.3:1
12	Np	*S*	**1.61**	100 %	1:0	8.3:1

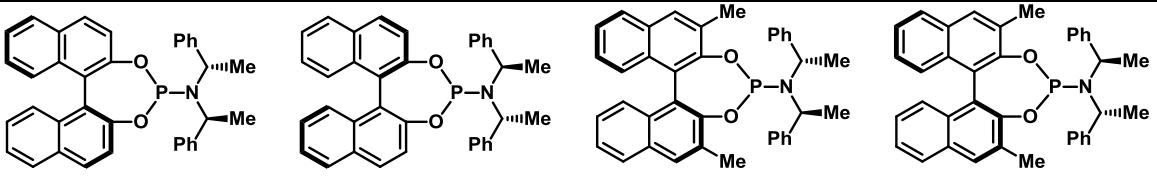

***ent*-1.37** **1.37** **1.60** **1.61**

Phosphoramidites **1.60** and **1.61**, diastereomeric ligands bearing methyl groups at the 3- and 3'-positions, were tested to see if the added steric bulk provided by the methyl substituents would improve diastereoselectivity (Table 1.1, entries 7 & 8). It was hypothesized that the diastereomeric relationship between phosphoramidites **1.60** and

1.61 would provide insight into the importance of the ligand amine moiety with regards to reaction diastereoselectivity. Of note is that ligands **1.60** and **1.61** have the opposite configuration at the biaryl stereocenter to phosphoramidite **1.37**. As such, cyanoformamide **1.57b** (Ar = Ph, *S* configuration) was chosen as the substrate to maintain the matched relationship between catalyst and substrate. Consistent with the hypothesis that increased steric bulk at the 3- and 3'-positions would lead to greater diastereoselectivity, phosphoramidites **1.60** and **1.61** both led to dramatically-improved d.r. and chemoselectivity, providing δ-lactam **1.58b** as a 8.1-to-1 and 8.7-to-1 mixture of diastereomers, respectively (Table 1.1, entries 7 & 8).

With the added steric bulk present in phosphoramidites **1.60** and **1.61** showing improved reaction diastereoselectivity, it was hypothesized that increasing the steric bulk on the substrate might also lead to more favorable reaction outcomes. To that end, the (*S*)-naphthyl(ethyl) protecting group was tested with achiral and chiral phosphine ligands (Table 1.1, entries 9-12). Consistent with the hypothesis that the bulkier (*S*)-napthyl(ethyl) protecting group would improve diastereoselectivity, alkene cyanoamidation of cyanoformamide **1.53c** (Ar = Np, *S* configuration) with achiral PPh_3 ligand produced δ-lactam **1.58c** as a slightly improved 4.1-to1 mixture of diastereomers (entry 9). Unfortunately, the use of both phosphoramidites ***ent*-1.37** and **1.37** resulted in reduced reaction chemoselectivity (entries 10 & 11). Interestingly, phosphoramidites ***ent*-1.37** and **1.37** both provided δ-lactam **1.58c** as a mixture of diastereomers favoring the same diastereomer, albeit at dramatically different ratios. These results suggest that while phosphoramidites ***ent*-1.37** and **1.37** still exhibit a matched/mis-matched relationship with

cyanoformamide **1.53c**, the bulky naphthyl substituent prohibited catalyst control from overturning substrate control in these cases.

Finally, the bulkier phosphoramidite **1.61** was tested with the bulkier cyanoformamide **1.53c** (Table 1.1, entry 12). This combination resulted in the formation of δ-lactam **1.58c** as a 8.3-to-1 ratio of diastereomers with complete chemoselectivity.

1.4.3 Reaction Scope Results

A limited substrate scope exploration for these diastereoselective cyanoamidation reactions was performed by Matt Eastwood, the results of which are shown below in Table 1.2.

Table 1.2. Substrate scope for diastereoselective intramolecular alkene cyanoamidation.

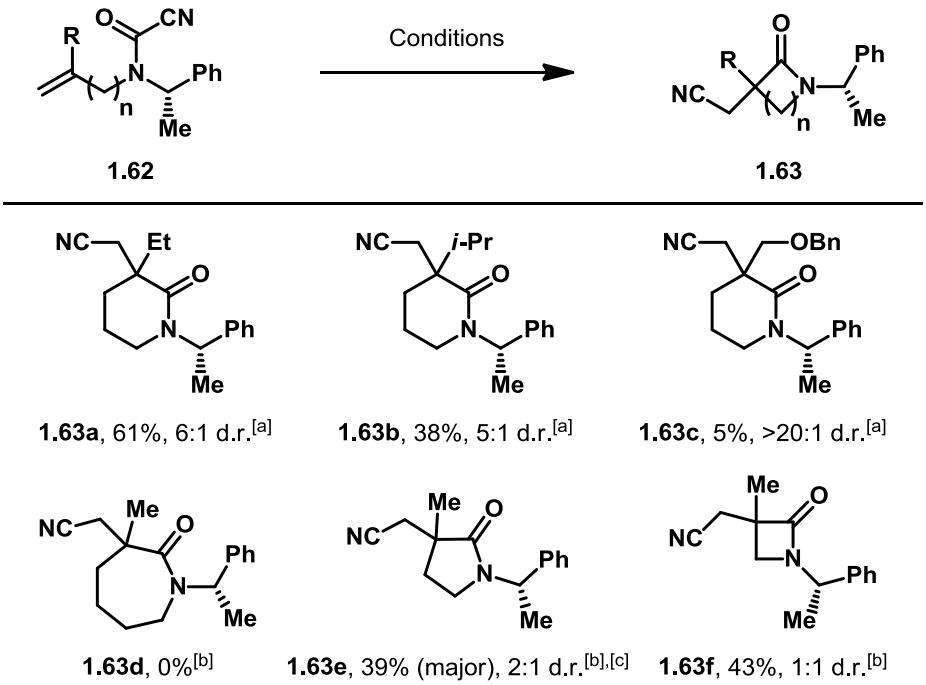

[a] Conditions: $Pd(dba)_2$ (8 mol%.), BPh_3 (100 mol%), phosphoramidite **1.61** (16 mol%), toluene, 130 °C, 48 h. [b] Conditions: $Pd(PPh_3)_4$ (8 mol%), BPh_3 (100 mol%), toluene, 130 °C, 48 h. [c] reaction run for 24 h.

A brief investigation into the substrate score revealed that the presence of an alkene ethyl substituent was tolerated (**1.63a**, Table 1.2), as was the bulkier isopropyl group (**1.63b**, Table 1.2), albeit with a slightly diminished yield. An electron deficient methylbenzyloxy substituents, however, was not tolerated (**1.63c**). Cyclization to afford a 7-membered ring was unsuccessful (**1.63d**), but 5- and 4-membered rings were produced in moderate yield (**1.63e** and **1.63f**, resprectively).

1.4.4 Cleavage of the Chiral Protecting Group

Work on the cleavage of the chiral protecting group was performed by Sadie Otte, Elizabeth Alonzi, and myself. Results have largely been unsuccessful, and this section will only describe my brief efforts to effect this transformation.

Our efforts to remove the chiral protecting group in δ-lactam **1.58** began with the synthesis of racemic material. This was done to avoid potential waste of valuable enantioenriched material. My contribution to this synthesis was the preparation of racemic phenyl(ethyl)amine **1.65** (Scheme 1.26). This was accomplished in 2 steps from commercially-available acetophenone. First, condensation with hydroxylamine afforded oxime **1.64** in excellent yield on relatively large scale. Subsequent palladium-catalyzed hydrogenation of oxime **1.64** provided phenyl(ethyl)amine **1.65** in good yield as the racemate. Initial attempts to reduce oxime **1.64** via a literature procedure[44] that involved palladium-catalyzed hydrogenation with the addition of HCl resulted in a complex mixture of phenyl(ethyl)amine **1.65**, acetophenone, and partially-reduced species. Other attempts to reduce oxime **1.64** using a reported[45] zinc and ammonium formate procedure resulted in a mixture of starting material, phenyl(ethyl)amine **1.65**, and formylated phenyl(ethyl)amine **1.65.**

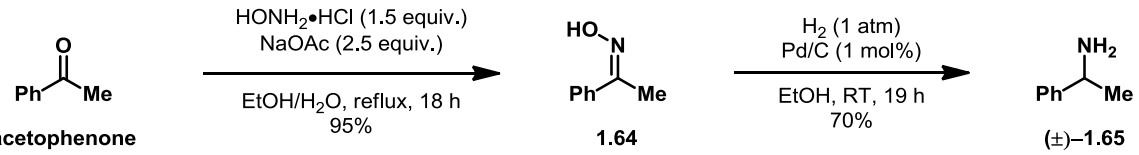

Scheme 1.26. Preparation of racemic phenyl(ethyl)amine **1.65**.

Sadie Otte, Matt Eastwood, and Elizabeth Alonzi used the prepared phenyl(ethyl)amine **1.65** racemate to synthesize racemic δ-lactam **1.58a** using the previously-established synthetic route, and optimized conditions for intramolecular alkene cyanoamidation. With δ-lactam **(±)-1.58a** in hand, attempts to remove the chiral

protecting group via hydrogenolysis and BBr_3-mediated cleavage resulted in no reaction taking place (Scheme 1.27).

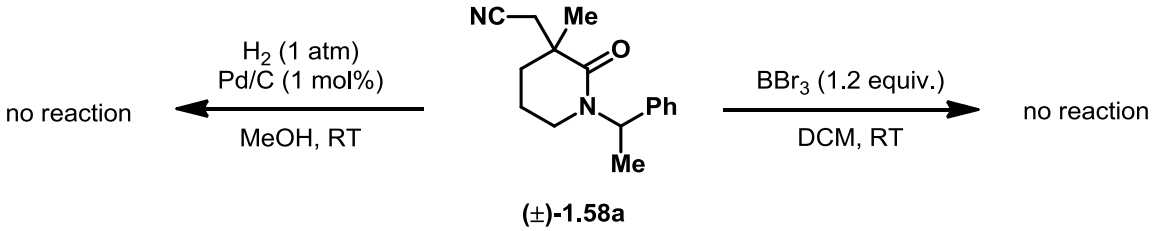

Scheme 1.27. Attempts to remove a chiral protecting group that resulted in no reaction occurring.

It was hypothesized that elevated temperatures would enable a BBr_3-mediated cleavage to occur. Indeed, treatment of δ-lactam **1.58a** with BBr_3 in refluxing chloroform did result in the consumption of starting material. However, ^{1}H NMR analysis of the crude reaction mixture suggested that the phenyl(ethyl) protecting group was left untouched. A slight upfield shift in the diastereotopic methylene protons adjacent to the nitrile suggested that a reaction had occurred at the nitrile moiety. As such, the product of this reaction has been tentatively assigned as amide **1.66** (Scheme 1.28).

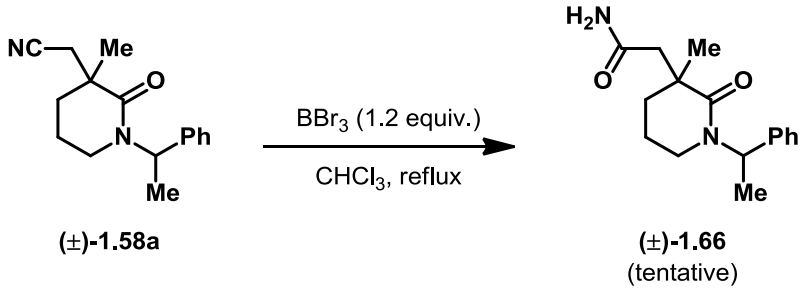

Scheme 1.28. Attempt to remove chiral protecting group leading to undesired reaction.

It is envisioned that this diastereoselective intramolecular alkene cyanoamidation methodology would be applicable in natural product syntheses. This would require the

development of conditions capable of removing the chiral protecting group. As such, efforts to remove this functionality are ongoing in our lab.

1.5. Intramolecular Alkene Aminocyanation via the Activation and Functionalization of N–CN Bonds

The following section describes work that received contributions from Zhonda Pan, Shengyang Wang, myself, and Christopher J. Douglas. This work is currently being reviewed for publication.

1.5.1 Background

Inspired by a report[46] from Nakao in 2012 on the intramolecular oxycyanation of alkenes, our group sought to extend our expertise with C–CN bond activation to the activation of N–CN bonds. Initial investigations into an intramolecular alkene aminocyanation methodology with rhodium catalysts gave promising results. A series of control experiments, however, showed that alkene aminocyanation could be effected solely with the Lewis acid $B(C_6F_5)_3$. These reported[47] metal-free reactions converted tosyl-protected cyanamides **1.67** into indolines and tetrahydroquinolines **1.68** (n = 1 and n = 2, respectively) in good to excellent yields and tolerated a variety of functional groups on the aromatic ring, including aryl halides (Scheme 1.29).

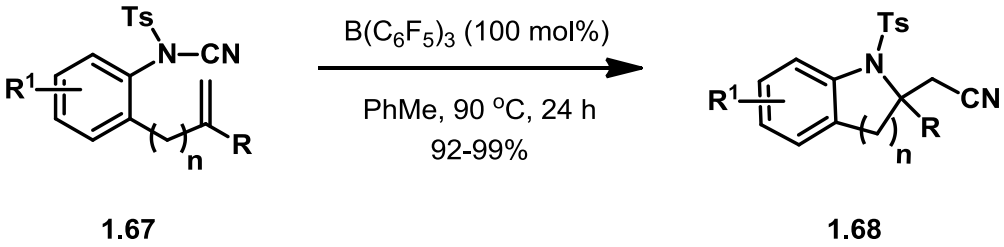

1.67 **1.68**

Scheme 1.29. Transition metal free intramolecular aminocyanation of alkenes reported by the Douglas group.

Concurrent with the publication on a metal-free alkene aminocyanation methodology by the Douglas group, Nakao reported[48] a similar reaction using palladium/boron cooperative catalysis. In this report, acyl-protected cyanamides **1.68** were cyclized to indolines **1.69** in moderate to excellent yields (Scheme 1.30).

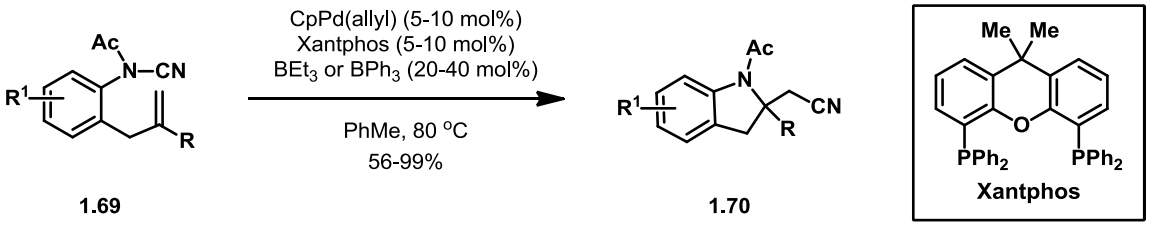

1.69 **1.70**

Scheme 1.30. Nakao's report on alkene aminocyanation using Pd/B cooperative catalysis

Notably, substrates containing a mono-substituted alkene (R = H) were also effectively converted to the corresponding indolines. This substitution pattern is atypical of bond activation substrates as the hydrogen present on the internal alkene carbon can allow for beta–hydride elimination after migratory insertion has occurred, which can then detrimentally compete with reductive elimination. Nakao attributed the success of these substrates to coordinating of Pd by the *N*-acyl protecting group after migratory insertion. This intramolecular coordination may prevent the metal from adopting the *syn*-coplanar arrangement required for beta–hydride elimination.

1.5.2 Research Proposal

The previously described work by both the Douglas and Nakao groups represents a novel alkene functionalization reaction. A shortcoming of both methodologies is the use of an aromatic linker to facilitate reactivity between the cyanamide and alkene moieties, which severely limits their scope. The report[48] from Nakao, however, did include a small number of examples wherein the reacting partners were not linked by an aromatic tether (Scheme 1.31). In these examples, the aliphatic linker contains a quaternary carbon. This demonstrated that the Thorpe-Ingold effect[49] may be an alternative way to increase intramolecular reactivity in these reactions, which would allow for an expansion of scope.

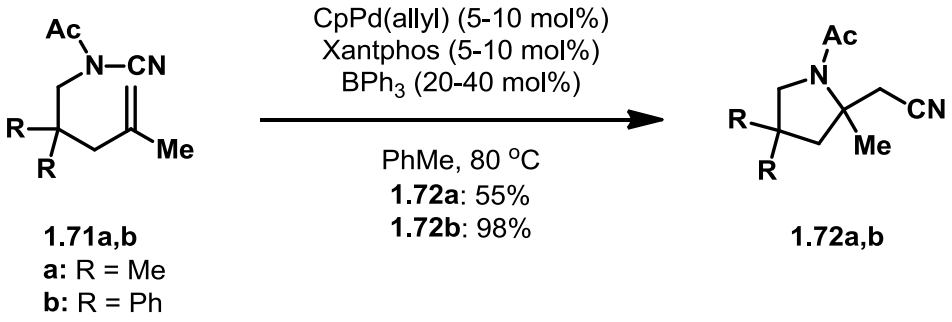

Scheme 1.31. Successful aliphatic substrates in intramolecular alkene aminocyanation reported by Nakao.

It was hypothesized that a simple alteration of functional group placement would lead to both increased intramolecular cyclization efficiency and more useful product scaffolds. Cyanamides **1.73** could take advantage of the Thorpe-Ingold effect[49] through the quaternary carbon adjacent to the carbonyl (see Scheme 1.32 below). Such structures would be easy to synthesize via traditional enolate chemistry and would provide lactams **1.74**, bearing two quaternary carbons, with at least one of those carbons being

stereogenic. Finally, if the quaternary carbon adjacent to the carbonyl were stereogenic, the reaction could potentially occur in a diastereoselective manner.

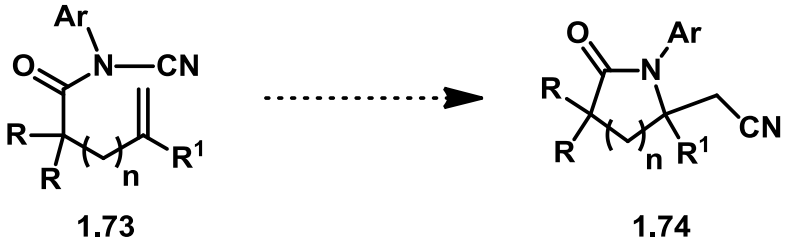

Scheme 1.32. Proposed scaffold for new intramolecular alkene aminocyanation substrates.

1.5.3 Initial Screening Results

Initial screening of reaction conditions for cyanamide **1.73a** (optimizing for yield of lactam **1.74a**) was carried out by Zhonda Pan. Initial testing of metal-free conditions with boron Lewis acids provided only starting material **1.73a** and decyanation product **1.75** (see Table 1.3 below, entries 1 & 2), whereas an aluminum Lewis acid led to unidentified decomposition (entry 3). Investigation into palladium/Lewis acid cooperative catalysis conditions provided the desired lactam **1.74a** in moderate-to-good yields (entries 4–7), with the combination of CpPd(1-phenylallyl) and Xantphos providing the best yield. A series of bidentate phosphines were chosen for screening based on their reported[50] bite angles (entries 8–14). A general correlation between increased bite angle and increased yield emerged with Xantphos (bite angle = 111°) providing the best result. Further increase in bite angle led to severely diminished reactivity. A control experiment was performed in which no Lewis acid was added (entry 15) and this resulted in a complex reaction mixture with a low yield of lactam **1.74a**.

Isolated yields were also established for reactions using BPh_3 and BEt_3 Lewis acids (entries 16 & 17, respectively) with BEt_3 giving superior results.

Table 1.3. Reaction optimization for intramolecular alkene aminocyanation of cyanamide **1.73a**.

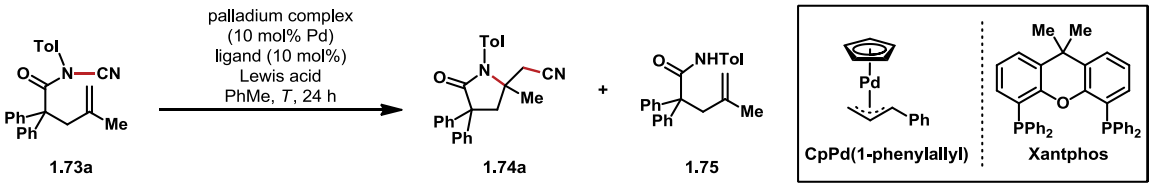

Entry	Palladium source	Ligand	Lewis acid (equiv.)	*T* (°C)	Yield of **1.74a** (%)[a]
1	–	–	BPh_3 (0.5)	100	0[b]
2	–	–	$B(C_6F_5)_3$ (0.5)	80	0[b]
3	–	–	$AlCl_3$ (0.5)	80	0[c]
4	CpPd(1-phenylallyl)	Xantphos	BPh_3 (0.5)	90	87
5	$Pd(PPh_3)_4$	–	BPh_3 (0.5)	90	81
6	$Pd(OAc)_2$	Xantphos	BPh_3 (0.5)	90	67
7	Pd_2dba_3	Xantphos	BPh_3 (0.5)	90	69
8	CpPd(1-phenylallyl)	dppe[d]	BPh_3 (0.4)	80	0[b]
9	CpPd(1-phenylallyl)	dppp	BPh_3 (0.4)	80	23
10	CpPd(1-phenylallyl)	dppb	BPh_3 (0.4)	80	49
11	CpPd(1-phenylallyl)	DPEphos	BPh_3 (0.4)	80	72
12	CpPd(1-phenylallyl)	Xantphos	BPh_3 (0.4)	80	93
13	CpPd(1-phenylallyl)	Nixantphos	BPh_3 (0.4)	80	81
14	CpPd(1-phenylallyl)	DBFphos	BPh_3 (0.4)	80	0[b]
15	CpPd(1-phenylallyl)	Xantphos	–	80	< 20[e]
16[g]	CpPd(1-phenylallyl)	Xantphos	BPh_3 (0.4)	80	89[f]

Entry	Palladium source	Ligand	Lewis acid (equiv.)	*T* (°C)	Yield of **1.74a** (%)[a]
1	–	–	BPh_3 (0.5)	100	0[b]
2	–	–	$B(C_6F_5)_3$ (0.5)	80	0[b]
3	–	–	$AlCl_3$ (0.5)	80	0[c]
17[g]	CpPd(1-phenylallyl)	Xantphos	BEt_3 (0.4)	80	99[f]

[a]Determined by ^{1}H NMR analysis using *p*-methoxyacetophenone as the internal standard. [b]Only **1.73a** and **1.75** detected by NMR spectroscopy. [c]Decomposition of **1.73a**. [d]Bite-angle values obtained from ref. 50: dppe 85°; dppp 91°; dppb 98°; DPEphos 102°; Xantphos 111°; Nixantphos 114°; DBFphos 131°. [e]Complex reaction mixture. [f]Yield after column chromatography. [g]Conditions applied to further substrate scope study.

1.5.4 Reaction Scope Results

After establishing efficient palladium/Lewis acid cooperative catalysis conditions, the scope of this reaction was investigated (see Table 1.4 below). The work on substrate scope exploration was performed by Zhongda Pan, Shengyang Wang and myself.

Substituents on the *N*-aryl ring of cyanamides **1.73** were generally well-tolerated (**1.74b-q**) with the exceptions of: 1) an acetyl group at the *para* position (**1.74h**); 2) substitution at the *ortho* position (**1.74n**); 3) an *N*-acetyl group at the *para* position (**1.74ak**); and 4) an aryl bromide (**1.74aj**). Notably, a pendant alkene (**1.74o**) was not isomerized under the reaction conditions and a heterocyclic aromatic ring also gave the desired lactam **1.74p** in excellent yield. A variety of geminal di-substituents at the α–amide carbon allowed for successful cyclization (**1.74r-v**), but a lack of substitution (**1.74w**) resulted in drastically lower yield. This suggests that Thorpe-Ingold effects are indeed important in the reaction. Substitution at the alkene (R^1) was less tolerated, as electron-withdrawing groups severely inhibited reactivity (**1.74z** and **1.74ai**), as did the absence of substitution (**1.74ab**).

Table 1.4. Substrate scope for the intramolecular aminocyanation of cyanamides **1.73.**

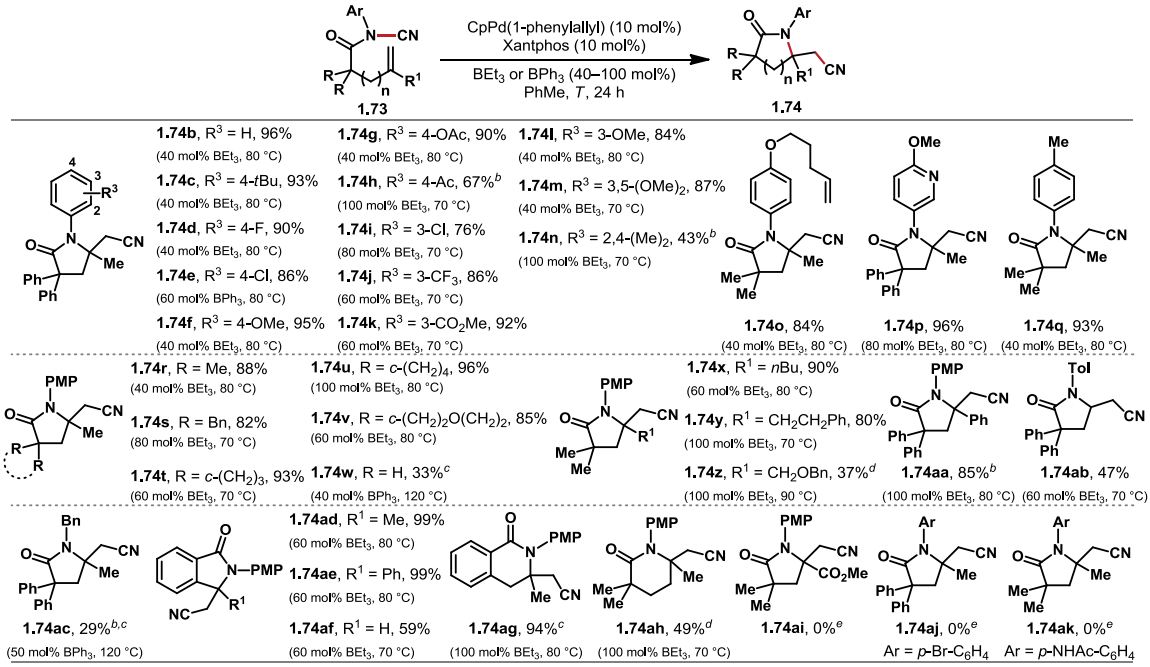

[a]Reaction conditions: CpPd(1-phenylallyl) (10 mol %), Xantphos (10 mol %), BPh_3 or BEt_3, PhMe (1.0 mL). Reaction time: 30 h (**1.74h**, **1.74m**); 36 h (**1.74u**, **1.74y**, **1.74aa**); 48 h (**1.74n**, **1.74s**, **1.74ab**, **1.74ah**); 24 h (all other entries). All yields are isolated yields. [b]Run with 15 mol % Pd/Xantphos. [c]Run in *m*-xylene. [d]Run with 20 mol % Pd/Xantphos. [e] Unconsumed staring material.

1.5.5 Diastereoselective Alkene Aminocyanation Results

Substrates bearing a stereocenter within the aliphatic tether were also used to test for diastereoselective variants of these intramolecular alkenes aminocyanation reactions. This work was performed by Zhongda Pan, Shengyang Wang, and myself. Indeed, substrates bearing a stereocenter at the α–amide carbon generally gave the desired lactam in excellent diastereomeric ratios (**1.77a-d** in Table 1.5 below). The exception to this was a substrate bearing an α–alkoxy group, which gave the corresponding lactam **1.77e** with only a moderate d.r. of 3.2:1. A substrate bearing an allylic stereocenter efficiently underwent cyclization, but produced the desired lactam **1.77f** with a d.r. of only 4.4:1.

Table 1.5. Diastereoselectivity in intramolecular alkene aminocyanation.

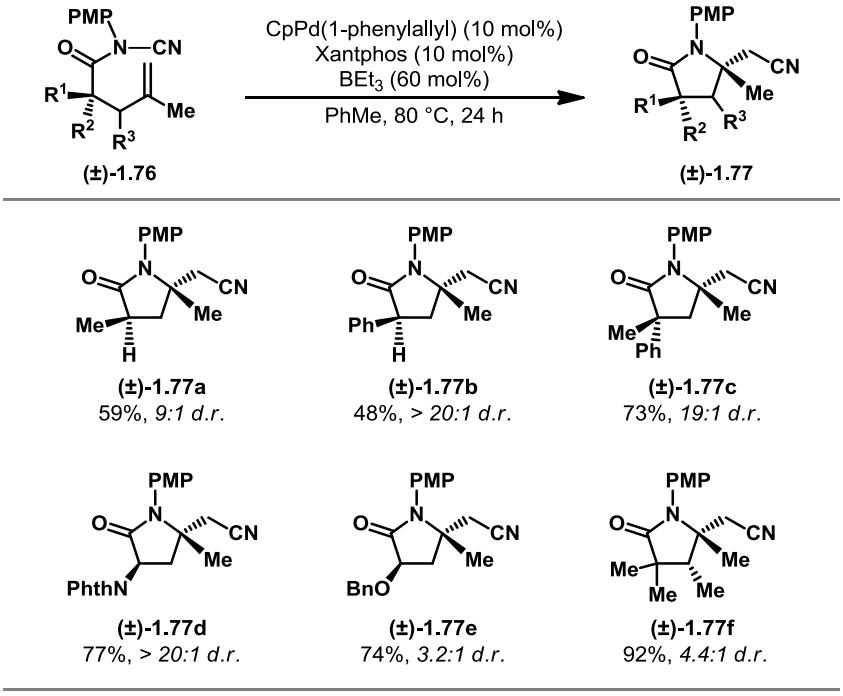

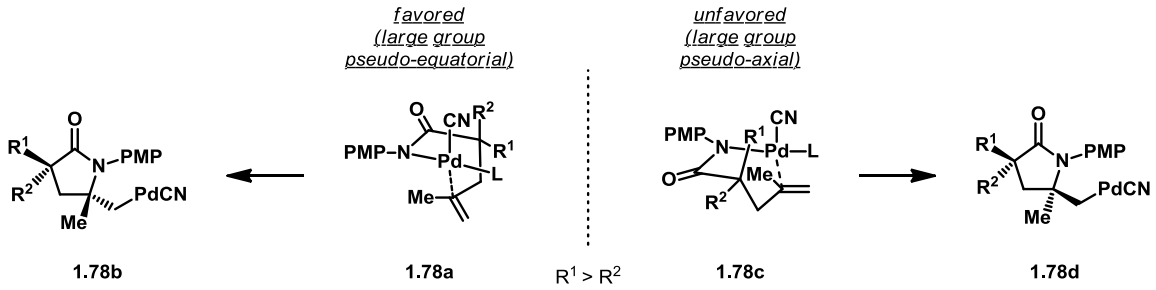

Scheme 1.33. Proposed model for diastereoselectivity in intramolecular alkene aminocyanation reactions.

I have proposed a model to account for the observed diastereoselectivity in these reactions (Scheme 1.33). To that end I have suggest the following: 1) after oxidative addition into the N–CN bond, intramolecular coordination of palladium to the alkene prior to migratory insertion generates a pseudo-six-membered ring. This results in two possible chair conformations, one with the large R^1 group axial and one with it equatorial,

as well as two possible boat conformations. Each of these conformations also allow palladium to bind to either prochiral face of the alkene, i.e. the *re* or *si* face, leading to 8 total possibilities. 2) Stereoelectronic requirements for migratory insertion, i.e. a *syn*-coplanar arrangement between the N–Pd bond and C–C π–bond, eliminates one possibility for each conformation, as coordination to one of the prochiral alkene faces does not allow for this geometric relationship. 3) Boat conformers may be favored over chair conformers in this case due to the large amount of planarity necessary for maintaining the amide bond. 4) Of the two possible boat conformers that fulfill the stereoelectronic requirements for migratory insertion, conformer **1.78a** positions the large R^1 group in a favorable pseudo-equatorial position and generates alkylpalladium intermediate **1.78b**. Reductive elimination of alkylpalladium **1.78b** then generates the observed major product from the reaction. Conversely, conformer **1.78c** places the large R^1 group in an unfavorable pseudo-axial position and generates alkylpalladium intermediate **1.78d**, from which reductive elimination provides the observed minor products. It is worth noting that this model would appear to conflict with the diastereoselectivity observed with lactam **1.77c** (see Table 1.5 above), as the larger R^1 group would be the methyl substituent and the smaller R^2 group would be the phenyl substituent in this case. However, it has been shown[51] that cyclohexane carbons bearing both methyl and phenyl substituents actually favor conformations wherein the phenyl group occupies the axial position. It could then be said that in this case the phenyl substituent may behave as the smaller group, preferring to adopt an axial or pseudo-axial position over an equatorial or pseudo-equatorial one.

1.5.6 Functionalization of alkene aminocyanation products

To demonstrate the versatility of the products generated from these intramolecular alkene aminocyanation reactions, Zhongda Pan, Shengyang Wang, and myself subjected lactam **1.74ad** to a variety of reaction conditions yielding functionalized products **1.79a-l** (Table 1.6). The nitrile moiety was efficiently converted to other carboxylic acid derivates (**1.79a-d**) as well as to alkyl and aryl ketones (**1.79e** and **1.79f**, respectively). Selective reductions of the nitrile to the primary- and Boc-protected amines were also effective (**1.79g** and **1.79h**, respectively). Interestingly, lactam **1.74ad** also underwent a formal [3+2] cycloaddition at the nitrile moiety to give tetrazole **1.72i** in good yield. Functionalization of the amide moiety was also demonstrated. This included removal of the *N*-substituted *para*-methoxy phenyl group (**1.79j**), conversion to thioamide **1.79k**, and reduction to secondary amine **1.79l**.

Table 1.6. Transformations of alkene aminocyanation product **1.74ad**.

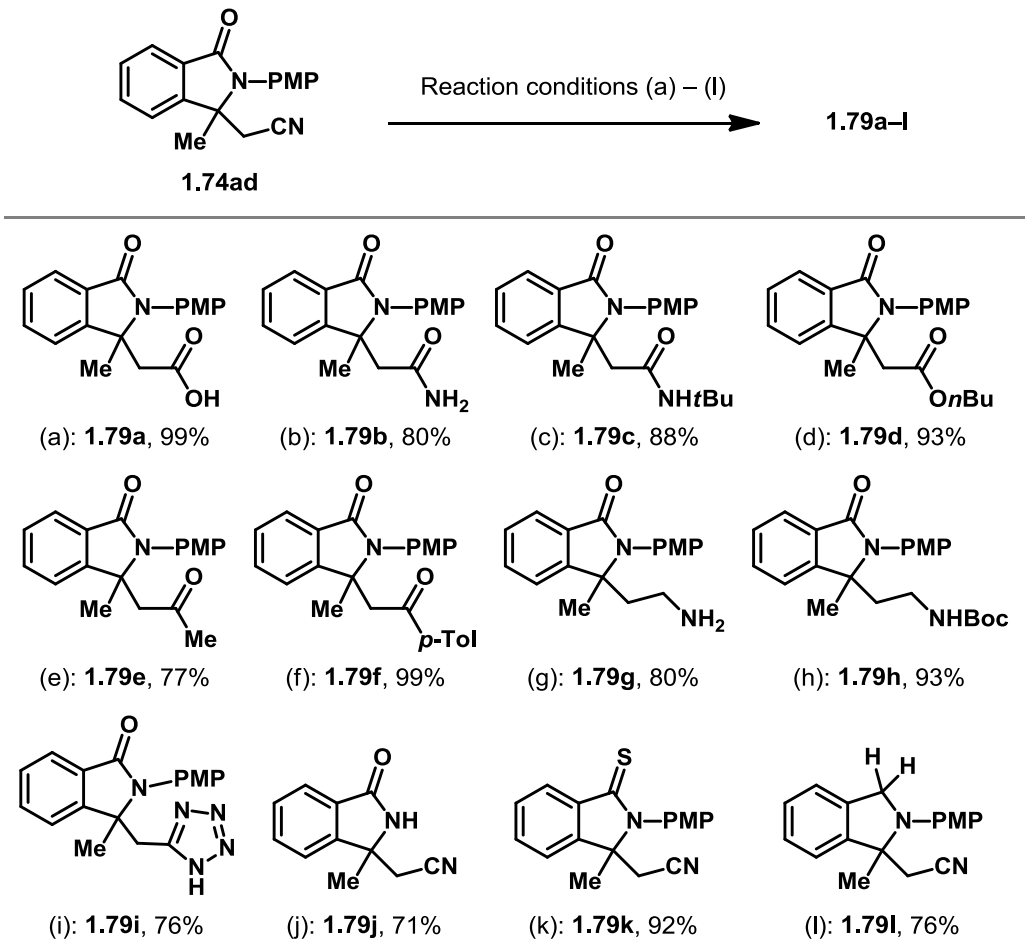

[a]All yields are of isolated material. Reaction conditions: (a) KOH, EtOH/H_2O, 90 °C, 40 h; (b) KOH, MeOH/H_2O, 90 °C, 2 h; (c) H_2SO_4 (1.2 equiv), *t*BuOH, 80 °C, 12 h; (d) TsOH·H_2O (2 equiv), *n*BuOH, 120 °C, 20 h; (e) $Ni(acac)_2$ (10 mol %), $AlMe_3$ (3 equiv), benzene, 50 °C, 5 h; (f) $Pd(OAc)_2$ (10 mol %), *p*-tolylboronic acid (2 equiv), 2,2′-bipyridyl (20 mol %), CF_3CO_2H (10 equiv), THF/H_2O, 90 °C, 28 h; (g) $NaBH_4$ (4 equiv), $CoCl_2·6H_2O$ (1.5 equiv), MeOH, 0 °C, 2 h; (h) $(Boc)_2O$ (2.5 equiv), $NaBH_4$ (4 equiv), $CoCl_2·6H_2O$ (1.5 equiv), MeOH, 0 °C, 3 h; (i) $TMSN_3$ (3 equiv), $nBu_2Sn(O)$ (0.5 equiv), PhMe, 100 °C, 48 h; (j) cerium (IV) ammonium nitrate (6 equiv), CH_3CN/H_2O, rt, 2 h; (k) Lawesson's reagent (1 equiv), PhMe, 100 °C, 2.5 h; (l) Tf_2O (1.2 equiv), CH_2Cl_2, 0 °C to rt, 30 min, then Hantzsch ester (3 equiv), RT, 4 h.

1.6. Chapter 1 Concluding Remarks

Bond activation and functionalization methodologies provide novel ways to form molecular scaffolds that may be difficult to synthesize in other ways. The ability to manipulate carbon frameworks in a more direct manner not only allows for atom-

economical transformations, but may even provide chemists with new perspectives on how to construct complex molecules. The activation and functionalization of C–CN and N–CN bonds has demonstrated the ability to simultaneously form cyclic structures while generating quaternary stereocenters. While enantioselective variants of these transformations remain elusive, diastereoselective methodologies have provided an alternative way to generate quaternary stereocenters asymmetrically. The medicinal relevance of the products from N–CN activation and functionalization has also been demonstrated.

1.7. Chapter 1 Experimental

1.7.1 General Details

Unless otherwise noted, all reactions were carried out using oven-dried glassware under a nitrogen atmosphere. Dichloromethane (DCM) and toluene were distilled from CaH_2 prior to use. Tetrahydrofuran (THF) was distilled from Na/benzophenone prior to use. *m*-Xylene and toluene were further degassed by bubbling a stream of argon through the liquid in a Strauss flask and then stored in a nitrogen-filled glove box. Acetonitrile (CH_3CN), benzene, methanol (MeOH), anhydrous *N*,*N*-dimethylformamide (DMF) and anhydrous diethyl ether (Et_2O) were purchased from Sigma-Aldrich and Alfa Aesar, and used without further purification. Unless otherwise noted, all chemicals were purchased from commercial sources and used as received. All transition-metal complexes, except for CpPd(1-phenylallyl), were purchased from Sigma-Aldrich or Strem and used as received. CpPd(1-phenylallyl) was synthesized following a known procedure.[52] Triphenylborane (BPh_3) was purchased from Strem and recrystallized from anhydrous

heptanes under nitrogen.[53] Tris(pentafluorophenyl)borane [$B(C_6F_5)_3$] was purchased from Strem and used as received.

Analytical thin-layer chromatography (TLC) and preparative thin-layer chromatography were carried out using 250 μm and 1000 μm silica plates (SiliCycle), respectively. Eluted plates were visualized first with a UV lamp (254 nm) and then stained with potassium permanganate, iodine, or bromocresol green. Flash column chromatography was performed using 230–400 mesh (particle size 40–63 μm) silica gel purchased from SiliCycle.

^{1}H-NMR (400 and 500 MHz), ^{13}C-NMR (75 and 125 MHz), and ^{19}F-NMR (375 and 470 MHz) spectra were obtained on Varian Inova and Bruker Avance instruments. ^{1}H NMR spectra data were reported as δ values in ppm relative to TMS (δ 0.00) or chloroform (δ 7.26). ^{13}C-NMR spectra data were reported as δ values in ppm relative to chloroform (δ 77.00). ^{19}F-NMR spectra data were reported as δ values in ppm using instrument standard. ^{1}H-NMR coupling constants were reported in Hz, and multiplicity was indicated as follows: s (singlet); d (doublet); t (triplet); q (quartet); quint (quintet); m (multiplet); dd (doublet of doublets); ddd (doublet of doublet of doublets); dddd (doublet of doublet of doublet of doublets); dt (doublet of triplets); td (triplet of doublets); ddt (doublet of doublet of triplets); dq (doublet of quartets); app (apparent); br (broad). Infrared (IR) spectra were obtained on a MIDAC FT-IR spectrometer. A thin-film of sample was prepared by evaporating solvent (DCM or $CDCl_3$) on NaCl plates. High-resolution mass spectra (HRMS) in electrospray ionization (ESI) experiments were

performed on a Bruker BioTOF II (Time-of-flight) instrument using PEG-300, PEG-400 or PPG-400 as an internal standard.

1.7.2 Diastereoselective Alkene Cyanoamidation – Synthesis of Racemic phenyl(ethyl)amine 1.65

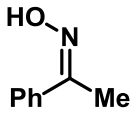

1.64

Oxime **1.64** was prepared using a known procedure.[54] ^{1}H-NMR data was in agreement with literature values. **^{1}H-NMR** (400 MHz; $CDCl_3$): δ 9.11 (s, 1H), 7.62 (dd, *J* = 6.7, 3.0 Hz, 2H), 7.40-7.37 (m, 3H), 2.30 (s, 3H).

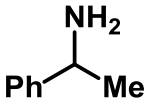

(±)–1.65

A 100 mL round-bottom flask was evacuated and back-filled with nitrogen 3 times before being charged with Pd/C (158 mg of 10% solid; 0.148 mmol Pd; 1 mol%). The solid was suspended in EtOH (10 mL) and oxime 1.64 (2.00 g; 14.8 mmol; 1 equiv.) was added as a solution in EtOH (40 mL). The mixture was degassed with nitrogen before purging with H_2. The mixture was stirred under a H_2 balloon atmosphere for 19 h and then degassed with nitrogen. The mixture was filtered through Celite®, rinsing with EtOAc. Concentration *in vacuo* afforded phenylethylamine **1.65** in 70% yield. ^{1}H-NMR data was consistent with literature values.[55] **^{1}H-NMR** (400 MHz; $CDCl_3$): δ 7.36-7.31 (m, 4H), 7.26-7.21 (m, 1H), 4.12 (q, *J* = 6.6 Hz, 1H), 1.59 (br s, 2H), 1.39 (d, *J* = 6.6 Hz, 3H).

1.7.3 Intramolecular Alkene Aminocyanation Substrate Synthesis

All *N*-acyl cyanamide substrates **1.76** were synthesized in 3 steps. Step 1 synthesizes aryl cyanamides **1.81** from the corresponding anilines **1.80**. Step 2 synthesizes carboxylic acids **1.83**. Step 3 synthesizes substrates **1.73** by coupling cyanamides **1.81** with acids **1.83**.

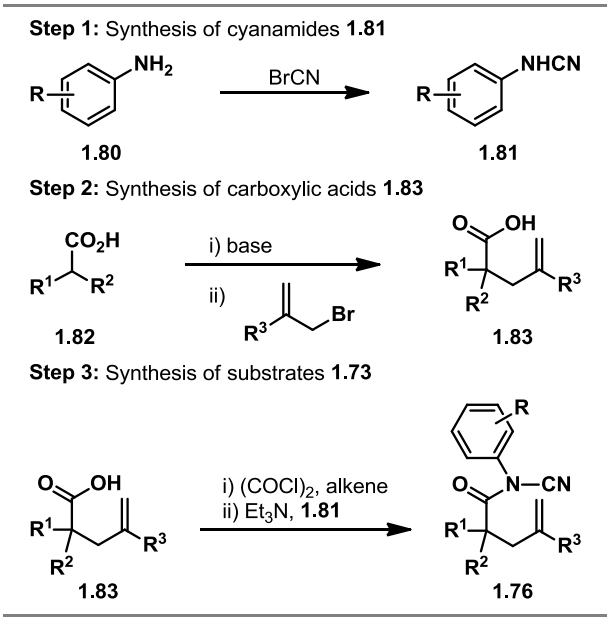

Step 1: Synthesis of cyanamides **1.81**

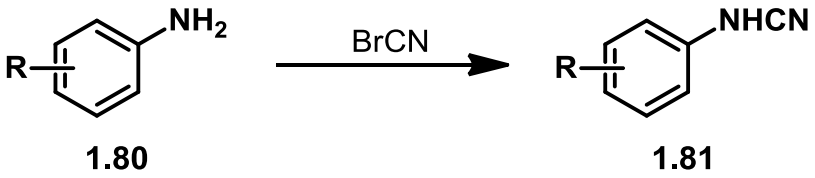

CAUTION! Cyanogen bromide (BrCN) is highly toxic and hydrolyzes readily to release hydrogen cyanide. The related preparation must be carried out in a well-ventilated fume hood. Excess BrCN should be destroyed with aqueous NaOH solution and the resulting aqueous solution should be disposed of properly.

General procedure for the synthesis of cyanamides **1.81:** a solution of BrCN (1271 mg, 12 mmol) in Et_2O (10 mL) was slowly added to aniline 1**.80** (20 mmol) in Et_2O (20 mL) at 0 °C. The reaction mixture was allowed to warm to room temperature and stir for 24 h. Upon completion, the mixture was diluted with Et_2O (40 mL) and filtered through a pad of Celite®. The filtrate was washed with 1 M HCl (10 mL), saturated aqueous $NaHCO_3$ (10 mL), and brine (10 mL), and was dried over anhydrous $MgSO_4$, and concentrated *in vacuo*. The crude product was purified by precipitation from Et_2O/Hex at 0 °C.

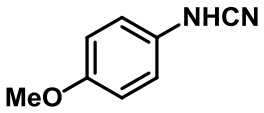

1.81a

Cyanamide **1.81a** is a known compound and the ^{1}H-NMR data matched that of the reported compound.[56] **^{1}H-NMR** (500 MHz; $CDCl_3$): δ 6.97-6.94 (m, 2H), 6.89-6.86 (m, 2H), 6.14 (br s, 1H), 3.79 (s, 3H).

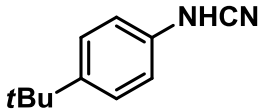

1.81b

Cyanamide **1.81b** was further purified by flash column chromatography (2:100 MeOH/DCM) as an off-white solid in 94% yield. R_f = 0.44 (5:95 MeOH/CH_2Cl_2); mp 86–88 °C; **^{1}H NMR** (500 MHz, $CDCl_3$) δ 7.38 – 7.32 (m, 2H), 7.00 – 6.90 (m, 2H), 6.10 (br s, 1H), 1.30 (s, 9H); **^{13}C NMR** (125 MHz, $CDCl_3$) δ 146.8, 134.4, 126.6, 115.1, 111.3, 34.3, 31.3; **HRMS** (ESI) calcd for $[C_{11}H_{14}N_2 + Na]^+$ 197.1049, found 197.1047; **IR** (thin film) 3159, 2227, 1517, 1253.

Step 2: Synthesis of carboxylic acids **1.83**

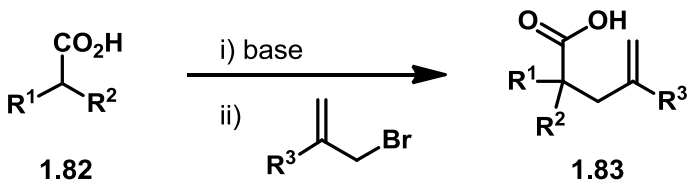

1.82 **1.83**

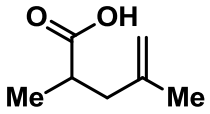

1.83a

To a flame-dried 100 mL round-bottom flask was added *i*-Pr_2NH (2.23 g; 22 mmol; 2.2 equiv.) and THF (30 mL). The flask was cooled to -78 ^oC and *n*BuLi (8.6 mL of 2.45 M, 21 mmol, 2.1 equiv.) was added. The reaction was stirred for 30 min. at -78 ^oC before propionic acid (0.741 g; 10 mmol; 1 equiv.) was added slowly as a THF (10 mL) solution. The flask was allowed to warm to RT and stirred for 1 h before being cooled to -78 ^oC. Methallyl bromide (2.70 g; 20 mmol; 2.0 equiv.) was added slowly as a THF (10 mL) solution. After complete addition the flask was allowed to gradually warm to RT overnight. The reaction was quenched with H_2O, made basic (pH ≥10) with 1 M NaOH, and extracted with Et_2O. The aqueous phase was then made acidic (pH = 1) with 1 M HCl and extracted with Et_2O. The combined organic layers from the acidic extraction were washed with H_2O and brine, dried over Na_2SO_4, filtered and concentrated *in vacuo* to give carboxylic acid **1.83a** in 95% yield as a pale yellow oil, which was sufficiently pure without column chromatography purification. R_f = 0.35 (1:4 EtOAc/Hex); ^{1}H-NMR data was consistent with literature values.[57] **^{1}H NMR** (500 MHz, $CDCl_3$) δ 4.80 (app s, 1H), 4.74 (d, *J* = 1.0 Hz, 1H), 2.67 (sextet, *J* = 7.1 Hz, 1H), 2.45 (ddd, *J* = 14.2, 7.1, 1.2

Hz, 1H), 2.10 (ddd, *J* = 14.1, 7.8, 1.1 Hz, 1H), 1.72 (s, 3H), 1.17 (d, *J* = 7.0 Hz, 3H); ^{13}C NMR (125 MHz, $CDCl_3$) δ 182.9, 142.5, 112.5, 41.5, 37.6, 22.1, 16.5.

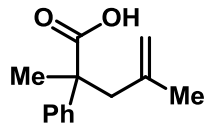

1.83c

To a flame-dried 100 mL round-bottom flask was added *i*-Pr_2NH (1.59 g; 15.7 mmol; 2.2 equiv.) and THF (26 mL). The flask was cooled to -78 ^{o}C and *n*BuLi (6.11 mL of 2.45 M, 15.0 mmol, 2.1 equiv.) was added. The reaction was stirred for 30 min. at -78 ^{o}C before 2-phenylpropanoic acid[58] (1.07 g; 7.13 mmol; 1 equiv.) was added slowly as a THF (10 mL) solution. The flask was stirred at -78 ^{o}C for 1 h before being allowed to warm to RT. The flask was then placed in a pre-heated oil bath and stirred at 50 ^{o}C for 40 min. before allowing to cool to RT. The flask was then further cooled to -78 ^{o}C and methallyl bromide (2.53 g; 14.3 mmol; 2.0 equiv.) was added slowly. After complete addition the flask was allowed to gradually warm to RT overnight. The reaction was quenched with NH_4Cl (sat. aq.) (pH = 1) and acidified with 1 M HCl. The mixture was extracted with Et_2O and the combined organic layers were washed with H_2O and brine, dried over Na_2SO_4, filtered and concentrated *in vacuo*. Purification via silica gel flash chromatography (1:9 EtOAc:hexanes) gave carboxylic acid **1.83c** in 68% yield as a pale yellow oil. R_f = 0.35 (1:4 EtOAc/Hex); **^{1}H NMR** (500 MHz, $CDCl_3$) δ 7.46 – 7.37 (m, 2H), 7.33 (dd, *J* = 8.5, 6.9 Hz, 2H), 7.29 – 7.22 (m, 1H), 4.85 – 4.79 (m, 1H), 4.66 (d, *J* = 1.2 Hz, 1H), 2.94 (d, *J* = 13.5 Hz, 1H), 2.65 (d, *J* = 13.5 Hz, 1H), 1.57 (s, 3H), 1.47 (s, 3H); **^{13}C NMR** (125 MHz, $CDCl_3$) δ 182.4, 142.9, 141.9, 128.4, 127.1, 126.2, 115.4,

49.2, 46.8, 23.8, 21.7; **MS** (ESI) calcd for $[(C_{13}H_{15}O_2)_2 + Na]^-$ 429.2, found 429.2. **IR** (thin film) 2941, 1690, 1449, 1408, 1375, 1320, 1274.

Step 3: Synthesis of substrates **1.76**

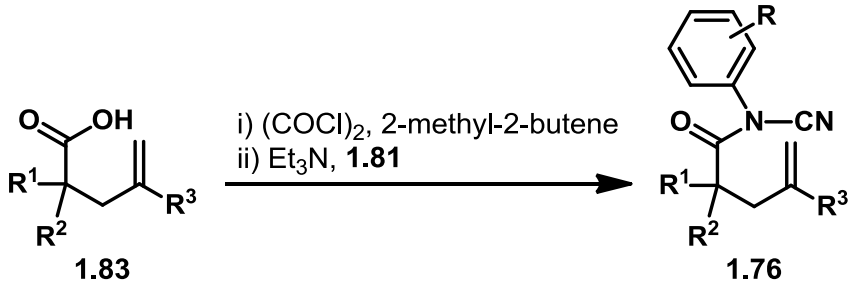

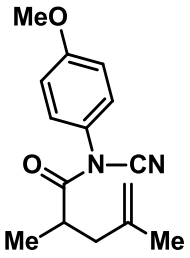

1.76a

A 50 mL round-bottom flask was flame-dried and charged with carboxylic acid **1.83a** (0.461 g, 3.6 mmol; 1.2 equiv.), 2-methyl-2-butene (1.05 g; 15 mmol; 5 equiv.) and DCM (4.3 mL). $(COCl)_2$ (1.32 mL of 2.0 M; 3.3 mmol; 1.1 equiv.) was added at room temperature and the flask was stirred for 20 min. before cooling to –12 °C in an ethylene glycol/dry ice bath. A solution of Et_3N (0.304 g; 3.0 mmol; 1 equiv.) in DCM (1 mL) was added dropwise and stirred for 10 min. at –12 °C before a solution of cyanamide **1.81a** (0.444 g; 3.0 mmol; 1 equiv.) and Et_3N (0.425 g; 4.2 mmol; 1.4 equiv.) in DCM (3.0 mL) was slowly added at the same temperature. The resulting mixture was allowed to warm up to room temperature and stir for 20 h. The mixture was poured over Et_2O (150 mL) to force precipitation of triethylamine hydrochloride, which was filtrated through Celite®

The filtrate was concentrated *in vacuo* and the crude material purified by silica gel flash column chromatography (1:9 EtOAc:hexanes). This afforded substrate **1.76a** as a pale yellow oil in 49% yield. R_f = 0.56 (3:7 EtOAc/Hex); **^{1}H NMR** (500 MHz, $CDCl_3$) δ 7.26 – 7.20 (m, 2H), 6.99 – 6.88 (m, 2H), 4.88 – 4.82 (m, 1H), 4.77 (app s, 1H), 3.82 (s, 3H), 3.35 (br app s, 1H), 2.55 (dd, *J* = 14.0, 7.6 Hz, 1H), 2.17 (dd, *J* = 14.0, 6.9 Hz, 1H), 1.77 (s, 3H), 1.28 (d, *J* = 7.0 Hz, 3H); **^{13}C NMR** (125 MHz, $CDCl_3$) δ 175.5, 160.0, 141.9, 127.3, 127.1, 114.9, 113.2, 110.1, 55.5, 41.8, 36.6 (br), 22.3, 17.0; **HRMS** (ESI) calcd for $[C_{15}H_{18}N_2O_2 + Na]^+$ 281.1260, found 281.1266; **IR** (thin film) 2231, 1736, 1509, 1251, 1180.

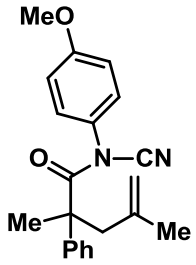

1.76c

Prepared analogously to substrate **1.76a** from carboxylic acid **1.83c** and cyanamide **1.81a** on a 2.4 mmol scale. Substrate **1.76c** was purified by silica gel flash column chromatography (1:9 EtOAc/Hex) as an off-white tacky solid in 36% yield. R_f = 0.42 (1:4 EtOAc/Hex); **^{1}H NMR** (500 MHz, $CDCl_3$) δ 7.46 – 7.42 (m, 2H), 7.39 – 7.31 (m, 3H), 7.16 – 7.10 (m, 2H), 6.96 – 6.87 (m, 2H), 4.95 (t, *J* = 1.8 Hz, 1H), 4.80 (dd, *J* = 2.1, 1.0 Hz, 1H), 3.81 (s, 3H), 3.19 (d, *J* = 14.0 Hz, 1H), 2.79 (d, *J* = 13.7 Hz, 1H), 1.80 (s, 3H), 1.48 (s, 3H); **^{13}C NMR** (125 MHz, $CDCl_3$) δ 175.3, 159.9, 141.6, 141.0, 129.0, 128.6, 127.8, 127.5, 126.4, 116.6, 114.8, 109.5, 100.0, 55.6, 52.2, 46.3, 24.1; **HRMS** (ESI)

calcd for $[C_{21}H_{22}N_2O_2 + Na]^+$ 357.1573, found 357.1578; **IR** (thin film) 2229, 1719, 1507, 1245, 1220.

1.7.4 Diasteroselective Aminocyanation Reaction

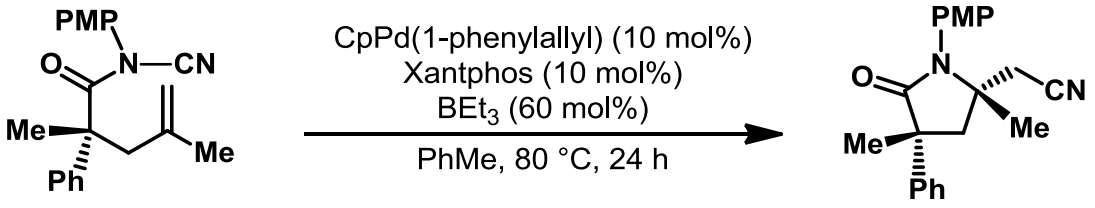

(±)-1.76c **(±)-1.77c**

In a nitrogen-filled glove box, a one-dram vial was charged with a magnetic stirring bar, substrate **1.76c** (100 mg; 0.30 mmol; 1 equiv.), BEt_3 (0.18 mL of 1.0 M; 0.18 mmol; 60 mol%), Xantphos (17 mg, 0.030 mmol; 10 mol%), and a solution of CpPd(1-phenylallyl) (8.7 mg; 0.030 mmol; 10 mol%) in toluene (1.5 mL, 0.20 M). The reaction mixture was sealed with a PTFE lined cap, removed from the glove box, and heated at 80 °C in an aluminum heating block for 24 h. The resulting mixture was allowed to cool to room temperature, diluted with DCM (5 mL), and filtered through Celite®. Lactam **1.77c** was purified by silica gel flash chromatography (1:4 → 3:7 EtOAc/Hex) to yield a mixture of diastereomers as an off-white solid (0.146 mmol, 73% yield). R_f = 0.25 (2:3 EtOAc/Hex); 19:1 d.r. based on ^{1}H NMR spectroscopy. The major and minor diastereomers could be separated as a saturated solution in 1:1 isopropanol:hexanes via HPLC using an Agilent Eclipse XDB-CN column, with an injection volume of 50 μL, flow rate of 5 mL/min., and eluting with an isocratic 15:85 isopropanol:hexanes solvent system. R_t major diastereomer = 6.93 min; R_t minor diastereomer = 9.36 min. *Major diastereomer:* **^{1}H NMR** (500 MHz, $CDCl_3$) δ 7.56 – 7.51 (m, 2H), 7.40 (dd, *J* = 8.4, 7.2 Hz, 2H), 7.33 –

7.25 (m, 1H), 7.07 – 7.00 (m, 2H), 7.00 – 6.93 (m, 2H), 3.83 (s, 3H), 3.07 (d, *J* = 13.7 Hz, 1H), 2.31 (app t, *J* = 15.5 Hz, 2H), 2.18 (d, *J* = 16.4 Hz, 1H), 1.64 (s, 3H), 1.45 (s, 3H); *Major diastereomer:* **^{13}C NMR** (125 MHz, $CDCl_3$) δ 177.0, 159.7, 144.0, 130.7, 129.2, 127.4, 127.2, 125.9, 116.9, 114.9, 59.8, 55.5, 48.5, 47.4, 28.4, 28.2, 27.3; *Major diastereomer*: **^{1}H-NMR** (500 MHz; CD_3CN): δ 7.54-7.53 (m, 2H), 7.40 (t, *J* = 7.7 Hz, 2H), 7.31-7.29 (m, 1H), 7.16-7.14 (m, 2H), 7.03-7.02 (m, 2H), 3.83 (s, 3H), 2.80 (d, *J* = 13.8 Hz, 1H), 2.51 (d, *J* = 16.9 Hz, 1H), 2.40 (d, *J* = 13.8 Hz, 1H), 2.33 (d, *J* = 16.9 Hz, 1H), 1.62 (s, 3H), 1.41 (s, 3H).; *Minor diastereomer*: **^{1}H-NMR** (500 MHz; CD_3CN): δ 7.49-7.48 (m, 1H), 7.39 (t, *J* = 7.8 Hz, 1H), 7.28 (t, *J* = 7.4 Hz, 1H), 7.17-7.15 (m, 1H), 7.04-7.02 (m, 1H), 3.83 (s, 1H), 2.70 (d, *J* = 13.7 Hz, 1H), 2.62 (d, *J* = 16.9 Hz, 1H), 2.59 (d, *J* = 17.1 Hz, 1H), 2.51 (d, *J* = 13.7 Hz, 1H), 1.60 (s, 1H), 1.11 (s, 1H). **HRMS** (ESI) calcd for $[C_{21}H_{22}N_2O_2 + Na]^+$ 357.1573, found 357.1595; **IR** (thin film) 2235, 1688, 1513, 1452, 1388, 1250.

1.7.5 Transformation of Aminocyanation Product 1.74ad

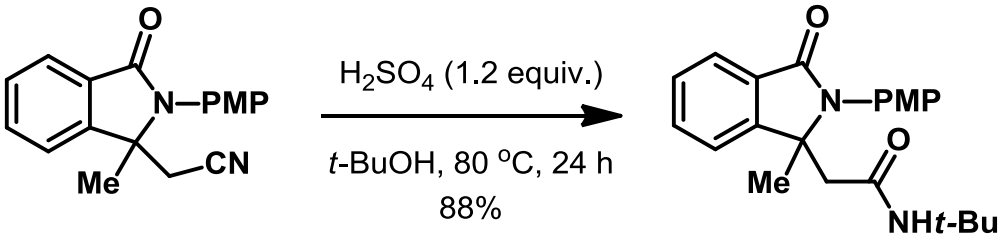

1.74ad **1.79c**

To a one-dram reaction vial was added lactam **1.74ad** (58 mg, 0.2 mmol), *tert*-butyl alcohol (0.40 mL; 0.50 M), and conc. H_2SO_4 (3 drops via glass pipiet; approx. 60 mg; 0.6 mmol). The vial was sealed with a PTFE-lined cap and heated at 80 °C for 24 h. The

reaction was allowed to cool to RT, diluted with DCM (3 mL), and washed with saturated aqueous $NaHCO_3$ (5 mL). The aqueous phase was extracted with DCM (3x 3 mL). The combined organic extracts were washed with brine (5 mL), dried over anhydrous Na_2SO_4, and concentrated *in vacuo*. The resulting mixture was purified by silica gel flash chromatography (1:1 EtOAc:hexanes) to afford amide **1.79c** as a white foam in 88% yield. R_f = 0.16 (1:1 EtOAc/Hex); **^{1}H NMR** (500 MHz, $CDCl_3$) δ 7.95 (dd, *J* = 7.5, 0.9 Hz, 1H), 7.63 (dd, *J* = 7.4, 1.1 Hz, 1H), 7.59 – 7.49 (m, 2H), 7.37 – 7.31 (m, 2H), 7.04 – 6.97 (m, 2H), 4.77 (s, 1H), 3.85 (s, 3H), 2.70 (d, *J* = 14.3 Hz, 1H), 2.56 (d, *J* = 14.4 Hz, 1H), 1.59 (s, 3H), 1.06 (s, 9H); **^{13}C NMR** (125 MHz, $CDCl_3$) δ 167.4, 159.4, 149.0, 132.1, 131.6, 131.0, 128.7, 127.8, 124.9, 124.5, 121.7, 114.8, 65.7, 55.5, 51.1, 46.4, 28.3, 26.1; **HRMS** (ESI) calcd for $[C_{22}H_{26}N_2O_3 + Na]^+$ 389.1836, found 389.1845; **IR** (thin film) 3330, 1680, 1656, 1512, 1391, 1247.

1.8. Chapter 1 References

1) Souillart, L.; Cramer, N. *Chem. Rev.* **2015**, *115*, 9410–9464.

2) Rybtchinski, B.; Milstein, D. *Angew. Chem. Int. Ed.* **1999**, *38*, 870-883.

3) Ruhland, K. *Eur. J. Org. Chem.* **2012**, *2012*, 2683-2706.

4) Murakami, M.; Matsuda, T. *Chem. Comm.* **2011**, *47*, 1100-1105.

5) Jun, C.-H. *Chem. Soc. Rev.* **2004**, *33*, 610-618.

6) Crabtree, R.H. *Chem. Rev.* **1985**, *85*, 245-269.

7) Chen, F.; Wang, T.; Jiao, N. *Chem. Rev.* **2014**, *114*, 8613–8661.

8) Jun, C.-H.; Park, J.-W. Directed C – C Bond Activation by Transition Metal Complexes In *Directed Metallation*; Chantani, N., Ed.; Springer: Berlin-Heidelberg, 2007; Vol. 24, p 117-143.

9) Dreis, A. M.; Douglas, C. J. Carbon–Carbon Bond Activation with 8-Acylquinolines In *C-C Bond Activation*; Dong, G., Ed.; Springer: Berlin, 2014, p 85–110.

10) Rahimi, N.; Karimzadeh, R. *Applied Catalysis A: General* **2011**, *398*, 1–17.

11) Vaska, L. *Acc. Chem. Res.* **1968**, *1*, 335–344.

12) Kliman, J. P.; Dubeck, M. *J. Am. Chem. Soc.* **1963**, *85*, 1544-1545.

13) Blanksby, S.J.; Ellison, G.B. *Acc. Chem. Res.* **2003**, *36*, 255-263.

14) Simoes, J. A. M.; Beauchamp, J. L. *Chem. Rev.* **1990**, *90*, 629-688.

15) Seiser, T., Saget, T., Tran, D. N.; Cramer, N. *Angew. Chem. Int. Ed.* **2011**, *50*, 7740–7752.

16) Wiberg, K. B. *Acc. Chem. Res.* **1996**, *29*, 229-234.

17) Tipper, C. F. H. *J. Chem. Soc.* **1955**, 2045-2046.

18) Adams, D. M.; Chatt, J.; Guy, R. G.; Sheppard, N. *J. Chem. Soc.* **1961**, 738-742.

19) Periana, R. A.; Bergman, R. G. *J. Am. Chem. Soc.* **1984**, *106*, 7272-7274.

20) Seiser, T.; Cramer, N. *Org. Biomol. Chem.* **2009**, *7*, 2835–2840.

21) Matsuda, T.; Tsuboi, T.; Murakami, M. *J. Am. Chem. Soc.* **2007**, *129*, 12596-12597.

22) Crabtree, R. H.; Dion, R. P. *J. Chem. Soc., Chem. Commun.* **1984**, 1260-1261.

23) Urbanos, F.; Fernandez-Baeza, J.; Chaudret, B. *J. Chem. Soc., Chem. Commun.* **1991**, 1739-1741.

24) Halcrow, M. A.; Urbanos, F.; Chaudret, B. *Organometallics* **1993**, *12*, 955-957.

25) Bruce, M. I. *Angew. Chem. Int. Ed.* **1977**, *16*, 73-86.

26) Omae, I. *Coord.Chem. Rev.* **2004**, *248*, 995–1023.

27) Suggs, J. W.; Jun, C.-H. *J. Am. Chem. Soc.* **1984**, *106*, 3054-3056.

28) Suggs, J. W.; Jun, C.-H. *J. Chem. Soc., Chem. Commun.* **1985**, 92-93.

29) Suggs, J. W.; Jun, C.-H. *J. Am. Chem. Soc.* **1986**, *108*, 4679-4681.

30) Gozin, M.; Weisman, A.; Ben-David, Y.; Milstein, D. *Nature* **1993**, *364*, 699-701.

31) McMillen, D. F.; Golden, D. M. *Rev. Phys. Chem.* **1982**, *33*, 493-532.

32) Nakao, Y. Catalytic C–CN Bond Activation In *C-C Bond Activation*; Dong, G., Ed.; Springer: Berlin, 2014, p 33–58.

33) Gerlach, D. H.; Kane, A. R.; Parshall, G. W.; Jesson, J. P.; Muetterties, E. L. *J. Am. Chem. Soc.* **1971**, *93*, 3543–3544.

34) Nakao, Y.; Oda, S.; Hiyama, T. *J. Am. Chem. Soc.* **2004**, *126*, 13904-13905.

35) Yasui, Y.; Kamisaki, H.; Takemoto, Y. *Org. Lett.* **2008**, *10*, 3303-3306.

36) Dreis, A. M.; Douglas, C. J. *J. Am. Chem. Soc.* **2009**, *131*, 412-413.

37) Wentzel, M.; Reddy, V. K.; Hyster, T. K.; Douglas, C. J. *Angew. Chem. Int. Ed.* **2009**, *48*, 6121 –6123.

38) Hoang, G. T.; Reddy, V. J.; Nguyen, H. H. K.; Douglas, C. J. *Angew. Chem. Int. Ed.* **2011**, *50*, 1882 –1884.

39) Rondla, N. R.; Levi, S. M.; Ryss, J. M.; Vanden Berg, R. A.; Douglas, C. J. *Org. Lett.* **2011**, *13*, 1940–1943.

40) Rondla, N. R.; Ogilvie, J. M.; Pan, Z.; Douglas, C. J. *Chem. Commun.* **2014**, *50*, 8974--8977.

41) Frost, G. B.; Serratore, N. A.; Ogilvie, J. M.; Douglas, C. J. *J. Org. Chem.* **2017**, *82*, 3721−3726.

42) Kamlet, M. J.; Abboud, J. L. M.; Abraham, M. H.; Taft, R. W. *J. Org. Chem.* **1983**, *48*, 2877–2887.

43) Dreis, A. M.; Otte, S. C.; Eastwood, M. S.; Alonzi, E. R.; Brethorst, J. T.; Douglas, C. J. *Eur. J. Org. Chem.* **2017**, 45–48.

44) Shi, J.; Zhang, J.; Yue, Z.; Li, M.; Zhu, C.; Zhang, Y.; Zi, J.; Wang, Y.; Fan, X.; Xu, R.; Lin, S.; Li, Y.; Yang, Y.; Sheng, L. N6-Substituted adenosine derivatives, N6-substituted adenine derivatives and uses thereof. WO 2011/069294, 2012

45) Abiraj, K.; Gowda, D. C. *J. Chem. Research (S)* **2003**, 332–334.

46) Koester, D. C.; Kobayashi, M.; Werz, D. B.; Nakao, Y. *J. Am. Chem. Soc.* **2012**, *134*, 6544–6547.

47) Pan, Z.; Pound, S. M.; Rondla, N. R.; Douglas, C. J. *Angew. Chem. Int. Ed.* **2014**, *53*, 5170 –5174.

48) Miyazaki, Y.; Ohta, N.; Semba, K.; Nakao, Y. *J. Am. Chem. Soc.* **2012**, *134*, 6544–6547.

49) Jung, M. E.; Piizzi, G. *Chem. Rev.* **2005**, *105*, 1735-1766.

50) Kamer, P. C. J.; van Leeuwen, P. W. N. M.; Reek, J. N. H. *Acc. Chem. Res.* **2001**, *34*, 895–904.

51) Eliel, E. L.; Manoharan, M. *J. Org. Chem.* **1981**, *46*, 1959-1962.

52) Fraser, A. W.; Besaw, J. E.; Hull, L. E.; Baird, M. C. *Organometallics* **2012**, *31*, 3928−3935.

53) Köster, R.; Binger, P.; Fenzl, W. *Inorg. Synth.* **1974**, *15*, 134-136.

54) Zhang, G.; Wen, X.; Wang, Y.; Mo, W.; Ding, C. *J. Org. Chem.* **2011**, *76*, 4665–4668.

55) Wang, C.; Pettman, A.; Bacsa, J.; Xiao, J. *Angew. Chem. Int. Ed.* **2010**, *49*, 7548 –7552.

56) Li, J.; Neuville, L. *Org. Lett.* **2013**, *15*, 6124–6127.

57) Tannert, R.; Milroy, L.; Ellinger, B.; Hu, T.; Arndt, H.; Waldmann, H. *J. Am. Chem. Soc.* **2010**, *132*, 3063–3077.

58) Kundig, P. E.; Seidel, T. M.; Jia, Y.; Bernardinelli, G. *Angew. Chem., Int. Ed.* **2007**, *46*, 8484 –8487.

CHAPTER 2:METAL–ORGANIC COOPERATIVE CATALYSIS AS A STRATEGY FOR BOND ACTIVATION

2.1. The Development of Metal-Organic Cooperative Catalysis as a Strategy for Bond Activation

2.1.1 Introduction

The difficulties of C–C bond activation were outlined in Chapter 1, as well as a few strategies chemists have taken to overcome the kinetic and enthalpic challenges associated with the activation of unreactive C–C bonds. While all of the aforementioned

strategies have contributed to growth in the field of C–C activation, they have for the most part served simply as proof-of-concept exercises with limited applications in complex molecule synthesis. One prominent limitation is that of substrate scope. Most of the C–C activation strategies previously discussed depend on carefully structured substrates in order to be effective, which hinders their application in the synthesis of complex molecules. If a complex molecular target does not accommodate the structural features necessary for efficient bond activation and functionalization, then the advantages these methodologies provide, such as generating molecular complexity in a fast and efficient manner, are rendered useless.

Chelation assistance, which requires an imbedded functional group capable of directing the transition metal through chelation, is arguably the most versatile strategy in achieving C–C activation. While early examples of chelation-assisted bond activation relied on directing groups embedded within the molecule, this same concept has been extended to methodologies wherein the directing group is transiently formed to facilitate bond activation and functionalization. This was first demonstrated by Suggs in 1978, when he reported the use of 2-amino-3-picoline (**2.2a**) in the net hydroacylation of alkenes from simple aldehyde substrates (Scheme 2.1).[1]

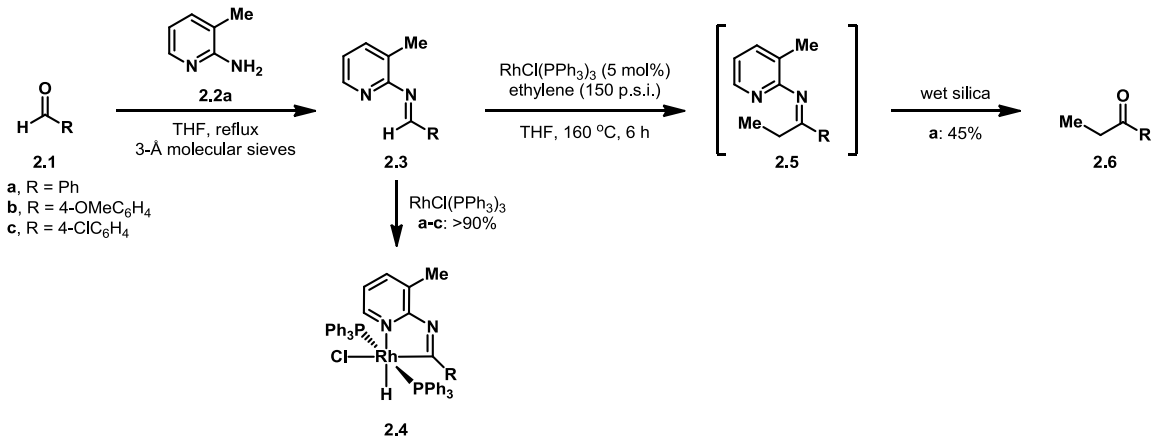

Scheme 2.1. Suggs' stoichiometric use of aminopicoline **2.2a** in the hydroacylation of alkenes from simple aldehydes.

In Suggs' 1978 report, aromatic aldehydes **2.1a-c** underwent condensation with aminopicoline **2.2a** to generate the corresponding aldimine **2.3**, while noting that condensations with aldehydes bearing α–hydrogens were not successful. When treated with stoichiometric Wilkinson's catalyst ([$RhCl(PPh_3)_3$]), aldimines **2.3a-c** provided the C–H activation complexes **2.4a-c** in excellent yield. More importantly, aldimine **2.3a** underwent catalytic bond activation with rhodium and subsequent functionalization under a high pressure of ethylene. The reaction between aldimine **2.3a** and ethylene presumably gave ketimine **2.5a**, but the crude reaction mixture was directly treated with wet silica gel and distilled to give the product of hydrolysis, propiophenone (**2.6a**), in 45% isolated yield.

Cyclometalation, afforded by chelation of the pyridyl nitrogen in aldimine **2.3**, was essential for accomplishing the bond activation reactions reported by Suggs. Besides lowering kinetic and enthalpic barriers for bond activation, cyclometallation helped avoid decarbonylation, which is a common and problematic side-reaction (Scheme 2.2a).[2]

Aldehydes such as **2.1** are capable of undergoing activation of the C_{acyl}–H bond with transition metals, but the resulting metal complex **2.7** tends to undergo α–elimination (i.e. decarbonylation) to generate the corresponding metal-carbonyl **2.8**.[3] Reductive elimination to release an alkane regenerates the metal in its original oxidation state (**2.9**), but the large amount of back-bonding to the CO ligand in complex **2.9** takes electron density away from the metal center. As a result, oxidative addition becomes unfavorable and inhibits the ability of complex **2.9** to further participate in bond activation processes, which stops catalytic turnover. The formation of a metallacycle (e.g. **2.4**) via intramolecular chelation (i.e. cyclometallation) stabilizes the metal complex and prevents α–elimination from occurring. As such, the formation of a deactivated metal complex is avoided and catalytic turnover is maintained (Scheme 2.2b). Furthermore, the presence of the methyl group *ortho* to the amine moiety in aminopicoline **2.2a** (refer to Scheme 2.1) is also important, as it biases the resulting imines (**2.3**) toward a conformation wherein the pyridyl nitrogen (which coordinates to the transition metal) is directed towards the imine C–H bond.

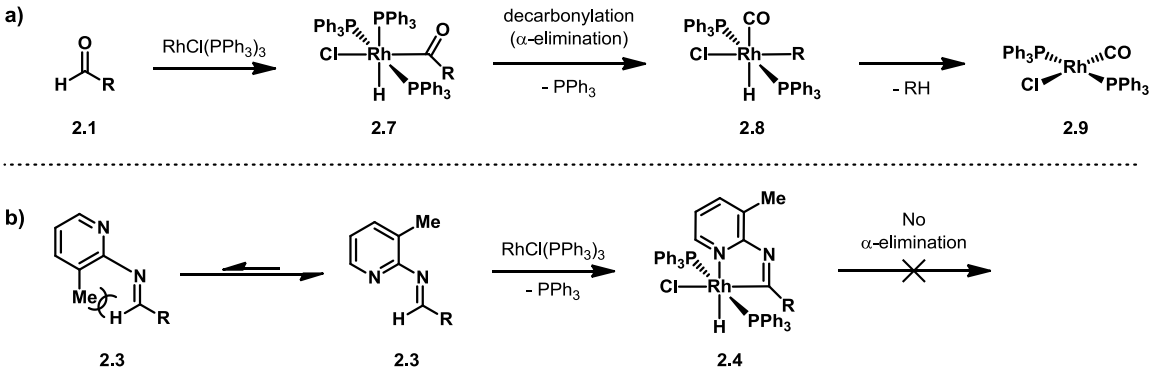

Scheme 2.2. a) transition metal mediated decarbonylation of aldehydes. **b)** conformational preference of imines derived from amino-picoline **2.2** and prevention of α -elimination via metallacycle formation.

2.1.2 Development of Metal-Organic Cooperative Catalysis Systems For C–H Activation and Functionalization

Jun, a student of Suggs', took the concept described above a step further in 1997 when he reported the intermolecular hydroacylation of alkenes directly from aldehydes, in the presence of a catalytic amount of aminopicoline **2.2a** (Scheme 2.3).[4] A variety of aliphatic alkenes (**2.10**) were shown to undergo hydroacylation with aromatic and aliphatic aldehydes **2.1** in moderate to excellent yield with only a catalytic amount of aminopicoline **2.2a** present.

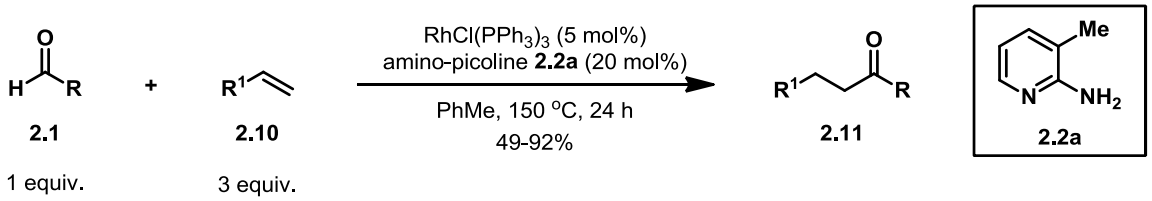

Scheme 2.3. Jun's catalytic use of amino-picoline **2.2a** in alkene hydroacylation directly from aldehydes.

In the same report, Jun also described the effect of aminopicoline **2.2a** catalyst loading on the product distribution (Table 2.1). Aryl ketone **2.11a** (see Scheme in Table 2.1) resulted from the desired alkene hydroacylation while anisole resulted from

decarbonylation. In the absence of aminopicoline **2.2a** (Table 2.1, entry 1) the reaction exclusively provided anisole due to the decarbonylation pathway (Table 2.1, entry 1). In the presence of 10 mol% of aminopicoline **2.2a** (Table 2.1, entry 2), a nearly-even ratio of **2.11a** and anisole was obtained, while 20 mol% of the co-catalyst (Table 2.1, entry 3) led to a drastically-improved 85:15 ratio of **2.11a**:anisole. Further increasing the loading of aminopicoline **2.2a** led to slight improvements in product distribution, but substantially increased the yield of ketone **2.11a** (Table 2.1, entries 4-6).

Table 2.1. Effect of amino-picoline **2.2a** on product distribution.

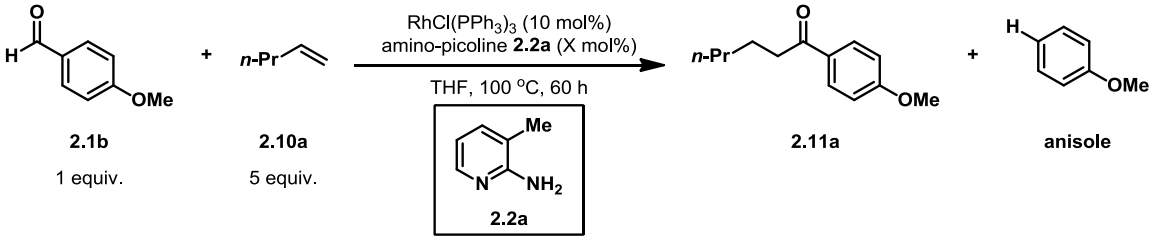

Entry	Loading of **2.2a** (mol%)	**2.11a**:anisole	Isolated Yield of **2.11a** (%)
1	0	0:100	0
2	10	58:42	14
3	20	85:15	57
4	50	85:15	70
5	70	90:10	80
6	100	93:7	83

Two integrated catalytic cycles, one organic in nature and one mediated by a transition metal, were proposed by Jun to account for the ability of aminopicoline **2.2a** to enable these C–H functionalization reactions in sub-stoichiometric amounts (Scheme 2.4). He would later refer to this dual catalytic system as metal-organic cooperative

catalysis (MOCC). First, a condensation between aldehyde **2.1** and aminopicoline **2.2a** generates the aldimine **2.3**, which enters into the transition metal mediated catalytic cycle on the right. Following ligand exchange, directed oxidative addition into the aldimine C–H bond gives C–H activation complex **2.12**. Dissociation of phosphine and association of alkene **2.10** provides coordination complex **2.13**, and migratory insertion into the alkene generates alkyl rhodium **2.14**. Reductive elimination followed by ligand exchange produces ketimine **2.15** and regenerates the transition metal catalyst. Hydrolysis of ketimine **2.15** gives the product ketone **2.11** and regenerates aminopicoline **2.2a**.

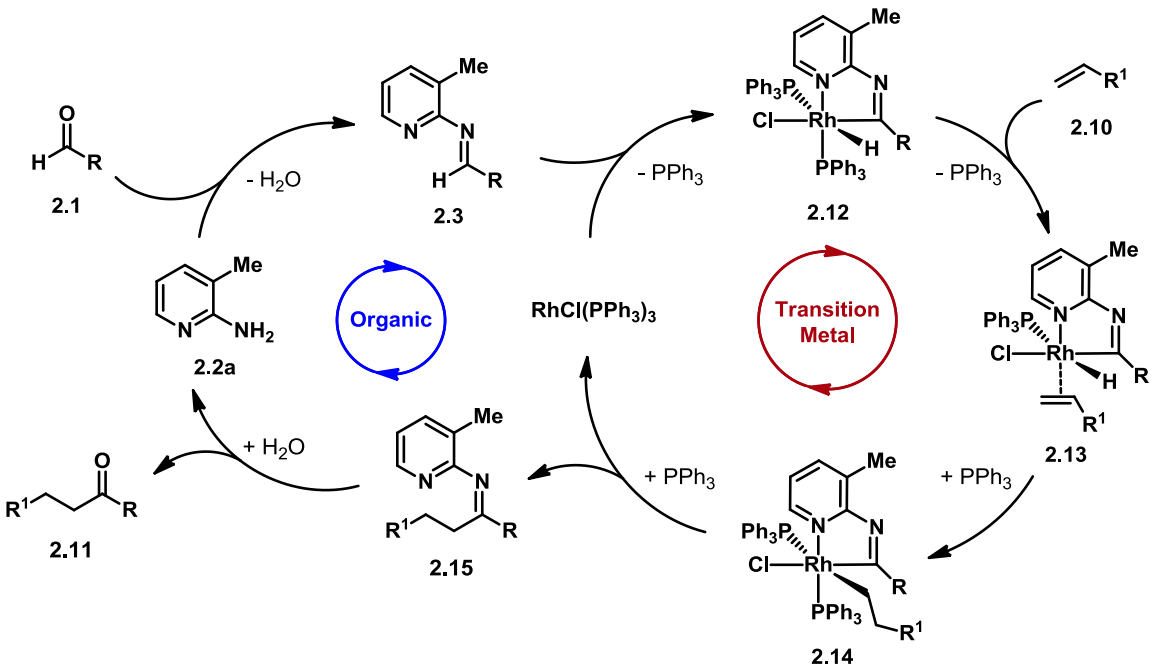

Scheme 2.4. Duel catalytic cycle proposed for amino-picoline **2.2a** and rhodium co-catalyzed intermolecular alkene hydroacylation.

A couple of aspects of the duel catalytic cycle are worth further discussion. First, the overall reaction is enthalpically downhill: a weak C–H bond (BDE ≈ 89 kcal/mol)[5] and a C–C π-bond (BDE ≈ 58 kcal/mol)[5] are exchanged for a weak C–C sigma bond

(BDE ≈ 84 kcal/mol)[5] and a strong C–H bond (BDE ≈ 101 kcal/mol)[5]. Therefore, no additional driving force is needed from an enthalpy standpoint. Secondly, the condensation and hydrolysis processes in the organic catalytic cycle are presumably reversible. General reactivity trends would suggest that the equilibrium between aldehyde **2.1** and aldimine **2.3** favors imine formation to a greater extent than the analogous equilibrium between.ketone **2.11** and ketimine **2.15**. In other words, aminopicoline **2.2a** has a greater propensity to react with aldehyde **2.1** (to form aldimine **2.3**) than it does to react with ketone **2.11** (to form ketimine **2.15**). This inherent reactivity trend then helps catalytic turnover of aminopicoline **2.2a** as the concentration of ketone **2.11** increases over the course of the reaction while the concentration of aldehyde **2.1** decreases.

Jun later showed that pre-formed aldimines were improved substrates for a metal-organic cooperative catalysis approach to alkene hydroacylation (Scheme 2.5).[6] With even lower catalyst loadings of aminopicoline **2.2a**, pre-formed aldimines **2.16** were converted to the corresponding ketimine **2.17** via hydroacylation of alkene **2.10**. Acidic hydrolysis of the reaction mixture gave ketones **2.11** in improved yields.

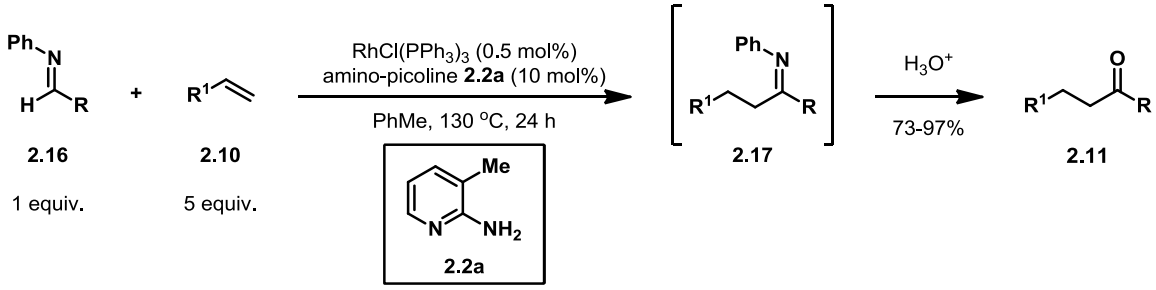

Scheme 2.5. Formal alkene hydroacylation with pre-formed aldimines as substrates.

The ability of aminopicoline **2.2a** to suppress decarbonylation (as outlined in Table 2.1 above), presumably occurs by increasing the rate of C–H activation for aldimine **2.3** relative to the non-co-catalyzed C–H activation pathway of the substrate aldehyde **2.1** (see Scheme 2.4 above). However, starting with a pre-formed aldimine avoids decarbonylation pathways altogether, which explains the marked improvement in yields with lower co-catalyst loadings. In the absence of aminopicoline **2.2a**, however, aldimines **2.16** underwent no reaction under otherwise identical conditions. Jun proposed a transimination cycle to account for the conversion of aldimines **2.16** to the chelating aldimines **2.3** *in situ* (Scheme 2.6).[6]

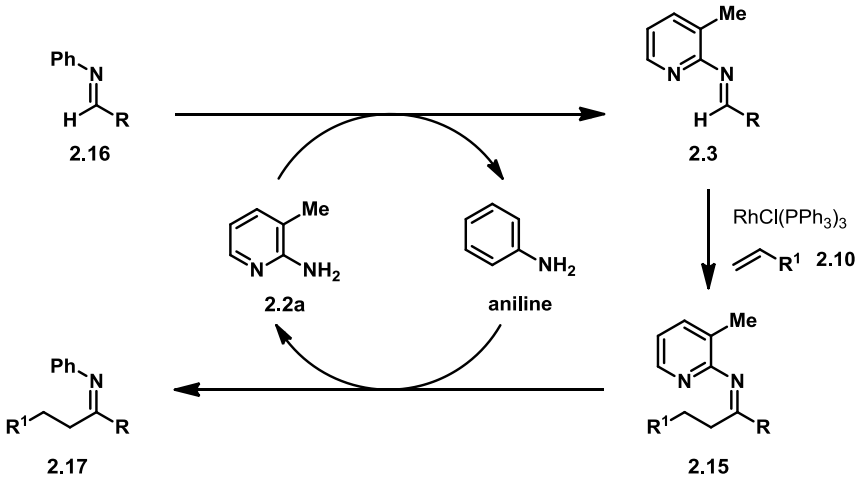

Scheme 2.6. Transimination as an alternative organic catalytic cycle for alkene hydroacylation.

The observation that pre-formed aldimines were superior substrates in MOCC alkene hydroacylation led Jun to develop a catalytic system in which aldehyde substrates were converted to their aldimine counterparts via *in situ* condensation with aniline. The *in situ* formation of simple aldimines, aided by the addition of benzoic acid, led to improved reaction yields and efficiencies, with reaction times going from 24 hours to 1 h (Scheme

2.7).[7] I would speculate that protection of aldehyde **2.1** as aldimine **2.16** (see Scheme 2.6 above) prevents decarbonylation, and the improved reaction outcomes are the result of this detrimental pathway being suppressed. Although benzoic acid likely acts as an acid catalyst for aldimine formation, carboxylates are also known as important η^2-ligands for transition metals, especially in C–H functionalization processes.[8-10] Thus, benzoic acid could possibly serve other roles in this system that are not yet understood.

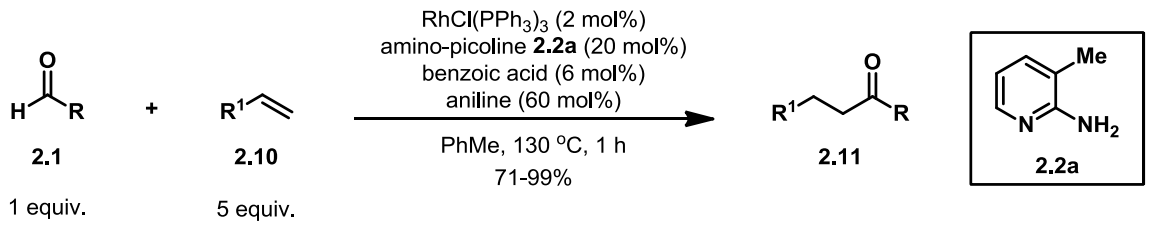

Scheme 2.7. Improved catalytic system for alkene hydroacylation enabled by metal-organic cooperative catalysis.

A competition study between aldimine and aldehyde substrates was also described in Jun's report (Table 2.2).[7] When an equal mixture of aldimine **2.17a** and electron-rich aldehyde **2.1b** were subjected to alkene hydroacylation conditions the product distribution after 5 minutes was heavily skewed toward ketone **2.11b**, arising from C–H functionalization of the aldimine. Interestingly, the reaction still favored aldimine C–H functionalization of an electron-rich aldimine (**2.17b**) in the presence of an electronically-neutral aldehyde (**2.1a**). These results suggest that transimination between aldimine **2.17** and aminopicoline **2.2a** may be faster than condensation between aldehyde **2.1** and aminopicoline **2.2a**, as one would expect the electronically-neutral substrate to be favored in both cases if transimination and condensation were competitive.

Table 2.2. Competition between aldimines and aldehydes in alkene hydroacylation via metal-organic cooperative catalysis.

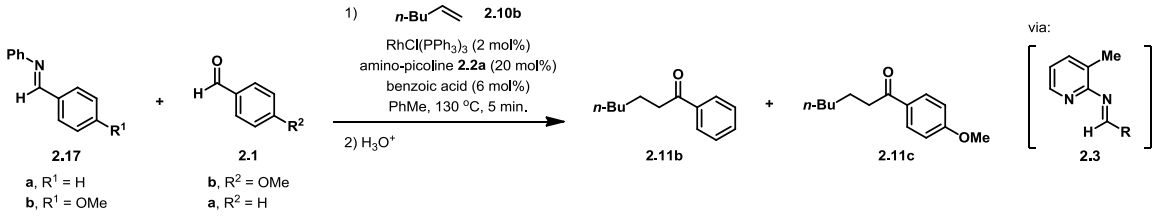

Entry	Aldimine	Aldehyde	Yield **2.11b** (%)	Yield **2.11c** (%)
1	**2.17a** (R^1 = H)	**2.1b** (R^2 = OMe)	21	5
2	**2.17b** (R^1 = OMe)	**2.1a** (R^2 = H)	5	26

In 2011, Breit reported the use of a modified aminopicoline co-catalyst in efforts to develop an intramolecular alkene hydroacylation from simple aldehydes (Scheme 2.8).[11] Amino-picoline **2.2b** includes the pyridyl nitrogen and a phosphine "arm" that are both able to ligate the rhodium metal catalyst. The bidentate nature of aminopicoline **2.2b** is thought to increase the likelihood that the metal catalyst and organic co-catalyst remain in close proximity, which in turn effectively increases the local concentration of metal catalyst upon aldimine formation. Aldehydes **2.18** were cyclized to the corresponding indanones **2.19** in excellent yields over short reaction times, all without the need for additional additives.

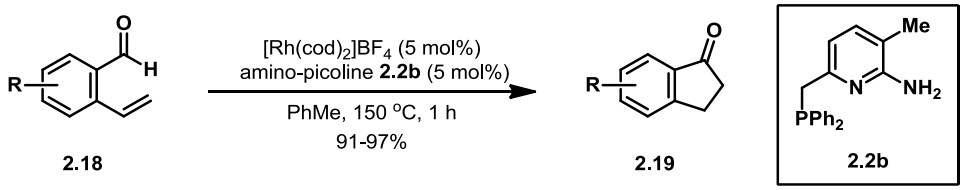

Scheme 2.8. Breit's use of a bidentate organic co-catalyst for intramolecular alkene hydroacylation.

2.1.3 Expansion of Metal-Organic Cooperative Catalysis Systems to C–C Activation and Functionalization

After having successfully demonstrated the ability to catalytically activate and functionalize C–H bonds via metal-organic cooperative catalysis, Jun expanded the methodology to the activation and functionalization of unstrained C–C bonds. In the presence of aminopicoline **2.2a** and Wilkinson's catalyst, ketones **2.11** were reacted with excess alkene **2.20** to give the product formally arising from alkene hydroacylation, ketone **2.21**, as well as alkene **2.10** as a by-product (Scheme 2.9).[12] Alkene **2.10** was thought to arise via a beta-hydride elimination pathway, which will be discussed in more detail in the following paragraphs. To avoid competitive bond activation and functionalization between the two carbonyl substituents, ketones **2.11** were designed such that one of the two substituents was devoid of beta hydrogens (e.g. R = Me, Ph). This substrate design led to the formation of ketones **2.21** in moderate-to-excellent yield. Compared to their alkene hydroacylation counterparts, these alkene carboacylation reactions required higher catalyst loadings and extended reaction times. Furthermore, the alkene hydroacylation reaction reported by Jun required solvent-level quantities of alkene **2.20**. The significance of this will be addressed upon further discussion below.

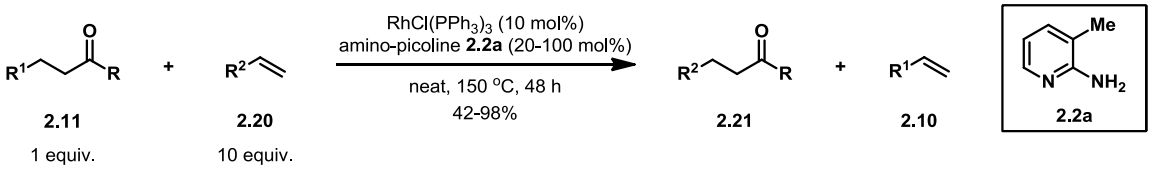

Scheme 2.9. Alkene hydroacylation via C–C bond activation using metal-organic cooperative catalysis.

Jun proposed a mechanism for alkene hydroacylation with ketone **2.11** and alkene **2.20** that parallels the mechanism proposed for alkene hydroacylation previously discussed (see Scheme 2.4 above).[12] The proposed mechanism includes ketimine formation (**2.15**, Scheme 2.10) via condensation of ketone **2.11** and aminopicoline **2.2a**, followed by C–C activation to provide alkylrhodium **2.14**. Beta-hydride elimination of alkylrhodium **2.14** generates rhodium hydride **2.12**, which is a common intermediate to alkene hydroacylation. Alkene **2.10** is also generated as a by-product of beta-hydride elimination. Reductive elimination of rhodium hydride **2.12**, followed by hydrolysis of the resulting ketimine (**2.23**) gives new ketone product **2.21**.

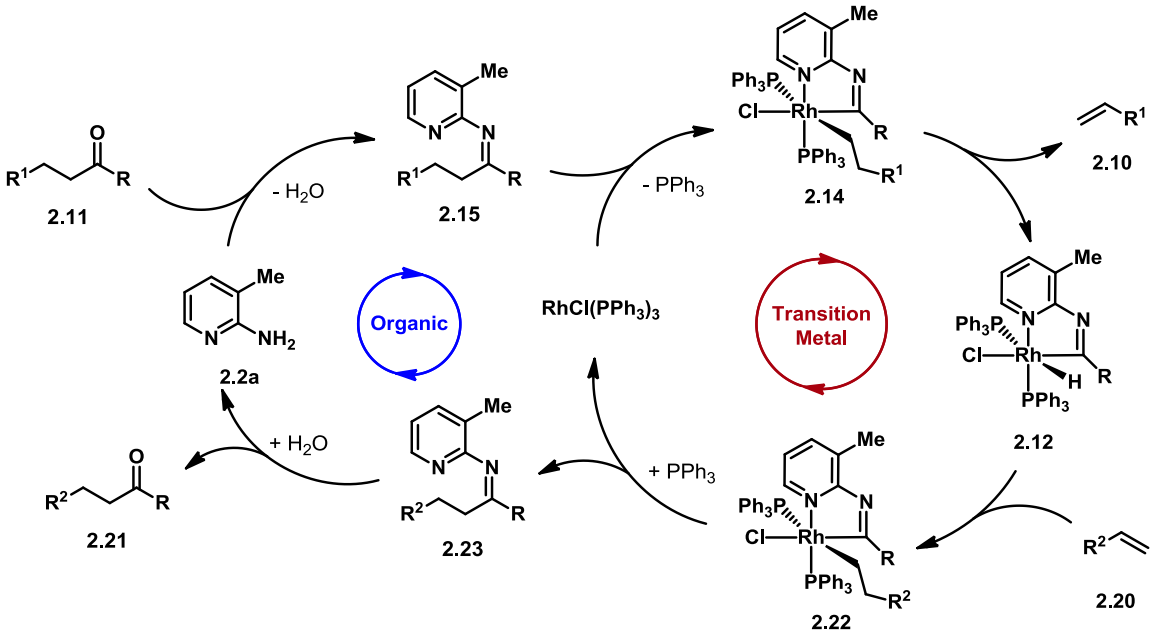

Scheme 2.10. Proposed mechanism for alkene carboacylation via metal-organic cooperative catalysis.

While the two catalytic cycles proposed for alkene hydroacylation with aldehydes **2.1** and ketones **2.11** appear similar (Scheme 2.4 and Scheme 2.10, respectively), there is

an important difference between them. As discussed in Section 2.1.2, alkene hydroacylation is enthalpically downhill, which provides a driving force for the reaction. Carboacylation, however, has virtually no enthalpy difference since one C–C sigma bond is traded for another of similar strength, and one C–C pi bond is traded for another of similar strength. Consequently, alkene carboacylation actually reaches an equilibrium between ketones **2.11** and **2.21** and alkenes **2.10** and **2.20**. The use of excess alkene then serves to drive this equilibrium towards products based on Le Chatelier's Principle. Interestingly, an additional way to drive the reaction is to have a phenyl group as the substituent R^1 in ketone **2.11**. When this is the case the alkene byproduct (**2.10**) is styrene, and since styrene polymerizes at the reaction temperatures, alkene **2.10** is pulled from equilibrium as polystyrene.

Dong recently used metal-organic cooperative catalysis in a ring-expanding C–C bond activation and functionalization methodology based on Jun's work.[13] Cyclobutanones **2.24** were treated with a Rh(I) precatalyst, an electron-deficient phosphine, and amino-picoline **2.2a** at high temperatures to give bridged rings **2.25** in moderate-to-good yield (Scheme 2.11). The authors note that such [3.3.1]-bridged ring products are similar to those that, in theory, could be prepared from a type-II intramolecular Diels-Alder reaction.[14] Therefore, Dong speculated that this C–C bond activation and functionalization methodology may be viewed as a retrosynthetic equivalent to the intramolecular Diels-Alder reaction.

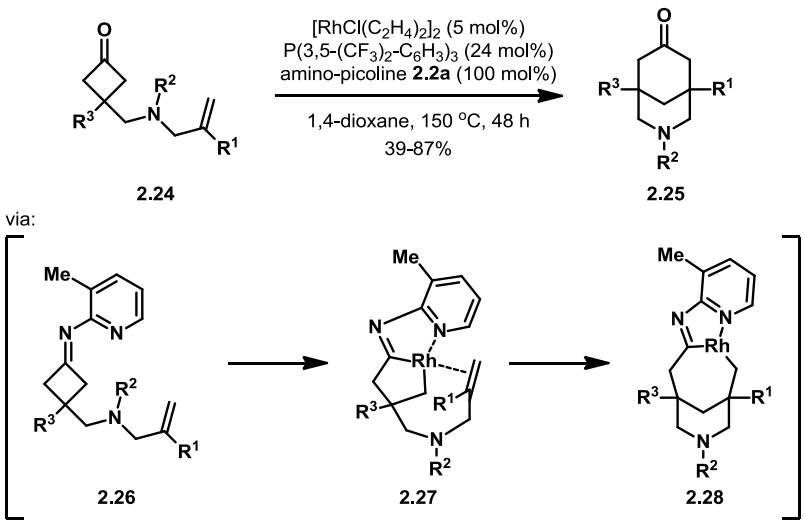

Scheme 2.11. C–C activation and functionalization of cyclobutanones in the formation of bridged ring systems.

Dong proposed that these reactions proceed through chelating imine **2.26**, after which rhodacycle **2.27** is formed via C–C bond activation. Intramolecular migratory insertion across the appended alkene forms the expanded rhodacycle **2.28**, which undergoes reductive elimination and hydrolysis to give bicyclic ketone **2.25**. Since activation of cyclobutanone C–C bonds has been reported without the need for chelation assistance,[15] it is not likely that aminopicoline **2.2a** is required for bond activation, but rather it is necessary to prevent decarbonylation in rhodacycles **2.27** and **2.28**. The amount of strain generated in the bicyclic system of rhodacycle **2.28** likely slows down the migratory insertion step that is required to form it. Therefore without protection as the cyclometallated imine, decarbonylation of the C–C activated intermediate would likely outcompete migratory insertion, leading to a metal carbonyl catalyst that can no longer engage in bond activation processes.

2.2. The Douglas Group's Application of Metal-Organic Cooperative Catalysis for Bond Activation

2.2.1 Intramolecular Alkene Hydroacylation via Metal-Organic Cooperative Catalysis

The Douglas group expanded the work developed by Jun to include metal-organic cooperative catalysis in intramolecular alkene hydroacylation.[16] Aldehydes **2.29**, which bear an appended alkene, were successfully converted to carbocycles **2.30** (see Scheme in Table 2.3 below). Intramolecular alkene hydroacylation, in this context, is particularly notable because it allows for the synthesis of 7-membered carbocycles. The formation of 7-membered rings is challenging in general, but a lack of embedded heteroatoms makes 7-membered carbocycles even more challenging. Furthermore, many intramolecular alkene hydroacylation strategies rely on a chelating group, permanently embedded within the substrate, to prevent decarbonylation. In contrast, we use a transiently-formed directing group, thereby increasing the scope to which this methodology can be applied.

Table 2.3. Substrate scope for intramolecular alkene hydroacylation enabled by metal-organic cooperative catalysis.

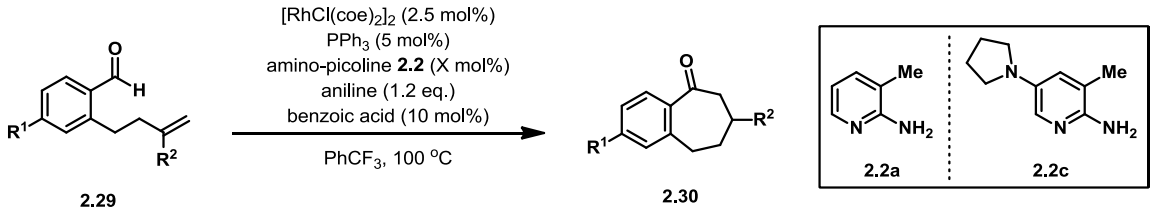

Entry[a]	Starting Material	R^1	R^2	Amino-picoline (mol%)	Product	Yield (%)[b]
1	**2.29a**	H	Me	**2.2a** (10%)	**2.30a**	81
2	**2.29b**	Me	Me	**2.2a** (10%)	**2.30b**	84[c]
3	**2.29c**	CF_3	Me	**2.2a** (10%)	**2.30c**	76
4	**2.29d**	OMe	Me	**2.2a** (10%)	**2.30d**	85
5	**2.29e**	F	Me	**2.2a** (10%)	**2.30e**	80[c]
6	**2.29f**	H	Et	**2.2a** (10%)	**2.30f**	86
7	**2.29g**	H	Ph	**2.2c** (25%)	**2.30g**	77
8	**2.29h**	H	CH_2OTBS	**2.2c** (10%)	**2.30h**	78
9[d]	**2.29i**	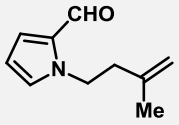		**2.2c** (25%)	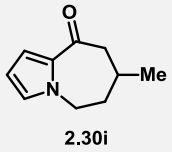 **2.30i**	63
10[d]	**2.29j**	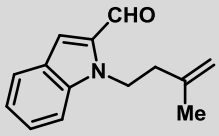		**2.2c** (25%)	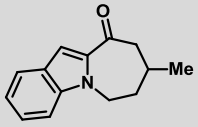 **2.30j**	66

[a]Conditions: $[RhCl(coe)_2]_2$ (2.5 mol %), PPh_3 (5 mol %), $PhNH_2$ (1.2 equiv), BzOH (10 mol %), $PhCF_3$, 100 °C. [b]Isolated yield after silica gel chromatography. Except where noted, regioisomeric hydroacylation products were not observed, indicating regioselectivity was >10:1. [c]Contaminated with a minor <5% of the corresponding indanone; pure sample could be obtained by preparative TLC. [d]Conditions: $[RhCl(coe)_2]_2$ (5 mol %), PPh_3 (10 mol %), $PhNH_2$ (1.2 equiv), BzOH (10 mol %).

During initial reaction optimization studies (not shown), aminopicoline **2.2a** performed poorly when used catalytically in dichloroethane as the reaction solvent. As was discussed in previous sections, decarbonylation has often been suggested as a source

of poor reaction outcomes in alkene hydroacylation methodologies, with imine formation being a viable strategy to avoid this detrimental reaction pathway. If the rate of intramolecular migratory insertion were to slow down significantly, which is likely true when such an insertion leads to the formation of 7-membered rings, non-co-catalyzed C–H activation of free aldehyde becomes competitive. It was hypothesized that a more nucleophilic aminopicoline co-catalyst would promote imine formation, thereby decreasing the amount of free aldehyde in solution, which in turn would decrease the rate of decarbonylation. To test this, a strongly electron-donating pyrrolidine group was placed *para* to the primary amine to give amino-picoline **2.2c** (see Scheme in Table 2.3 above). The electron-rich aminopicoline **2.2c** outperformed aminopicoline **2.2a** when used catalytically in dichloroethane. However, aminopicoline **2.2a** was shown to be a viable co-catalyst when trifluorotoluene was used as the reaction solvent instead of dichloroethane. As such, the modified aminopicoline **2.2c** was only used for intramolecular alkene hydroacylation substrates when aminopicoline **2.2a** was not an effective co-catalyst.

In this report,[16] aromatic substituents *para* to the aldehyde moiety did not demonstrate a large effect on the reaction (Table 2.3 above, entries 1–5). Even a strong electron-withdrawing $–CF_3$ group provided ketone **2.30c** in only slightly diminished yield (entry 3). Substituents on the alkene were also well-tolerated (entries 6–8), as an electron-withdrawing allylic ether also provided the cyclized product in good yield (entry 8). Aromatic heterocycles were demonstrated to be viable tethers, albeit at the expense of diminished yields (entries 9 & 10).

The intramolecular alkene hydroacylation reactions discussed above also generate a stereocenter in the ketone product. As such, chiral ligands were tested to see what effects they would have on both enantioselectivity and reaction efficiency. Surprisingly, chiral phosphoramidites MONOPHOS and **2.31a** (Table 2.4, entries 1 & 2) and chiral phosphines **2.31b** and **2.31c** (entries 3 & 4) all resulted in drastically diminished reaction yields, while also providing little enantioselectivity.

Table 2.4. Effects of chiral ligands for enantioselective intramolecular alkene hydroacylation.

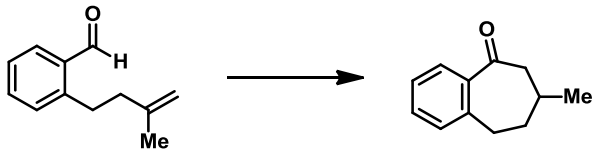

2.29a **2.30a**

Entry[a]	Ligand	Yield **2.30a** (%)[b]	*ee*[c]
1	(+)-MONOPHOS	0	N/A
2[d]	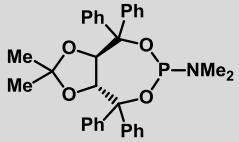 **2.31a**	30	23
3	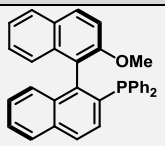 **2.31b**	10	24
4	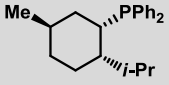 **2.31c**	3	18

[a]Conditions: $[RhCl(coe)_2]_2$ (2.5 mol %), ligand (5 mol %), **2.2a** (10 mol%), $PhNH_2$ (1.2 equiv), BzOH (10 mol %), $PhCF_3$, 100 °C. [b]Yield after silica gel chromatography. [c]Determined by HPLC (Chiralcel OD-H, *n*-hexane/IPA (9:1), λ = 220 nm). [d]**2.29a**, $PhNH_2$, and BzOH in $PhCF_3$ were premixed before adding $[RhCl(coe)_2]_2$, ligand, and **2.2a**.

Given the poor results using chiral ligands to induce enantioselectivity in the reaction, the possibility of using a chiral aminopicoline co-catalyst for enantioinduction was explored (Scheme 2.12). Unlike the chiral ligands described above, aminopicoline **2.2d** did not affect the efficiency of the reaction, but provided carbocycle **2.30a** in only moderate *ee*. Despite the poor enantioselectivity, these results were promising as they suggested enantioselective reactions may be possible with the right chiral aminopicoline co-catalyst.

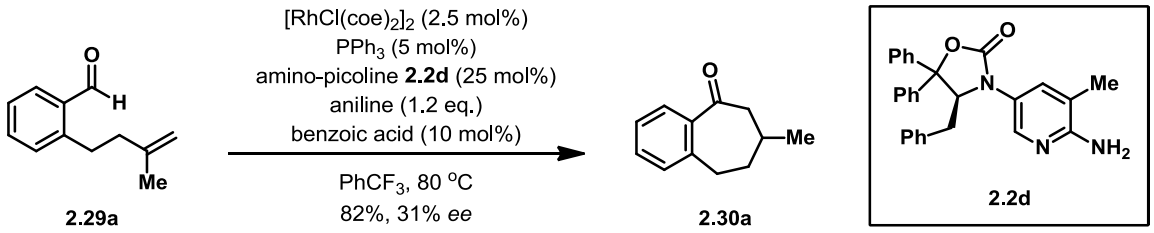

Scheme 2.12. Enantioselective intramolecular alkene hydroacylation using aminopicoline **2.2d**.

2.3. Enantioselective Intramolecular Alkene Hydroacylation

2.3.1 Research Proposal: Co-catalysts bearing a chiral, C_2-symmetrical substituent

After obtaining promising results with aminopicoline **2.2d** in enantioselective variants of the MOCC intramolecular alkene hydroacylation methodology (see Scheme 2.12 above), it was envisioned that alternative chiral scaffolds attached to the amino-picoline core could provide more effective enantio-induction. A serious drawback to the design of aminopicoline **2.2d** is that rotation about the N–C bond linking the chiral appendage to the aminopicoline core allows for a conformer that would likely provide enantio-induction opposite that of the original conformer (Figure 2.1a). If the populations of the two conformers are approximately equal, and if each conformer is equally efficient

at providing enantio-induction, then one would expect an equal amount of each enantiomer. The moderate *ee* (31%) obtained with aminopicoline **2.2d** is likely then the result of either non-equal populations of the two conformers, unequal efficiency of the two conformers at providing enantio-induction, or a combination of the two.

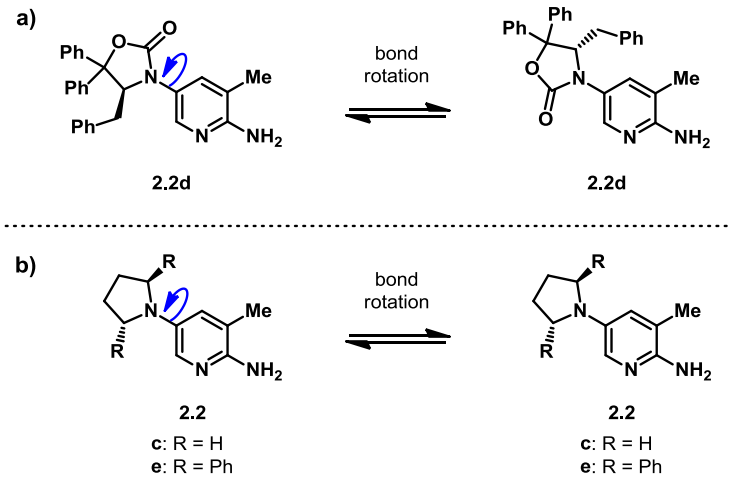

Figure 2.1. Effects of bond rotation in chiral aminopicoline co-catalysts leading to a) conformers with opposing stereo-induction and b) redundant conformers.

A plausible solution to this problem is to incorporate an element of C_2-symmetry within the chiral appendage (Figure 2.1b). This symmetry element then makes bond rotation result in redundant conformers, thereby eliminating the issue present in aminopicoline **2.2d**.

2.3.2 Results: Co-catalysts bearing a chiral, C_2-symmetrical substituent

Work on this project began with synthesizing the previously-prepared achiral aminopicoline **2.2c** (see Scheme 2.13 below for synthesis). It was envisioned that chiral aminopicoline **2.2e** could be synthesized in a manner analogous to **2.2c**. As such, synthesizing the simpler analog would allow for familiarization of the chemistry involved

while also proving useful material. Aminopicoline **2.2c** can be prepared in two steps from commercially-available aminopicoline **2.2a**. The synthesis starts with an electrophilic aromatic substitution[17] to install the iodine moiety, giving aminopicoline **2.2f** in a moderate 65% yield. This reaction is typically run on >5 g scale, so despite the modest yield, aminopicoline **2.2f** could easily be prepared in sufficient quantities. A modified Ullmann coupling[18] was then be used to install the pyrrolidine appendage, giving aminopicoline **2.2c** in good yield. Purification of aminopicoline **2.2c** was a point of concern. Different batches gave solids with drastically different colors, even after chromatographic purification and despite identical ^{1}H NMR spectra. It was hypothesized that this color difference was due to varying amounts of copper ligated to the pyridyl nitrogen in the product. Acid-base extractions of the crude reaction mixture followed by column chromatography consistently provided **2.2c** as a light-brown solid, which was deemed acceptable for subsequent use.

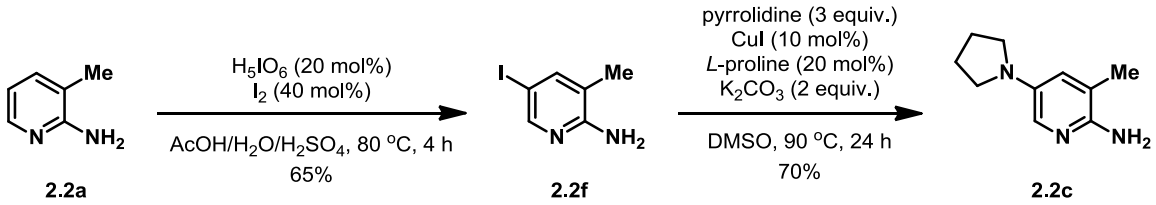

Scheme 2.13. Synthesis of aminopicoline **2.2c.**

Having successfully made aminopicoline **2.2c**, we turned our attention to the synthesis of chiral aminopicoline **2.2e** (Scheme 2.14). Chiral 2,5-diphenylpyrrolidine **2.32** was provided by Christopher Douglas, and was used in a series of modified Ullmann coupling reactions. Using 1.5 equivalents of pyrrolidine **2.32** under previously-established reaction conditions led only to hydrodehalogenated aminopicoline **2.2a**

(Scheme 2.14a). Increased catalyst loading and increased base equivalents prevented this hydrodehalogenation, but still only returned starting materials (Scheme 2.14b). Alternative conditions had been previously used to synthesis chiral aminopicoline **2.2d**,[16] as the oxazolidinone coupling partner in that case was much less nucleophilic than the usual pyrrolidine coupling partner. Those conditions were attempted with diphenylpyrrolidine **2.32** as the coupling partner, but resulted in only a minor amount of what was tentatively assigned as the product arising from homo-coupling (**2.2g**, Scheme 2.14c). This result suggests that diphenylpyrrolidine **2.32** is poorly nucleophilic, as the electron-deficient amine in aminopicoline **2.2f** was able to out-compete it as a nucleophile. Our hypothesis is that the steric bulk around the pyrrolidine nitrogen is actually much greater than it would appear to be at first glance. Since each of the phenyl rings in pyrrolidine **2.32** is projected to a different face of the pyrrolidine ring, there is no approach to the nitrogen that isn't hindered by one of the two phenyl substituents.

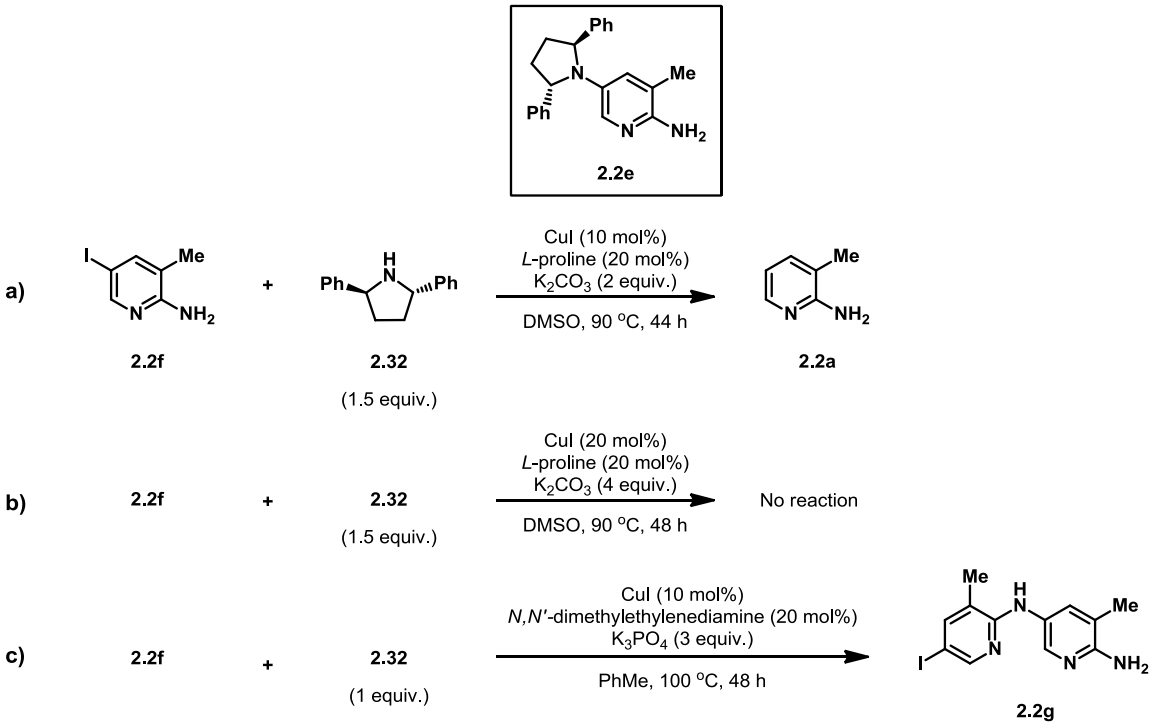

Scheme 2.14. Attempted synthesis of amino-picoline **2.2e** via modified Ullmann coupling resulting in a) hydrodehalogenation b) no reaction and c) homo-coupling.

Based on the above results, it was suggested that nucleophilic aromatic substitution (S_NAr) might be an alternative way to make the desired N–C bond. Since the electrophile in S_NAr is planar, the steric hindrance around the pyrrolidine nitrogen in **2.32** might be less influential on the outcome of such a reaction. We started with commercially-available amino-pyridine **2.33** (Scheme 2.15). This amino-pyridine was desirable not only because it contained a fluorine substituent in the 5-position, but also because the bromide at the 3-position would allow for modification at that site via cross-coupling or lithium-halogen exchange chemistry.

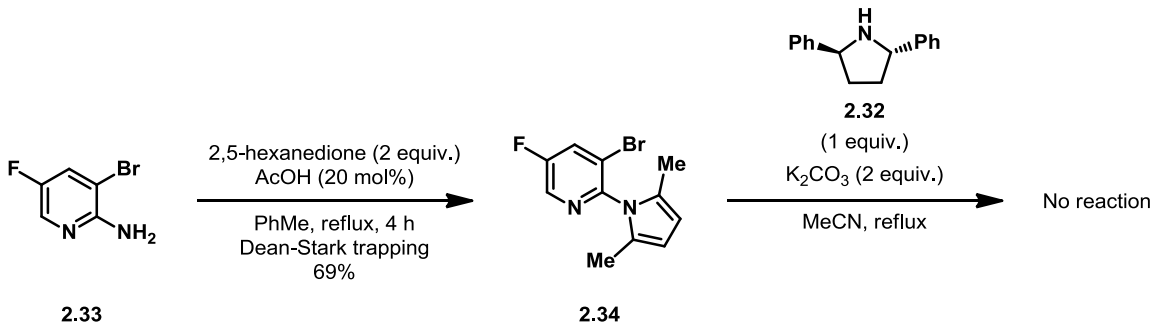

Scheme 2.15. Attempted coupling of pyrrolidine **2.32** to fluoro-pyridine **2.34** via S_NAr

The first step in this synthesis was protection of the primary nitrogen in aminopyridine **2.33** as the pyrrole. Pyrrole was chosen as the protecting group because it protects both N–H bonds, and provides some electron-withdrawing character due to the aromaticity gained through lone-pair donation. This was achieved via condensation of aminopyridine **2.33** with 2,5-hexanedione to give fluoropyridine **2.34** in modest yield. Unfortunately, attempts to couple pyrrolidine **2.32** to fluoropyridine **2.34** were unsuccessful. Attempts to couple aminopyridine **2.33** with pyrrolidine via S_NAr were also unsuccessful (not shown).

Due to an inability to synthesize chiral amino-picoline **2.2e**, our original hypothesis has not been able to be tested. We therefore turned to other scaffolds for aminopicoline co-catalysts to see if enantioselective intramolecular alkene hydroacylation might be effected by chiral co-catalysts.

2.3.3 Research Proposal: Biaryl co-catalysts with axial chirality

The design of new organic co-catalysts prompted a return to the drawing board. The pyridine nitrogen and the primary amine at the 2-position in the ring are prerequisites for generating an imine capable of directing a metal catalyst to the appropriate bond, thus

they needed to be kept intact (Figure 2.2a). The methyl group at the 3-position is also needed to bias the metal towards the desired bond (refer to Scheme 2.2b above), but in theory any substitution at the 3-position should accomplish this. This leaves the 4-, 5-, and 6-positions open to install the chiral portion of the catalyst. To achieve maximum enantio-induction, chirality should be positioned as close to the metal center as possible, meaning that the 6-position (substituent X) would ideally bear the source of chirality. This leaves the 4- and 5-positions (substituents Z and Y, respectively) open to either be modified or left unsubstituted.

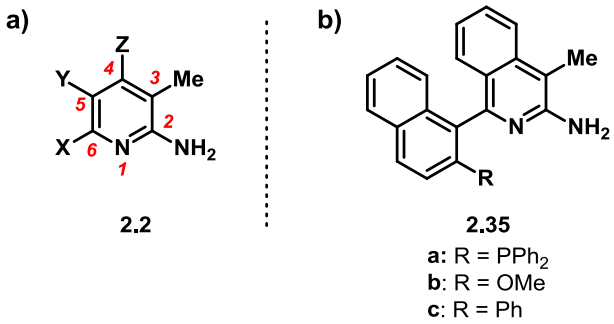

Figure 2.2. a) general design outline for organic co-catalysts and b) amino-isoquinoline framework proposed for new co-catalysts.

If substituents Y and Z are covalently connected, a bulky aryl group at the 6-position (substituent X) would allow an axis of chirality to be established. This led to my proposal of aminoisoquinolines **2.35** as new chiral organic co-catalysts for MOCC bond activation methodologies (Figure 2.2b). In addition to introducing a new mode of chirality for these organic co-catalysts, the biaryl linkage allows further modifications to be made. For example, substitution of a $–PPh_2$ group at the 2'-position creates a bidentate co-catalyst (**2.35a**) similar to aminopicoline **2.2b** reported by Breit (see Scheme 2.8 above).[11] Substitution of a –OMe group at the same position allows for a hemi-labile

bidentate co-catalyst (**2.35b**), and substitution with a bulky substituent, such as a phenyl group (**2.35c**), could allow for longer "reach" to help improve enantio-induction.

A retrosynthesis of the newly designed aminoisoquinoline co-catalysts is shown below (Scheme 2.16). Aminoisoquinolines **2.35a** and **2.35c** should be available from aminoisoquinoline **2.35b** by way of converting the aryl methoxy ether to the aryl triflate, followed by cross-coupling with either diphenylphosphine[19] or phenylboronic acid (yielding aminoisoquinolines **2.35a** and **2.35c**, respectively). Aminoisoquinoline **2.35b** should be available via a Suzuki cross-coupling of known arylboronic acid **2.36**[19] and known bromoisoquinoline **2.37**.[20] Cross-coupling reactions that form similar axially-chiral biaryl linkages enantioselectively are known,[21] so this route could eventually provide enantio-enriched aminoisoquinolines **2.35a-c**, if they prove to be viable organic co-catalysts.

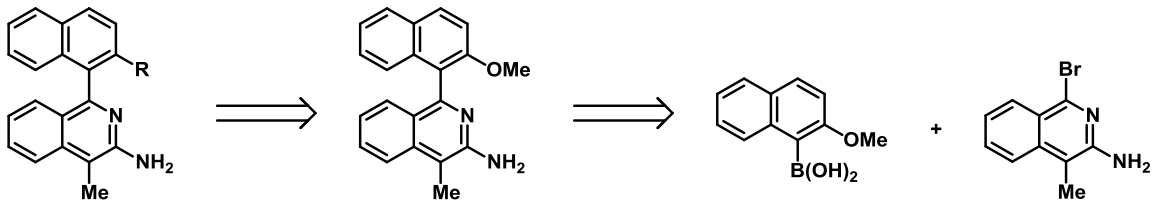

2.35 **2.35b** **2.36** **2.37**

a: R = PPh_2
c: R = Ph

Scheme 2.16. Retrosynthetic analysis for aminoisoquinolines **2.35**.

2.3.4 Results: Biaryl co-catalysts with axial chirality

Arylboronic acid **2.36** has been previously reported[19] and is available in 2 steps from commercially-available 2-methoxynaphthalene (**2.38**, Scheme 2.17). Arene **2.38** is treated with bromine in acetic acid to give aryl bromide **2.39** in excellent yield.

Conversion of aryl bromide **2.39** to the corresponding Grignard reagent followed by the addition of trimethyl borate gives arylboronic acid **2.36** in 58% yield.

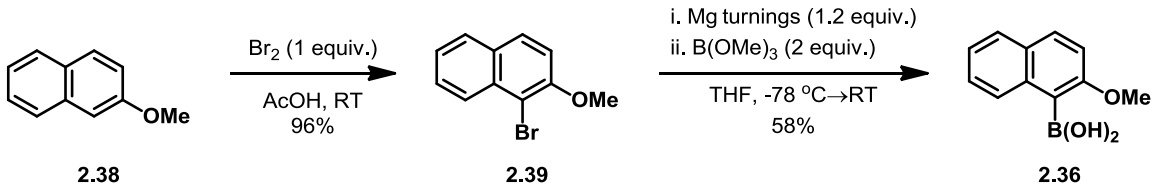

2.38 **2.39** **2.36**

Scheme 2.17. Synthesis of arylboronic acid **2.36**.

Bromoisoquinoline **2.37** has also been previously reported[20] and can be prepared in two steps from commercially available 2-cyanophenylacetonitrile (**2.40**, Scheme 2.18). Phenylacetonitrile **2.40** can be deprotonated with LDA which, upon treatment with iodomethane, gives the dinitrile **2.41** in good yield.[22] Over-alkylation was a common issue with this reaction, but could be mitigated with an inverse addition of reagents (deprotonated **2.40** added to iodomethane). When treated with an acetic acid solution of HBr, dinitrile **2.41** cyclized to give a mixture of bromoisoquinoline **2.37** and *N*-acyl-bromoisoquinoline **2.42**.[20] Amide bond formation likely occurs via an acid-catalyzed acylation of bromoisoquinoline **2.37** with acetic acid. However, the acetate group in **2.42** could be readily cleaved with aqueous acid to provide additional bromoisoquinoline **2.37** in excellent yield.

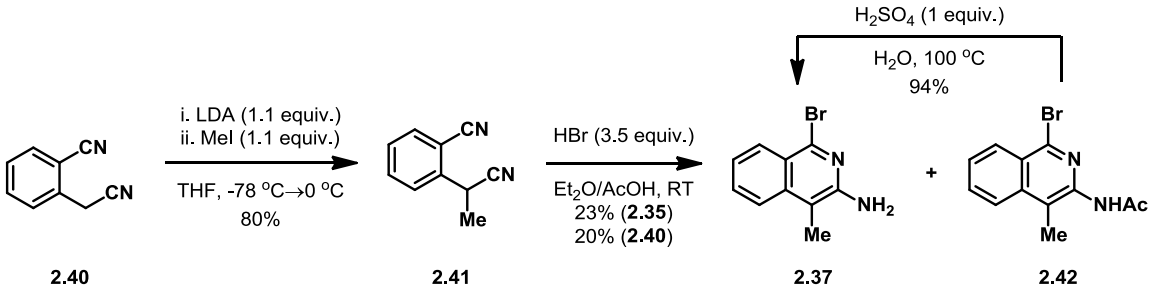

Scheme 2.18. Synthesis of bromoisoquinoline **2.37**.

With arylboronic acid **2.36** and bromoisoquinoline **2.37** in hand, Suzuki coupling could be used to efficiently form the biaryl linkage, providing aminoisoquinoline **2.35b** in good yield (Scheme 2.19). Due to compatibility issues during a future triflation step, the amine moiety needed to be protected at this point. This was achieved by conversion to

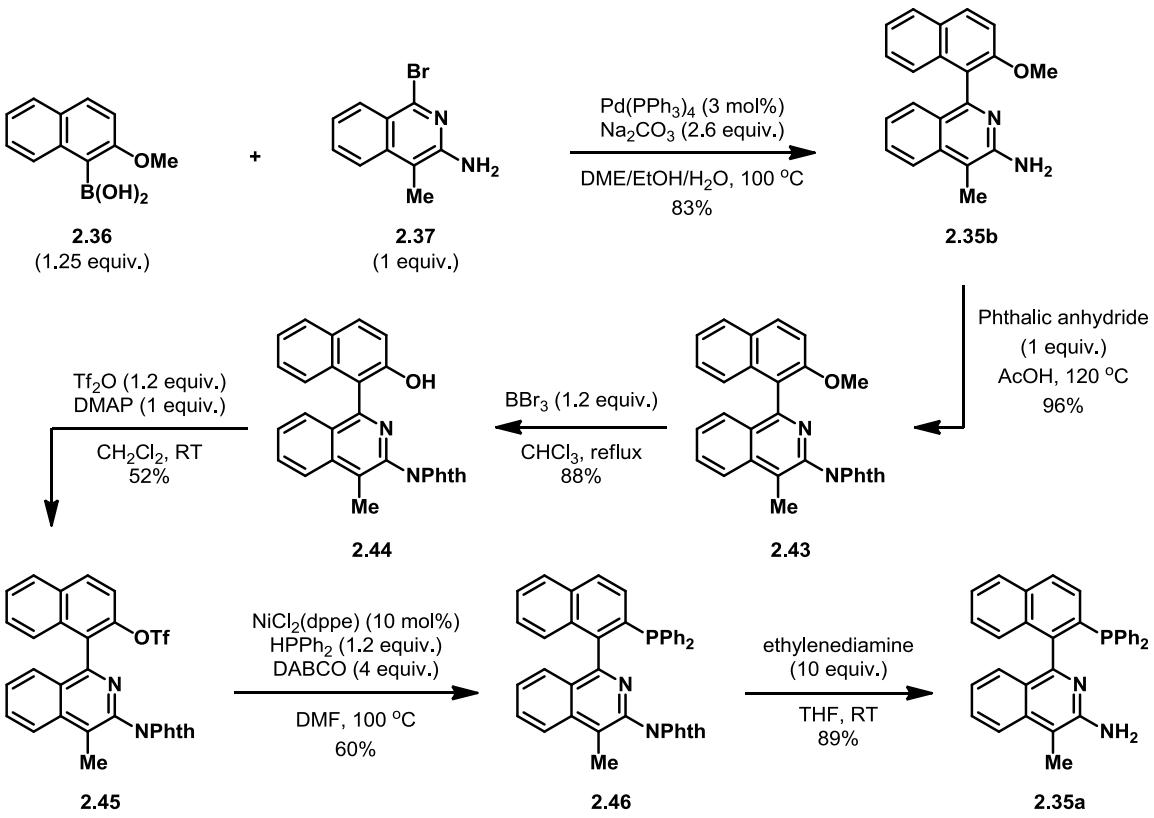

Scheme 2.19. Synthesis of aminoisoquinolines **2.35b** and **2.35a**.

phthalimide **2.43**, which could be made efficiently via a condensation of aminoisoquinoline **2.35b** with phthalic anhydride. Arylmethyl ether **2.43** could then be converted to aryl triflate **2.45** in two steps via cleavage of the O–Me bond with boron tribromide followed by triflation of the resulting phenol (**2.44**) with triflic anhydride. Nickel-catalyzed cross coupling of aryl triflate **2.45** with diphenylphosphine was able to install the phosphine moiety at the 2'-position in 60% yield.[19] Finally, removal of the phthalimide group gave aminoisoquinoline **2.35a**. Initial attempts using hydrazine were successful in removing the phthalimide protecting group, but purification proved challenging. It is hypothesized that the by-product from this hydrazine-mediated removal is capable of forming a strong hydrogen-bond adduct with aminoisoquinoline **2.35a**. This issue was obviated by switching from hydrazine to ethylenediamine[23] as the nucleophile, allowing for a clean removal of the phthalimide protecting group.

With bidentate aminoisoquinoline **2.35a** in hand, we screened for reactivity under intramolecular alkene hydroacylation conditions similar to those reported by Breit.[11] These conditions were chosen because of the similarity between aminoisoquinoline **2.35a** and the bidentate co-catalyst used by Breit (aminopicoline **2.2b**, refer to Scheme 2.8 above). Additionally, our previous work on intramolecular alkene hydroacylation reported that bidentate phosphines shut down reactivity.[16] This lack of reactivity is hypothesized to be caused by a saturated coordination environment of the metal center after C–H activation. Using a non-coordinating counterion, such as BF_4^- or SbF_6^-, should mitigate this by opening up a coordination site, allowing for easier alkene binding.

The results of this screening are shown below (Table 2.5). With $[Rh(cod)_2]BF_4$ in toluene at 150 °C, aminoisoquinoline **2.35a** did not give any of the desired 7-membered carbocycle **2.30a**, but did generate a substantial amount of the known indanone **2.48**[24] (entry 1). This likely occurs by isomerization of the alkene, presumably to the extent that it becomes conjugated to the aromatic ring, followed by hydroacylation of the alkene. Due to concerns about the solubility of $[Rh(cod)_2]BF_4$ in toluene, the solvent was changed to trifluorotoluene. In addition to the change in solvent, lowering the temperature to 130 °C resulted in a lesser amount of cyclized products and produced a mixture of known tetralone **2.47**[25] and indanone **2.48** (entry 2). Again, both of these cyclized products are likely formed via alkene isomerization followed by hydroacylation. Further lowering of the temperature only gave back starting material (entry 3).

Table 2.5. Initial screening of aminoisoquinoline **2.35a** with rhodium(I) precatalysts.

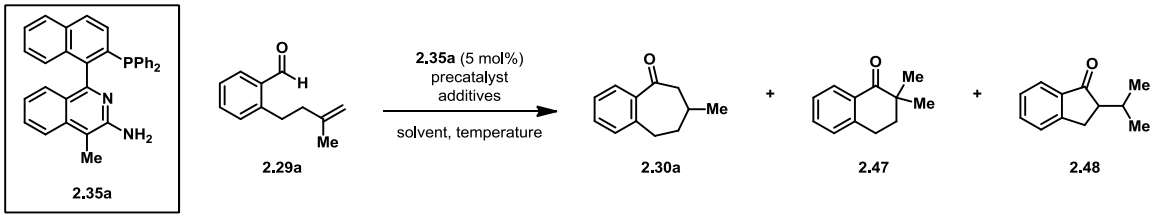

Entry[a]	Precatalyst (mol%)	Additives (mol %)	Solvent	Temp (°C)	S.M. and Product Ratios[b]			
					2.29a	**2.30a**	**2.47**	**2.48**
1	$[Rh(cod)_2]BF_4$ (5 mol%)	–	PhMe	150	1.7	0	0	1
2	$[Rh(cod)_2]BF_4$ (5 mol%)	–	$PhCF_3$	130	8.4	0	1.9	1
3	$[Rh(cod)_2]BF_4$ (5 mol%)	–	$PhCF_3$	100	1	0	0	0
4	$[Rh(cod)Cl]_2$ (2.5 mol%)	–	PhMe	130	1	0	0	0
5	$[Rh(cod)Cl]_2$ (2.5 mol%)	$AgBF_4$ (5 mol%)	PhMe	130	1	0	0	0

6	$[Rh(cod)Cl]_2$ (2.5 mol%)	$AgSbF_6$ (5 mol%)	PhMe	130	1	0	0	0
7	$[Rh(coe)_2Cl]_2$ (2.5 mol%)	–	PhMe	130	1	0	0	0
8	$[Rh(coe)_2Cl]_2$ (2.5 mol%)	$AgBF_4$ (5 mol%)	PhMe	130	1	0	0	0

[a]Reactions were performed in a nitrogen-filled glovebox and stirred at the indicated temperature overnight.
[b]Determined via ^{1}H NMR integrations from crude reaction mixtures.

Still concerned about potential solubility issues, we sought to use more soluble rhodium(I) chloride precatalysts and generate cationic rhodium *in situ* via halide abstraction with silver(I) additives.[26] Initial attempts employed $[Rh(cod)Cl]_2$ as the precatalyst and this was first used without additives as a control experiment (Table 2.5, entry 4). Consistent with our hypothesis regarding coordinative saturation of the metal center, no cyclized products were obtained under these conditions. $AgBF_4$ and $AgSbF_6$ were screened as additives to see if the counterion (BF_4^- and SbF_6^-, respectively) might also play some role in the reaction, whether from catalyst solubility enhancement or otherwise. Unexpectedly, neither $AgBF_4$ nor $AgSbF_6$ lead to the formation of any cyclized products (Table 2.5, entries 5 & 6, respectively). The result with $AgBF_4$ as an additive was particularly worrisome as it should, in theory, generate the same active metal species used in entries 1-3.

We began to question whether the bidentate nature of the cyclooctadiene (cod) ligands, while not as strongly-coordinating as phosphines, could still prevent the substrate alkene moiety from binding effectively to the metal center, thereby preventing migratory insertion. Double bond isomerization of the substrate could allow for better binding of the substrate alkene, as more favorably-sized metallacycles would be formed. This could

explain why the 5- and 6-membered carbocycles (**2.48** and **2.47**, respectively) were able to be formed, while the desired 7-membered carbocycle **2.30a** was not. To test this hypothesis we switched to $[Rh(coe)_2Cl]_2$ as the precatalyst, and ran the reaction both without additives and with $AgBF_4$ (Table 2.5, entries 7 & 8). These conditions, however, also resulted in no formation of cyclized products.

Despite the lack of reactivity observed with the precatalyst $[Rh(cod)Cl]_2$, an encouraging sign was that the addition of $AgSbF_6$ gave back starting material very cleanly. This result suggested to us that alkene isomerization, among other non-productive pathways, were not competitive. This led us to examine these same conditions, albeit at much higher temperatures. At 170 ^oC, the combination of $[Rh(cod)Cl]_2$, $AgSbF_6$ and aminoisoquinoline **2.35a** gave significant conversion of starting material (Table 2.6, entry 1). The product, however, was not a product arising from alkene hydroacylation, but instead has been tentatively assigned as keto-styrene **2.49**.

Table 2.6. Screening of aminoisoquinoline **2.35a** at elevated temperatures with control experiments.

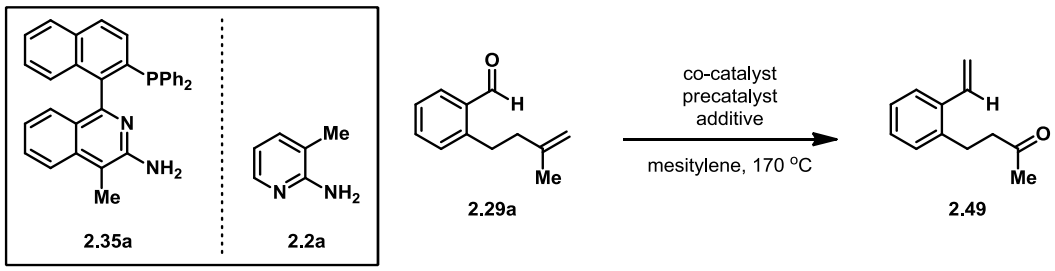

Entry[a]	Co-catalyst (mol%)	Precatalyst (mol%)	Additive (mol%)	S.M. to Product Ratio[b]	
				2.29a	**2.49**
1	**2.35a** (5 mol%)	$[Rh(cod)Cl]_2$ (2.5 mol%)	$AgSbF_6$ (5 mol%)	1	3.5

2	–	$[Rh(cod)Cl]_2$ (2.5 mol%)	$AgSbF_6$ (5 mol%)	1	8.6
3	–	$[Rh(cod)Cl]_2$ (2.5 mol%)	–	1	0
4[c]	–	–	$AgSbF_6$ (5 mol%)	0	0
5[d]	–	–	AgCl (10 mol%)	1	0
6	**2.2a** (5 mol%)	$[Rh(cod)Cl]_2$ (2.5 mol%)	PPh_3 (5 mol%) $AgSbF_6$ (5 mol%)	1	0

[a]Reactions were performed in a nitrogen-filled glovebox and stirred at 170 °C overnight. [b]Determined via ^1H NMR integrations from crude reaction mixtures. [c]Reaction produced a complex mixture. [d]Another as-yet unidentified product was formed instead of **2.49**.

This unexpected transformation occurred relatively cleanly. As such, a series of control experiments were performed to elucidate what components of the reaction were important for this new mode of reactivity. The use of $[Rh(cod)Cl]_2$ and $AgSbF_6$ without an organic co-catalyst resulted in even better conversion to keto-styrene **2.49** (Table 2.6, entry 2), which suggests that aminoisoquinoline **2.35a** actually inhibits this reaction. Further control experiments using either $[Rh(cod)Cl]_2$ or $AgSbF_6$ as the sole reagent did not result in any conversion to keto-styrene **2.49** (entries 3 & 4, respectively). This shows that the combination of $[Rh(cod)Cl]_2$ and $AgSbF_6$ is necessary for reactivity. However, treatment of $[Rh(cod)Cl]_2$ with $AgSbF_6$ also produces AgCl as a by-product. To ensure that this new reaction was not mediated by AgCl, aldehyde **2.29a** was treated with 10 mol% of AgCl and heated in mestiylene at 170 °C overnight (entry 5). This resulted in clean conversion to a minor amount of a new product that is not keto-styrene **2.49**, but has not yet been identified. As aminoisoquinoline **2.35a** had inhibited, but not shut down entirely, this new mode of reactivity, we wanted to examine if the bidentate nature of aminoisoquinoline **2.35a** was playing some role. Surprisingly, the use of aminopicoline

2.2a and triphenylphosphine in place of aminoisoquinoline **2.35a** resulted in no conversion to keto-styrene **2.49** (entry 6).

While the previous results are interesting and possibly worth exploring further, we wanted to get back to answering our hypothesis about the viability of aminoisoquinolines **2.35** as co-catalysts for intramolecular alkene hydroacylation. To determine if the apparent lack of reactivity was an attribute of the rhodium precatalysts or aminoisoquinoline **2.35a**, side-by-side experiments were run using aminoisoquinoline **2.35a** and aminopicoline **2.2a** under conditions similar to those previously reported by our group (see Table 2.7 below). With added triphenylphosphine, benzoic acid, and aniline, amino-isoquinoline **2.35a** only returned starting material (entry 1) while aminopicoline **2.2a** gave the desired 7-membered carbocycle as the major product (entry 2).

Given the poor results we have obtained with bidentate ligands in alkene hydroacylation in general, we attributed the lack of success of aminoisoquinoline **2.35a** to its strong bidentate nature. As such, we turned to aminoisoquinoline **2.35b** as an alternative co-catalyst. The hemi-labile nature of the 2'–methoxy group was intriguing and sufficient quantities of aminoisoquinoline **2.35b** were more readily available than other derivatives (refer to Scheme 2.19 above).

Table 2.7. Side-by-side comparison of aminosoquinoline **2.35a** and aminopicoline **2.2a**.

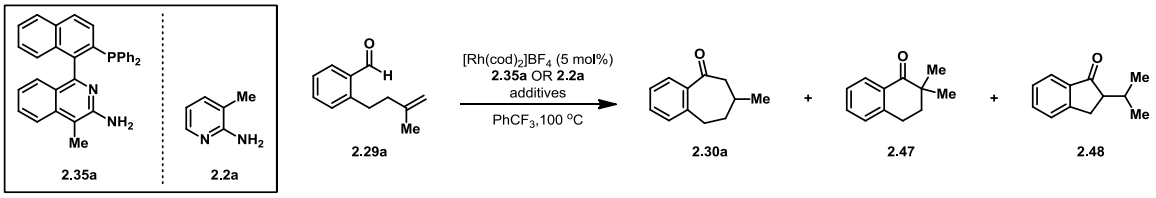

Entry[a]	Co-catalyst (mol%)	Additives (mol %)	S.M. and Product Ratios[b]			
			2.29a	**2.30a**	**2.47**	**2.48**
1	**2.35a** (5 mol%)	PPh_3 (10 mol%) BzOH (12 mol%) aniline (120 mol%)	1	0	0	0
2	**2.2a** (120 mol%)	PPh_3 (10 mol%) BzOH (12 mol%) aniline (120 mol%)	10.3	54.8	1	0

[a]Reactions were performed in a nitrogen-filled glovebox and stirred at 100 °C overnight. Work-up included washing with 1 M HCl to hydrolyze any imines present and to remove aniline. [b]Determined via ^{1}H NMR integrations from crude reaction mixtures (after HCl washing).

We began by running side-by-side reactions with aminoisoquinoline **2.35b** and aminopicoline **2.2a** under conditions similar to those previously reported for our enantioselective intramolecular alkene hydroacylation (see scheme in Table 2.8).[16] Gratifyingly, aminoisoquinoline **2.35b** did produce a significant amount of the desired 7-membered carbocycle **2.30a** (Table 2.8, entry 1). Under the same conditions, aminopicoline **2.2a** resulted in full conversion to carbocycle **2.30a** (entry 2).

Table 2.8. Screening of amino-isoquinoline **2.35b** as a co-catalyst for intramolecular alkene hydroacylation.

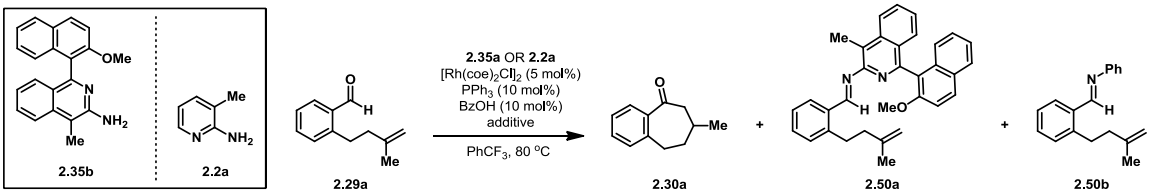

Entry[a]	Co-catalyst (mol%)	Additive (mol%)	S.M. to Product Ratio[b]			
			2.29a	**2.30a**	**2.50a**	**2.50b**
1[c]	**2.35b** (25 mol%)	aniline (120 mol%)	29.5	11.4	1	0
2[c]	**2.2a** (25 mol%)	aniline (120 mol%)	0	1	0	0
3	**2.35b** (120 mol%)	–	1	0	9.5	0
4	–	aniline (120 mol%)	0	0	0	1

[a]Reactions were performed in a nitrogen-filled glovebox and stirred at 80 °C overnight. [b]Determined via ^{1}H NMR integrations from crude reaction mixtures. [c]Work-up included washing with 1 M HCl prior to ^{1}H NMR analysis.

Interestingly, the conversion to the desired product with aminoisoquinoline **2.35b** was nearly equivalent to the loading of the co-catalyst. This could result from a lack of catalytic turnover which could occur, for example, if hydrolysis of the initially-formed ketimine was problematic under the reaction conditions. To probe this, the reaction was performed using stoichiometric amounts of aminoisoquinoline **2.35a** (entry 3). Surprisingly, this resulted only in formation of aldimine **2.50a** with no conversion to the desired carbocycle **2.30a**. It occurred to us that if imine formation with aminoisoquinolines **2.35** was so slow that non-catalyzed C–H activation was competitive, deactivation of the rhodium catalyst via decarbonylation could explain nearly all of our previous results where aniline was not used as an additive to protect the aldehyde *in situ*.

Another possibility for the low conversion to desired carbocycle **2.30a** using aminoisoquinoline **2.35b**, albeit one that seemed unlikely to us, was that aniline itself

could act as an organic co-catalyst in these reactions (perhaps directing the metal via coordination to the phenyl π–system). To the best of our knowledge, a control experiment wherein aniline was used in the absence of another organic co-catalyst had not been reported (previous reports on the necessity of aminopicoline **2.2a** had been performed prior to the development of systems containing benzoic acid and aniline as additives).[4] As such, we performed this control experiment and found that only aldimine **2.50b** was formed (Table 2.8, entry 4).

To test our hypothesis regarding diminished imine formation with aminoisoquinolines **2.35**, we re-subjected aldimine **2.50a** to rhodium-catalyzed alkene hydroacylation conditions (Scheme 2.20). Unfortunately, no cyclized product was observed under these conditions.

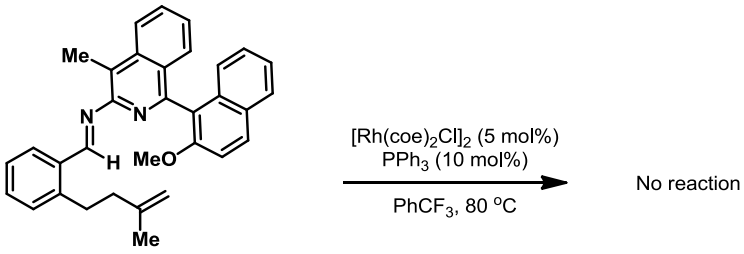

2.50a

Scheme 2.20. Attempted intramolecular alkene hydroacylation of aldimine **2.50a**.

This result led us to hypothesize that the benzoic acid and/or aniline additives may play a role in the C–H activation step, in addition to their other roles to facilitate aldimine formation. As a result, C–H activation of aldimine **2.50a** may not occur at 80 °C in the absence of additives.

To test this hypothesis, a control experiment was performed in which aldimine **2.50a** was treated with $[Rh(coe)_2Cl]_2$ in the presence of aniline and benzoic acid. This resulted in moderate conversion to the 7-membered carbocycle, as well as near-complete transimination to the *N*-phenyl aldimine. An additional control experiment in which aldimine **2.50a** was treated with $[Rh(coe)_2Cl]_2$ and benzoic acid resulted in even greater conversion to the 7-membered carbocycle. An important note is that triphenylphosphine was unintentionally omitted from these control experiments. While this does not allow for a direct comparison to previous results, the observation of cyclized product formation in these cases would suggest that the addition of phosphine ligands may not be necessary.

2.3.5 Future Work

The results obtained using pre-formed aldimine **2.50a**, with and without additives, suggest that benzoic acid and aniline may play a larger role in intramolecular alkene hydroacylation than previously thought. The observation of cyclized products without the addition of triphenylphosphine would also suggest that exogenous phosphine ligands may not be necessary. The combination of benzoic acid and aniline additives with added phosphine ligand warrants further exploration (Scheme 2.21). It is also worth noting that the reactions performed with aminoisoquinolines **2.35a** and **2.35b** were done at relatively low reaction temperatures. Additional control experiments focusing on reaction temperatures should also be performed.

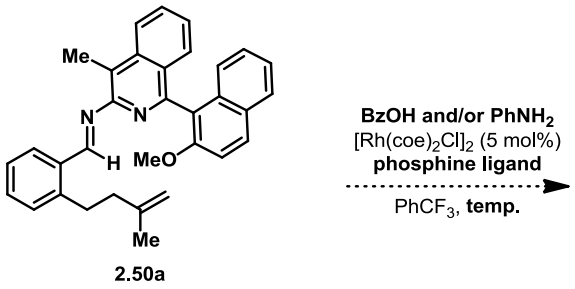

Scheme 2.21. Control experiments proposed for examining alkene hydroacylation reactivity of aldimine **2.50a**.

The results from Table 2.1, entry 1 could indicate that hydrolysis of the initially-formed ketone is turnover limiting under the reaction conditions. We hypothesize that this is the result of the steric hindrance created by the biaryl linkage. Since imine formation adjacent to the heterocyclic nitrogen is necessary for the reaction, co-catalysts should be re-designed such that the biaryl linkage is as far from the primary nitrogen as possible. This could be achieved with alternative aminoisoquinolines **2.51** (Figure 2.3). As mentioned previously in Section 2.3.3, the methyl group adjacent to the primary nitrogen in these co-catalysts is necessary to bias imine conformation such that the heterocyclic nitrogen is directed toward the desired C–H bond. However, this can also be achieved by introducing any sort of steric hindrance at that position. In aminoisoquinolines **2.51**, it is the benzo-fused ring that provides the steric bulk needed to bias imine conformation. This allows the biaryl linkage to be placed 4 bonds away from the primary nitrogen, which should allow for less-hindered approach of a nucleophile to the imine carbon.

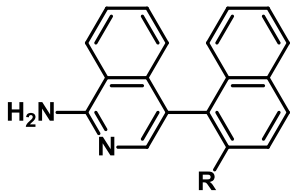

2.51
a: R = OMe

Figure 2.3. Alternative chiral aminoisoquinolines **2.51.**

Future work on this project will focus on testing the viability of aminoisoquinolines **2.51** as co-catalysts in intramolecular alkene hydroacylation methodologies. Aminoisoquinolines **2.51** should be available in a manner analogous to aminoisoquinolines **2.35** (Scheme 2.21). The biaryl linkage should be available through a Suzuki cross-coupling of arylboronic acid **2.36** and haloisoquinoline **2.52**. Haloisoquinoline **2.52** should in turn be available from isoquinoline via *N*-oxide formation followed by a one-pot *ortho*-amination protocol.[27] Once the amine moiety is installed, electrophilic aromatic substitution should allow for halogenation at the desired position.[28] Once synthesized, amino-isoquinolines **2.51** will be tested for viability as intramolecular alkene hydroacylation co-catalysts in the same manner as aminoisoquinolines **2.35**.

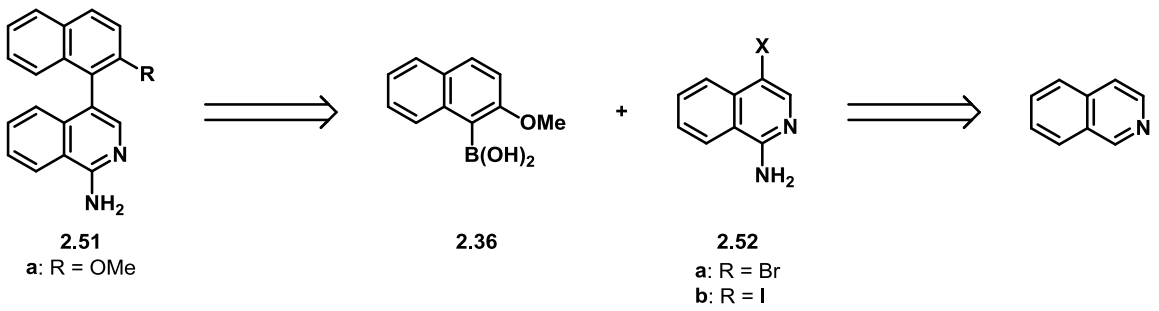

2.51
a: R = OMe

2.36

2.52
a: R = Br
b: R = **I**

Scheme 2.22. Retrosynthetic analysis for aminoisoquinolines **2.51**.

2.4. Chapter 2 Concluding Remarks

Metal-organic cooperative catalysis is a relatively unexplored strategy used to overcome the inherent challenges involved in the activation and functionalization of unreactive bonds. Such an approach may greatly expand the scope of C–C and C–H bond activation and functionalization methodologies, as the careful design of substrates becomes less necessary. This has been demonstrated through the use of metal-organic cooperative catalysis as a way to prevent decarbonylation in intramolecular alkene hydroacylations, obviating the need for a substrate-embedded directing group. The use of an aminoisoquinoline based organic co-catalyst has provided a new scaffold from which enantioselective methodologies may be developed. Further control experiments need to be performed to gain insight into the role of benzoic acid and aniline additives. A new co-catalyst scaffold may also be beneficial, should *in situ* ketimine hydrolysis prove problematic.

2.5. Chapter 2 Experimental

2.5.1 General procedures

Unless otherwise noted, all reactions were carried out under a nitrogen atmosphere. Dichloromethane (DCM), acetonitrile (MeCN), and toluene were distilled from CaH_2 prior to use. Tetrahydrofuran (THF) was distilled from Na/benzophenone prior to use. Benzene, methanol (MeOH), ethanol (EtOH), dimethoxyethane (DME), anhydrous *N*,*N*-dimethylformamide (DMF) and anhydrous diethyl ether (Et_2O) were purchased from Sigma-Aldrich and Alfa Aesar, and used without further purification. Unless otherwise noted, all chemicals were purchased from commercial sources and used as received.

Analytical thin-layer chromatography (TLC) and preparative thin-layer chromatography were carried out using 250 μm and 1000 μm silica plates (SiliCycle), respectively. Eluted plates were visualized first with a UV lamp (254 nm) and then stained with ceric ammonium molybdate, potassium permanganate, or iodine. Flash column chromatography was performed using 230–400 mesh (particle size 40–63 μm) silica gel purchased from SiliCycle.

^{1}H NMR (400 and 500 MHz), ^{13}C NMR (75 and 125 MHz), and ^{19}F NMR (375 and 470 MHz) spectra were obtained on Varian Inova and Bruker Avance instruments. ^{1}H NMR spectra data were reported as δ values in ppm relative to TMS (δ 0.00) or chloroform (7.26) if collected in $CDCl_3$. ^{13}C NMR spectra data were reported as δ values in ppm relative to chloroform (δ 77.00) if collected in $CDCl_3$. ^{19}F NMR spectra data were

reported as δ values in ppm using instrument standard. ^{1}H NMR coupling constants were reported in Hz, and multiplicity was indicated as follows: s (singlet); d (doublet); t (triplet); q (quartet); quint (quintet); m (multiplet); dd (doublet of doublets); ddd (doublet of doublet of doublets); dddd (doublet of doublet of doublet of doublets); dt (doublet of triplets); td (triplet of doublets); ddt (doublet of doublet of triplets); dq (doublet of quartets); app (apparent); br (broad). Infrared (IR) spectra were obtained on a Thermo Scientific Nicolet iS5 FT-IR spectrometer with an iD5 ATR probe. High-resolution mass spectra (HRMS) in electrospray ionization (ESI) experiments were performed on a Bruker BioTOF II (Time-of-flight) instrument using PEG-300, PEG-400 or PPG-400 as an internal standard.

2.5.2 Procedures for co-catalysts bearing a chiral, C_2-symmetrical substituent

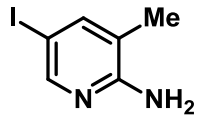

2.2f

Iodopicoline **2.2f** was prepared from commercially-available 2-amino-3-picoline using a known procedure.[17] ^{1}H-NMR data was in agreement with literature values. **^{1}H-NMR** (300 MHz; $CDCl_3$): δ 8.07 (d, *J* = 1.0 Hz, 1H), 7.53 (d, *J* = 1.1 Hz, 1H), 4.72 (br s, 2H), 2.09 (s, 3H).

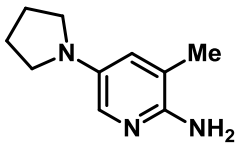

2.2c

To a 25 mL round-bottom flask was added iodopicoline **2.2f** (1.50 g; 6.41 mmol; 1 equiv.), *L*-proline (0.147 g; 1.28 mmol; 0.20 equiv.), CuI (0.122 g; 0.641 mmol; 0.10 equiv.), K_2CO_3 (1.77 g; 12.8 mmol; 2.0 equiv.), pyrrolidine (1.37 g; 19.2 mmol; 3.0 equiv.), and DMSO (4.5 mL; 1.4 M). The flask was then fitted with a reflux condenser, placed under a nitrogen atmosphere, and heated to 90 ^oC. After stirring for 25 h at 90 ^oC, the flask was allowed to cool to RT and the mixture was diluted with EtOAc (approx. 150 mL) and partioned over H_2O (approx. 100 mL). The mixture was filtered through Celite® and the organic layer was further washed with H_2O (3x approx. 100 mL). The organic layer was then dried over Na_2SO_4, filtered, and concentrated *in vacuo*. The crude material was taken up in DCM and washed with 1 M HCl until no product was observed in the organic layer via TLC. The aqueous layer was then treated with 10 % NaOH (aq.) until pH $\geq$ 10 was achieved. The basic aqueous layer was extracted with DCM, and the combined organic layers were dried over Na_2SO_4, filtered, and concentrated *in vacuo*. Material obtained from acid-base extraction was further purified by silica gel flash chromatography (0.5:4:96 Et_3N, MeOH, EtOAc) to give aminopicoline **2.2c** as a light brown solid in 70% yield. R_f = 0.11 (20:1 EtOAc:MeOH); **^{1}H-NMR** (300 MHz; $CDCl_3$): δ 7.39 (d, *J* = 2.7 Hz, 1H), 6.72 (d, *J* = 2.7 Hz, 1H), 3.91 (s, 2H), 3.22-3.18 (m, 4H), 2.14 (s, 3H), 2.00-1.96 (m, 4H);**^{13}C NMR** (75 MHz, $CDCl_3$) δ 148.3, 139.4, 128.9, 123.5,

117.7, 48.3, 25.2, 17.7; **IR** (neat film NaCl) 3377, 3319, 3176, 2906, 2829, 1646, 1474, 1437 cm^{-1}; **HRMS** (ESI) calcd for $[C_{10}H_{15}N_3 + H]^+$ 178.1339, found 178.1326.

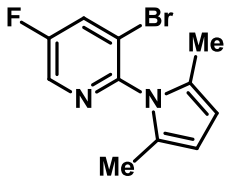

2.34

To a 10 mL round-bottom flask was added commercially-available 2-amino-3-bromo-5-fluoropyridine (250 mg; 1.31 mmol; 1 equiv.), 2,5-hexanedione (300 mg; 2.62 mmol; 2.0 equiv.), toluene (3 mL; 0.4 M), and AcOH (1 drop). The flask was fitted with a Dean-Stark trap and reflux condenser and placed in a pre-heated oil bath. The reaction was refluxed for 4 h before allowing to cool to RT. The mixture was then poured over $NaHCO_3$ (sat. aq.) and extracted with EtOAc (3x approx. 10 mL). The combined organic layers were washed with brine, dried over Na_2SO_4, filtered, and concentrated *in vacuo*. Purification via silica gel flash chromatography (3:7 EtOAc:hexanes) provided pyrrolyl pyridine **2.34** in 69% yield as a dark solid. **^{1}H-NMR** (500 MHz; $CDCl_3$): δ 8.46 (d, *J* = 2.7 Hz, 1H), 7.85 (dd, *J* = 6.9, 2.7 Hz, 1H), 5.92 (s, 2H), 1.99 (s, 8H). For an example of H-F coupling in fluoropyridines see ref. [29]. [29]

2.5.3 Procedures for biaryl co-catalysts with axial chirality

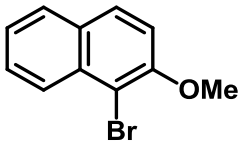

2.39

Aryl bromide **2.39** was prepared from 2-methoxylnaphthalene using a known procedure.[19] ^{1}H-NMR data were in agreement with literature values. **^{1}H-NMR** (500 MHz; $CDCl_3$): δ 8.22 (d, *J* = 8.6 Hz, 1H), 7.81 (d, *J* = 9.0 Hz, 1H), 7.78 (d, *J* = 8.2 Hz, 1H), 7.56 (ddd, *J* = 8.4, 7.0, 1.3 Hz, 1H), 7.39 (ddd, *J* = 8.1, 6.9, 1.1 Hz, 1H), 7.27 (d, *J* = 9.0 Hz, 1H), 4.03 (s, 3H).

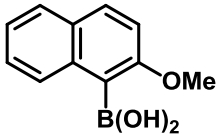

2.36

Arylboronic acid **2.36** was prepared from aryl bromide **2.39** using a known procedure.[19] ^{1}H-NMR data was consistent with literature values. **^{1}H-NMR** (500 MHz; $CDCl_3$): δ 8.84 (dd, *J* = 8.7, 0.7 Hz, 1H), 7.94 (d, *J* = 9.0 Hz, 1H), 7.78 (dt, *J* = 8.1, 0.6 Hz, 1H), 7.51 (ddd, *J* = 8.6, 6.9, 1.6 Hz, 1H), 7.37 (ddd, *J* = 8.1, 6.8, 1.2 Hz, 1H), 7.28 (d, *J* = 9.1 Hz, 1H), 6.18 (s, 2H), 4.03 (s, 3H).

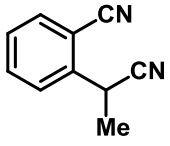

2.41

Two 250 mL round-bottom flasks were flame dried and charged with 20 mL THF. To one flask was added *i*-$PrNH_2$ (4.10 g; 40.5 mmol; 1.15 equiv.). The flask was cooled to -

78 ^{o}C and *n*BuLi (15.5 mL 2.5 M; 38.7 mmol; 1.1 equiv.) was added. The flask was stirred at -78 ^{o}C for 20 min. before commercially-available (2-cyano)phenylacetonitrile (5.00 g; 35.2 mmol; 1 equiv.) was added slowly as a solution in THF (20 mL). After complete addition, the flask was allowed to warm to 0 ^{o}C through a change of cooling baths. To the second 250 mL round-bottom flask containing 20 mL of THF was added iodomethane (5.49 g; 38.7 mmol; 1.1 equiv.) and the flask was cooled to 0 ^{o}C. The flask containing deprotonated (2-cyano)phenylacetonitrile was then cannulated into the flask containing iodomethane over the course of 1 h. After stirring for 2.5 h at 0 ^{o}C the reaction was quenched with NH_4Cl (sat. aq., approx. 100 mL) and extracted with EtOAc (3x approx. 100 mL). The combined organic layers were washed with brine, dried over Na_2SO_4, filtered, and concentrated *in vacuo*. Purification via silica gel chromatography (1:9 EtOAc:hexanes) afforded dinitrile **2.41** as a colorless liquid in 80% yield. **^{1}H-NMR** (500 MHz; $CDCl_3$): δ 7.73-7.68 (m, 3H), 7.47 (td, *J* = 7.5, 1.5 Hz, 1H), 4.33 (q, *J* = 7.2 Hz, 1H), 1.72 (d, *J* = 7.2 Hz, 3H).

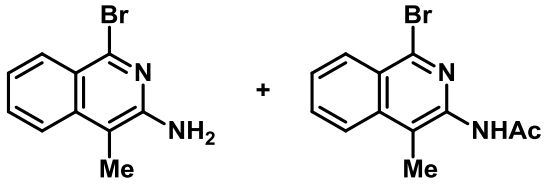

2.37 **2.42**

To a flame-dried 100 mL round-bottom flask was added HBr (3.62 g 33% in AcOH; 44.8 mmol; 3.5 equiv.) and AcOH (11 mL). The flask was cooled to 0 ^{o}C and dinitrile **2.41** (2.00 g; 12.8 mmol; 1 equiv.) was added as a solution in AcOH (10 mL). The reaction was allowed to warm to RT and was stirred for 16 h before hexanes was added to force

precipitation. The slurry was filtered and the solid material was collected and taken up in DCM. The organic layer was partitioned over H_2O and $NaHCO_3$ (sat. aq.) was washed in until pH ≥ 7 was achieved. The aqueous phase was extracted with DCM (3x approx. 50 mL) and the combined organic layers were washed with brine, dried over Na_2SO_4, filtered, and concentrated *in vacuo*. Purification via gradient silica gel flash chromatography (2:8 to 1:1 EtOAc:hexanes) afforded bromoisoquinolines **2.37** and **2.42** in 23% and 20% yield, respectively. Bromoisoquinoline **2.37**: **^{1}H-NMR** (500 MHz; $CDCl_3$): δ 8.11 (d, *J* = 8.5 Hz, 1H), 7.75 (d, *J* = 8.6 Hz, 1H), 7.59 (t, *J* = 7.6 Hz, 1H), 7.33 (t, *J* = 7.6 Hz, 1H), 4.46 (br s, 2H), 2.33 (s, 3H); **^{13}C-NMR** (126 MHz; CDCl3): δ 151.4, 141.5, 139.1, 130.9, 129.5, 123.94, 123.83, 122.1, 105.3, 11.6; **IR** (neat) 3490, 3315, 3188, 1622, 1573, 1551, 1452, 1320. Bromoisoquinoline **2.42**: **^{1}H-NMR** (500 MHz; $CDCl_3$): δ 8.26 (d, *J* = 8.4 Hz, 1H), 8.02 (d, *J* = 8.5 Hz, 1H), 7.99 (br s, 1H), 7.77 (t, *J* = 7.6 Hz, 1H), 7.65 (t, *J* = 7.6 Hz, 1H), 2.50 (s, 3H), 2.25 (s, 3H); **IR** (neat) 3246, 1661, 1584, 1486, 1310, 1257; **MS** (ESI) calcd for $[C_{12}H_{11}BrN_2O + Na]^+$ 300.99 + 302.99 (M+2), found 301.10 + 303.10 (M+2).

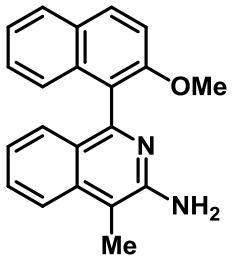

2.35b

A 20 dram vial was charged with $Pd(PPh_3)_4$ (73 mg; 0.063 mmol; 3 mol%). Bromoisoquinoline **2.37** (0.500 g; 2.11 mmol; 1 equiv.) was dissolved in

dimethoxyethane (3.0 mL), de-gassed wit Ar, and added to the reaction vial with $Pd(PPh_3)_4$. Boronic acid **2.36** (0.533 g; 2.64 mmol; 1.25 equiv.) was dissolved in EtOH (2.5 mL), de-gassed with Ar, and added to the reaction vial. Na_2CO_3 (0.582 g; 5.49 mmol; 2.6 equiv.) was dissolved in a minimal amount of de-ionized H_2O and added to the reaction mixture. The mixture was further de-gassed with Ar, sealed with a PTFE-lined cap and placed in a pre-heated (100 ^oC) aluminum heating block. The reaction was heated at 100 ^oC for 21 h before allowing to cool to RT. The reaction mixture was filtered and rinsed with DCM until no color remained in the precipitate. The filtrate was further diluted with DCM and washed with H_2O and brine. The organic layer was dried over Na_2SO_4, filtered, and concentrated *in vacuo*. Crude material was then suspended in Et2O and stirred for 15 min., after which point the mixture was filtered and rinsed with Et_2O. This provided aminoisoquinoline **2.35b** as a bright yellow powder in 83% yield. **^{1}H-NMR** (500 MHz; $CDCl_3$): δ 7.98 (d, *J* = 9.0 Hz, 1H), 7.89 (d, *J* = 8.7 Hz, 1H), 7.84 (d, *J* = 8.1 Hz, 1H), 7.54 (app t, *J* = 7.7 Hz, 1H), 7.42 (d, *J* = 9.0 Hz, 1H), 7.31 (app t, *J* = 7.7 Hz, 2H), 7.24 (app t, *J* = 7.2 Hz, 1H, partially overlapped with $CHCl_3$), 7.10 (d, *J* = 8.5 Hz, 1H), 7.04 (app t, *J* = 7.4 Hz, 1H), 4.51 (br s, 2H), 3.79 (s, 3H), 2.49 (s, 3H); **^{13}C-NMR** (126 MHz; CDCl3): δ 154.97, 154.87, 151.9, 137.8, 134.0, 130.4, 130.0, 129.3, 128.2, 128.0, 126.8, 125.2, 124.2, 123.8, 122.5, 122.1, 121.9, 113.7, 104.8, 56.8, 11.8; **IR** (neat) 3280, 3160, 1618, 1576, 1267; **MS** calc for $[C_{21}H_{18}N_2O + H]^+$ 315.15, found 315.28.

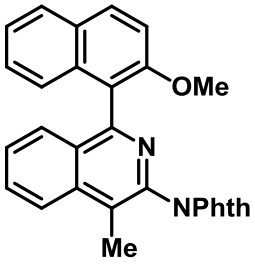

2.43

To a 20 dram reaction vial were added aminoisoquinoline **2.35b** (400 mg; 1.3 mmol; 1 equiv.) and phthalic anhydride (193 mg; 1.3 mmol, 1 equiv.). The solids were dissolved in AcOH (3.7 mL; 0.35 M) and placed in a pre-heated (120 ^{o}C) aluminum heating block. The reaction was stirred at 120 ^{o}C for 17 h before being allowed to cool to RT. The mixture was taken up in EtOAc and H_2O and $NaHCO_3$ was added until pH $\geq$ 7 was achieved. The aqueous phase was extracted with EtOAc (3x approx. 10 mL) and the combined organic layers were washed with brine, dried over Na_2SO_4, filtered, and concentrated *in vacuo*. This gave aminoisoquinoline **2.43** as a dark yellow powder in 96% yield. **^{1}H-NMR** (500 MHz; $CDCl_3$): δ 8.18 (d, *J* = 8.5 Hz, 1H), 7.99 (d, *J* = 9.0 Hz, 1H), 7.94 (m, 2H), 7.83 (dt, *J* = 6.3, 3.1 Hz, 1H), 7.80-7.76 (m, 3H, overlapping peaks), 7.61 (d, *J* = 8.4 Hz, 1H), 7.48 (app t, *J* = 7.5 Hz, 1H), 7.41 (d, *J* = 9.1 Hz, 1H), 7.32 (dt, *J* = 6.3, 3.1 Hz, 2H), 7.27-7.26 (m, 1H, overlapping with $CHCl_3$), 3.79 (s, 3H), 2.68 (s, 3H); **^{13}C-NMR** (126 MHz; CDCl3): δ 167.6, 167.4 (diastereotopic phthalimide carbonyl carbons), 156.9, 155.2, 138.3, 137.4, 134.4, 134.0, 132.55, 132.52 (diastereotopic phthalimide *ipso* aromatic carbons), 130.89, 130.73, 129.4, 128.9, 128.3, 127.95, 127.78, 127.2, 126.6, 125.1, 124.3, 123.96, 123.90, 121.3, 114.0, 57.1, 13.8; **IR** (neat) 1717, 1620, 1592, 1556, 1389, 1360, 1339, 1266, 1251; **MS** (ESI) calc for $[C_{29}H_{20}N_2O_3 + H]^+$ 445.15, found 445.33.

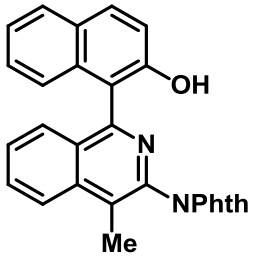

2.44

A 25 mL round-bottom flask was fitted with a dropping funnel and flame-dried. Aminoisoquinoline **2.43** (0.500 g; 1.12 mmol; 1 equiv.) was added and dissolved in anhydrous $CHCl_3$ (5.6 mL, 0.2 M). BBr_3 (1.34 mL, 1.0 M in DCM; 1.34 mmol; 1.2 equiv.) was slowly added via dropping funnel with stirring at RT. After complete addition, the dropping funnel was replaced with a reflux condenser and the reaction was placed in a pre-heated oil bath. The reaction was heated at reflux for 16 h after which point the flask was allowed to cool to RT. The reaction was quenched with H_2O and diluted with EtOAc. $NaHCO_3$ was added until pH ≥ 7 was achieved. The aqueous phase was extracted with EtOAc (3x approx. 50 mL) and the combined organic layers were washed with brine, dried over Na_2SO_4, filtered, and concentrated *in vacuo*. This provided aminoisoquinoline **2.44** in 88% yield as a burnt orange powder. Aminoisoquinoline **2.44** prepared this way was of sufficient purity to be take on without additional purification. **^{1}H-NMR** (500 MHz; $CDCl_3$): δ 8.21 (d, *J* = 8.5 Hz, 1H), 7.98 (m, 2H), 7.88 (d, *J* = 8.8 Hz, 1H), 7.83-7.80 (m, 4H, overlapping peaks), 7.73 (d, *J* = 8.5 Hz, 1H), 7.48 (app t, *J* = 7.8 Hz, 1H), 7.37 (d, *J* = 9.1 Hz, 1H), 7.33-7.24 (m, 3H, overlapped with $CHCl_3$), 2.70 (s, 3H); **^{13}C-NMR** (126 MHz; CDCl3): δ 168.3, 166.8 (diastereotopic phthalimide carbonyl carbons), 155.5, 153.8, 138.4, 138.1, 134.76, 134.69 (diastereotopic phthalimide *ipso* aromatic carbons), 132.9, 132.4, 132.1, 131.39, 131.33 (diastereotopic phthalimide

aromatic carbons), 129.07, 128.88, 128.3, 128.03, 127.89, 126.89, 126.71, 125.3, 124.5, 124.21 (diastereotopic phthalimide aromatic carbons), 124.14, 123.5, 119.5, 116.8, 14.1; **IR** (neat) 3061, 1715, 1621, 1585, 1556, 1347

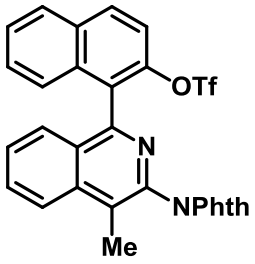

2.45

A 25 mL round-bottom flask was flame-dried and charged with aminoisoquinoline 2.44 (400 mg; 0.93 mmol; 1 equiv.) and DMAP (114 mg; 0.93 mmol; 1 equiv.). The solids were dissolved in DCM (9.3 mL; 0.1 M) and triflic anhydride (0.17 mL; 1.02 mmol; 1.1 equiv.) was added with stirring at RT. Solution was maintained at RT for 14 h before the reaction was quenched with $NaHCO_3$ (sat. aq.). The aqueous layer was extracted with DCM (3x approx. 20 mL) and the combined organic layers were washed with brine, dried over Na_2SO_4, filtered, and concentrated *in vacuo*. Purification via silica gel flash chromatography (0.1:2:8 Et_3N:AcMe:hexanes) gave aminoisoquinoline **2.45** in 52% yield as a dark yellow powder. **^{1}H-NMR** (500 MHz; $CDCl_3$): δ 8.23 (d, *J* = 8.6 Hz, 1H), 8.08 (d, *J* = 9.0 Hz, 1H), 7.97-7.93 (m, 3H), 7.83 (td, *J* = 5.5, 2.6 Hz, 1H), 7.78 (m, 2H), 7.60 (d, *J* = 9.1 Hz, 1H), 7.55 (m, 3H), 7.47 (app s, 2H), 2.71 (s, 3H); **^{13}C-NMR** (126 MHz; CDCl3): δ 167.6, 166.8, 152.6, 145.1, 138.5, 137.5, 134.51, 134.42, 133.4, 132.7, 132.47, 132.43, 131.6, 131.2, 128.37, 128.31, 128.26, 128.14, 128.10, 127.6, 127.4, 126.7, 124.5, 124.08, 123.90, 119.6, 117.0, 13.9; **^{19}F-NMR** (471 MHz; CDCl3): δ -74.24.

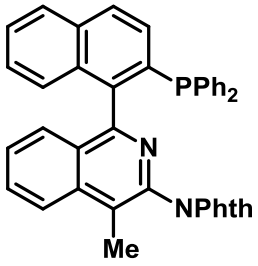

2.46

In a nitrogen-filled glovebox, a 20 dram reaction vial was charged with $NiCl_2$(dppe) (47 mg; 0.089 mmol; 10 mol%) and DMF (1.8 mL) was added. A portion of $HPPh_2$ (50 mg; 0.27 mmol; 0.3 equiv.) was added and the flask was sealed with a PTFE-lined cap. The reaction vial was placed in a pre-heated aluminum block and heated at 100 ^oC for 10 min. before allowing to cool to RT. Aminoisoquinoline **2.45** (0.500 g; 0.89 mmol; 1 equiv.) and DABCO (0.404 g; 3.6 mmol; 4.0 equiv.) were then added with the aid of DMF (3.0 mL) and the solution was heated to 100 ^oC. After 1 h an additional portion of $HPPh_2$ (50 mg; 0.27 mmol; 0.3 equiv.) was added. Two more portions of $HPPh_2$ (50 mg; 0.27 mmol; 0.3 equiv.). were added after 3 h and 6 h from the start of the reaction. The reaction was stirred at 100 ^oC for a total time of 48 h. After allowing the vial to cool to RT, it was removed from the glovebox and the solution was diluted with DCM (approx. 50 mL) and poured over $NaHCO_3$ (sat. aq.). The organic layer was washed with 2 M LiCl (2x approx. 75 mL) and brine, and was then dried over Na_2SO_4, filtered, and concentrated *in vacuo*. Purification via silica gel flash chromatogrphy (3:7 EtOAc:hexanes) provided solid material that was further purified by rinsing with a minimal amount of cold EtOAc to provide aminoisoquinoline **2.46** as a dark yellow powder in 60% yield. **^{1}H-NMR** (500 MHz; $CDCl_3$): δ 8.16 (d, *J* = 8.4 Hz, 1H), 7.94-7.92 (m, 1H), 7.90-7.89 (m, 1H), 7.87 (d, *J* = 6.6 Hz, 1H), 7.85 (d, *J* = 6.2 Hz, 1H)., 7.77-7.75 (m, 2H)., 7.71 (ddd, *J* = 8.4, 7.0, 1.4

Hz, 1H), 7.47 (ddd, *J* = 8.2, 6.8, 1.3 Hz, 1H), 7.43 (td, *J* = 5.7, 2.7 Hz, 2H), 7.33-7.28 (m, 5H), 7.23-7.18 (m, 5H), 7.15-7.12 (m, 2H), 7.08-7.05 (m, 1H), 2.67 (s, 3H); **^{31}P-NMR** (203 MHz; CDCl3): δ -13.9

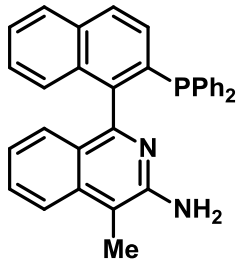

2.35a

A 10 ml pear-shaped flask was charged with aminoisoquinoline **2.46** (100 mg; 0.17 mmol; 1 equiv.) and THF (3.4 mL; 0.05 M) and the solution was de-gassed with nitrogen. Ethylene diamine (102 mg; 1.7 mmol; 10 equiv.) was added and the solution was stirred at RT for 3 h. The reaction mixture was diluted with DCM and washed with H_2O and brine, dried over Na_2SO_4, filtered, and concentrated *in vacuo*. This provided aminoisoquinoline **2.35a** as a bright yellow powder in 89% yield. **^{1}H-NMR** (500 MHz; $CDCl_3$): δ 7.87-7.85 (m, 3H), 7.47 (dddd, *J* = 13.5, 8.3, 6.8, 1.4 Hz, 2H), 7.40 (dd, *J* = 8.6, 3.1 Hz, 1H), 7.28-7.26 (m, 7H, overlapping peaks), 7.23-7.15 (m, 6H, overlapping peaks), 6.91 (ddd, *J* = 8.2, 6.9, 1.2 Hz, 1H), 4.28 (br s, 2H), 2.47 (s, 3H); **^{13}C-NMR** (126 MHz; $CDCl_3$): δ 160.6, 157.13, 157.08, 151.5, 137.91, 137.84, 137.82, 137.5, 137.2, 135.07, 134.97, 133.88, 133.72, 133.66, 133.51, 130.2, 129.9, 128.6, 128.43, 128.36, 128.30, 128.25, 128.14, 127.99, 127.03, 127.01, 126.95, 126.7, 122.4, 121.9, 105.1, 11.9; **^{31}P-NMR** (203 MHz; $CDCl_3$): δ -13.7; **IR** (neat) 3280, 3149, 3063, 1621, 1577, 1555, 738, 695; **MS** calcd for $[C_{32}H_{25}N_2P + H]^+$ 469.18, found 469.37.

2.6. Chapter 2 References

1) Suggs, J. W. *J. Am. Chem. Soc.* **1979**, *101*, 489.

2) Tsuji, J.; Ohno, K. *Tetrahedron Lett.* **1965**, *6*, 3969.

3) Willis, M. C. *Chem. Rev.* **2010**, *110*, 725–748 and references therein.

4) Jun, C.-H.; Lee, H.; Hong, J.-B. *J. Org. Chem.* **1997**, *62*, 1200-1201.

5) Blanksby, S.J.; Ellison, G.B. *Acc. Chem. Res.* **2003**, *36*, 255-263.

6) Jun, C.-H.; Hong, J.-B. *Org. Lett.* **1999**, *1*, 887-889.

7) Jun, C.-H.; Lee, D.-Y.; Lee, H.; Hong, J.-B. *Angew. Chem. Int. Ed.* **2000**, *39*, 3070-3072.

8) Maleckis, A.; Kampf, J. W.; Sanford, M. S. *J. Am. Chem. Soc.* **2013**, *135*, 6618−6625.

9) Lafrance, M.; Gorelsky, S. I.; Fagnou, K. *J. Am. Chem. Soc.* **2007**, *129*, 14570−14571.

10) Rhinehart, J. L.; Manbeck, K. A.; Buzak, S. K.; Lippa, G. M.; Brennessel, W. W.; Goldberg, K. I.; Jones, W. D. *Organometallics* **2012**, *31*, 1943−1952.

11) Vautravers, N. R.; Regent, D. D.; Bernhard Breit, B. *Chem. Commun.* **2011**, *47*, 6635–6637.

12) Jun, C.-H.; Lee, H. *J. Am. Chem. Soc.* **1999**, *121*, 880-881.

13) Ko, H. M.; Dong, G. *Nature Chem.* **2014**, *6*, 739–744.

14) Bear, B. R.; Sparks, S. M.; Shea, K. J. *Angew. Chem. Int. Ed.* **2001**, *40*, 820–849.

15) Seiser, T., Saget, T., Tran, D. N.; Cramer, N. *Angew. Chem. Int. Ed.* **2011**, *50*, 7740–7752 and references therein.

16) Beletskiy, E. V.; Sudheer, Ch; Douglas, C. J. *J. Org. Chem.* **2012**, *77*, 5884-5893.

17) Hsieh, H.-P.; McLaughlin, L. W. *J. Org. Chem.* **1995**, *60*, 5356-5359.

18) Zhang, H.; Cai, Q; Ma, D. *J. Org. Chem.* **2005**, *70*, 5164-5173.

19) Lim, C. W.; Tissot, O.; Mattison, A.; Hooper, M. W.; Brown, J. M.; Cowley, A. R.; Hulmes, D. I.; Blacker, A. J. *Org. Process Res. Dev.* **2003**, *7*, 379-384.

20) Johnson, F.; Nasutavicus, W. A. *J. Org. Chem.* **1962**, *27*, 3953–3958.

21) Bhat, V.; Wang, S.; Stoltz, B. M.; Virgil, S. C. *J. Am. Chem. Soc.* **2013**, *135*, 16829−16832.

22) Guin, J.; Varseev, G.; List, B. *J. Am. Chem. Soc.* **2013**, *135*, 2100–2103.

23) Das, J.; Natesan, S.; Trehan, S.; Iqbal, J.; Magadi, S. K. Antiifective 1,2,3-Triazole Derivatives, Process for Their Preparation and Pharmaceutical Compositions Containing Them. WO 2004/101531 A1, 2004

24) Malosh, C. F.; Ready, J. M. *J. Am. Chem. Soc.* **2004**, *126*, 10240–10241.

25) Hoshimoto, Y.; Hayashi, Y.; Suzuki, H.; Ohashi, M.; Ogoshi, S. *Angew. Chem. Int. Ed.* **2012**, *51*, 10812 –10815.

26) Liston, D. J.; Lee, Y. J.; Scheidt, W. R.; Reed, C. A. *J. Am. Chem. Soc.* **1989**, *111*, 6643-6648.

27) Yin, J.; Xiang, B.; Huffman, M. A.; Raab, C. E.; Davies, I. W. *J. Org. Chem.* **2007**, *72*, 4554–4557.

28) Sharma, K. K.; Patel, D. I.; Jain, R. *Chem. Commun.* **2015**, *51*, 15129-15132.

29) de Viedma, A. G.; Martınez-Barrasa, V.; Burgos, C.; Izquierdo, M. L.; Alvarez-Builla, J. *J. Org. Chem.* **1999**, *64*, 1007-1010.

CHAPTER 3:THE DRAGMACIDIN FAMILY OF NATURAL PRODUCTS

3.1. Introduction to the Dragmacidins

The dragmacidins are a family of bis(indole) alkaloids that have been isolated from a variety of sea sponges, including those from the *Dragmacidon*,[1] *Hexadella*,[2] and *Spongosorites*[3,4] genera. The family can be subdivided into members that contain a piperazine linker (dragmacidin and dragmacidins A–C, Figure 3.1a) and members that contain a pyrazinone linker (dragmacidins D–F, Figure 3.1b).

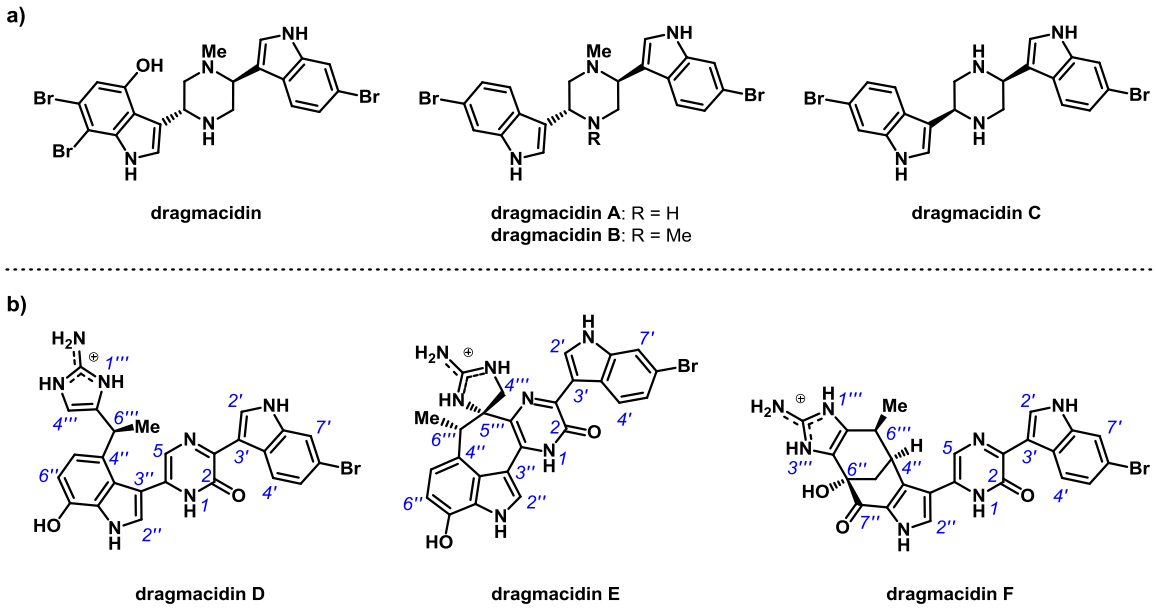

Figure 3.1. Dragmacidin family of natural products featuring: a) a piperazine linker and b) a pyrazinone linker.

The sponges from which these compounds have been isolated have shown wide variability in the profiles of dragmacidins and other bis(indole) alkaloids present. This even includes variations in secondary metabolite profiles based on the depth at which the sponges were harvested.[2] Because of this, it has been suggested that the dragmacidins may actually have microbial origins.

Interest in the dragmacidins has, in part, stemmed from their wide range of biological activity. The dragmacidins containing a pyrazinone linker (dragmacidins D–F) have demonstrated cytotoxicity towards a number of cancer cell lines, anti-inflammatory properties, and protein phosphatase inhibition.[5] Dragmacidin D has also been shown to selectively inhibit neural nitric oxide synthase,[6] which has implications for the treatment of neurodegenerative disorders such as Alzheimer's disease, Parkinson's disease, and

Huntington's disease.[7] Meanwhile, dragmacidin F has shown activity against HSV-I (herpes simplex virus) and HIV-I (human immunodeficiency virus).[8]

The dragmacidins have routinely been isolated in low natural abundance from their difficult-to-obtain host organisms.[3,4,8] The combination of relevant biological activity and low natural abundance makes the dragmacidins excellent total synthesis candidates. Furthermore, early isolation work was able to establish the relative stereochemical configurations of dragmacidins D–F, but absolute configurations were not able to be determined. There has also been speculation regarding the enantiopurity of natural dragmacidin samples. Successful synthetic efforts have already proven useful for addressing these stereochemical issues.

3.2. Select Total Syntheses of Dragmacidins D and F

After the initial isolation of dragmacidin D in 1992,[4] nearly a decade went by before a successful synthesis was reported for any of the pyrazinone-linked dragmacidins (although dragmacidins E and F weren't isolated until 1998 and 2000, respectively). This section will discuss some of the more significant synthetic work related to dragmacidins D and F, with the following section describing the reported work related to dragmacidin E.

3.2.1 Stoltz's Total Synthesis of (±)–Dragmacidin D

The first successful synthesis of a pyrazinone-linked dragmacidin came from Stoltz et al. in 2002, when they reported the total synthesis of racemic dragmacidin D.[9] The authors noted that while they were interested in each of the pyrazinone-linked

dragmacidins, dragmacidin D seemed the most suitable target for initial synthetic endeavors. This was, in part, because of the hypothesis that dragmacidin D could serve as a biosynthetic precursor to both dragmacidins E and F (Scheme 3.1).[3,8] Additionally, despite its relatively simple structure, dragmacidin D shares a number of synthetic challenges present in dragmacidins E and F. The authors therefore suggested that whatever knowledge could be gained about constructing the core of dragmacidin D, and installing the requisite functional groups therein, might also be applicable to synthetic efforts towards dragmacidins E and F.

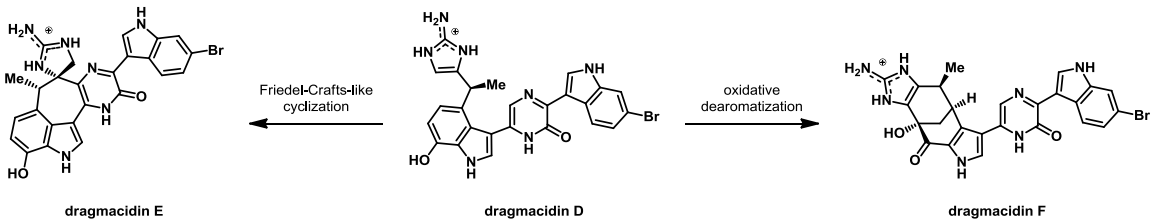

Scheme 3.1. Biosynthetic relationships between dragmacidins D–F proposed by Stoltz.

The authors identified four main synthetic challenges present in dragmacidin D: 1) the presence of seven nitrogen atoms within the compact structure; 2) four uniquely-substituted heterocycles; 3) the 3,6-disubstitution and 3,4,7-trisubstitution patterns on the indole heterocycles; and 4) the highly-polar and reactive aminoimidazolium subunit. The authors suspected that the aminoimidazolium moiety would be particularly troublesome, so they sought to install this functionality after having built the core of the molecule.

Initial considerations for construction of the dragmacidin D core spawned two different approaches. The first approach relied on forming bis(indolyl)pyrazinone **3.1** via a cyclocondensation between indole **3.2** and indole **3.3** (Scheme 3.2a). An important

benefit of this strategy is that it would allow for a highly convergent synthesis. The second approach to the core structure would require the formation of bis(indolyl)pyrazine **3.4** through a 3-component coupling of indolylboronic ester **3.5**, dihalopyrazine **3.6**, and indolylboronic acid **3.7** (Scheme 3.2b).

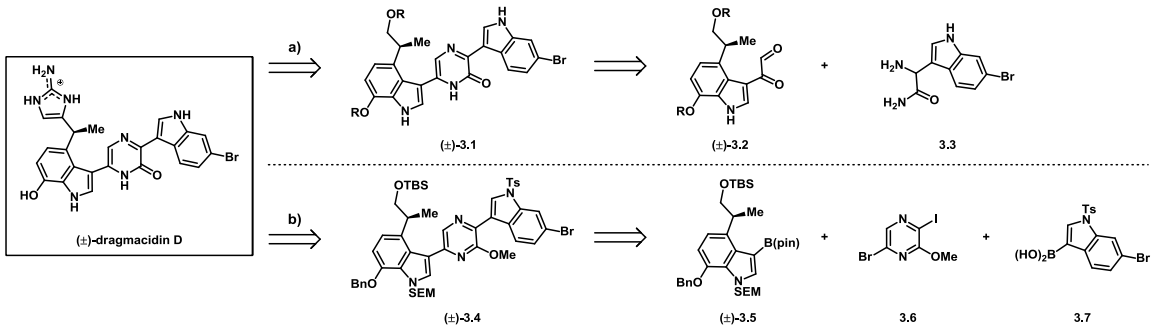

Scheme 3.2. Stoltz's retrosynthetic analyses for dragmacidin D featuring a) cyclocondensation to form the pyrazinone linker and b) sequential cross-coupling of dihalopyrazine **3.6** to link the two indole fragments.

Stoltz et al. first performed a model study to test the viability of their cyclocondensation approach to form the pyrazinone ring. Ketoacid chloride **3.8**, which is readily available by treatment of indole with oxalyl chloride,[10] provided both ketoaldehyde **3.9** and aminoamide **3.10** in 1 and 3 steps, respectively (Scheme 3.3). Cyclocondensation between ketoaldehyde **3.9** and aminoamide **3.10** was accomplished under basic conditions, providing bis(indolyl)pyrazinone **3.11** in 75% yield.

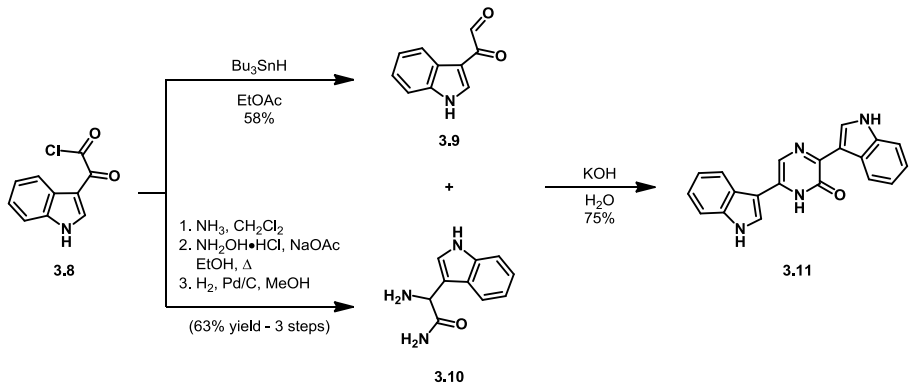

Scheme 3.3. Model reaction for pyrazinone formation via cyclocondensation.

Having successfully demonstrated a cyclocondensation approach to form the pyrazinone ring, albeit with highly-simplified substrates, the authors sought to test the viability of this strategy on true dragmacidin D substrates. Unfortunately, ketoaldehydes **3.12** did not undergo cyclocondensation with aminoamide **3.13** (Scheme 3.4). The authors note that while ketoaldehydes **3.12** are electronically dissimilar to those used in previous model studies due to the methoxy group at the indole 7-position, they attribute the failure of ketoaldehydes **3.12** to substitution at the indole 4-position. This is based on a result (not shown) wherein a ketoaldehyde similar to **3.12**, but with no substitution at the indole 4-position, did react with aminoamide **3.13** to give the corresponding pyrazinone.

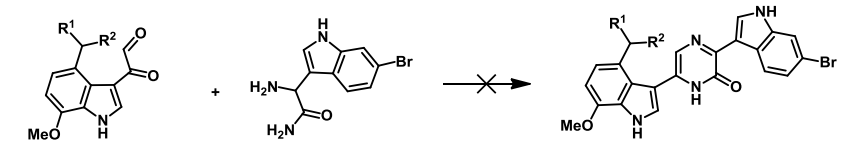

Scheme 3.4. Failed attempts at cyclocondensation for ketoaldehydes **3.12**.

Having demonstrated that a cyclocondensation approach to dragmacidin D was ineffective, the authors turned to their second approach based on selective cross-couplings of dihalopyrazine **3.6** with indolylboronic ester **3.5** and indolylboronic acid **3.7** (refer to Scheme 3.2b). They began with the synthesis of indolylboronic ester **3.5** (Scheme 3.5). Nitro arene **3.14** was converted to indole **3.15** through a Bartoli indole synthesis,[11] albeit in relatively low yield. Protection of the indole nitrogen, followed by a lithium-halogen exchange and electrophilic borylation provided indolylboronic ester **3.16** in moderate yield over two steps. Suzuki cross-coupling between indolylboronic ester **3.16** and vinylbromide **3.17** then provided substituted indole **3.18** in good yield. Completion of indolylboronic ester **3.5** was achieved through a 3-step sequence consisting of: 1) hydrogenation of the alkene moiety to establish the stereogenic methyl group; 2) electrophilic bromination of the indole at the 3-position; and 3) lithium-halogen exchange, followed by quenching with isopropoxyboronic acid pinacol ester. This sequence provided racemic indolylboronic ester **3.5** in 66% yield over 3 steps.

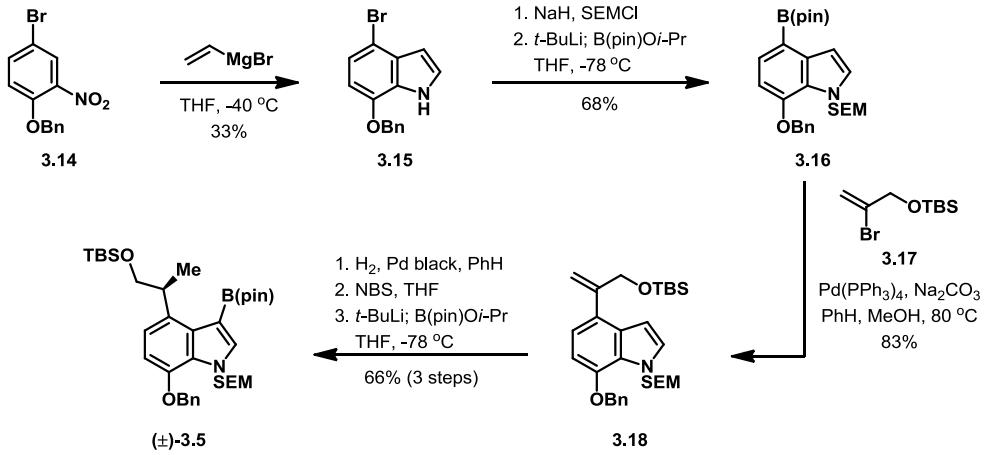

Scheme 3.5. Synthesis of racemic indolylboronic ester **3.5**.

With one of the organometallic coupling partners in hand, dihalopyrazine **3.6** was then generated in a single step from the known aminopyrazine **3.19**[12] via substitution of the diazonium salt formed *in situ* (Scheme 3.6a). The other organometallic coupling partner, indolylboronic acid **3.7**, was then synthesized in 3 steps from bromoindole **3.20** (Scheme 3.6b). This 3-step synthesis was accomplished by: 1) protecting the indole nitrogen as the tosyl sulfonamide; 2) electrophilic mercuration at the indole 3-position to give idolylmercurial **3.21**; 3) treatment of indolylmercurial **3.21** with borane, followed by hydrolytic workup.

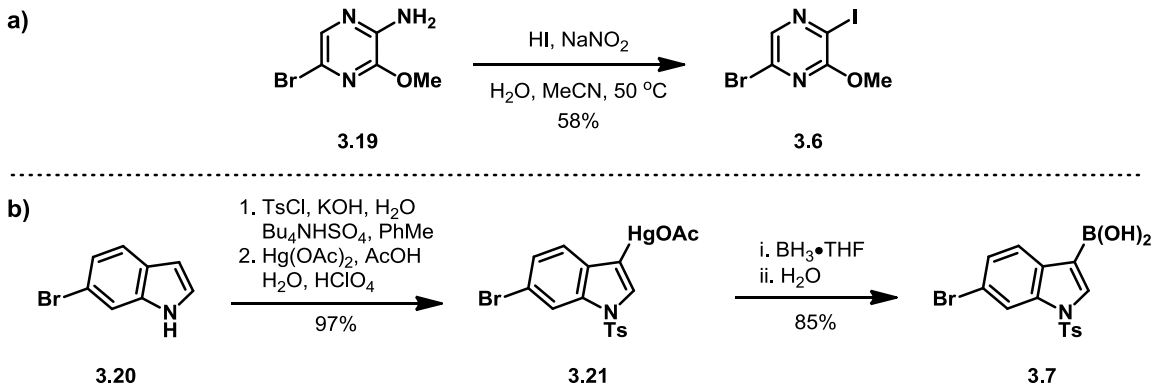

Scheme 3.6. Synthesis of a) dihalopyrazine **3.6** and b) indolylboronic acid **3.7**.

Stoltz et al. then screened cross-coupling conditions on model substrates (not shown). From this screening, suitable conditions were developed to enable sequential cross-couplings of indolylboronic acid **3.7** and indolylboronic ester **3.5** to dihalopyrazine **3.6** (Scheme 3.7). The first cross-coupling occurred chemoselectively at room temperature to give halopyrazine **3.22** in good yield. It is notable, although not entirely surprising, that the pyrazinyl iodide bond was selectively activated in the presence of two other aryl halide bonds in this system. The second cross-coupling, however, would be

more important to the success of this strategy overall. In the cross-coupling of indolylboronic ester **3.5** and halopyrazine **3.22**, the metal catalyst must be able to selectively activate one aryl bromide over another in halopyrazine **3.22**. The authors noted that at temperatures approaching 80 °C, coupling to the indolyl bromide becomes competitive with coupling to the pyrazinyl bromide. This selectivity issue, however, was mitigated by running the reaction at the lowest possible temperature (50 °C) for extended periods of time, which furnished the desired bis(indolyl)pyrazine **3.4** in good yield.

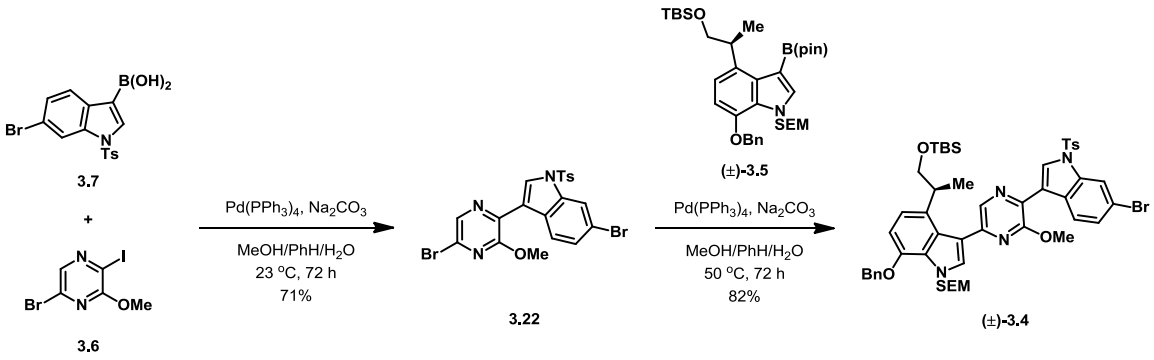

Scheme 3.7. Chemoselective cross-coupling of dihalopyrazine **3.6** with indolylboronic acid **3.7**, followed by regioselective cross-coupling of halopyrazine **3.22** with indolylboronic ester **3.5**.

Stoltz et al. attempted to convert bis(indolyl)pyrazine **3.4** to dragmacidin D through a strategy that relied on multiple late-stage deprotections (Scheme 3.8). Installation of the aminoimidazole moiety was achieved from bis(indolyl)pyrazine **3.4**, but all attempts to remove the protecting groups present in dragmacidin D precursor **3.23** resulted in non-specific cleavage of the aminoimidazole moiety. As such, the authors adjusted their endgame such that installation of the aminoimidazole group would occur after protecting group removal.

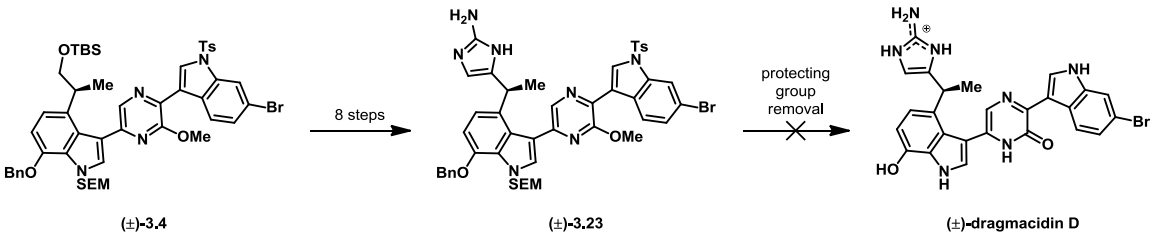

Scheme 3.8. Unsuccessful endgame for the completion of dragmacidin D based on late-stage deprotection.

The new endgame approach began with a homologation of bis(indolyl)pyrazine **3.4**. This was enacted by the conversion of bis(indolyl)pyrazine **3.4** to aldehyde **3.24** via silyl ether cleavage followed by Dess-Martin oxidation[13] (Scheme 3.9). Following this, a Henry reaction[14] of aldehyde **3.24** with nitromethane, followed by another Dess-Martin oxidation[13] gave the homologated nitro ketone **3.25** in excellent yield.

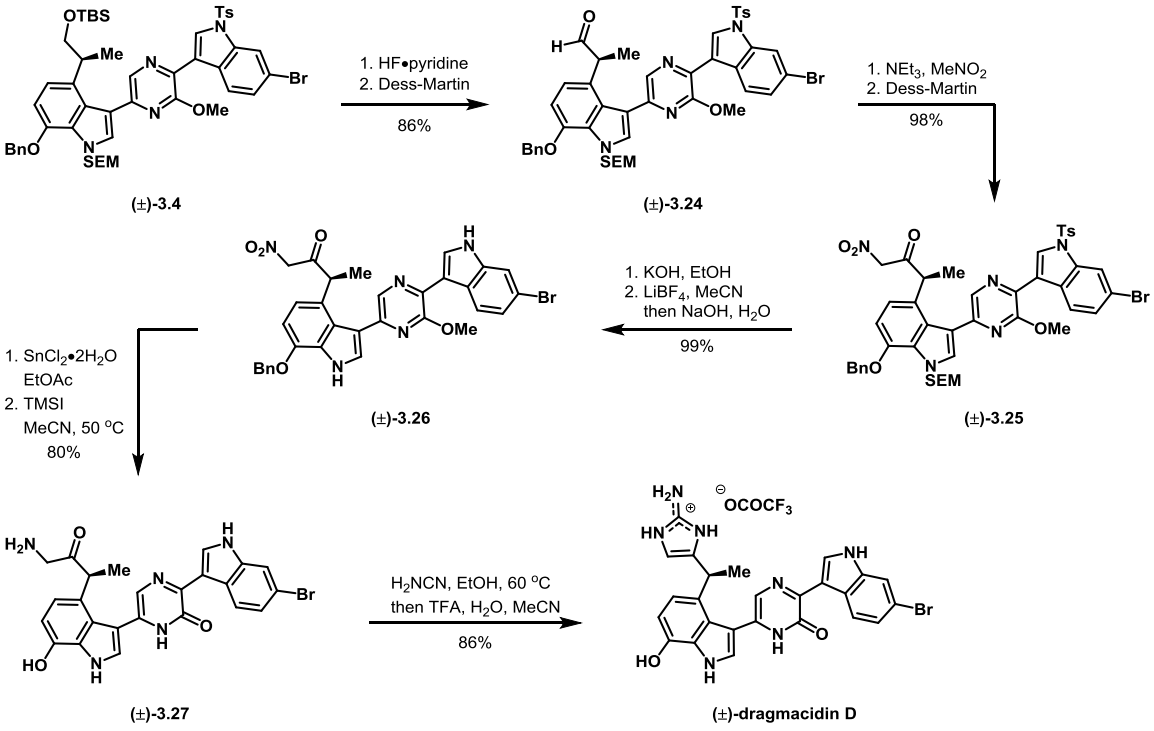

Scheme 3.9. Stoltz's successful completion of racemic dragmacidin D.

It was at this point in the synthesis that the authors sought to remove the remaining protecting groups. The *N*–tosyl group on the indole was the first to be removed, and this was accomplished through basic hydrolysis (see Scheme 3.9 above). Fluoride-mediated desilylation of the SEM group, followed by hydrolysis of the resulting acetal then provided bis(indolyl)pyrazine **3.26** in excellent yield over 2 steps. Having removed the protecting groups on each of the indole nitrogens, Stoltz et al. then unveiled the masked amine moiety through a tin-mediated reduction of the nitro group. Subsequent cleavage of the aromatic methyl and benzyl ethers provided the fully deprotected pyrazinone **3.27** in good yield.

The authors noted that the exact order of synthetic sequencing from nitro ketone **3.25** to pyrazinone **3.27** was crucial for success. Attempts to either reduce the nitro group or remove the SEM group prior to de-tosylation of the indole nitrogen resulted in a large amount of non-specific decomposition. Similarly, attempts to remove the aromatic methyl and benzyl ethers prior to reduction of the nitro group also resulted in decomposition of the nitro ketone moiety.

Installation of the aminoimidazolium moiety completed the total synthesis of dragmacidin D. This was accomplished through a condensation of deprotected pyrazinone **3.27** with cyanamide, followed by treatment with trifluoroacetic acid (see Scheme 3.9 above). Stoltz et al. note that the synthetically-prepared dragmacidin D, as its previously-reported trifluoroacetate salt, was identical to natural samples in ^{1}H NMR, ^{13}C NMR, IR, HRMS, and UV-Vis characterization. However, since this route only provided

racemic dragmacidin D, the absolute configuration of the natural product was not able to be determined.

3.2.2 Stoltz's Enantiospecific Total Synthesis of (+)–Dragmacidin F

Only 2 years after publishing the first reported total synthesis of dragmacidin D, the Stoltz lab successfully completed an enantiospecific synthesis of (+)–dragmacidin F.[15] In addition to the synthetic challenges previously discussed for dragmacidin D, dragmacidin F also contains a tri-substituted pyrrole and a [3.3.1] bicyclic ring system. Furthermore, this bridged ring system is fused to both the pyrrole and aminoimidazole heterocycles.

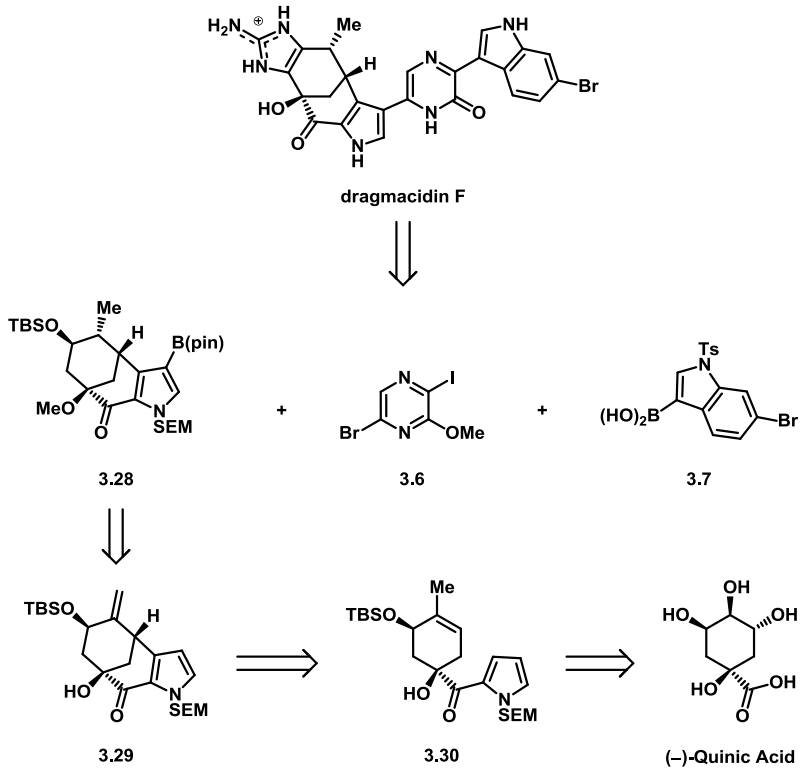

Scheme 3.10. Stoltz's retrosynthetic approach to dragmacidin F.

Stoltz et al.'s retrosynthetic analysis of dragmacidin F borrowed from their previous sequential cross-coupling approach to dragmacidin D. They envisioned the core of dragmacidin F being available through the same cross-coupling of dihalopyrazine **3.6** and indolylboronic acid **3.7**, followed by an analogous cross-coupling with arylboronic ester **3.28** (Scheme 3.10). They anticipated arylboronic ester **3.28** being readily available from bicycle **3.29**, which would serve as the key intermediate for this synthesis. Based on their previous work with palladium-catalyzed dehydrogenation methodologies,[16] Stoltz et al. hypothesized that the key bicycle **3.29** could arise from an oxidative carbocyclization of pyrrole **3.30**. Pyrrole **3.30**, in turn, could be made enantiospecifically from commercially available (–)–quinic acid.

The total synthesis of dragmacidin F began from known bridged lactone **3.31**, which is available from (–)–quinic acid in only 2 steps (Scheme 3.11).[17] Oxidation of the secondary alcohol present in bridged lactone **3.31**, followed by Wittig olefination of the resulting ketone installed the *exo*-methylene group, giving alkene **3.32** in 69% yield over two steps.

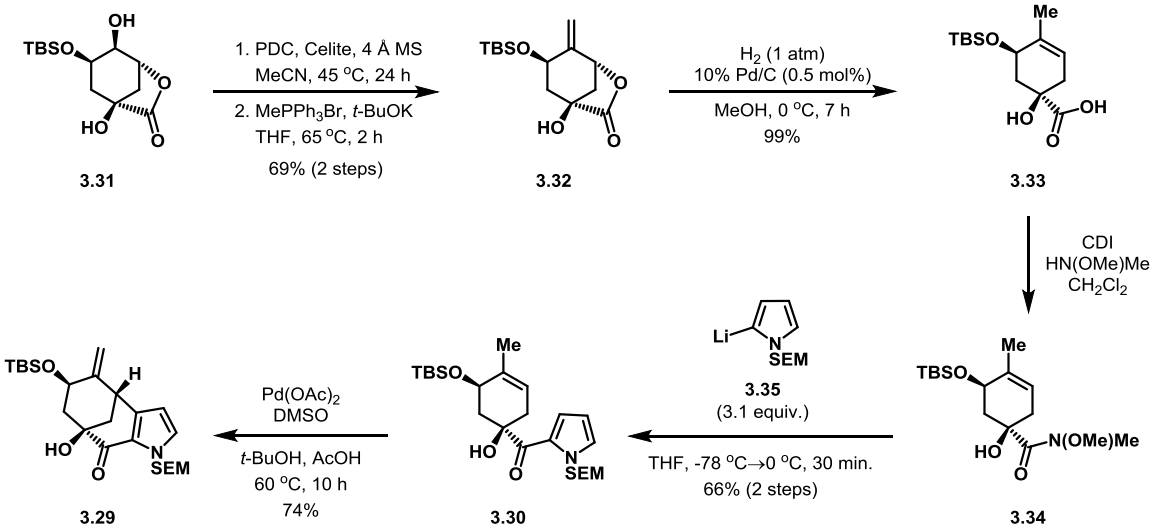

Scheme 3.11.Successful application of Pd-mediated oxidative cyclization to give bicycle **3.29**

Stoltz et al. sought to utilize homogenous Pd π–allyl chemistry to isomerize exocyclic alkene **3.32** to trisubstituted alkene **3.33**, taking advantage of the allylic acetate-like functionality present in alkene **3.32** (Scheme 3.11). Extensive efforts to affect this transformation with homogenous catalysts, while unsusccessful, led to the discovery of a simple heterogeneous catalytic system that was able to efficiently convert exocyclic alkene **3.32** to trisubstituted alkene **3.33**. This transformation is quite remarkable since one might expect hydrogenation of the alkene moiety, present in both the substrate and the product, to be competitive under the reaction conditions. Substitution at the allylic position in both substrate **3.32** and product **3.33** may provide enough steric hindrance to slow their reduction by a metal catalyst. However, alkene coordination is also thought to be necessary for π–allyl substitution pathways.[18] While the authors do not give specific information, they do note that preliminary mechanistic investigations suggest that reduction of a Pd π–allyl species is not operative.

Having successfully obtained alkene **3.33**, Stoltz et al. turned to installing the pyrrole moiety. This was accomplished by conversion of the carboxylic acid to Weinreb amide **3.34** (Scheme 3.11), followed by addition of lithiopyrrole **3.35** to give the precursor for oxidative cyclization, acylpyrrole **3.30**, in good yield over two steps.

To their delight, the authors found that a variety of conditions allowed for the desired oxidative cyclization to take place, with optimal conditions converting acylpyrrole **3.30** to bicycle **3.29** in 74% yield (refer to Scheme 3.11 above). It is worth noting, however, that this oxidative cyclization requires stoichiometric $Pd(OAc)_2$. The presence of the pyrrole moiety may have been problematic for developing conditions catalytic in palladium, as the electron-rich heterocycle may have been incompatible with a stoichiometric oxidant that would be required for catalyst turnover.

Having successfully made their key synthetic intermediate, Stoltz et al. continued their synthesis by converting bicycle **3.29** to arylboronic ester **3.28** (Scheme 3.12). This was accomplished in 4 steps. First, bicycle **3.29** underwent palladium-on-carbon catalyzed hydrogenation to reduce the exocyclic alkene to the stereogenic methyl group, which was followed by protection of the tertiary alcohol as the methyl ether. The authors make no comment to the extent of stereoselectivity for the hydrogenation reaction, but it must be substantial considering the high yield reported for this two step sequence. While one might expect hydrogenation of the alkene to occur on the opposite face of the relatively bulky –OTBS group, approach of the metal from the less-hindered *exo* face of

the bicyclic ring system would provide the *endo*-methyl substituent as shown, which is likely the source of selectivity in this case.

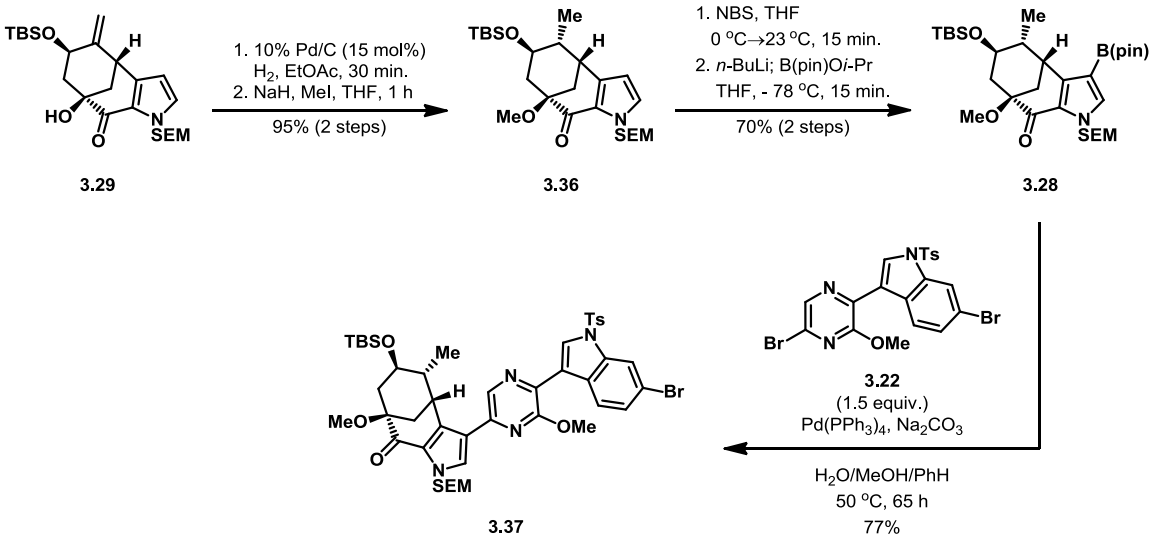

Scheme 3.12. Completion of dragmacidin F core structure **3.37** via selective Suzuki cross-coupling with halopyrazine **3.22**.

Pyrrole **3.36** was then regioselectively brominated at the 3-position , after which point lithium-halogen exchange/electrophilic borylation provided arylboronic ester **3.28** in good yield (see Scheme 3.12 above). Consistent with their previous efforts towards dragmacidin D, Stoltz et al. were able to effect the regioselective cross-coupling of arylboronic ester **3.28** with halopyrazine **3.22** through careful temperature control and extended reaction times. This cross-coupling gave pyrazine **3.37** in good yield, and provided the authors with the core framework for dragmacidin F

Stoltz et al. began their endgame approach to the natural product by converting the TBS-protected alcohol to the corresponding ketone (Scheme 3.13). This was achieved through fluoride-mediated deprotection of the silyl ether, followed by Dess-Martin

oxidation to give ketone **3.38** in excellent yield. The authors had envisioned installing the aminoimidazole moiety in a manner similar to that used in their prior synthesis of dragmacidin D (refer to Scheme 3.9 above). This required installation of an amino group alpha to the ketone in **3.38**. After attempts to accomplish this with traditional enolate and enol ether chemistry proved unsuccessful, Stoltz et al. examined the possibility of using a Neber rearrangement[19] to accomplish this task instead.

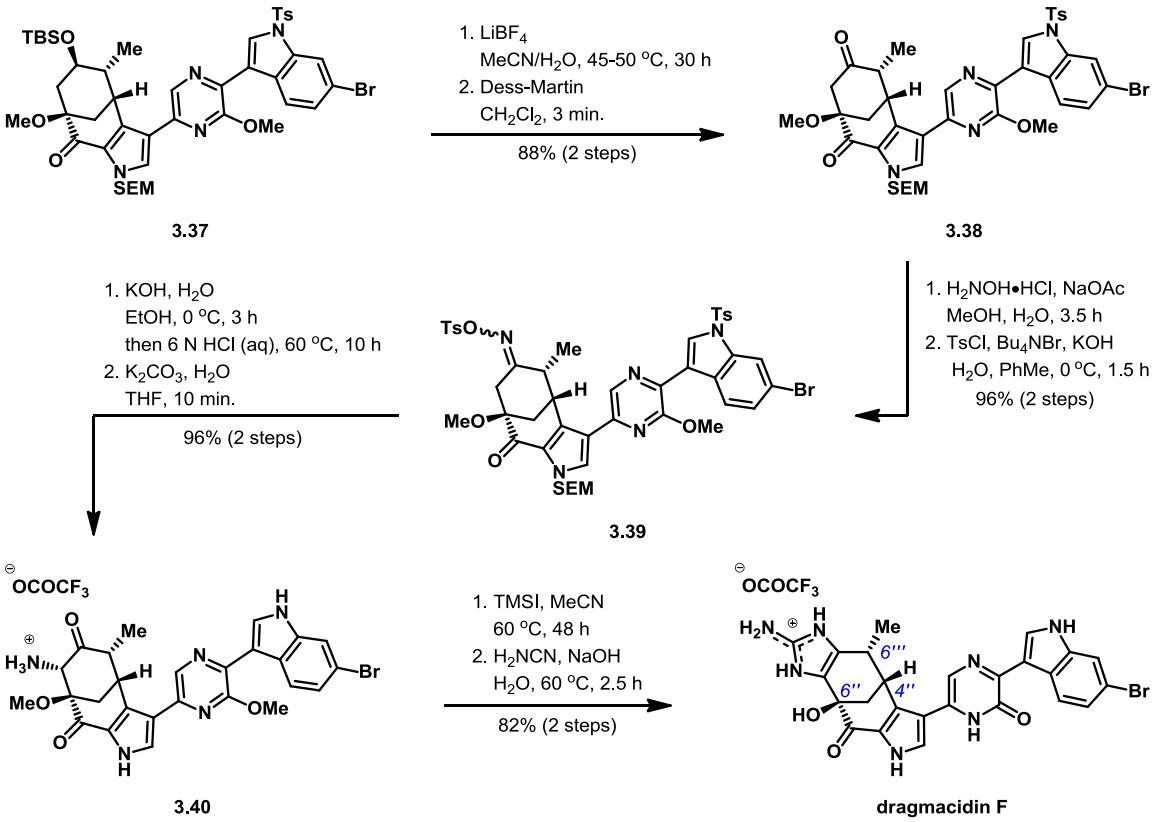

Scheme 3.13.Elaboration of core structure **3.37** to give dragmacidin F.

To test the proposed Neber rearrangement, ketone **3.38** was converted to tosyloxime **3.39** via a two-step sequence consisting of oxime formation followed by tosylation (see Scheme 3.13 above). Remarkably, a Neber rearrangement protocol not

only gave the desired α-aminoketone **3.40** as a single regio- and stereoisomer, but also removed the tosyl and SEM protecting groups. Considering the harsh conditions used in the acidic hydrolysis stage (6 N HCl at 60 ^{o}C for 10 h), one might suspect epimerization at the methyl-substituted ketone α-position to be problematic. The fact that this was not an issue could suggest that the *endo* position of the methyl group is favored from a thermodynamic perspective. If the *endo* position is the preferred position for the α-methyl group, it may be the favored position for the α–amino group as well.

As an aside, the trifluoroacetate counterion present in aminoketone **3.40** is introduced during purification: reverse-phase chromatography was performed using trifluoroacetic acid as an eluent additive. This method of purification was also used in the remaining steps, and ensured that the trifluoroacetate counterion remained intact.

Completion of the total synthesis of dragmacidin F from aminoketone **3.40** was achieved through a 2-step sequence consisting of: 1) removal of the alkyl and aryl methyl ether protecting groups; and 2) Condensation of the α-aminoketone moiety with cyanamide. The authors note that the enantiopure synthetic dragmacidin F was spectroscopically identical to natural samples via ^{1}H NMR, ^{13}C NMR, IR, UV, and HPLC characterization. However, the sign of optical rotation for the synthetic sample of dragmacidin F was opposite to that of natural samples (natural: $[\alpha]^{25}_{D}$ –159° (*c* 0.4, MeOH); synthetic: $[\alpha]^{25}_{D}$ +146° (*c* 0.45, MeOH)). From this optical rotation measurement, Stoltz et al. concluded that their synthetically-prepared dragmacidin F was the enantiomer of the natural product. As such, they assigned the absolute configuration

for natural dragmacidin F as (4’’*S*, 6’’*S*, 6’’’*S*) (see Figure 3.1 above for numbering conventions of dragmacidins D–F). Furthermore, based on the assumption that dragmacidins D–F are biosynthetically related, Stoltz et al. hypothesized that the absolute configurations for dragmacidins D and E should be (6’’’*S*) and (5’’’*R*, 6’’’*S*), respectively.

3.2.3 Jia’s Asymmetric Total Synthesis of (+)–Dragmacidin D

Jia et al. recently reported an asymmetric total synthesis of dragmacidin D.[20] Their retrosynthetic approach to the natural product is outlined below in Scheme 3.14. Borrowing from Stoltz’s previous synthesis of racemic dragmacidin D, Jia et al. envisioned installing the aminoimidazole moiety near the end of the synthesis. As such, they anticipated the natural product being available through late-stage manipulations of bis(indolyl)pyrazine **3.41**. The authors hypothesized that the pyrazine linker could be formed through a cyclocondensation between acid chloride **3.42** and diamine **3.43**.

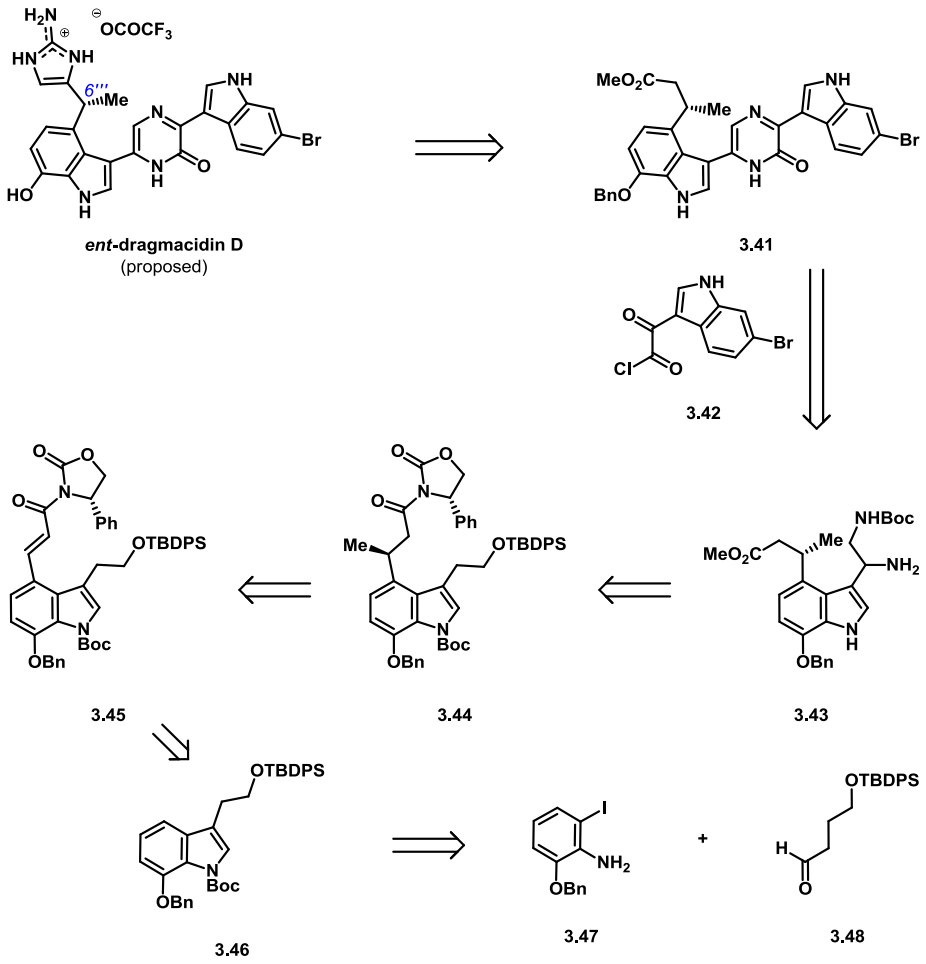

Scheme 3.14. Jia's retrosynthetic approach to *ent*-dragmacidin D.

While Stoltz had previously demonstrated ineffective cyclocondensation approaches with 4-substituted indoles, the disconnect presented by Jia is different in an important way. The unsuccessful cycloaddition substrates reported by Stoltz featured 4-substituted indoles bearing the electrophilic components of the reaction, whereas the substrates proposed by Jia bear the nucleophilic components on the 4-substituted indole.

To this end, the nucleophilic diamine **3.43** was thought to be available from indole **3.44** (see Scheme 3.14 above). Jia et al. envisioned the stereogenic methyl group in indole **3.44** being introduced through an Evans auxiliary controlled asymmetric

conjugate addition[21] to enamide **3.45**. Enamide **3.45**, in turn, was expected to be available via halogenation of indole **3.46** followed by Heck coupling with the appropriate *N*-acryl-oxazolidinone. Finally, indole **3.46** was predicted to be formed through a Pd-catalyzed annulation of iodoaniline **3.47** with aldehyde **3.48**.[22]

Jia et al. began their synthetic efforts toward dragmacidin F with the Pd-catalyzed annulation of iodoaniline **3.47** with aldehyde **3.48** (Scheme 3.15). This annulation occurred as expected, giving the authors unprotected indole **3.49** in good yield. Subsequent treatment with Boc-anhydride afforded protected indole **3.46** in excellent yield, and was followed by iodination to give the Heck coupling precursor iodoindole **3.50**. A ligand-free Heck protocol formed the desired C–C bond at the indole C4 position, but the corresponding enamide **3.45** was generated as a 7:2 mixture of *E*- and *Z*-isomers, respectively. The authors noted that added phosphine ligands did not improve the ratio of alkene isomers, but resulted in diminished product yield. Furthermore, these double bond isomers were not able to be separated by chromatographic purification.

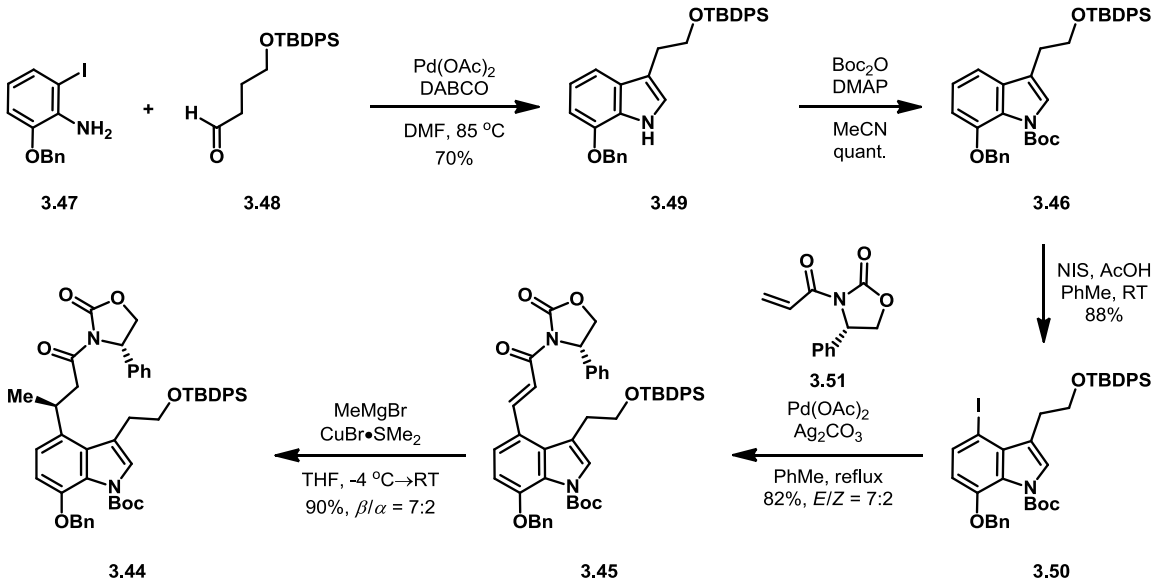

Scheme 3.15. Jia's asymmetric synthesis of indole fragment **3.44**.

Having successfully installed the chiral auxiliary through a Heck coupling of iodoindole **3.50** and *N*-acryl-oxazolidine **3.51**, Jia et al. examined the key enantio-determining step of the synthesis. Upon exposure of α,β-unsaturated amide **3.45** to a cooled solution of methyl Grignard and cuprous bromide-dimethylsulfide, conjugate addition of the methyl nucleophile occurred with excellent selectivity and yield to give indole **3.44** as a 7:2 mixture of diastereomers in 90% combined yield. It is interesting that the alkene isomer ratio present in the starting material was identical to the ratio of diastereomers generated in this reaction. This could suggest that the two alkene isomers provided the same level of diastereoselectivity, although this could just be a coincidence since these ratios were only reported to 1 significant figure.

With the key stereocenter set, the authors turned their attention to preparing the cycloaddition precursor diamine **3.43**. This was accomplished in 8 steps from indole **3.44** (Scheme 3.16). First, methanolysis allowed for efficient removal of the chiral auxiliary

and provided methyl ester **3.52** in quantitative yield. As an aside, the absolute configuration of the sole stereocenter was determined by degradation studies of ester **3.52**. Auxiliary cleavage was followed by removal of the TBDPS silyl ether, and the resulting alcohol was converted to the azide via a Mitsunobu reaction. Azide **3.53** was converted to Boc-protected amine **3.54** through a 3-step sequence consisting of: 1) Staudinger reduction of the azide; 2) deprotection of the indole nitrogen; and 3) Boc protection of the primary amine. Installation of the second amine functionality was achieved through a DDQ-mediated benzylic azidation procedure, originally reported by Feldman et al. in their efforts towards dragmacidin E analogs,[23] which gave benzylic azide **3.55** in excellent yield. Finally, nickel borohydride reduction of the azide provided the desired diamine **3.43** in quantitative yield.

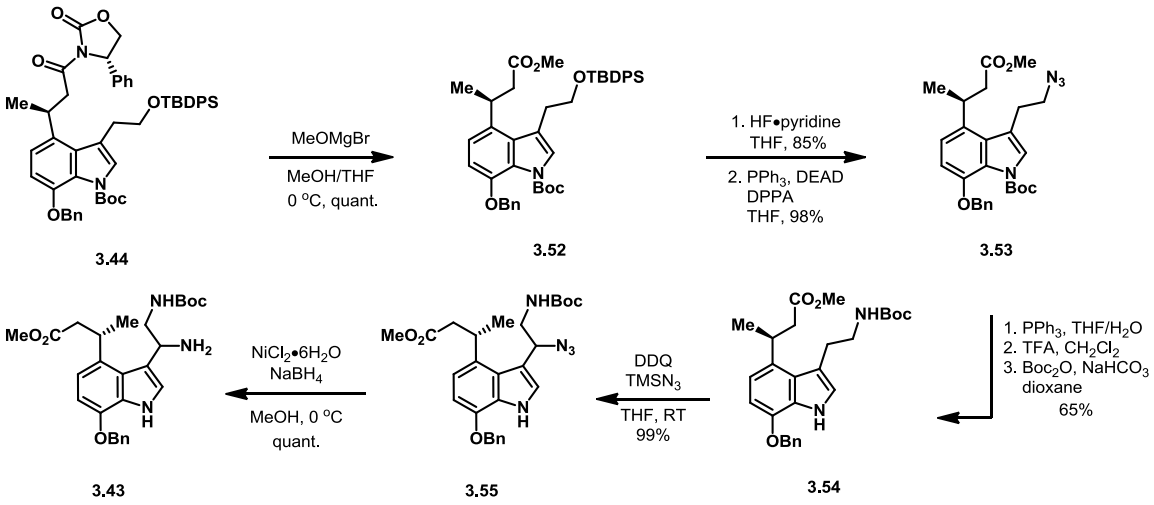

Scheme 3.16. Synthesis of cycloaddition precursor **3.43**.

To form the pyrazinone ring, Jia et al. first acylated the unprotected primary amine in diamine **3.43** with the readily-available acid chloride **3.42** to give amide **3.56** in good yield (Scheme 3.17). Completion of pyrazinone **3.41** was then achieved through a

3-step sequence consisting of: 1) deprotection of the Boc-protected amine; 2) intramolecular condensation of the newly-formed primary amine with the indolyl ketone; and 3) DDQ-mediated oxidative aromatization. From here, attempts to introduce heteroatoms alpha to the ester in pyrazine **3.41** resulted only in the recovery of starting material. The authors reasoned that the installation of protecting groups in pyrazinone **3.41** would be necessary to circumvent this issue. To that end, the indole nitrogens were protected with Boc groups, after which point the pyrazinone was protected as the pyrazinyl SEM ether to give protected pyrazine **3.57** in good yield over two steps.

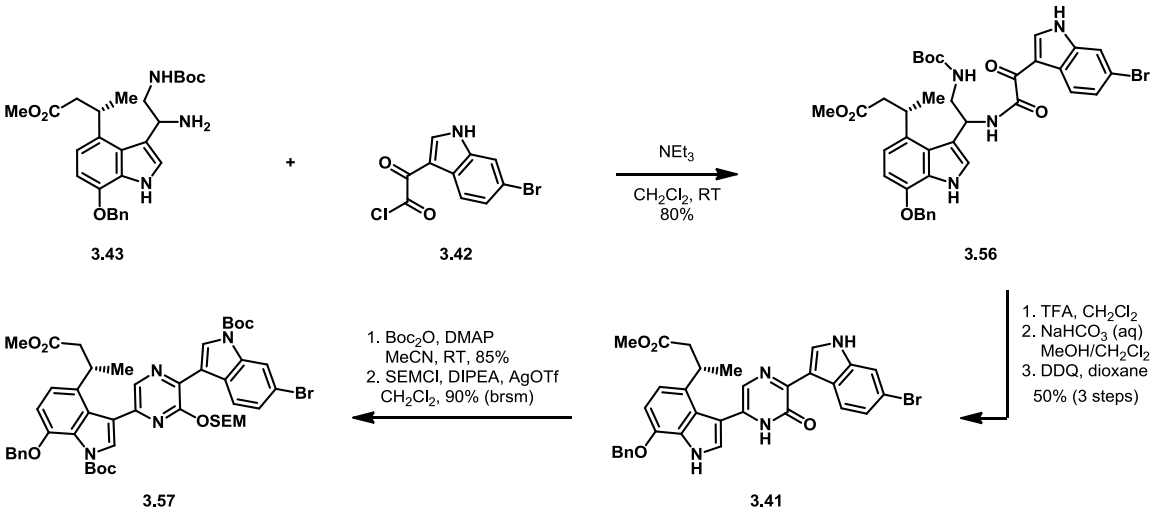

Scheme 3.17. Completion of the pyrazinone **3.41** core of dragmacidin D and subsequent functional group protections.

From pyrazine **3.57**, two objectives remained to complete the synthesis of dragmacidin D : 1) installation of the aminoimidazole moiety, and 2) protecting group removal. Installation of the aminoamidazole moiety was accomplised in 6 steps. Jia et al. installed the requisite heteroatom functionality alpha to the ester via electrophilic bromination of the enolate derived from pryazine **3.57** (Scheme 3.18). This gave halo-

ester **3.58** as a single diastereomer in poor yield, although a significant amount of starting material was also recovered. While the authors do not comment on this reaction, it seems likely that enolate formation was problematic. The substitution present at the beta position in ester **3.57** should dramatically slow down deprotonation with a bulky base such as LDA. Additionally, treatment of pyrazine **3.57** with LDA was only done for 30 min. at a temperature of -40 ^{o}C. The low yield and large amount of starting material recovered from this reaction would support this hypothesis.

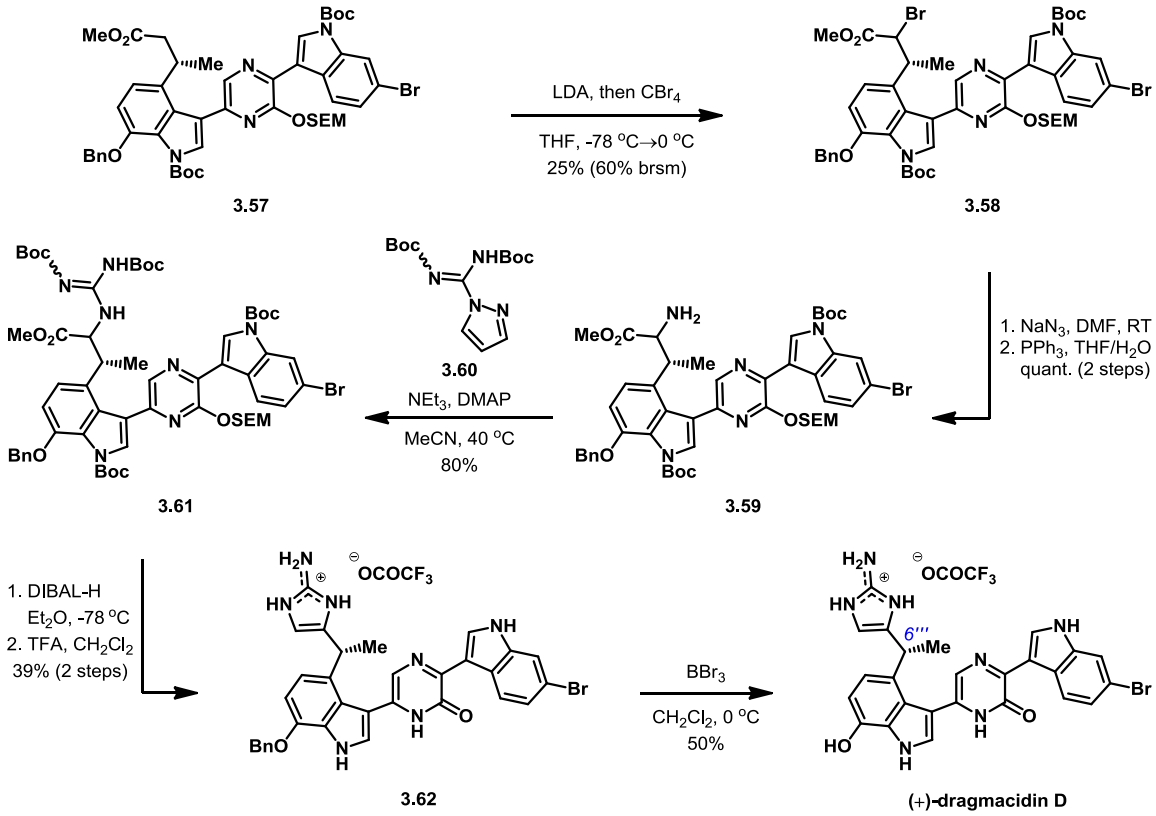

Scheme 3.18. Jia's endgame for the completion of (+)-dragmacidin D.

Halo-ester **3.58** was then converted to amino-ester **3.59** through a two-step azide substitution and Staudinger reduction sequence (see Scheme 3.18 above). The newly-

installed amine was then incorporated into a guanidine subunit via acyl-like substitution with amidinyl pyrazole **3.60**, which gave guanidine **3.61** in good yield. DIBAL reduction of the ester, followed by treatment with trifluoroacetic acid not only installed the aminoimidazolium moiety but also achieved a global Boc-deprotection and revealed the unprotected pyrazinone functionality. This resulted in the formation of pyrazinone **3.62** in 39% yield over the two steps. Despite the relatively low yield, this two-step conversion of guanidine **3.61** to pyrazinone **3.62** is impressive considering how much was accomplished. This is especially true when one considers that a global deprotection strategy attempted by Stoltz on a very similar substrate (refer to pyrazine **3.23**, Scheme 3.8) was unsuccessful.

Jia et. al. completed their synthesis of dragmacidin D via boron tribromide mediated deprotection of the benzyl ether in pyrazinone **3.62** (see Scheme 3.18 above). Based on Stoltz's proposed (6'''*S*) configuration for natural dragmacidin D (refer to Section 3.2.2), the (6'''*R*) configuration present in Jia et al.'s synthetic dragmacidin D should be enantiomeric to the natural configuration. However, optical rotation measurements for Jia's synthetic dragmacidin D gave the same (+) sign as that reported[3] for natural samples (synthetic: $[\alpha]^{25}_{D}$ +18.8° (*c* 0.10, EtOH); natural: $[\alpha]^{25}_{D}$ +12° (*c*, 0.95, EtOH). It should be noted, however, that there has been some discrepancy in the optical rotation measurements provided in the isolation reports for dragmacidin D. The initially reported isolation[4] of dragmacidin D in 1992 was unable to measure any optical activity for the natural sample, while a later isolation[3] in 1998 reported an optical rotation of

+12°. It is also worth mentioning that the concentration used by Jia et al. to determine optical rotation was significantly more dilute than that reported for the natural sample.

This unexpected stereochemical discrepancy led Jia et al. to analyze their synthetic dragmacidin D and natural samples via chiral HPLC (Figure 3.2). Before coming to any conclusions about Jia's HPLC analysis, it should be noted that the HPLC chromatograms reported have poor resolution of the two enantiomers. As such, quantitative measurements are likely not reliable. With this in mind, the HPLC data reported by Jia provided some interesting qualitative insight. Chromatogram (a) in Figure 3.2 is that of the synthetic dragmacidin D prepared in this report. While an accurate quantification of enantiomeric excess is not possible due to the poor resolution, qualitatively, one can surmise that some amount of *ee* is present in the synthetic sample, which the authors labeled as **(+)–1**. Chromatogram (b) is that of an archived sample of isolated dragmacidin D, which was reported by Jia et al. to have 39% *ee*. Based on the co-elution of the major synthetic enantiomer with the major enantiomer from the natural sample, Jia et al. concluded that the natural configuration of dragmacidin D is likely (6'''*R*). They also note that a potential issue with the biosynthetic relationships proposed by Stoltz is that dragmacidin F has not yet been reported to be co-isolated with either dragmacidins D or E.

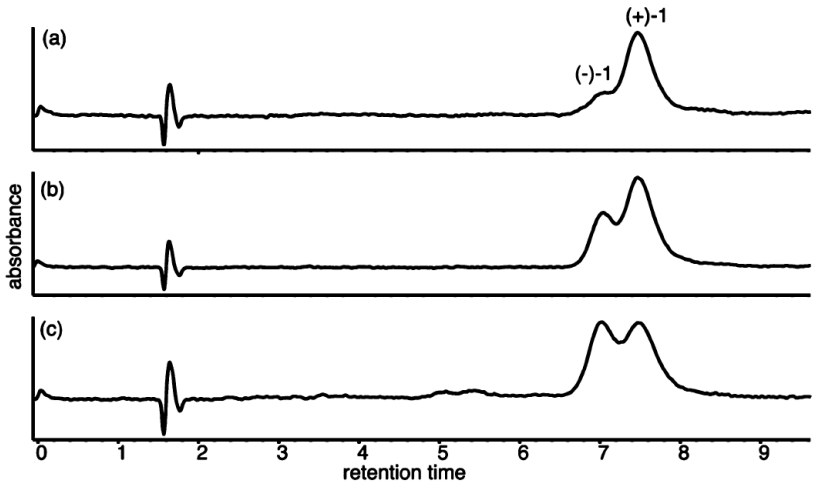

Figure 3.2. Jia's chiral HPLC-DAD analyses for a) synthetic (+)-dragmacidin D; b) natural dragmacidin D from archived specimen RJC-91-011; and c) natural dragmacidin D from a younger specimen, RJC-98-305.[20]

Concerned that long-term storage may have resulted in some racemization of the natural sample, the authors analyzed a more recent extract of natural dragmacidin D, the chiral HPLC chromatogram of which is shown in Figure 3.2c. Much to their surprise, this sample of natural dragmacidin D had even lower *ee* than that of the older specimen. From this observation, Jia et al. suggested that the dragmacidins may be produced naturally either as racemates or scalemic mixtures. This finding further complicated the issues surrounding the biosynthesis, configuration of, and even bioactivity of the dragmacidins.

3.2.4 Zakarian's Total Synthesis of (+)–Dragmacidin D

Very shortly after Jia's reported synthesis of (+)–dragmacidin D, Zakarian et al. reported their own enantioselective synthesis of the natural product.[24] Impressively, this synthesis consisted of a longest linear sequence of only 10 steps. The retrosynthetic analysis of dragmacidin D by Zakarian et al. is shown below in Scheme 3.19.

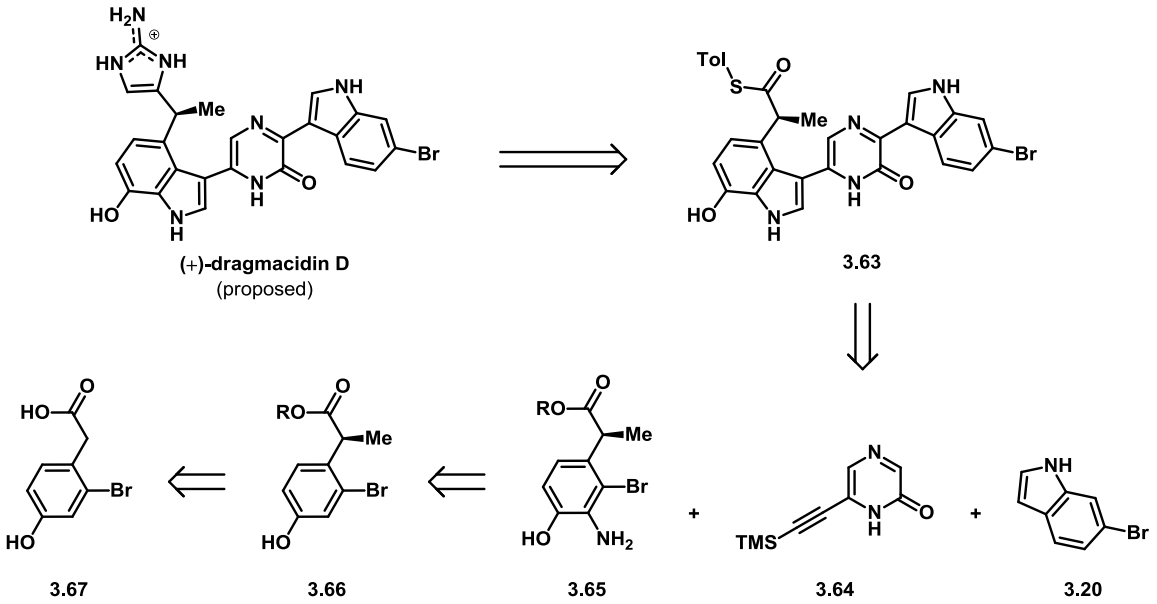

Scheme 3.19. Zakarian's retrosynthetic approach towards (+)–dragmacidin D.

In line with previous efforts, installation of the aminoimidazole moiety was envisioned to occur at the end of the synthesis following the formation of thioester **3.63**. Unlike previous efforts towards dragmacidin D, Zakarian et al. sought to introduce synthetic convergence via the trisubstituted indole, as well as the pyrazinone. As such, they envisioned thioester **3.63** being available through a Larock indole synthesis[25] of haloaniline **3.65** with alkynyl pyrazinone **3.64**, at which point the second indole could be installed. The authors foresaw haloaniline **3.65** being available from aryl halide **3.66**, which in turn might be made enantioselectively from carboxylic acid **3.67** through an asymmetric alkylation strategy developed by the Zakarian group.[26]

The authors' synthesis started with the enantioselective alkylation of carboxylic acid **3.68** (Scheme 3.20). Preliminary investigations, focused solely on reactivity, showed that *n*BuLi and LDA were poor enolization reagents as they led to decomposition of

starting material. The authors hypothesized that this was due to competitive lithiation of the aromatic ring at the C3 position. Lithiation at this position would allow for a 1,2-elimination to form benzyne, which could open decomposition pathways. Use of the less basic LHMDS ($HN(SiMe_3)_2$ $pK_a = 26$; $HN(i\text{-}Pr)_2$ $pK_a = 37$)[24] as the enolization reagent in this reaction avoided starting material decomposition, but resulted in lower conversion. The use of $LiN(t\text{-}Bu)SiMe_3$ ($HN(t\text{-}Bu)SiMe_3$ $pK_a = 33$)[24], an enolization reagent of intermediate basicity, solved the reactivity issues that had been encountered as it avoided starting material decomposition while providing near-complete conversion. When applied to the enantioselective alkylation of carboxylic acid **3.68**, formation of the enediolate using $LiN(t\text{-}Bu)SiMe_3$ in combination with the mixed-aggregate chiral scaffolding reagent (*R*)–$^1TALi_2$ (see Scheme 3.20 for structure) provided branched carboxylic acid **3.69** in moderate yield with 81% *ee*. Impressively, this reaction was performed on scales using nearly 5 grams of carboxylic acid **3.68**. Less impressively, this reaction required stoichiometric use of the mixed-aggregate chiral scaffolding reagent (*R*)–$^1TALi_2$. The absolute configuration of the newly-formed stereocenter was determined by LAH reduction to the known alcohol (not shown).

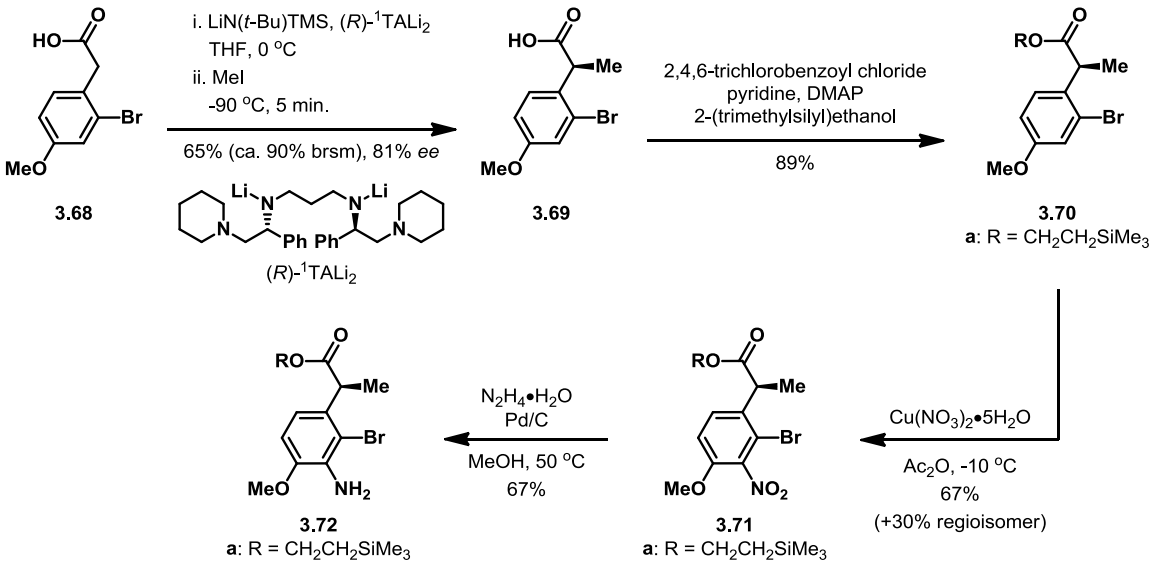

Scheme 3.20. Zakarian et al.'s enantioselective synthesis of Larock indole precursor **3.72**.

The authors were concerned that the stereocenter generated with the enantioselective alkylation protocol would be labile to epimerization. As such, they anticipated that mild conditions would be needed throughout the remainder of the synthesis to avoid racemization. With that in mind, Zakarian et al. looked to introduce the amino group at the arene C3 position. This was accomplished by protection of the carboxylic acid as (trimethylsilyl)ethyl ester **3.70** followed by nitration of the arene using Cu(II) nitrate in acetic anhydride (Scheme 3.20). This 2-step procedure provided nitroarene **3.71** as a 2-to-1 mixture of regioisomers, with the desired 3-nitro isomer being favored over the undesired 5-nitro isomer. The authors noted that careful temperature control was needed under these conditions to avoid racemization of the benzylic stereocenter. Zakarian et al.'s completion of their anticpated Larock indole synthesis precursor was achieved through a palladium-catalyzed reduction of the nitro group using hydrazine, which provided haloaniline **3.72** in moderate yield. The authors noted that

careful control of both temperature and hydrazine stoichiometry were important to avoid over-reduction (presumably of the aryl bromide).

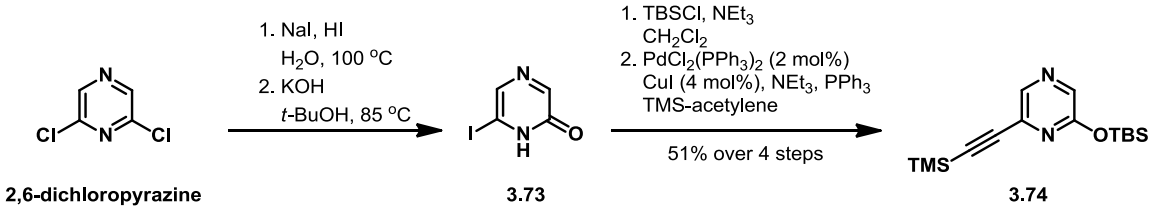

Scheme 3.21. Synthesis of Larock indole synthesis coupling partner alkyne **3.74**.

With haloaniline **3.72** in hand, the authors turned to making the alkyne coupling partner needed for their proposed Larock indole synthesis. This was achieved in 4 steps from commercially-available 2,6-dichloropyrazine. Acid-mediated halogen exchange of 2,6-dichloropyrazine to the diiodopyrazine followed by substitution with potassium hydroxide provided iodopyrazinone **3.73** (see Scheme 3.21 above). The pyrazinone moiety was then protected as the pyrazinyl TBS ether, after which point Sonogashira cross-coupling with TMS-acetylene gave the desired alkynyl pyrazine **3.74** in 51% total yield over 4 steps.

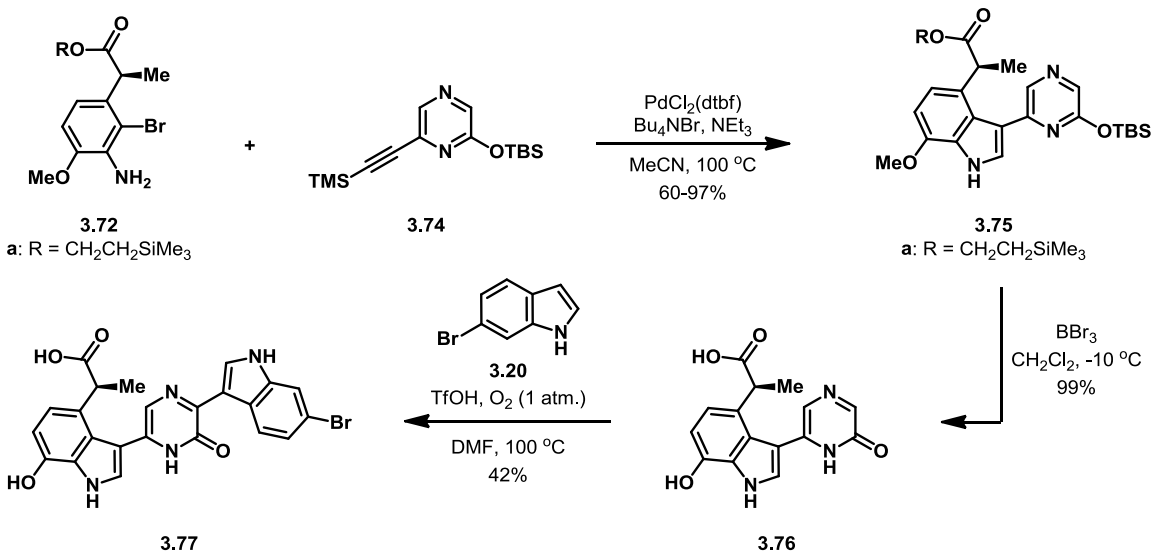

Scheme 3.22. Synthesis of indolylpyrazine **3.75** and elaboration to bis(indolyl)pyrazinone **3.77**.

The Pd-catalyzed coupling of haloaniline **3.72** and alkyne **3.74** gave the desired indolylpyrazine **3.75** in variable yields (see Scheme 3.22 above). The authors noted that best results were obtained with freshly-prepared substrates and freshly-purified solvents. Additionally, the use of tetrabutylammonium bromide (TBAB) was crucial for ensuring reproducibility as it prevented the formation of palladium black.

Global deprotection of indolylpyrazine **3.75** occurred smoothly upon treatment with boron tribromide and provided pyrazinone **3.76** in excellent yield (see Scheme 3.22 above). To install the 6-bromoindole fragment, Zakarian et al. used a procedure from a previous synthesis of dragmacidin D reported by Itami in 2011.[27] With this procedure, indole **3.20** was directly coupled to pyrazinone **3.76** using triflic acid at high temperatures and under an atmosphere of oxygen. The mechanism for this type of reaction was hypothesized by Itami et al. to occur through a Friedel-Crafts-like substitution of the

electron-rich aromatic ring, followed by air oxidation and elimination to re-form the double bond.

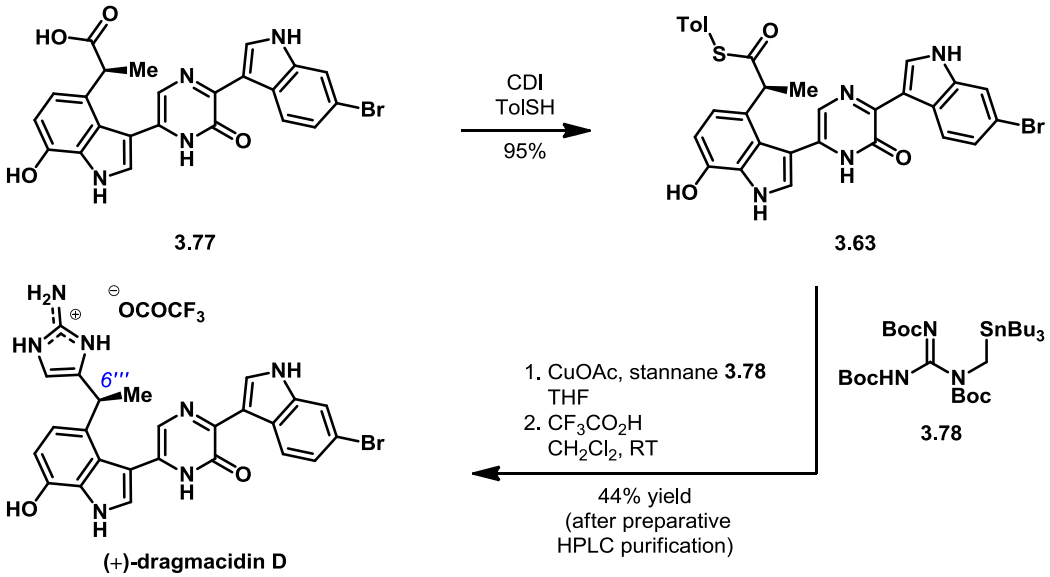

Scheme 3.23. Zakarian et al.'s completion of the total synthesis of (+)–dragmacidin D.

With bis(indolyl) pyrazinone **3.77** in hand, the authors impressively completed the synthesis of (+)–dragmacidin D in only 3 steps. Conversion of the carboxylic acid moiety to the thioester was affected by treatment of bis(indolyl)pyrazinone **3.77** with carbonyldiimidazole (CDI), followed by the addition of thiocresol (see Scheme 3.23 above). This transformation provided thioester **3.63** in excellent yield. Thioester **3.63** then underwent a Fukuyama-like cross-coupling[28] with guanidinyl stannane **3.78** to give the desired ketone, which was subsequently treated with trifluoroacetic acid to give (+)–dragmacidin D in 44% yield after reverse-phase preparative HPLC purification.

Zakarian et al. used a previously-prepared sample of racemic dragmacidin D to develop an effective chiral HPLC analytical method to assess the *ee* of their product.

Despite the 81% *ee* obtained during the enantio-determining step of the synthesis, the final dragmacidin D product was shown to have only 61% enantiomeric excess. The authors had been concerned about the lability of the sole stereocenter towards racemization throughout the synthesis, but they also noted that racemization of dragmacidin D itself could be an issue.

The optical rotation measurements for synthetic dragmacidin D, prepared in this report by Zakarian et al. with the (6’’’*S*) configuration, showed markedly higher and positive optical rotations ($[\alpha]^{25}_{D}$ +106° (c 0.95, EtOH); $[\alpha]^{25}_{D}$ +95° (c 0.10, EtOH) than measurements from previous reports (refer to Section 3.2.3). These results supported the original hypothesis put forth by Stoltz regarding the absolute configuration of natural dragmacidin D, and contradicted the results from the previous report by Jia et al.[20]

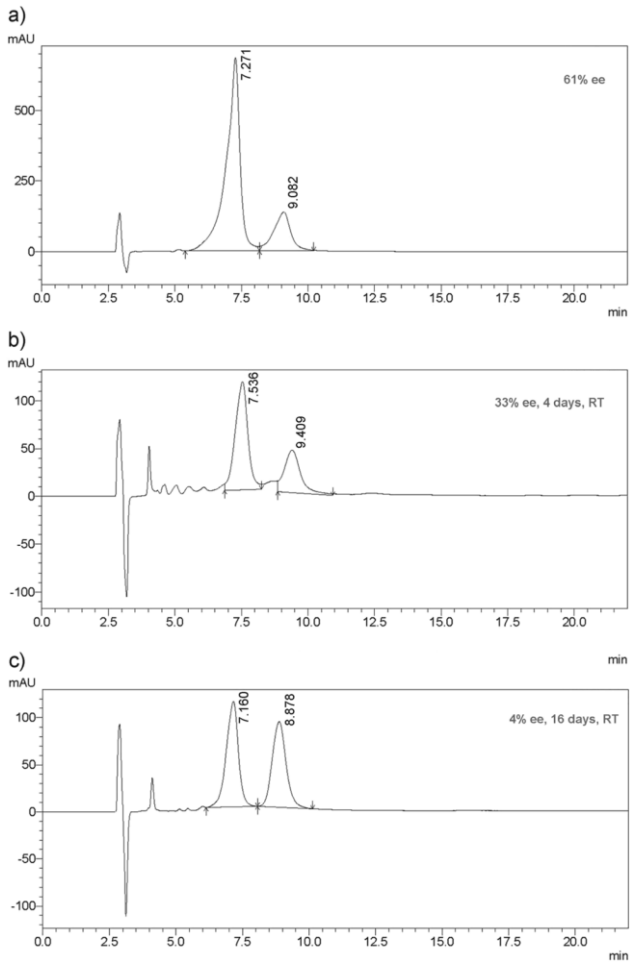

Figure 3.3. Enantiomeric excess of an aqueous solution of synthetic dragmacidin D after a) fresh preparation; b) 4 days at RT; and c) 16 days at RT.

Given the uncertainty about the configuration of dragmacidin D presented in the literature, Zakarian et al. performed what would be an important experiment to address this long-standing issue. The authors made an aqueous solution of their synthetic dragmacidin D (61% *ee*) and monitored the enantiomeric excess over time (see Figure 3.3 above). Notably, after only 16 days in solution at room temperature the enantiomeric excess had dropped to only 4%. The authors note that a mixed benzene solution stored at -20 ^{o}C showed no change in *ee* after as many as 40 days. Furthermore, they note that

exposure of an aqueous solution of dragmacidin D to light at room temperature led to rapid decomposition.

These results could explain many of the discrepancies found in the literature with regards to the optical rotation and enantiopurity of natural dragmacidin D. This result also has serious consequences for the reported biological activity observed for dragmacidin D (refer to section 3.1). Given the facile racemization observed for the natural product in solution and its rapid decomposition upon exposure to light, the true identity of the small molecule(s) responsible for the bioactivity in previous studies should be called into question. On a less serious note, as mentioned by Zakarian, this observation is also interesting in the context of the deep oceanic habitat in which the source organisms reside.

3.3. Synthetic Efforts Towards Dragmacidin E

Compared to dragmacidins D and F, reports of synthetic efforts towards dragmacidin E have been less common. The unique structure of dragmacidin E introduces a prominent synthetic challenge not present in the other dragmacidins: a 7-membered carbocyclic ring. Other considerations for synthetic approaches to dragmacidin E should include: 1) the molecule contains a cyclic guanidine subunit, rather than the aminoimidazole subunit found in the other pyrazinone-linked family members; 2) like dragmacidin F, but unlike dragmacidin D, dragmacidin E contains a quaternary stereocenter; and 3) steric bulk around the pyrazinone ring is much greater in dragmacidin E than it is in dragmacidins D or F.

A limited number of synthetic efforts towards dragmacidin E have been reported,[23,29-34] but only one of those has resulted in the successful synthesis of the natural product. The majority of the reported synthetic work, including the sole completed synthesis, has come from the lab of Ken Feldman and it is that work which will be the focus of the following section.

3.3.1 Feldman's Model Cycloheptannelated Indole Fragment

Feldman and Ngernmeesri were the first to report on synthetic efforts specifically targeted toward dragmaicin E.[30] In 2005, they disclosed their work that had been focused on solving the prominent synthetic issue present in the molecule: the 7-membered carbocycle.

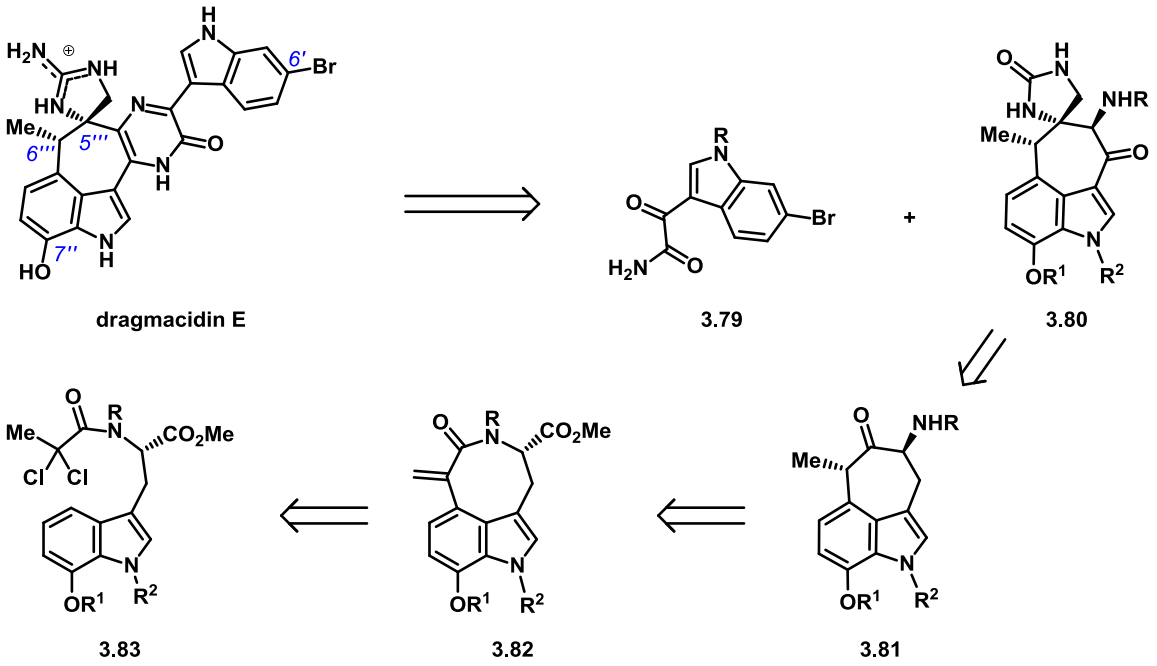

Scheme 3.24. Feldman and Ngernmeesri's retrosynthetic approach to dragmacidin E.

Feldman and Ngernmeesri's retrosynthetic analysis for dragmacidin E is shown above in Scheme 3.25. Similar to previous efforts towards dragmacidins D and F, they sought to install the sensitive guanidine subunit towards the end of the synthesis. As such, they envisioned the natural product being available through a cyclocondensation of ketoamide **3.79** and aminoketone **3.80**, a somewhat bold proposition considering the steric hindrance adjacent to the nucleophilic amino group, as well as the electronic deactivation of the electrophilic ketone in aminoketone **3.80**. They anticipated forming the quaternary stereocenter in aminoketone **3.80** via a Strecker reaction of ketone **3.81**, which they considered the key intermediate in their synthesis. Feldman and Ngernmeesri hypothesized that this key intermediate would be available from cyclooctane **3.82**through a trans-annular Dieckmann condensation/decarboxylation sequence. The annelated indole core of cyclooctane **3.82** was envisioned to be formed through a photocyclization of chloroamide **3.83**, similar to a photocyclization of chloroacetyl tryptophan reported by Witkop in 1966.[35]

The authors began their synthetic efforts towards dragmacidin E with a model study, wherein the 6'-bromo and 7''-hydroxyl substituents would not be included. This was primarily because the starting materials would then consist of tryptophan and indole, two cheap and readily-available starting materials. Furthermore, tryptophan would also allow entry into enantiospecific syntheses.

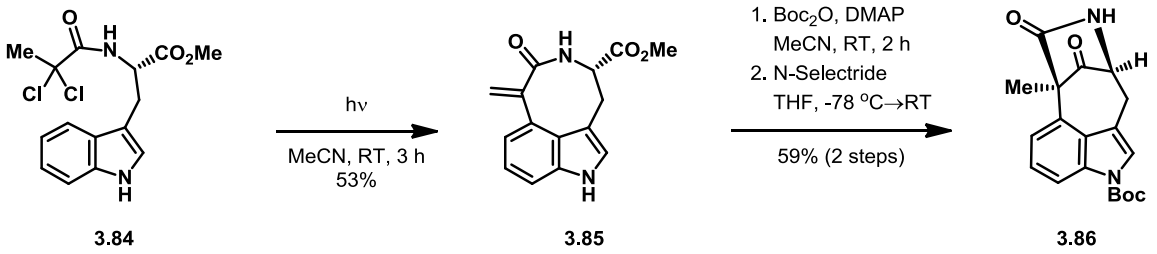

3.84 **3.85** **3.86**

Scheme 3.25. Feldman and Ngernmeesri's key Witkop cyclization and ring contraction to form a cycloheptannelated indole moiety.

Feldman and Ngernmeesri began work on this model study with the readily available *N*-dichloroacyl tryptophan derivative **3.84**, which underwent the desired Witkop photocyclization with relatively high efficiency (see Scheme 3.26 above). The authors suggested that the presence of the second chlorine atom may contribute to the relatively high yield for cyclooctane **3.85**, as it could stabilize radical intermediates that are formed prior to cyclization. The second chlorine atom also leads to alkene formation in the final product through the elimination of HCl (either through normal or excited state pathways).

With cyclooctane **3.85** in hand both the amide and indole nitrogens were Boc-protected. After the nitrogen protecting groups were installed, an intramolecular Dieckmann cyclization was initiated through a conjugate reduction of the acrylamide moiety with N-Selectride® (see Scheme 3.26 above). Loss of the amide Boc group also occurred during this reaction. As such, mono Boc-protected bridged lactam **3.86** was isolated in moderate yield over two steps. Notably, this Dieckmann condensation does not benefit from deprotonation of an acidic β-dicarbonyl in the product, which is usually considered the driving force for such reactions. The authors speculated that in this case

there may be some beneficial relief of steric strain, as the pendant ester group becomes incorporated into the bicyclic framework, which serves as an alternative driving force.

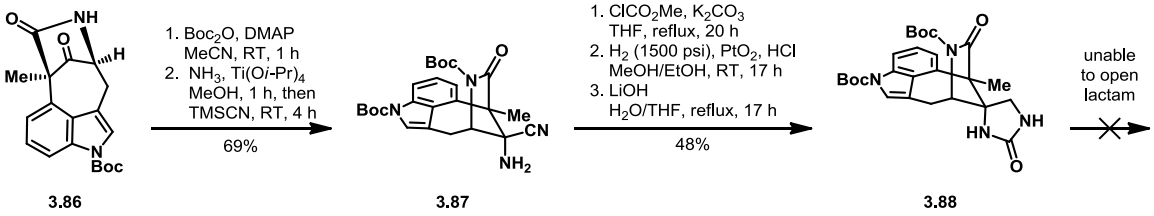

Scheme 3.26. Feldman and Ngernmeeri's unsuccessful approach to forming a cycloaddition precursor through ring-opening of lactam **3.88**.

Having made the key 7-membered carbocyle, Feldman and Ngernmeesri turned their attention toward the construction of the quaternary stereocenter. Since the amide Boc group had been lost in the Dieckmann condensation, they re-protected the amide nitrogen as the Boc carbamate (see Scheme 3.27 above). This was followed by a titanium-mediated Strecker reaction to give aminonitrile **3.87** as a single diastereomer in good yield. From aminonitrile **3.87**, tricyclic urea **3.88** was furnished through a 3-step sequence consisting of: 1) amine acylation; 2) nitrile reduction to the amine; and 3) intramolecular condensation. Unfortunately, all attempts to cleave the bridging lactam from this intermediate were unsuccessful.

Prior to the observation that lactam **3.88** was unable to be cleaved, Feldman and Ngernmeesri had considered an alternative sequence of transformations whereby cleavage of the lactam would be carried out prior to formation of the quaternary stereocenter. As their first attempts proved unsuccessful, the authors moved to the alternative sequence of transformations. As before, reprotecting the amide nitrogen in bridged lactam **3.86** with a Boc group was done first (Scheme 3.27). This was followed

by basic hydrolysis, which after decarboxylation provided the ring-opened cycloheptanone **3.89** in excellent yield. This also led to epimerization of the stereogenic methyl group, and cycloheptanone **3.89** was isolated as a 2-to-1 mixture of diastereomers favoring the undesired β-isomer. While unfortunate, the authors found that this issue was able to be obviated in the next step. Through forcing conditions, a Strecker reaction of cycloheptanone **3.89** provided aminonitrile **3.90** as a single diastereomer. The relative stereochemistry of aminonitrile **3.90** was not able to be determined at this point, but was determined after reduction of the nitrile provided a better handle for ^{1}H NMR analysis.

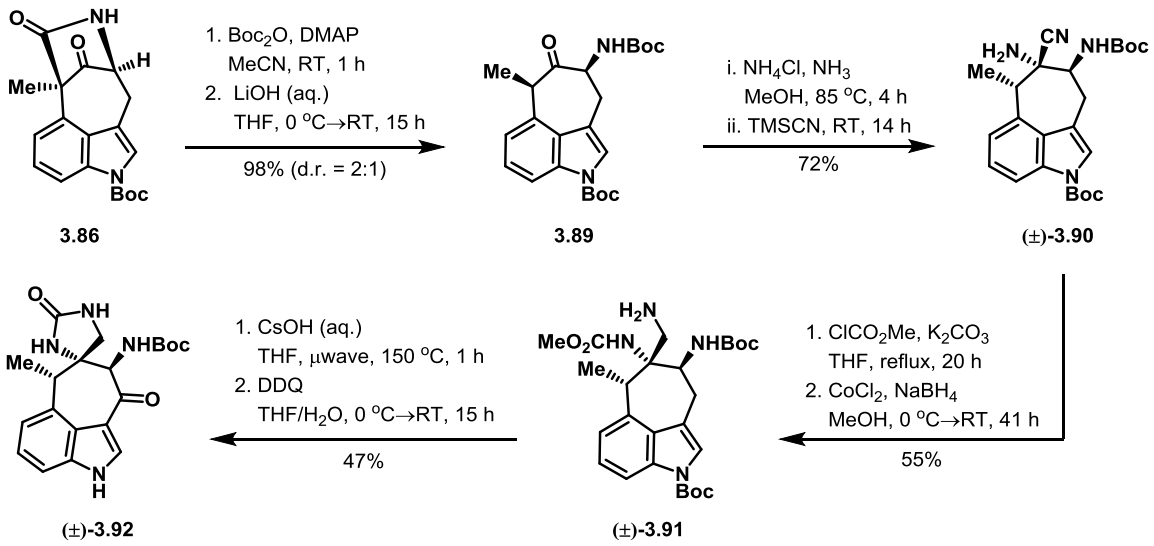

Scheme 3.27. Feldman and Ngernmeesri's successful lactam opening and further elaboration to form the core structure of a dragmacidin E analog.

To gain insight into the source of the diastereoselectivity observed in their Strecker reaction, the authors performed molecular mechanics calculations. These calculations suggested that the most favorable approach of a nucleophile towards the intermediate imine occurred when the adjacent methyl group was in the α-position. They reasoned that this is the result of unavoidable $A^{1,3}$ interactions present with the β-isomer.

Fledman and Ngernmeesri would later find out that the final product in this report was optically inactive, and they hypothesized that racemization had occurred during this transformation. This was further supported when they analyzed cycloheptanone **3.89** recovered from this reaction and found it to be optically inactive as well.

The completion of the core structure for a dragmacidin E analog was achieved from the diastereomerically pure, albeit racemic, aminonitrile **3.90** in 4 steps (see Scheme 3.27 above). Acylation of the primary amine followed by reduction of the nitrile provided aminocarbamate **3.91** in moderate yield. The authors noted that attempts to reduce the nitrile via hydrogenation were ineffective as either starting material or a secondary amine, likely the result of HCN elimination and reduction of the resulting imine, were obtained instead of the desired primary amine. The use of cobalt(II) chloride with sodium borohydride, however, was a successful alternative and provided the desired primary amine. Aminocarbamate **3.91** was then heated to high temperatures, under basic conditions, using microwave irradiation. Under these conditions, ring closure occurred to form the cyclic urea was accompanied by removal of the indole *N*-Boc protecting group. Subsequent DDQ oxidation was used to install the ketone substituent at the indole 3-position, and provided aminoketone **3.92** in moderate yield over this two step sequence.

Aminoketone **3.92** was the final product in this report by Feldman and Ngernmeesri. They anticipated future endeavors would be aimed at elaborating aminoketone **3.92** to a dragmacidin E analog, after which point their synthetic approach to such an analog could be translated to the total synthesis of the natural product itself.

3.3.2 Feldman's Completed Synthesis of a Dragmacidin E Analog

Five years after reporting the synthesis of the core structure, aminoketone **3.92**, Feldman and Ngernmeesri disclosed the completion of their dragmacidin E analog.[23] Starting from aminoketone **3.92**, only 9 synthetic steps were required to complete de(6'-bromo-7''-hydroxyl)-dragmacidin E (**3.98**, Scheme 3.28).

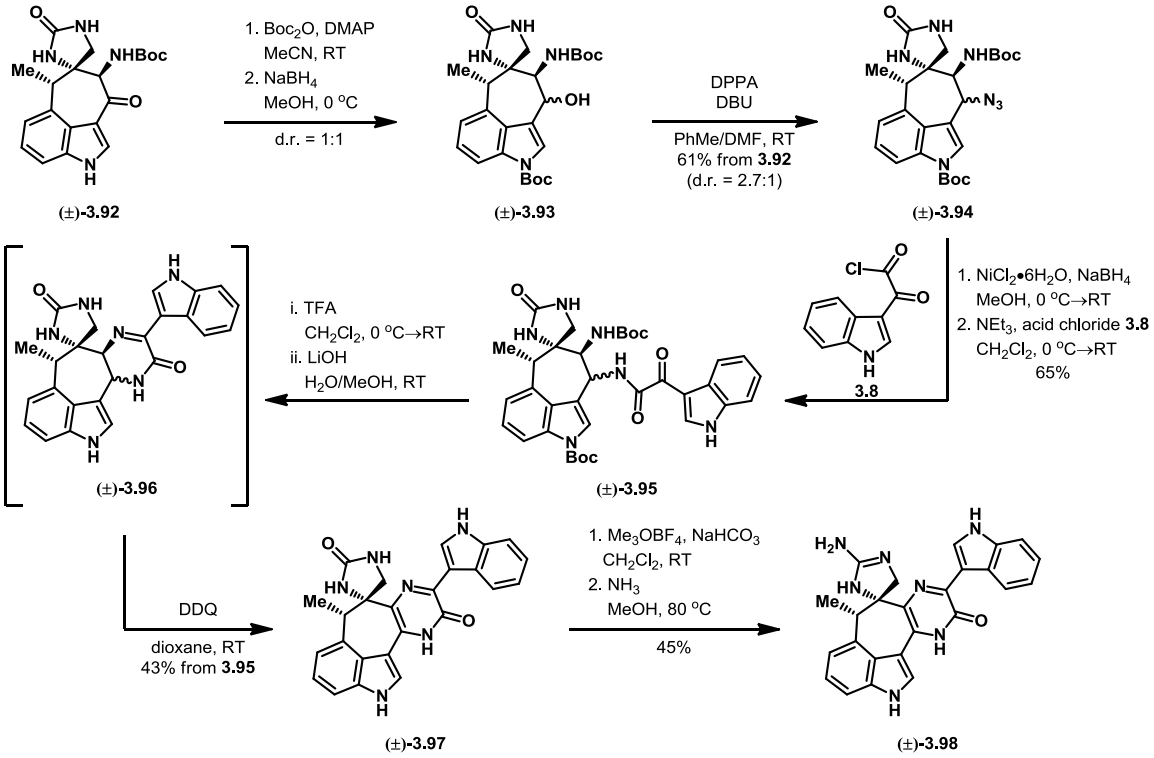

Scheme 3.28. Feldman and Ngernmeesri's completed synthesis of a dragmacidin E analog.

The first task undertaken by the authors in this report was the conversion of the ketone moiety into an amine. This is a notable change from their original retrosynthetic approach to dragmacidin E that sought to utilize a cyclocondensation of aminoketone **3.80** with ketoamide **3.79** (refer back to Scheme 3.24). This might suggest that such an approach was tried and met without success, however, the authors do not make any

comments related to this. With their new approach to forming the pyrazinone ring in mind, Feldman and Ngernmeesri discovered that attempts to install nitrogen functionality through imine formation or reductive amination only resulted in Boc deprotection of aminoketone **3.92** (Scheme 3.28). A 3-step sequence ultimately led to the installation of the desired nitrogen functionality as the azide, and this was accomplished by: 1) Boc-protection of the indole nitrogen; 2) reduction of the ketone by sodium borohydride; and 3) azide substitution of the resulting alcohol via a Mitsunobu-like protocol. Interestingly, while alcohol **3.93** was formed as an equal mixture of diastereomers in this sequence, azide **3.94** was formed in nearly a 3-to-1 ratio of diastereomers favoring the α–isomer. Pertinent to this observation is that roughly 15% of a single diastereomer of alcohol **3.93** was recovered from the Mitsunobu reaction. Eventually, the stereochemistry at this position would be ablated, so azide **3.94** was carried on as a mixture of diastereomers.

Nickel borohydride reduction of azide **3.94**, followed by amide coupling with acid chloride **3.8** provided the cycloaddition precursor **3.95** in moderate yield (see Scheme 3.28 above). Prior to carrying out this cyclocondensation, the authors were concerned about two aspects in particular: 1) finding conditions that would permit removal of the Boc group present on the primary nitrogen without concomitant loss of the oxalylindole fragment as a whole; and 2) the energetic barrier that would need to be overcome to form the requisite *s*-cis amide bond conformer. To that end, trifluoroacetic acid accomplished the task of Boc deprotection while avoiding decomposition. The resulting ammonium trifluoroacetate salt was then treated with base and furnished what was presumed to be dihydropyrazinone **3.96**. The authors noted that the crude product formed in this reaction

was too unstable to isolate, and that attempts to air oxidize the crude reaction mixture led to decomposition. DDQ oxidation of the crude iminoamide **3.96**, on the other hand, led to cleaner formation of the desired pyrazinone **3.97** and only a small amount of decomposition.

Completion of a dragmacidin E analog was achieved through a 2-step procedure consisting of: 1) conversion of the urea moiety in pyrazinone **3.97** to the methoxy amidine using Meerwein's salt, and 2) heating the methoxy amidine with ammonia at elevated temperatures in a sealed tube. This sequence provided dragmacidin E analog **3.98** in a moderate 45% yield.

3.3.3 Feldman's Synthesis of (±)–Dragmacidin E

Not long after having reported their successful synthesis of a dragmacidin E analog, Feldman and Ngernmeesri published the first and, to date, only completed total synthesis of dragmacidin E.[32] Given the similarity of their previously-made analog to the natural product, it comes as no surprise that the vast majority of the synthetic sequence was able to be kept intact.

Feldman and Ngernmeesri's synthesis of dragmacidin E required the synthesis of a new Witkop cyclization substrate. They began with known[36] indole **3.99** (Scheme 3.29). Installation of the aldehyde at the indole 3-position was accomplished with a Vilsmeier-Haack formylation. This was followed by protection of the indole nitrogen as the 2-(trimethylsilyl)ethoxycarbamate (TEOC), giving aldehyde **3.100** in moderate yield over two steps. Aldehyde **3.100** was then coupled with phosphorylacetate **3.101**via a Horner-

Wadsworth-Emmons olefination to give *Z*-alkene **3.102** in good yield. Wilkinson's catalyst was used to hydrogenate the alkene, which also resulted in cleavage of the phenolic diphenylmethyl ether protecting group. Subsequent deprotection of the indole nitrogen delivered Witkop cyclization precursor **3.83a** in excellent yield over two steps.

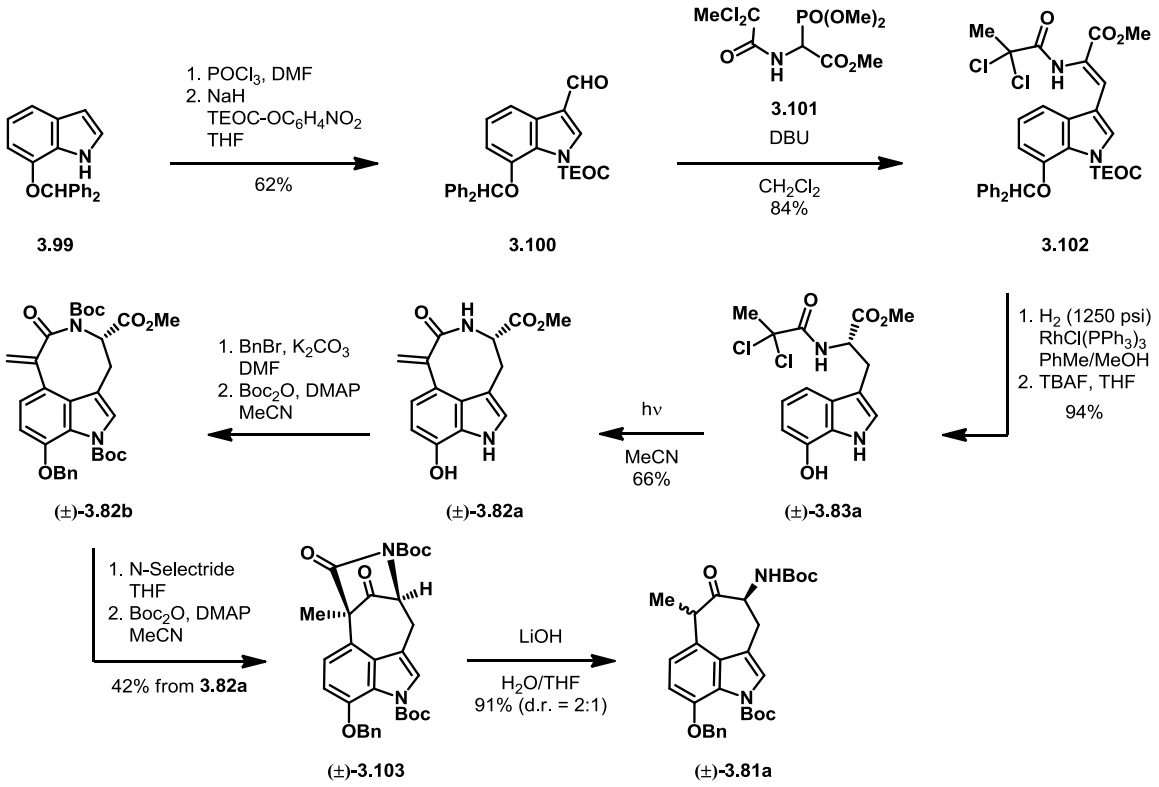

Scheme 3.29. Feldman and Ngernmeesri's synthesis of a dragmacidin E core structure, utilizing protocols previously established in their synthesis of a natural product analog.

Witkop cyclization of chloroamide **3.83a** gave the desired cyclooctane **3.82** in significantly higher yield compared to the previous analog, albeit at a modest 66% (see Scheme 3.29 above). Following a successful Witkop cyclization the phenol was protected as the benzyl ether, after which point the amide and indole nitrogens were also protected as the Boc carbamates. Conjugate reduction of enamide **3.82b** induced the desired

intramolecular Dieckmann condensation, which again resulted in the incidental removal of the amide Boc group. Re-protection of the amide nitrogen as the Boc carbamate gave bicycle **3.103** in good yield over this 4-step sequence. Ring opening of bicycle **3.103** through basic hydrolysis provided aminoketone **3.81a** as a mixture of diastereomers, which was inconsequential as epimerization of the α–stereocenter was anticipated to occur in the next transformation.

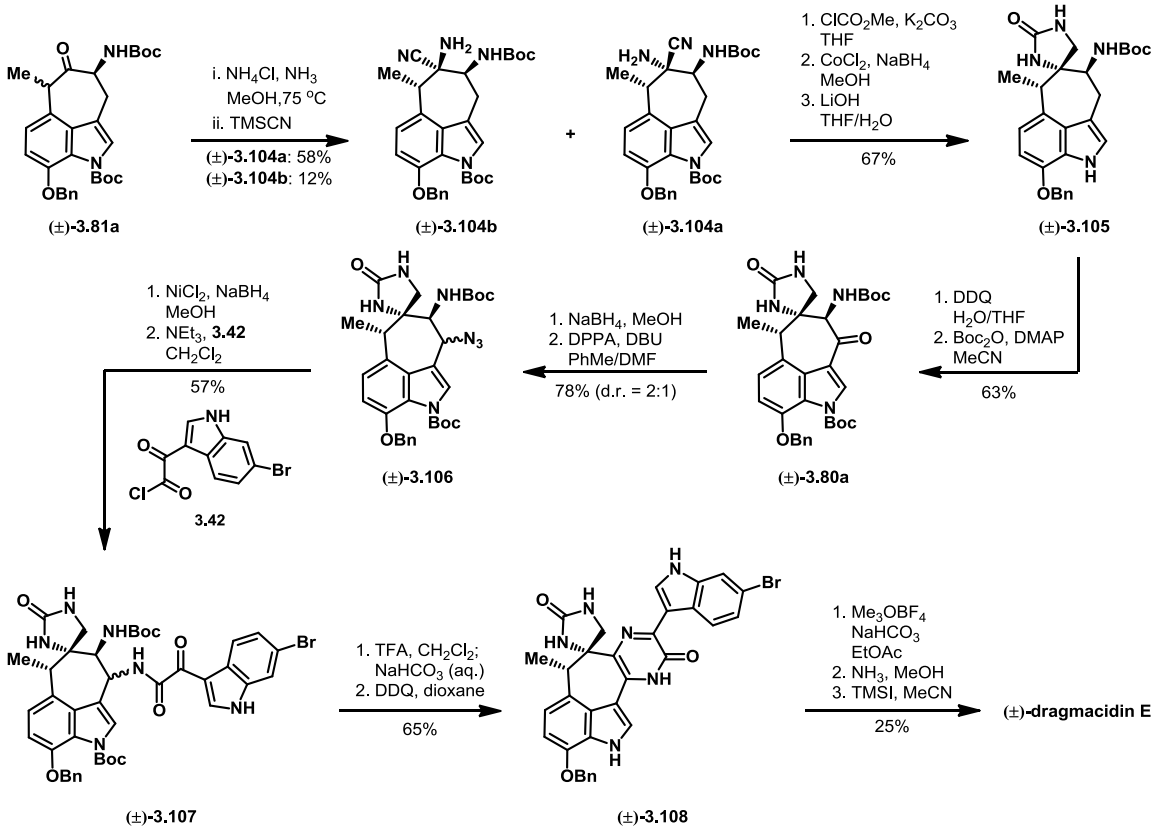

Scheme 3.30. Feldman and Ngernmeesri's successful completion of (±)–dragmacidin E.

A Strecker reaction of ketone **3.81a** did provide the desired aminonitrile **3.104**, but unlike the Strecker reaction used in the synthesis of a dragmacidin E analog, this reaction gave aminonitrile **3.104** as a mixture of diastereomers. The major diastereomer

was the desired aminonitrile **3.104a**, but it is nonetheless surprising that the presence of the remote 7-benzyloxy substituent on the indole had such a large effect on the outcome of this reaction. Fortunately, the two diastereomers could be chromatographically separated, after which point aminonitrile **3.104a** was efficiently converted to cyclic urea **3.105** through a 3-step synthetic sequence, similar to that used in the model study, consisting of: 1) acylation of the free amine; 2) reduction of the nitrile to the primary amine; and 3) base-promoted cyclization.

The endgame strategy previously developed in the synthesis of the natural product analog proved to be amenable to the completion of (±)–dragmacidin E. DDQ oxidation was again used to install the ketone moiety in (see Scheme 3.30 above). From aminoketone **3.80a**, sodium borohydride reduction and Mitsunobu substitution provided azide **3.106** as an inconsequential mixture of diastereomers. Reduction of azide **3.106** and coupling with acid chloride **3.42** provided the cyclocondensation precursor **3.107** in moderate yield. Similar to their previous report, treatment of aminoamide **3.107** with trifluoroacetic acid followed by basic quenching and DDQ oxidation provided Feldman and Ngernmeesri with pyrazinone **3.108**. Methylation of the urea moiety in pyrazinone **3.108** with Meerwein's salt and subsequent condensation with ammonia introduced the guanidine functionality. This was followed by removal of the benzyl protecting group with TMSI, giving (±)–dragmacidin E in moderate yield over the final three steps. The final structure was confirmed by the comparison of ^{1}H and ^{13}C NMR data to that of natural dragmacidin E, as well as HPLC analysis of coinjected synthetic and natural samples.

3.4. Chapter 3 Concluding Remarks

The dragmacidins are a biologically-relevant family of natural products that contain two indole moieties linked by either a piperazine or pyrazinone ring. Dragmacidins D, E, and F contain a pyrazinone linker and have been the subject of a number of synthetic and biological activity studies. Assignment of the absolute configuration of dragmacidin F was first determined by Stoltz, who hypothesized that dragmacidins D and E should have the same configuration as dragmacidin F based on a biosynthetic relationship. Following this, there have been conflicting reports in the literature regarding the absolute configuration of dragmacidin D. Recent reports have supported the hypothesis put forth by Stoltz and have also shed light on the stability and stereo-lability of dragmacidin D in solution, which has serious implications for the biological activity this molecule has displayed. The absolute configuration of dragmacidin E has still not been confirmed, as its preparation in an enantiopure form has yet to be reported. This is likely the result of the unique synthetic challenges present in the core structure of dragmacidin E.

3.5. Chapter 3 References

1) Kohmoto, S.; Kashman, Y.; McConnell, O. J.; Rinehart, K. L. Jr.; Wright, A.; Koehn, F. *J. Org. Chem.* **1988**, *53*, 3116-3118.

2) Morris, S. A.; Andersen, R. J. *Tetrahedron* **1990**, *46*, 715-720.

3) Capon, R. J.; Rooney, F.; Murray, L. M.; Collins, E.; Sim, A. T. R.; Rostas, J. A. P.; Butler, M. S.; Carrol, A. R. *J. Nat. Prod.* **1998**, *61*, 660-662.

4) Wright, A. E.; Pomponi, S. A.; Cross, S. S.; McCarthy, P. *J. Org. Chem.* **1992**, *57*, 4772-4775.

5) Garg, N. K.; Stoltz, B. M. *Chem. Commun.* **2006**, *0*, 3769–3779.

6) Longley, R. E.; Isbrucker, R. A.; Wright, A. E. Use of Imidazole And Indole Compounds as Inhibitors of Nitric Oxide Synthase. US006087363A, 1999

7) Molina, J. A.; Jimenez-Jimenez, F. J.; Orti-Pareja, M.; Navarro, J. A. *1998* **1998**, *12*, 251-259.

8) Cutignano, A.; Bifulco, G.; Bruno, I.; Casapullo, A.; Gomez-Paloma, L.; Riccio, R. *Tetrahedron* **2000**, *56*, 3743-3748.

9) Garg, N. K.; Sarpong, R.; Stoltz, B. M. *J. Am. Chem. Soc.* **2002**, *124*, 13179-13184.

10) Hashem, M. A.; Sultana, I.; Hai, M. A. *Indian J. Chem., Sect. B* **1999**, *38*, 789-794.

11) Bartoli, G.; Palmieri, G.; Bosco, M.; Dalpozzo, R. *Tetrahedron Lett.* **1989**, *30*, 2129-2132.

12) Barlin, G. B. *Aust. J. Chem.* **1983**, *36*, 983-992.

13) Dess, D. B.; Martin, J. C. *J. Org. Chem.* **1983**, *48*, 4155-4156.

14) Luzzio, F. A. *Tetrahedron* **2001**, *57*, 915-945.

15) Garg, N. K.; Caspi, D. D.; Stoltz, B. M. *J. Am. Chem. Soc.* **2004**, *126*, 9552-9553.

16) Stoltz, B. M. *Chem. Lett.* **2004**, *33*, 362-367.

17) Manthey, M. K.; Gonzalez-Bello, C.; Abell, C. *J. Chem. Soc., Perkin Trans. 1* **1997**, *5*, 625-628.

18) Poli, G.; Prestat, G.; Liron, F.; Kammerer-Pentier, C. Selectivity in Palladium-Catalyzed Allylic Substitution In *Transition Metal Catalyzed Enantioselective Allylic Substitution in Organic Synthesis*; Kazmaier, U., Ed.; Springer: Berlin, 2012, p 1-64.

19) Neber, P. W.; Friedolsheim, A. *Ann.* **1926**, *449*, 109–134.

20) Zhang, F.; Wang, B.; Prasad, P.; Capon, R. J.; Jia, Y. *Org. Lett.* **2015**, *17*, 1529 – 1532.

21) Qian, X.; Russel, K. C.; Boteju, L. W.; Hruby, V. J. *Tetrahedron* **1995**, *51*, 1033−1054.

22) Jia, Y.; Zhu, J. *J. Org. Chem.* **2006**, *71*, 7826−7834.

23) Feldman, K. S.; Ngernmeesri, P. *Org. Lett.* **2010**, *12*, 4502−4505.

24) Jackson, J. J.; Kobayashi, H.; Steffens, S. D.; Zakarian, A. *Angew.Chem. Int. Ed.* **2015**, *54*, 9971-9975.

25) Larock, R. C.; Yum, E. K. *J. Am. Chem. Soc.* **1991**, *113*, 6689 – 6690.

26) Stivala, C. E.; Zakarian, A. *J. Am. Chem. Soc.* **2011**, *133*, 1936–11939.

27) Mandal, D.; Yamaguchi, A. D.; Yamaguchi, J.; Itami, K. *J. Am. Chem. Soc.* **2011**, *133*, 19660–19663.

28) Tokuyama, H.; Yokoshima, S.; Yamashita, T.; Fukuyama, T. *Tetrahedron Lett.* **1998**, *39*, 3189-3192.

29) Feldman, K. S.; Ngernmeesrib, P. *Synlett* **2012**, *23*, 1882–1892.

30) Feldman, K. S.; Ngernmeesri, P. *Org. Lett.* **2005**, *7*, 5449-5452.

31) Huntley, R. J.; Funk, R. L. *Org. Lett.* **2006**, *8*, 4775-4778.

32) Feldman, K. S.; Ngernmeesri, P. *Org. Lett.* **2011**, *13*, 5704–5707.

33) Wang, B.; Qin, H.; Zhang, F.; Jia, Y. *Tetrahedron Lett.* **2014**, *55*, 1561–1563.

34) Inoue, N.; Nakano, S.-I.; Harada, S.; Hamada, Y.; Nemoto, T. *J. Org. Chem.* **2017**, *82*, 2787−2793.

35) Yonemitsu, O.; Cerutti, P.; Witkop, B. *J. Am. Chem. Soc.* **1966**, *88*, 3941-3945.

36) Dobson, D.; Todd, A.; Gilmore, J. *Synth. Commun.* **1991**, *21*, 611–617.

CHAPTER 4: EFFORTS TOWARD THE TOTAL SYNTHESIS OF DRAGMACIDIN E

4.1. Introduction

Chapter 3 introduced the dragmacidin family of natural products and elaborated on some of the more important syntheses reported in the literature for family members bearing a pyrazinone linker. Although there have been conflicting reports in the literature, recent evidence[1] would suggest a biosynthetic relationship between dragmacidins D, E, and F wherein the absolute configuration of the shared (6''') stereocenter is conserved. Given their widespread and often potent bioactivity, firm establishment of the absolute configuration of the dragmacidins is an important measure of control for further biological testing. While dragmacidins D and F have reasonable evidence for the

assignment of their absolute stereochemistry, dragmacidin E has never been made in an asymmetric manner.

The unique synthetic challenges present in dragmacidin E are likely contributing factors to the absence of its asymmetric synthesis. Perhaps the most significant difference between dragmacidin E and dragmacidins D and F is the presence of a 7-membered carbocyclic ring. Rings of this size are often difficult to produce through traditional ring-forming reactions, as such cyclizations are entropically unfavorable. Furthermore, 7-membered rings consisting of an all-carbon skeleton are an even greater challenge, as the absence of heteroatoms makes establishing appropriately reactive nucleophile-electrophile pairs more difficult.

We envisioned the intramolecular alkene hydroacylation methodology developed by our group (discussed in Chapter 2) being a potential solution to the challenging 7-membered carbocyclic motif present in dragmacidin E. Enantioselective variants of our methodology could allow for catalyst control if needed, but we also anticipated the possibility of using substrate control to direct a diastereoselective cyclization. Our approach to synthesizing dragmacidin E is outlined in the following section.

4.1. Retrosynthetic Analysis

Our retrosynthetic approach to dragmacidin E borrows from previous dragmacidin syntheses as we envisioned installing the sensitive guanidine subunit in the later stages of the synthesis (Scheme 4.1).

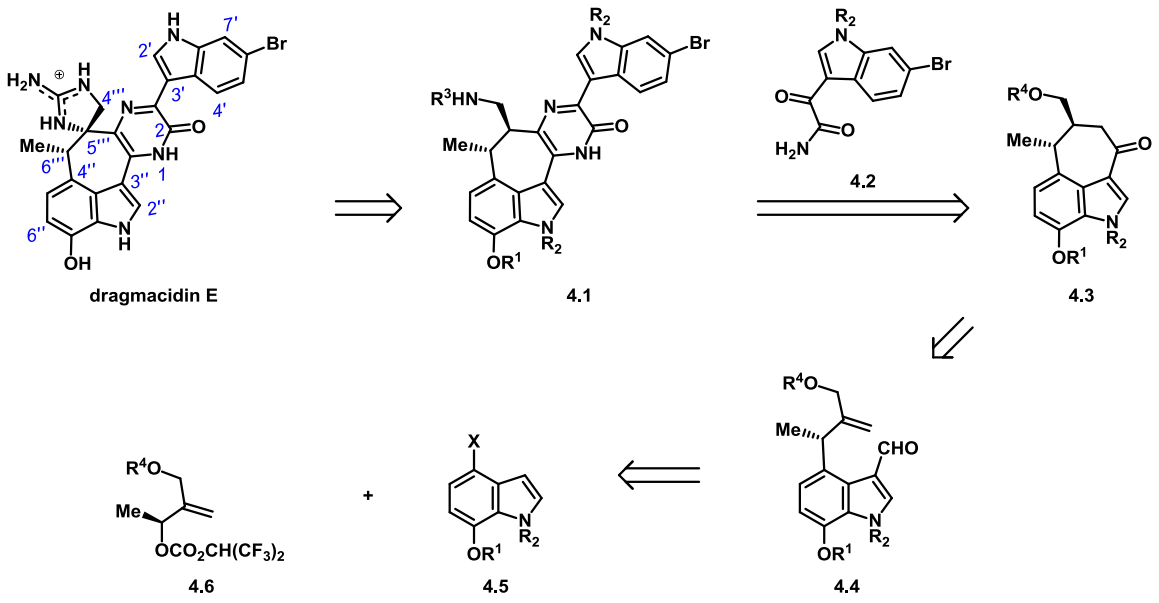

Scheme 4.1. Our retrosynthetic approach to the synthesis of dragmacidin E.

An acyclic guanidine moiety could be introduced via the protected amine in pyrazinone **4.1** (see Scheme 4.1 above). The acyclic guanidine could then be cyclized through an intramolecular C–H amination methodology developed by Du Bois.[2] Pyrazinone **4.1** was thought to be available through a cyclocondensation between ketoamide **4.2** and an α–aminoketone derived from cycloheptanone **4.3.** This disconnection, unlike those used in other dragmacidin syntheses, benefits from having the substrates in the same overall oxidation state as the desired pyrazinone **4.1**. This would obviate the need for subsequent oxidations, and the direct formation of the aromatic ring should provide an additional driving force for the reaction. As such, we viewed cycloheptanone **4.3** as a key intermediate for our synthesis. We anticipated intramolecular alkene hydroacylation of aldehyde **4.4** would provide the necessary cycloheptanone skeleton. If successful, this cyclization would represent the key step of

our synthesis and demonstrate the power of this methodology. The highly functionalized indolylaldehyde **4.4** was thought to be available through an allylic arylation methodology reported by Evans.[3] In this approach, haloindole **4.5** could be converted to the corresponding organozinc halide and coupled to allylic carbonate **4.6** through the use of a transition metal catalyst.

The allylic arylation methodology reported by Evans was shown to occur in a stereospecific manner.[3] If enantioenriched allylic carbonate **4.6** could be accessed, then an enantioselective synthesis should be possible. Considering that allylic carbonate **4.6** would, in all likelihood, be made from the corresponding secondary alcohol, accessing enantioenriched material through a Corey-Bakshi-Shibata (CBS) reduction[4] seemed reasonable. Furthermore, the allylic stereocenter present in aldehyde **4.4** may allow for a diastereoselective intramolecular alkene hydroacylation (Figure 4.1). This would require the C–H activation intermediate **4.7** to preferentially adopt a conformation wherein $A^{1,3}$ strain would be minimized. If $A^{1,2}$ strain was an equally-important or predominant factor, however, then catalyst control would be required to arrive at the necessary configuration for what would ultimately be the (5’’’) stereocenter.

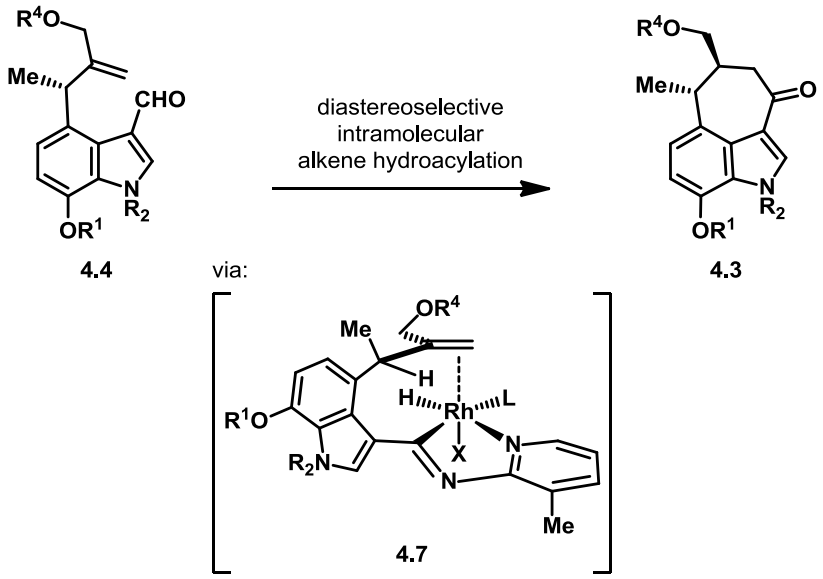

Figure 4.1. Minimization of $A^{1,3}$ strain, allowing for diastereoselective hydride insertion.

Before investing in an enantioselective synthesis of dragmacidin E, it seemed prudent to us to carry out a synthesis of racemic dragmacidin E first. As such, our first task was to obtain racemic indolylaldehyde **4.4** in order to test the key intramolecular alkene hydroacylation step.

4.2. Synthetic Attempts Toward an Alkene Hydroacylation Precursor Utilizing Allylic Arylation

4.2.1 Research Proposal

Allylic substitution is a well-known and powerful method for forming carbon–carbon and carbon–heteroatom bonds.[5] A principal concern in these reactions is the regioselectivity through which the substitution occurs (Scheme 4.2). Primary or secondary leaving groups (**4.8** and **4.9**, respectively) can both lead to either primary substituted products (**4.10**, sometimes referred to as the linear product) or secondary substituted products (**4.11**, sometimes referred to as the branched product). This is a

consequence of the formation of the electrophilic metal π–allyl intermediate, **4.12**. Both primary substrates **4.8** and secondary substrates **4.9** can lead to the same electrophilic metal π–allyl intermediate **4.12** through η^1–η^3–η^1 isomerization. Regioselectivity then depends primarily on: 1) the preference of the metal to adopt either **η^1-4.12a**, **η^3-4.12**, or **η^1-4.12b** coordination isomeric forms; and 2) the engagement of the nucleophile in either inner-sphere attack (i.e. direct attack at the metal center) or outer-sphere attack (i.e. attack at a carbon of the π–allyl ligand) of the electrophilic metal π–allyl intermediate **4.12**.

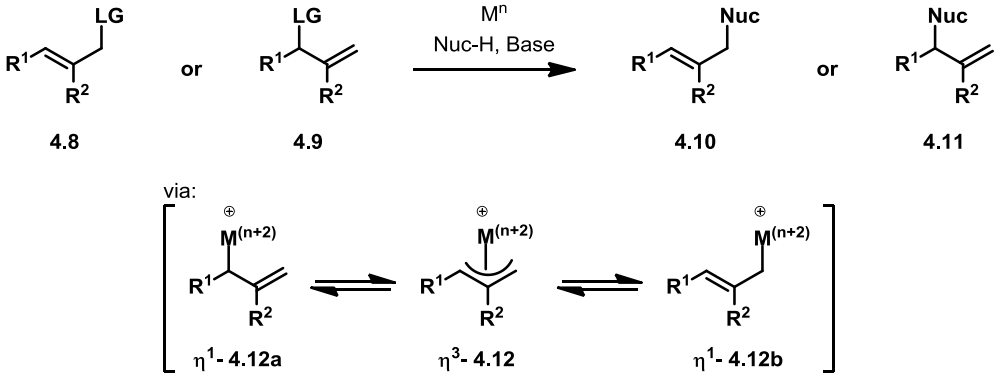

Scheme 4.2. Regioselectivity in transition metal catalyzed allylic substitution. LG = leaving group; Nuc = nucleophile; M = transition metal; n = oxidation state

In their 2003 report, Evans et al. disclosed the use of fluorinated allylic carbonates **4.13** as substrates for allylic substitution with organozinc nucleophiles (Scheme 4.3).[3] There are a number of aspects of this transformation worth discussing: 1) the regioselectivity highly favored the branched isomer **4.14** over the linear isomer **4.15**, which is hard to achieve with most transition metal catalysts. The use of fluorinated carbonates was said to help increase this selectivity for the branched isomer **4.14**. 2) The arylzinc nucleophiles used are regarded as non-stabilized carbon nucleophiles. This class of nucleophile is much less common in allylic substitution reactions due to their often

high level of non-catalyzed reactivity. 3) Rhodium is employed as the transition metal catalyst. Compared to other transition metals (such as Cu, Pd, and Ir), rhodium is less-commonly used in allylic substitution chemistry. 4) When an enantioenriched allylic carbonate (**4.13a**, Scheme 4.3b) was used, the branched product **4.14a** was formed with complete inversion of stereochemistry.

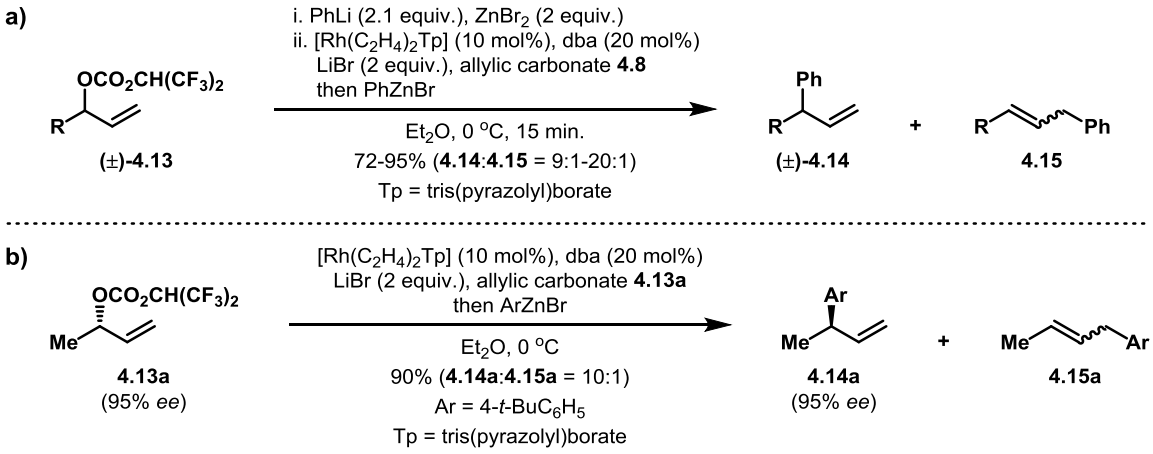

Scheme 4.3. Evans' report[3] on a) a general allylic arylation methodology featuring high branched-to-linear product ratios; b) a stereospecific arylation of an enantioenriched allylic carbonate.

We envisioned adopting the methodology reported by Evans toward the construction of our alkene hydroacylation precursor. To this end, we hypothesized that fluorinated allylic carbonate **4.6a** could undergo substitution with the organozinc nucleophile derived from haloindole **4.5a** to give the functionalized indole **4.16** (see Scheme 4.4 below).

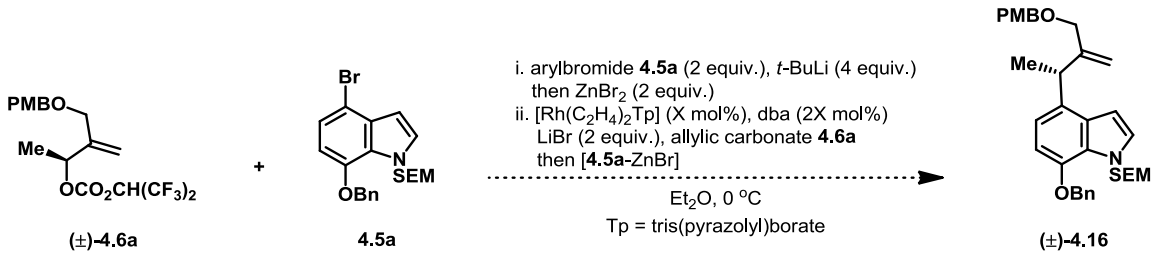

Scheme 4.4. Proposed arylation of allylic carbonate **4.6a**.

This strategy would constitute a convergent approach to the synthesis of indole **4.16**, with the added benefit of allylic carbonate **4.6a** and haloindole **4.5a** being nearly equal in molecular complexity. Furthermore, this would allow for an enantioselective synthesis of dragmacidin E, should enantiopure allylic carbonate **4.6a** be available.

4.2.2 Results

To test our hypothesis that an allylic arylation methodology would allow for efficient construction of an alkene hydroacylation precursor, the two coupling partners haloindole **4.5a** and allylic carbonate **4.6** would need to be synthesized. Haloindole **4.5a** was an intermediate used in Stoltz's synthesis of dragmacidin D (refer to Chapter 3, Section 3.2.1)[6] and was prepared according to the literature. Beginning with commercially-available phenol **4.17**, benzyl protection with benzyl bromide afforded arylnitro **4.18** in excellent yield without complication (Scheme 4.5).

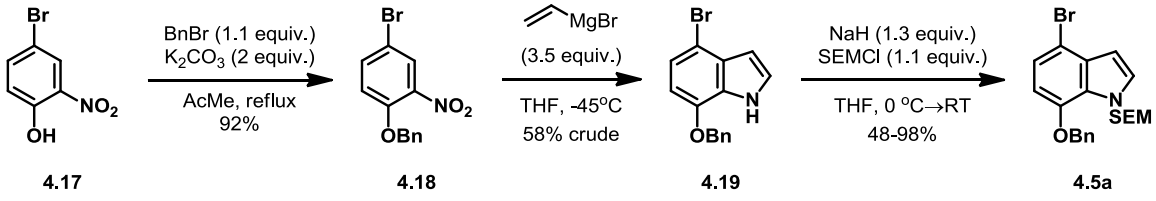

Scheme 4.5. Synthesis of haloidole **4.5a**.

Attempts at performing a Bartoli indole synthesis[7] with arylnitro **4.18**, however, were not as straightforward as the literature would suggest. It was found that temperature control in this reaction was critical to success, and the use of a cryogenic immersion cooler led to improved reaction outcomes. More importantly, it was found that the product of this reaction, indole **4.19**, was very unstable to silica gel chromatography. Despite the use of silica gel chromatography to purify indole **4.19** reported in the literature[6], in our hands silica gel chromatographic purification of indole **4.19** led to massive loss of material (often an order of magnitude less material, by mass, was recovered). Analysis of indole **4.19** by 2-dimensional TLC on both silica and alumina plates showed that decomposition was occurring. Indole **4.19** also happened to be a thick oil, which severely limited alternative methods of purification (e.g. distillation and/or recrystallization). This issue could be mitigated to a certain extent by simply carrying indole **4.19** forward in the synthesis without purification. Protection of the indole nitrogen as the [2-(trimethylsilyl)ethoxy]methyl *N*,*O* acetal (SEM) gave the desired indole **4.5a** in isolated yields that varied greatly. This discrepancy in isolated yield is also the result of decomposition that occurs during chromatographic purification.

Synthesis of allylic carbonate **4.6a** could be accomplished in 4 synthetic steps from methylvinylketone (see Scheme 4.6 below). A known Baylis-Hillman reaction[8] of methylvinyl ketone with formaldehyde gave allylic alcohol **4.20** in moderate yield after vacuum distillation.

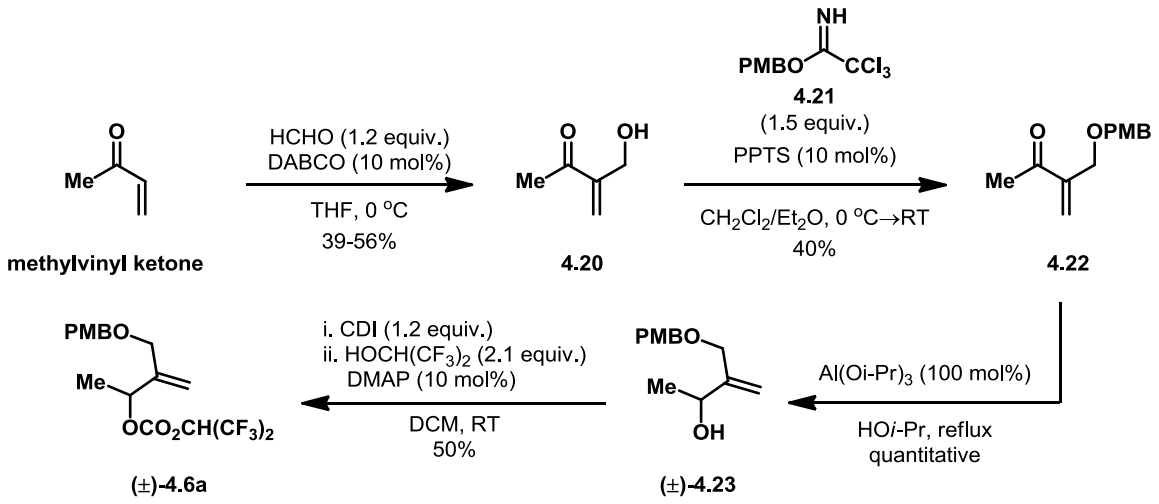

Scheme 4.6.Synthesis of allylic carbonate **4.6a**.

The alcohol moiety was then protected as the *para*-methoxybenzyl (PMB) ether (**4.22**) according to a modified literature procedure (Scheme 4.6).[9] Trichloroacetimidate **4.21** (available in a single step from trichloroacetonitrile and *para*-methoxybenzyl alcohol)[10] was used to allow for an acid-catalyzed transformation. The literature procedure utilized camphor sulfonic acid as the catalyst but, due to a lack of availability, pyridinium para-toluenesulfonate (PPTS) was used as an alternative organic-soluble acid catalyst. The use of PPTS as an acid catalyst met with limited success. An observable amount of precipitate developed as this reaction progressed, which was hypothesized to be the trichloroacetamide byproduct. A leveling-off of reaction conversion (around 80%) was also observed, which led to the hypothesis that perhaps the precipitate being formed was actually that of the protonated trichloroacetamide byproduct, as this would result in sequestration of the acid catalyst. As such, conversion was monitored over time using different catalyst loadings. Surprisingly, the leveling-off of reaction conversion seemed to be uniform, regardless of catalyst loading. Purification of enone **4.22** was also

complicated, as trichloroacetimidate **4.21** decomposes on silica gel to give multiple spots with retention factor (R_f) values near that of enone **4.22**. In hindsight, this could probably be mitigated by using lower stoichiometries of trichloroimidate **4.21** in this reaction.

Reduction of enone **4.22** through a Meerwein-Ponndorf-Verley protocol allowed for the efficient formation of allylic alcohol **4.23** (see Scheme 4.6 above). Allylic alcohol **4.23** could then be converted to the fluorinated allylic carbonate via the procedure outlined by Evans et al.[3] This gave allylic carbonate **4.6a** in a yield comparable to those for substrates in the literature report.

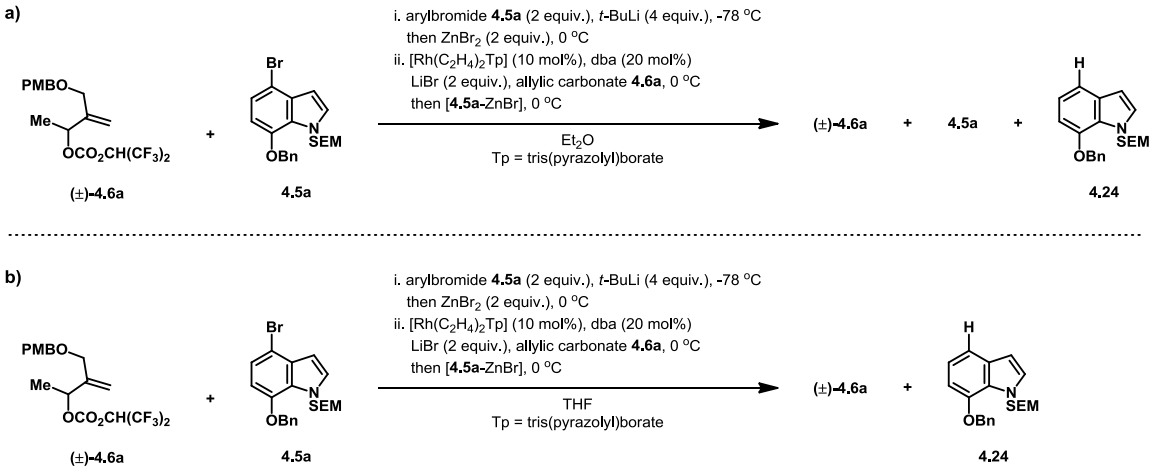

Scheme 4.7. Attemped coupling of allylic carbonate **4.6a** and haloindole **4.5a** using a) diethyl ether as the reaction solvent; and b) using THF as the reaction solvent..

With allylic carbonate **4.6a** and haloindole **4.5a** in hand, we attempted to couple the two together using Evan's protocol. The first attempt used diethyl ether as the solvent, which only gave back starting material and some of the dehalogenated indole **4.24** (Scheme 4.7a). This was likely the result of poor solubility of haloindole **4.5a** at low temperatures; while haloindole **4.5a** is soluble in diethyl ether at room temperature, it was

found to crash out of solution once cooled to -78 ^{o}C. Switching the solvent to THF obviated solubility issues, but still resulted in only the formation of dehalogenated indole **4.24** after workup.

The formation of dehalogenated indole **4.24** suggests that lithium-halogen exchange occurs smoothly, and thus it seemed to us that the problem likely involved the formation of the organozinc from the organolithium. Zinc halide salts tend to be very hygroscopic and even though rigorous drying was performed, it was possible that the $ZnBr_2$ reagent still contained some amount of water that was quenching the organolithium derived from haloindole **4.5a**. Furthermore, formation of the organolithium reagent from the arylhalide through lithium-halogen exchange was a departure from the procedure reported by Evans, as commercial sources of phenyllithium were used in those cases.

Since the formation of the organozinc reagent was hypothesized to be the source of reactivity issues, we began by examining the formation of phenylzinc bromide from bromobenzene using lithium halogen exchange, followed by treatment with $ZnBr_2$. To this end, No-D NMR proved to be invaluable. Treatment of a THF solution of bromobenzene with *t*-BuLi results in the formation of phenyllitium, along with a minor amount of benzene that results from protonation of the generated organolithium (see Figure 4.2a below). Of note is that the protons *ortho* to the metal center are shifted downfield relative to benzene. While counter-intuitive from an inductive effect standpoint, an anisotropic effect has been presented in the literature to account for this

phenomenon.[11] Furthermore, treatment of an aliquot of this reaction mixture with $ZnBr_2$ then results in a noticeable upfield chemical shift, relative to the organolithium, for the aromatic protons *ortho* to the metal (see Figure 4.2b below). This change in chemical shift for the organozinc is also in agreement with the literature.[11]

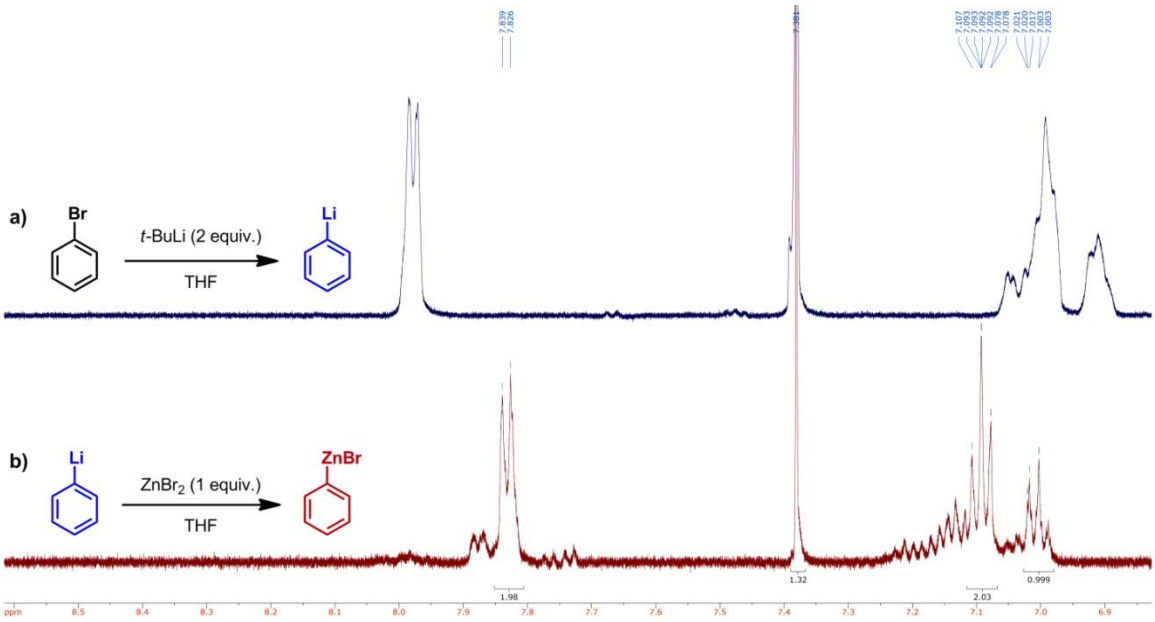

Figure 4.2. No-D NMR spectra for a) lithiation of bromobenzene; and b) transmetallation of *in situ* formed phenyllithium with $ZnBr_2$.

Confident that formation of the organozinc was not the source of the observed lack of reactivity, we sought to test various reaction parameters on a substrate reported by Evans. This would allow us to use less precious material, as well as provide us with a point of reference through which to compare reaction outcomes. As such, allylic carbonate **4.13b** was prepared in just two steps from commercially-available phenylacetaldehyde (Scheme 4.8). Treatment of phenylacetaldehyde with vinylmagnesium bromide afforded allylic alcohol **4.25** in excellent yield as the racemate.

Conversion of allylic alcohol **4.25** to the imidazole carbamate, followed by treatment with hexafluoroisopropanol furnished allylic carbonate **4.13b** in moderate yield.

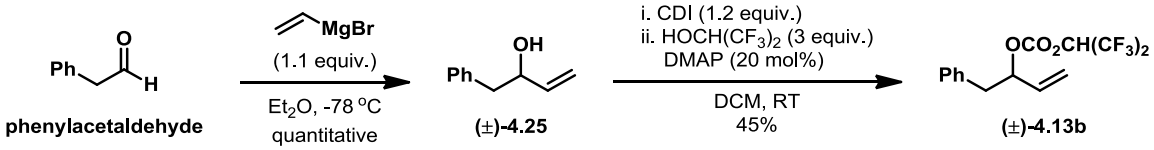

Scheme 4.8. Synthesis of the known allylic carbonate **4.13b**.

With allylic carbonate **4.13b** in hand, we began our examination by seeing if the use of THF as the solvent may have been a contributing factor for the lack of reactivity we had observed in our previous trials, as this was another notable deviation from the literature procedure. It should be noted that the use of lithium-halogen exchange to form the aryllithium does generate an equivalent of lithium bromide as a byproduct, which is another point of deviation from the methodology reported by Evans. Considering that 2 equivalents of lithium bromide were intentionally added in that methodology, however, we believed that this generation of lithium bromide byproduct would not be a significant factor in the outcome of the reaction.

To test our hypothesis that the use of THF as the reaction solvent was having a detrimental effect, side-by-side reactions were performed. Based on our previous results we knew that diethyl ether would not be a viable solvent for the generation of the organozinc (due to substrate solubility issues), but could still be used as part of a solvent system in the reaction. As such, both side-by-side reactions used diethyl ether as the solvent for the catalyst and allylic carbonate **4.13b** mixture (see Table 4.1 below, entries 1 & 2). The difference between the two was the use of either THF or diethyl ether as the

solvent in which phenylzinc bromide was being generated (entries 1 & 2, respectively). As can be seen in Table 4.1, the use of THF as a solvent did result in dramatically reduced conversion, as well as much poorer regioselectivity for the desired branched product **4.14b**.

We hypothesized that the coordinating ability of THF might be affecting the efficiency of the Rh(I) catalyst. To test this hypothesis, we ran a reaction where THF was part of the solvent system used to pre-form the active catalyst (Table 4.1, entry 3). Consistent with our hypothesis, no substituted products were observed in this case.

We hypothesized that *t*-butylmethyl ether (MTBE) might be a good alternative ethereal solvent, as the bulky *t*-butyl group might inhibit coordination to the Rh(I) catalyst. Formation of phenylzinc bromide in MTBE, contrary to our hypothesis, resulted in poorer conversion than when THF was used (Table 4.1, entry 4). Interestingly, better regioselectivity for the desired branched product **4.14b** was also observed in this case.

Table 4.1. Attempts at reproducing Evans' results with modified allylic arylation conditions.

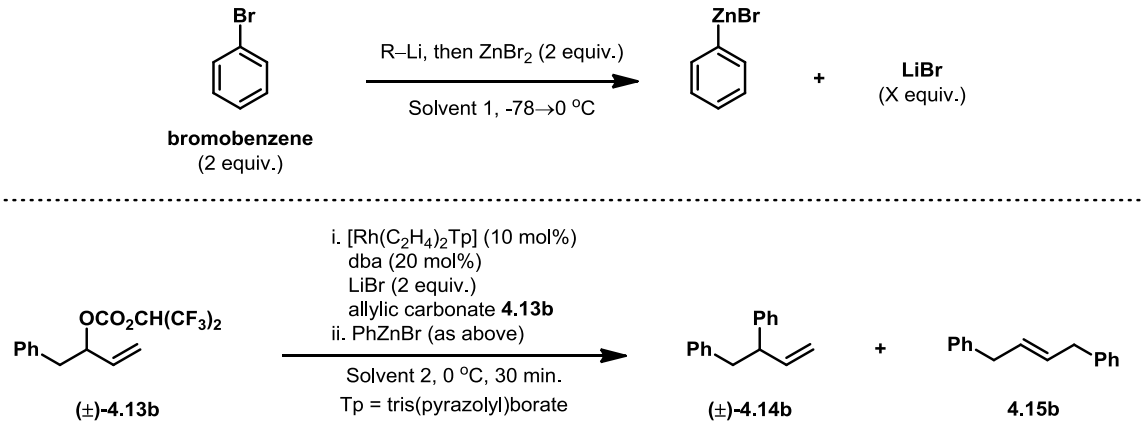

Entry[a]	R–Li (equiv.)	Byproduct LiBr equiv.	Solvent 1	Solvent 2	Product Distribution Ratios[b]		
					4.13b	**4.14b**	**4.15b**
1	*t*-BuLi (4 equiv.)	4	THF	Et_2O	13.1	1.1	1
2	*t*-BuLi (4 equiv.)	4	Et_2O	Et_2O	5.1	7.7	1
3	*t*-BuLi (4 equiv.)	4	Et_2O	Et_2O/THF (2:1)	1	0	0
4	*t*-BuLi (4 equiv.)	4	MTBE	Et_2O	37.6	6.41	1
5[c]	*n*BuLi (2.1 equiv.)	2	Et_2O	Et_2O	1	0	0

[a]The solution of *in situ* generated phenyllithium was cannulated into a solution of $ZnBr_2$. After allowing sufficient mix time, this solution was then slowly cannulated into a stirred solution of carbonate **4.13b**, $[Rh(C_2H_4)_2Tp]$, dba, and LiBr. [b]Determined via ^1H NMR integrations from crude reaction mixtures. [c]The formation of *n*BuBr as the byproduct of lithium halogen exchange may complicate results, as this alkyl halide may not be innocent in the presence of $[Rh(C_2H_4)_2Tp]$.

It was at this point that we began to question our assumption about the innocence of the lithium bromide byproduct being generated in the formation of phenyllithium. To test this hypothesis, we switched to using *n*BuLi as the lithium-halogen exchange reagent, as lithium bromide should not be produced in this exchange (Table 4.1, entry 5). Surprisingly, the formation of either substituted product was not observed in this case. In hindsight it would not be surprising if *n*BuBr, the byproduct of lithium-halogen exchange with *n*BuLi, was affecting the active Rh(I) catalyst more severely than lithium bromide.

As an additional means of testing the effect of metal-halogen salts on the reaction outcome, commercially-available phenylmagnesium bromide was used as the transmetallating reagent for the formation of phenylzinc bromide (Scheme 4.9). Diethyl ether was used as the sole reaction solvent in this case, and the results were comparable to those obtained when *t*-BuLi was used to facilitate lithium-halogen exchange in diethyl ether (see Table 4.1 above, entry 2), albeit with slightly less conversion.

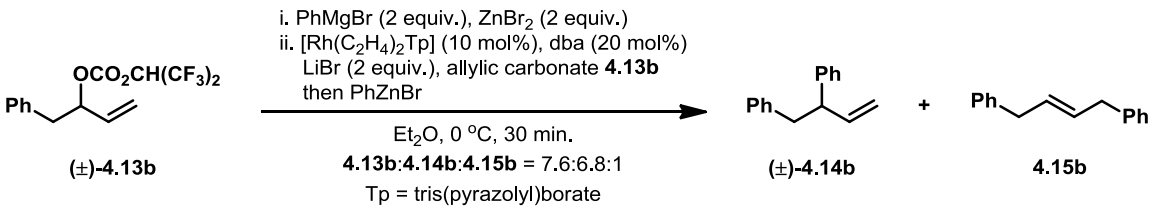

Scheme 4.9. Use of commercially-available phenylmagnesium bromide as the transmetallating agent in the arylation of allylic carbonate **4.13b**.

During our testing of Evans' methodology, another example was found in the literature where a similar allylic arylation was reported.[12] In this report by Martin et al., enantiopure allylic carbonate **4.26** underwent Rh(I)-catalyzed substitution with phenylzinc bromide to give substituted alkene **4.27** in excellent yield, with excellent regioselectivity and near-complete inversion of stereochemistry (see Scheme 4.10a below). This was attractive to us for a number of reasons: 1) the phenylzinc bromide nucleophile was formed through transmetallation with phenyllithium that was generated *in situ* through lithium-halogen exchange; 2) THF was used as the solvent in this reaction; 3) the reaction used a much simpler Rh(I) pre-catalyst that did not require additional additives.

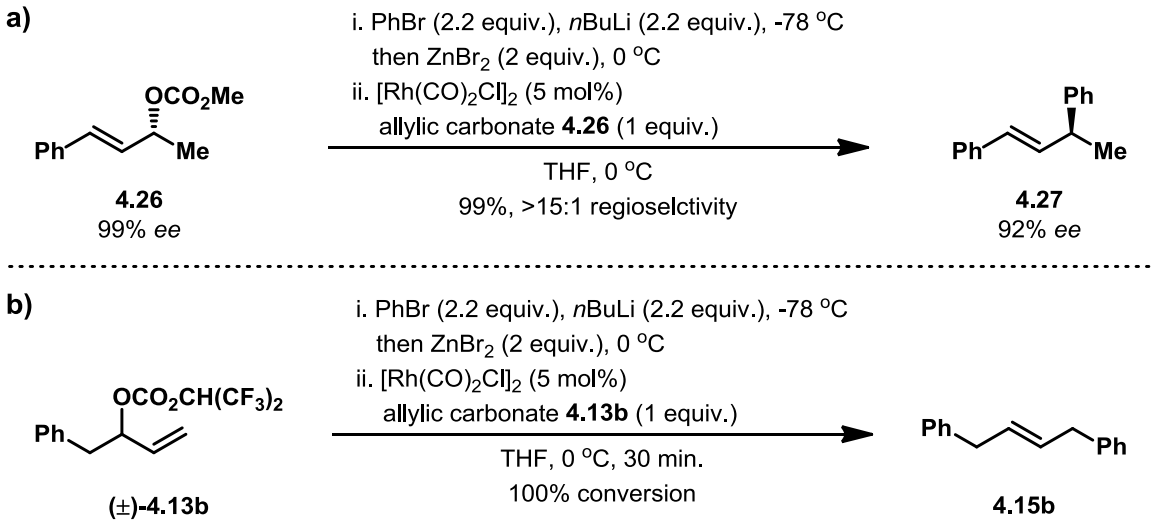

Scheme 4.10. a) Martin's report[12] on a regioselective and enantiospecific allylic arylation using a non-stabilized nucleophile; b) observed arylation of allylic carbonate **4.13b** using $[Rh(CO)_2Cl]_2$.

We then applied the methodology reported by Martin et al. to the substitution of allylic carbonate **4.13b** (Scheme 4.10b). This resulted in complete consumption of the starting allylic carbonate **4.13b**, but unfortunately led to the formation of the undesired alkene **4.15b** as the major product. Our results would seem to disagree with those reported by Martin, but this is likely just a consequence of different substrate biases. In Martin's case, substitution of allylic carbonate **4.26** at the terminus bearing the methyl group is likely favored for two reasons: 1) the methyl group poses less steric hindrance than the phenyl group, which could lead to a more favorable η^1-π-allyl intermediate bearing the metal at that site; 2) substitution at the terminus bearing the methyl group produces an alkene of greater stability, as conjugation with the phenyl ring is maintained. When allylic carbonate **4.13b** is used as a substrate, substitution at the methylene terminus is likely favored for similar reasons (in this case, substitution at the methylene

terminus results in the formation of the more stable disubstituted alkene, as opposed to the terminal alkene that would result from substitution at the benzyl terminus).

It was at this point that we began to assess all of our results for attempts at allylic arylation and considered if this route was still worth pursuing. For the following reasons, we viewed alternative courses of action prudent: 1) the dramatic and detrimental effect observed when diethyl ether, a solvent known to be incompatible with the actual synthetic substrate in this reaction, was not used as a solvent; 2) the observation of much lower conversion and regioselectivity than reported values[3]; 3) the use of an expensive [$Rh(C_2H_4)_2Tp$] pre-catalyst; 4) the subtle, yet dramatic, unknown effect that LiBr may have on both the active catalyst[13] and/or the organozinc nucleophile[14], as well as the possible interplay between these two effects; 5) the unknown scalability of this reaction, which could result in a bottle-neck of material throughput. Such a bottle-neck this early in the synthetic route would have more severe consequences than if it had occurred later on.

4.3. Synthetic Attempts Toward an Alkene Hydroacylation Precursor Utilizing an Indolyne Alder-Ene Reaction

4.3.1 Research Proposal

After our unsuccessful attempts to employ allylic arylation to construct the allylic stereocenter present in our alkene hydroacylation precursor, we looked to the literature for other ways that have been used to form stereogenic carbons with similar substitution patterns (e.g. stereogenic carbons bearing alkyl, vinyl, and aryl substituents). One example that piqued our interest was a report[15] by Liu et al. wherein benzyne

intermediates underwent Alder-Ene reactions with a number of alkene substrates. We were particularly interested in the reaction of benzyne precursor **4.28** with 2-methyl-2-butene to give allylic arene **4.30** upon treatment with a fluoride source (Scheme 4.11).

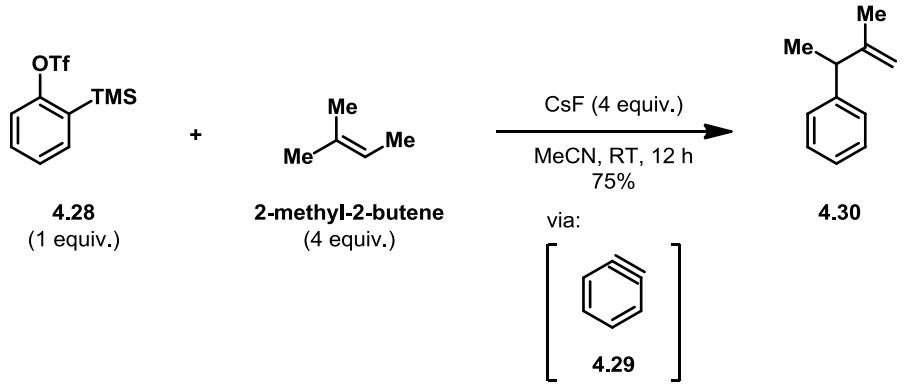

Scheme 4.11. Liu et al.'s report of a aryne-ene reaction to form an allylic and benzylic stereocenter.

We were interested in the possibility of utilizing an aryne-Alder-Ene reaction in part due to the work being done by Garg on the use of indolyne intermediates to generate functionalized indoles (see Scheme 4.12 below).[16-19] Following from benzyne formation protocols established by Kobashi[20], treatment of indolylsilyl triflate **4.31** with a fluoride source was able to generate indolyne **4.32**, which in the presence of furan produced Diels-Alder adduct **4.33** in good yield. The reaction of indolylsilyl triflate **4.31** with furan demonstrates an umpolung of the normal nucleophilic mode of indole reactivity, as indolyne **4.32** serves as an electrophile in this reaction. While this is not surprising, as benzyne is known to be a good electrophile, this methodology does provide a novel way to introduce substitution on the benzenoid ring of indole, which is difficult to do by traditional methods.

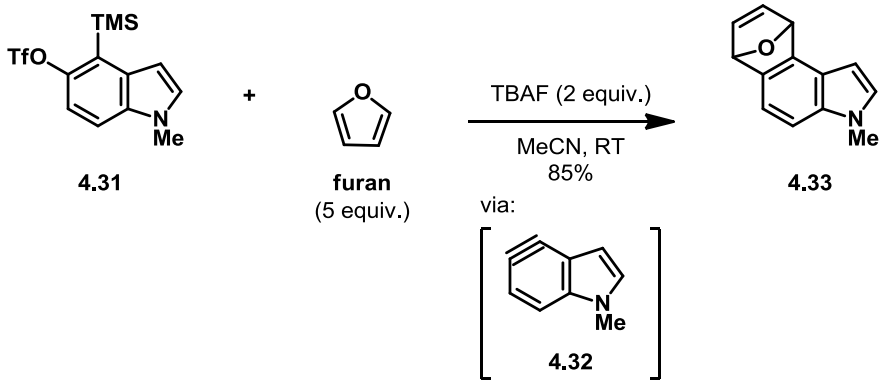

Scheme 4.12. Garg's use of indolyne as a dienophile in a Diels-Alder reaction with furan.

In that same report, Garg et al. reported the formal [2+2] and [3+2] cycloadditions of indolyne with ketene acetal **4.34** and benzylazide **4.37**, respectively (see Scheme 4.13 below). Unlike the cycloaddition reaction with furan, indolyne cycloaddition reactions with ketene acetal **4.34** or benzylazide **4.37** allowed for the formation of regioisomers. Upon treatment of indolylsilyl triflate **4.31** with fluoride in the presence of ketene acetal **4.34**, regioisomeric ketones **4.35** and **4.36** were produced in a 5.5-to-1 ratio (Scheme 4.13a).

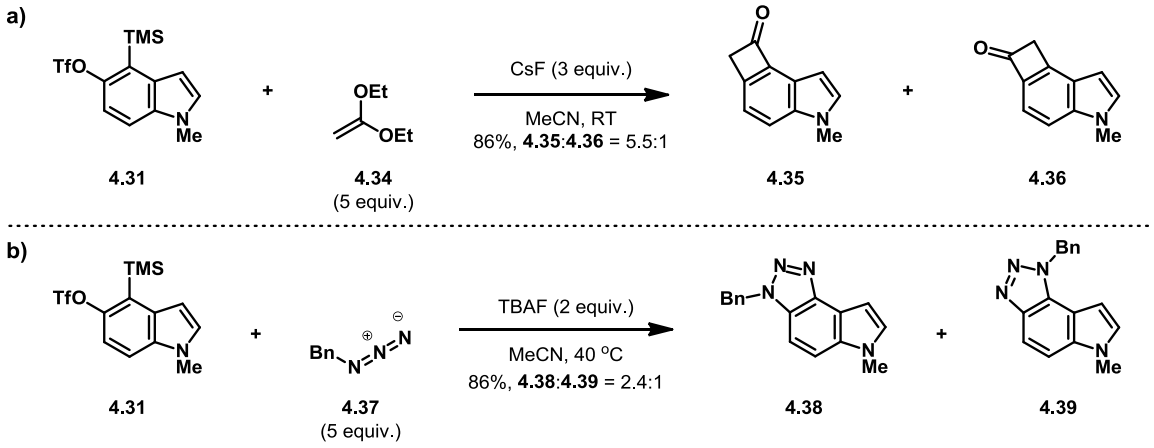

Scheme 4.13. Indolyne regioselectivity in a) a formal [2+2] cycloaddition with a highly polarized alkene; b) a formal [3+2] cycloaddition with a weakly polarized 1,3-dipole.

The major product in this formal [2+2] cycloaddition results from C–C bond formation between the terminal carbon in ketene acetal **4.34**, which bears a significant amount of partial negative charge due to electron donation from the two alcoxy subtituents, and C5 on the indole benzenoid ring. When the indolyne intermediate is formed in the presence of benzylazide **4.37**, a mixture of regioisomeric triazoles **4.38** and **4.39** are formed in only a 2.4-to-1 ratio. This is perhaps the result of a less electronically-biased nucleophile, as both the terminal and alkyl-bound nitrogens in benzylazide **4.37** bear a large amount of negative charge from electron delocalization, consistent with the 1,3-dipole nature of benzylazide **4.37**.

To gain insight into the source of the regioselectivity observed in indolyne reactions, a collaboration with Ken Houk was undertaken.[17] Density functional theory calculations from this collaboration suggested that there is significant distortion at the indole C3a ring juncture in indolyne **4.32**, which is accompanied by distortion of the internal C4 and C5 bond angles (Figure 4.3a).

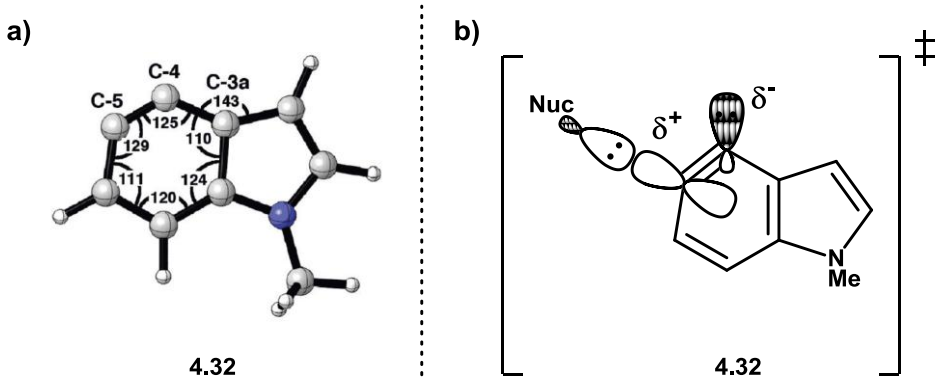

Figure 4.3. a) bond distortions in B3LYP/6-31G(d)-optimized structure for indolyne **4.32**; b) nucleophilic attack at indolyne **4.32** C5, leading to a flattening of the internal C5 bond angle and increased p-orbital character, along with constriction of the C4 internal bond angle and increased C4 s-orbital character.

Transition state calculations for nucleophilic attack on indolyne **4.32** suggested that a large amount of flattening (i.e. an increase in the internal bond angle) occurs at the site of attack, regardless of regioselectivity. This flattening leads to a large amount of p-orbital character development at the carbon being attacked, accompanied by a slight build-up of positive charge (see Figure 4.3b above). Consequent compression at the adjacent carbon results in greater s-character for that orbital, which helps to stabilize the negative charge build-up that occurs at that position. Nucleophilic attack at C5 in indolyne **4.32** would then be preferable, as the bond angle at that position is already distorted in a manner to accommodate the flattening that occurs in the transition state. As such, less distortion is needed to reach the necessary transition state geometry, which results in a lower energetic barrier.

The work reported by Garg and Houk shows a clear preference for nucleophilic attack at C5 for indolyne **4.32**. But as can be seen in Scheme 4.13, the regioselectivity for (formally) pericyclic reactions is correlated with an electronic bias of the arynophile. We

questioned what preference there might be, if any, for an arynophile lacking significant electronic bias. Specifically, we were curious what regiochemical preference might exist for indolyne **4.32** undergoing an Alder-Ene reaction with 2-methyl-2-butene (see Scheme 4.14a below), analogous to the benzyne Alder-Ene reaction reported by Liu et al. (refer to Scheme 4.11). We considered the hypothetical transition states for such regioisomeric pericyclic Alder-Ene reactions (**4.42a** and **4.42b**, Scheme 4.14b) and it was not clear to us which transition state might be preferred.

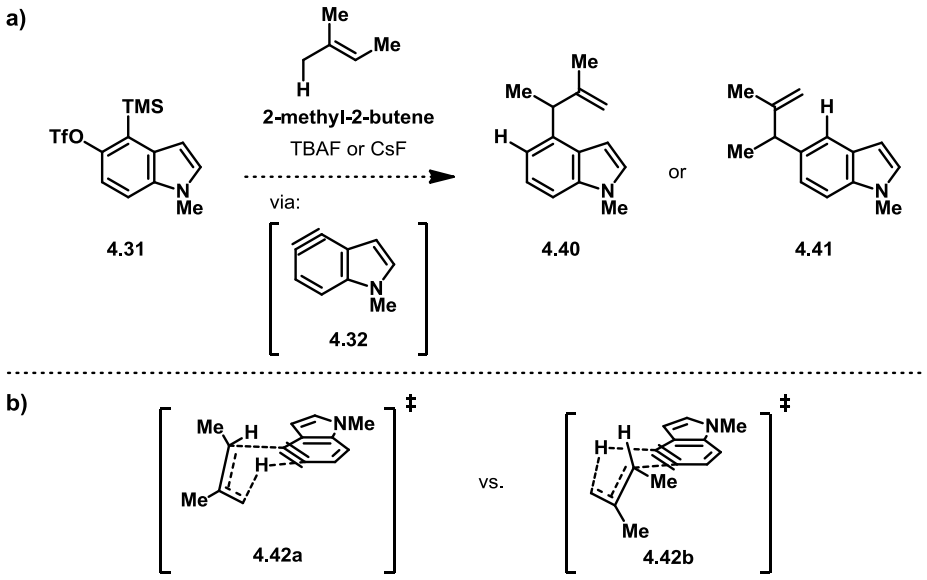

Scheme 4.14. a) regioisomeric products that could result from an indolyne-ene reaction with 2-methyl-2-butene; b) anticipated transition states leading to regioisomeric products.

Since there did not appear to be a clear regioisomeric preference, we thought this would be worth exploring. It should be noted, however, that this assessment does not take into account the possibility of a step-wise mechanism. If a step-wise mechanism were operative, then the alkene moiety would undoubtedly behave as the nucleophilic counterpart to the electrophilic aryne. It should also be noted that the use of 2-methyl-2-

butene as the arynophile opens up the possibility of regioisomerism for the alkene moiety, as multiple allylic hydrogens are present that could engage in an Alder-Ene reaction. The benzyne Alder-Ene reaction with 2-methyl-2-butene disclosed by Liu was reported to give only a single regioisomer;[15] however, since our principal concern was with the regiochemical preference for substitution on the indole ring, we sought to first explore this chemistry with an alkene substrate devoid of regioisomeric allylic hydrogens. To this end, we proposed to study an indolyne Alder-Ene reaction of indolylsilyl triflate **4.31** with 2,3-dimethyl-2-butene (see Scheme 4.15 below).

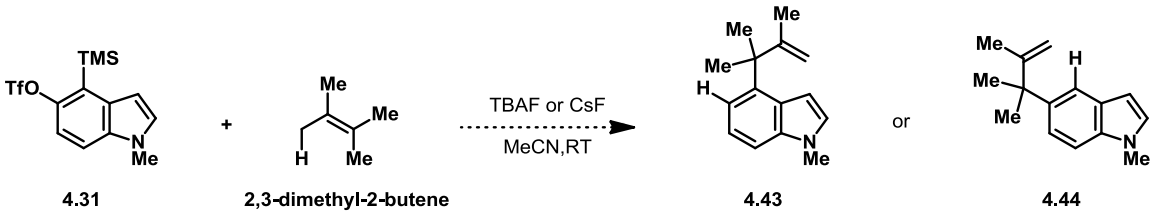

Scheme 4.15. Proposed indolyne-ene model substrate that avoids regioisomeric issues from the alkene moiety.

4.3.2 Results

Synthesis of indolylsilyl triflate **4.31** was completed in 5 steps using the protocols established by Garg et al. (Scheme 4.16). Benzyloxy indole **4.45** is commercially available and was treated with sodium hydride and iodomethane to give *N*-methyl indole **4.46** cleanly. Hydrogenolysis of the benzyl ether was not as efficient in our hands, as the reaction was plagued by slow conversion which led to decomposition of the product over extended reaction times.

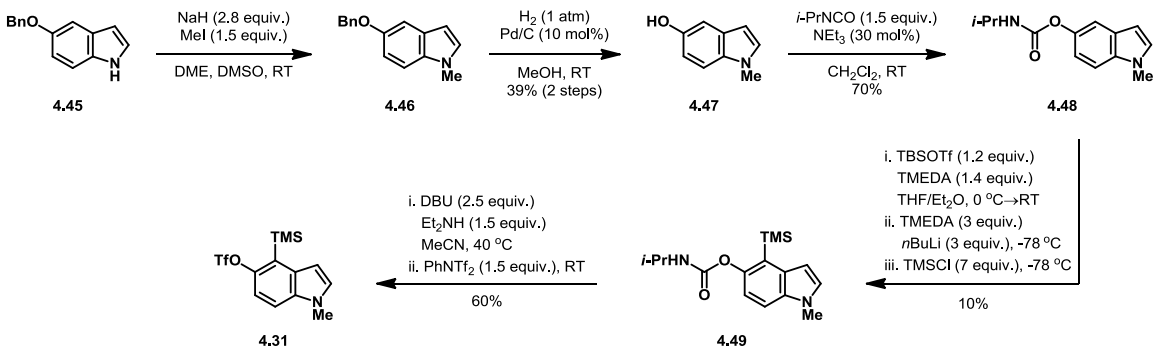

Scheme 4.16. Synthesis of indolylsilyl triflate **4.31** from commercially-available indole **4.45**

Regardless, treatment of hydroxyindole **4.47** with isopropyl isocyanate provided indolylcarbamate **4.48** in good yield. Protection of carbamate **4.48** *in situ*, followed by regioselective C–H lithiation with TMEDA-complexed *n*BuLi and subsequent quenching with TMSCl did provide indolylsilyl carbamate **4.49**, albeit in low isolated yield likely due to multiple chromatographic separations being required to obtain pure indolylsilyl carbamate **4.49**. Finally, base promoted cleavage of the carbamate and triflation of the resulting phenol provided indolylsilyl triflate **4.31** in moderate yield.

The difficulties encountered in the preparation of indolylsilyl triflate **4.31** resulted in obtaining just enough material to run a single experiment to test the viability of an indolyne Alder-Ene reaction with 2,3-dimethyl-2-butene. Treatment of indolylsilyl triflate **4.31** with TBAF in the presence of excess 2,3-dimethyl-2-butene resulted in the formation of a species with vinyl protons observable by ^{1}H NMR; unfortunately, attempts to isolate this species were met with failure.

Since the crude reaction mixture had shown promising signs of a successful indolyne Alder-Ene reaction, we opted to purchase a small amount of the commercially-

available (albeit expensive) indolylsilyl triflate **4.50** (Scheme 4.17). Upon treatment of indolylsilyl triflate **4.50** with TBAF in the presence of excess alkene, complete consumption of starting material was observed, along with the formation of substituted indoles **4.51** and **4.52**.

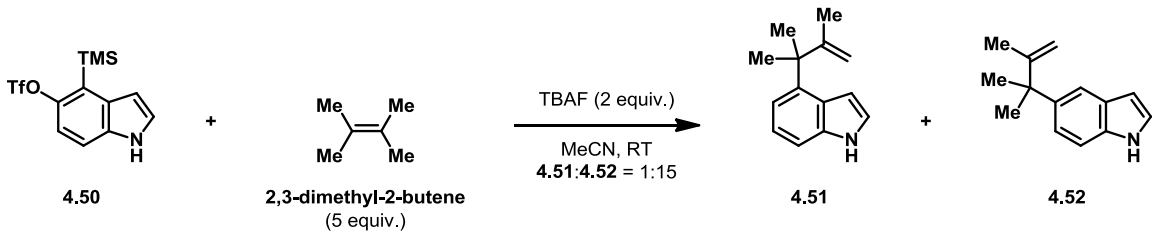

Scheme 4.17. Alder-Ene reaction of indolylsilyl triflate **4.50** with 2,3-dimethyl-2-butene to give the undesired regioisomeric indole **4.52** as the major product.

Analysis of the crude reaction mixture showed a 15:1 ratio of products containing vinyl protons. ^{1}H NMR analysis of an isolated mixture of the two Alder-Ene products revealed aromatic proton coupling constants consistent with the assignment of indole **4.52** as the major product of this reaction.

While the result of the indolyne Alder-Ene reaction was disappointing as it related to our use of such a strategy towards the total synthesis of dragmacidin E, it is still remarkable in the sense that the observed regioselectivity was greater than any of the examples reported by Garg et al. Furthermore, such a transformation may be useful in other areas of study. Given the widespread occurrence of indoles in Nature, this indolyne Alder-Ene reaction may enable the synthesis of prenylated indole frameworks that would otherwise be difficult to obtain.

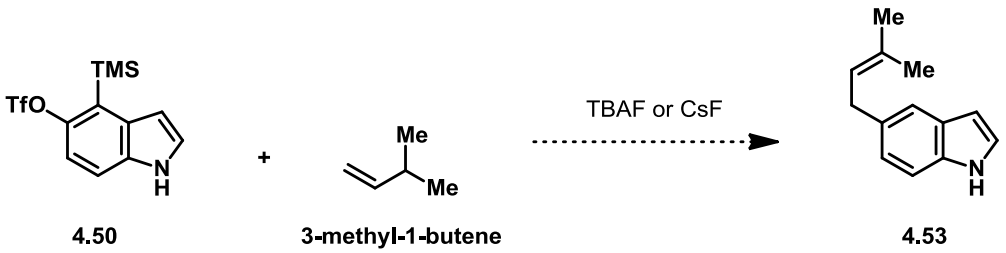

4.50 3-methyl-1-butene 4.53

Scheme 4.18. Potential application of the indolyne Alder-Ene reaction for the synthesis of prenylated indoles.

4.4. Synthetic Attempts Toward an Alkene Hydroacylation Precursor Utilizing Suzuki Cross-Coupling

4.4.1 Research Proposal

With our first two synthetic routes toward an alkene hydroacylation precursor meeting with little success, we opted to take a safer approach to forming the heretofore difficult carbon-carbon bond at the indole C5 position. In their efforts to synthesize dragmacidin D, Stoltz et al. had formed a carbon-carbon bond at the indole C5 position via the Suzuki cross-coupling of indolylboronic ester **4.54** and vinylbromide **4.55** (Scheme 4.19).[6] We anticipated that a similar approach to our alkene hydroacylation precursor would prove beneficial. We also thought that, at this juncture, a model alkene hydroacylation precursor would be a more prudent target. We viewed the testing of our key intramolecular alkene hydroacylation step as an important goal, and wanted to be able to test this as soon as possible.

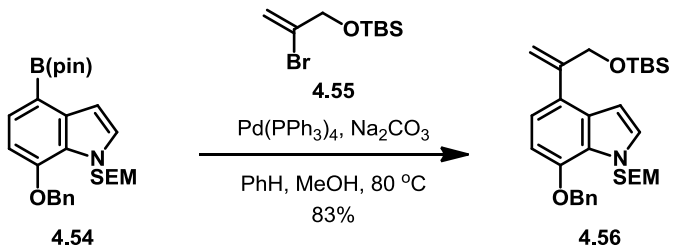

Scheme 4.19. Stoltz's use of a Suzuki coupling to form a C–C bond at the indole C5 position.

To that end, we targeted indole **4.57** as a model substrate on which to test our key intramolecular alkene hydroacylation step (Scheme 4.20). We envisioned indole **4.57** being available from ketone **4.58** via a Wittig olefination and Vilsmeier-Haack formylation[21] sequence. Ketone **4.58** would be available from allylic alcohol **4.59** through either a reduction-oxidation sequence or, more ideally, through isomerization of the double bond. Finally, allylic alcohol **4.59** would be available through Suzuki coupling of indolylboronic ester **4.54** and vinylbromide **4.60**.

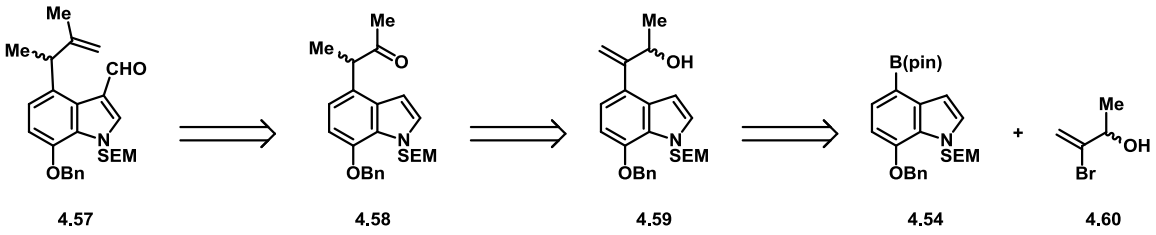

Scheme 4.20. Retrosynthetic approach to a model alkene hydroacylation precursor utilizing a Suzuki coupling to form the C–C bond at the indole C5 position.

4.4.2 Results

We began our studies by converting the in-hand bromoindole **4.5a** to indolylboronic ester **4.54** (see Scheme 4.21 below). Procedures involving lithium-halogen exchange with *t*-BuLi and trapping with isopropoxy pinacolborane afforded indolylboronic ester **4.54** in varying isolated yields. An unidentified by-product was often

observed, and the formation of this byproduct could be promoted by the inverse addition of bromoindole **4.5a** to a cooled solution of *t*-BuLi. Furthermore, significant amounts of material loss were encountered during attempts at chromatographic purification.

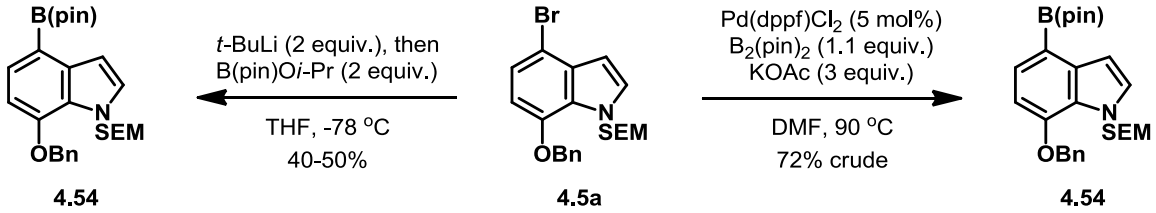

Scheme 4.21. Conversion of bromoindole **4.5a** to indolylboronic ester **4.54** through lithium-halogen exchange or Miyura borylation protocols.

It occurred to us that since the next synthetic step involving indolylboronic ester **4.54** was a Suzuki cross-coupling, a Miyura borylation of bromoindole **4.5a** may be an alternative way to generate indolylboronic ester **4.5a**. The benefit of this approach would be that the by-products formed in the Miyura borylation, such as pinacol boronate esters, would also be formed during a Suzuki cross-coupling. As such, purification of crude indolylboronic ester **4.5a** may not be necessary. Treatment of bromoindole **4.5a** with bis(pinacolato)diboron under palladium catalysis did provide indolylboronic ester **4.54** in relatively clean fashion. As such, we attempted to telescope this reaction with a Suzuki cross-coupling with vinylbromide **4.60** (refer to Scheme 4.20) in a one-pot protocol, but these attempts proved unsuccessful.

Vinylbromide **4.60**, the Suzuki cross-coupling partner for indolylboronic ester **4.54**, could be made in just 2 steps from methylvinyl ketone (see Scheme 4.22 below). Treatment of methylvinyl ketone with slightly less than 1 equivalent of bromine,

followed by careful addition of triethylamine, furnished enone **4.61** of sufficient purity that it could be carried on without purification. The Meerwein-Ponndorf-Verley protocol we had established for the reduction of enone **4.20** (refer to section 4.2.2) could not be successfully applied to the 1,2-reduction of enone **4.61**, as this species seemed to be much more prone to thermal decomposition. We had also attempted to use enone **4.61** directly in a Suzuki cross-coupling, but here too decomposition of enone **4.61** appeared to be problematic. Alternatively, Luche reduction of this ketone afforded vinylbromide **4.60** in moderate yield.

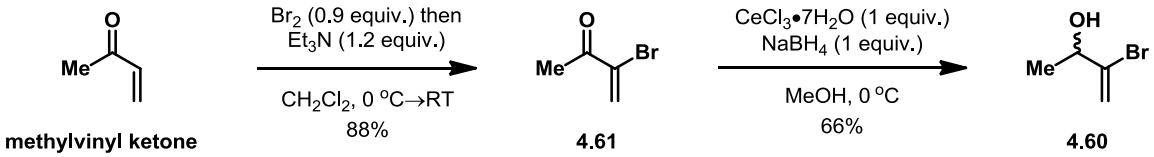

Scheme 4.22. Synthesis of vinylbromide **4.60**.

With indolylboronic ester **4.54** and vinylbromide **4.60** in hand, we were able to test our hypothesis on the viability of forming the carbon-carbon bond at the indole C5 position through a Suzuki cross-coupling. Substituted indole **4.59** was indeed able to be formed through a cross-coupling of indolylboronic ester **4.54** and vinylbromide **4.60** (see Scheme 4.23 below). Initial attempts at monitoring reaction progress suggested a leveling-off at around 50% conversion of indolylboronic ester **4.54**. Furthermore, additional catalyst loadings did not seem to result in further consumption of starting material.

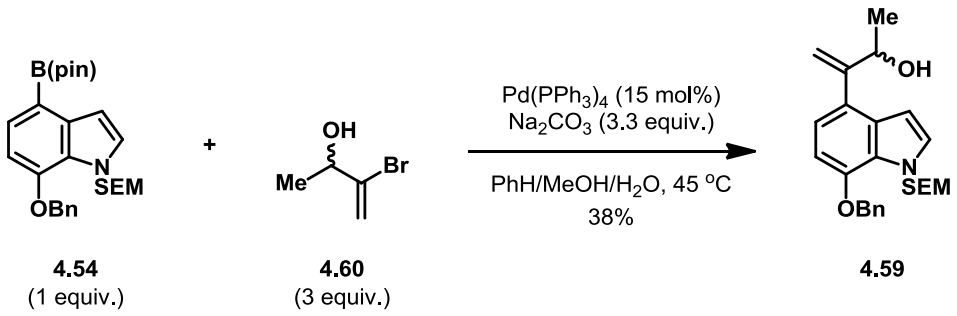

4.54 (1 equiv.) **4.60** (3 equiv.) **4.59**

Scheme 4.23. Suzuki coupling of indolylboronic ester **4.54** and vinylbromide **4.60**.

We hypothesized that the difficulties encountered in the purification of indolylboronic ester **4.54** were having a detrimental effect on the outcome of this Suzuki cross-coupling. It occurred to us that instead of converting bromoindole **4.5a** to indolylboronic ester **4.54**, we could perhaps instead convert vinylbromide **4.60** to vinylboronic ester **4.62** and perform an inverted Suzuki cross-coupling (Scheme 4.24).

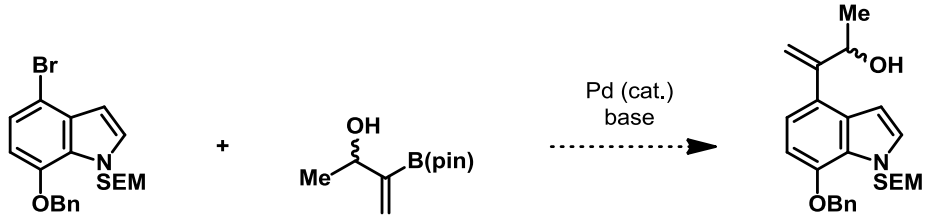

4.5a **4.62** **4.59**

Scheme 4.24. Proposed alternative Suzuki cross-coupling to form substituted indole **4.59**.

To that end, we envisioned vinylboronic ester **4.62** being available in a manner analogous to our conversion of bromoindole **4.5a** to vinylboronic ester **4.54** (refer to Scheme 4.21). We began by protecting allylic alcohol **4.60** as the silyl ether, which provided vinylbromide **4.61** in excellent yield (see Scheme 4.25 below). Lithium-halogen exchange with *t*-BuLi and quenching with isopropoxy pinacolborane resulted in the complete consumption of vinylbromide **4.61**, but resulted in the formation of a new, as-

yet unidentified compound (**4.62**). Diagnostic ^{1}H NMR signals for this species showed two new vinyl protons each with doublet of quartet splitting patterns, as well as a downfield-shifted methyl group coupled to each of the vinyl protons. Attempts to isolate this compound via chromatography, however, resulted in decomposition to a complex mixture.

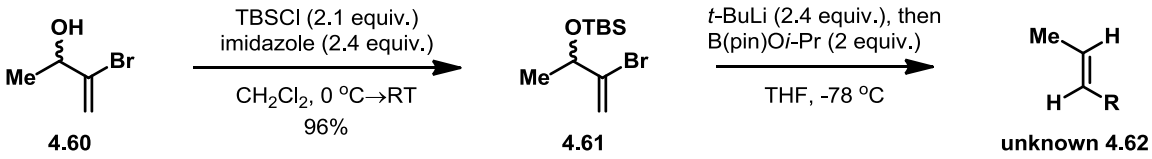

Scheme 4.25. Protection of allylic alcohol **4.60** and attempted lithium-halogen exchange of vinylbromide **4.61**.

It was hypothesized that an E_1cB-like mechanism may be operative, where lithium-halogen exchange of the vinyl bromide is followed by β–elimination of the silyl alkoxide. To circumvent this, we attempted to perform a Miyura borylation with vinyl bromide **4.60**, but this led to a complex reaction mixture that did not appear to produce the desired vinylboronic ester **4.62**. Alternatively, we considered that elimination of alkoxide could be prevented by treatment of vinyl bromide **4.60** with sodium hydride prior to lithium-halogen exchange, essentially protecting it as the alkoxide *in situ*. This was met with limited success, as vinylboronic ester **4.62** was able to be isolated in 10% yield through this deprotonation/lithium-halogen exchange/borylation sequence. This low yield was again shown to be due to decomposition of vinylboronic ester **4.62** on silica by 2-dimensional TLC.

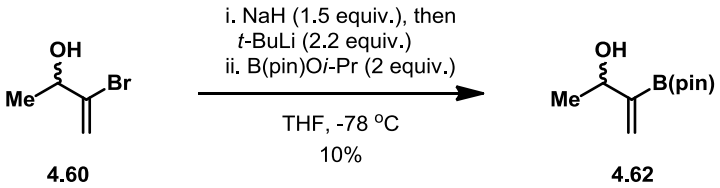

4.60 **4.62**

Scheme 4.26. Formation of vinyl bromide **4.62** by *in situ* protection of the alcohol as the alkoxide.

Having continually encountered low isolated yields due to chromatography-induced decomposition, particularly for indole-based compounds, we opted to take a different approach to forming our alkene hydroacylation precursor wherein the problematic indole moiety would be introduced late in the synthesis.

4.5. Synthetic Attempts Toward an Alkene Hydroacylation Precursor via Late-Stage Indole Formation

4.5.1 Research Proposal

We envisioned forming the indole moiety through a Bartoli indole synthesis[7], similar to previous synthetic routes, but would do so later on in this route (Scheme 4.27). As such, alkene hydroacylation precursor **4.4a** was expected to be available through a Bartoli indole synthesis of arylnitro **4.63**, followed by Vilsmeier-Haack formylation[21]. Arylnitro **4.63** in turn was anticipated to be made through a Wittig olefination/allylic oxidation sequence of ketone **4.64**. Ketone **4.64** should be available from alkene **4.65** via hydroboration/oxidation, and alkene **4.65** should be available from commercially-available 4'-methoxyacetophenone. Not only would this synthetic route allow for late-stage installation of the heretofore problematic indole ring, but using hydroboration in the stereo-determining step could eventually allow for an enantioselective synthesis using either chiral borane reagents or chiral rhodium catalysts.[22]

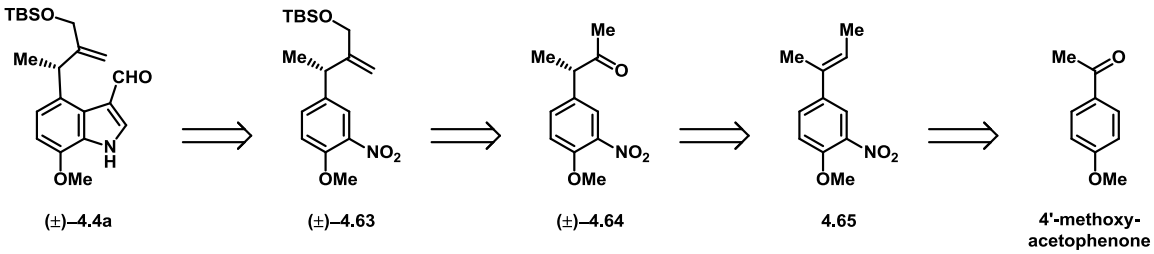

Scheme 4.27. Retrosynthetic approach to alkene hydroacylation precursor **4.4a** featuring late-stage introduction of the indole ring and a stereo-determining alkene hydroboration.

4.5.2 Results

To test our hypothesis, cheap and readily-available 4'-methoxyacetophenone was nitrated to give arylnitro **4.66** in good yield after recrystallization (Scheme 4.28). Wittig olefination of arylnitro **4.66** did not provide alkene **4.65** as smoothly as anticipated. This reaction did result in complete consumption of starting material, but mass recovery was a consistent issue. We hypothesized that the stoichiometric formation of triphenylphosphine oxide may have played a role in this mass recovery issue. The scalability of this reaction was also hindered by the large amount of ethyltriphenylphosphonium bromide required (due to its high molecular weight). Furthermore, alkene **4.65** was formed as a 2-to-1 mixture of geometric isomers. While this is inconsequential for the synthesis of racemic dragmacidin E, it would become an important factor once enantioselective synthetic endeavors are undertaken.

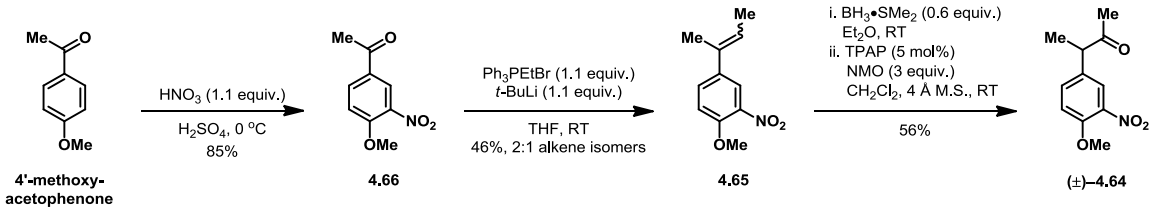

Scheme 4.28. Synthesis of ketone **4.64** via a one-pot hydroboration/oxidation of alkene **4.65**.

A one-pot hydroboration/oxidation sequence of alkene **4.65** was able to provide ketone **4.64** in moderate yield, along with a small amount (roughly 10 mol%) of ketone **4.66** (Scheme 4.28). We hypothesized the formation of ketone **4.66** in this reaction was due to either oxidation of the benzylic methine proton, followed by oxidative cleavage mediated by TPAP, or oxidation of the enol tautomer of ketone **4.64** followed by oxidative cleavage with TPAP.

Given the mass recovery and scalability issues encountered in the Wittig olefination of 4'-methoxyacetophenone, we realized an alternative olefination would likely be much more efficient, both from a synthetic planning perspective and a reaction yield perspective.

4.5.3 Research Proposal

We hypothesized that a Horner-Wadsworth-Emmons (HWE) olefination of 4'-methoxyacetophenone, followed by hydrogenation, would be a better alternative to the Wittig olefination/hydroboration route used previously (Scheme 4.29). Furthermore, asymmetric hydrogenation of the unsaturated ester would allow for enantioselective syntheses.

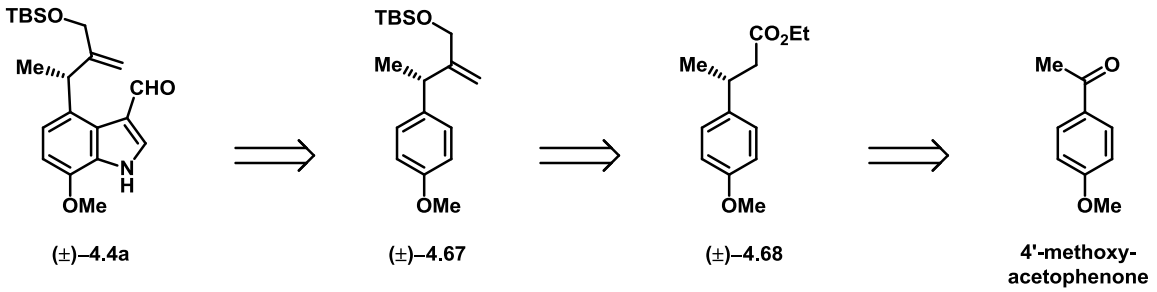

Scheme 4.29. Retrosynthetic approach to alkene hydroacylation precursor **4.4a**, featuring late-stage indole synthesis and a stereo-determining Horner-Wadsworth-Emmons olefination-hydrogenation sequence.

With this new route, late-stage introduction of the indole moiety would still be used to form alkene hydroacylation precursor **4.4a**. This was expected to arise via nitration of electron-rich arene **4.67**, followed by a Bartoli indole synthesis and Vilsmeier-Haack formylation (Scheme 4.29). Installation of the methylene group was anticipated to occur through traditional enolate chemistry at the α-position of ester **4.68**, after which reduction of the ester and protection of the resulting alcohol would give arene **4.67**. Ester **4.68** would then be available via a HWE olefination/hydrogenation sequence from 4'-methoxylacetophenone. This synthetic approach would only require one transformation of the indole and this transformation would introduce an electron-withdrawing group at the indole C3 position, with both aspects being beneficial to preventing decomposition.

4.5.4 Results

To test our hypothesis, 4'-methoxyacetophenone was treated with the anion of triethylphophonoacetate in refluxing THF, which provided unsaturated ester **4.69** in excellent yield as a 3.7-to-1 mixture of geometric isomers (see Scheme 4.30 below). Importantly, these isomers were able to be separated via silica gel chromatography.

While this has no bearing on our synthesis of racemic material, it will be important when enantioselective syntheses are undertaken. Palladium-catalyzed hydrogenation of unsaturated ester **4.69** provided the reduced ester **4.68** in quantitative yield and in a manner that did not require further purification. It is also worth mentioning that these reactions could be run on scales as large as 10-15 grams with no decrease in reaction efficiency.

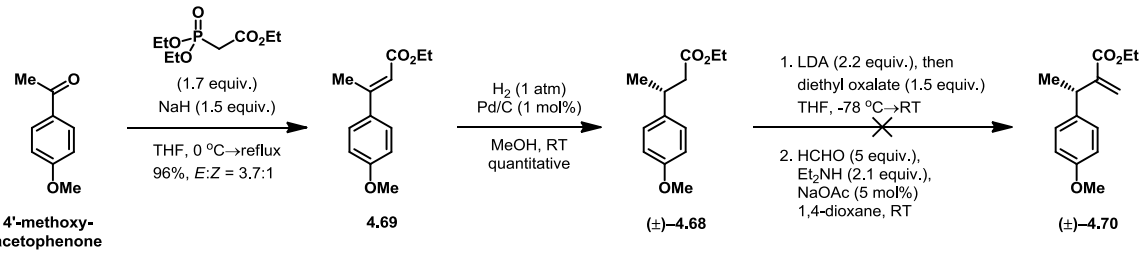

Scheme 4.30. Two-step synthesis of saturated ester **4.68** and an unsuccessful approach to installation of the alkene moiety.

Initial attempts at installing the methylene group involved a Claisen condensation to form a β-dicarbonyl moiety, followed by treatment with diethylamine and formaldehyde to induce an elimination[23] in what is presumed to be a retro-oxa-Michael-type mechanism (Scheme 4.30) . While this was able to provide some amount of alkene product via ^{1}H NMR analysis, the elimination reaction was not efficient and was difficult to monitor by ^{1}H NMR.

A much simpler method was discovered, which involved treatment of ester **4.68** with LDA followed by trapping with MEMCl to give the oxa-Michael product **4.71** in excellent yield (see Scheme 4.31 below). β-alkoxy ester **4.71** was not stable to chromatographic purification, but was clean enough to be taken on without purification.

Base-promoted elimination of β-alkoxy ester **4.71** with potassium *tert*-butoxide gave unsaturated ester **4.70**, again in excellent yield and with sufficient purity to be taken on as the crude mixture. DIBAL reduction of unsaturated ester **4.70** provided allylic alcohol **4.72** in 50% overall yield from the previous 3 steps. Again, these reactions were able to be run on scales as large as 5 grams consistently.

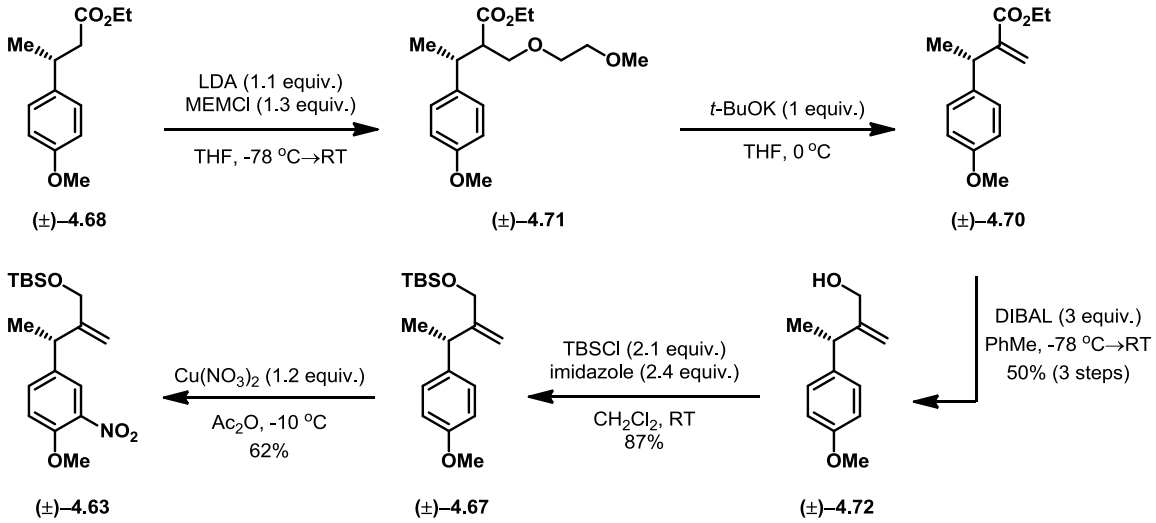

Scheme 4.31. Current synthetic route towards an alkene hydroacylation precursor.

Finally, protection of allylic alcohol as the TBS ether provided arene **4.67** in good yield, after which mild nitration conditions provided the desired arylnitro **4.63**. Even though the use of $Cu(NO_3)_2$ with acetic anhydride is significantly more mild than traditional conditions involving nitric and sulfuric acid, a significant amount of the allylic acetate was also formed during this reaction. This may actually occur upon workup, which involves the addition of methanol to remove the large excess of acetic anhydride by way of methanolysis. Removal of acetic anhydride in this way forms methyl acetate and acetic acid as by-products. The formation of acetic acid in the presence of acetic

anhydride could lead to removal of the acid-labile TBS group and *in situ* protection of the allylic alcohol as the acetate. Formation of the allylic acetate may be avoided through either the use of an alternative protecting group or by finding alternative work-up methods.

4.6. Chapter 4 Concluding Remarks

Our approach towards the synthesis of dragmacidin E hinges on the ability to form the challenging 7-membered carbocycle through the intramolecular alkene hydroacylation methodology developed in our group. Attempts to synthesize the appropriate substrate for this key step have met with very limited success. The stability of the electron-rich indole moiety is hypothesized to be the cause for the dramatic loss of material frequently encountered when attempting to purify synthetic intermediates. Our latest synthetic approach appears to have solved this problem by introducing the indole moiety late in the synthesis. This new route also allows for greater material throughput, as most of the reactions remain efficient upon scale-up. Furthermore, the stereogenic center is formed via the hydrogenation of an unsaturated ester, a reaction of which enantioselective variants are known. Late-stage formation of the indole via a Bartoli indole synthesis, however, has yet to be realized.

4.7. Chapter 4 Experimental

4.7.1 General Procedures

Unless otherwise noted, all reactions were carried out under a nitrogen atmosphere. Dichloromethane (DCM), acetonitrile (MeCN), and toluene were distilled

from CaH_2 prior to use. Tetrahydrofuran (THF) was distilled from Na/benzophenone prior to use. Benzene, methanol (MeOH), ethanol (EtOH), anhydrous *N*,*N*-dimethylformamide (DMF), anhydrous chloroform ($CHCl_3$), and anhydrous diethyl ether (Et_2O) were purchased from Sigma-Aldrich and Alfa Aesar, and used without further purification. Unless otherwise noted, all chemicals were purchased from commercial sources and used as received.

Analytical thin-layer chromatography (TLC) and preparative thin-layer chromatography were carried out using 250 μm and 1000 μm silica plates (SiliCycle), respectively. Eluted plates were visualized first with a UV lamp (254 nm) and then stained with ceric ammonium molybdate, potassium permanganate, or iodine. Flash column chromatography was performed using 230–400 mesh (particle size 40–63 μm) silica gel purchased from SiliCycle.

^{1}H NMR (400 and 500 MHz), ^{13}C NMR (75 and 125 MHz), and ^{19}F NMR (375 and 470 MHz) spectra were obtained on Varian Inova and Bruker Avance instruments. ^{1}H NMR spectra data were reported as δ values in ppm relative to TMS (δ 0.00) or chloroform (7.26) if collected in $CDCl_3$. ^{13}C NMR spectra data were reported as δ values in ppm relative to chloroform (δ 77.00) if collected in $CDCl_3$. ^{19}F NMR spectra data were reported as δ values in ppm using instrument standard. ^{1}H NMR coupling constants were reported in Hz, and multiplicity was indicated as follows: s (singlet); d (doublet); t (triplet); q (quartet); quint (quintet); m (multiplet); dd (doublet of doublets); ddd (doublet of doublet of doublets); dddd (doublet of doublet of doublet of doublets); dt (doublet of

triplets); td (triplet of doublets); ddt (doublet of doublet of triplets); dq (doublet of quartets); app (apparent); br (broad). Infrared (IR) spectra were obtained on a Thermo Scientific Nicolet iS5 FT-IR spectrometer with an iD5 ATR probe. High-resolution mass spectra (HRMS) in electrospray ionization (ESI) experiments were performed on a Bruker BioTOF II (Time-of-flight) instrument using PEG-300, PEG-400 or PPG-400 as an internal standard.

4.7.2 Dragmacidin E allylic arylation route procedures

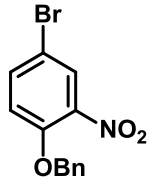

4.18

Commercially-available 4-bromo-2-nitrophenol (10.0 g; 45.9 mmol; 1 equiv.) was added to a flame-dried 250 mL round-bottom flask with a magnetic stir bar and dissolved in acetone (92 mL; 0.5 M). K_2CO_3 (12.7 g; 91.8 mmol; 2 equiv.) was added, followed by benzyl bromide (8.64g; 50.5 mmol; 1.1 equiv.). The flask was fitted with a reflux condenser and placed in a pre-heated oil bath. After the solution had refluxed for 5 h, the reaction was allowed to cool to RT and then quenched with 1 M HCl until pH $\leq$ 4 was obtained. The mixture was extracted with EtOAc and concentrated *in vacuo*. Crude material was recrystallized with a MeOH–H_2O solvent pair to give arylnitro **4.18** in 92% yield. The ^{1}H NMR data for **4.18** was consistent with literature values.[24] **^{1}H-NMR** (500 MHz; $CDCl_3$): δ 7.97 (d, *J* = 2.5 Hz, 1H), 7.58 (dd, *J* = 8.9, 2.5 Hz, 1H), 7.44-7.32 (m, 5H), 7.00 (d, *J* = 9.0 Hz, 1H), 5.22 (s, 2H).

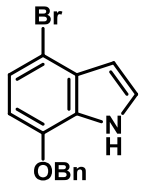

4.19

A 3-neck 500 mL round-bottom flask with a magnetic stir bar was fitted with a septum, dropping funnel, and an internal temperature thermometer and then flame-dried. Arylnitro **4.18** (5.00 g; 16.2 mmol; 1 equiv.) was added as a solid under a positive pressure of nitrogen, and was then dissolved in THF (162 mL; 0.1 M). Vinylmagnesium bromide (56.7 mL; 56.7 mmol; 3.5 equiv.) was added to the dropping funnel and the flask was placed in a Dewar cooled by an immersion cooler until an internal temp. of -45 ^{o}C was achieved. Vinylmagnesium bromide was then added dropwise, keeping the internal temp. below -40 ^{o}C. After complete addition of vinylmagnesium bromide the solution was stirred at -45 ^{o}C for 4 hours, at which point the reaction was quenched with 1 M HCl (50 mL) and allowed to warm to RT. The mixture was extracted with Et_2O (3x100 mL) and the combined organic layers were dried over $MgSO_4$, filtered, and concentrated *in vacuo*. The crude material was taken up in DCM and filtered through Celite® to provide crude indole **4.19** in approximately 58% yield. The crude sample could then be purified via silica gel flash chromatography (1:9 Et_2O:hexanes) to provide isolated indole **4.19** in 31% yield. 1H NMR data for indole **4.19** was consistent with literature values.[6] **^{1}H-NMR** (500 MHz; $CDCl_3$): δ 8.53 (s, 1H), 7.46-7.45 (m, 2H), 7.42-7.36 (m, 3H), 7.20 (t, *J* = 2.8 Hz, 1H), 7.15 (d, *J* = 8.2 Hz, 1H), 6.59 (d, *J* = 8.2 Hz, 1H), 6.56 (dd, *J* = 3.1, 2.4 Hz, 1H), 5.18 (s, 2H).

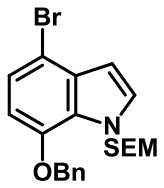

4.5a

To a flame-dried 100 mL round bottom flask was added NaH (160 mg; 4.0 mmol; 1.3 equiv.) and THF (15 mL). This suspension was stirred and cooled to 0 ^{o}C, after which point a THF (15 mL) solution of indole **4.19** (0.930 g; 3.1 mmol; 1 equiv.) was slowly added. After complete addition, the flask was allowed to warm to RT and stirred for 30 min. before cooling to 0 ^{o}C. SEMCl (632 μL; 3.4 mmol; 1.1 equiv.) was added at 0 ^{o}C and the reaction was allowed to warm to RT. After stirring for 7 hours at RT the reaction was quenched with NH_4Cl (20 mL, sat. aq.) and extracted with Et_2O (3x 20 mL). The combined organic layers were washed with brine (20 mL), dried over Na_2SO_4, filtered, and concentrated *in vacuo*. The crude material was purified via silica gel flash chromatography (7:93 EtOAc/hexanes) to give protected indole **4.5a** in variable yields. ^{1}H NMR data for protected indole **4.5a** was consistent with literature values.[6] **^{1}H-NMR** (500 MHz; $CDCl_3$): δ 7.49 (d, *J* = 6.9 Hz, 2H), 7.42-7.34 (m, 3H), 7.19 (d, *J* = 3.2 Hz, 1H), 7.16 (d, *J* = 8.3 Hz, 1H), 6.62 (d, *J* = 8.3 Hz, 1H), 6.56 (d, *J* = 3.2 Hz, 1H), 5.72 (s, 2H), 5.19 (s, 2H), 3.43 (t, *J* = 8.2 Hz, 2H), 0.81 (t, *J* = 8.2 Hz, 2H), -0.09 (s, 9H).

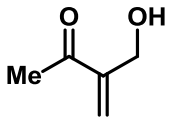

4.20

A 2-neck 25 mL round bottom flask containing a magnetic stir bar was fitted with a septum and an internal temperature thermometer adapter. The flask was purged with nitrogen, charged with methylvinyl ketone (1.75 g; 25 mmol; 1 equiv.) and THF (10 mL), and cooled to 0 ^{o}C. Formaldehyde (0.901 g; 30 mmol; 1.2 equiv.) was then added as a 37% aq. soln. A THF (2 mL) solution of DABCO (0.28 g; 2.5 mmol; 0.10 equiv.) was added slowly and the reaction was stirred at 0 ^{o}C for 6 h. The solution was then poured over an aq. soln of NaCl and $NaHCO_3$ (basified brine, 20 mL) and extracted with Et_2O (3x 20 mL). The combined organic layers were dried over Na_2SO_4, filtered, and concentrated *in vacuo*. The crude material was purified through high-vacuum distillation (pressure = 0.05 mmHg) to give allylic alcohol **4.20** in 56% yield. ^{1}H NMR data for allylic alcohol **4.20** was consistent with literature values.[8] **^{1}H-NMR** (500 MHz; $CDCl_3$): δ 6.13 (s, 1H), 6.06 (s, 1H), 4.32 (d, *J* = 5.9 Hz, 2H), 2.52 (bs, 1H), 2.38 (s, 3H).

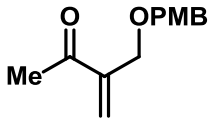

4.22

To a flame-dried 100 mL round-bottom flask was added allylic alcohol **4.20** (1.00 g; 10 mmol; 1 equiv.) and DCM (20 mL). 4-methoxybenzyl 2,2,2-trichloroacetimidate (4.24 g; 15 mmol; 1.5 equiv.) was added as a DCM solution (10 mL) and the flask was cooled to 0 ^{o}C. PPTS (0.251 g; 1.0 mmol; 0.10 equiv.) was dissolved in DCM (10 mL) and added

slowly to the reaction mixture. After complete addition the flask was allowed to warm to RT and was stirred for 1 h, after which point MeOH (4 mL; 10 equiv.) was added and the solution was stirred for an additional 30 min. The reaction was then quenched with $NaHCO_3$ (sat. aq., 50 mL) and extracted with DCM (2x 40 mL). The combined organic layers were washed with brine (50 mL), dried over Na_2SO_4, filtered, and concentrated *in vacuo*. Silica gel flash chromatography (20:80 EtOAc:hexanes) gave allylic ether **4.22** as a yellow oil in 40% yield. R_f = 0.64 (80:20 Et_2O:hexanes) **^{1}H-NMR** (500 MHz; $CDCl_3$): δ 7.28-7.26 (m, 2H), 6.89-6.87 (m, 2H), 6.16 (app. q, *J* = 1.5 Hz, 1H), 6.12 (td, *J* = 1.5, 0.5 Hz, 1H), 4.51 (s, 2H), 4.21 (t, *J* = 1.6 Hz, 2H), 3.80 (s, 3H), 2.35 (s, 3H).

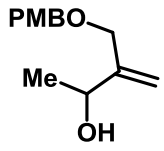

(±)-4.23

Enone **4.22** (1.00 g; 4.54 mmol; 1 equiv.) was added to a flame-dried 100 mL round-bottom flask and dissolved in *i*PrOH (52 mL; 0.1 M). Aluminum isopropoxide (0.927 g, 4.54 mmol; 1 equiv.) was added and the flask was fitted with a reflux condenser. The reaction was heated to reflux and stirred overnight. After allowing to cool to RT, the reaction mixture was acidified with 1 M HCl until pH ≤ 4 was obtained and extracted with EtOAc (3x approx. 50 mL). The combined organic layers were then stirred with Rhochelle salt (sat. aq., approx. 100 mL). The mixture was filtered and the organic layer was washed with brine, dried over Na_2SO_4, filtered, and concentrated *in vacuo* to give allylic alcohol **4.23** as a pale yellow oil in quantitative yield. Material prepared this way required no additional purification. R_f = 0.42 (1:1 EtOAc:hexanes); **^{1}H-NMR** (500 MHz;

CDCl3): δ 7.27 (d, *J* = 8.6 Hz, 2H), 6.88 (d, *J* = 8.6 Hz, 2H), 5.19 (s, 1H), 5.10 (s, 1H), 4.46 (s, 2H), 4.39 (q, *J* = 6.5 Hz, 1H), 4.13 (d, *J* = 11.9 Hz, 1H), 4.06 (d, *J* = 11.9 Hz, 1H), 3.81 (s, 4H), 1.33 (d, *J* = 6.5 Hz, 3H); **^{13}C-NMR** (126 MHz; CDCl3): δ 159.4, 148.6, 130.0, 129.6, 114.0, 112.8, 72.2, 71.4, 69.6, 55.4, 22.1; **MS** (ESI) calcd for $[C_{13}H_{18}O_3 + Na]^+$ 245.27, found 245.21; **IR** (neat) 3392, 1612, 1512, 1245.

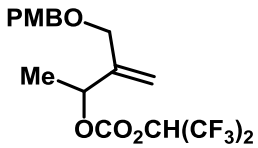

(±)-4.6a

To a flame-dried 10 mL pear-shaped flask was added allylic alcohol **4.23** (200 mg; 0.90 mmol; 1 equiv.) and DCM (0.9 mL). Carbonyl diimidazole (175 mg; 1.08 mmol; 1.2 equiv.) was then added and the flask was stirred at RT for 5 h. The reaction mixture was then diluted with DCM and washed with H_2O and brine, dried over Na_2SO_4, filtered, and concentrated *in vacuo*. The crude product was taken up in DCM (0.9 mL). DMAP (33 mg; 0.27 mmol; 0.3 equiv.) and hexafluoro-2-propanol (0.38 mL; 3.6 mmol; 4.0 equiv.) were added and the solution was stirred at RT overnight. The reaction mixture was diluted with DCM and washed with H_2O (3x approx. 5 mL). The organic layer was then dried over Na_2SO_4, filtered, and concentrated *in vacuo*. Silica gel flash chromatography (2:8 EtOAc:hexanes) afforded allylic carbonate **4.6a** in 50% yield as a yellow oil. **^{1}H-NMR** (500 MHz; $CDCl_3$): δ 7.26 (d, *J* = 7.6 Hz, 2H), 6.88 (d, *J* = 7.6 Hz, 2H), 5.59-5.52 (m, 1H), 5.38 (q, *J* = 6.6 Hz, 1H), 5.28 (s, 1H), 5.26 (s, 1H), 4.46 (d, *J* = 11.4 Hz, 1H), 4.41 (d, *J* = 11.4 Hz, 1H), 4.05 (d, *J* = 12.7 Hz, 1H), 4.02 (d, *J* = 12.7 Hz, 1H), 3.81 (s, 3H), 1.49 (d, *J* = 6.7 Hz, 3H); **^{13}C-NMR** (126 MHz; CDCl3): δ 159.4, 152.3, 144.1,

130.1, 129.6, 114.8, 114.0, 78.1, 72.0, 70.4 (q, *J* = 34.7 Hz), 70.1 (q, *J* = 34.7 Hz), 70.1, 55.4, 19.4 (a signal appears to overlap with a $CDCl_3$ peak at 77.37 ppm); **IR** (neat) 1773, 1514, 1249, 1197.

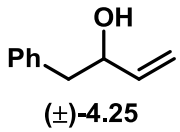

(±)-4.25

To a flame-dried 100 mL round-bottom flask was added vinylmagensium bromide (24 mL; 24 mmol; 1.1 equiv.). Another flask was charged with phenylacetaldehyde (2.6 g; 21.8 mmol; 1 equiv.) and anhydrous Et_2O (16 mL; 1.4 M). Both flasks were cooled to -78 ^oC, after which point the phenylacetaldehyde solution was cannulated into vinylmagnesium bromide. The reaction flask was stirred at -78 ^oC for 40 min., and then was allowed to warm to RT. The reaction was quenched with NH_4Cl (sat. aq., approx. 30 mL) and extracted with EtOAc (3x approx. 30 mL). The combined organic extracts were dried over Na_2SO_4, filtered, and concentrated *in vacuo* to give crude allylic alcohol **4.25** in quantitative yield with sufficient purity to be carried forward. ^{1}H-NMR data for allylic alcohol 4.25 was consistent with literature values.[25] **^{1}H-NMR** (500 MHz; $CDCl_3$): δ 7.33-7.30 (m, 2H), 7.24-7.22 (m, 3H), 5.93 (ddd, *J* = 17.0, 10.7, 6.0 Hz, 1H), 5.25 (app. dt, *J* = 17.0, 1.5 Hz, 1H), 5.13 (app. dt, *J* = 10.5, 1.0 Hz, 1H), 4.35 (m, 1H), 2.88 (dd, *J* = 13.6, 5.1 Hz, 1H), 2.79 (dd, *J* = 13.6, 8.0 Hz, 1H), 1.69 (bs, 1H).

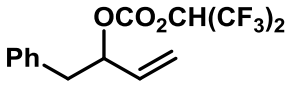

(±)-4.13b

Allylic carbonate **4.13b** was prepared from allylic alcohol **4.25** using a literature procedure. [1]H-NMR data was in agreement with literature values.[3] **^{1}H-NMR** (500 MHz; $CDCl_3$): δ 7.30 (t, *J* = 7.0 Hz, 2H), 7.25-7.23 (m, 1H), 7.20 (d, *J* = 7.0 Hz, 2H), 5.85 (ddd, *J* = 17.2, 10.5, 6.7 Hz, 1H), 5.47 (septet, *J* = 6.0 Hz, 1H), 5.35 (br. q, *J* = 6.9 Hz, 1H), 5.31 (app. dt, *J* = 17.2, 1.0 Hz, 1H), 5.28 (app. dt, *J* = 10.6, 0.9 Hz, 1H), 3.07 (dd, *J* = 14.0, 7.6 Hz, 1H), 2.98 (dd, *J* = 14.0, 6.0 Hz, 1H).

4.7.3 Dragmacidin E indolyne Alder-ene route procedures

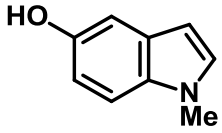

4.47

Hydroxyindole **4.47** was prepared from commercially-available 5-benzyloxyindole using a known two-step procedure.[16] Hydroxyindole **4.47** was isolated as a mixture with *N*-methyl-5-benzyloxyindole, and was taken further without purification due to the observation of silica-promoted decomposition.

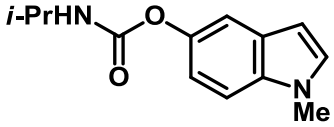

4.48

Indole carbamate **4.48** was prepared from hydroxyindole **4.47** using a known procedure.[16] [1]H-NMR data was in agreement with literature values. **^{1}H-NMR** (500 MHz; $CDCl_3$): δ 7.34 (d, *J* = 2.2 Hz, 1H), 7.26 (d, *J* = 8.5 Hz, 2H), 7.06 (d, *J* = 3.1 Hz, 1H), 6.99 (dd, *J* =

8.8, 2.2 Hz, 1H), 6.44 (d, *J* = 3.0 Hz, 1H), 4.84 (br s, 1H), 3.95-3.88 (m, 1H), 3.78 (s, 3H), 1.23 (d, *J* = 6.5 Hz, 6H).

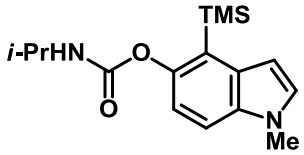

4.49

Silylindole **4.49** was prepared using a known procedure,[16] but was unable to be isolated pure. It was carried forward as a mixture with its 5-trimethylsilyl regioisomer.

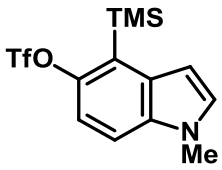

4.31

Indolylsilyl triflate **4.31** was prepared from silylindole **4.49** using a known procedure.[16] **^{1}H-NMR** data were in agreement with literature values. **^{1}H-NMR** (500 MHz; $CDCl_3$): δ 7.33 (d, *J* = 9.0 Hz, 1H), 7.17 (d, *J* = 3.0 Hz, 1H), 7.16 (d, *J* = 9.0 Hz, 1H), 6.68 (d, *J* = 3.2 Hz, 1H), 3.80 (s, 3H), 0.50 (s, 9H).

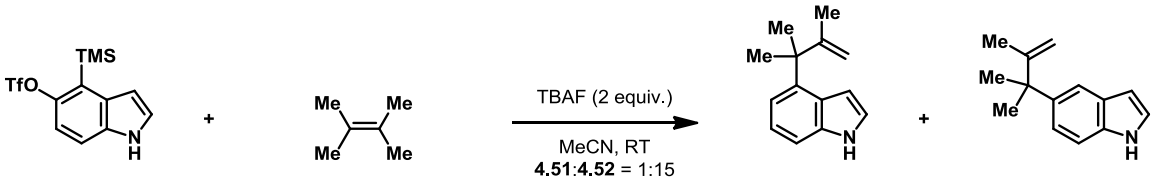

4.50 | **2,3-dimethyl-2-butene** (5 equiv.) | **4.51** | **4.52**

A 1-dram vial was charged with TBAF (60 μL 1.0 M THF soln; 0.060 mmol; 2.0 equiv.), 2,3-dimethyl-2-butene (12.6 mg; 0.15 mmol; 5.0 equiv.) and MeCN (0.15 mL). The mixture was stirred for 5 min. before commercially-available indolylsilyl triflate **4.50**

(0.15 mL 0.20 M MeCN; 0.030 mmol; 1 equiv.) was added as a stock solution. The reaction mixture was stirred at RT overnight, after which point it was diluted with Et_2O and passed through a small plug of Celite® and silica. The crude product was analyzed by ^{1}H-NMR and GC/MS. Micro-scale silica gel chromatography (15:15:70 Et_2O:DCM:hexanes) afforded alkylindole **4.52**, the substitution pattern of which was confirmed via ^{1}H-NMR coupling constants. **^{1}H-NMR** (500 MHz; $CDCl_3$): δ 8.07 (br s, 1H), 7.59 (d, *J* = 1.5 Hz, 1H), 7.31 (d, *J* = 8.6 Hz, 1H), 7.19 (app t, *J* = 2.8 Hz, 1H), 7.15 (dd, *J* = 8.6, 1.5 Hz, 1H), 6.53-6.51 (m, 1H), 5.02 (d, *J* = 1.6 Hz, 1H), 4.88 (t, *J* = 1.4 Hz, 1H), 1.53 (d, *J* = 0.6 Hz, 3H), 1.49 (s, 6H).

4.7.4 Dragmacidin E Suzuki cross-coupling route procedures

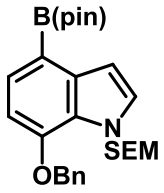

4.54

Indolylboronic ester **4.54** was prepared from bromoindole **4.5a** using a known procedure.[6] ^{1}H-NMR data was in agreement with literature values. **^{1}H-NMR** (500 MHz; CDCl3): δ 7.57 (d, J = 7.8 Hz, 1H), 7.52-7.50 (m, 2H), 7.41-7.37 (m, 2H), 7.35-7.32 (m, 1H), 7.18 (d, J = 3.1 Hz, 1H), 7.03 (d, J = 3.1 Hz, 1H), 6.77 (d, J = 7.9 Hz, 1H), 5.74 (s, 2H), 5.24 (s, 2H), 3.43-3.40 (m, 2H), 1.37 (s, 12H), 0.82-0.78 (m, 2H), -0.10 (s, 9H).

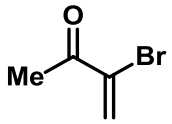

4.61

A 250 mL 3-neck round-bottom flask was fitted with a dropping funnel, internal temperature thermometer and a septum and the apparatus was flame-dried. The flask was charged with methylvinyl ketone (4.5 mL; 55 mmol; 1 equiv.) and DCM (28 mL). The flask was cooled to -5 ^{o}C and the dropping funnel was charged with Br_2 (2.6 mL; 51 mmol; 0.9 equiv.) and DCM (26 mL). The Br_2 solution was then added such that the internal temperature of the reaction did not exceed 0 oC. The reaction was stirred at -5 ^{o}C for 30 min. before distilled Et_3N (9.0 mL; 65 mmol; 1.2 equiv.) was added via syringe. After complete addition the flask was allowed to warm to RT and stirred for 19 h. The mixture was poured over 1 M HCl and diluted with DCM. The aqueous phase was extracted with DCM (3x approx. 100 mL) and the combined organic layers were dried over Na_2SO_4, filtered, and concentrated *in vacuo*. This provided vinyl bromide **4.61** in 88% yield and no further purification was necessary. ^{1}H-NMR data for vinyl bromide **4.61** was consistent with literature values.[26] **^{1}H-NMR** (500 MHz; $CDCl_3$): δ 6.80 (d, *J* = 2.4 Hz, 1H), 6.42 (d, *J* = 2.4 Hz, 1H), 2.48 (s, 3H).

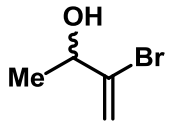

4.60

A 250 mL round-bottom flask was flame-dried and charged with vinyl bromide **4.61** (3.6 g; 24.2 mmol; 1 equiv.). MeOH (37 mL) was added, followed by $CeCl_3 \cdot 7H_2O$ (9.02 g;

24.2 mmol; 1 equiv.) as a solution in MeOH (73 mL). The flask was cooled to 0 ^{o}C and $NaBH_4$ (0.915 g; 24.2 mmol; 1 equiv.) was added slowly in portions. The reaction was stirred at 0 ^{o}C for 2.5 h before quenching with 1 M HCl. The mixture was extracted with EtOAc and combined organic layers were dried over Na_2SO_4, filtered, and concentrated *in vacuo*. This provided allylic alcohol **4.60** in 66% yield with sufficient purity to be carried forward. ^{1}H-NMR data for allylic alcohol **4.60** were in agreement with literature values.[27] **^{1}H-NMR** (500 MHz; $CDCl_3$): δ 5.90 (s, 1H), 5.52 (d, *J* = 1.8 Hz, 1H), 4.33 (d, *J* = 6.0 Hz, 1H), 2.08 (s, 1H), 1.39 (d, *J* = 6.3 Hz, 3H).

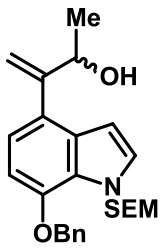

4.59

A 50 mL round-bottom flask was charged with vinyl bromide **4.60** (95 mg; 0.63 mmol; 3 equiv.) and MeOH (2.9 mL). Indolylboronic ester **4.54** (100 mg; 0.21 mmol; 1 equiv.) was added as a solution in benzene (9 mL), along with Na_2CO_3 (0.35 mL of 2.0 M aq.; 0.69 mmol; 3.3 equiv.). The mixture was degassed with Ar and $Pd(PPh_3)_4$ (37 mg; 0.032 mmol; 15 mol%) was added with the aid of benzene (3 mL). The mixture was further degassed with Ar and placed in a pre-heated oil bath. The reaction was stirred under a positive Ar pressure at 45 ^{o}C for 11 h and was then poured over H_2O (15 mL). The aqueous phase was extracted with Et_2O (3x 15 mL) and the combined organic layers were dried over Na_2SO_4, filtered, and concentrated *in vacuo*. Purification via silica gel flash

chromatography (1:9 EtOAc:hexanes) afforded substituted indole **4.59** as a colorless oil in 38% yield. **^{1}H-NMR** (500 MHz; $CDCl_3$): δ 7.53-7.51 (m, 2H), 7.42-7.39 (m, 3H), 7.37-7.34 (m, 1H), 7.15 (d, *J* = 3.2 Hz, 1H), 6.92 (d, *J* = 8.0 Hz, 1H), 6.73 (d, *J* = 8.0 Hz, 1H), 6.57 (d, *J* = 3.2 Hz, 1H), 5.74 (s, 2H), 5.51 (app t, *J* = 1.5 Hz, 1H), 5.26 (dd, *J* = 1.4, 0.7 Hz, 1H), 5.21 (s, 2H), 4.83 (app quintet, *J* = 5.7 Hz, 1H), 3.46-3.43 (m, 2H), 1.72 (d, *J* = 4.3 Hz, 1H), 1.30 (d, *J* = 6.4 Hz, 3H), 0.81 (t, *J* = 8.1 Hz, 2H), -0.11 (s, 9H); **MS** (ESI) calcd for $[C_{25}H_{33}NO_3Si + Na]^+$ 446.21, found 446.39.

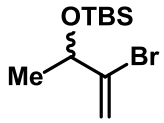

4.61

A 100 mL round-bottom flask was flame-dried and charged will allylic alcohol **4.60** (1.00 g; 6.6 mmol; 1 equiv.) and imidazole (1.08 g; 15.8 mmol; 2.4 equiv.). The reagents were dissolved in DCM (33 mL; 0.2 M) and cooled to 0 ^oC. TBSCl (2.10 g; 13.9 mmol; 2.1 equiv.) was added using a minimal amount of DCM. After complete addition, the flask was allowed to warm to RT and stirred for 3 h before quenching with NH_4Cl (sat. aq., approx. 100 mL). The mixture was extracted with DCM (3x approx. 75 mL) and the combined organic layers were dried over Na_2SO_4, filtered, and concentrated *in vacuo*. Crude material was filtered through a plug of silica gel eluting with hexanes to give allylic ether **4.61** as a colorless liquid in 96% yield. **^{1}H-NMR** (500 MHz; $CDCl_3$): δ 5.90 (t, *J* = 1.3 Hz, 1H), 5.46 (app s, 1H), 4.29 (q, *J* = 6.3 Hz, 1H), 1.34 (d, *J* = 6.3 Hz, 3H), 0.91 (s, 9H), 0.08 (s, 3H), 0.08 (s, 3H); **^{13}C-NMR** (126 MHz; $CDCl_3$): δ 138.4, 114.9,

72.8, 25.9, 23.5, 18.4, -4.7, -4.9 (diastereotopic TBS methyl carbons); **IR** (neat) 2955, 2930, 2857, 1253, 1098, 1079.

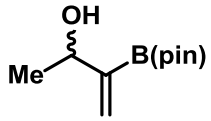

4.62

A flame-dried 250 mL round-bottom flask was charged with NaH (159 mg 60% in mineral oil; 6.62 mmol; 2.0 equiv.). THF (45 mL) was added and the suspension was cooled to 0 ^{o}C. Allylic ether **4.61** (500 mg; 3.31 mmol; 1 equiv.) was added slowly as a solution in THF (10 mL). After complete addition, the flask was allowed to warm to RT and stirred for 30 min. The flask was then cooled to -78 ^{o}C and *t*-BuLi (5.52 mL of 1.32 M; 7.28 mmol; 2.2 equiv.) was added dropwise. The solution was stirred at -78 oC for 15 min. before B(pin)O*i*-Pr (925 mg; 4.97 mmol; 1.5 equiv.) was added. The reaction was stirred at -78 ^{o}C for 1.5 h before quenching with NH_4Cl (sat. aq.; 25 mL) at -78 ^{o}C. The flask was allowed to warm to RT and the contents were poured into EtOAc. 1 M HCl was added until a pH < 7 was obtained. The aqueous phase was extracted with EtOAc (3x approx. 100 mL) and the combined organic layers were dried over Na_2SO_4, filtered, and concentrated *in vacuo*. Purification via silica gel flash chromatography (1:9 AcMe:hexanes) afforded vinylboronic ester **4.62** as off-white needles in 10% yield. 1H-NMR data for vinylboronic ester **4.62** was consistent with literature values.[28] **^{1}H-NMR** (500 MHz; $CDCl_3$): δ 5.82 (d, *J* = 2.3 Hz, 1H), 5.78 (s, 1H), 4.38 (app quintet, *J* = 6.4 Hz, 1H), 2.26 (d, *J* = 6.7 Hz, 1H), 1.31 (d, *J* = 6.4 Hz, 3H), 1.29 (s, 12H).

4.7.5 Dragmacidin E Wittig olefination route procedures

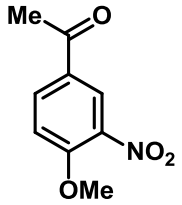

4.66

A 100 mL 3-neck round-bottom flask was fitted with an internal temperature thermometer and a glass stopper, leaving 1 neck open. 4'-methoxyacetophenone (5.00 g; 33.3 mmol; 1 equiv.) was added and dissolved in concentrated H_2SO_4 (28 mL; 1.2 M) before cooling to 0 ^oC. Nitric acid (2.34 mL of 70% aq.; 36.6 mmol; 1.1 equiv.) was added to a test tube and diluted with concentrated H_2SO_4 (2.34 mL) before cooling to 0 ^oC. The nitric acid solution was then added to the reaction flask via pipet at such a rate as to keep the internal temperature below 10 ^oC. The reaction mixture was stirred open to air at 0 oC for 30 min. before allowing to warm to RT. The mixture was poured over cold H_2O to give a precipitate that was collected by vacuum filtration and rinsed with cold H_2O. The crude solid was recrystallized using EtOH/H_2O to give aryl nitro **4.66** in 85% yield. ^{1}H-NMR data was consistent with literature values.[29] **^{1}H-NMR** (500 MHz; $CDCl_3$): δ 8.44 (d, *J* = 2.2 Hz, 1H), 8.18 (dd, *J* = 8.8, 2.2 Hz, 1H), 7.17 (d, *J* = 8.8 Hz, 1H), 4.05 (s, 3H), 2.61 (s, 3H).

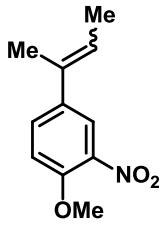

4.65

A 25 mL round-bottom flask was flame-dried and charged with ethyltriphenylphosphonium bromide (1.08 g; 2.9 mmol; 1.1 equiv.). THF (4.1 mL) was added and the flask was cooled to -78 ^{o}C. *t*-BuLi (2.3 mL of 1.24 M; 2.9 mmol; 1.1 equiv.) was added dropwise at -78 ^{o}C and after complete addition the flask was allowed to warm to RT. Arylnitro **4.66** (0.500 g; 2.6 mmol; 1 equiv.) was added dropwise as a solution in THF (5.2 mL) at RT. The reaction was stirred for 2 h at RT before quenching with NH_4Cl (sat. aq.). The aqueous phase was extracted with DCM (3x approx. 50 mL) and the combined organic layers were washed with brine, dried over Na_2SO_4, filtered, and concentrated *in vacuo*. Purification via silica gel flash chromatography (5:95 AcMe:hexanes) afforded alkene **4.65** as an orange oil in a 2.1:1 ratio of alkene isomers. Alkene **4.65** major isomer: **^{1}H-NMR** (500 MHz; $CDCl_3$): δ 7.84 (s, 1H), 7.53 (d, *J* = 8.8 Hz, 1H), 7.02 (d, *J* = 8.8 Hz, 1H), 5.87 (q, *J* = 6.8 Hz, 1H), 3.95 (s, 3H), 2.01 (s, 3H, overlapped with minor isomer), 1.80 (d, *J* = 6.9 Hz, 3H), Alkene **4.65** minor isomer: **^{1}H-NMR** (500 MHz; $CDCl_3$): δ 7.69 (s, 1H), 7.38 (d, *J* = 8.6 Hz, 1H), 7.06 (d, *J* = 8.6 Hz, 1H), 5.62 (q, *J* = 6.9 Hz, 1H), 3.96 (s, 3H), 2.01 (s, 3H, overlapped with major isomer), 1.60 (d, *J* = 6.9 Hz, 3H).

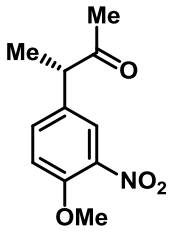

(±)–**4.64**

A 10 mL pear-shaped flask was flame-dried and charged with alkene **4.65** (50 mg; 0.24 mmol; 1 equiv.). The oil was dissolved in Et_2O (2.4 mL; 0.1 M) and $BH_3{\cdot}SMe_2$ (11 mg; 0.14 mmol; 0.6 equiv.) was added via microsyringe. The reaction was stirred at RT for 20 h before solvent was evaporated *in vacuo*. Crude material was redissolved in DCM (2.4 mL; 0.1 M) and activated 4 Å molecular sieves were added (approx. 650 mg). NMO (84 mg; 0.72 mmol; 3 equiv.) was added and the flask was stirred at RT for 2.5 h. TPAP (4.2 mg; 0.012 mmol; 5 mol%) was then added and the reaction was stirred at RT for an additional 2.5 h. The reaction mixture was diluted with EtOAc and filtered through a plug of silica gel, rinsing with EtOAc. The solvent was concentrated *in vacuo* and silica gel flash chromatography (2:8 EtOAc:hexanes) afforded ketone **4.64** in 56% yield as an off-white solid. **^{1}H-NMR** (500 MHz; $CDCl_3$): δ 7.73 (d, *J* = 2.2 Hz, 1H), 7.40 (dd, *J* = 8.7, 2.2 Hz, 1H), 7.08 (d, *J* = 8.7 Hz, 1H), 3.96 (s, 3H), 3.77 (q, *J* = 7.0 Hz, 1H), 2.11 (s, 3H), 1.42 (d, *J* = 7.1 Hz, 3H); **^{13}C-NMR** (126 MHz; $CDCl_3$): δ 207.9, 152.3, 139.8, 133.5, 132.9, 125.2, 114.2, 56.8, 52.3, 28.6, 17.5; **IR** (neat) 1705, 1621, 1530, 1341, 1274.

4.7.6 Dragmacidin E HWE olefination route procedures

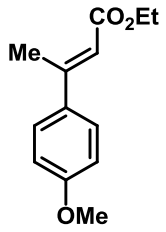

4.69

A 1 L round-bottom flask was evacuated and back-filled with nitrogen three times, then charged with NaH (2.4 g; 99.9 mmol; 1.5 equiv.). THF (400 mL) was added and the suspension was cooled to 0 ^{o}C. Triethylphosphonoacetate (25.3 g; 113 mmol; 1.7 equiv.) was added slowly and the mixture was stirred at 0 oC for 30 min. before 4'methoxyacetophenone (10.0 g; 66.6 mmol; 1 equiv.) was added as a solution in THF (100 mL). After complete addition the flask was allowed to warm to RT, was fitted with a reflux condenser, and was placed in a pre-heated oil bath. The reaction was refluxed for 24 h before allowing to cool to RT. The mixture was quenched with NH4Cl (sat. aq.) and extracted with Et_2O (3x approx. 200 mL). The combined organic layers were dried over Na_2SO_4, filtered, and concentrated *in vacuo*. Purification via silica gel flash chromatography (1:9 EtOAc:hexanes) afforded enoate **4.69** as a 3.7:1 mixture of alkene isomers in a combined 99% yield. ^{1}H-NMR data was in agreement with literature values.[30] Enoate **4.69** major isomer: **^{1}H-NMR** (400 MHz; $CDCl_3$): δ 7.47-7.44 (m, 2H), 6.91-6.87 (m, 2H, overlapping with minor isomer), 6.11 (q, *J* = 1.2 Hz, 1H), 4.21 (q, *J* = 7.1 Hz, 2H), 3.83 (s, 3H), 2.56 (d, *J* = 1.2 Hz, 3H), 1.31 (t, *J* = 7.1 Hz, 3H). Enoate **4.69** minor isomer: **^{1}H-NMR** (400 MHz; $CDCl_3$): δ 7.21-7.17 (m, 2H), 6.88-6.86 (m, 2H,

overlapping with major isomer), 5.87 (q, *J* = 1.4 Hz, 1H), 4.03 (q, *J* = 7.1 Hz, 2H), 3.81 (s, 3H), 2.16 (d, *J* = 1.4 Hz, 3H), 1.14 (t, *J* = 7.1 Hz, 4H).

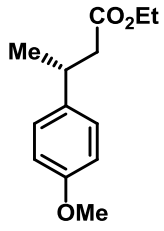

(±)–4.68

A 1 L round-bottom flask was evacuated and back-filled with nitrogen 3 times and then charged with Pd/C (0.70 g of 10% mix.; 0.658 mmol; 1 mol% Pd), followed by MeOH (200 mL). Enoate **4.69** (14.5 g; 65.8 mmol; 1 equiv.) was added as a solution in MeOH (130 mL). The mixture was purged with nitrogen for 5 min. before purging with H_2. The reaction was then stirred under a hydrogen balloon atmosphere at RT for 18 h. The solution was purged with nitrogen and filtered through Celite®, using EtOAc to aid transfer. The filtrate was concentrated in vacuo to afford ester **4.68** in 99% yield. 1H-NMR data was in agreement with literature values.[31] **^{1}H-NMR** (400 MHz; $CDCl_3$): δ 7.16-7.12 (m, 2H), 6.85-6.82 (m, 2H), 4.07 (q, *J* = 7.2 Hz, 2H), 3.78 (s, 3H), 3.23 (app sextet, *J* = 7.3 Hz, 1H), 2.57 (dd, *J* = 14.9, 7.2 Hz, 1H), 2.50 (dd, *J* = 14.9, 8.0 Hz, 1H). 1.27 (d, *J* = 7.0 Hz, 3H), 1.18 (t, *J* = 7.1 Hz, 3H).

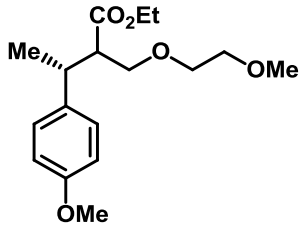

(±)–4.70

A 250 mL round-bottom flask was flame-dried and charged with *i*-Pr_2NH (2.51 g; 24.8 mmol; 1.1 equiv.) and THF (26 mL). The flask was cooled to -78 ^oC and *n*BuLi (9.47 mL of 2.62 M; 24.8 mmol; 1.1 equiv.) was added. The reaction was stirred at -78 ^oC for 45 min. before ester **4.68** (5.00 g; 22.5 mmol; 1 equiv.) was added as a solution in THF (30 mL). The mixture was stirred at -78 ^oC for 1 h before MEMCl (3.65 g; 29.3 mmol; 1.3 equiv.) was added dropwise. The reaction was slowly brought to RT overnight and then quenched with NH_4Cl (sat. aq.). The mixture was extracted with EtOAc (3x approx. 100 mL) and the combined organic layers were dried over Na_2SO_4, filtered, and concentrated *in vacuo*. Crude ester **4.70** was taken on as an inconsequential mixture of diastereomers without further purification due to observed decomposition when exposed to silica gel.

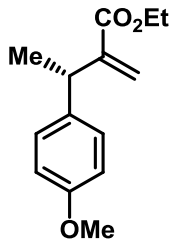

(±)–4.71

A 250 mL round-bottom flask was flame-dried and charged with solid KO*t*-Bu (2.52 g; 22.5 mmol; 1 equiv.). THF (50 mL) was added and the suspension was cooled to 0 ^oC. A THF (60 mL) solution of crude ester **4.70** was cooled to 0 ^oC and slowly transferred to the reaction flask. The reaction was stirred at 0 ^oC for 3 h before quenching with NH_4Cl

(sat. aq.) and was extracted with Et_2O (3x approx. 100 mL). The combined organic layers were dried over Na_2SO_4, filtered, and concentrated *in vacuo*. Crude enoate **4.71** was taken on without further purification.

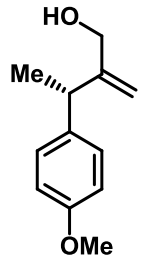

(±)–4.72

A 250 mL round-bottom flask was fitted with a dropping funnel and the apparatus was flame-dried. Crude enoate **4.71** was transferred to the reaction flask with the aid of toluene (75 mL; 0.3 M) and the flask was cooled to -78 ^oC. DIBAL (67.5 mL of 1.0 M; 67.5 mmol; 3 equiv.) was added to the dropping funnel, then added to the reaction dropwise at -78 ^oC. After complete addition, the flask was allowed to warm to RT overnight. The flask was cooled to -78 ^oC and the reaction was quenched with EtOAc (20 mL). The flask was allowed to warm to RT after which point the mixture was poured over an aqueous solution of Rochelle salt (250 mL) and stirred vigorously for 75 min. The mixture was diluted with EtOAc and filtered through Celite®, rinsing with EtOAc. The filtrate was extracted with EtOAc and the combined organic layers were stirred with an aqueous solution of Rochelle salt (100 mL) for a second time. After stirring for 45 min. the mixture was separated and the organic layer was washed with H_2O and brine, dried over Na_2SO_4, filtered, and concentrated *in vacuo*. Purification via silica gel flash chromatography (2:8 EtOAc:hexanes) provided allylic alcohol **4.72** as a pale yellow

liquid in 50% yield over 3 steps. **^{1}H-NMR** (500 MHz; $CDCl_3$): δ 7.14-7.11 (m, 2H), 6.84-6.81 (m, 2H), 5.18 (t, *J* = 1.0 Hz, 1H), 5.06 (t, *J* = 1.1 Hz, 1H), 3.96 (app t, *J* = 16.7 Hz, 2H, overlapped diastereotopic protons), 3.78 (s, 3H), 3.46 (q, *J* = 7.0 Hz, 1H), 1.38 (d, *J* = 7.1 Hz, 3H); **^{13}C-NMR** (126 MHz; CDCl3): δ 158.2, 152.8, 136.9, 128.4, 114.0, 109.0, 65.3, 55.4, 41.6, 20.7; **IR** (neat) 3358, 1610, 1509, 1242.

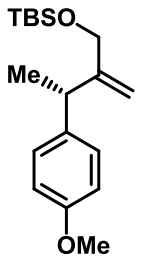

(±)–4.67

A 100 mL round-bottom flask was evacuated and back-filled with nitrogen 3 times, then charged with imidazole (0.851 g; 12.5 mmol; 2.4 equiv.) and a DCM (16 mL) solution of allylic alcohol **4.72** (1.00 g; 5.20 mmol; 1 equiv.). The flask was cooled to 0 ^{o}C and TBSCl (1.64 g; 10.9 mmol; 2.1 equiv.) was added as a DCM solution (10 mL). After complete addition the flask was allowed to warm to RT and stirred for 1 h before being quenched with NH_4Cl (sat. aq.). The mixture was extracted with DCM (3x approx. 50 mL) and the combined organic layers were washed with H_2O (2x approx. 50 mL) and brine (2x approx. 50 mL). The organic phase was then dried over Na_2SO_4, filtered, and concentrated *in vacuo*. Purification via silica gel flash chromatography (5:95 EtOAc:hexanes) afforded allylic ether **4.67** as a colorless liquid in 87% yield. **^{1}H-NMR** (500 MHz; $CDCl_3$): δ 7.11 (d, *J* = 8.5 Hz, 2H), 6.82 (d, *J* = 8.5 Hz, 2H), 5.19 (d, *J* = 0.5 Hz, 1H), 4.99 (d, *J* = 1.0 Hz, 1H), 3.97-3.91 (m, 2H), 3.79 (s, 3H), 3.40 (q, *J* = 7.1 Hz,

1H), 1.36 (d, *J* = 7.1 Hz, 3H), 0.88 (s, 9H), -0.02 (s, 6H); **^{13}C-NMR** (126 MHz; $CDCl_3$): δ 158.1, 152.5, 137.3, 128.5, 113.8, 108.3, 65.3, 55.4, 41.2, 26.1, 21.0, 18.5, -5.3; **IR** (neat) 2955, 2929, 2856, 1510, 1246.

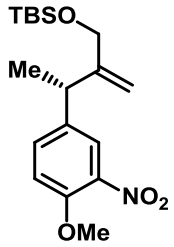

(±)–4.63

A 50 mL round-bottom flask was flame-dried and charged with $Cu(NO_3)_2 \cdot 5H_2O$ (1.45 g; 6.24 mmol; 1.2 equiv.) and acetic anhydride (10.4 mL). The flask was stirred at RT open to air for 1 h to dissolve $Cu(NO_3)_2 \cdot 5H_2O$ before cooling to -10 ^oC. Allylic ether **4.67** (1.00 g; 5.20 mmol; 1 equiv.) was dissolved in acetic anhydride (6.5 mL) and added to the open reaction flask such that the internal temperature did not exceed -5 ^oC. After complete addition the reaction was stirred at -10 ^oC for 2 h before quenching with H_2O and extracting with EtOAc. The combined organic layers were concentrated *in vacuo*, dissolved in MeOH (100 mL) and stirred at RT for 1 h before pouring over EtOAc and neutralizing with $NaHCO_3$ (sat. aq.). until a pH ≥ 8 was achieved. The aqueous phase was extracted with EtOAc and the combined organic layers were then dried over Na_2SO_4, filtered, and concentrated *in vacuo*. Purification via silica gel flash chromatography (15:85 EtOAc:hexanes) afforded arylnitro **4.63** as a yellow oil in 62% yield. **^{1}H-NMR** (500 MHz; $CDCl_3$): δ 7.68 (d, *J* = 1.9 Hz, 1H), 7.38 (dd, *J* = 8.6, 1.9 Hz, 1H), 7.00 (d, *J* = 8.6 Hz, 1H), 5.23 (s, 1H), 5.01 (s, 1H), 3.96 (d, 14 Hz, 1H), 3.94 (s, 3H), 3.92 (d, 14 Hz,

1H), 3.50 (q, *J* = 7.1 Hz, 1H), 1.38 (d, *J* = 7.1 Hz, 3H), 0.88 (s, 9H), -0.01 (s, 6H); **^{13}C-NMR** (126 MHz; $CDCl_3$): δ 151.5, 151.2, 139.6, 137.8, 133.4, 124.5, 113.6, 109.8, 65.3, 56.7, 40.7, 26.0, 20.6, 18.4, -5.3; **IR** (neat) 2929, 2856, 1620, 1529, 1258

4.8. Chapter 4 References

1) Jackson, J. J.; Kobayashi, H.; Steffens, S. D.; Zakarian, A. *Angew.Chem. Int. Ed.* **2015**, *54*, 9971-9975.

2) Kim, M.; Mulcahy, J. V.; Espino, C. G.; Du Bois, J. *Org. Lett.* **2006**, *8*, 1073-1076.

3) Evans, P. A.; Uraguchi, D. *J. Am. Chem. Soc.* **2003**, *125*, 7158-7159.

4) Corey, E. J.; Bakshi, R. K.; Shibata, S. *J. Am. Chem. Soc.* **1987**, *109*, 5551–5553.

5) Poli, G.; Prestat, G.; Liron, F.; Kammerer-Pentier, C. Selectivity in Palladium-Catalyzed Allylic Substitution In *Transition Metal Catalyzed Enantioselective Allylic Substitution in Organic Synthesis*; Kazmaier, U., Ed.; Springer: Berlin, 2012, p 1-64.

6) Garg, N. K.; Sarpong, R.; Stoltz, B. M. *J. Am. Chem. Soc.* **2002**, *124*, 13179-13184.

7) Bartoli, G.; Palmieri, G.; Bosco, M.; Dalpozzo, R. *Tetrahedron Lett.* **1989**, *30*, 2129-2132.

8) Graupner, P. R.; Gerwick, B. C.; Fields, S. C.; Scmitzer, P. R.; Brewster, W. K. Methylidene Mevalonates and Their use as Herbicides. 2006

9) Nicolaou, K. C.; Postema, M. H. D.; Miller, N. D.; Yang, G. *Angew. Chem. Int. Ed.* **1997**, *36*, 2821-2823.

10) Joly, G. D.; Jacobsen, E. N. *Org. Lett.* **2002**, *4*, 1795-1798.

11) Ladd, J. A. *Spectrochim. Acta* **1966**, *22*, 1157-1163.

12) Ashfeld, B. L.; Miller, K. A.; Smith, A. J.; Tran, K.; Martin, S. F. *J. Org. Chem.* **2007**, *72*, 9018-9031.

13) Aullon, G.; Esquius, G.; Lledos, A; Maseras, F.; Pons, J.; Ros, J. *Organometallics* **2004**, *23*, 5530-5539.

14) McCann, L. C.; Organ, M. G. *Angew. Chem. Int. Ed.* **2014**, *53*, 4386 –4389.

15) Chen, Z.; Liang, J.; Yin, J.; Yu, G.-A.; Liu, S. H. *Tetrahedron Lett.* **2013**, *54*, 5785–5787.

16) Bronner, S. M.; Bahnck, K. B.; Garg, N. K. *Org. Lett.* **2009**, *11*, 1007-1010.

17) Im, G.-Y. J.; Bronner, S. M.; Goetz, A. E.; Paton, R. S.; Cheong, P. H.-Y.; Houk, K. N.; Garg, N. K. *J. Am. Chem. Soc*. **2010**, *132*, 17933–17944.

18) Bronner, S. M.; Goetz, A. E.; Garg, N. K. *J. Am. Chem. Soc.* **2011**, *133*, 3832–3835.

19) Huters, A. D.; Quasdorf, K. W.; Styduhar, E. D.; Garg, N. K. *J. Am. Chem. Soc*. **2011**, *133*, 15797–15799.

20) Himeshima, Y.; Sonoda, T.; Kobayashi, H. *Chem. Lett.* **1983**, *12*, 1211–1214.

21) Vilsmeier, A.; Haack, A. *Chem. Ber*. **1927**, *60B*, 119-122.

22) Thomas, S. P.; Aggarwal, V. K. *Angew. Chem. Int. Ed.* **2009**, *48*, 1896 – 1898.

23) Mechelke, M. F.; Brethorst, J. T.; Crookston, C.; Klinkhammer, C.; Miller, B. N.; Payne, C.; Pillsbury, M.; Ringsmuth, C. R.; Traut, M. *J. Undergrad. Chem. Res.* **2014**, *13*, 12-14.

24) Ji, J.; Li, T.; Mortell, K. H.; Schrimpf, M. R.; Nersesian, D. L.; Pan, L. Fused bicycloheterocycle substituted quinuclidine derivatives. WO 2006/065233 A1, 2006

25) Kyne, R. E.; Ryan, M. C.; Kliman, L. T.; Morken, J. P. *Org. Lett.* **2010**, *12*, 3796-3799.

26) Rickerby, J.; Vallet, M.; Bernardinelli, G.; Viton, F.; Kuendig, E. P. *Chem. Eur. J.* **2007**, *13*, 3354 – 3368.

27) Murphy, J. A.; Scott, K. A.; Sinclair, R. S.; Martin, C. G.; Kennedy, A. R.; Lewis, N. *J. Chem. Soc., Perkin Trans. 1* **2000**, 2395–2408.

28) Moure, A. L; Mauleon, P.; Arrayas, R. G.; Carretero, J. C. *Org. Lett.* **2013**, *15*, 2054–2057.

29) Aridoss, G.; Laali, K. K. *J. Org. Chem.* **2011**, *76*, 8088–8094.

30) Thanh Nguyen, T. N.;Thiel, N. O.; Pape, F.; Teichert, J. F. *Org. Lett.* **2016**, *18*, 2455−2458.

31) Linsenmeier, A. M.; Braje, W. M. *Tetrahedron* **2015**, *71*, 6913-6919.

BIBLIOGRAPHY

(1) Shi, J.; Zhang, J.; Yue, Z.; Li, M.; Zhu, C.; Zhang, Y.; Zi, J.; Wang, Y.; Fan, X.; Xu, R.; Lin, S.; Li, Y.; Yang, Y.; Sheng, L. N6-Substituted adenosine derivatives, N6-substituted adenine derivatives and uses thereof. WO 2011/069294, 2012

(2) Zhang, G.; Wen, X.; Wang, Y.; Mo, W.; Ding, C. Sodium Nitrite Catalyzed Aerobic Oxidative Deoximation under Mild Conditions *J. Org. Chem.* **2011**, *76*, 4665–4668.

(3) Yasui, Y.; Kamisaki, H.; Takemoto, Y. Enantioselective Synthesis of 3,3-Disubstituted Oxindoles through Pd-Catalyzed Cyanoamidation *Org. Lett.* **2008**, *10*, 3303-3306.

(4) Wiberg, K. B. Bent Bonds in Organic Compounds *Acc. Chem. Res.* **1996**, *29*, 229-234.

(5) Wentzel, M.; Reddy, V. K.; Hyster, T. K.; Douglas, C. J. Chemoselectivity in Catalytic C-C and C-H Bond Activation: Controlling Intermolecular Carboacylation and Hydroarylation of Alkenes *Angew. Chem. Int. Ed.* **2009**, *48*, 6121 –6123.

(6) Wang, C.; Pettman, A.; Bacsa, J.; Xiao, J. A Versatile Catalyst for Reductive Amination by Transfer Hydrogenation *Angew. Chem. Int. Ed.* **2010**, *49*, 7548 –7552.

(7) Vaska, L. Reversible activation of covalent molecules by transition-metal complexes. The role of the covalent molecule *Acc. Chem. Res.* **1968**, *1*, 335–344.

(8) Urbanos, F.; Fernandez-Baeza, J.; Chaudret, B. Selective Aromatization of the A Ring of Steroids through Demethylation by an Electrophilic Ruthenium Fragment *J. Chem. Soc., Chem. Commun.* **1991**, 1739-1741.

(9) Tipper, C. F. H. Some Reactions of cyclopropane, and a Comparison with the Lower Olefins. Part II. Some Platinous-cyclopropane Complexes. *J. Chem. Soc.* **1955**, 2045-2046.

(10) Tannert, R.; Milroy, L.; Ellinger, B.; Hu, T.; Arndt, H.; Waldmann, H. Synthesis and Structure−Activity Correlation of Natural-Product Inspired Cyclodepsipeptides Stabilizing F-Actin *J. Am. Chem. Soc.* **2010**, *132*, 3063–3077.

(11) Suggs, J. W.; Jun, C.-H. Synthesis of a Chiral Rhodium Alkyl via Metal Insertion into an Unstrained C–C Bond and Use of the Rate of Racemization at Carbon to Obtain a Rhodium-Carbon Bond Dissociation Energy *J. Am. Chem. Soc.* **1986**, *108*, 4679-4681.

(12) Suggs, J. W.; Jun, C.-H. Metal-Catalysed Alkyl Ketone to Ethyl Ketone Conversions in Chelating Ketones via Carbon-Carbon Bond Cleavage *J. Chem. Soc., Chem. Commun.* **1985**, 92-93.

(13) Suggs, J. W.; Jun, C.-H. Directed Cleavage of Carbon-Carbon Bonds by Transition Metals: The alpha-Bonds of Ketones *J. Am. Chem. Soc.* **1984**, *106*, 3054-3056.

(14) Souillart, L.; Cramer, N. Catalytic C–C Bond Activations via Oxidative Addition to Transition Metals *Chem. Rev.* **2015**, *115*, 9410–9464.

(15) Simoes, J. A. M.; Beauchamp, J. L. Transition Metal-Hydrogen and Metal-Carbon Bond Strengths: The Keys to Catalysis *Chem. Rev.* **1990**, *90*, 629-688.

(16) Seiser, T.; Cramer, N. Enantioselective metal-catalyzed activation of strained rings *Org. Biomol. Chem.* **2009**, *7*, 2835–2840.

(17) Seiser, T., Saget, T., Tran, D. N.; Cramer, N. Cyclobutanes in Catalysis *Angew. Chem. Int. Ed.* **2011**, *50*, 7740–7752.

(18) Rybtchinski, B.; Milstein, D. Metal Insertion into C–C Bonds in Solution *Angew. Chem. Int. Ed.* **1999**, *38*, 870-883.

(19) Ruhland, K. Transition-Metal-Mediated Cleavage and Activation of C-C Single Bonds *Eur. J. Org. Chem.* **2012**, *2012*, 2683-2706.

(20) Rondla, N. R.; Ogilvie, J. M.; Pan, Z.; Douglas, C. J. Palladium catalyzed intramolecular acylcyanation of alkenes using α-iminonitriles *Chem. Commun.* **2014**, *50*, 8974--8977.

(21) Rondla, N. R.; Levi, S. M.; Ryss, J. M.; Vanden Berg, R. A.; Douglas, C. J. Palladium-Catalyzed C-CN Activation for Intramolecular Cyanoesterification of Alkynes *Org. Lett.* **2011**, *13*, 1940–1943.

(22) Rahimi, N.; Karimzadeh, R. Catalytic cracking of hydrocarbons over modified ZSM-5 zeolites to produce lightolefins: A review *Applied Catalysis A: General* **2011**, *398*, 1–17.

(23) Periana, R. A.; Bergman, R. G. Rapid Intramolecular Rearrangement of a Hydridocyclopropylrhodium Complex to a Rhodacyclobutane. Independent Synthesis of the Metallacycle by Addition of Hydride to the Central Carbon Atom of a Cationic Rhodium pi-Allyl Complex *J. Am. Chem. Soc.* **1984**, *106*, 7272-7274.

(24) Pan, Z.; Pound, S. M.; Rondla, N. R.; Douglas, C. J. Intramolecular Aminocyanation of Alkenes by N-CN Bond Cleavage *Angew. Chem. Int. Ed.* **2014**, *53*, 5170 –5174.

(25) Omae, I. Intramolecular five-membered ring compounds and their applications *Coord.Chem. Rev.* **2004**, *248*, 995–1023.

(26) Nakao, Y.; Oda, S.; Hiyama, T. Nickel-Catalyzed Arylcyanation of Alkynes *J. Am. Chem. Soc.* **2004**, *126*, 13904-13905.

(27) Murakami, M.; Matsuda, T. Metal-catalysed cleavage of carbon-carbon bonds *Chem. Comm.* **2011**, *47*, 1100-1105.

(28) Miyazaki, Y.; Ohta, N.; Semba, K.; Nakao, Y. Intramolecular Aminocyanation of Alkenes by Cooperative Palladium/Boron Catalysis *J. Am. Chem. Soc.* **2012**, *134*, 6544–6547.

(29) McMillen, D. F.; Golden, D. M. Hydrocarbon Bond Dissociation Energies *Rev. Phys. Chem.* **1982**, *33*, 493-532.

(30) Matsuda, T.; Tsuboi, T.; Murakami, M. Rhodium-Catalyzed Carbonylation of Spiropentanes *J. Am. Chem. Soc.* **2007**, *129*, 12596-12597.

(31) Li, J.; Neuville, L. Copper-Catalyzed Oxidative Three-Component Synthesis of N, N′,N″-Trisubstituted Guanidines *Org. Lett.* **2013**, *15*, 6124–6127.

(32) Kundig, P. E.; Seidel, T. M.; Jia, Y.; Bernardinelli, G. Bulky Chiral Carbene Ligands and Their Application in the PalladiumCatalyzed Asymmetric Intramolecular a-Arylation of Amides *Angew. Chem., Int. Ed.* **2007**, *46*, 8484 –8487.

(33) Köster, R.; Binger, P.; Fenzl, W. Triphenylborane *Inorg. Synth.* **1974**, *15*, 134-136.

(34) Koester, D. C.; Kobayashi, M.; Werz, D. B.; Nakao, Y. Intramolecular Oxycyanation of Alkenes by Cooperative Pd/BPh3 Catalysis *J. Am. Chem. Soc.* **2012**, *134*, 6544–6547.

(35) Kliman, J. P.; Dubeck, M. The Preparation of Cyclopentadienyl[o-(phenylazo)phenyl]nickel *J. Am. Chem. Soc.* **1963**, *85*, 1544-1545.

(36) Kamlet, M. J.; Abboud, J. L. M.; Abraham, M. H.; Taft, R. W. Linear solvation energy relationships. 23. A comprehensive collection of the solvatochromic parameters, .pi.*, .alpha., and .beta., and some methods for simplifying the generalized solvatochromic equation *J. Org. Chem.* **1983**, *48*, 2877–2887.

(37) Kamer, P. C. J.; van Leeuwen, P. W. N. M.; Reek, J. N. H. Wide Bite Angle Diphosphines: Xantphos Ligands in Transition Metal Complexes and Catalysis *Acc. Chem. Res.* **2001**, *34*, 895–904.

(38) Jung, M. E.; Piizzi, G. gem-Disubstituent Effect: Theoretical Basis and Synthetic Applications *Chem. Rev.* **2005**, *105*, 1735-1766.

(39) Jun, C.-H. Transition metal-catalyzed carbon-carbon bond activation *Chem. Soc. Rev.* **2004**, *33*, 610-618.

(40) Hoang, G. T.; Reddy, V. J.; Nguyen, H. H. K.; Douglas, C. J. Insertion of an Alkene into an Ester: Intramolecular Oxyacylation Reaction of Alkenes through Acyl C-O Bond Activation *Angew. Chem. Int. Ed.* **2011**, *50*, 1882 –1884.

(41) Halcrow, M. A.; Urbanos, F.; Chaudret, B. Aromatization of the B-Ring of 5,7-Dienyl Steroids by the Electrophilic Ruthenium Fragment "$[Cp^*Ru]^+$" *Organometallics* **1993**, *12*, 955-957.

(42) Gozin, M.; Weisman, A.; Ben-David, Y.; Milstein, D. Activation of a carbon-carbon bond in solution by transition-metal insertion *Nature* **1993**, *364*, 699-701.

(43) Gerlach, D. H.; Kane, A. R.; Parshall, G. W.; Jesson, J. P.; Muetterties, E. L. Reactivity of Trialkylphosphine Complexes of Platinum(0) *J. Am. Chem. Soc.* **1971**, *93*, 3543–3544.

(44) Frost, G. B.; Serratore, N. A.; Ogilvie, J. M.; Douglas, C. J. Mechanistic Model for Enantioselective Intramolecular Alkene Cyanoamidation via Palladium-Catalyzed C−CN Bond Activation *J. Org. Chem.* **2017**, *82*, 3721−3726.

(45) Fraser, A. W.; Besaw, J. E.; Hull, L. E.; Baird, M. C. Pd(η3-1-PhC3H4)(η5-C5H5) as a Catalyst Precursor for Buchwald−Hartwig Amination Reactions *Organometallics* **2012**, *31*, 3928−3935.

(46) Eliel, E. L.; Manoharan, M. Conformational Analysis. 40. Conformation of 1-Methyl-1-phenylcyclohexane and the Conformational Energies of the Phenyl and Vinyl Groups *J. Org. Chem.* **1981**, *46*, 1959-1962.

(47) Dreis, A. M.; Otte, S. C.; Eastwood, M. S.; Alonzi, E. R.; Brethorst, J. T.; Douglas, C. J. Diastereoselective Intramolecular Cyanoamidation with Alkenes *Eur. J. Org. Chem.* **2017**, 45–48.

(48) Dreis, A. M.; Douglas, C. J. Catalytic Carbon-Carbon sigma Bond Activation: An Intramolecular Carbo-Acylation Reaction with Acylquinolines *J. Am. Chem. Soc.* **2009**, *131*, 412-413.

(49) Crabtree, R. H.; Dion, R. P. Selective alkane C-C bond Cleavage via Prior Dehydrogenation by a Transition Metal Complex *J. Chem. Soc., Chem. Commun.* **1984**, 1260-1261.

(50) Crabtree, R.H. The Organometallic Chemistry of Alkanes *Chem. Rev.* **1985**, *85*, 245-269.

(51) Chen, F.; Wang, T.; Jiao, N. Recent Advances in Transition-Metal-Catalyzed Functionalization of Unstrained Carbon–Carbon Bonds *Chem. Rev.* **2014**, *114*, 8613–8661.

(52) Bruce, M. I. Cyclometalation Reactions *Angew. Chem. Int. Ed.* **1977**, *16*, 73-86.

(53) Blanksby, S.J.; Ellison, G.B. Bond Dissociation Energies of Organic Molecules *Acc. Chem. Res.* **2003**, *36*, 255-263.

(54) Adams, D. M.; Chatt, J.; Guy, R. G.; Sheppard, N. The Structure of "Cyclopropane Platinous Chloride." *J. Chem. Soc.* **1961**, 738-742.

(55) Abiraj, K.; Gowda, D. C. Zinc/ammonium formate: a new facile system for the rapid and selective reduction of oximes to amines *J. Chem. Research (S)* **2003**, 332–334.

(56) Nakao, Y. Catalytic C–CN Bond Activation In *C-C Bond Activation*; Dong, G., Ed.; Springer: Berlin, 2014, p 33–58.

(57) Jun, C.-H.; Park, J.-W. Directed C – C Bond Activation by Transition Metal Complexes In *Directed Metallation*; Chantani, N., Ed.; Springer: Berlin-Heidelberg, 2007; Vol. 24, p 117-143.

(58) Dreis, A. M.; Douglas, C. J. Carbon–Carbon Bond Activation with 8-Acylquinolines In *C-C Bond Activation*; Dong, G., Ed.; Springer: Berlin, 2014, p 85–110.

(59) Das, J.; Natesan, S.; Trehan, S.; Iqbal, J.; Magadi, S. K. Antiifective 1,2,3-Triazole Derivatives, Process for Their Preparation and Pharmaceutical Compositions Containing Them. WO 2004/101531 A1, 2004

(60) Zhang, H.; Cai, Q; Ma, D. Amino Acid Promoted CuI-Catalyzed C-N Bond Formation between Aryl Halides and Amines or N-Containing Heterocycles *J. Org. Chem.* **2005**, *70*, 5164-5173.

(61) Yin, J.; Xiang, B.; Huffman, M. A.; Raab, C. E.; Davies, I. W. A General and Efficient 2-Amination of Pyridines and Quinolines *J. Org. Chem.* **2007**, *72*, 4554–4557.

(62) Willis, M. C. Transition Metal Catalyzed Alkene and Alkyne Hydroacylation *Chem. Rev.* **2010**, *110*, 725–748.

(63) Vautravers, N. R.; Regent, D. D.; Bernhard Breit, B. Inter- and intramolecular hydroacylation of alkenes employing a bifunctional catalyst system *Chem. Commun.* **2011**, *47*, 6635–6637.

(64) Tsuji, J.; Ohno, K. Organic syntheses by means of noble metal compounds XXI. Decarbonylation of aldehydes using rhodium complex *Tetrahedron Lett.* **1965**, *6*, 3969.

(65) Suggs, J. W. Activation of Aldehyde C-H Bonds to Oxidative Addition via Formation of 3-Methyl-2-aminopyridyl Aldimines and Related Compounds: Rhodium Based Catalytic Hydroacylation *J. Am. Chem. Soc.* **1979**, *101*, 489.

(66) Sharma, K. K.; Patel, D. I.; Jain, R. Metal-free synthesis of N-fused heterocyclic iodides via C–H functionalization mediated by tert-butylhydroperoxide *Chem. Commun.* **2015**, *51*, 15129-15132.

(67) Rhinehart, J. L.; Manbeck, K. A.; Buzak, S. K.; Lippa, G. M.; Brennessel, W. W.; Goldberg, K. I.; Jones, W. D. Catalytic Arene H/D Exchange with Novel Rhodium and Iridium Complexes *Organometallics* **2012**, *31*, 1943−1952.

(68) Malosh, C. F.; Ready, J. M. Catalytic Cross-Coupling of Alkylzinc Halides with α-Chloroketones *J. Am. Chem. Soc.* **2004**, *126*, 10240–10241.

(69) Maleckis, A.; Kampf, J. W.; Sanford, M. S. A Detailed Study of Acetate-Assisted C−H Activation at Palladium(IV) Centers *J. Am. Chem. Soc.* **2013**, *135*, 6618−6625.

(70) Liston, D. J.; Lee, Y. J.; Scheidt, W. R.; Reed, C. A. Observations on Silver Salt Metathesis Reactions with Very Weakly Coordinating Anions *J. Am. Chem. Soc.* **1989**, *111*, 6643-6648.

(71) Lim, C. W.; Tissot, O.; Mattison, A.; Hooper, M. W.; Brown, J. M.; Cowley, A. R.; Hulmes, D. I.; Blacker, A. J. Practical Preparation and Resolution of 1-(2'-Diphenylphosphino-1'-naphthyl)isoquinoline: A Useful Ligand for Catalytic Asymmetric Synthesis *Org. Process Res. Dev.* **2003**, *7*, 379-384.

(72) Lafrance, M.; Gorelsky, S. I.; Fagnou, K. High-Yielding Palladium-Catalyzed Intramolecular Alkane Arylation: Reaction Development and Mechanistic Studies *J. Am. Chem. Soc.* **2007**, *129*, 14570−14571.

(73) Ko, H. M.; Dong, G. Cooperative activation of cyclobutanones and olefins leads to bridged ring systems by a catalytic [4 + 2] coupling *Nature Chem.* **2014**, *6*, 739–744.

(74) Jun, C.-H.; Lee, H.; Hong, J.-B. Chelation-Assisted Intermolecular Hydroacylation: Direct Synthesis of Ketone from Aldehyde and 1-Alkane *J. Org. Chem.* **1997**, *62*, 1200-1201.

(75) Jun, C.-H.; Lee, H. Catalytic Carbon−Carbon Bond Activation of Unstrained Ketone by Soluble Transition-Metal Complex *J. Am. Chem. Soc.* **1999**, *121*, 880-881.

(76) Jun, C.-H.; Lee, D.-Y.; Lee, H.; Hong, J.-B. A Highly Active Catalyst System for Intermolecular Hydroacylation *Angew. Chem. Int. Ed.* **2000**, *39*, 3070-3072.

(77) Jun, C.-H.; Hong, J.-B. Catalytic Transformation of Aldimine to Ketimine by Wilkinson's Complex through Transimination *Org. Lett.* **1999**, *1*, 887-889.

(78) Johnson, F.; Nasutavicus, W. A. The Cyclization of Dinitriles by Anhydrous Halogen Acids. A New Synthesis of Isoquinolines *J. Org. Chem.* **1962**, *27*, 3953–3958.

(79) Hsieh, H.-P.; McLaughlin, L. W. Syntheses of Two Pyridine C-Nucleosides as "Deletion-Modified'' Analogues of dT and dC *J. Org. Chem.* **1995**, *60*, 5356-5359.

(80) Hoshimoto, Y.; Hayashi, Y.; Suzuki, H.; Ohashi, M.; Ogoshi, S. Synthesis of Five- and Six-Membered Benzocyclic Ketones through Intramolecular Alkene Hydroacylation Catalyzed by Nickel(0)/N-Heterocyclic Carbenes *Angew. Chem. Int. Ed.* **2012**, *51*, 10812 –10815.

(81) Guin, J.; Varseev, G.; List, B. Catalytic Asymmetric Protonation of Silyl Ketene Imines *J. Am. Chem. Soc.* **2013**, *135*, 2100–2103.

(82) de Viedma, A. G.; Martınez-Barrasa, V.; Burgos, C.; Izquierdo, M. L.; Alvarez-Builla, J. N-Azinylpyridinium N-Aminides: Intermediates for the Regioselective Synthesis of 3-Fluoro-2-aminopyridine Derivatives *J. Org. Chem.* **1999**, *64*, 1007-1010.

(83) Bhat, V.; Wang, S.; Stoltz, B. M.; Virgil, S. C. Asymmetric Synthesis of QUINAP via Dynamic Kinetic Resolution *J. Am. Chem. Soc.* **2013**, *135*, 16829−16832.

(84) Beletskiy, E. V.; Sudheer, Ch; Douglas, C. J. Cooperative catalysis approach to intramolecular hydroacylation *J. Org. Chem.* **2012**, *77*, 5884-5893.

(85) Bear, B. R.; Sparks, S. M.; Shea, K. J. The type 2 intramolcular Diels–Alder reaction: synthesis and chemistry of bridgehead alkene *Angew. Chem. Int. Ed.* **2001**, *40*, 820–849.

(86) Longley, R. E.; Isbrucker, R. A.; Wright, A. E. Use of Imidazole And Indole Compounds as Inhibitors of Nitric Oxide Synthase. US006087363A, 1999

(87) Zhang, F.; Wang, B.; Prasad, P.; Capon, R. J.; Jia, Y. Asymmetric Total Synthesis of (+)-Dragmacidin D Reveals Unexpected Stereocomplexity *Org. Lett.* **2015**, *17*, 1529 – 1532.

(88) Yonemitsu, O.; Cerutti, P.; Witkop, B. Photoreductions and Photocyclizations of Tryptophan *J. Am. Chem. Soc.* **1966**, *88*, 3941-3945.

(89) Wright, A. E.; Pomponi, S. A.; Cross, S. S.; McCarthy, P. A New Bis(indole) Alkaloid from a Deep-Water Marine Sponge of the Genus Spongosorites *J. Org. Chem.* **1992**, *57*, 4772-4775.

(90) Wang, B.; Qin, H.; Zhang, F.; Jia, Y. Synthesis of the cycloheptannelated indole fragment of dragmacidin E *Tetrahedron Lett.* **2014**, *55*, 1561–1563.

(91) Tokuyama, H.; Yokoshima, S.; Yamashita, T.; Fukuyama, T. A Novel Ketone Synthesis by a Palladium-Catalyzed Reaction of Thiol Esters and Organozinc Reagents *Tetrahedron Lett.* **1998**, *39*, 3189-3192.

(92) Stoltz, B. M. Palladium Catalyzed Aerobic Dehydrogenation: From Alcohols to Indoles and Asymmetric Catalysis *Chem. Lett.* **2004**, *33*, 362-367.

(93) Stivala, C. E.; Zakarian, A. Highly Enantioselective Direct Alkylation of Arylacetic Acids with Chiral Lithium Amides as Traceless Auxiliaries *J. Am. Chem. Soc.* **2011**, *133*, 1936–11939.

(94) Qian, X.; Russel, K. C.; Boteju, L. W.; Hruby, V. J. Stereoselective Total Synthesis of Topographically Constrained Designer Amino Acids: 2', 6'-Dimethyl-β-methyltyrosines *Tetrahedron* **1995**, *51*, 1033−1054.

(95) Neber, P. W.; Friedolsheim, A. New kind of rearrangement of oximes *Ann.* **1926**, *449*, 109–134.

(96) Morris, S. A.; Andersen, R. J. Brominated Bis(indole) Alkaloids From the Marine Sponge Hexadella sp. *Tetrahedron* **1990**, *46*, 715-720.

(97) Molina, J. A.; Jimenez-Jimenez, F. J.; Orti-Pareja, M.; Navarro, J. A. The Role of Nitric Oxide in Neurodegeneration Potential for Pharmacological Intervention *1998* **1998**, *12*, 251-259.

(98) Manthey, M. K.; Gonzalez-Bello, C.; Abell, C. Synthesis of (2R)-2-bromodehydroquinic acid and (2R)-2-fluorodehydroquinic acid *J. Chem. Soc., Perkin Trans. 1* **1997**, *5*, 625-628.

(99) Mandal, D.; Yamaguchi, A. D.; Yamaguchi, J.; Itami, K. Synthesis of Dragmacidin D via Direct C-H Couplings *J. Am. Chem. Soc.* **2011**, *133*, 19660–19663.

(100) Luzzio, F. A. The Henry reaction: recent examples *Tetrahedron* **2001**, *57*, 915-945.

(101) Larock, R. C.; Yum, E. K. Synthesis of Indoles via Palladium-Catalyzed Heteroannulation of Internal Alkynes *J. Am. Chem. Soc.* **1991**, *113*, 6689 – 6690.

(102) Kohmoto, S.; Kashman, Y.; McConnell, O. J.; Rinehart, K. L. Jr.; Wright, A.; Koehn, F. Dragmacidin, a New Cytotoxic Bis(indole) Alkaloid from a Deep Water Marine Sponge, Dragmacidon sp. *J. Org. Chem.* **1988**, *53*, 3116-3118.

(103) Jia, Y.; Zhu, J. Palladium-Catalyzed, Modular Synthesis of Highly Functionalized Indoles and Tryptophans by Direct Annulation of Substituted *o*-Haloanilines and Aldehydes *J. Org. Chem.* **2006**, *71*, 7826−7834.

(104) Jackson, J. J.; Kobayashi, H.; Steffens, S. D.; Zakarian, A. 10-Step Asymmetric Total Synthesis and Stereochemical Elucidation of (+)-Dragmacidin D *Angew.Chem. Int. Ed.* **2015**, *54*, 9971-9975.

(105) Inoue, N.; Nakano, S.-I.; Harada, S.; Hamada, Y.; Nemoto, T. Synthetic Study of Dragmacidin E: Construction of the Core Structure Using Pd-Catalyzed Cascade Cyclization and Rh-Catalyzed Aminoacetoxylation *J. Org. Chem.* **2017**, *82*, 2787−2793.

(106) Huntley, R. J.; Funk, R. L. A Strategy for the Total Synthesis of Dragmacidin E. Construction of the Core Ring System *Org. Lett.* **2006**, *8*, 4775-4778.

(107) Hashem, M. A.; Sultana, I.; Hai, M. A. Synthesis of an analogue of the naturally occurring Aristotelia indole alkaloid, fruticosoline *Indian J. Chem., Sect. B* **1999**, *38*, 789-794.

(108) Garg, N. K.; Stoltz, B. M. A unified synthetic approach to the pyrazinone dragmacidins *Chem. Commun.* **2006**, *0*, 3769–3779.

(109) Garg, N. K.; Sarpong, R.; Stoltz, B. M. The First Total Synthesis of Dragmacidin D *J. Am. Chem. Soc.* **2002**, *124*, 13179-13184.

(110) Garg, N. K.; Caspi, D. D.; Stoltz, B. M. The Total Synthesis of (+)-Dragmacidin F *J. Am. Chem. Soc.* **2004**, *126*, 9552-9553.

(111) Feldman, K. S.; Ngernmeesrib, P. Total Synthesis of (±)-Dragmacidin E; Problems Solved and Lessons Learned *Synlett* **2012**, *23*, 1882–1892.

(112) Feldman, K. S.; Ngernmeesri, P. Total Synthesis of (±)-Dragmacidin E *Org. Lett.* **2011**, *13*, 5704–5707.

(113) Feldman, K. S.; Ngernmeesri, P. Dragmacidin E Synthesis Studies. Preparation of a Model Heptacyclic Core Structure *Org. Lett.* **2010**, *12*, 4502−4505.

(114) Feldman, K. S.; Ngernmeesri, P. Dragmacidin E Synthesis Studies. Preparation of a Model Cycloheptannelated Indole Fragment *Org. Lett.* **2005**, *7*, 5449-5452.

(115) Dobson, D.; Todd, A.; Gilmore, J. The Synthesis of 7-Alkoxyindoles *Synth. Commun.* **1991**, *21*, 611–617.

(116) Dess, D. B.; Martin, J. C. Readily accessible 12-I-5 oxidant for the conversion of primary and secondary alcohols to aldehydes and ketones *J. Org. Chem.* **1983**, *48*, 4155-4156.

(117) Cutignano, A.; Bifulco, G.; Bruno, I.; Casapullo, A.; Gomez-Paloma, L.; Riccio, R. Dragmacidin F: A New Antiviral Bromoindole Alkaloid from the Mediterranean Sponge Halicortex sp. *Tetrahedron* **2000**, *56*, 3743-3748.

(118) Capon, R. J.; Rooney, F.; Murray, L. M.; Collins, E.; Sim, A. T. R.; Rostas, J. A. P.; Butler, M. S.; Carrol, A. R. Dragmacidins: New Protein Phosphatase Inhibitors from a Southern Australian Deep-Water Marine Sponge, Spongosorites sp. *J. Nat. Prod.* **1998**, *61*, 660-662.

(119) Bartoli, G.; Palmieri, G.; Bosco, M.; Dalpozzo, R. The Reaction of Vinyl Grignard Reagents With 2-Substituted Nitroarenes: A New Approach to the Synthesis of 7-Substituted Indoles *Tetrahedron Lett.* **1989**, *30*, 2129-2132.

(120) Barlin, G. B. Purine analogues as amplifiers of phleomycin. VIII. Some Thiazolo[4,5-b]pyrazines and related compounds *Aust. J. Chem.* **1983**, *36*, 983-992.

(121) Poli, G.; Prestat, G.; Liron, F.; Kammerer-Pentier, C. Selectivity in Palladium-Catalyzed Allylic Substitution In *Transition Metal Catalyzed Enantioselective Allylic Substitution in Organic Synthesis*; Kazmaier, U., Ed.; Springer: Berlin, 2012, p 1-64.

(122) Ji, J.; Li, T.; Mortell, K. H.; Schrimpf, M. R.; Nersesian, D. L.; Pan, L. Fused bicycloheterocycle substituted quinuclidine derivatives. WO 2006/065233 A1, 2006

(123) Graupner, P. R.; Gerwick, B. C.; Fields, S. C.; Scmitzer, P. R.; Brewster, W. K. Methylidene Mevalonates and Their use as Herbicides. 2006

(124) Vilsmeier, A.; Haack, A. Action of phosphorous halides on alkylformanilides. A new method for the preparation of secondary and tertiary p-alkylaminobenzaldehydes *Chem. Ber.* **1927**, *60B*, 119-122.

(125) Thomas, S. P.; Aggarwal, V. K. Asymmetric Hydroboration of 1,1-Disubstituted Alkenes *Angew. Chem. Int. Ed.* **2009**, *48*, 1896 – 1898.

(126) Thanh Nguyen, T. N.;Thiel, N. O.; Pape, F.; Teichert, J. F. Copper(I)-Catalyzed Allylic Substitutions with a Hydride Nucleophile *Org. Lett.* **2016**, *18*, 2455−2458.

(127) Rickerby, J.; Vallet, M.; Bernardinelli, G.; Viton, F.; Kuendig, E. P. Ruthenium–Lewis Acid Catalyzed Asymmetric Diels–Alder Reactions between Dienes and α,β-Unsaturated Ketones *Chem. Eur. J.* **2007**, *13*, 3354 – 3368.

(128) Nicolaou, K. C.; Postema, M. H. D.; Miller, N. D.; Yang, G. A Novel Approach to the CP-225,917 and CP-263,114 Core *Angew. Chem. Int. Ed.* **1997**, *36*, 2821-2823.

(129) Murphy, J. A.; Scott, K. A.; Sinclair, R. S.; Martin, C. G.; Kennedy, A. R.; Lewis, N. A radical based addition–elimination route for the preparation of indoles *J. Chem. Soc., Perkin Trans. 1* **2000**, 2395–2408.

(130) Moure, A. L; Mauleon, P.; Arrayas, R. G.; Carretero, J. C. Formal Regiocontrolled Hydroboration of Unbiased Internal Alkynes via Borylation/Allylic Alkylation of Terminal Alkynes *Org. Lett.* **2013**, *15*, 2054–2057.

(131) Mechelke, M. F.; Brethorst, J. T.; Crookston, C.; Klinkhammer, C.; Miller, B. N.; Payne, C.; Pillsbury, M.; Ringsmuth, C. R.; Traut, M. Design and Synthesis of a Novel Alpha-methylene Lactone Chemotherapeutic Agent *J. Undergrad. Chem. Res.* **2014**, *13*, 12-14.

(132) McCann, L. C.; Organ, M. G. On The Remarkably Different Role of Salt in the Cross-Coupling of Arylzincs From That Seen With Alkylzincs *Angew. Chem. Int. Ed.* **2014**, *53*, 4386 –4389.

(133) Linsenmeier, A. M.; Braje, W. M. Efficient one-pot synthesis of dihydroquinolinones in water at room temperature *Tetrahedron* **2015**, *71*, 6913-6919.

(134) Ladd, J. A. The nuclear magnetic resonance spectra of phenylithium, diphenylmagnesium and diphenylzinc *Spectrochim. Acta* **1966**, *22*, 1157-1163.

(135) Kyne, R. E.; Ryan, M. C.; Kliman, L. T.; Morken, J. P. Allylation of Nitrosobenzene with Pinacol Allylboronates. A Regioselective Complement to Peroxide Oxidation *Org. Lett.* **2010**, *12*, 3796-3799.

(136) Kim, M.; Mulcahy, J. V.; Espino, C. G.; Du Bois, J. Expanding the Substrate Scope for C-H Amination Reactions: Oxidative Cyclization of Urea and Guanidine Derivatives *Org. Lett.* **2006**, *8*, 1073-1076.

(137) Joly, G. D.; Jacobsen, E. N. Catalyst-Controlled Diastereoselective Hetero-Diels-Alder Reactions *Org. Lett.* **2002**, *4*, 1795-1798.

(138) Im, G.-Y. J.; Bronner, S. M.; Goetz, A. E.; Paton, R. S.; Cheong, P. H.-Y.; Houk, K. N.; Garg, N. K. Indolyne Experimental and Computational Studies: Synthetic Applications and Origins of Selectivities of Nucleophilic Additions *J. Am. Chem. Soc.* **2010**, *132*, 17933–17944.

(139) Huters, A. D.; Quasdorf, K. W.; Styduhar, E. D.; Garg, N. K. Total Synthesis of (-)-*N*-Methylwelwitindolinone C Isothiocyanate *J. Am. Chem. Soc.* **2011**, *133*, 15797–15799.

(140) Himeshima, Y.; Sonoda, T.; Kobayashi, H. Fluoride-induced 1,2-elimination of *o*-trimethylsilyl-phenyl triflate to benzyne under mild conditions *Chem. Lett.* **1983**, *12*, 1211–1214.

(141) Evans, P. A.; Uraguchi, D. Regio- and Enantiospecific Rhodium-Catalyzed Arylation of Unsymmetrical Fluorinated Acyclic Allylic Carbonates: Inversion of Absolute Configuration *J. Am. Chem. Soc.* **2003**, *125*, 7158-7159.

(142) Corey, E. J.; Bakshi, R. K.; Shibata, S. Highly enantioselective borane reduction of ketones catalyzed by chiral oxazaborolidines. Mechanism and synthetic implications *J. Am. Chem. Soc.* **1987**, *109*, 5551–5553.

(143) Chen, Z.; Liang, J.; Yin, J.; Yu, G.-A.; Liu, S. H. Alder-ene reaction of aryne with olefins *Tetrahedron Lett.* **2013**, *54*, 5785–5787.

(144) Bronner, S. M.; Goetz, A. E.; Garg, N. K. Overturning Indolyne Regioselectivities and Synthesis of Indolactam V *J. Am. Chem. Soc.* **2011**, *133*, 3832–3835.

(145) Bronner, S. M.; Bahnck, K. B.; Garg, N. K. Indolynes as Electrophilic Indole Surrogates: Fundamental Reactivity and Synthetic Applications *Org. Lett.* **2009**, *11*, 1007-1010.

(146) Bartoli, G.; Palmieri, G.; Bosco, M.; Dalpozzo, R. The reaction of vinyl Grignard reagents with 2-substituted nitroarenes: a new approach to the synthesis of 7-substitued indoles *Tetrahedron Lett.* **1989**, *30*, 2129-2132.

(147) Aullon, G.; Esquius, G.; Lledos, A; Maseras, F.; Pons, J.; Ros, J. Unexpected Influence of the Counteranion in the κ2 vs κ3 Hapticity of Polydentate N-Donor Ligands in [RhI(N-ligand)L2]+ Complexes *Organometallics* **2004**, *23*, 5530-5539.

(148) Ashfeld, B. L.; Miller, K. A.; Smith, A. J.; Tran, K.; Martin, S. F. Features and Applications of [Rh(CO)2Cl]2-Catalyzed Alkylations of Unsymmetrical Allylic Substrates *J. Org. Chem.* **2007**, *72*, 9018-9031.

(149) Aridoss, G.; Laali, K. K. Ethylammonium Nitrate (EAN)/Tf2Oand EAN/TFAA: Ionic Liquid Based Systems for Aromatic Nitration *J. Org. Chem.* **2011**, *76*, 8088–8094.

APPENDIX

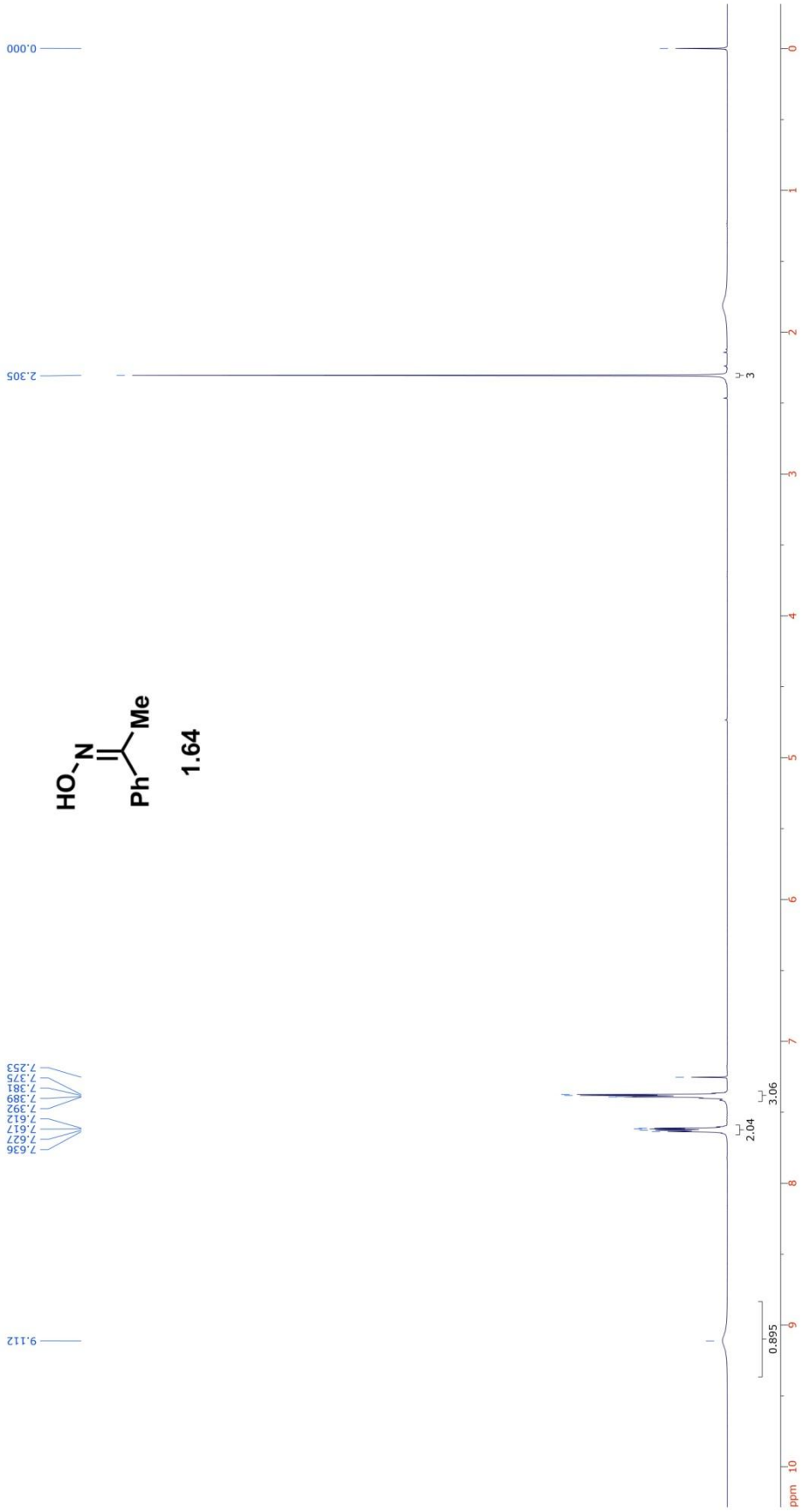
0.000
2.305
9.112
7.636
7.627
7.617
7.612
7.392
7.389
7.381
7.375
7.253
3
3.06
2.04
0.895
ppm
HO
N
Ph
Me
1.64

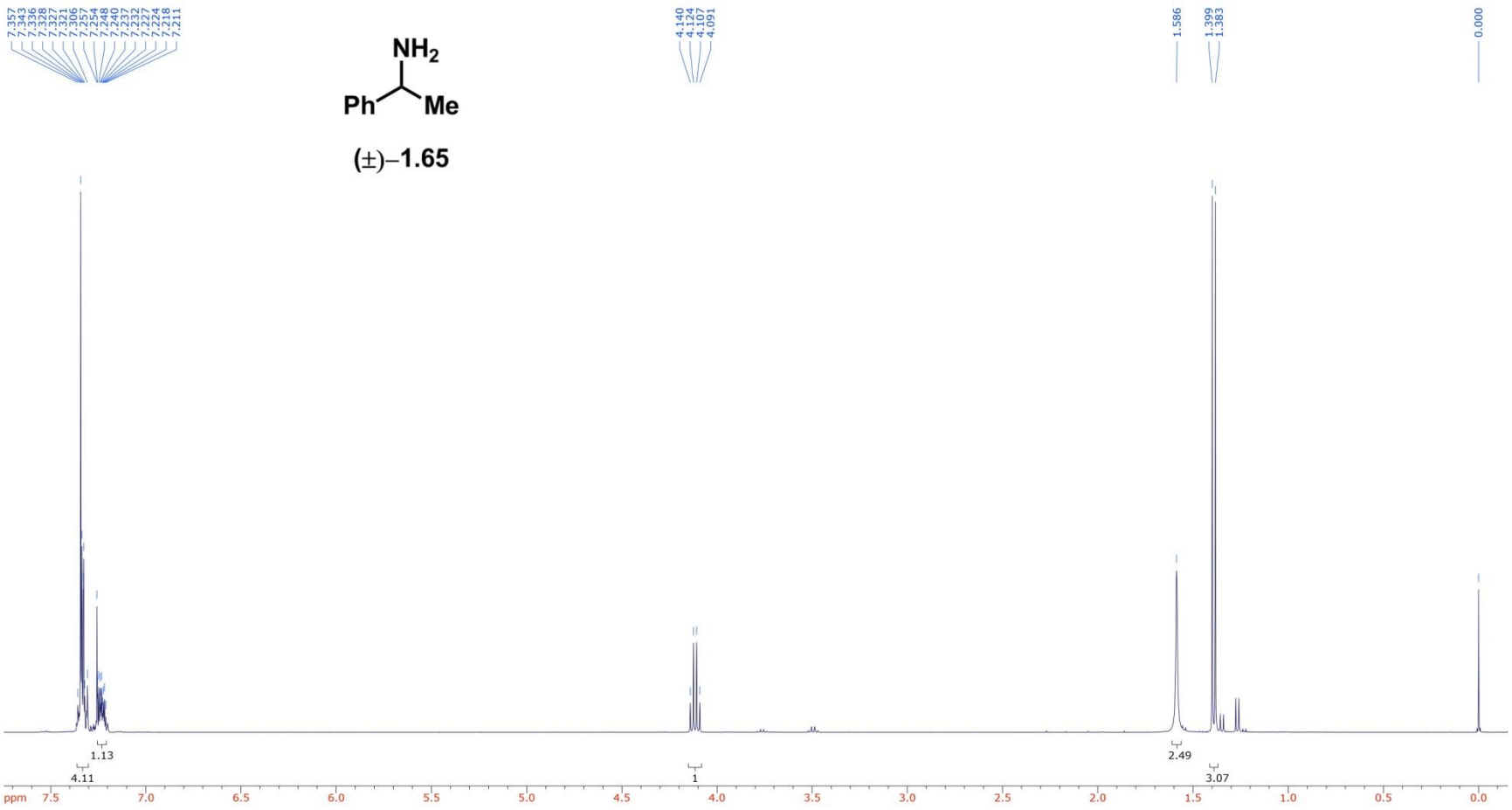
7.357
7.343
7.336
7.328
7.327
7.321
7.306
7.257
7.254
7.248
7.240
7.237
7.232
7.227
7.224
7.218
7.211
4.140
4.124
4.107
4.091
1.586
1.399
1.383
0.000
NH2
Ph
Me
(±)–1.65
4.11
1.13
1
2.49
3.07
ppm
7.5
7.0
6.5
6.0
5.5
5.0
4.5
4.0
3.5
3.0
2.5
2.0
1.5
1.0
0.5
0.0

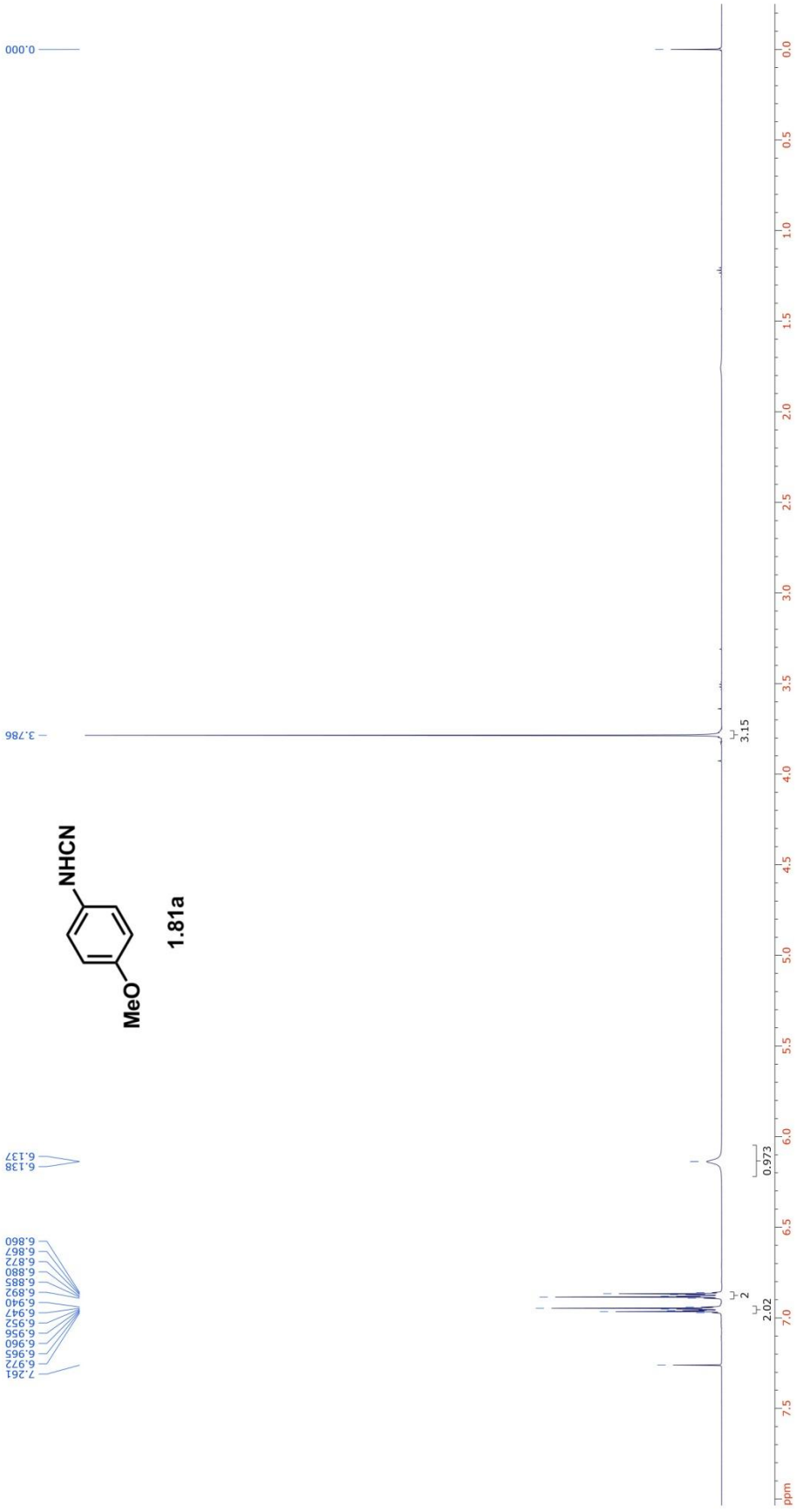
0.000
3.786
6.138
6.137
6.860
6.867
6.872
6.880
6.885
6.892
6.940
6.947
6.952
6.956
6.960
6.965
6.972
7.261
NHCN
MeO
1.81a
3.15
0.973
2
2.02
ppm

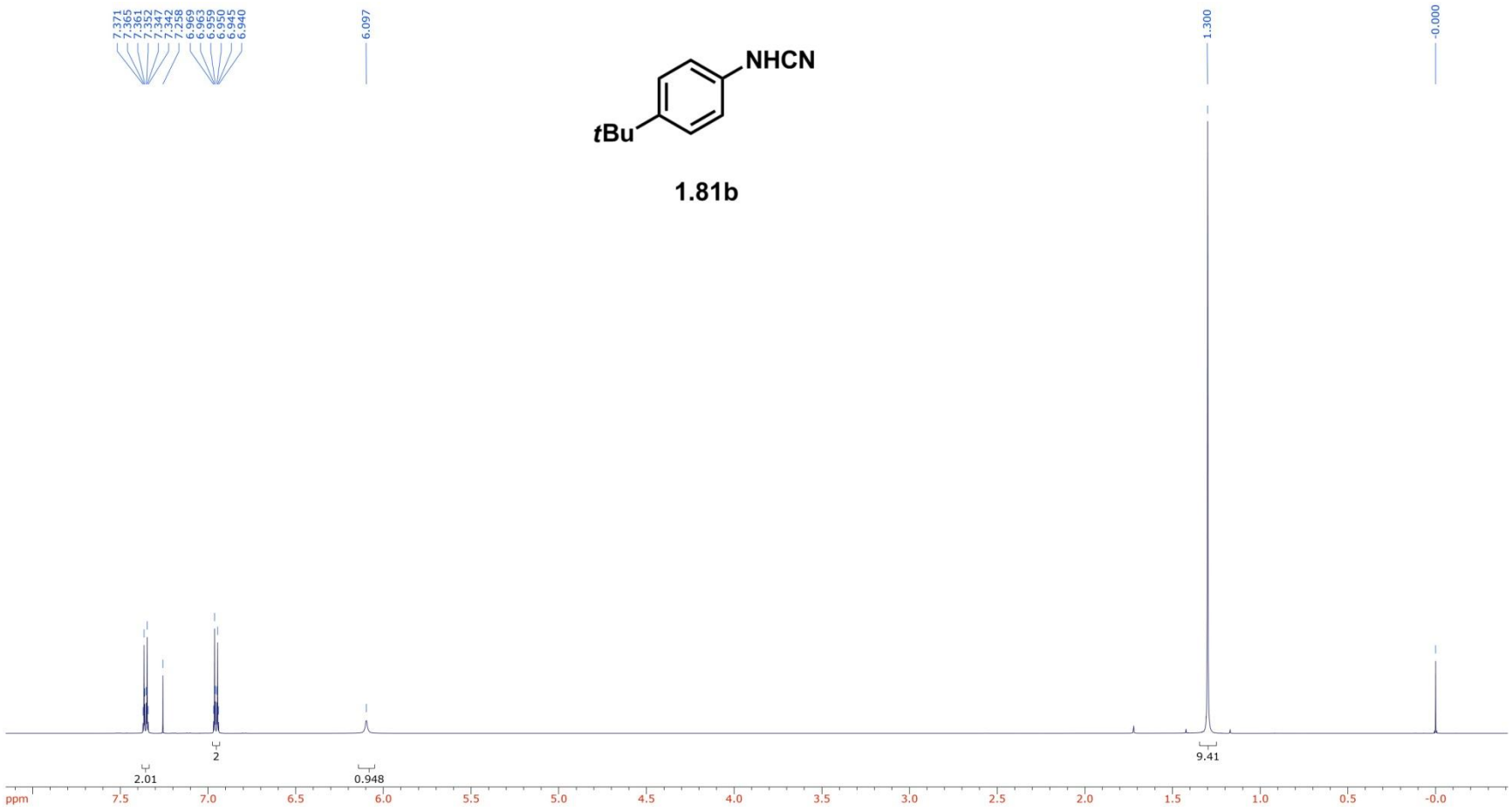
7.371
7.365
7.361
7.352
7.347
7.342
7.338
6.969
6.963
6.959
6.950
6.945
6.940
6.097
1.300
-0.000
NHCN
tBu
1.81b
2.01
2
0.948
9.41
ppm
7.5
7.0
6.5
6.0
5.5
5.0
4.5
4.0
3.5
3.0
2.5
2.0
1.5
1.0
0.5
-0.0

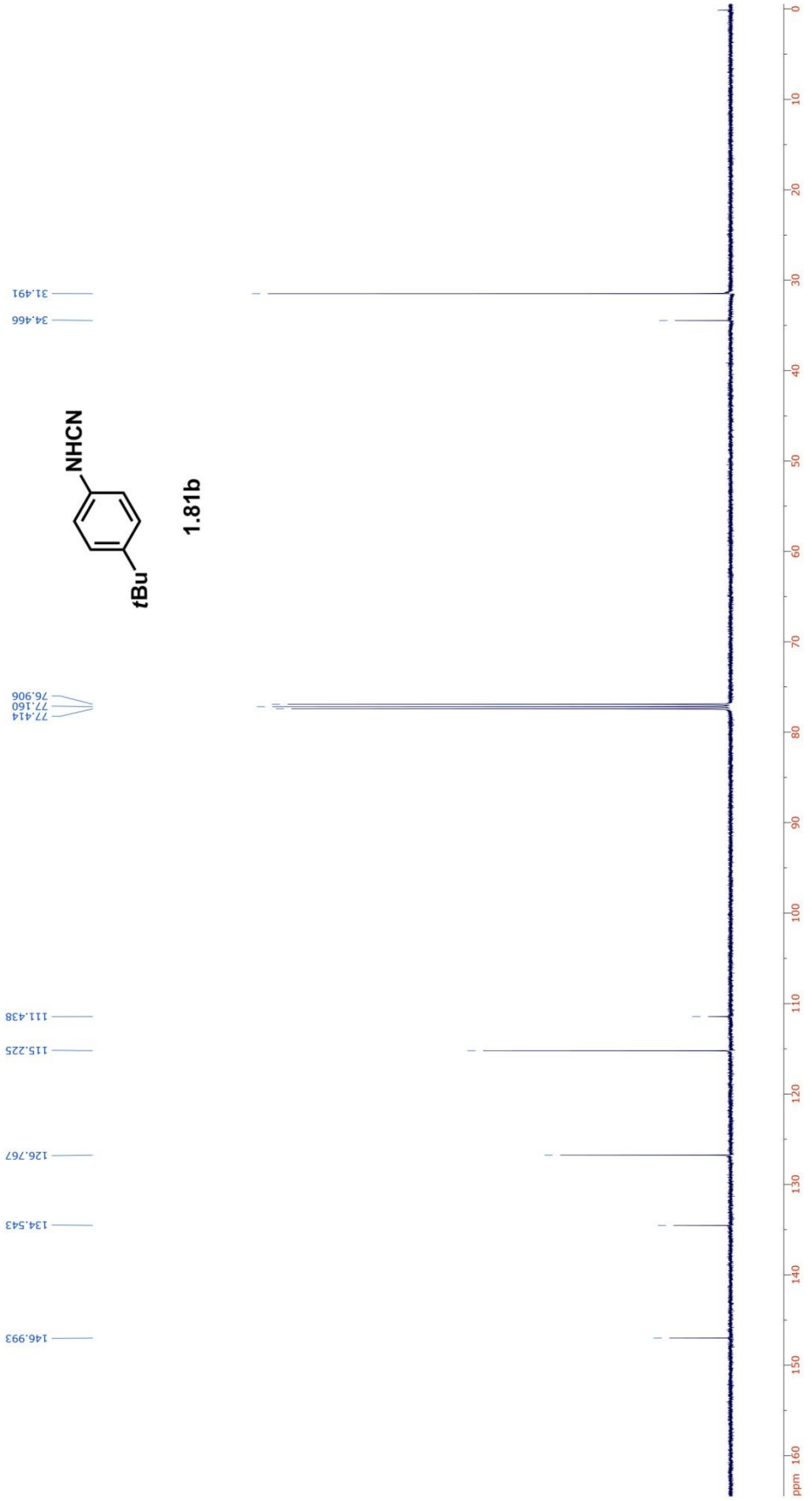
NHCN
tBu
1.81b
31.491
34.466
76.906
77.160
77.414
111.438
115.225
126.767
134.543
146.993
ppm

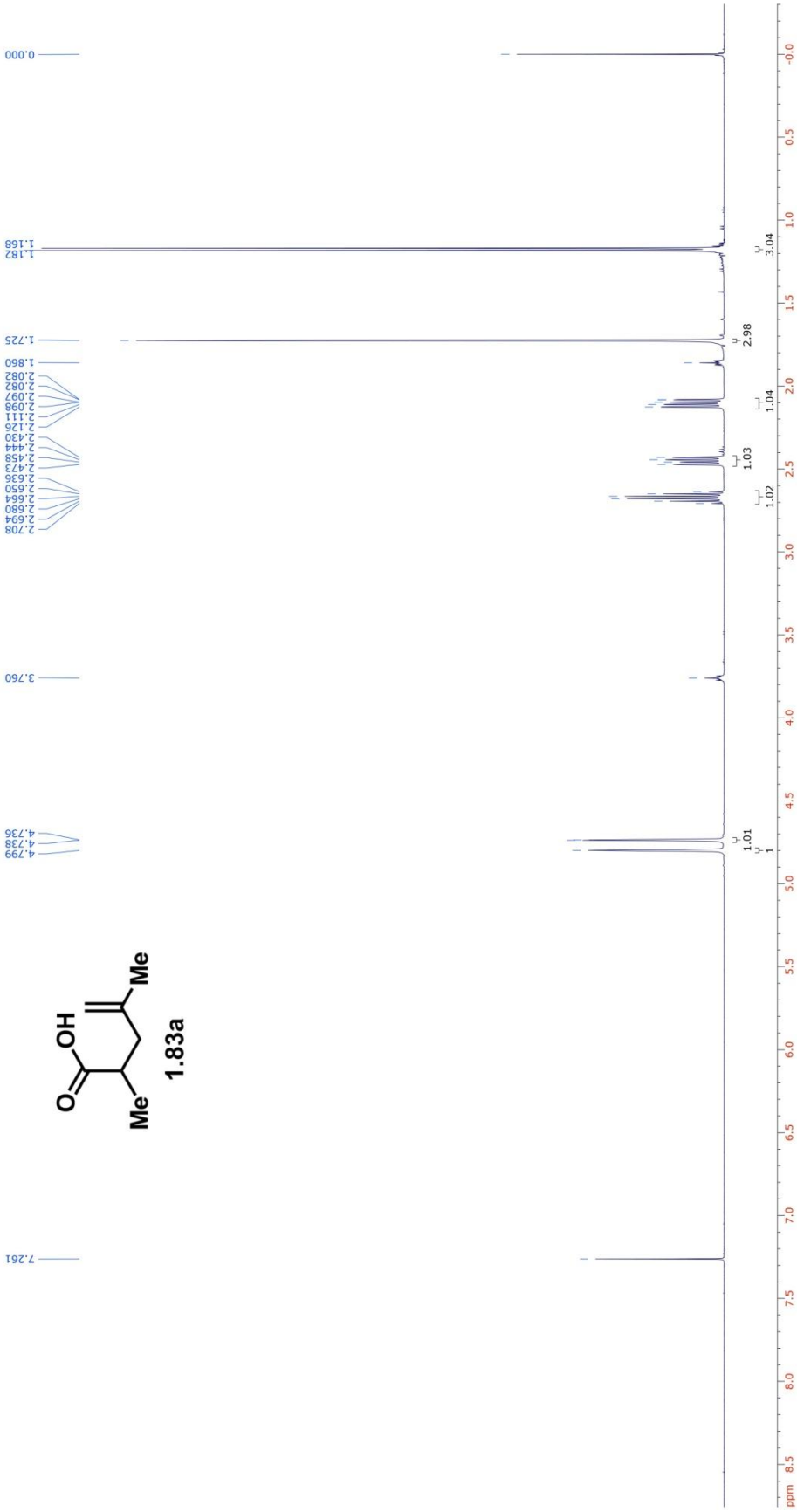
0.000
1.168
1.182
1.725
1.860
2.082
2.082
2.097
2.098
2.111
2.126
2.430
2.444
2.458
2.473
2.636
2.650
2.664
2.680
2.694
2.708
3.760
4.736
4.738
4.799
7.261
2.98
3.04
1.04
1.03
1.02
1.01
1
ppm
Me
OH
O
Me
1.83a

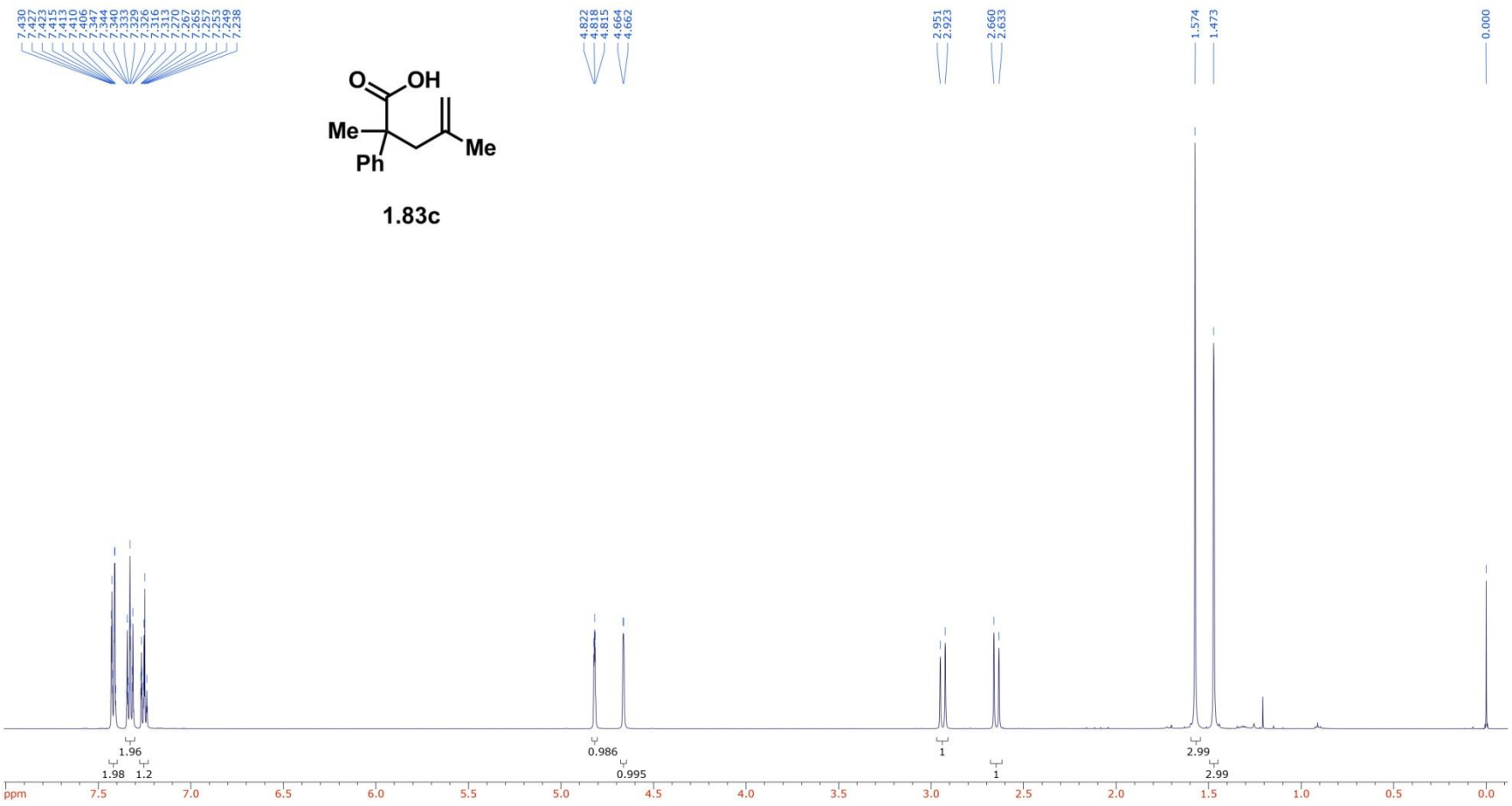
7.430
7.427
7.423
7.415
7.413
7.410
7.406
7.347
7.344
7.340
7.333
7.329
7.326
7.316
7.313
7.270
7.267
7.265
7.257
7.253
7.249
7.238
4.822
4.818
4.815
4.664
4.662
2.951
2.923
2.660
2.633
1.574
1.473
0.000
O
OH
Me
Me
Ph
1.96
1.98
1.2
0.986
0.995
1
1
2.99
2.99
ppm
7.5
7.0
6.5
6.0
5.5
5.0
4.5
4.0
3.5
3.0
2.5
2.0
1.5
1.0
0.5
0.0

1.83c

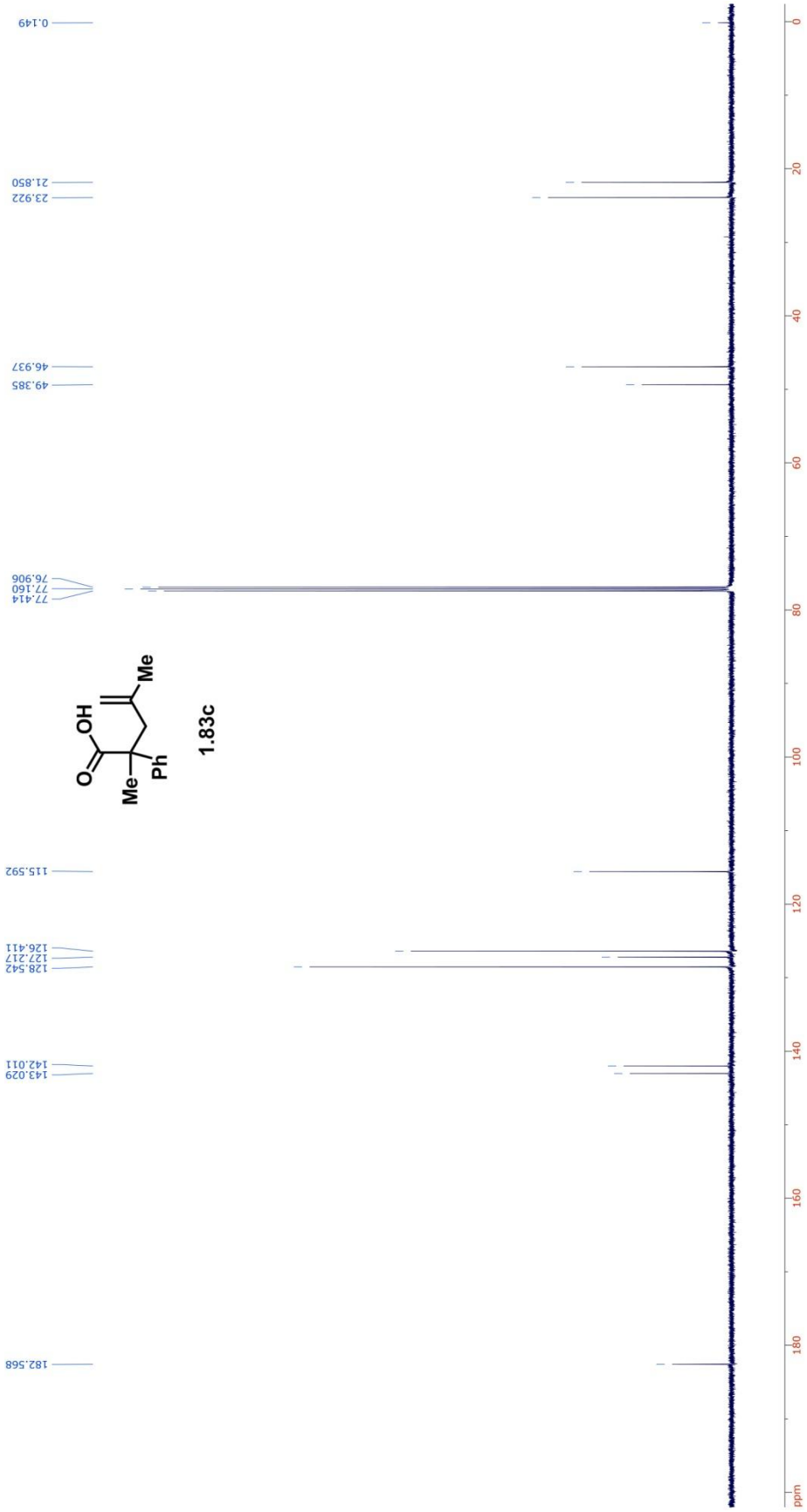
0.149
21.850
23.922
46.937
49.385
76.906
77.160
77.414
115.592
126.411
127.217
128.542
142.011
143.029
182.568
ppm
0
20
40
60
80
100
120
140
160
180
OH
O
Me
Me
Ph
1.83c

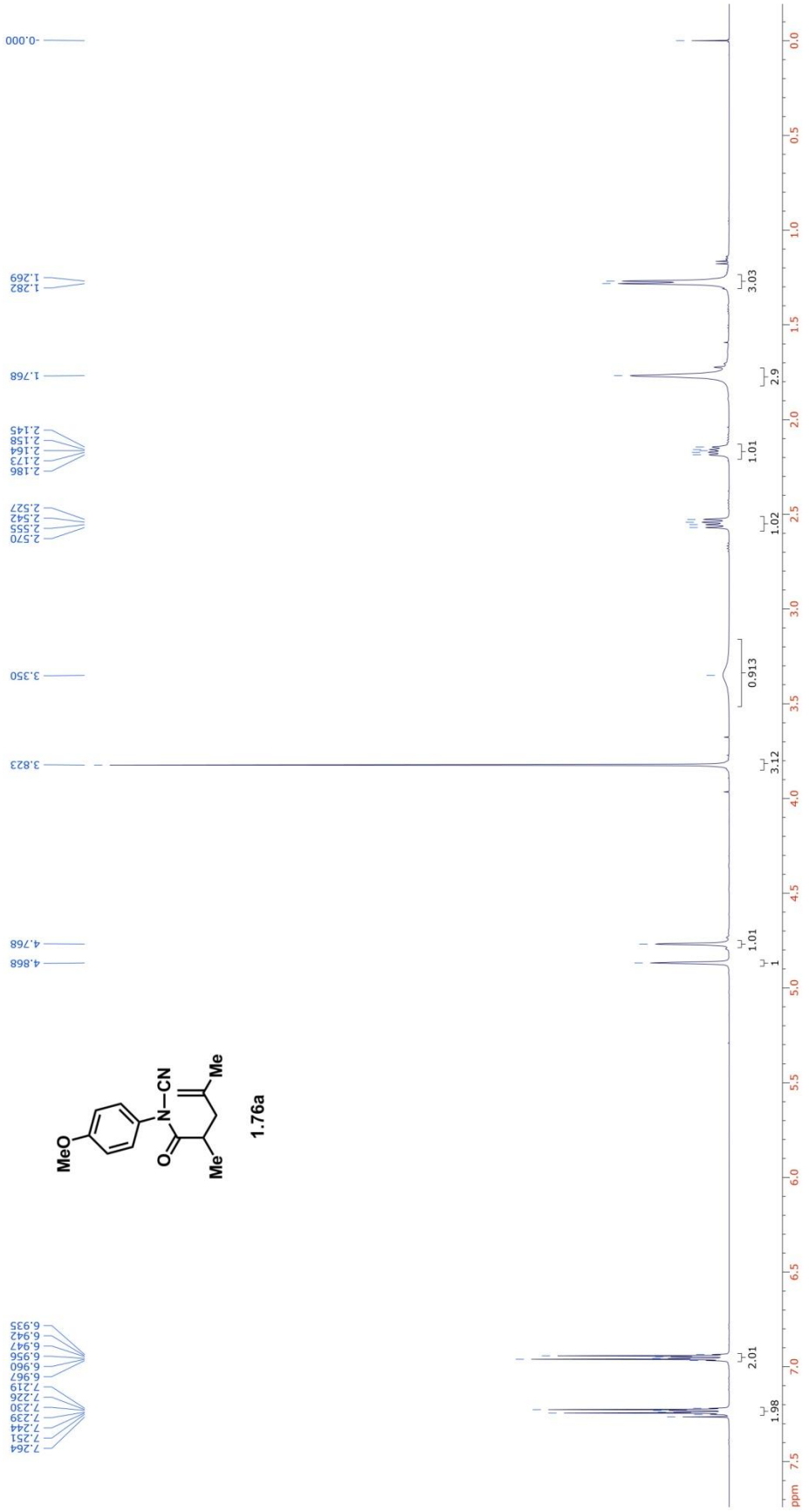
-0.000
1.269
1.282
1.768
2.145
2.158
2.164
2.173
2.186
2.527
2.542
2.555
2.570
3.350
3.823
4.768
4.868
6.935
6.942
6.947
6.956
6.960
6.967
7.219
7.226
7.230
7.239
7.244
7.251
7.264
3.03
2.9
1.01
1.02
0.913
3.12
1.01
1
2.01
1.98
ppm
MeO
N
CN
O
Me
Me
1.76a

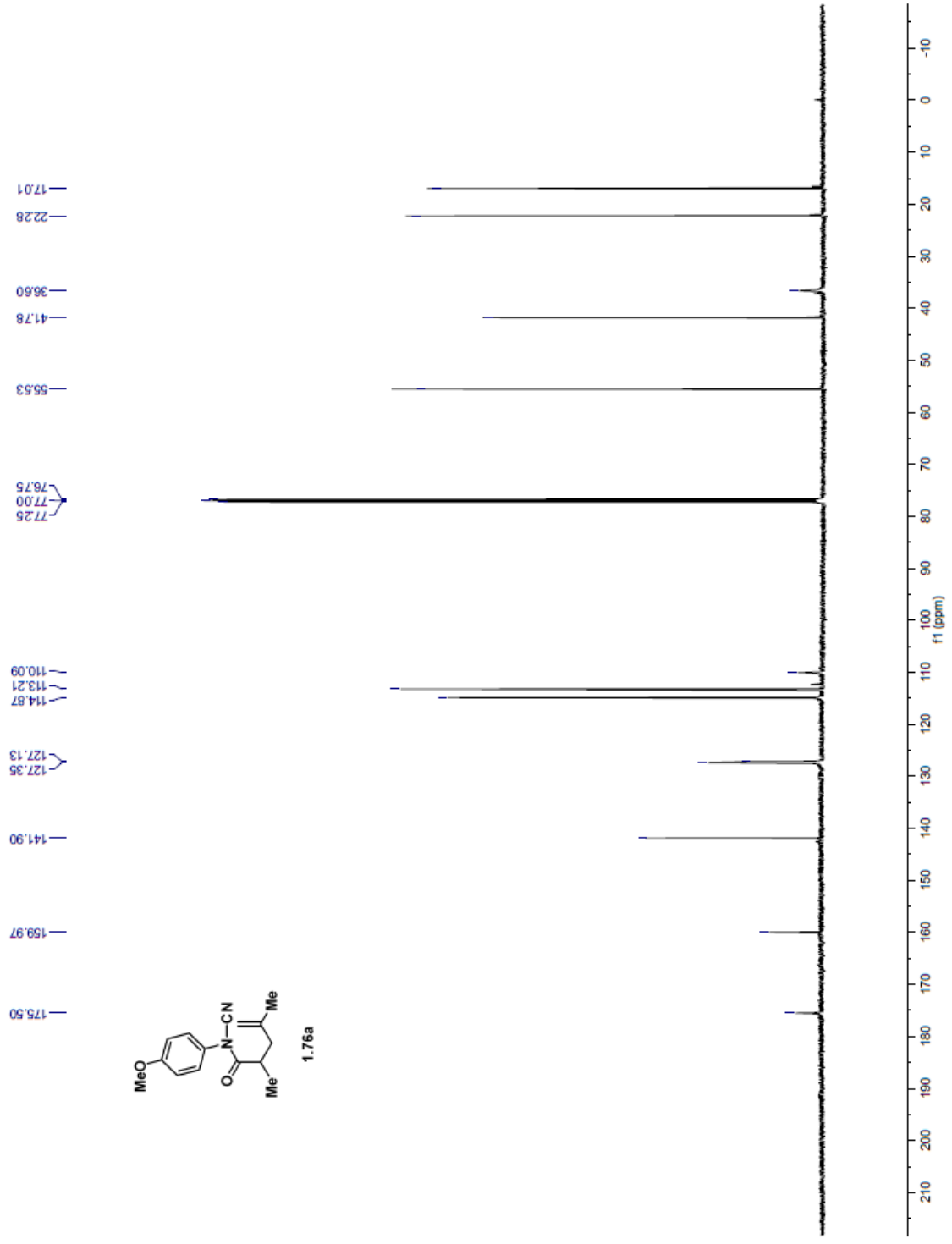
175.50
159.97
141.90
127.35
127.13
114.87
113.21
110.09
77.25
77.00
76.75
55.53
41.78
36.60
22.28
17.01
MeO
N
O
CN
Me
Me
1.76a
f1 (ppm)

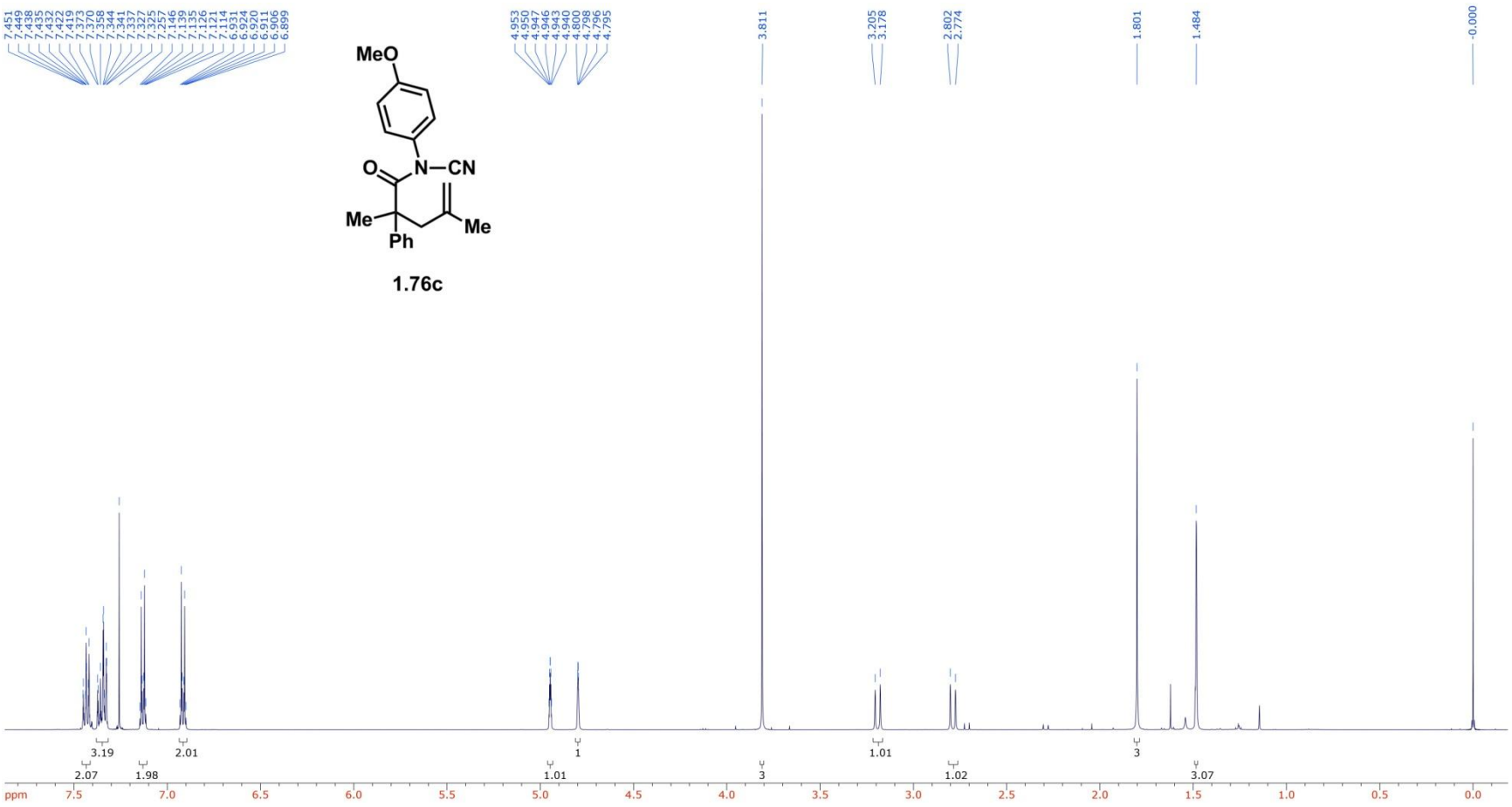
7.451
7.449
7.438
7.435
7.432
7.422
7.419
7.373
7.370
7.358
7.344
7.341
7.337
7.327
7.325
7.257
7.146
7.139
7.135
7.126
7.121
7.114
6.931
6.924
6.920
6.911
6.906
6.899
4.953
4.950
4.947
4.946
4.943
4.940
4.800
4.798
4.796
4.795
3.811
3.205
3.178
2.802
2.774
1.801
1.484
-0.000
MeO
O
N—CN
Me
Me
Ph
1.76c
3.19
2.01
1
1.01
3
1.01
3
2.07
1.98
1.01
3
1.02
3.07
ppm
7.5
7.0
6.5
6.0
5.5
5.0
4.5
4.0
3.5
3.0
2.5
2.0
1.5
1.0
0.5
0.0

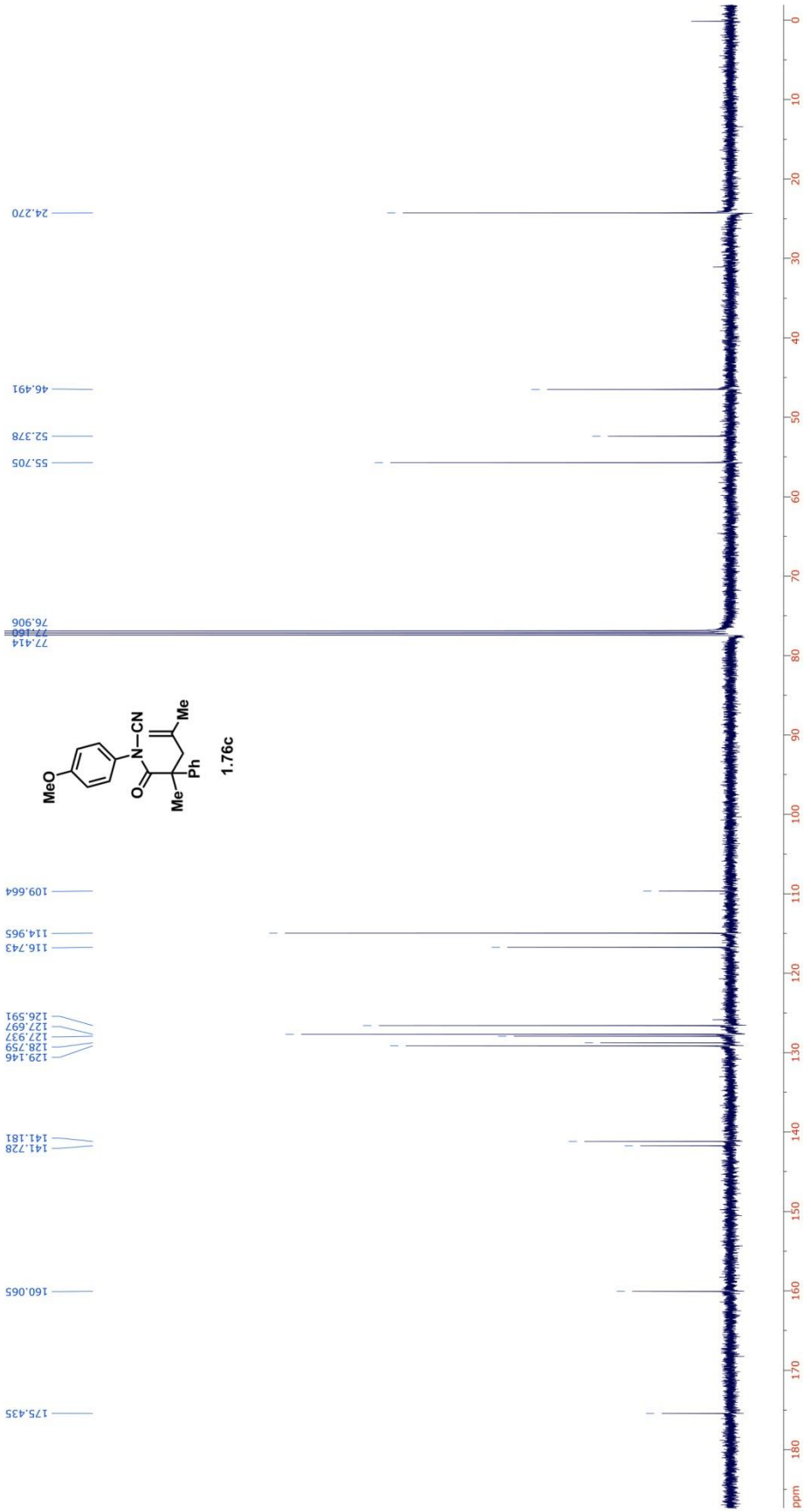
24.270
46.491
52.378
55.705
76.906
77.160
77.414
109.664
114.965
116.743
126.591
127.697
127.937
128.759
129.146
141.728
141.181
160.065
175.435
MeO
N
CN
Me
O
Me
Ph
1.76c
0
10
20
30
40
50
60
70
80
90
100
110
120
130
140
150
160
170
180
ppm

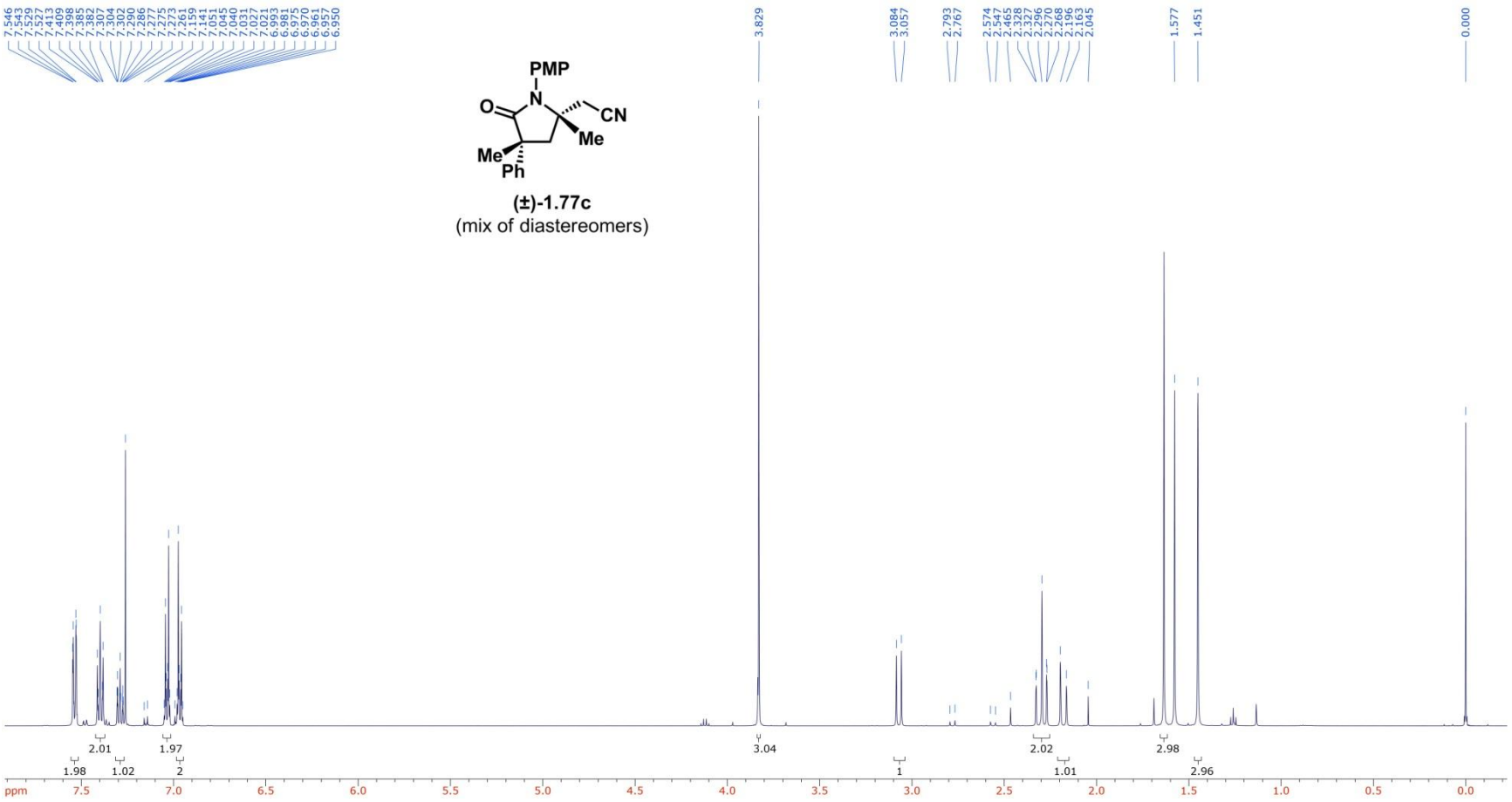
7.546
7.543
7.529
7.527
7.413
7.409
7.398
7.388
7.382
7.307
7.304
7.302
7.290
7.286
7.277
7.275
7.273
7.261
7.159
7.141
7.051
7.045
7.040
7.031
7.027
7.021
6.993
6.981
6.975
6.970
6.961
6.957
6.950
3.829
3.084
3.057
2.793
2.767
2.574
2.547
2.465
2.328
2.327
2.296
2.270
2.268
2.196
2.163
2.045
1.577
1.451
0.000
PMP
N
O
CN
Me
Me
Ph
(±)-1.77c
(mix of diastereomers)
2.01
1.97
3.04
2.02
2.98
1.98
1.02
2
1
1.01
2.96
ppm
7.5
7.0
6.5
6.0
5.5
5.0
4.5
4.0
3.5
3.0
2.5
2.0
1.5
1.0
0.5
0.0

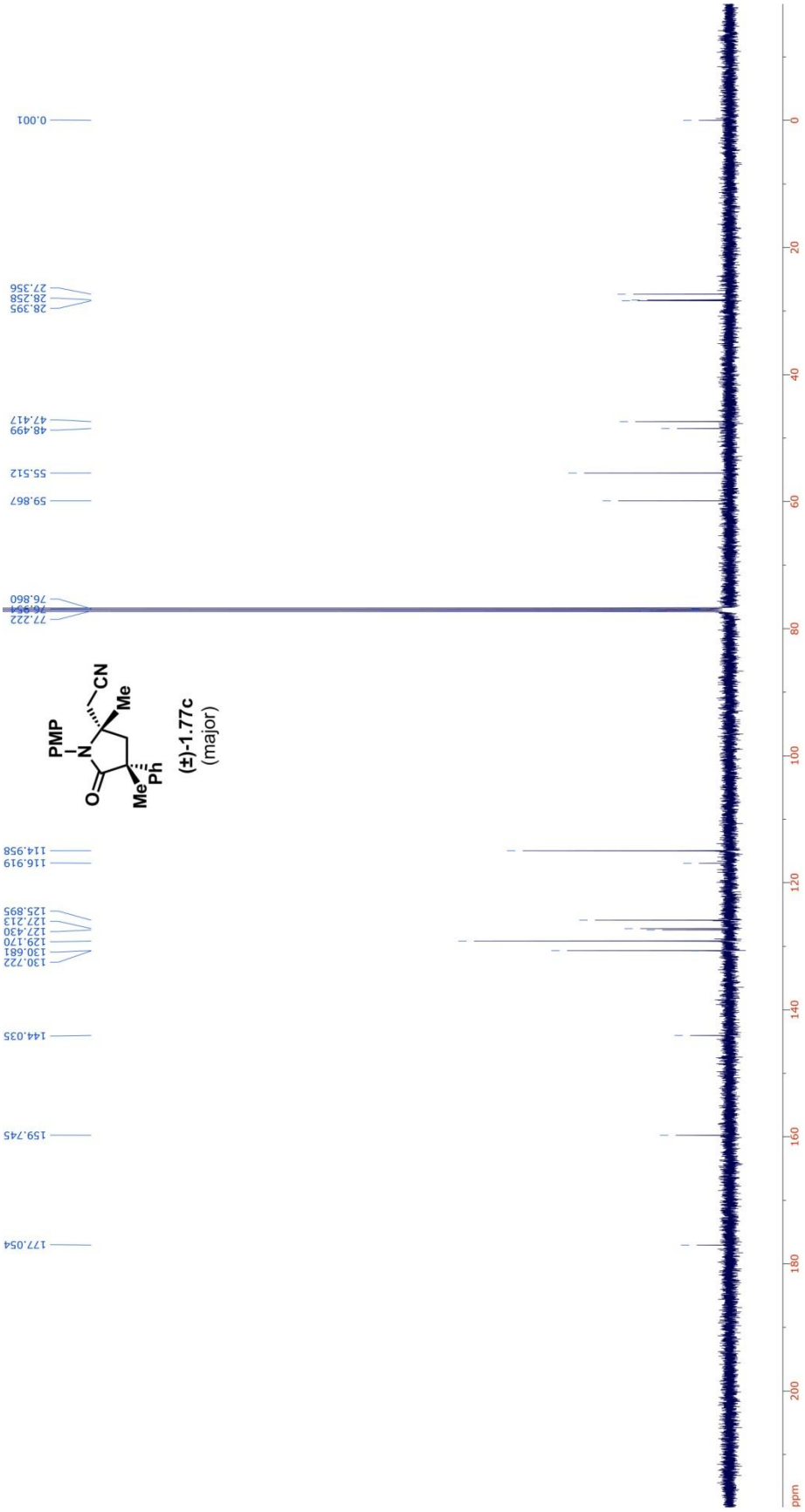
0.001
27.356
28.258
28.395
47.417
48.499
55.512
59.867
76.860
76.954
77.222
114.958
116.919
125.895
127.213
127.430
129.170
130.681
130.722
144.035
159.745
177.054
PMP
N
O
CN
Me
Me
Ph
(±)-1.77c
(major)
0
20
40
60
80
100
120
140
160
180
200
ppm

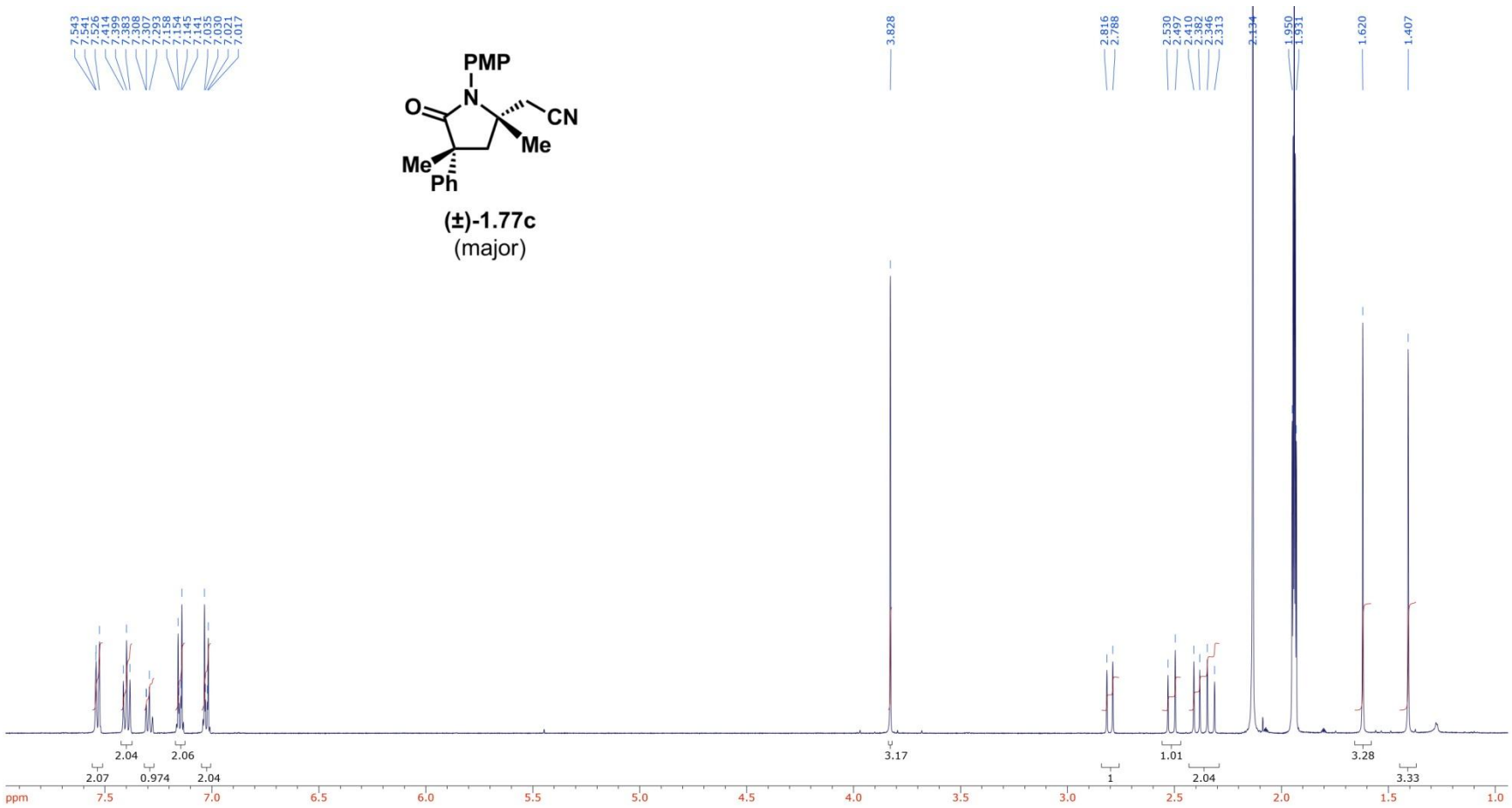
7.543
7.541
7.526
7.414
7.399
7.383
7.308
7.307
7.293
7.158
7.154
7.145
7.141
7.035
7.030
7.021
7.017
PMP
N
O
CN
Me
Me
Ph
3.828
2.816
2.788
2.530
2.497
2.410
2.382
2.346
2.313
2.134
1.950
1.931
1.620
1.407
2.04
2.06
3.17
1.01
3.28
2.07
0.974
2.04
1
2.04
3.33
ppm
7.5
7.0
6.5
6.0
5.5
5.0
4.5
4.0
3.5
3.0
2.5
2.0
1.5
1.0

(±)-1.77c
(major)

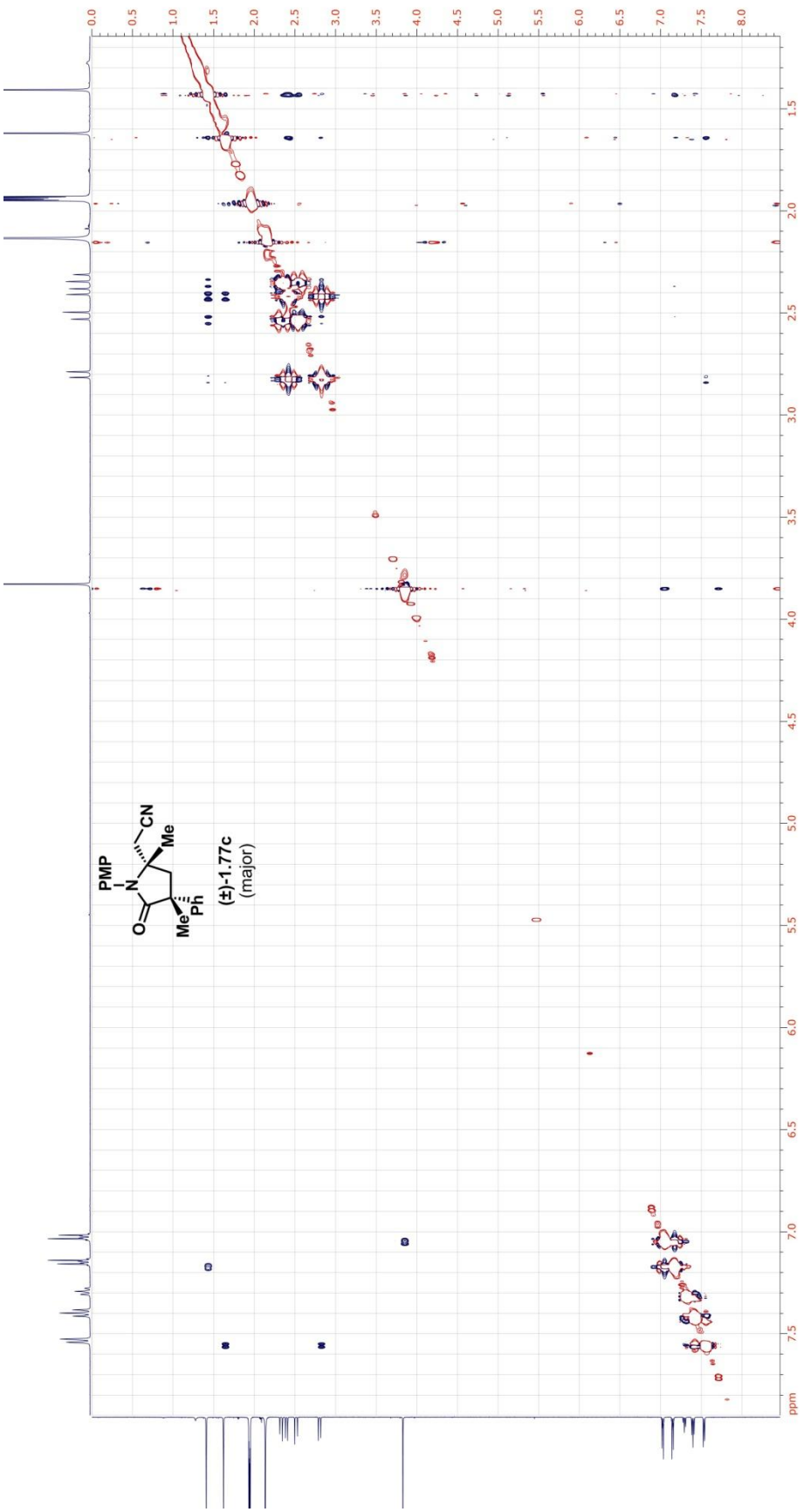
PMP
N
O
CN
Me
Me
Ph
(±)-1.77c
(major)
ppm

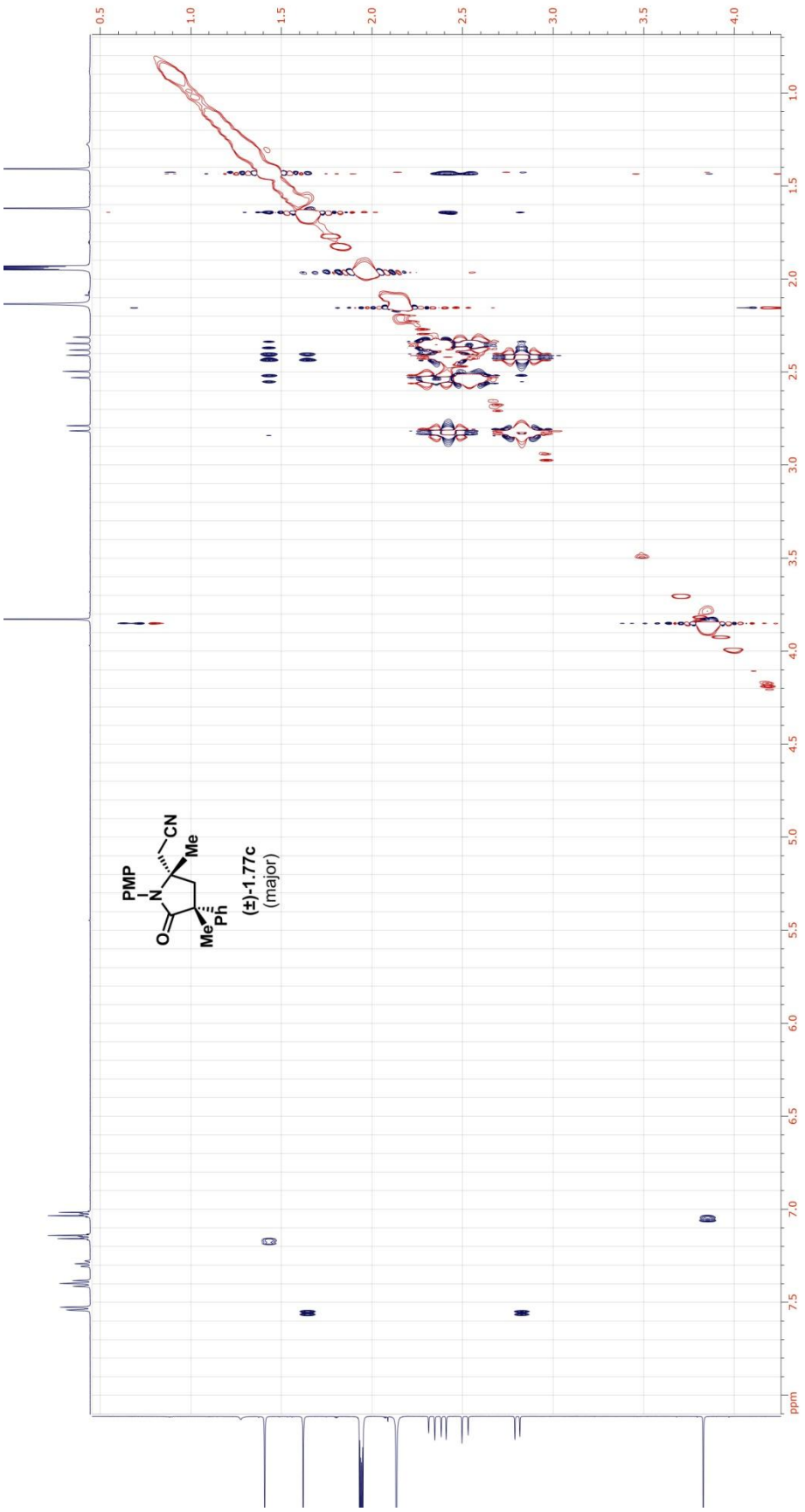
PMP
N
O
CN
Me
Me
Ph
(±)-1.77c
(major)
ppm

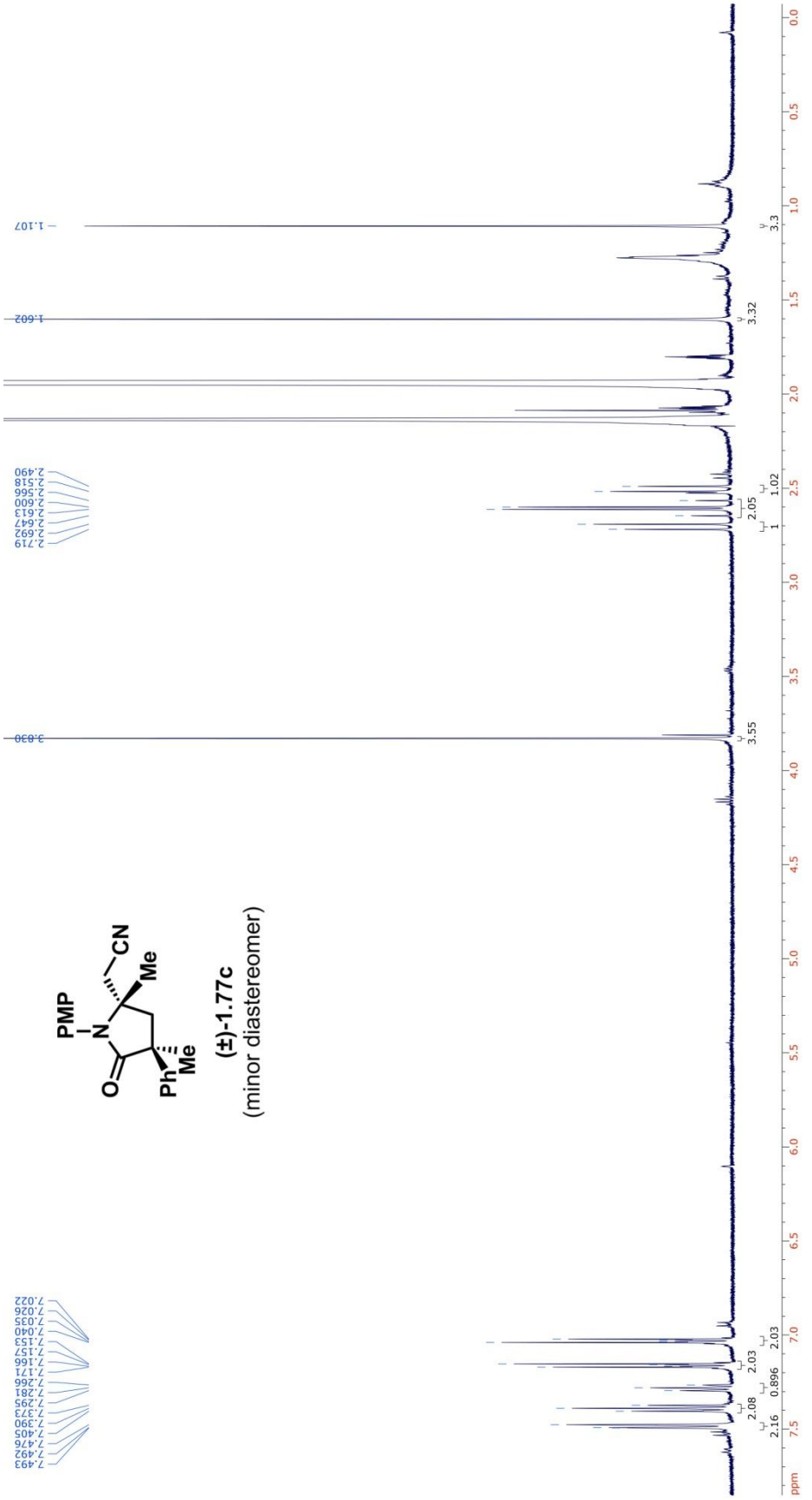
PMP
N
O
CN
Me
Ph
Me
(±)-1.77c
(minor diastereomer)
7.493
7.492
7.476
7.405
7.390
7.373
7.295
7.281
7.266
7.171
7.166
7.157
7.153
7.040
7.035
7.026
7.022
2.719
2.692
2.647
2.613
2.600
2.566
2.518
2.490
3.830
1.602
1.107
2.16
2.08
0.896
2.03
2.03
2.05
1
1.02
3.55
3.32
3.3
ppm

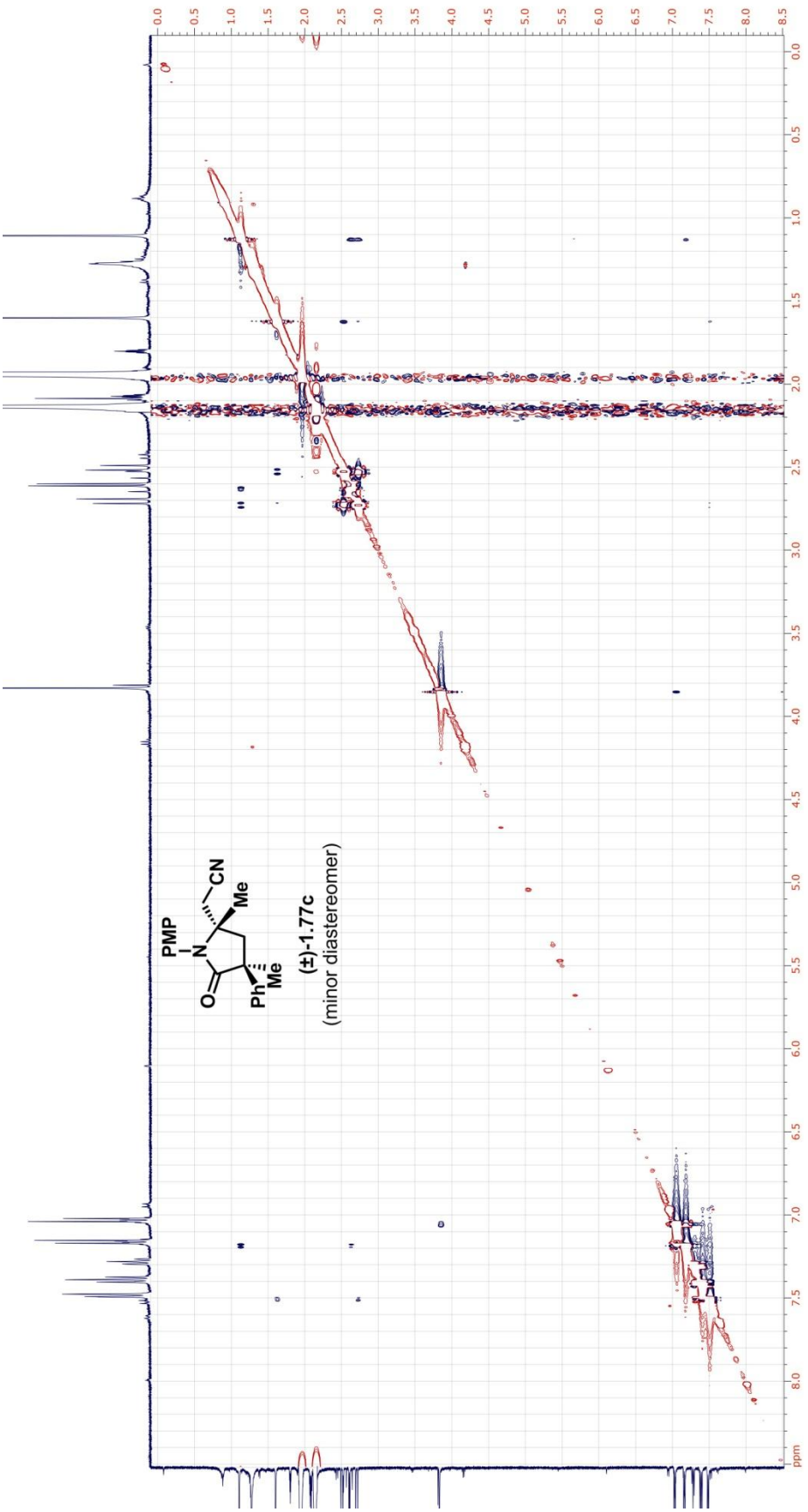
PMP
N
O
CN
Me
Ph
Me
(±)-1.77c
(minor diastereomer)
ppm

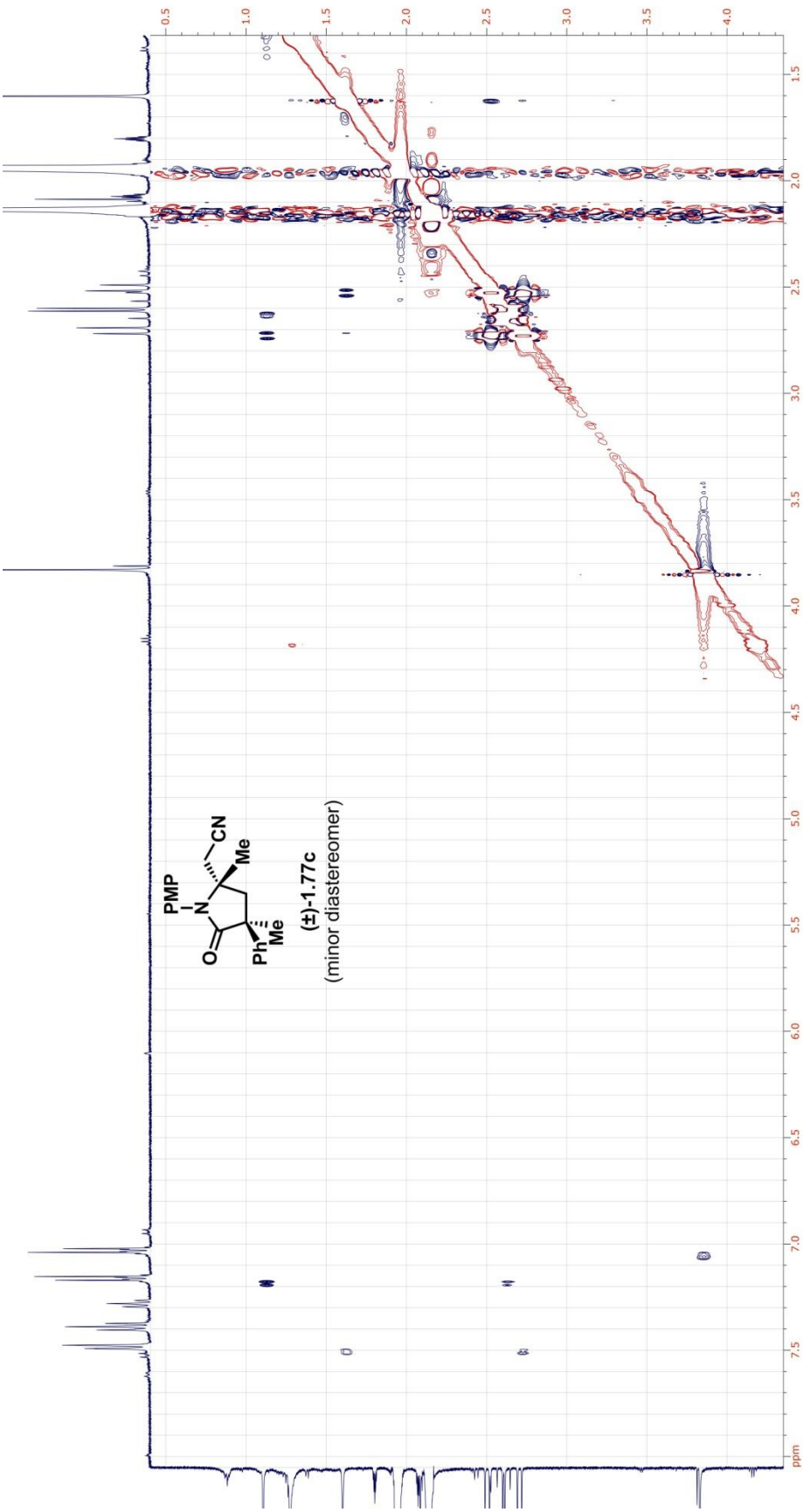
PMP
N
O
CN
Me
Ph
Me
(±)-1.77c
(minor diastereomer)
ppm

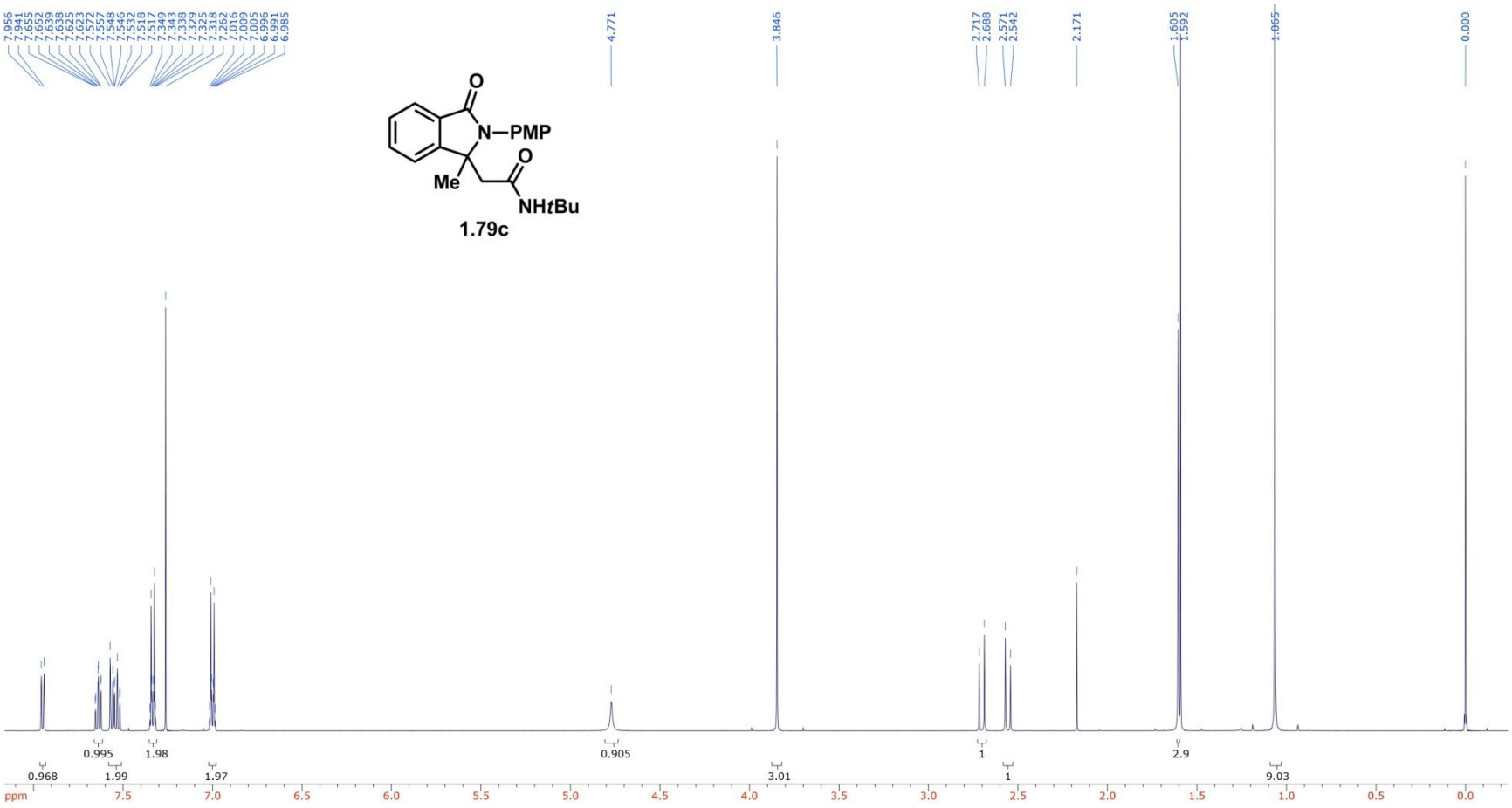
7.956
7.941
7.655
7.652
7.639
7.638
7.625
7.623
7.572
7.557
7.548
7.546
7.532
7.518
7.517
7.349
7.343
7.338
7.329
7.325
7.318
7.262
7.016
7.009
7.005
6.996
6.991
6.985
4.771
3.846
2.717
2.688
2.571
2.542
2.171
1.605
1.592
1.065
0.000
O
N—PMP
O
Me
NHtBu
1.79c
0.995
1.98
0.905
1
2.9
0.968
1.99
1.97
3.01
1
9.03
ppm
7.5
7.0
6.5
6.0
5.5
5.0
4.5
4.0
3.5
3.0
2.5
2.0
1.5
1.0
0.5
0.0

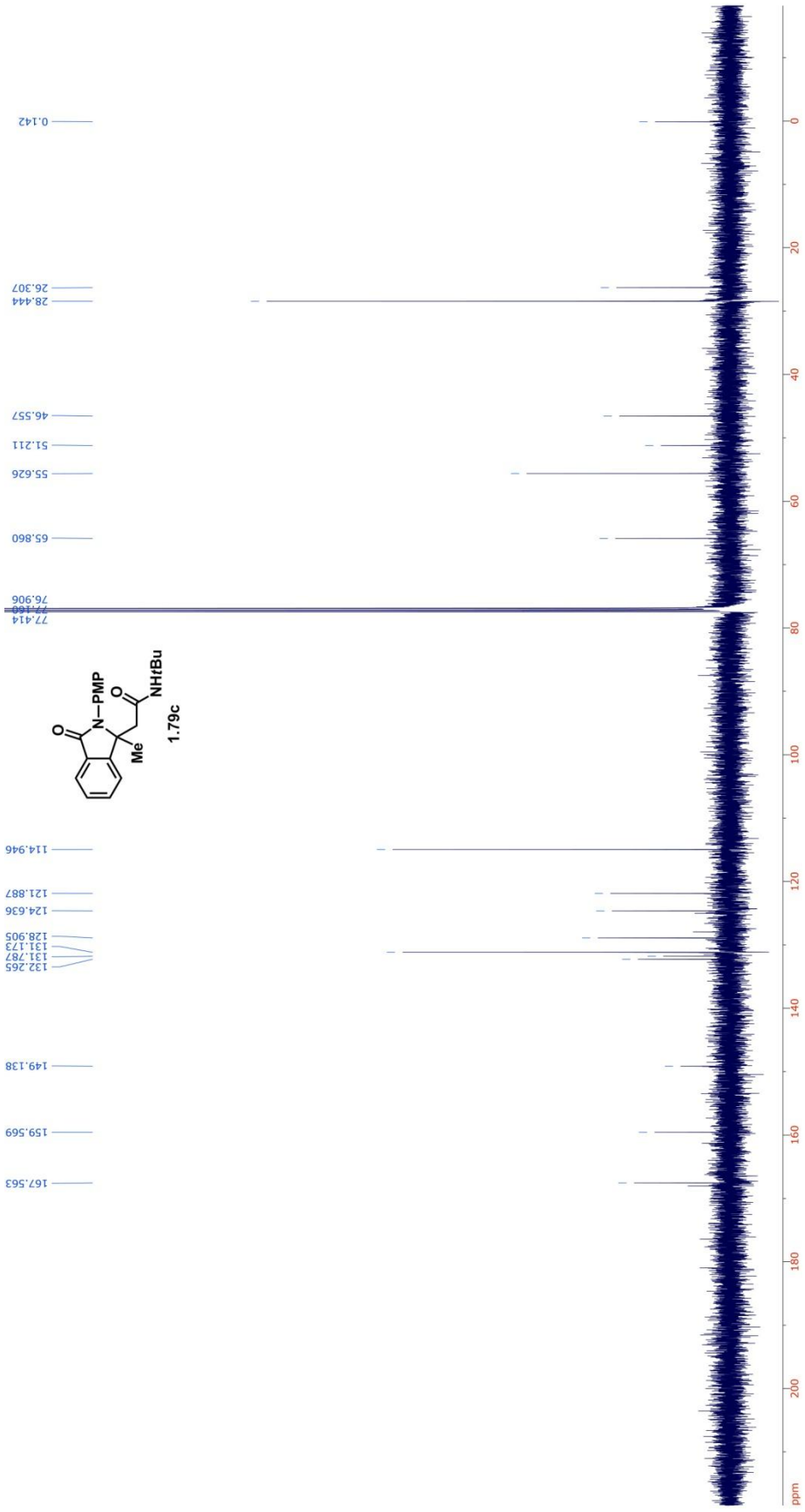
0.142
26.307
28.444
46.557
51.211
55.626
65.860
76.906
77.160
77.414
114.946
121.887
124.636
128.905
131.173
131.787
132.265
149.138
159.569
167.563
N–PMP
O
O
NHtBu
Me
1.79c
0
20
40
60
80
100
120
140
160
180
200
ppm

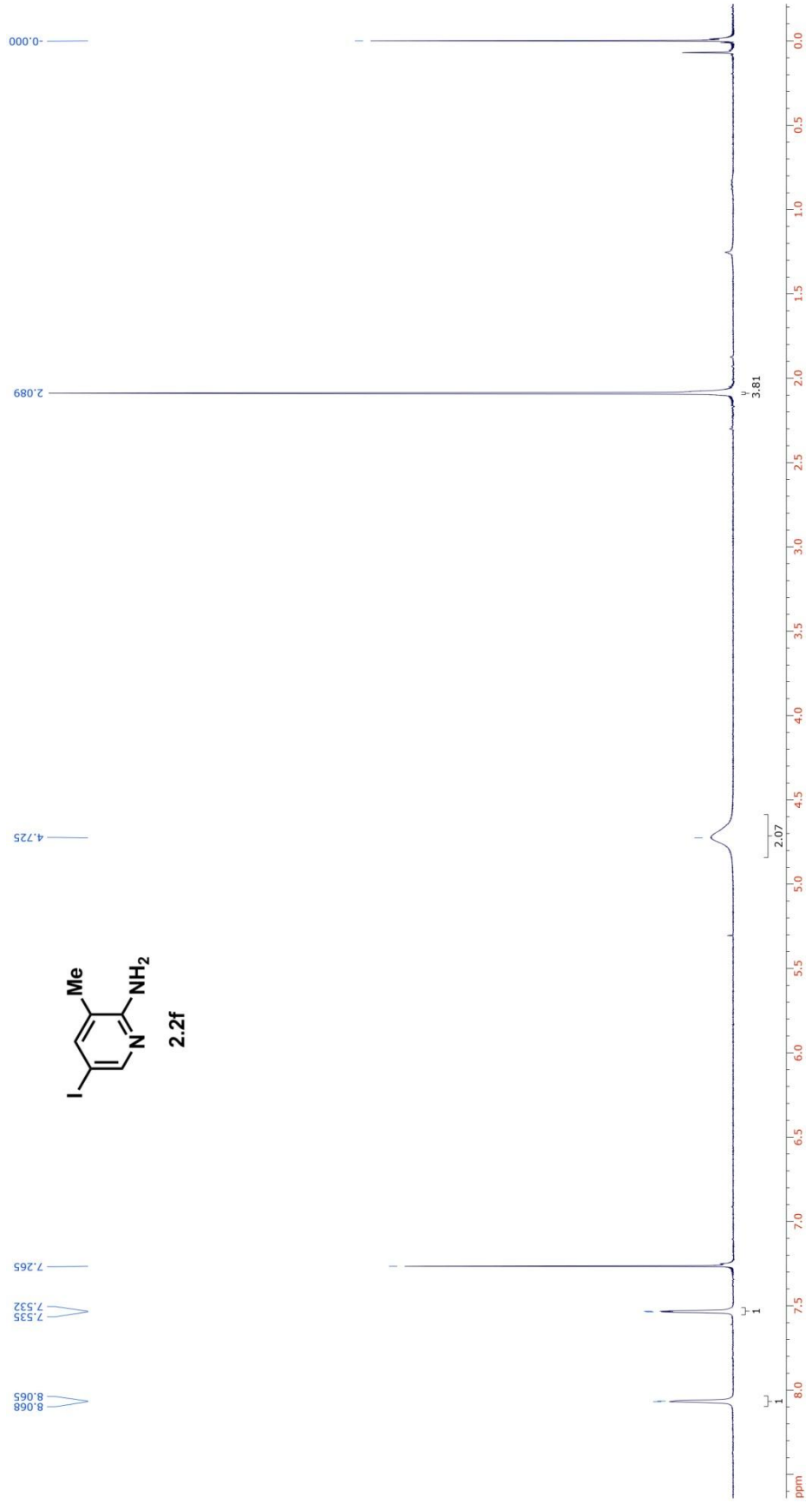
-0.000
2.089
4.725
7.265
7.535
7.532
8.068
8.065
3.81
2.07
1
1
Me
NH2
I
N
2.2f
ppm

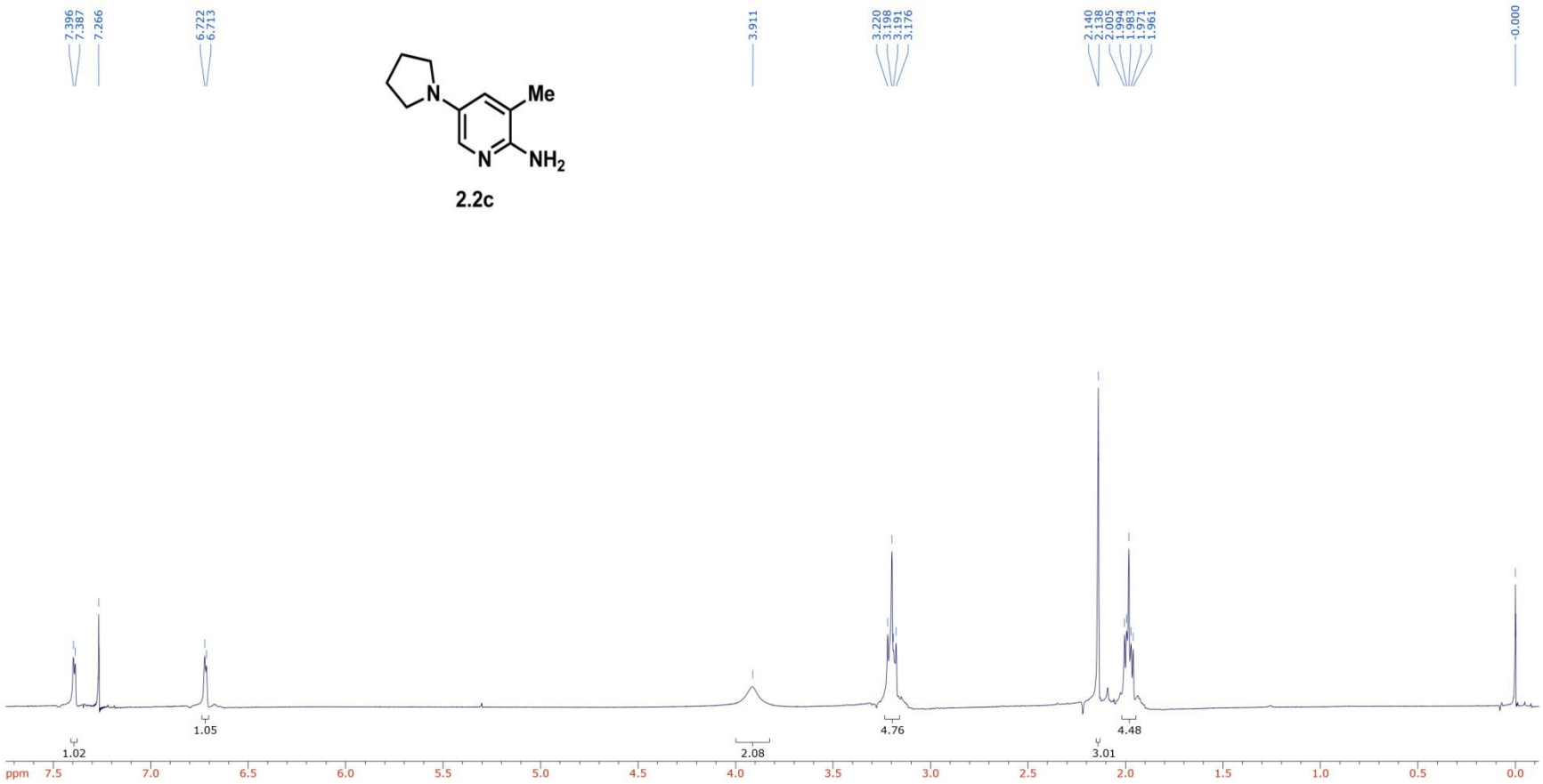
7.396
7.387
7.266
6.722
6.713
3.911
3.220
3.198
3.191
3.176
2.140
2.138
2.005
1.994
1.983
1.971
1.961
0.000
Me
N
N
NH2
2.2c
1.02
1.05
2.08
4.76
3.01
4.48
ppm 7.5 7.0 6.5 6.0 5.5 5.0 4.5 4.0 3.5 3.0 2.5 2.0 1.5 1.0 0.5 0.0

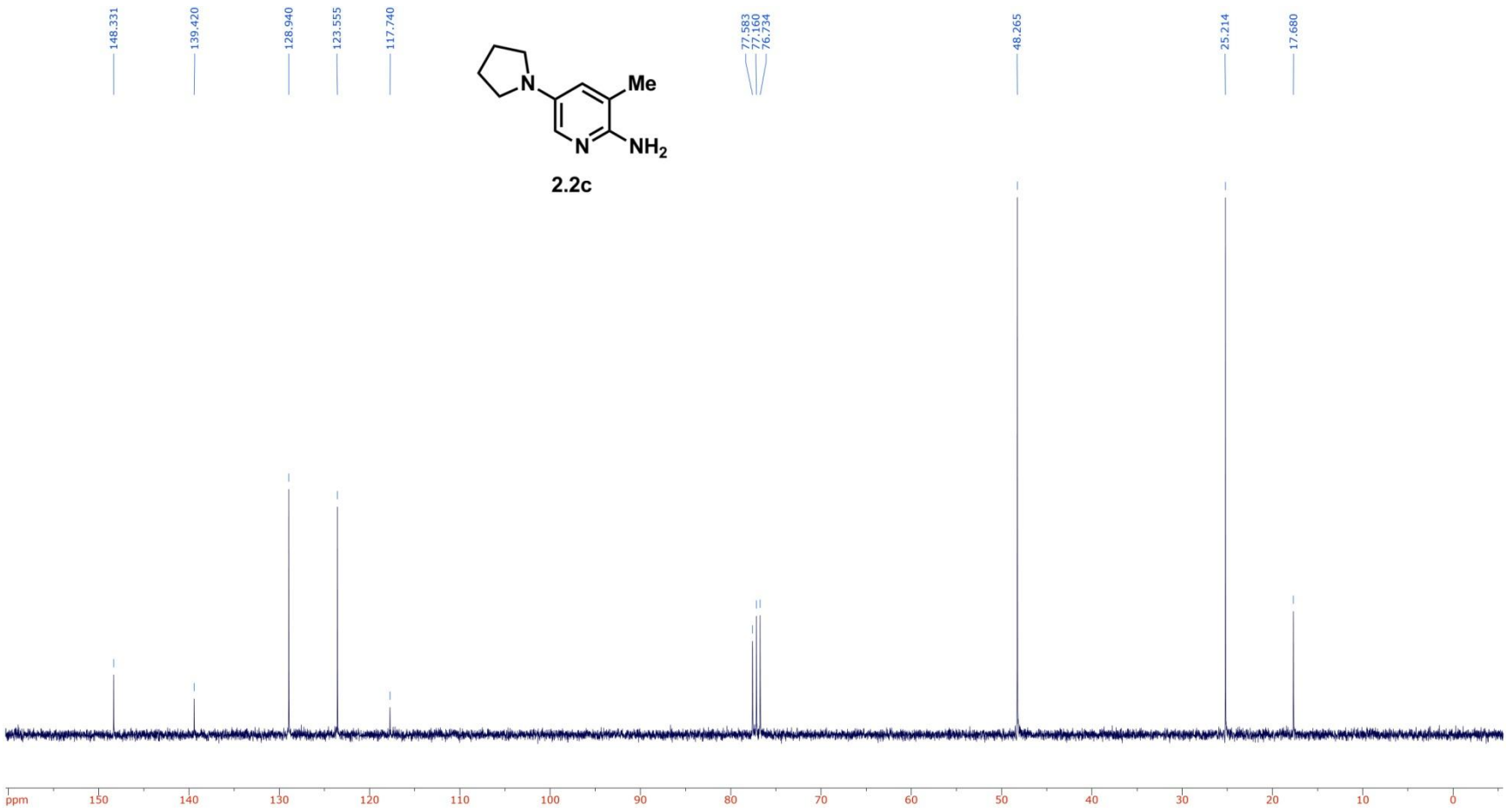
148.331
139.420
128.940
123.555
117.740
77.583
77.160
76.734
48.265
25.214
17.680
Me
N
N
NH2
2.2c
ppm
150
140
130
120
110
100
90
80
70
60
50
40
30
20
10
0

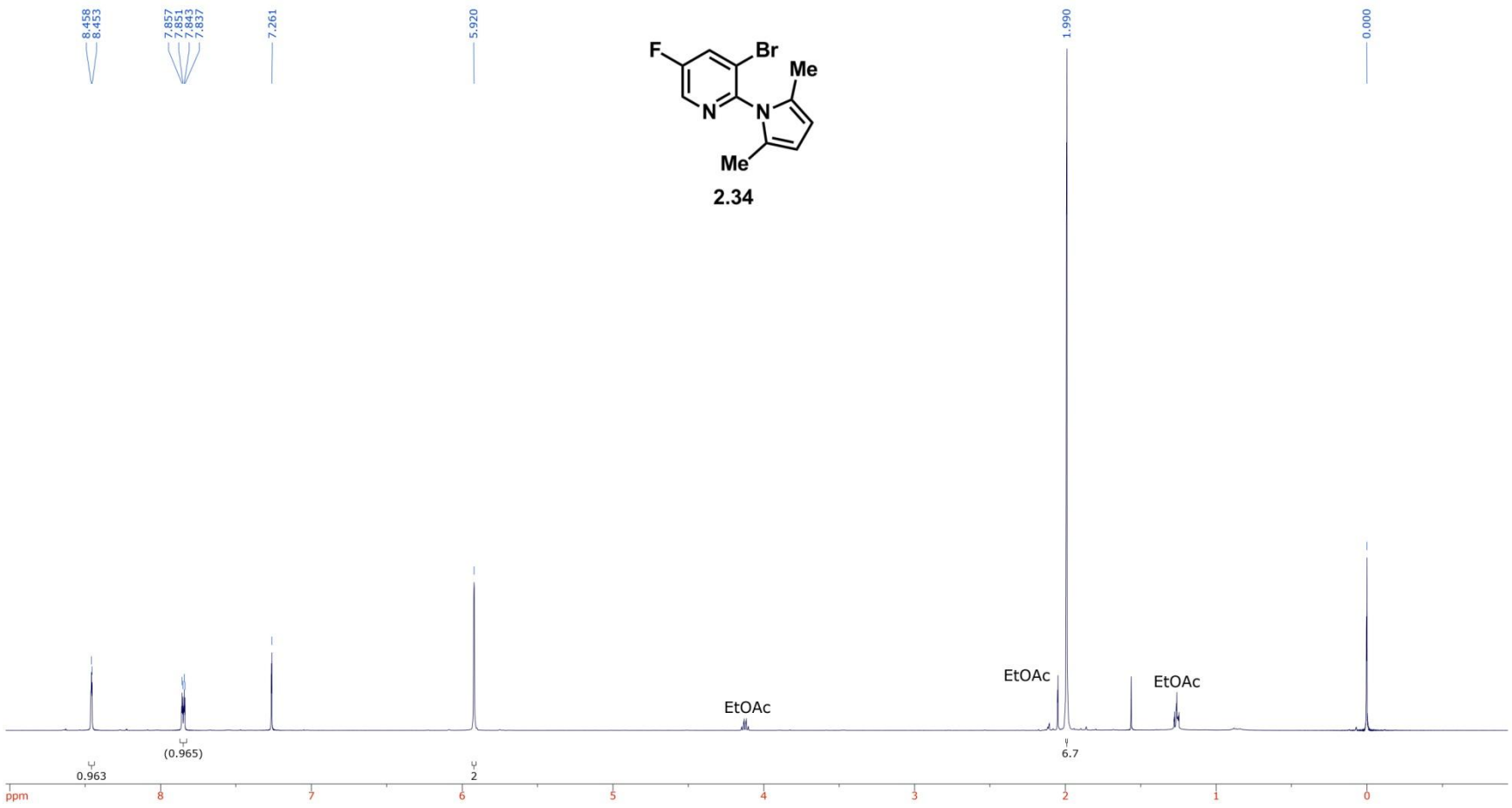
8.458
8.453
7.857
7.851
7.843
7.837
7.261
5.920
1.990
0.000
F
Br
Me
N
N
Me
2.34
EtOAc
EtOAc
EtOAc
0.963
(0.965)
2
6.7
ppm
8
7
6
5
4
3
2
1
0

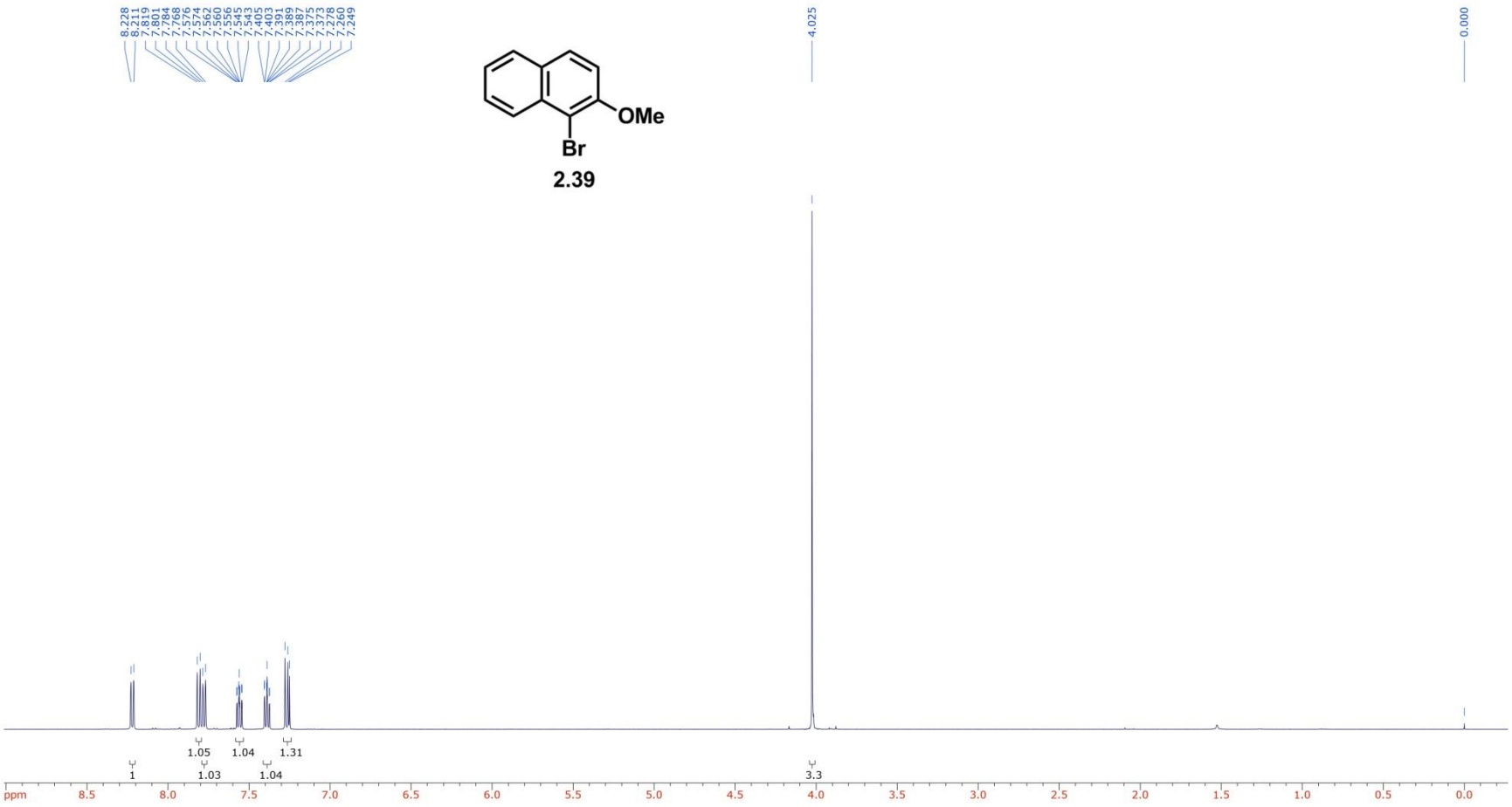
8.228
8.211
7.819
7.801
7.784
7.768
7.576
7.574
7.562
7.560
7.556
7.545
7.543
7.405
7.403
7.391
7.389
7.387
7.375
7.373
7.278
7.260
7.249
OMe
Br
2.39
4.025
0.000
1.05
1.04
1.31
1
1.03
1.04
3.3
ppm
8.5
8.0
7.5
7.0
6.5
6.0
5.5
5.0
4.5
4.0
3.5
3.0
2.5
2.0
1.5
1.0
0.5
0.0

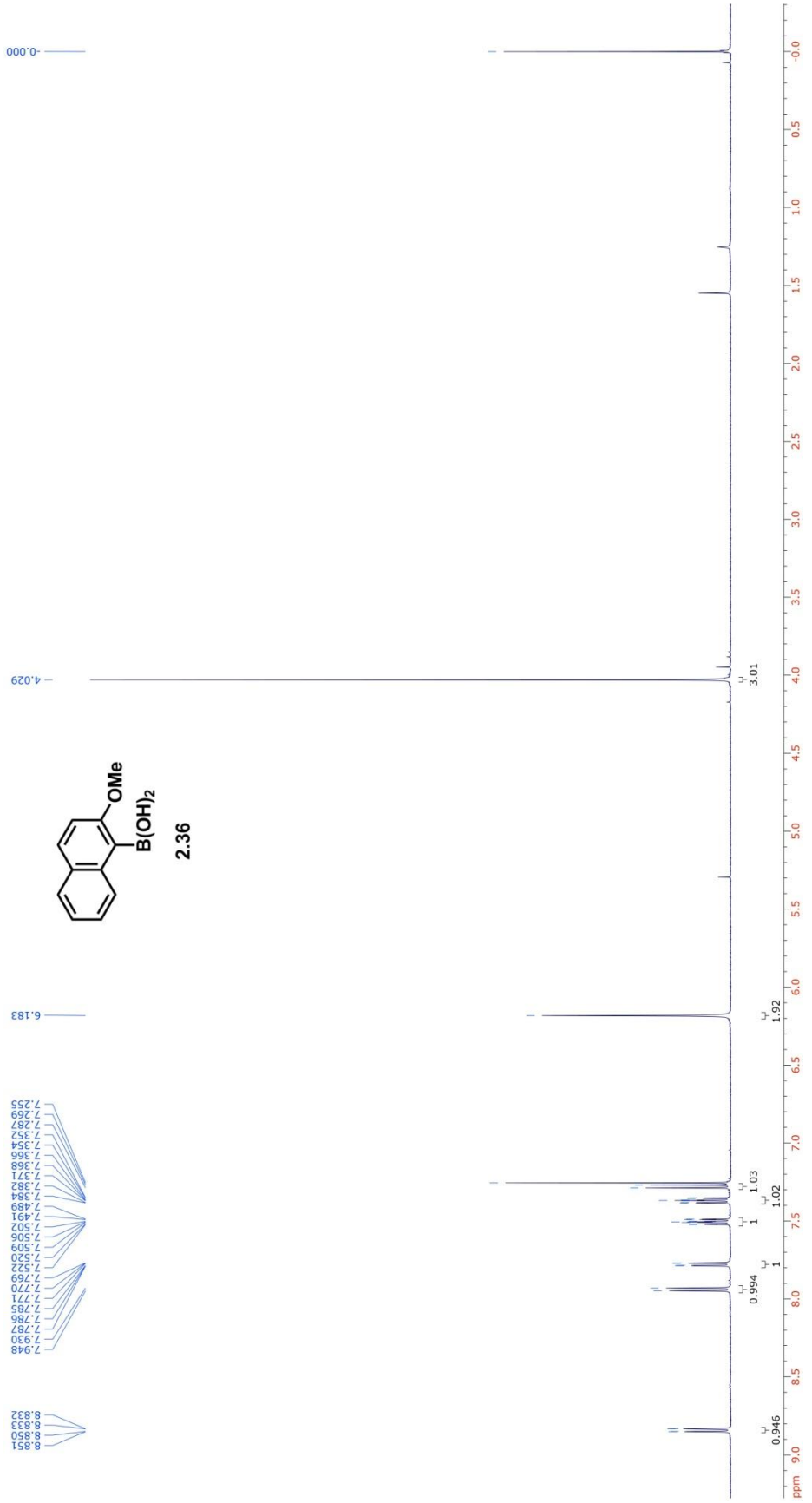
OMe
B(OH)2
2.36
8.851
8.850
8.833
8.832
7.948
7.930
7.787
7.786
7.785
7.771
7.770
7.769
7.522
7.520
7.509
7.506
7.502
7.491
7.489
7.384
7.382
7.371
7.368
7.366
7.354
7.352
7.287
7.269
7.255
6.183
4.029
-0.000
0.946
0.994
1
1
1.03
1.02
1.92
3.01
ppm

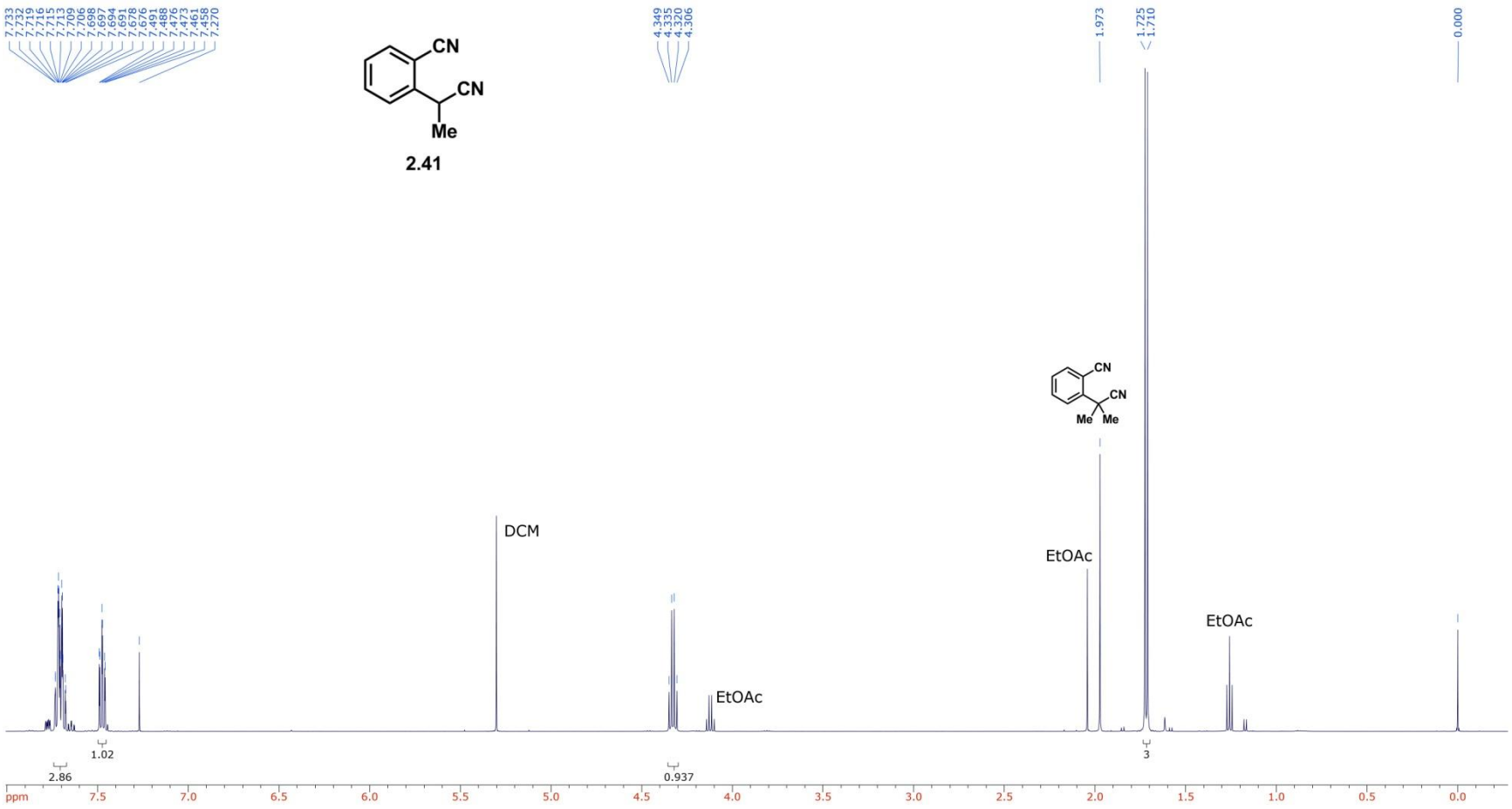
7.733
7.732
7.719
7.716
7.715
7.713
7.709
7.706
7.698
7.697
7.694
7.691
7.678
7.676
7.491
7.488
7.476
7.473
7.461
7.458
7.270
CN
CN
Me
2.41
4.349
4.335
4.320
4.306
1.973
1.725
1.710
0.000
CN
CN
Me
Me
DCM
EtOAc
EtOAc
EtOAc
1.02
2.86
0.937
3
ppm
7.5
7.0
6.5
6.0
5.5
5.0
4.5
4.0
3.5
3.0
2.5
2.0
1.5
1.0
0.5
0.0

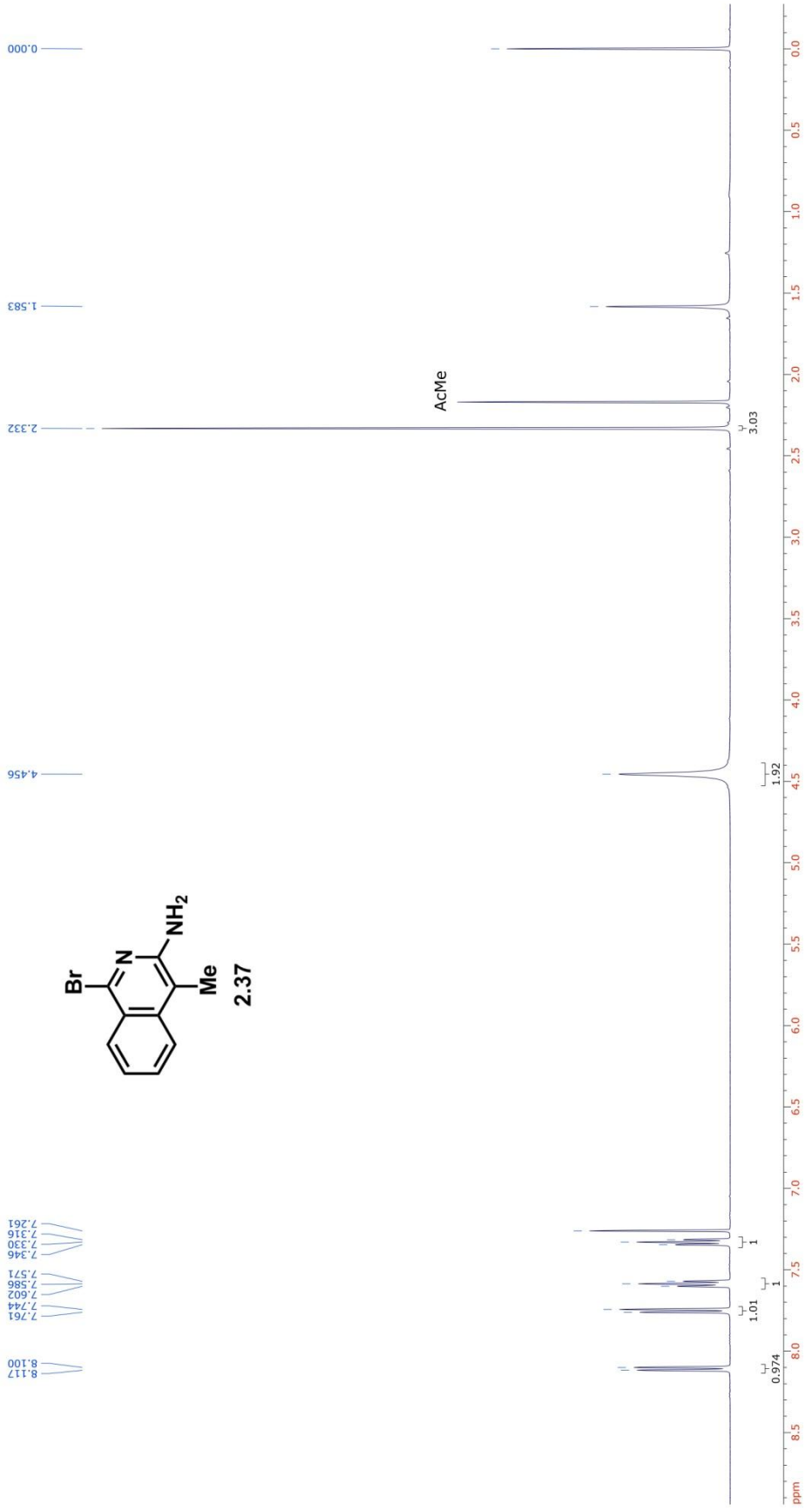
0.000
1.583
2.332
4.456
7.261
7.316
7.330
7.346
7.571
7.586
7.602
7.744
7.761
8.117
8.100
AcMe
3.03
1.92
1
1
1.01
0.974
ppm
Br
N
NH2
Me
2.37

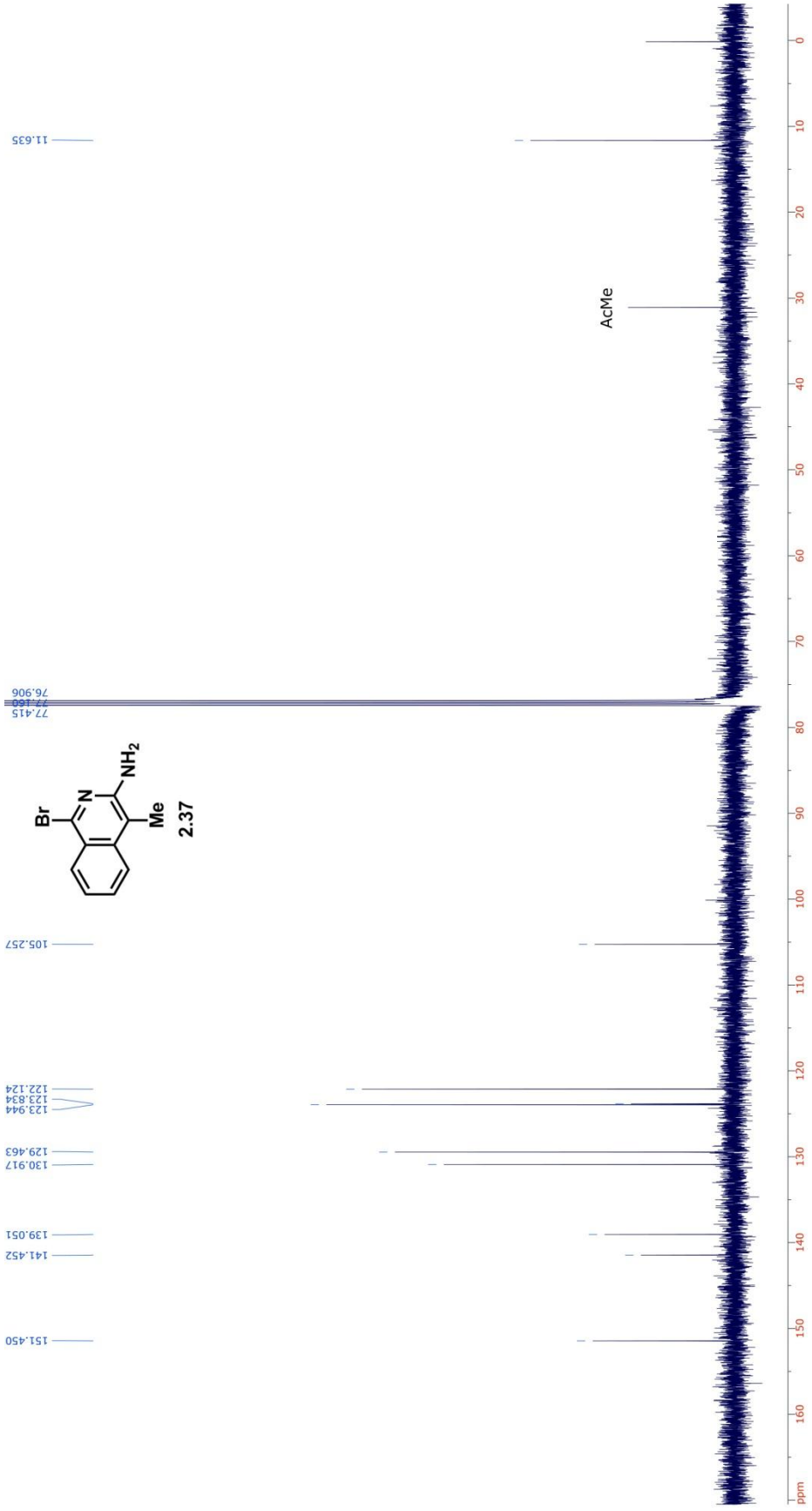
11.635
AcMe
77.415
77.160
76.906
Br
N
NH2
Me
2.37
105.257
122.124
123.834
123.944
129.463
130.917
139.051
141.452
151.450
ppm

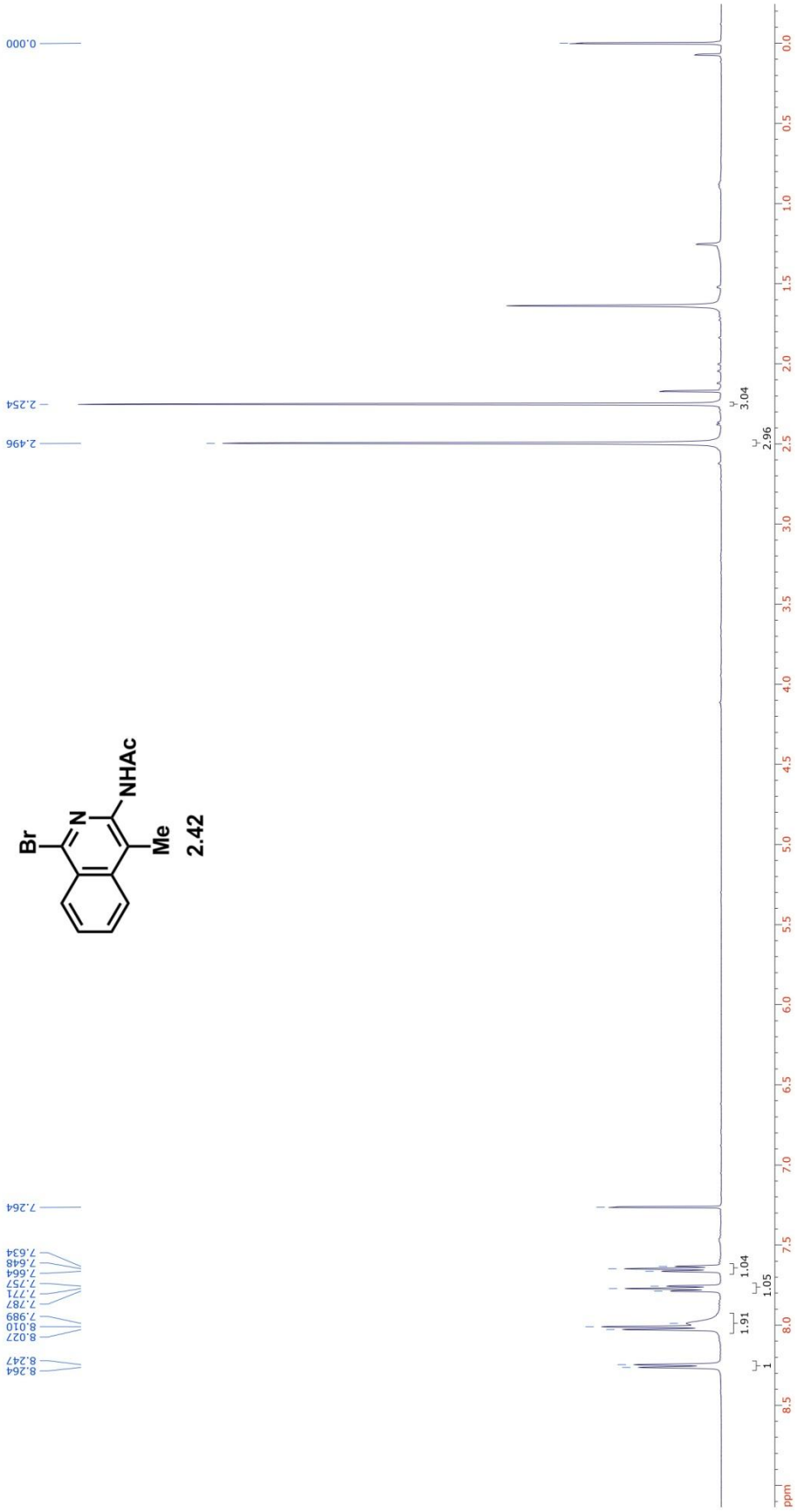
0.000
2.254
2.496
7.264
7.634
7.648
7.664
7.757
7.771
7.787
7.989
8.010
8.027
8.247
8.264
3.04
2.96
1.04
1.05
1.91
1
Br
N
NHAc
Me
2.42
ppm

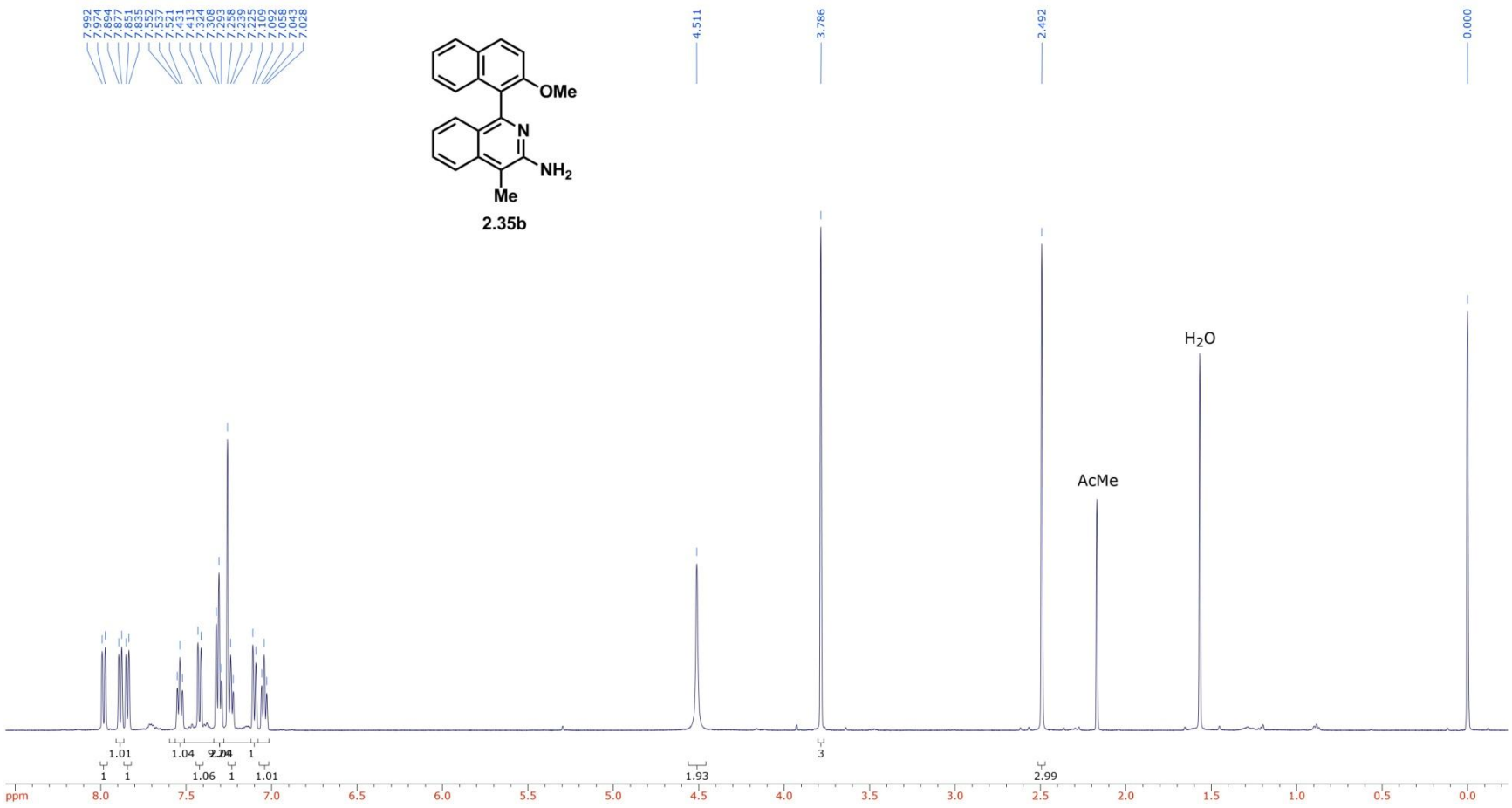
7.992
7.974
7.894
7.877
7.851
7.835
7.552
7.537
7.321
7.311
7.413
7.324
7.308
7.293
7.258
7.225
7.109
7.092
7.058
7.043
7.028
4.511
3.786
2.492
0.000
OMe
N
NH2
Me
2.35b
H2O
AcMe
1.01
1
1
1.04
1.06
2.24
1
1
1.01
1.93
3
2.99
ppm
8.0
7.5
7.0
6.5
6.0
5.5
5.0
4.5
4.0
3.5
3.0
2.5
2.0
1.5
1.0
0.5
0.0

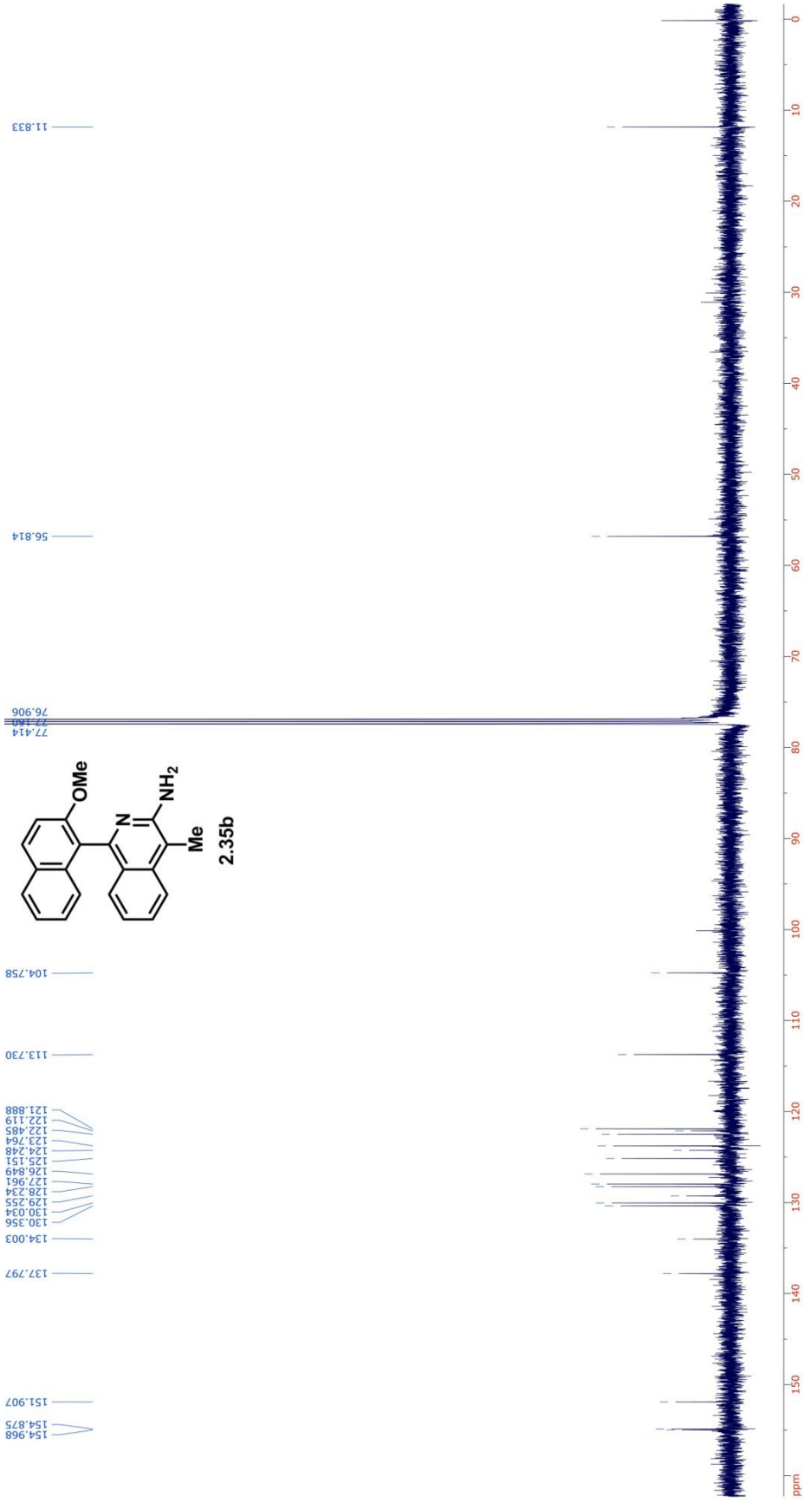
11.833
56.814
76.906
77.414
104.758
113.730
121.888
122.119
122.485
123.764
124.248
125.151
126.849
127.961
128.234
129.255
130.034
130.356
134.003
137.797
151.907
154.875
154.968
OMe
N
NH2
Me
2.35b
ppm

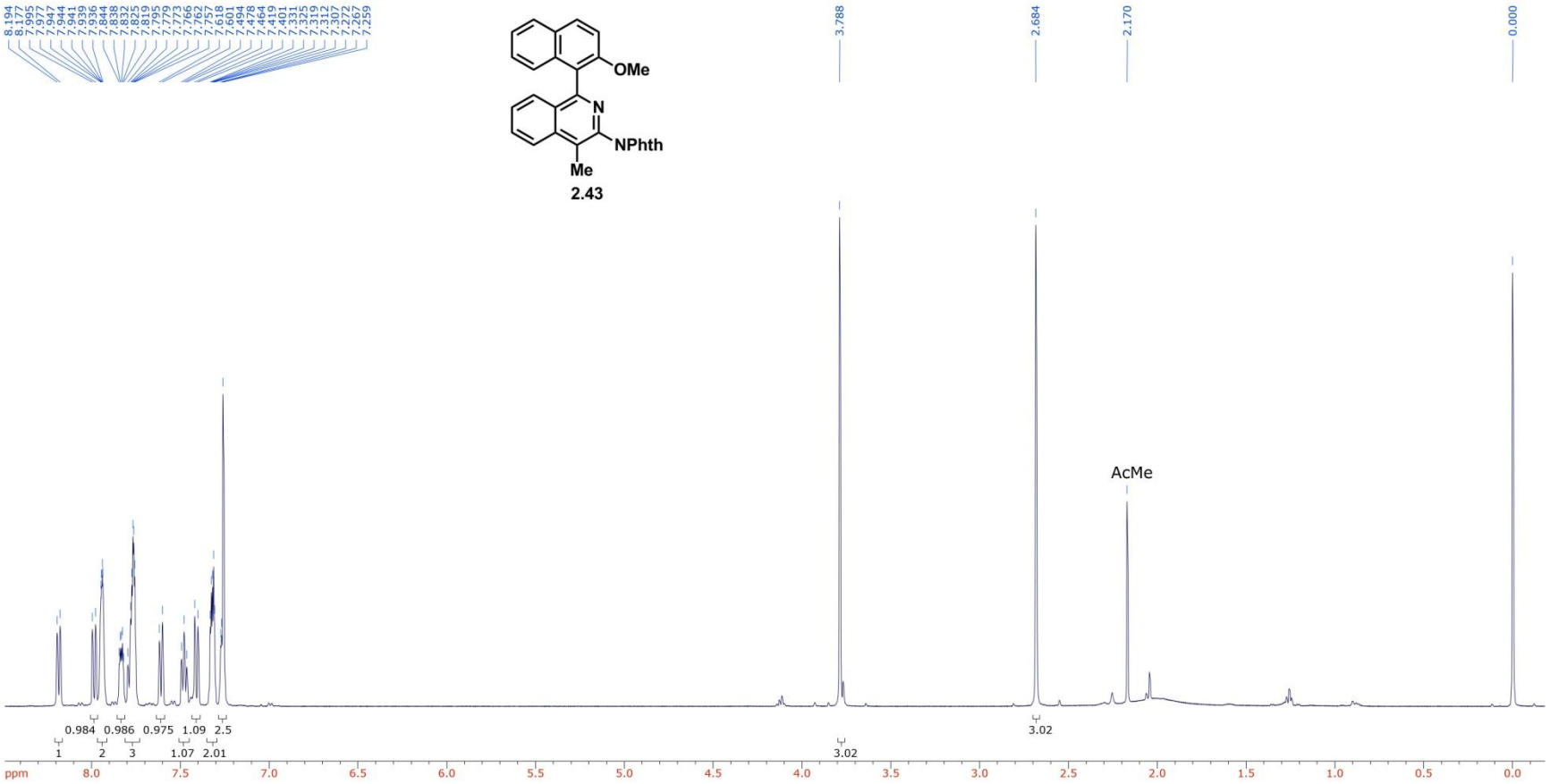
8.194
8.177
7.995
7.977
7.947
7.944
7.941
7.939
7.936
7.844
7.838
7.832
7.825
7.819
7.795
7.779
7.773
7.766
7.762
7.757
7.618
7.601
7.494
7.478
7.464
7.419
7.401
7.331
7.325
7.319
7.312
7.307
7.272
7.267
7.259
OMe
N
NPhth
Me
2.43
3.788
2.684
2.170
0.000
AcMe
0.984
0.986
0.975
1.09
2.5
1.07
2.01
3.02
3.02
ppm
8.0
7.5
7.0
6.5
6.0
5.5
5.0
4.5
4.0
3.5
3.0
2.5
2.0
1.5
1.0
0.5
0.0

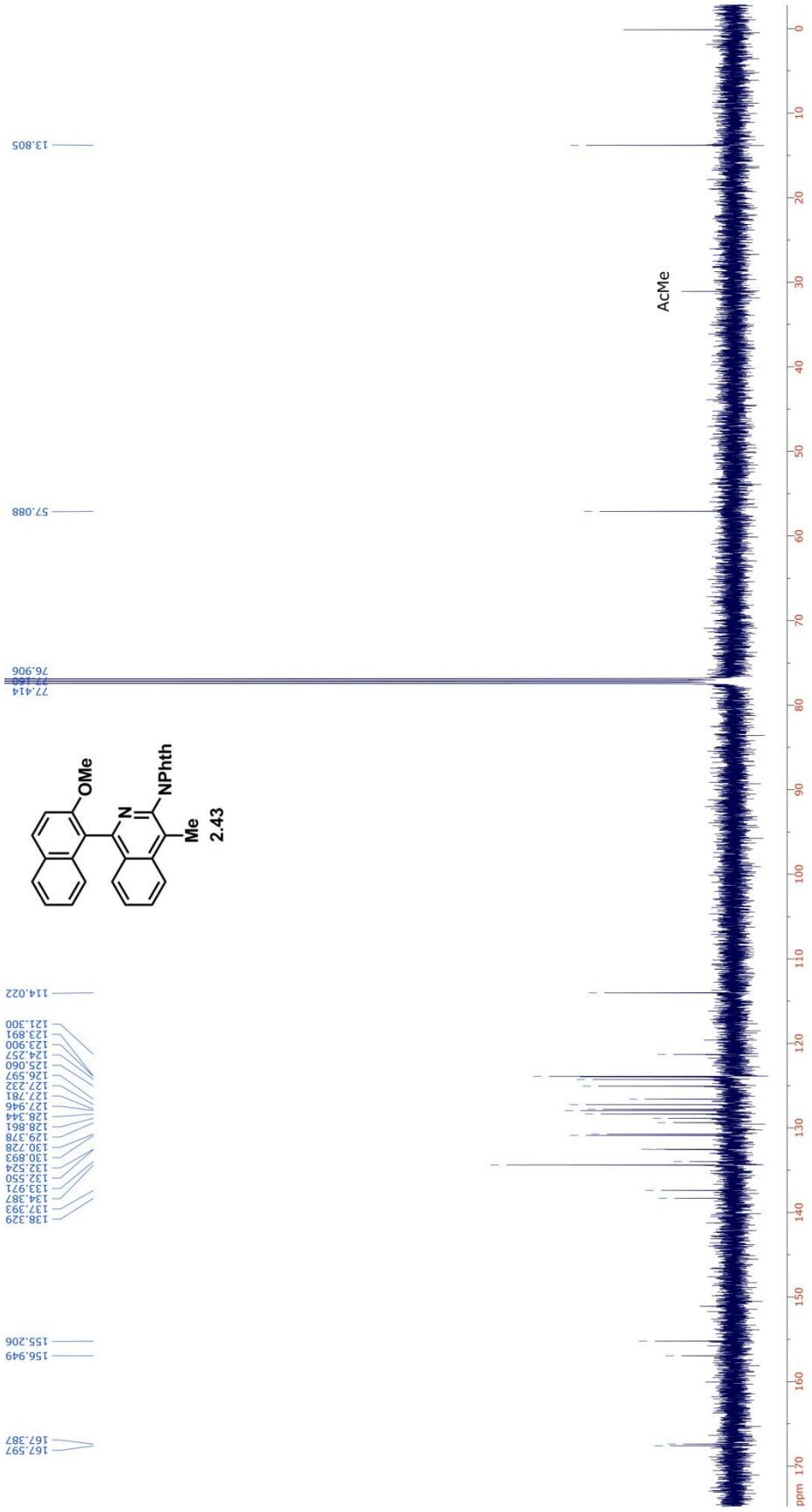
13.805
57.088
76.906
77.160
77.414
114.022
121.300
123.891
123.900
124.257
125.060
126.597
127.232
127.781
127.946
128.344
128.861
129.378
130.728
130.893
132.524
132.550
133.971
134.387
137.393
138.329
155.206
156.949
167.387
167.597
OMe
N
NPhth
Me
2.43
AcMe
ppm

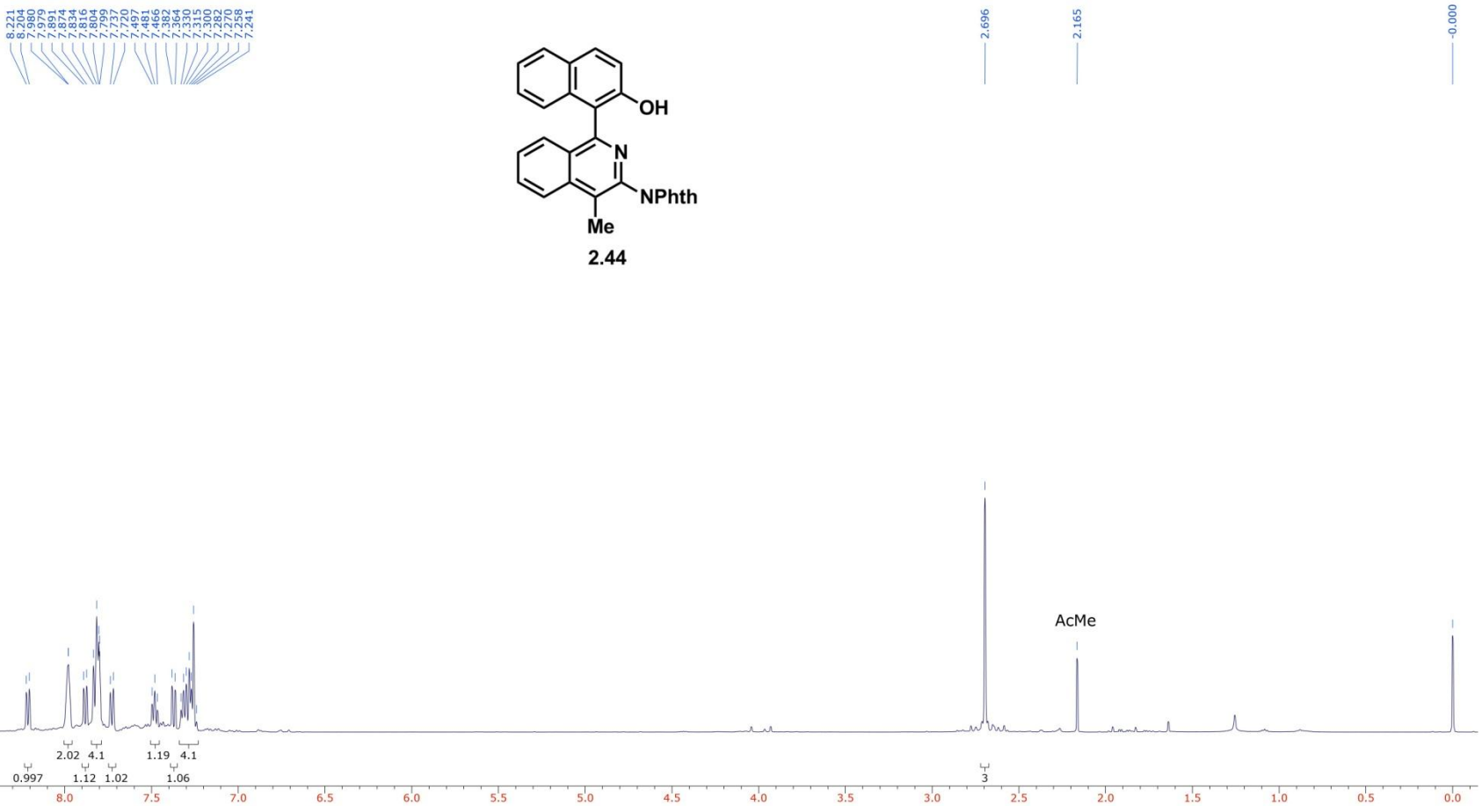
8.221
8.204
7.980
7.979
7.971
7.874
7.834
7.816
7.804
7.799
7.737
7.720
7.497
7.481
7.466
7.382
7.364
7.330
7.315
7.300
7.282
7.270
7.258
7.241
2.696
2.165
-0.000
OH
N
NPhth
Me
2.44
AcMe
2.02
4.1
1.19
4.1
0.997
1.12
1.02
1.06
3
ppm
8.0
7.5
7.0
6.5
6.0
5.5
5.0
4.5
4.0
3.5
3.0
2.5
2.0
1.5
1.0
0.5
0.0

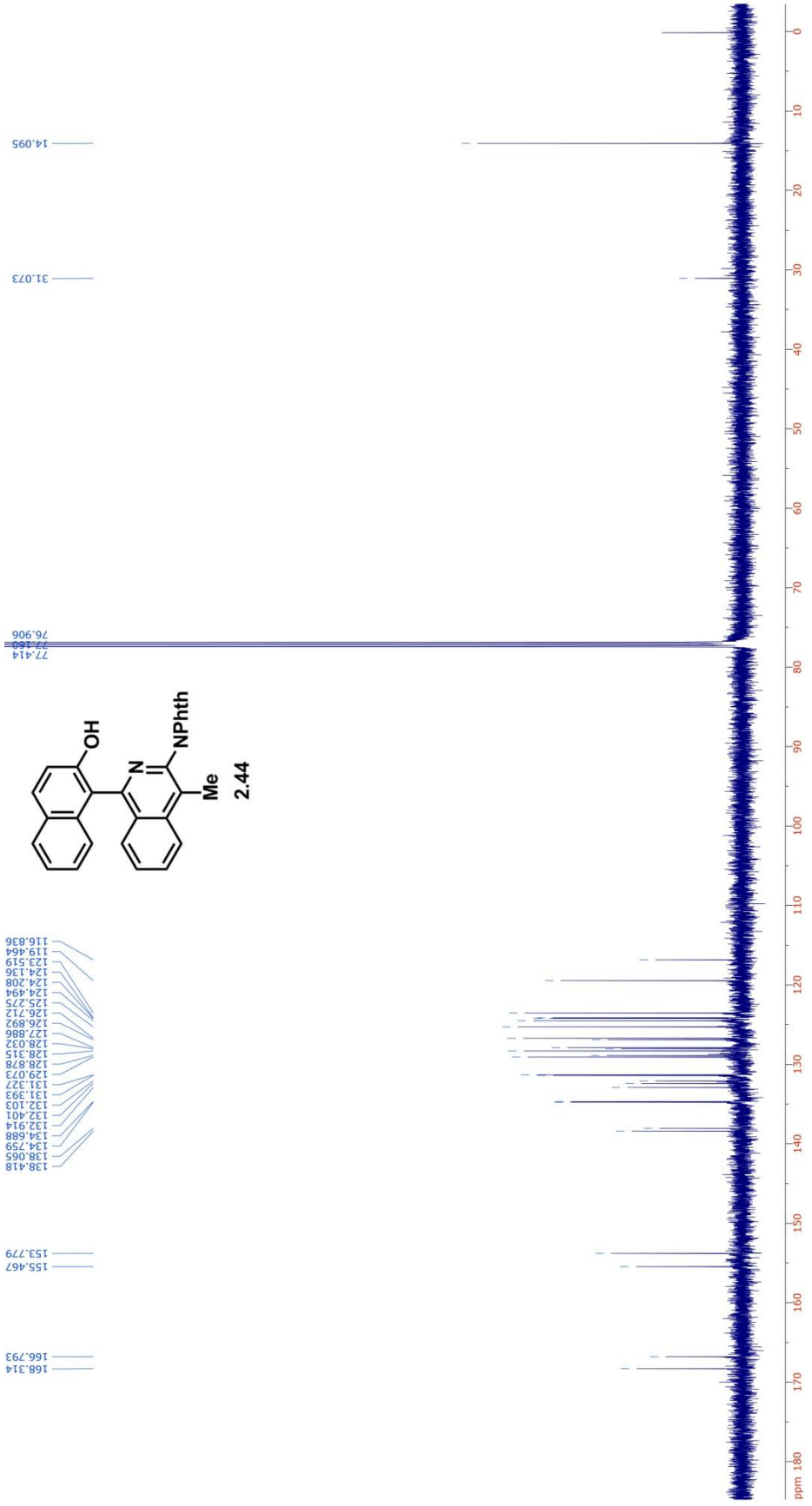
OH
N
NPhth
Me
2.44
14.095
31.073
77.414
77.160
76.906
116.836
119.464
123.519
124.136
124.208
124.494
125.275
126.712
126.892
127.886
128.032
128.315
128.878
129.073
131.327
131.393
132.103
132.401
132.914
134.688
134.759
136.065
138.418
153.779
155.467
166.793
168.314
ppm

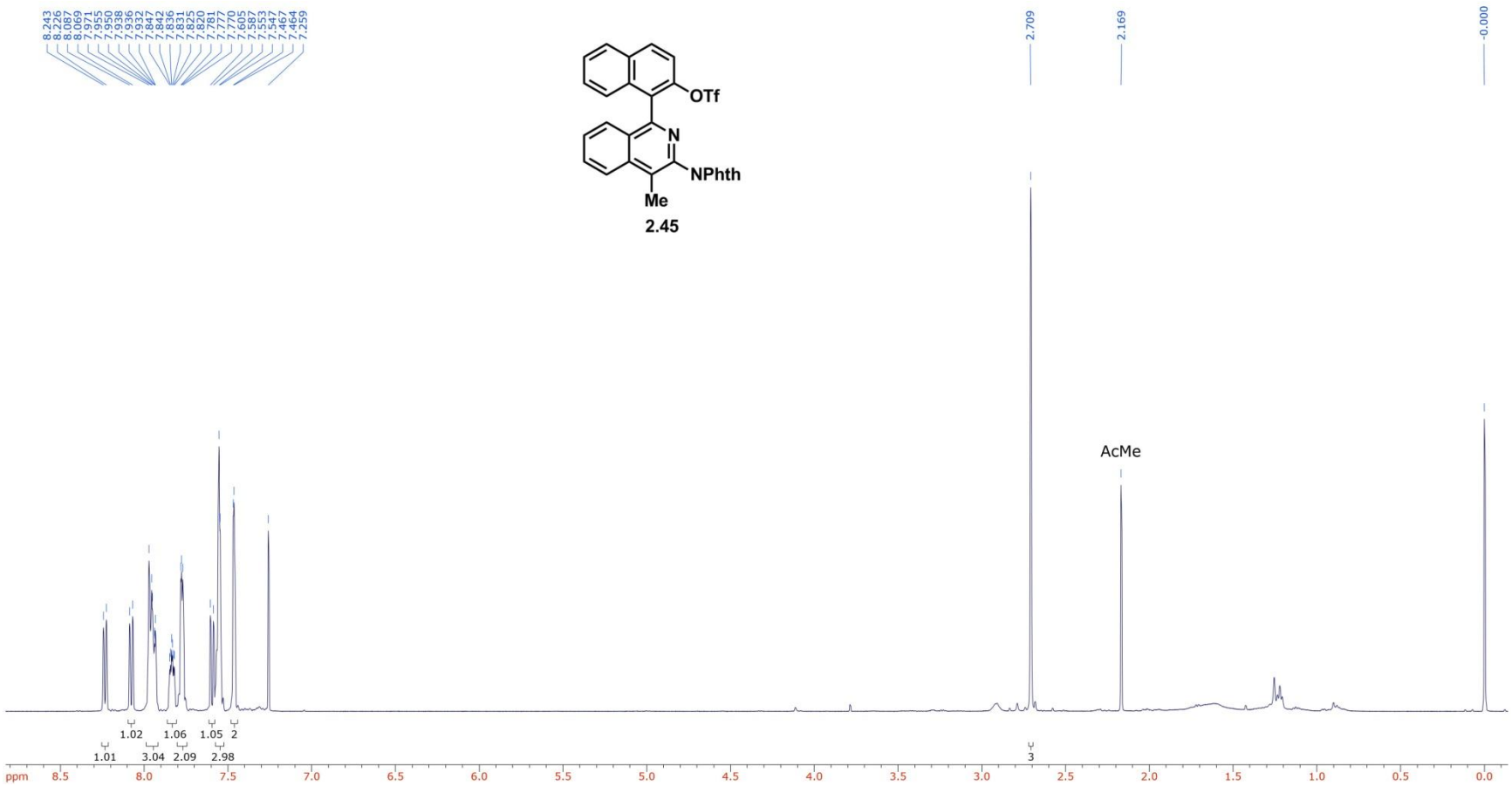
8.243
8.236
8.087
8.069
7.971
7.955
7.950
7.938
7.936
7.932
7.847
7.842
7.836
7.831
7.825
7.820
7.781
7.777
7.770
7.605
7.597
7.553
7.547
7.467
7.464
7.259
OTf
N
NPhth
Me
2.45
2.709
2.169
-0.000
AcMe
1.01
1.02
3.04
1.06
2.09
1.05
2.98
2
3
ppm
8.5
8.0
7.5
7.0
6.5
6.0
5.5
5.0
4.5
4.0
3.5
3.0
2.5
2.0
1.5
1.0
0.5
0.0

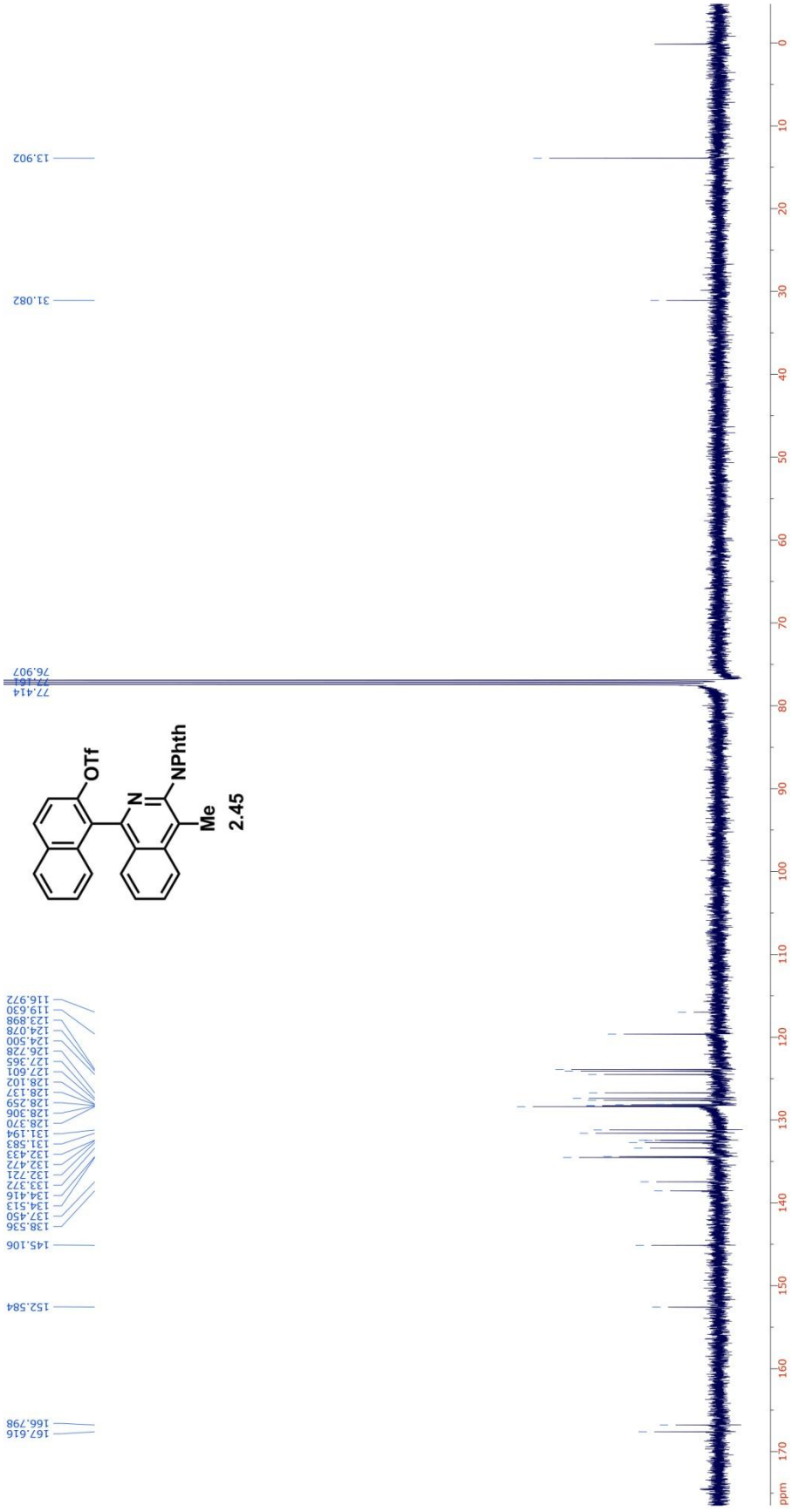
13.902
31.082
76.907
77.161
77.414
OTf
N
NPhth
Me
2.45
116.972
119.630
123.898
124.078
124.300
126.728
127.365
127.601
128.102
128.137
128.259
128.306
128.370
131.194
131.583
132.433
132.472
132.721
133.372
134.416
134.513
137.450
138.536
145.106
152.584
166.798
167.616
ppm

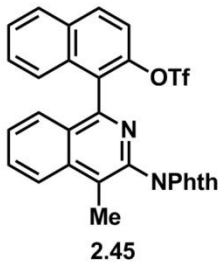
OTf
N
NPhth
Me

2.45

-74.242
-78.290
ppm
-10
-20
-30
-40
-50
-60
-70
-80
-90
-100
-110
-120
-130
-140
-150

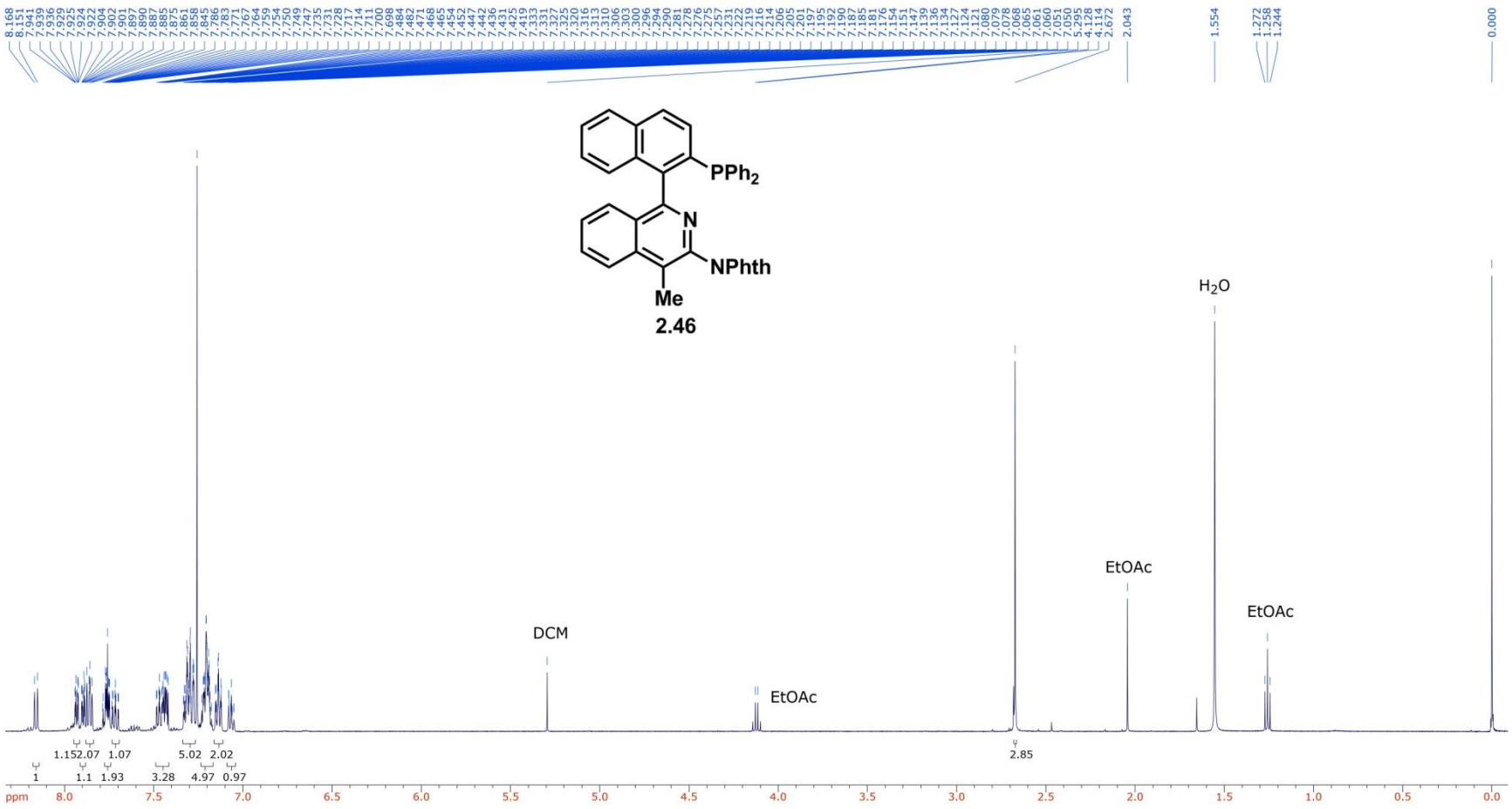
PPh2
N
NPhth
Me
2.46
H2O
EtOAc
EtOAc
DCM
EtOAc
1.15
2.07
1.07
5.02
2.02
1
1.1
1.93
3.28
4.97
0.97
2.85
ppm

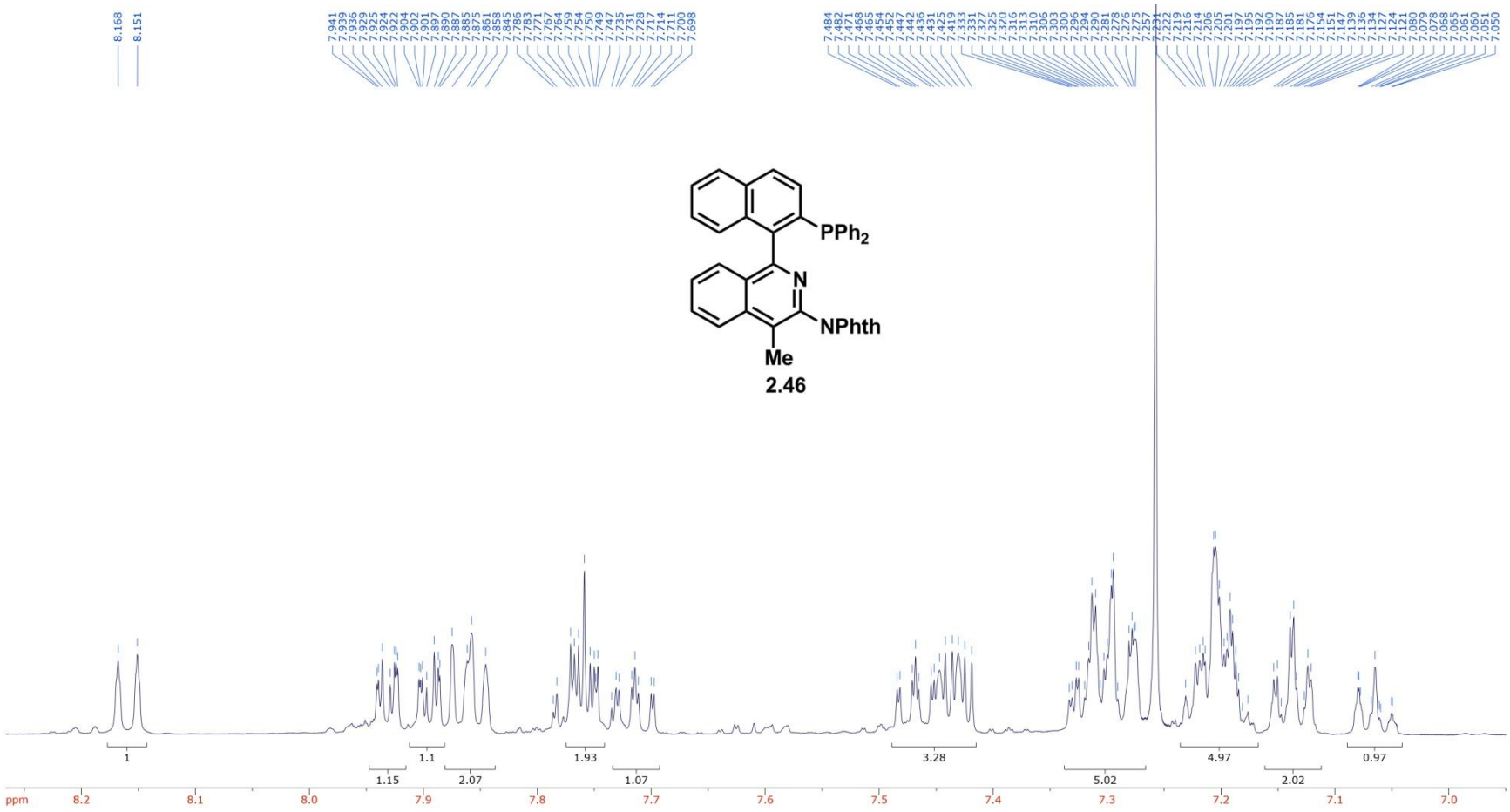
8.168
8.151
7.941
7.939
7.936
7.929
7.925
7.924
7.922
7.904
7.902
7.901
7.897
7.890
7.887
7.885
7.875
7.861
7.858
7.845
7.786
7.783
7.771
7.767
7.764
7.759
7.754
7.750
7.749
7.747
7.735
7.731
7.728
7.717
7.714
7.711
7.700
7.698
7.484
7.482
7.471
7.468
7.465
7.454
7.452
7.447
7.442
7.436
7.431
7.425
7.419
7.333
7.331
7.327
7.325
7.320
7.316
7.313
7.310
7.306
7.303
7.300
7.296
7.294
7.280
7.278
7.276
7.275
7.257
7.221
7.219
7.216
7.214
7.206
7.205
7.201
7.197
7.195
7.192
7.190
7.187
7.185
7.181
7.176
7.154
7.151
7.147
7.139
7.136
7.134
7.127
7.124
7.121
7.080
7.079
7.078
7.068
7.065
7.061
7.060
7.051
7.050
PPh2
N
NPhth
Me
2.46
1
1.15
1.1
2.07
1.93
1.07
3.28
5.02
4.97
2.02
0.97
ppm
8.2
8.1
8.0
7.9
7.8
7.7
7.6
7.5
7.4
7.3
7.2
7.1
7.0

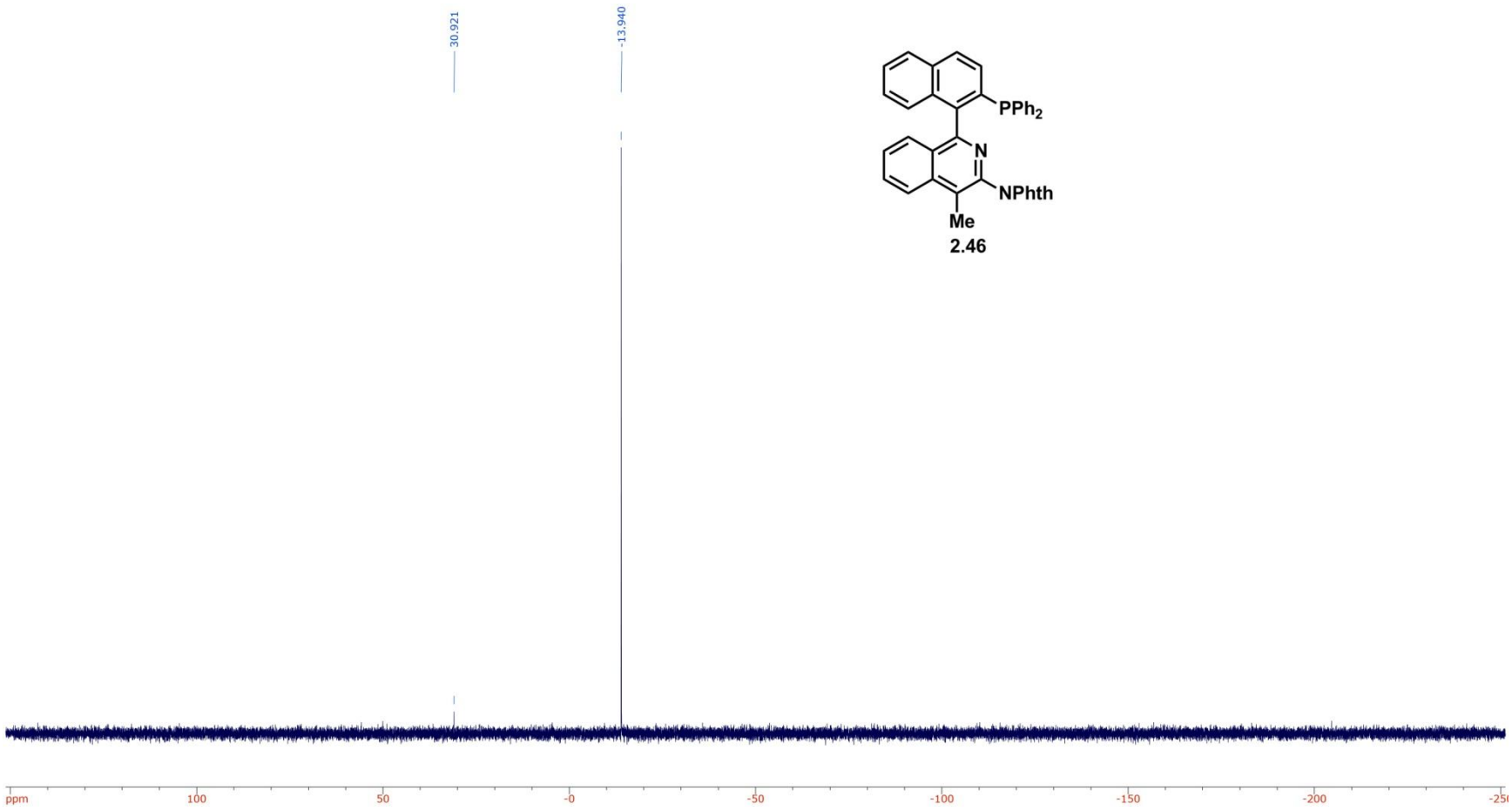
30.921
-13.940
PPh2
N
NPhth
Me
2.46
ppm
100
50
-0
-50
-100
-150
-200

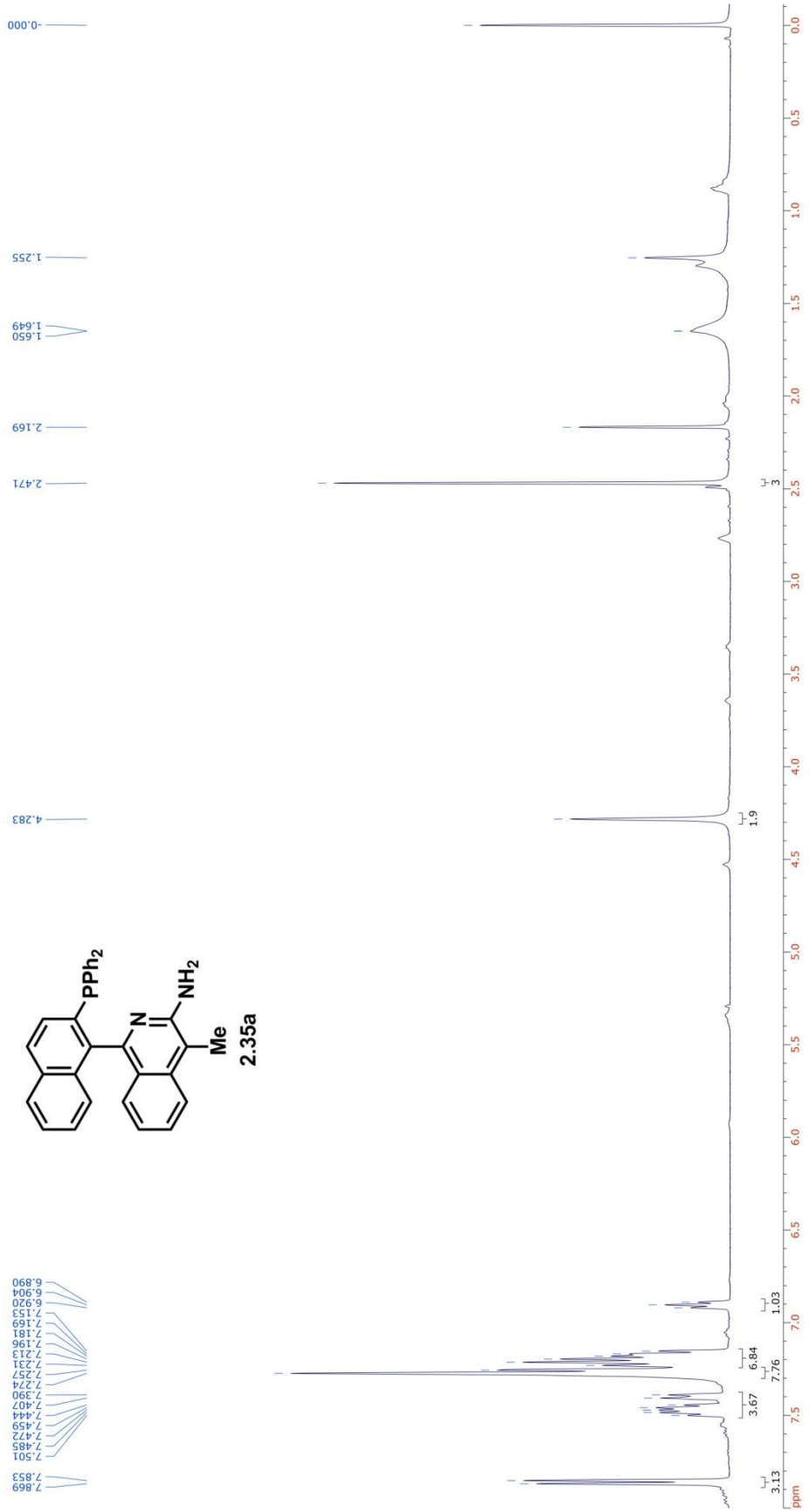
PPh2
NH2
N
Me
2.35a
-0.000
1.255
1.650
1.649
2.169
2.471
4.283
6.890
6.904
6.920
7.153
7.169
7.181
7.196
7.213
7.231
7.257
7.274
7.390
7.407
7.444
7.459
7.472
7.485
7.501
7.853
7.869
3.13
3.67
6.84
7.76
1.03
1.9
3
ppm

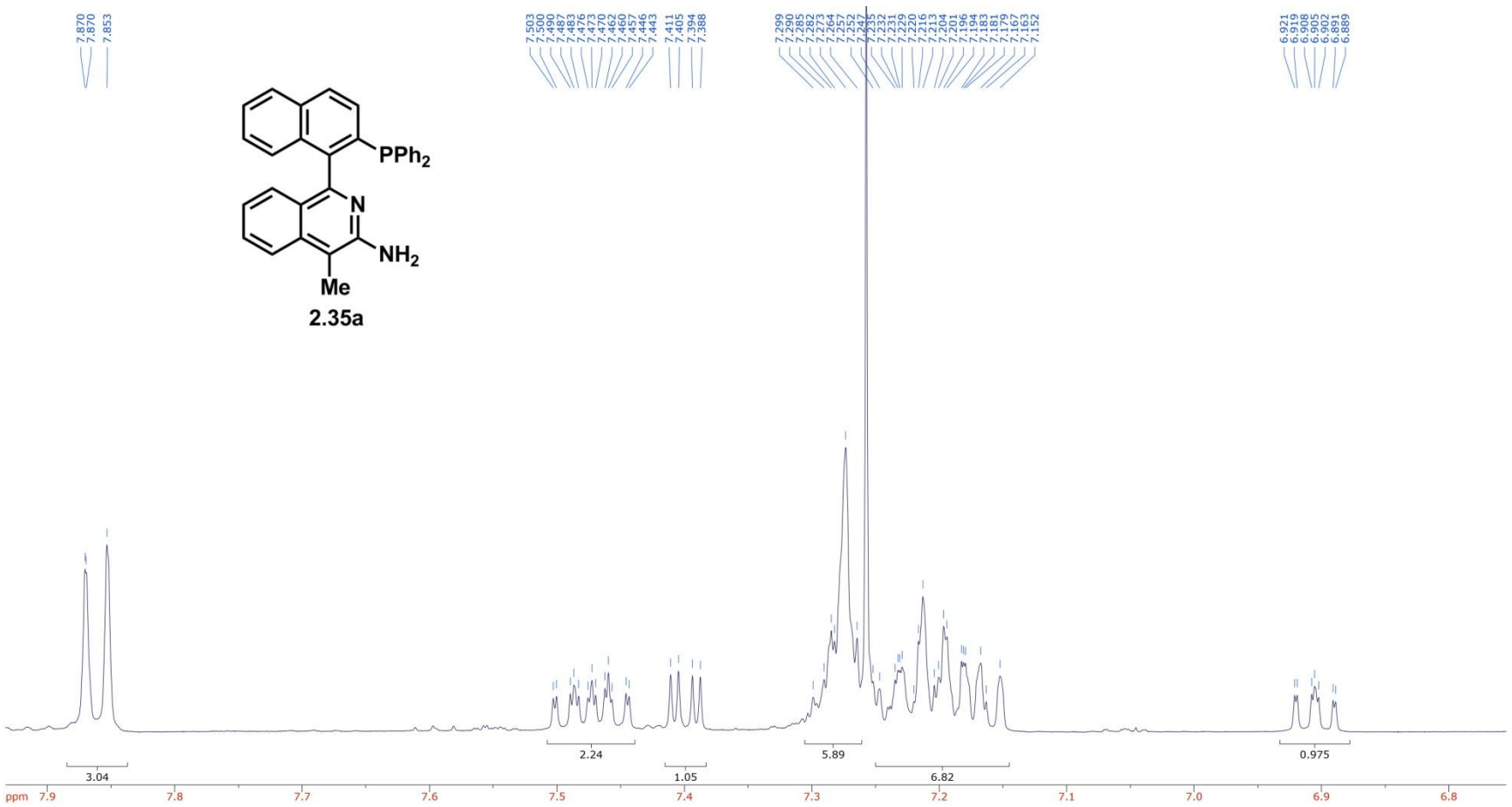
7.870
7.870
7.853
7.503
7.500
7.490
7.487
7.483
7.476
7.473
7.470
7.462
7.460
7.457
7.446
7.443
7.411
7.405
7.394
7.388
7.299
7.290
7.285
7.282
7.273
7.264
7.257
7.252
7.242
7.235
7.232
7.231
7.229
7.220
7.216
7.213
7.204
7.201
7.196
7.194
7.183
7.181
7.179
7.167
7.163
7.152
6.921
6.919
6.908
6.905
6.902
6.891
6.889
PPh2
N
NH2
Me
2.35a
3.04
2.24
1.05
5.89
6.82
0.975
ppm 7.9
7.8
7.7
7.6
7.5
7.4
7.3
7.2
7.1
7.0
6.9
6.8

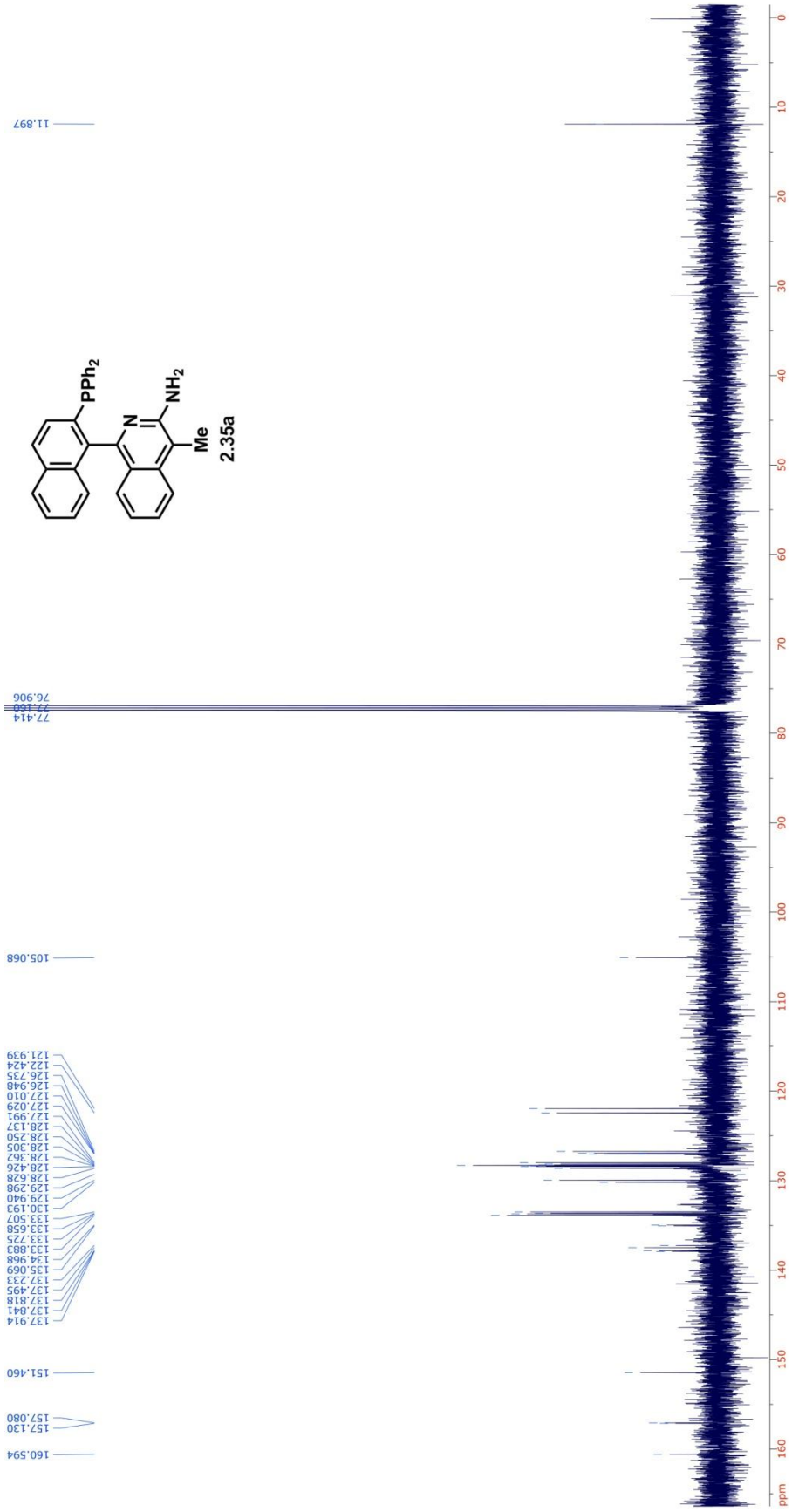
PPh2
NH2
N
Me
2.35a
11.897
77.414
77.160
76.906
105.068
121.939
122.424
126.735
126.948
127.010
127.029
127.991
128.137
128.250
128.305
128.362
128.426
128.628
129.298
129.940
130.193
133.507
133.658
133.725
133.883
134.968
135.069
137.233
137.495
137.818
137.841
137.914
151.460
157.080
157.130
160.594
0
10
20
30
40
50
60
70
80
90
100
110
120
130
140
150
160
ppm

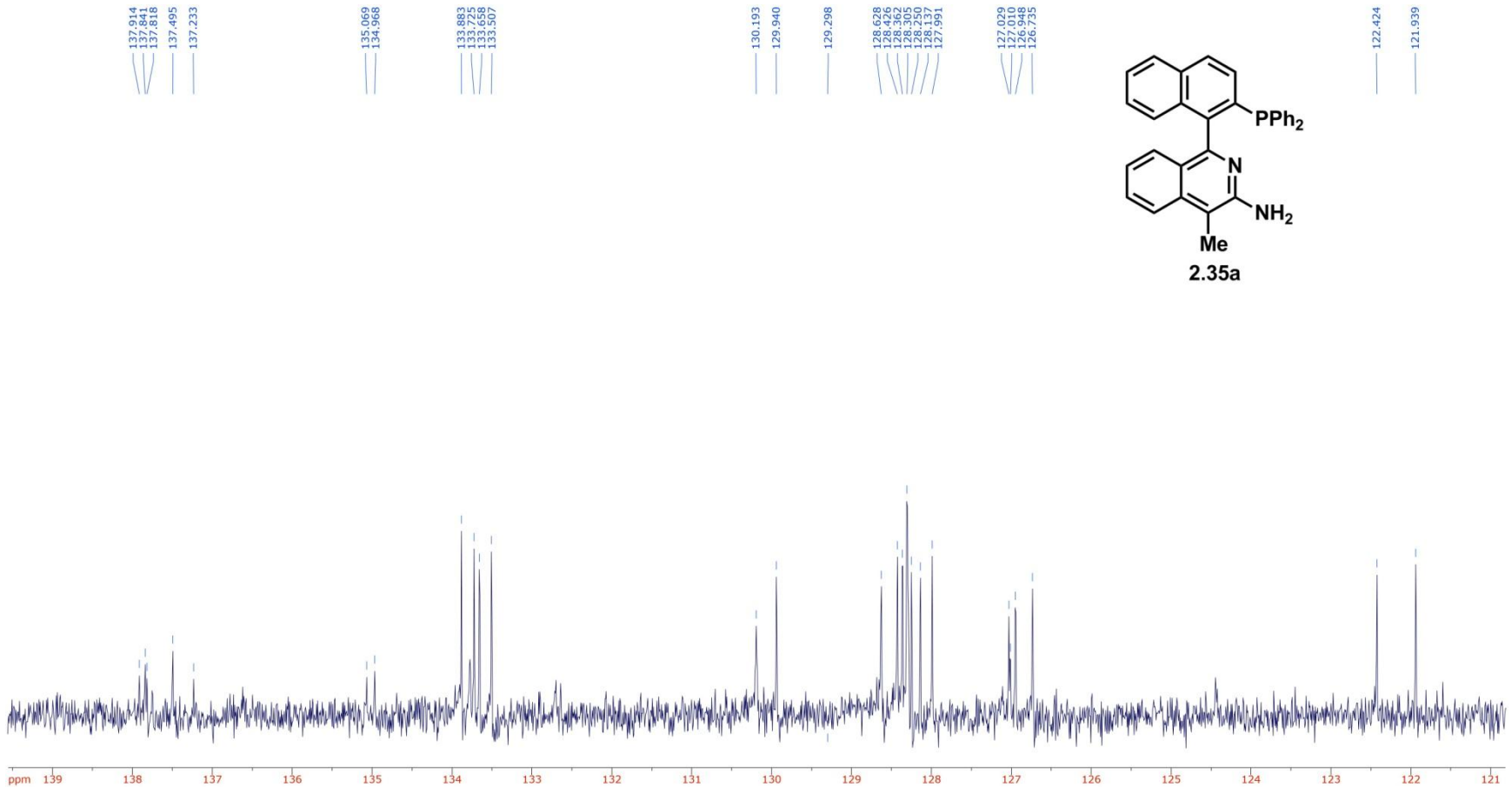
137.914
137.841
137.818
137.495
137.233
135.069
134.968
133.883
133.725
133.658
133.507
130.193
129.940
129.298
128.628
128.426
128.362
128.305
128.250
128.137
127.991
127.029
127.010
126.948
126.735
122.424
121.939
PPh2
N
NH2
Me
2.35a
ppm 139
138
137
136
135
134
133
132
131
130
129
128
127
126
125
124
123
122
121

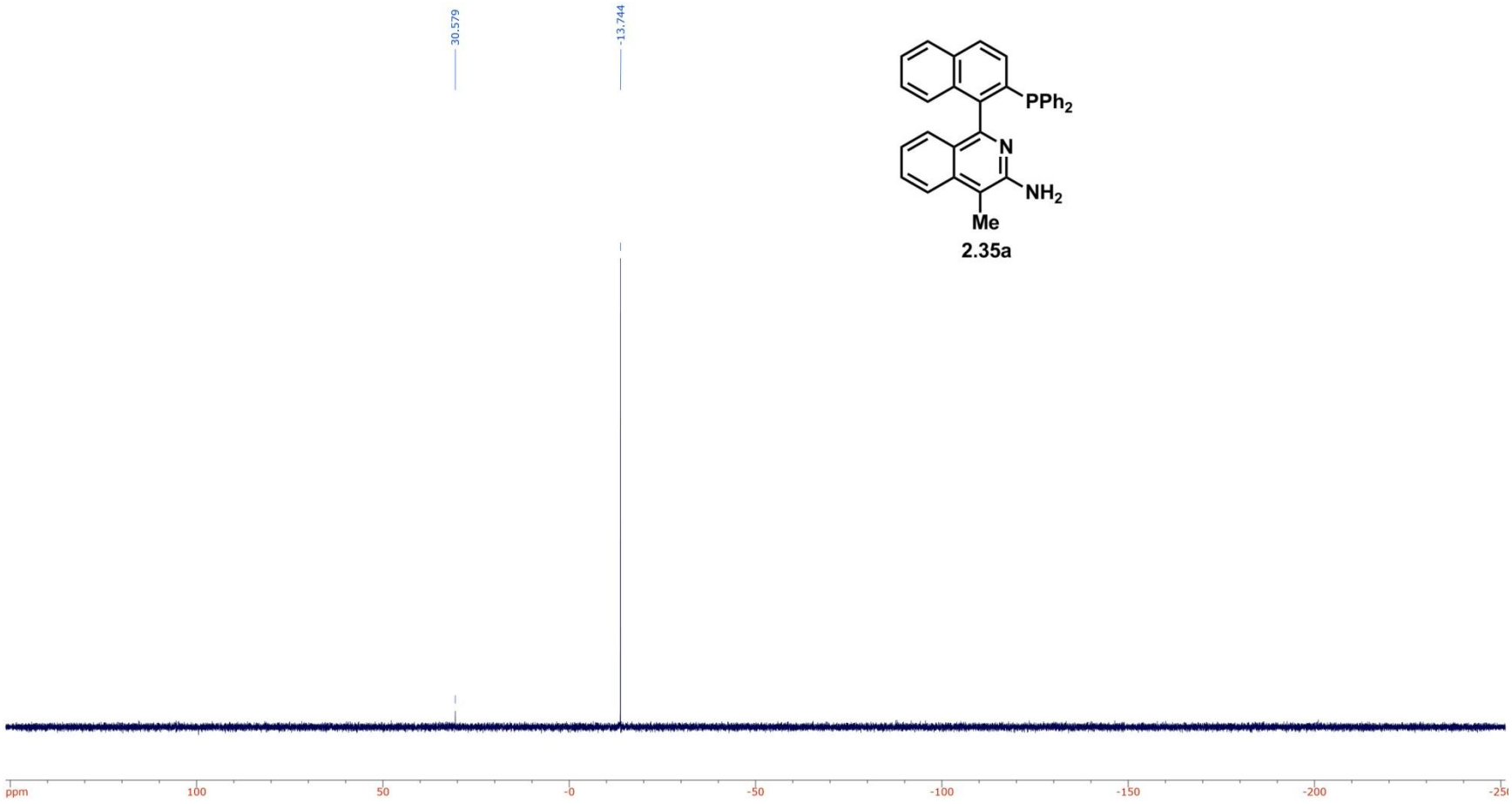
30.579
-13.744
PPh2
N
NH2
Me
2.35a
ppm
100
50
-0
-50
-100
-150
-200

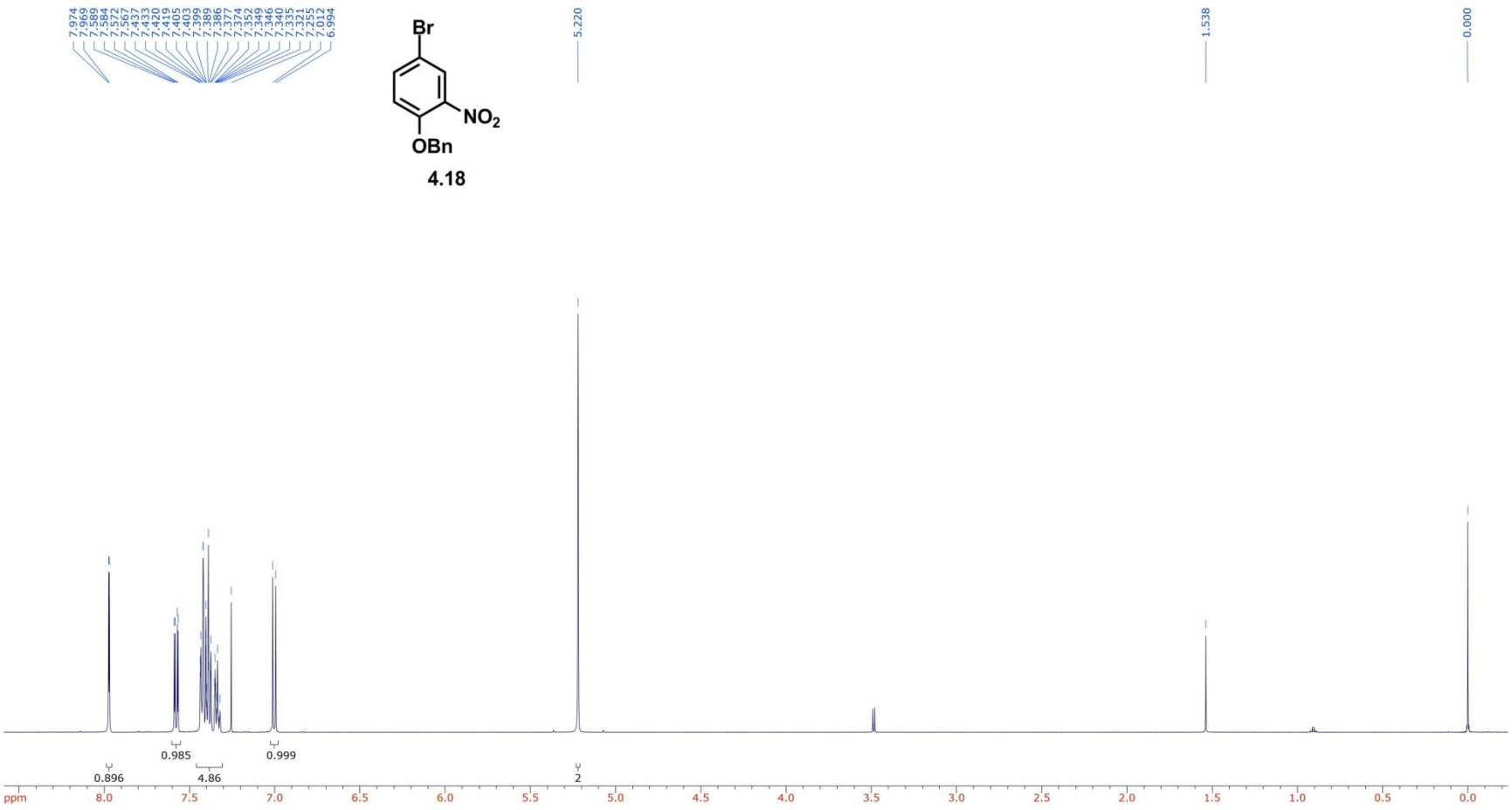
7.974
7.969
7.589
7.584
7.572
7.567
7.437
7.433
7.420
7.419
7.405
7.403
7.399
7.389
7.386
7.377
7.374
7.352
7.349
7.346
7.340
7.335
7.331
7.255
7.012
6.994
Br
NO2
OBn
4.18
5.220
1.538
0.000
0.896
0.985
4.86
0.999
2
ppm
8.0
7.5
7.0
6.5
6.0
5.5
5.0
4.5
4.0
3.5
3.0
2.5
2.0
1.5
1.0
0.5
0.0

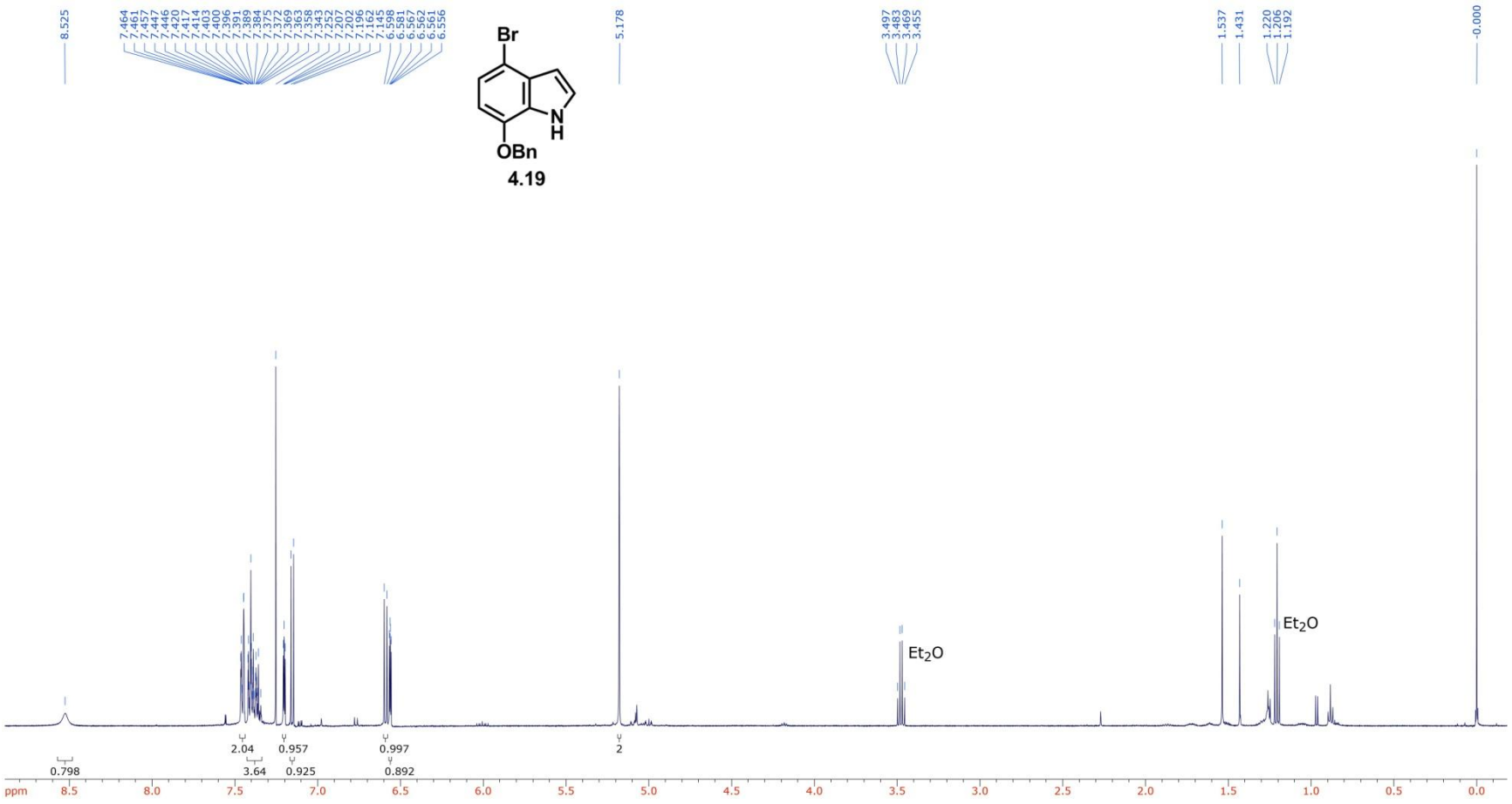
8.525
7.464
7.461
7.457
7.447
7.446
7.420
7.417
7.414
7.403
7.400
7.396
7.391
7.389
7.384
7.375
7.372
7.369
7.363
7.358
7.343
7.252
7.207
7.200
7.196
7.162
7.145
6.598
6.581
6.567
6.562
6.561
6.556
Br
N
H
OBn
4.19
5.178
3.497
3.483
3.469
3.455
1.537
1.431
1.220
1.206
1.192
0.000
Et2O
Et2O
2.04
0.957
0.997
2
0.798
3.64
0.925
0.892
ppm
8.5
8.0
7.5
7.0
6.5
6.0
5.5
5.0
4.5
4.0
3.5
3.0
2.5
2.0
1.5
1.0
0.5
0.0

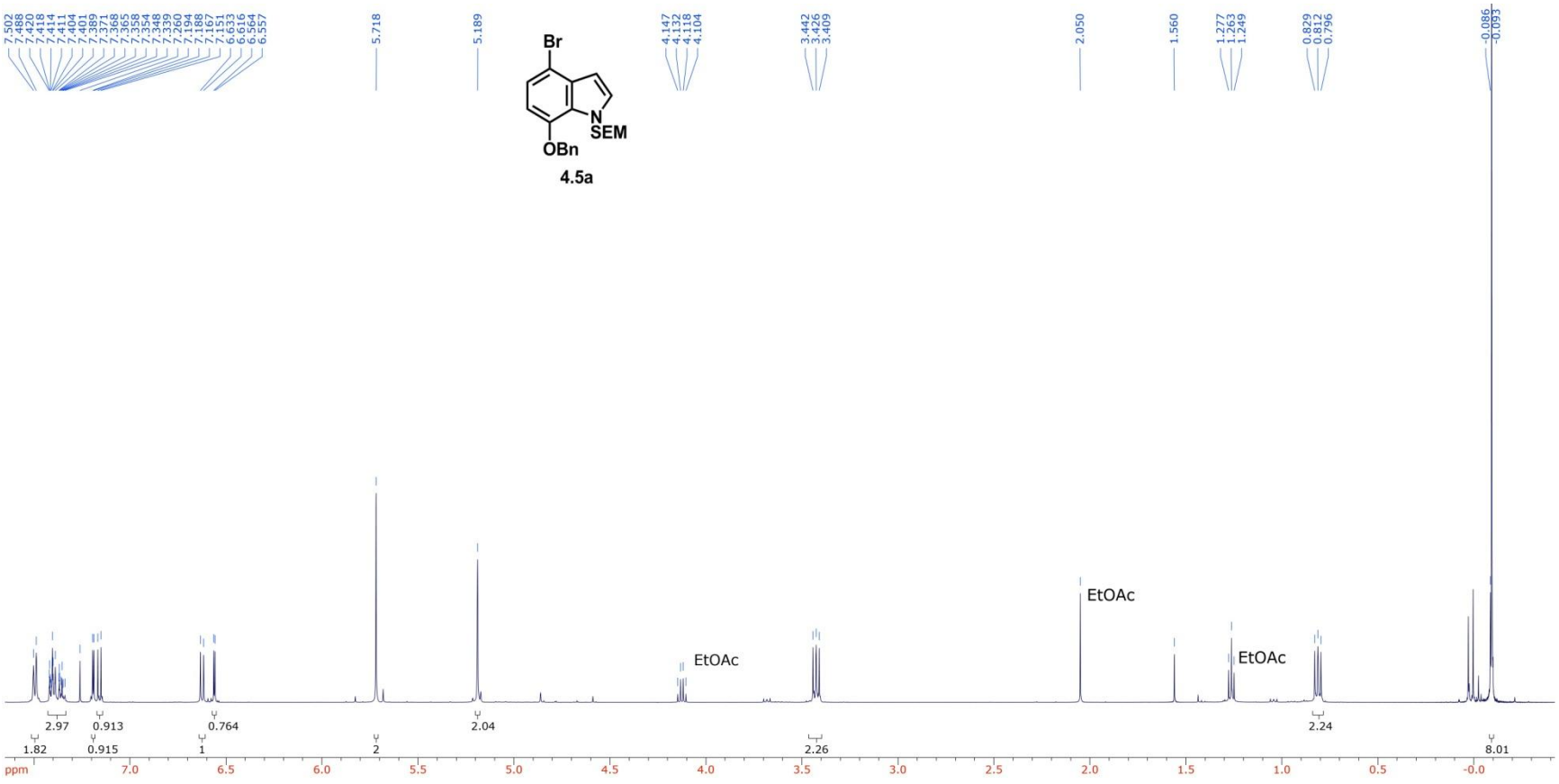
7.502
7.488
7.420
7.418
7.414
7.411
7.404
7.401
7.389
7.371
7.368
7.365
7.358
7.354
7.348
7.339
7.260
7.194
7.188
7.167
7.151
6.633
6.616
6.564
6.557
5.718
5.189
4.147
4.132
4.118
4.104
3.442
3.426
3.409
2.050
1.560
1.277
1.263
1.249
0.829
0.812
0.796
-0.086
-0.093
Br
N
SEM
OBn
4.5a
EtOAc
EtOAc
EtOAc
2.97
0.913
0.764
2.04
2.24
1.82
0.915
1
2
2.26
8.01
ppm
7.0
6.5
6.0
5.5
5.0
4.5
4.0
3.5
3.0
2.5
2.0
1.5
1.0
0.5
-0.0

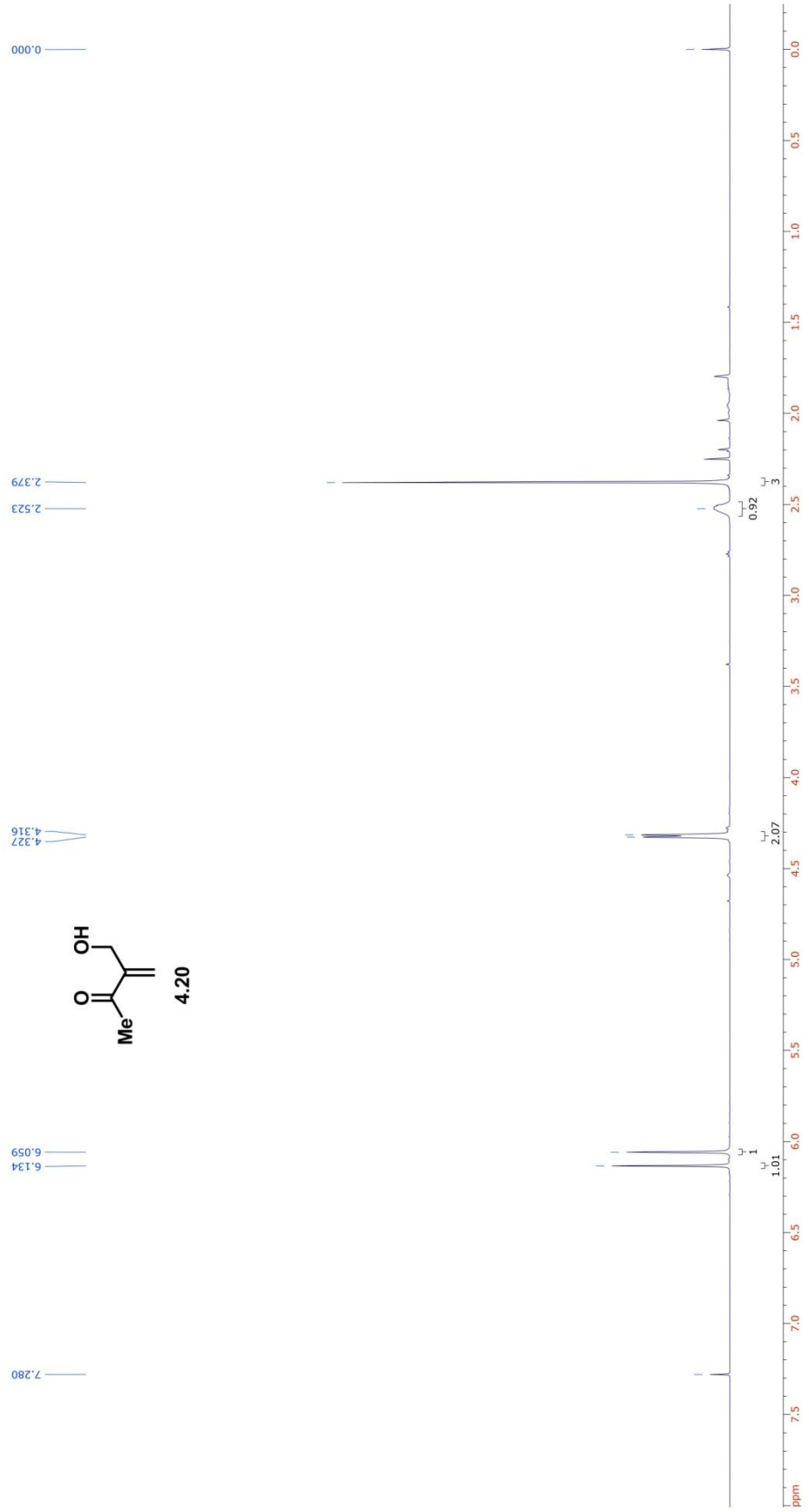
0.000
2.379
2.523
4.316
4.327
6.059
6.134
7.280
3
0.92
2.07
1
1.01
ppm
OH
O
Me
4.20

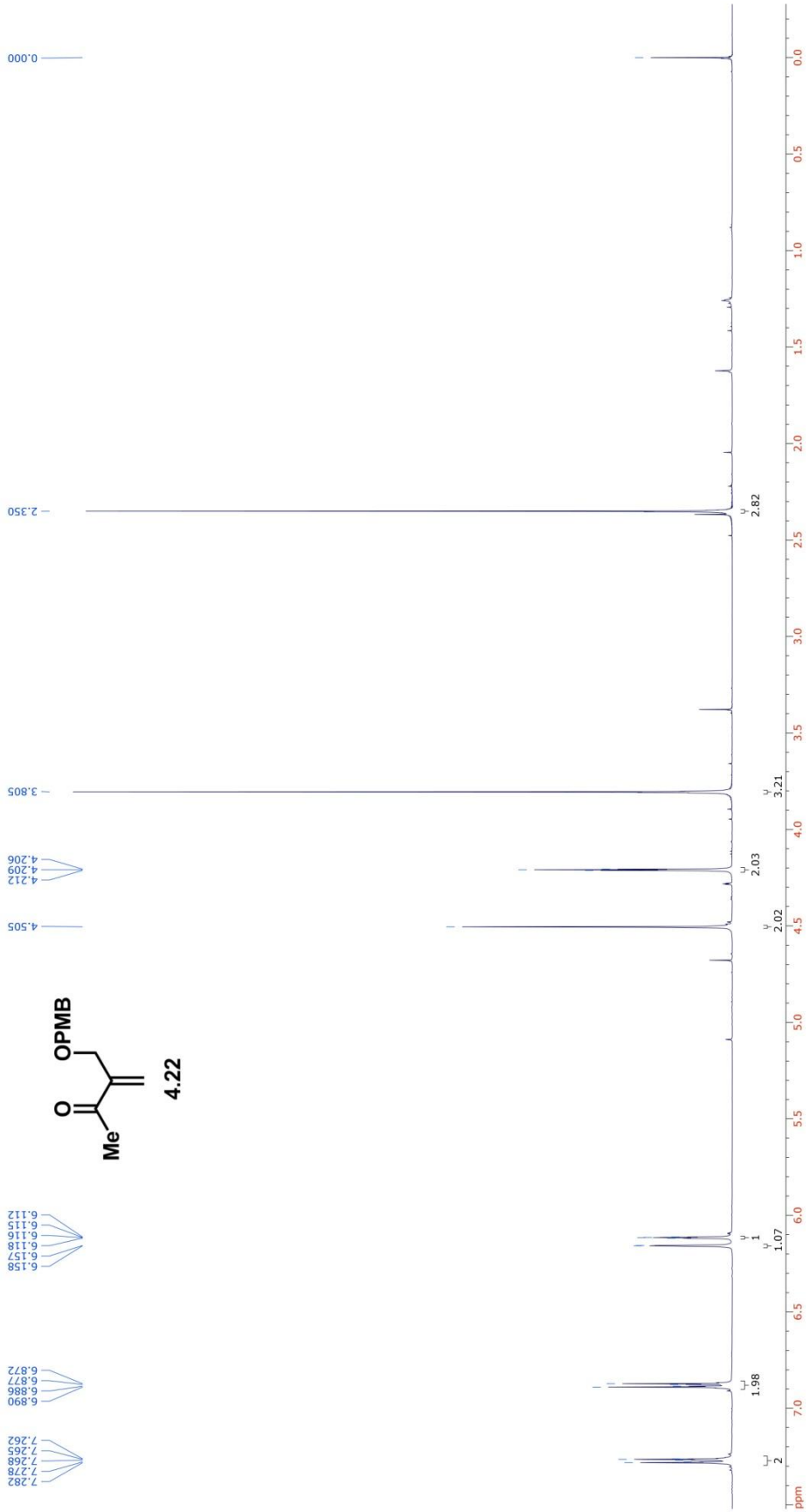
OPMB
O
Me
4.22

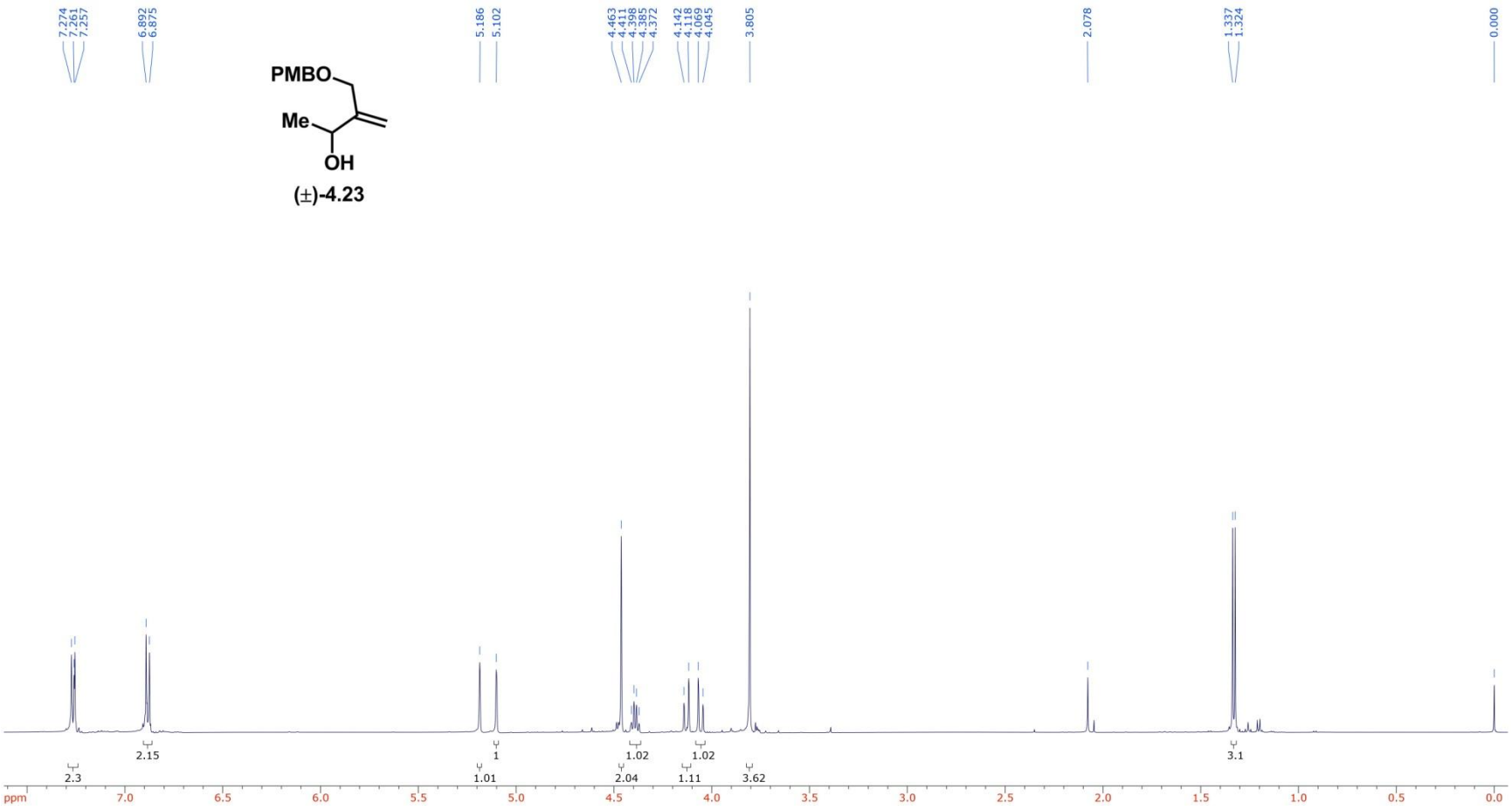
7.274
7.261
7.257
6.892
6.875
5.186
5.102
4.463
4.411
4.398
4.385
4.372
4.142
4.118
4.069
4.045
3.805
2.078
1.337
1.324
0.000
PMBO
Me
OH
(±)-4.23
2.3
2.15
1
1.01
1.02
2.04
1.02
1.11
3.62
3.1
ppm
7.0
6.5
6.0
5.5
5.0
4.5
4.0
3.5
3.0
2.5
2.0
1.5
1.0
0.5
0.0

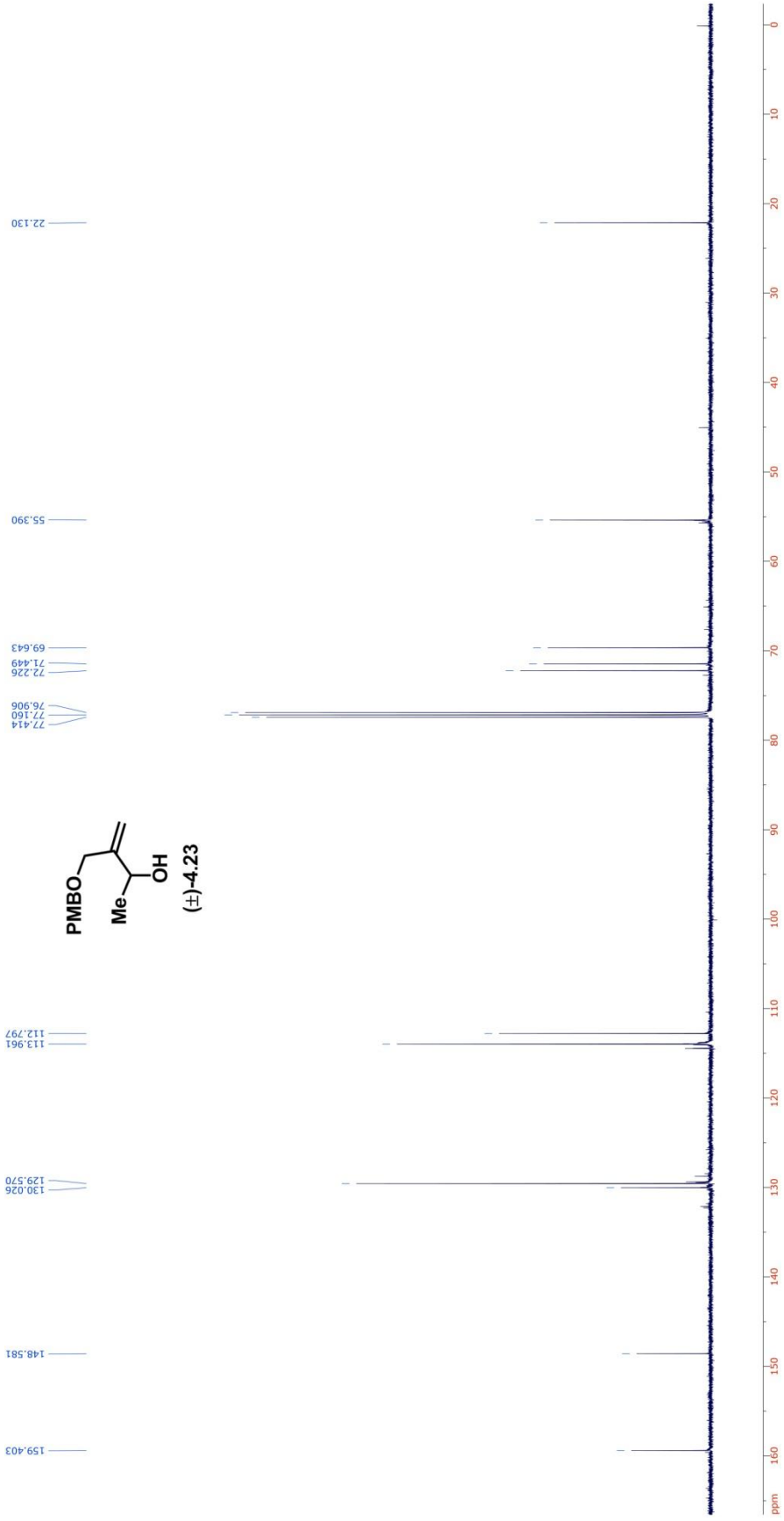
159.403
148.581
129.570
130.026
112.797
113.961
77.414
77.160
76.906
72.226
71.449
69.643
55.390
22.130
PMBO
Me
OH
(±)-4.23
ppm

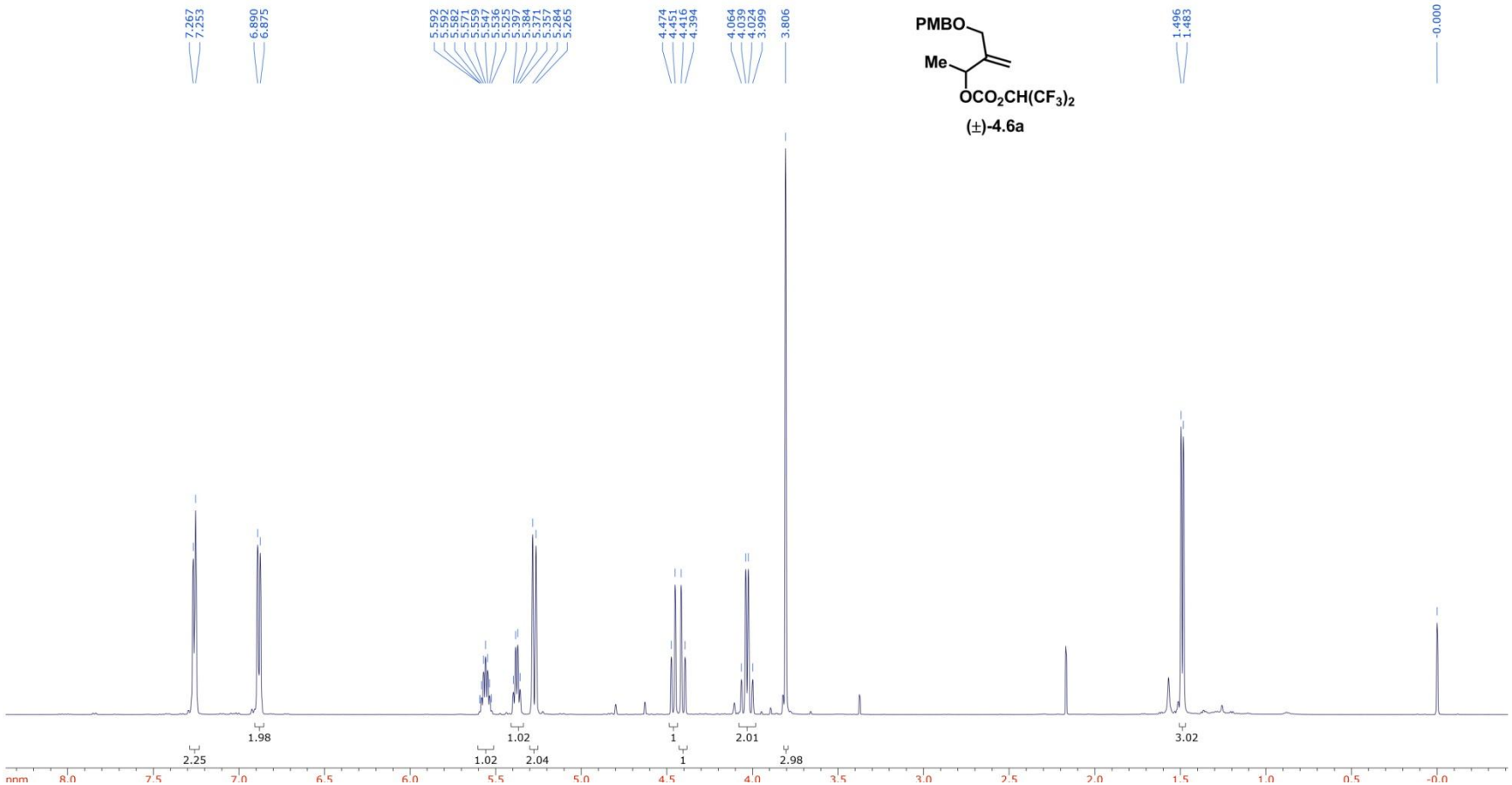
7.267
7.253
6.890
6.875
5.592
5.592
5.582
5.571
5.559
5.547
5.536
5.525
5.397
5.384
5.371
5.357
5.344
5.265
4.474
4.451
4.416
4.394
4.064
4.039
4.024
3.999
3.806
PMBO
Me
OCO2CH(CF3)2
(±)-4.6a
1.496
1.483
-0.000
1.98
1.02
1
2.01
3.02
2.25
1.02
2.04
1
2.98
ppm

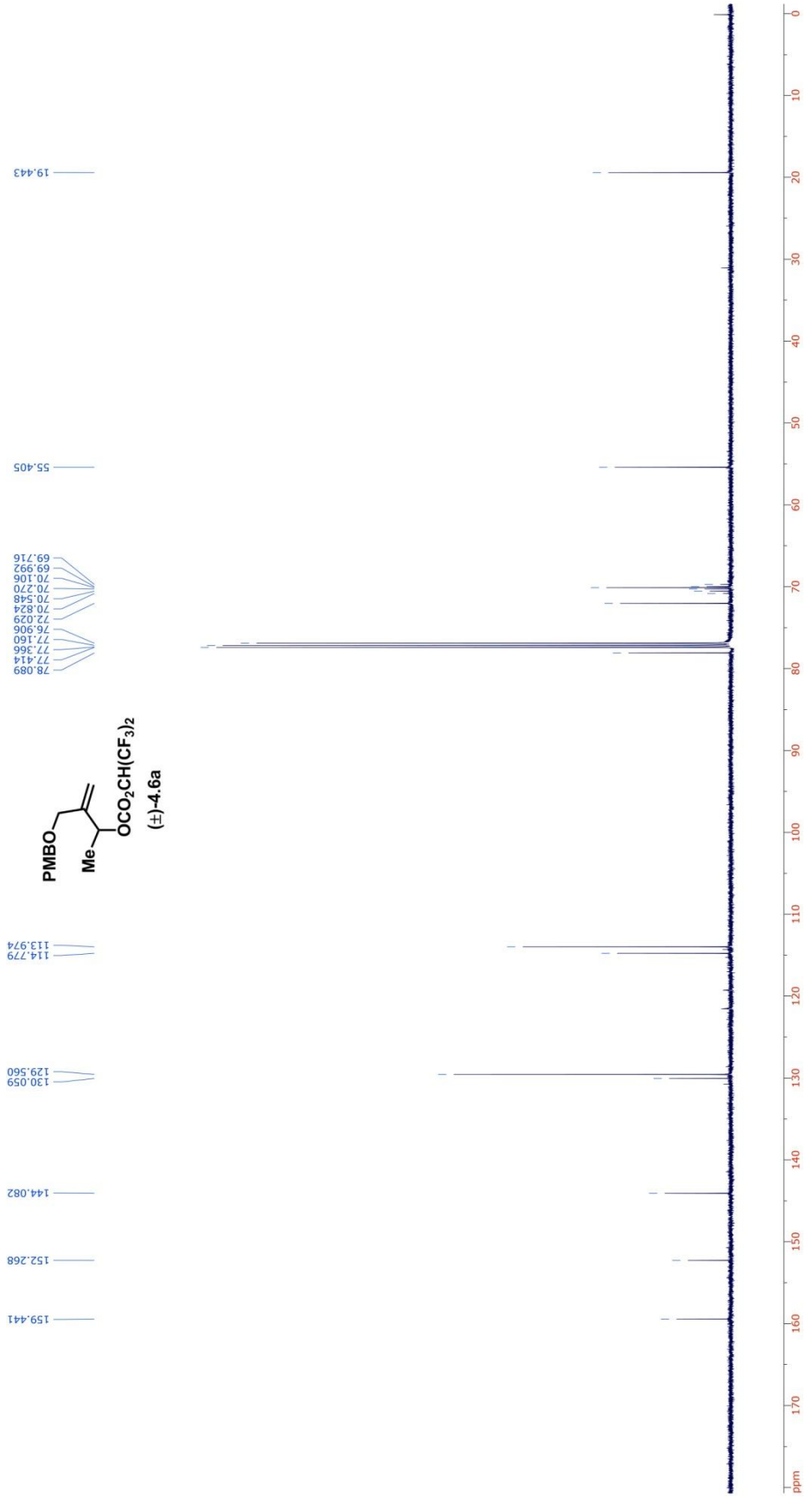
19.443
55.405
69.716
69.992
70.106
70.270
70.548
70.824
72.029
76.906
77.160
77.366
77.414
78.089
113.974
114.779
129.560
130.059
144.082
152.268
159.441
PMBO
Me
OCO2CH(CF3)2
(±)-4.6a
ppm

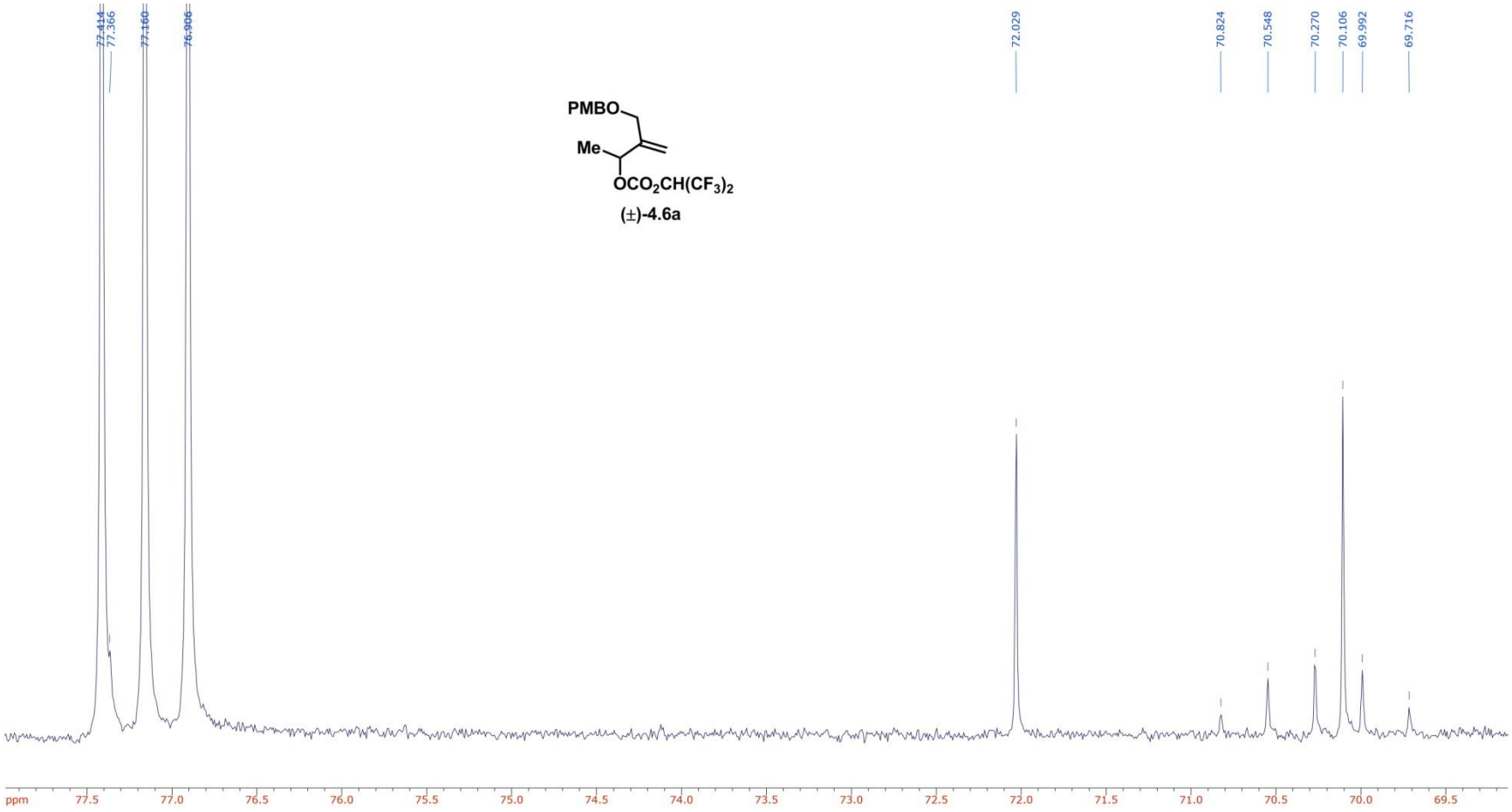
77.414
77.366
77.160
76.906
72.029
70.824
70.548
70.270
70.106
69.992
69.716
PMBO
Me
OCO2CH(CF3)2
(±)-4.6a
ppm
77.5
77.0
76.5
76.0
75.5
75.0
74.5
74.0
73.5
73.0
72.5
72.0
71.5
71.0
70.5
70.0
69.5


7.331
7.315
7.301
7.254
7.239
7.236
7.223
5.967
5.955
5.946
5.933
5.921
5.911
5.900
5.268
5.265
5.262
5.231
5.228
5.144
5.142
5.139
5.138
5.123
5.121
5.118
5.117
4.354
4.345
2.896
2.886
2.869
2.859
2.791
2.790
2.783
2.767
1.689
0.000

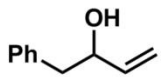
OH
Ph

(±)-4.25

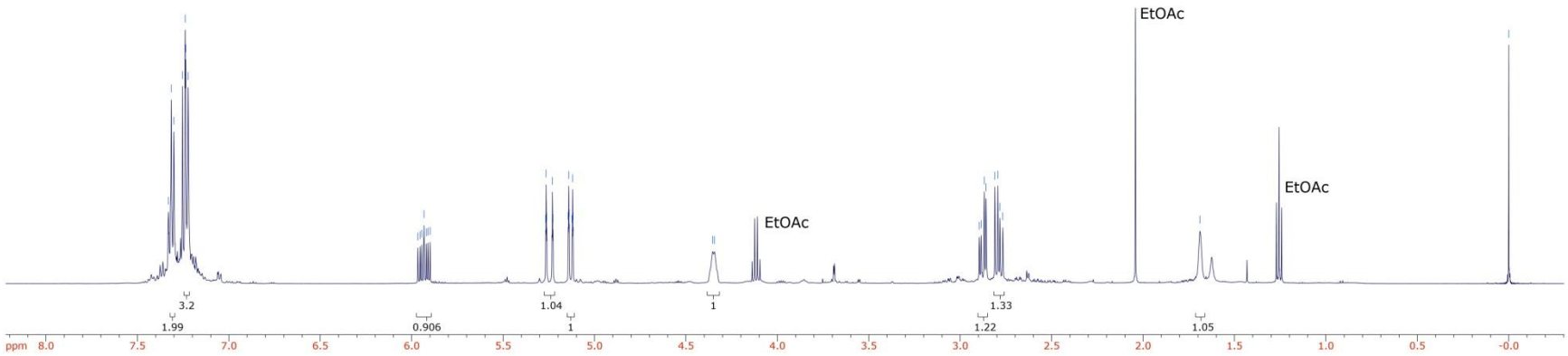
EtOAc
EtOAc
EtOAc
3.2
1.99
0.906
1.04
1
1
1.33
1.22
1.05
ppm 8.0
7.5
7.0
6.5
6.0
5.5
5.0
4.5
4.0
3.5
3.0
2.5
2.0
1.5
1.0
0.5
-0.0

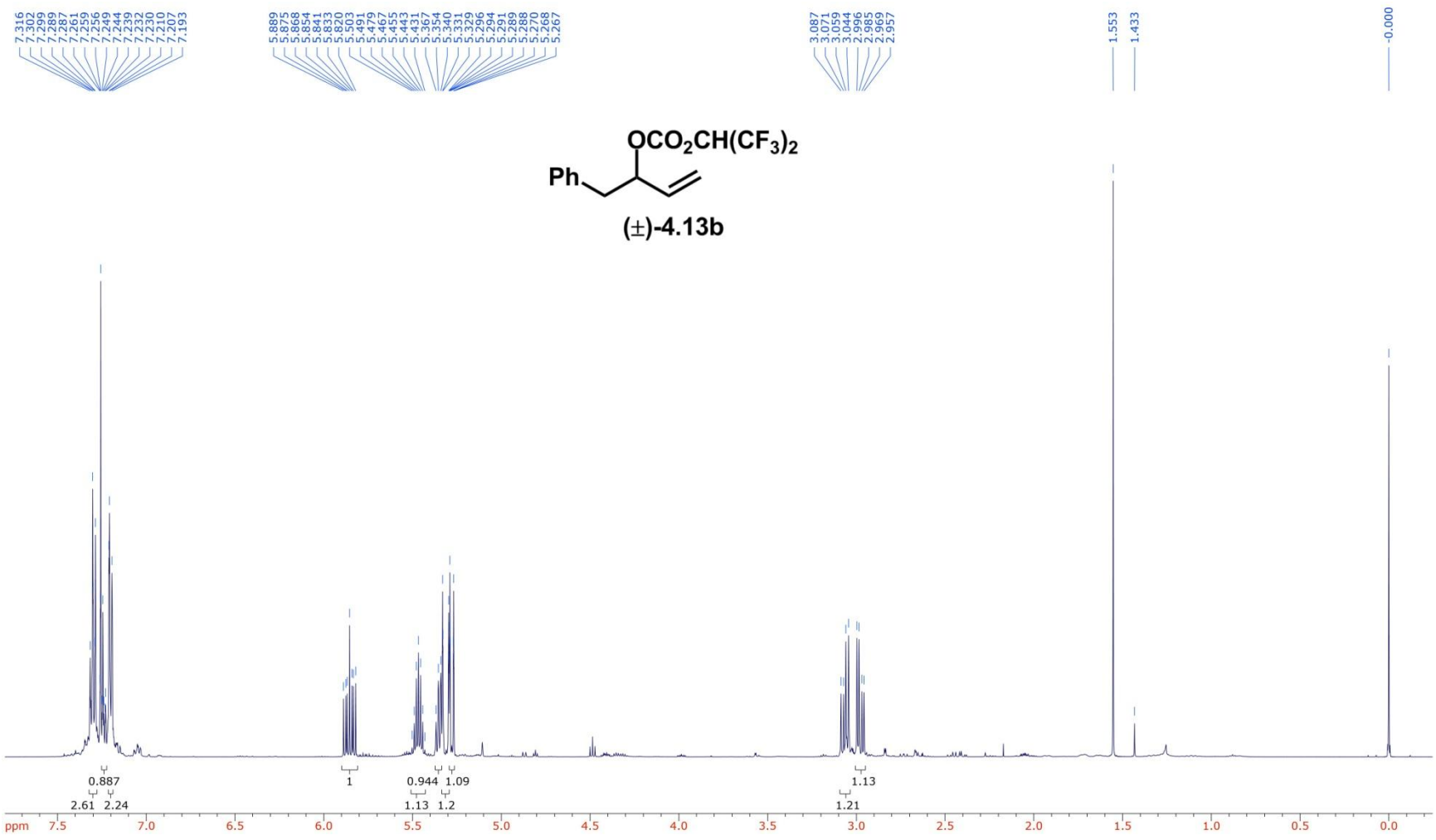
7.316
7.302
7.292
7.289
7.287
7.261
7.259
7.256
7.249
7.244
7.239
7.232
7.230
7.210
7.207
7.193
5.889
5.875
5.868
5.854
5.841
5.833
5.820
5.503
5.491
5.479
5.467
5.455
5.443
5.431
5.417
5.354
5.340
5.331
5.329
5.296
5.294
5.291
5.289
5.288
5.270
5.268
5.267
3.087
3.071
3.059
3.044
2.996
2.985
2.969
2.957
1.553
1.433
-0.000
OCO2CH(CF3)2
Ph
(±)-4.13b
0.887
2.61
2.24
1
0.944
1.13
1.09
1.2
1.13
1.21
ppm
7.5
7.0
6.5
6.0
5.5
5.0
4.5
4.0
3.5
3.0
2.5
2.0
1.5
1.0
0.5
0.0

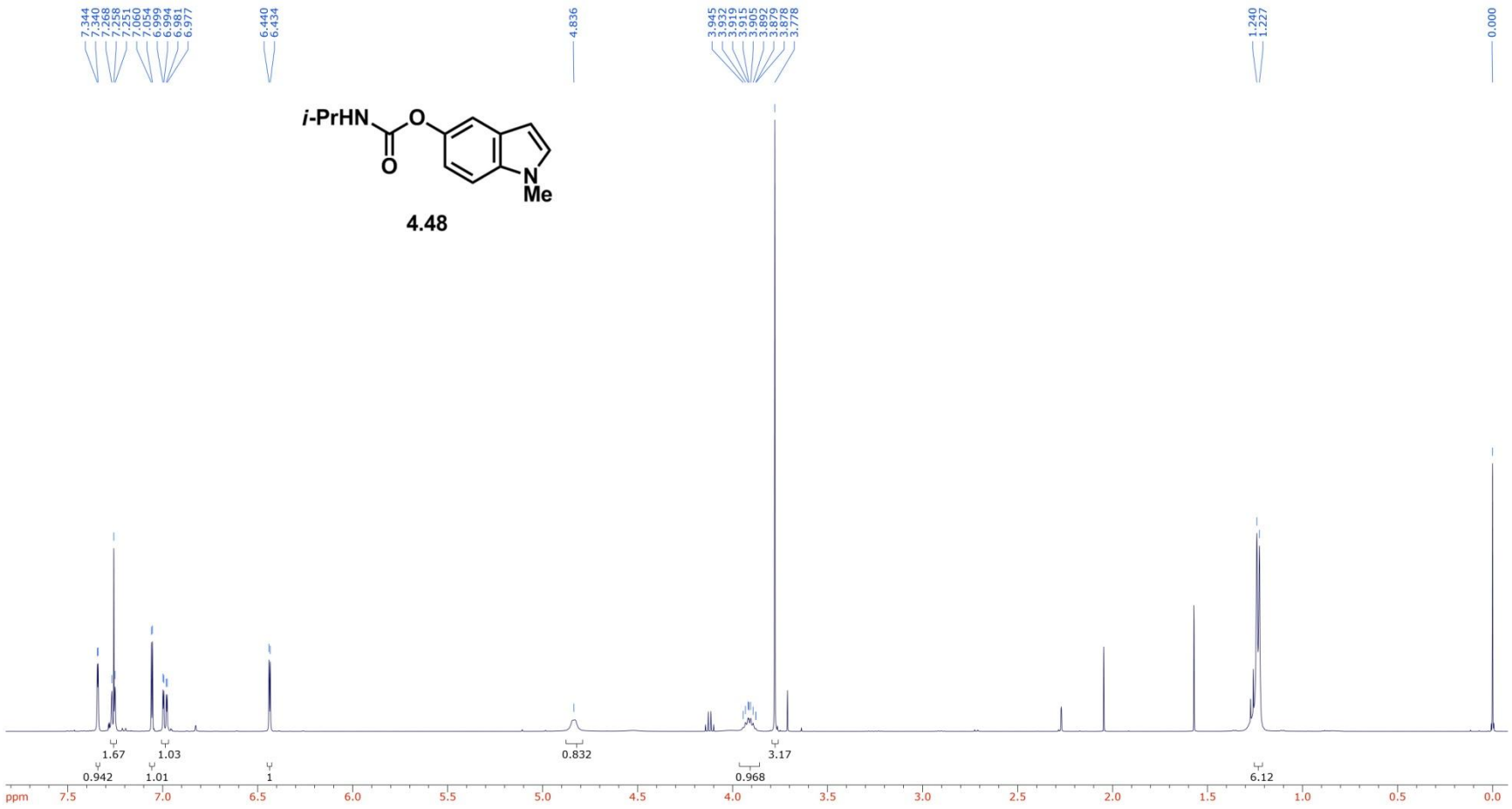
7.344
7.340
7.268
7.258
7.251
7.060
7.054
6.999
6.994
6.981
6.977
6.440
6.434
4.836
3.945
3.932
3.919
3.915
3.905
3.892
3.879
3.878
3.778
1.240
1.227
0.000
i-PrHN
O
O
N
Me
4.48
1.67
1.03
0.832
3.17
0.942
1.01
1
0.968
6.12
ppm
7.5
7.0
6.5
6.0
5.5
5.0
4.5
4.0
3.5
3.0
2.5
2.0
1.5
1.0
0.5
0.0

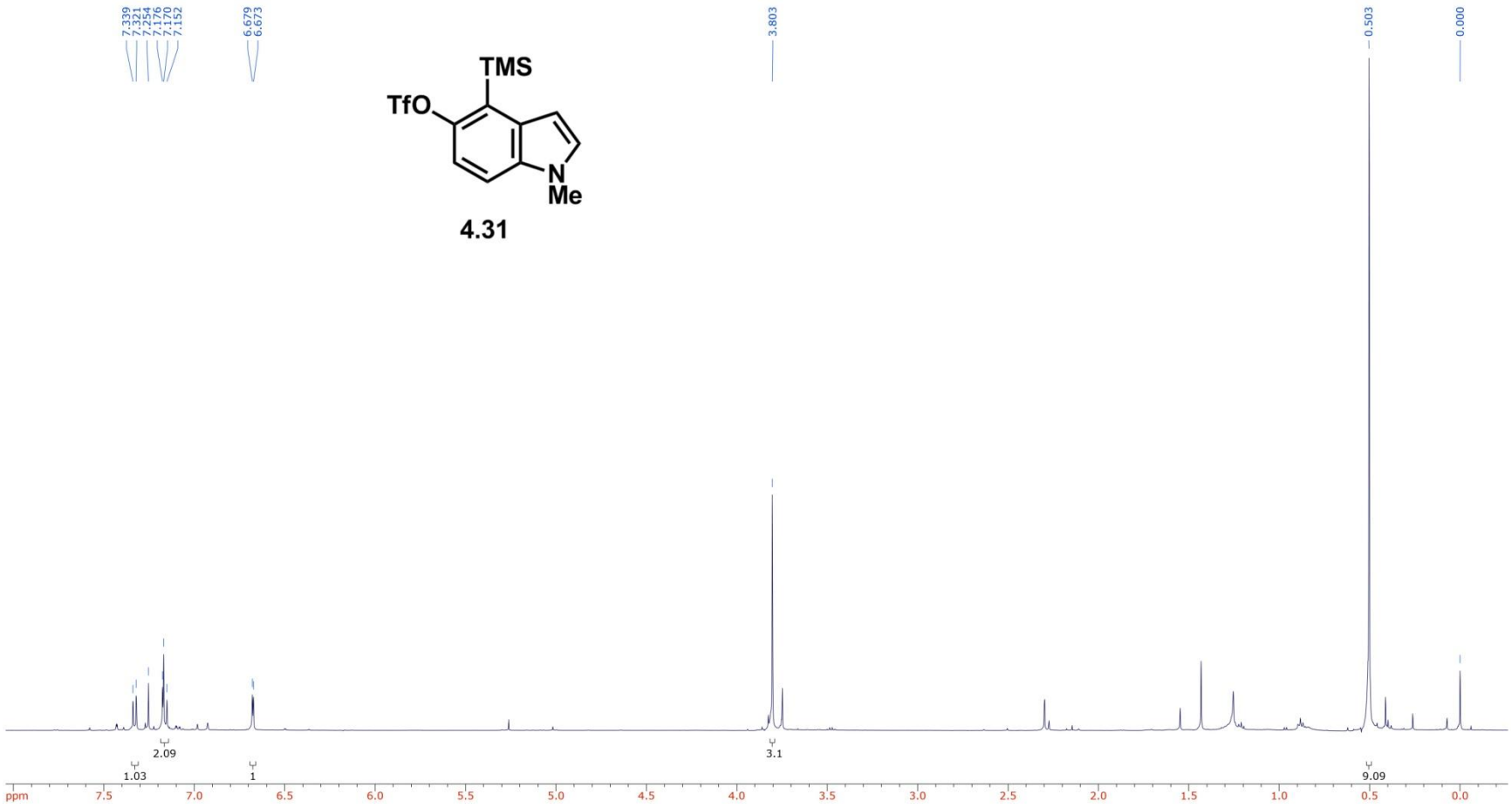
7.339
7.321
7.254
7.176
7.170
7.152
6.679
6.673
3.803
0.503
0.000
TMS
TfO
N
Me
4.31
2.09
1.03
1
3.1
9.09
ppm
7.5
7.0
6.5
6.0
5.5
5.0
4.5
4.0
3.5
3.0
2.5
2.0
1.5
1.0
0.5
0.0

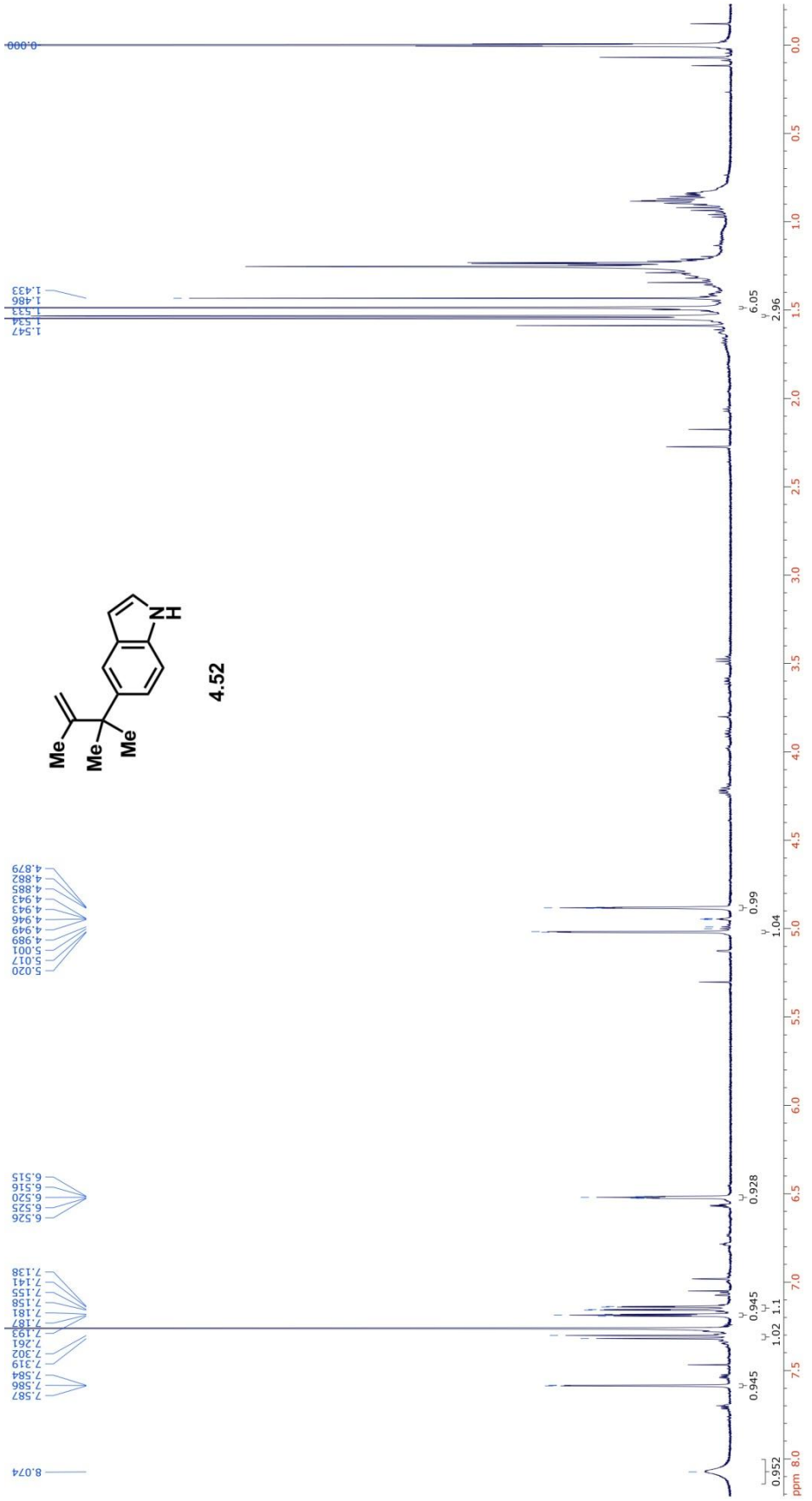
8.074
7.587
7.586
7.584
7.319
7.302
7.261
7.193
7.187
7.181
7.158
7.155
7.141
7.138
6.526
6.525
6.520
6.516
6.515
5.020
5.017
5.001
4.989
4.949
4.946
4.943
4.943
4.885
4.882
4.879
1.547
1.534
1.533
1.486
1.433
0.000
0.952
0.945
1.02
0.945
1.1
0.928
0.99
1.04
6.05
2.96
ppm 8.0
7.5
7.0
6.5
6.0
5.5
5.0
4.5
4.0
3.5
3.0
2.5
2.0
1.5
1.0
0.5
0.0
Me
Me
Me
H
N

4.52

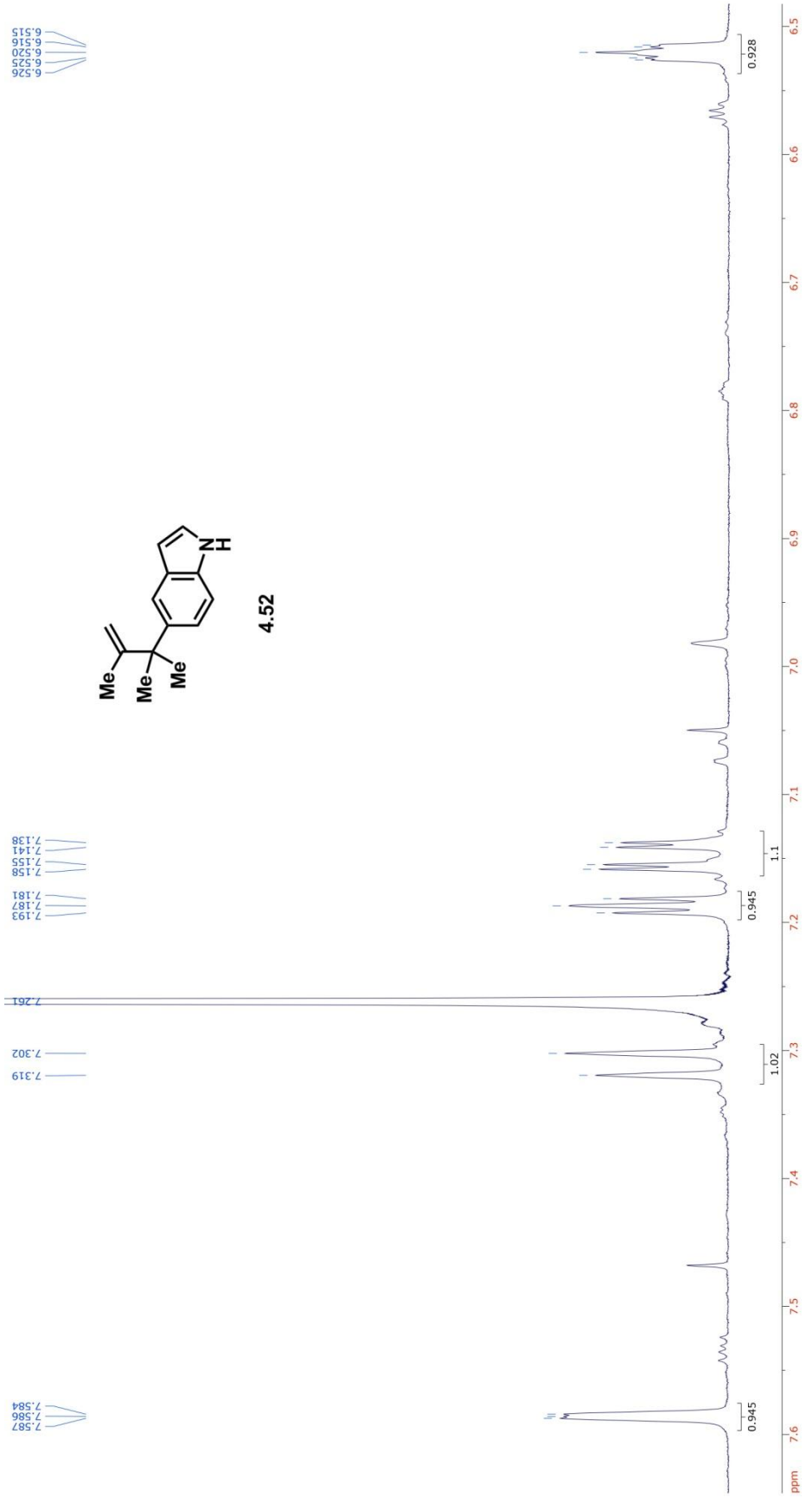
6.526
6.525
6.520
6.516
6.515
7.587
7.586
7.584
7.261
7.193
7.187
7.181
7.158
7.155
7.141
7.138
7.319
7.302
0.928
1.1
0.945
1.02
0.945
6.5
6.6
6.7
6.8
6.9
7.0
7.1
7.2
7.3
7.4
7.5
7.6
ppm
Me
Me
Me
N
H
4.52

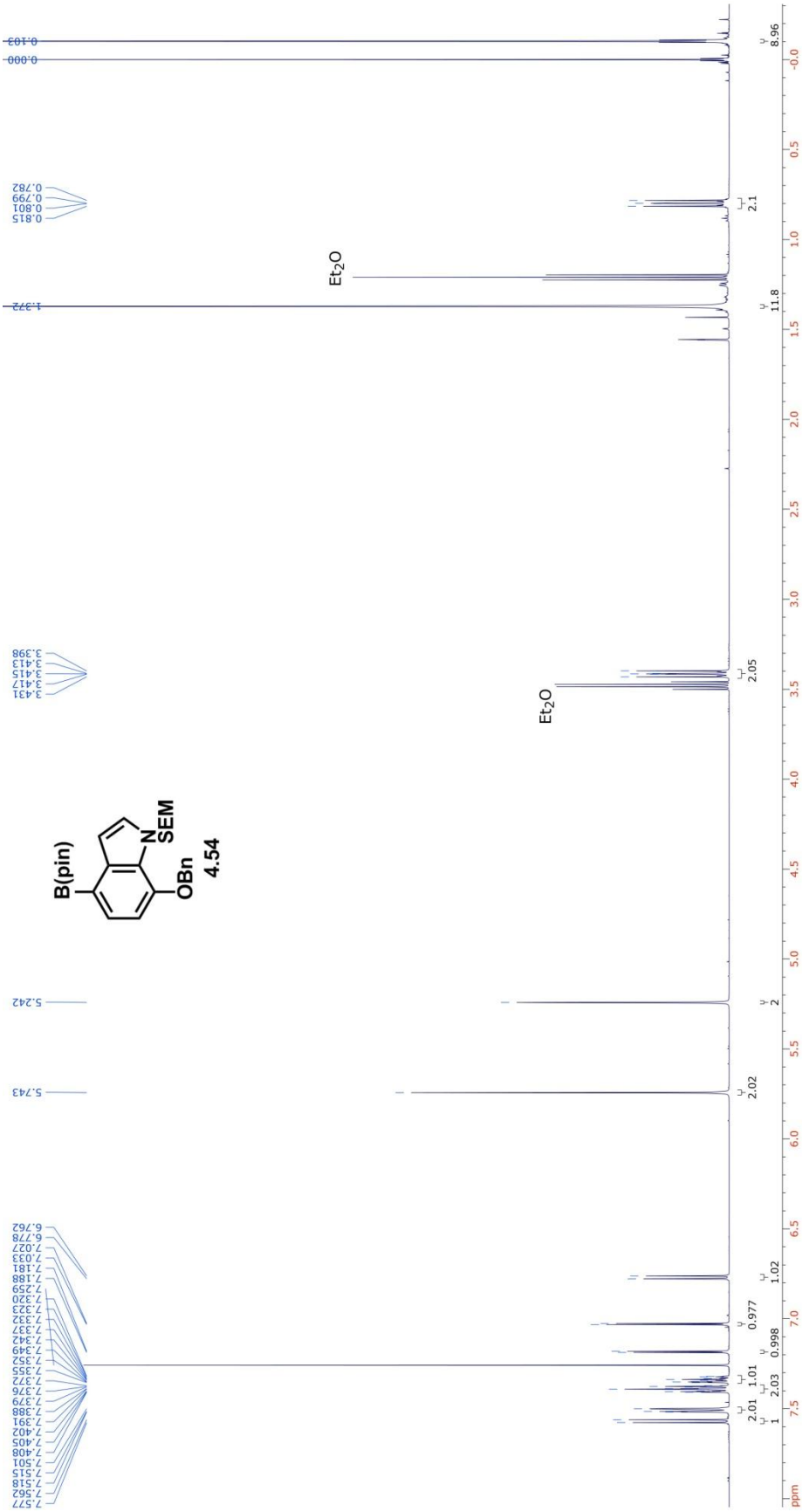
B(pin)
N
SEM
OBn
4.54
Et2O
Et2O

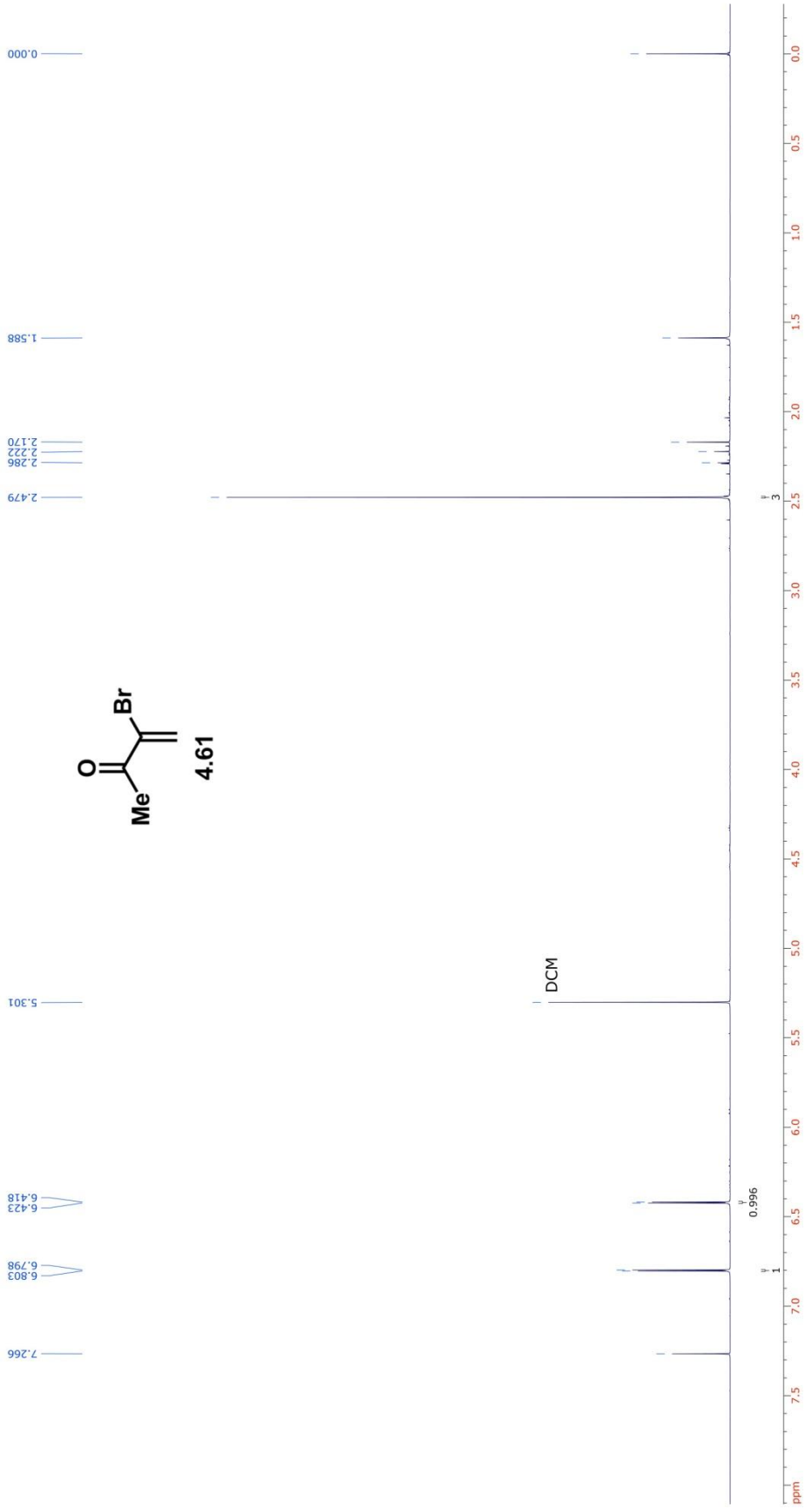
0.000
1.588
2.170
2.222
2.286
2.479
5.301
6.418
6.423
6.798
6.803
7.266
DCM
Br
O
Me
4.61
ppm

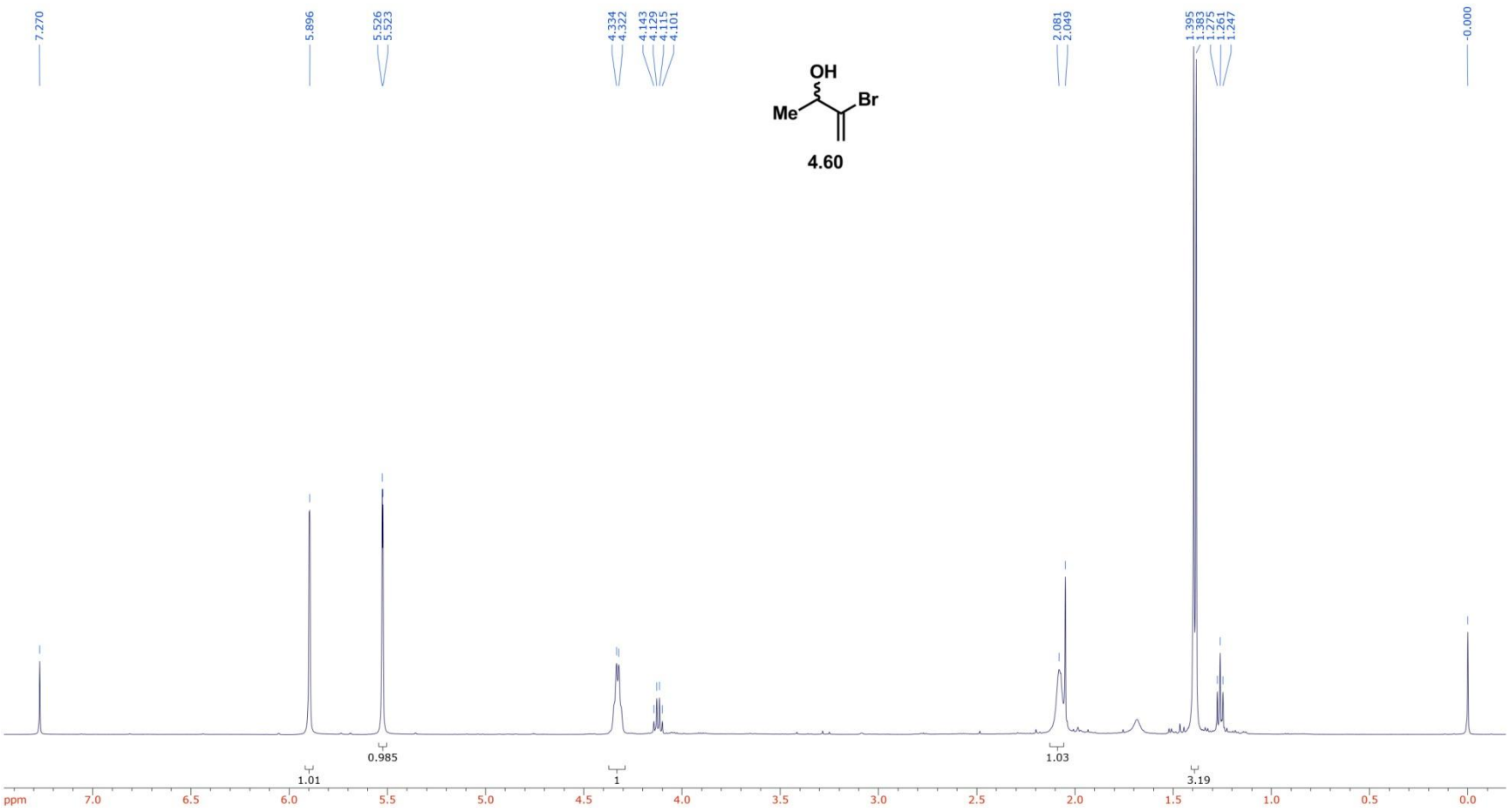
7.270
5.896
5.526
5.523
4.334
4.322
4.143
4.129
4.115
4.101
2.081
2.049
1.395
1.383
1.275
1.261
1.247
-0.000
OH
Me
Br
4.60
1.01
0.985
1
1.03
3.19
ppm
7.0
6.5
6.0
5.5
5.0
4.5
4.0
3.5
3.0
2.5
2.0
1.5
1.0
0.5
0.0

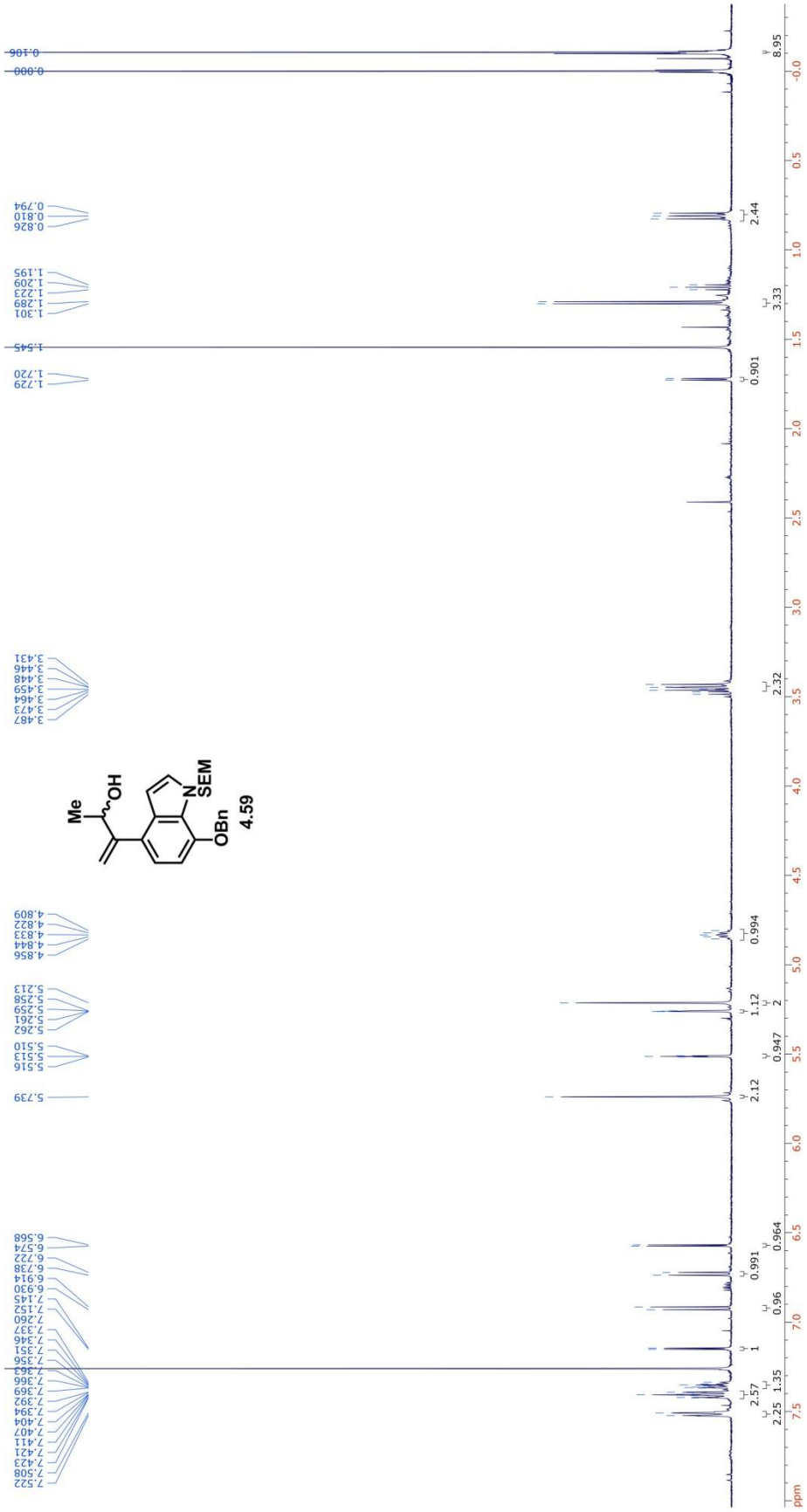
Me
OH
N
SEM
OBn
4.59

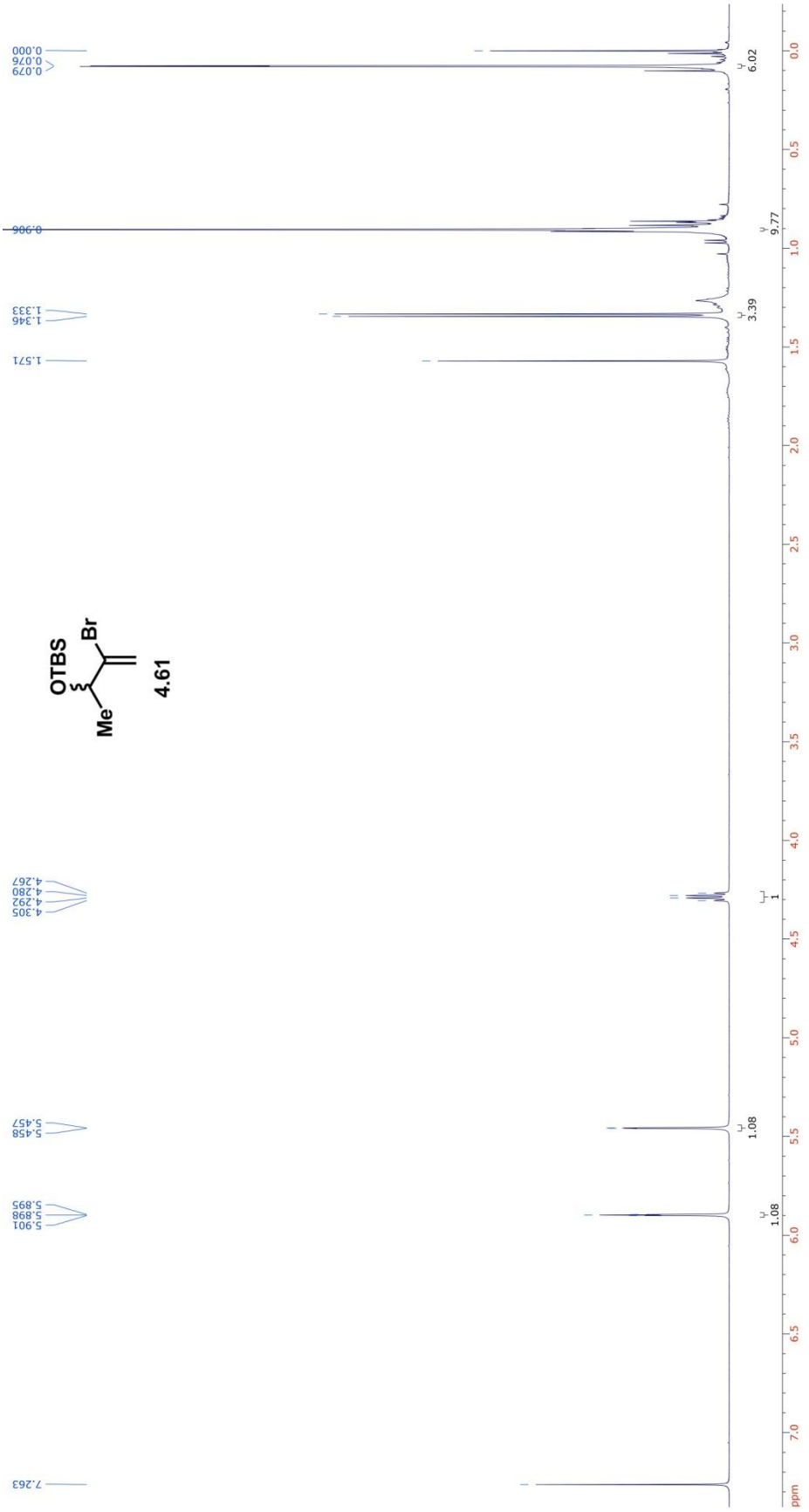
OTBS
Br
Me
4.61
0.000
0.076
0.079
0.906
1.333
1.346
1.571
4.267
4.280
4.292
4.305
5.457
5.458
5.895
5.898
5.901
7.263
6.02
9.77
3.39
1
1.08
1.08
ppm

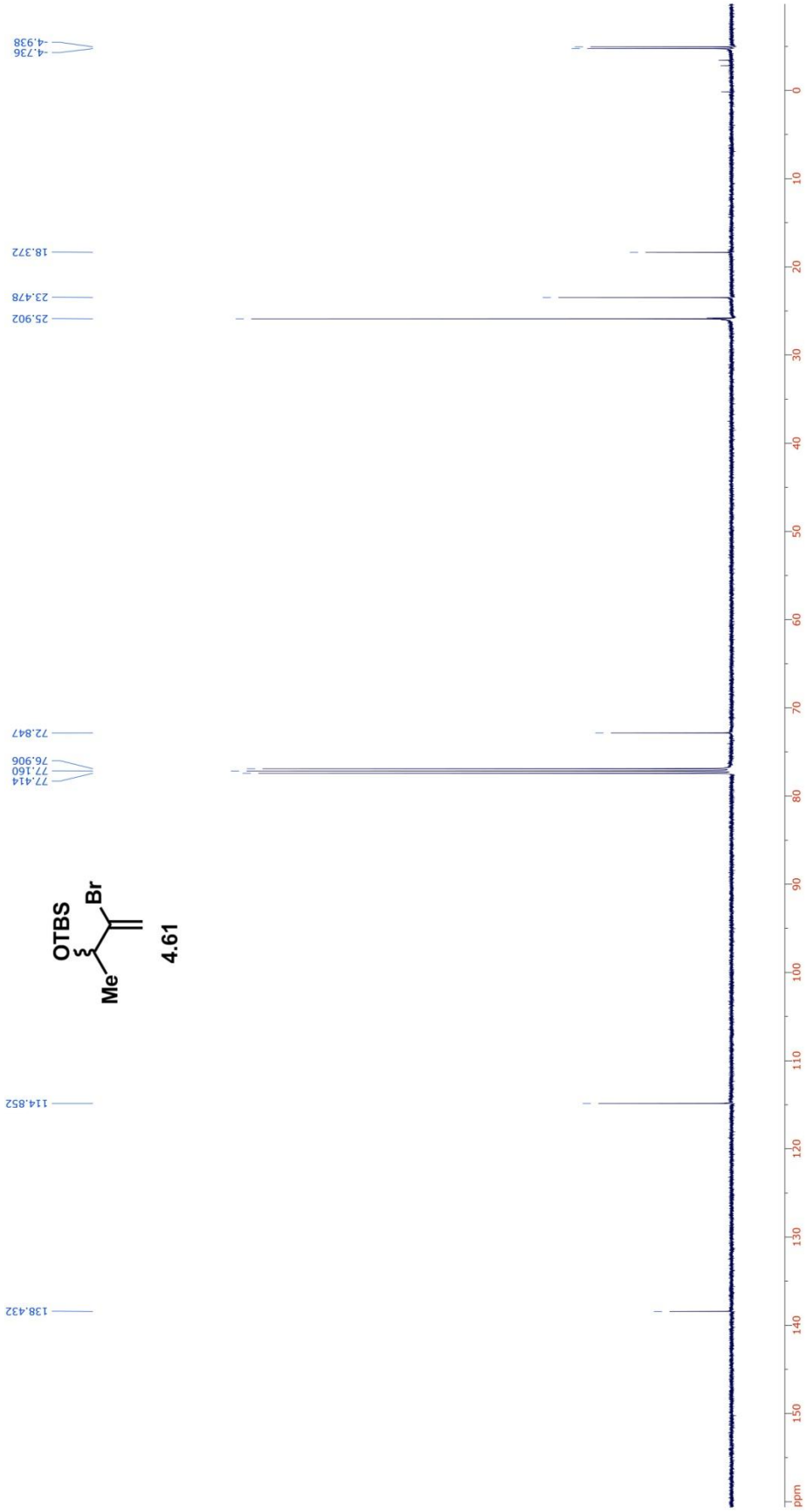
-4.736
-4.938
18.372
23.478
25.902
72.847
77.414
77.160
76.906
114.852
138.432
OTBS
Br
Me
4.61
ppm

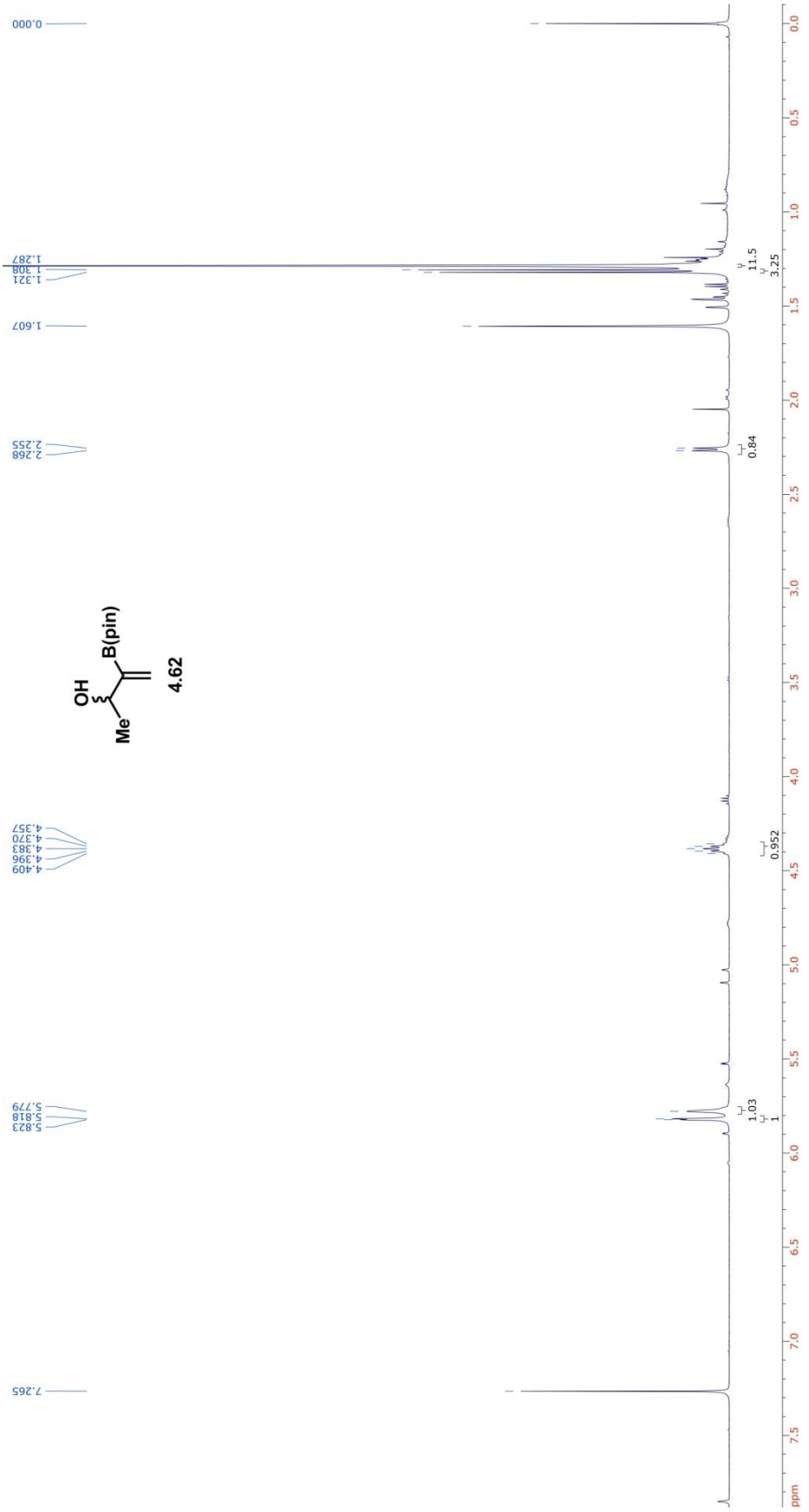
0.000
1.287
1.308
1.321
1.607
2.255
2.268
4.357
4.370
4.383
4.396
4.409
5.779
5.818
5.823
7.265
B(pin)
OH
Me
4.62
11.5
3.25
0.84
0.952
1.03
1
ppm

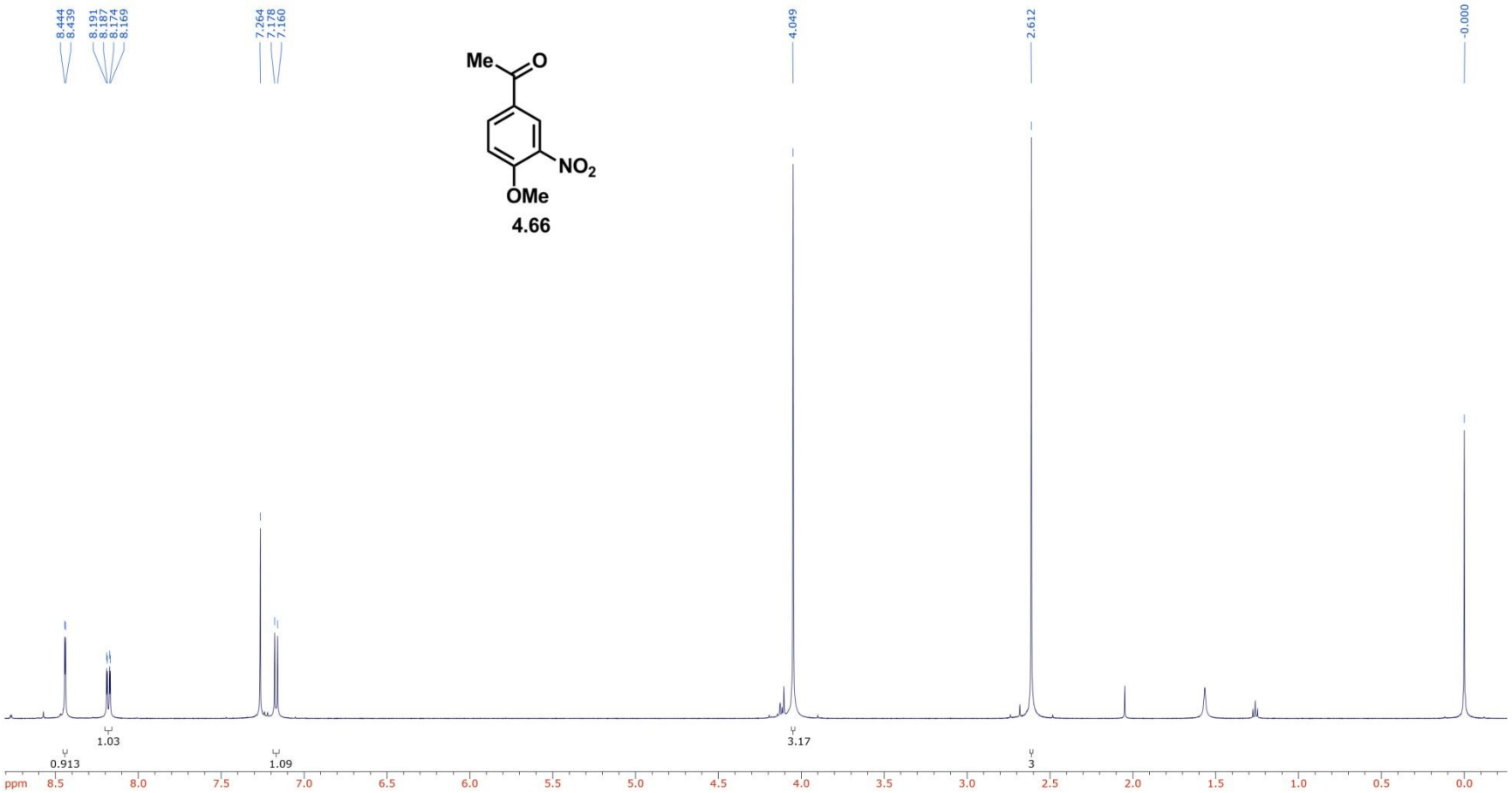
8.444
8.439
8.191
8.187
8.174
8.169
7.264
7.178
7.160
4.049
2.612
-0.000
Me
O
NO2
OMe
4.66
1.03
0.913
1.09
3.17
3
ppm
8.5
8.0
7.5
7.0
6.5
6.0
5.5
5.0
4.5
4.0
3.5
3.0
2.5
2.0
1.5
1.0
0.5
0.0

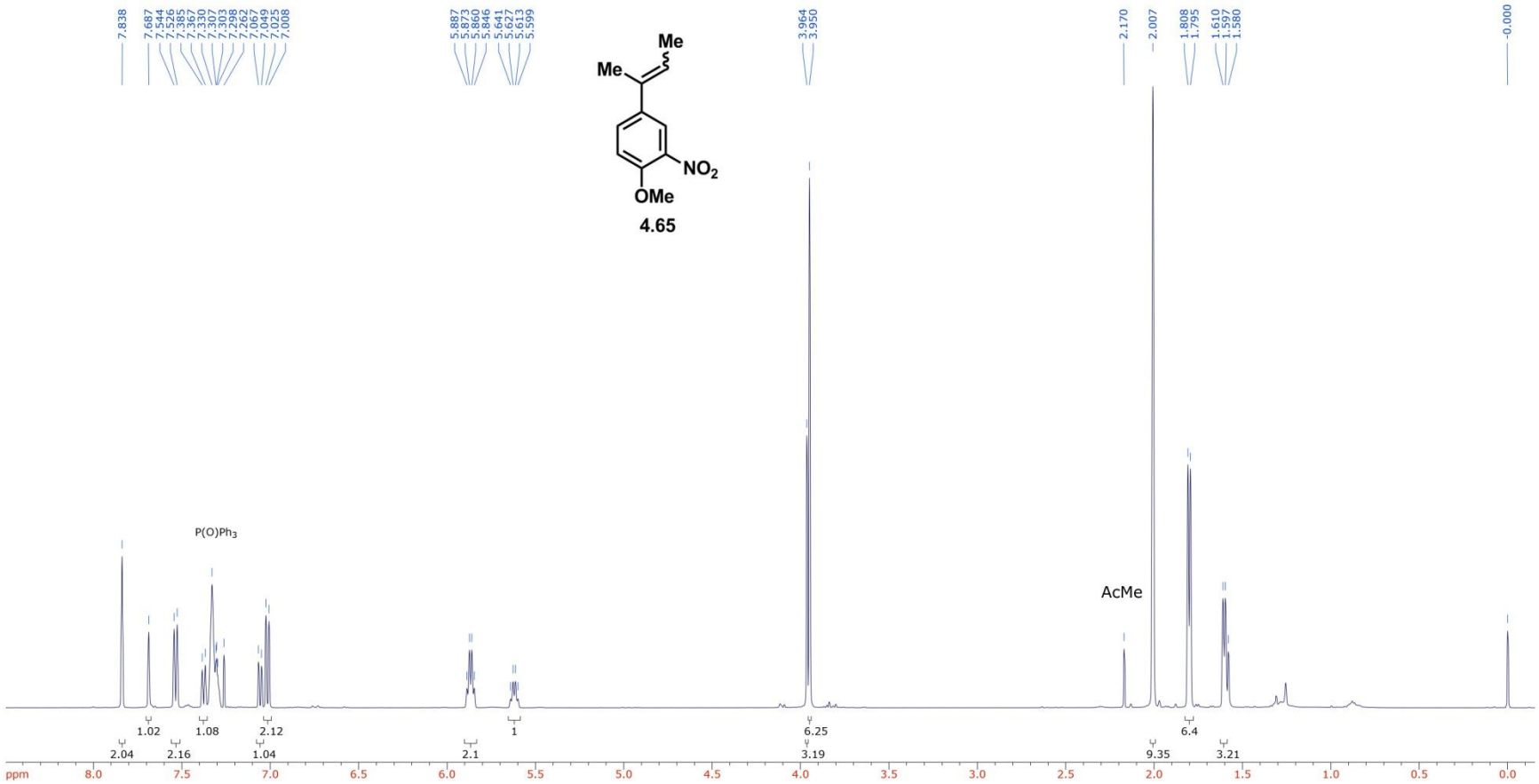
7.838
7.687
7.544
7.536
7.385
7.367
7.330
7.307
7.303
7.288
7.282
7.067
7.049
7.025
7.008
5.887
5.873
5.860
5.846
5.641
5.627
5.613
5.599
3.964
3.950
2.170
2.007
1.808
1.795
1.610
1.597
1.580
-0.000
Me
Me
NO2
OMe
4.65
P(O)Ph3
AcMe
1.02
1.08
2.12
1
6.25
6.4
2.04
2.16
1.04
2.1
3.19
9.35
3.21
ppm
8.0
7.5
7.0
6.5
6.0
5.5
5.0
4.5
4.0
3.5
3.0
2.5
2.0
1.5
1.0
0.5
0.0

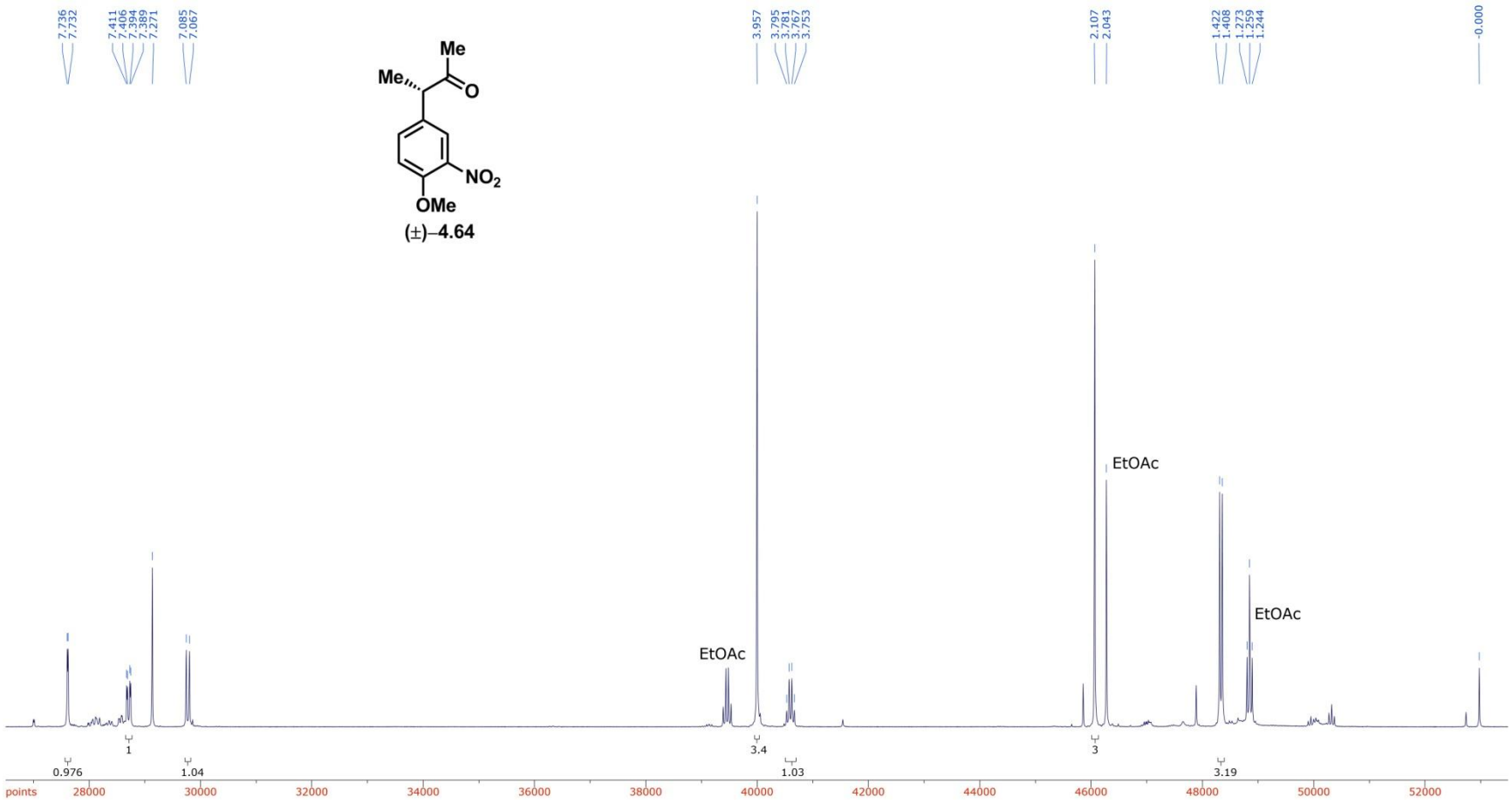
7.736
7.732
7.411
7.406
7.394
7.389
7.271
7.085
7.067
3.957
3.795
3.781
3.767
3.753
2.107
2.043
1.422
1.408
1.273
1.259
1.244
-0.000
Me
Me
O
NO2
OMe
(±)–4.64
EtOAc
EtOAc
EtOAc
1
0.976
1.04
3.4
1.03
3
3.19
points
28000
30000
32000
34000
36000
38000
40000
42000
44000
46000
48000
50000
52000

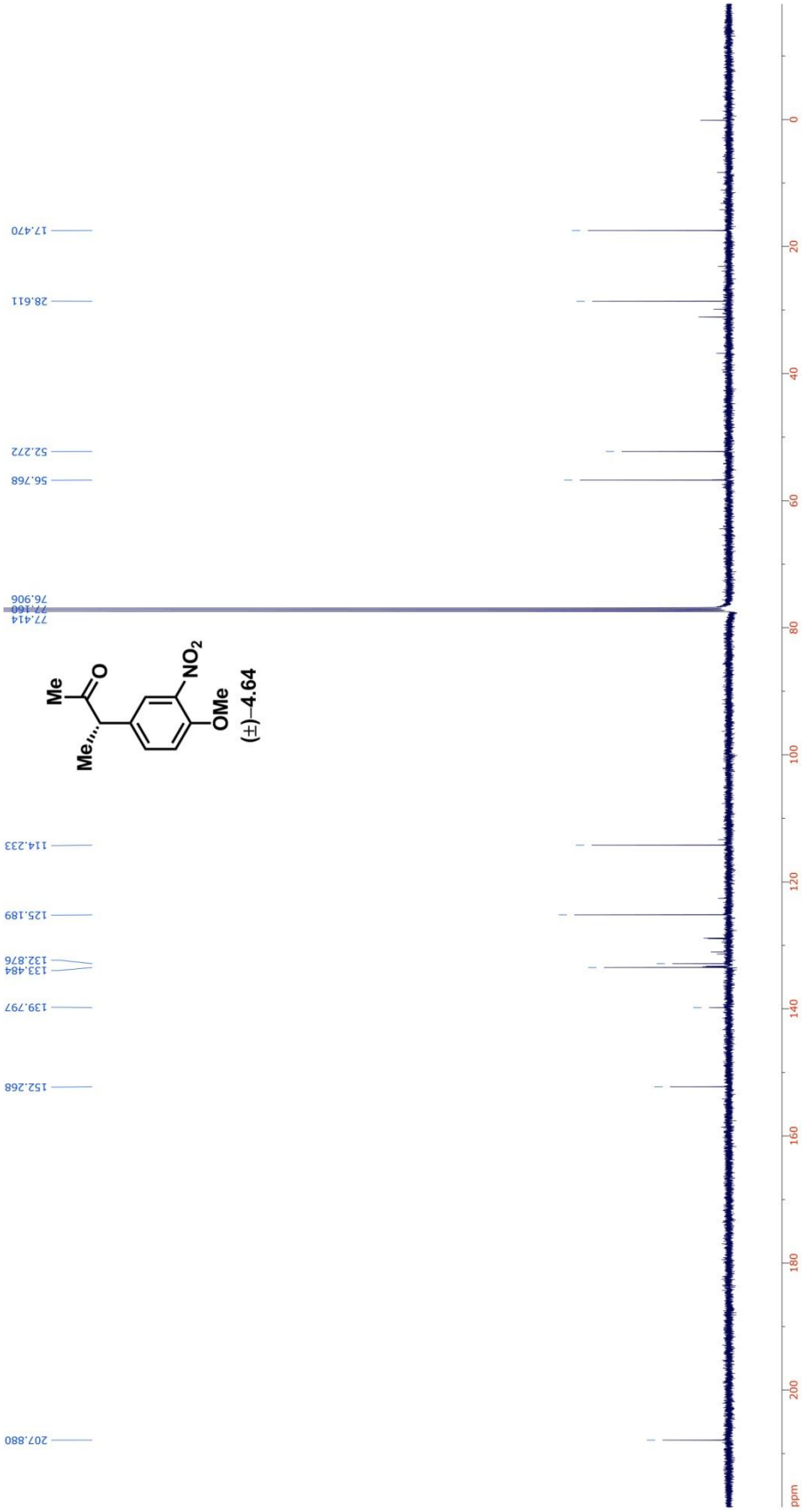
17.470
28.611
52.272
56.768
76.906
77.160
77.414
114.233
125.189
132.876
133.484
139.797
152.268
207.880
Me
O
NO2
OMe
Me
(±)-4.64
0
20
40
60
80
100
120
140
160
180
200
ppm

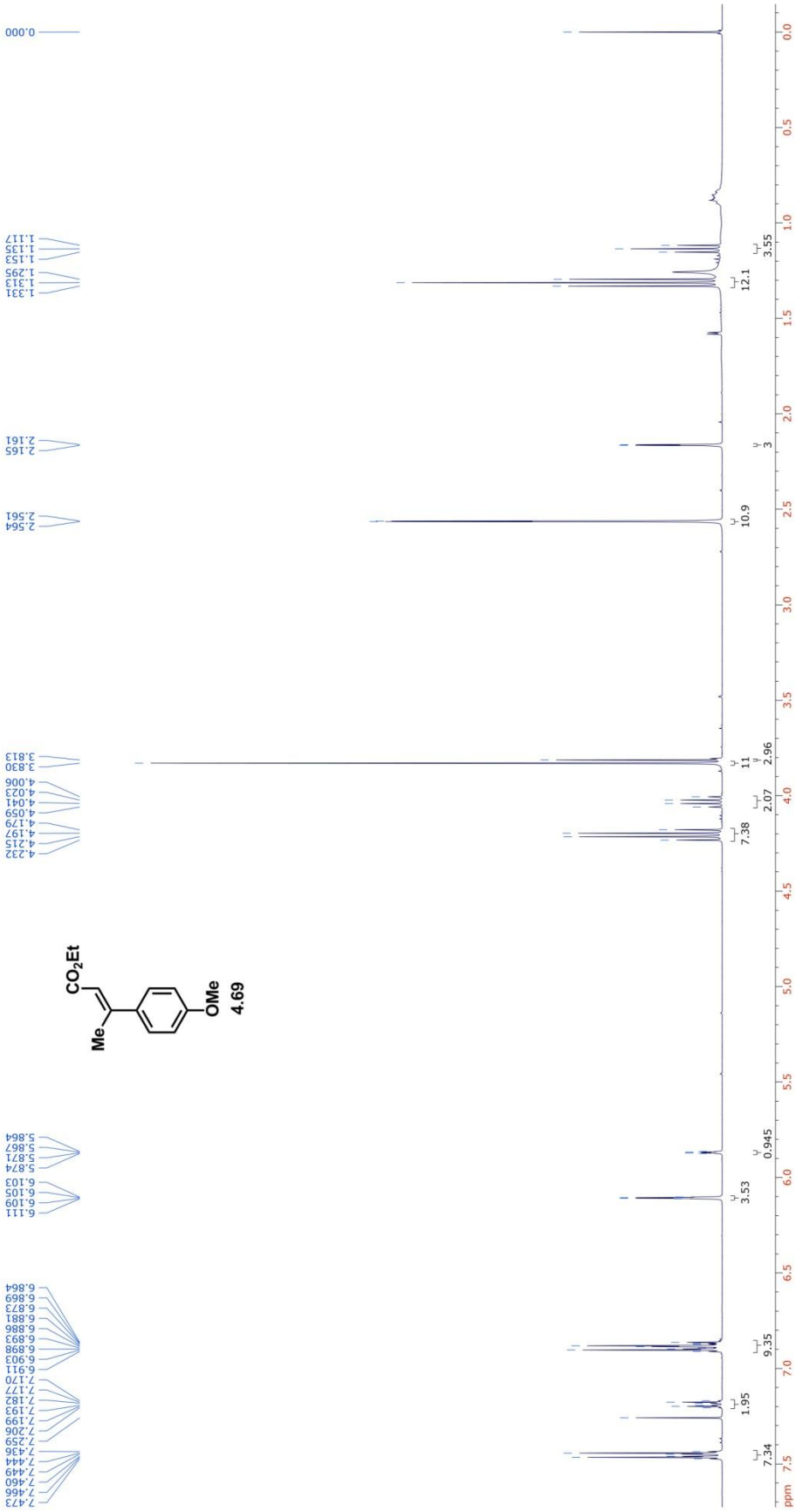
CO2Et
Me
OMe
4.69

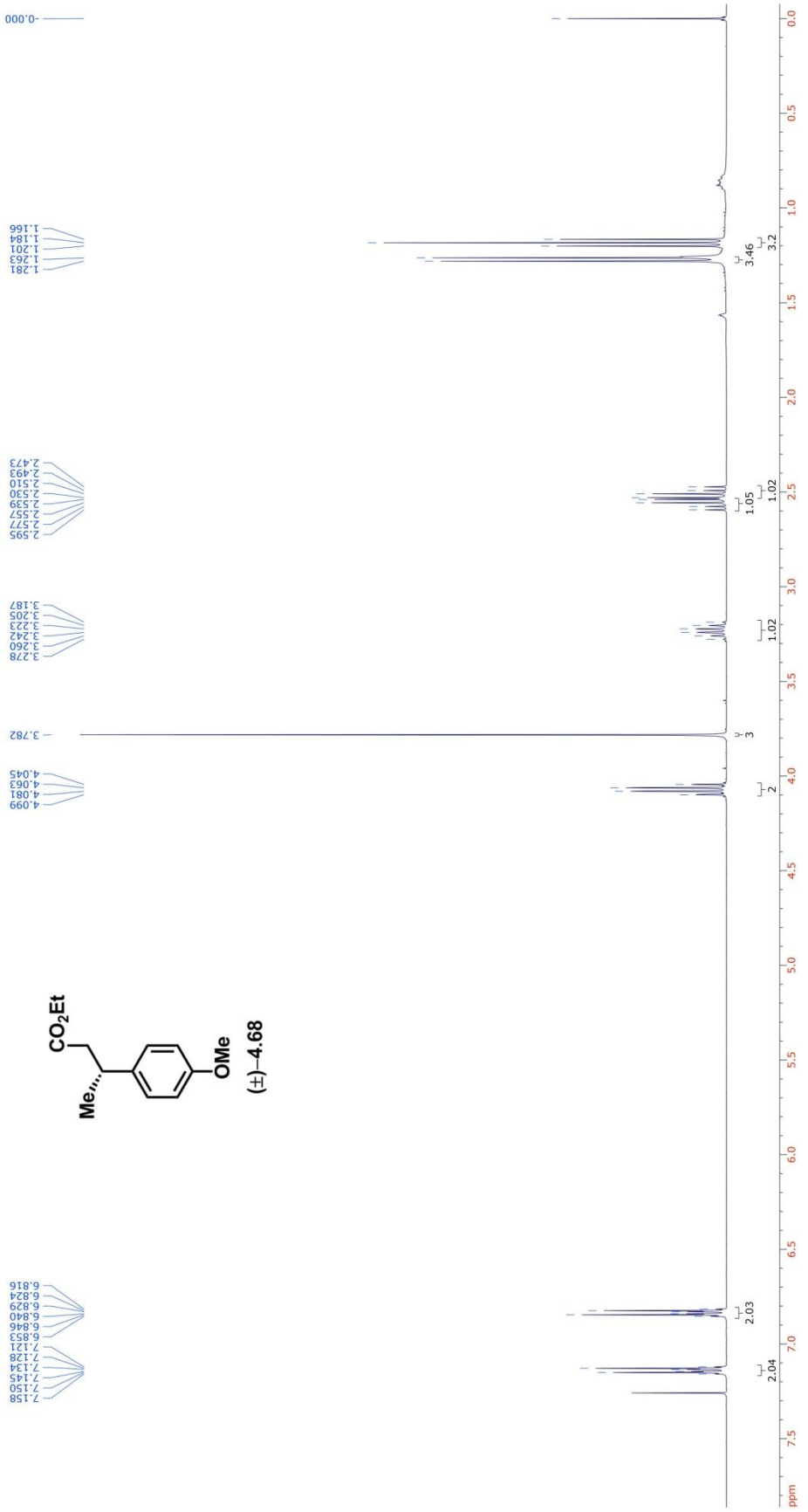
CO2Et
Me
OMe
(±)-4.68

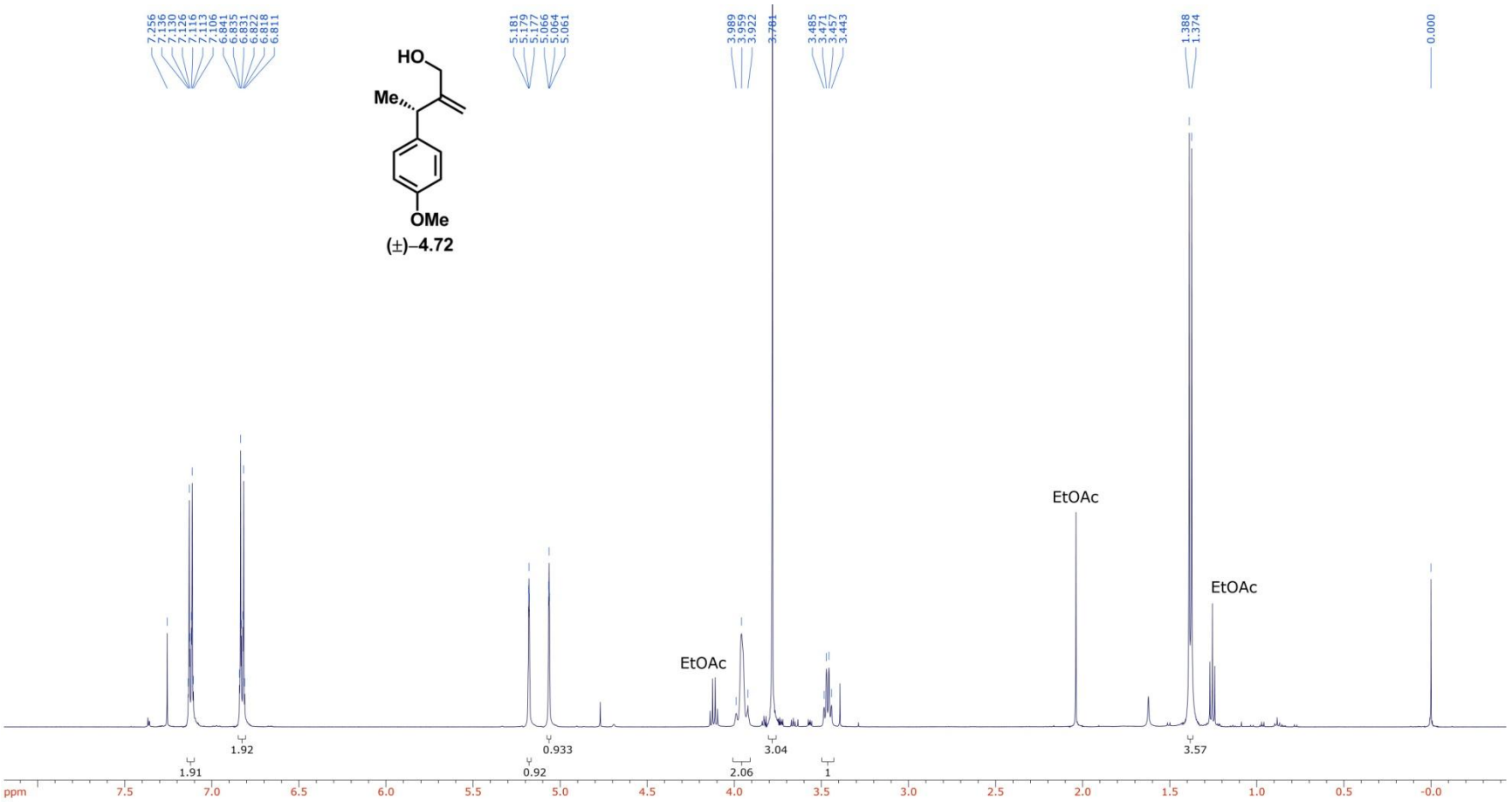
7.256
7.136
7.130
7.126
7.115
7.113
7.106
6.841
6.835
6.831
6.822
6.818
6.811
5.181
5.179
5.177
5.066
5.064
5.061
3.989
3.959
3.922
3.781
3.485
3.471
3.457
3.443
1.388
1.374
0.000
HO
Me
OMe
(±)–4.72
EtOAc
EtOAc
EtOAc
1.91
1.92
0.92
0.933
2.06
3.04
1
3.57
ppm
7.5
7.0
6.5
6.0
5.5
5.0
4.5
4.0
3.5
3.0
2.5
2.0
1.5
1.0
0.5
-0.0

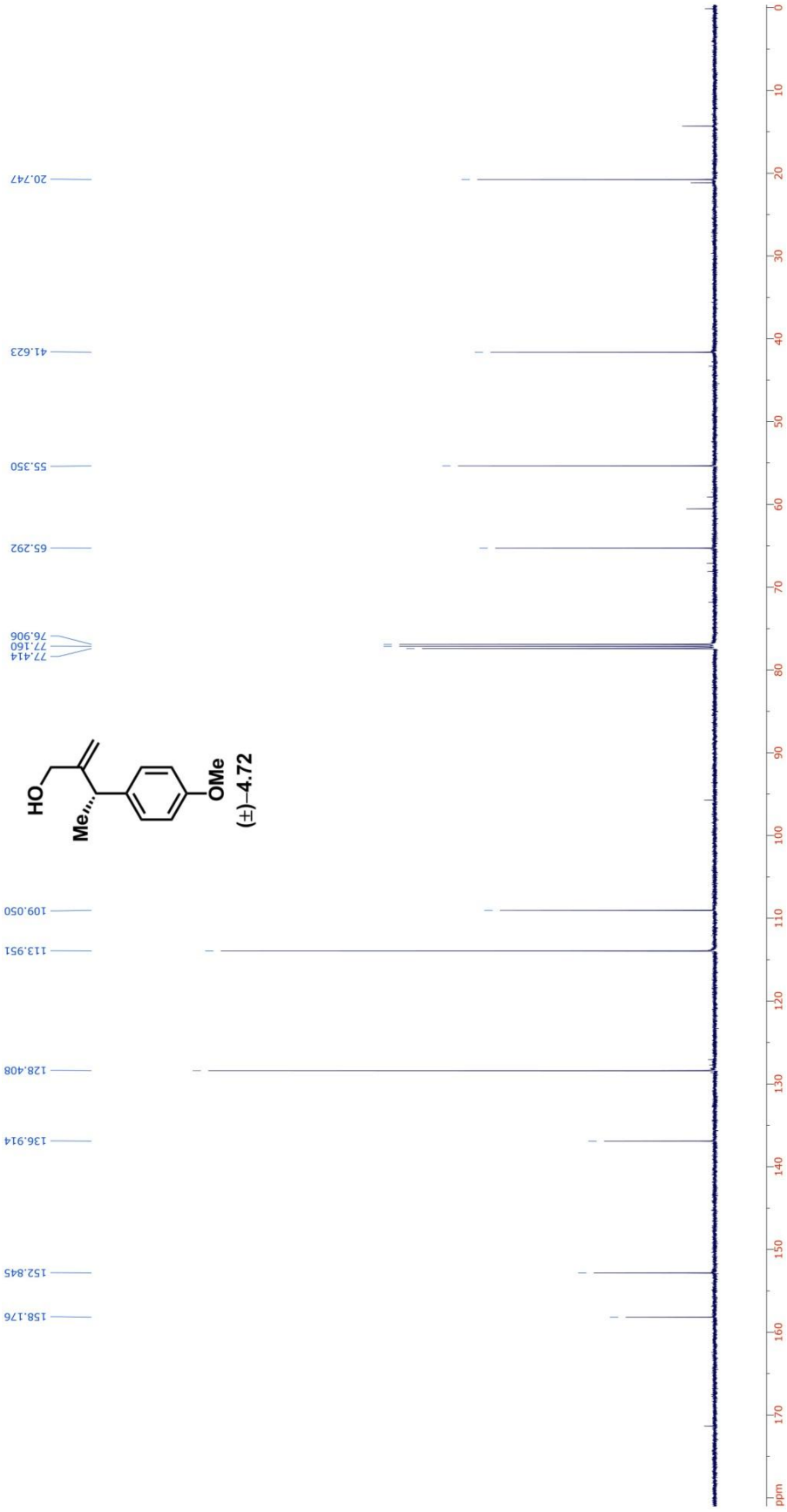
20.747
41.623
55.350
65.292
77.414
77.160
76.906
109.050
113.951
128.408
136.914
152.845
158.176
HO
Me
OMe
(±)-4.72
ppm

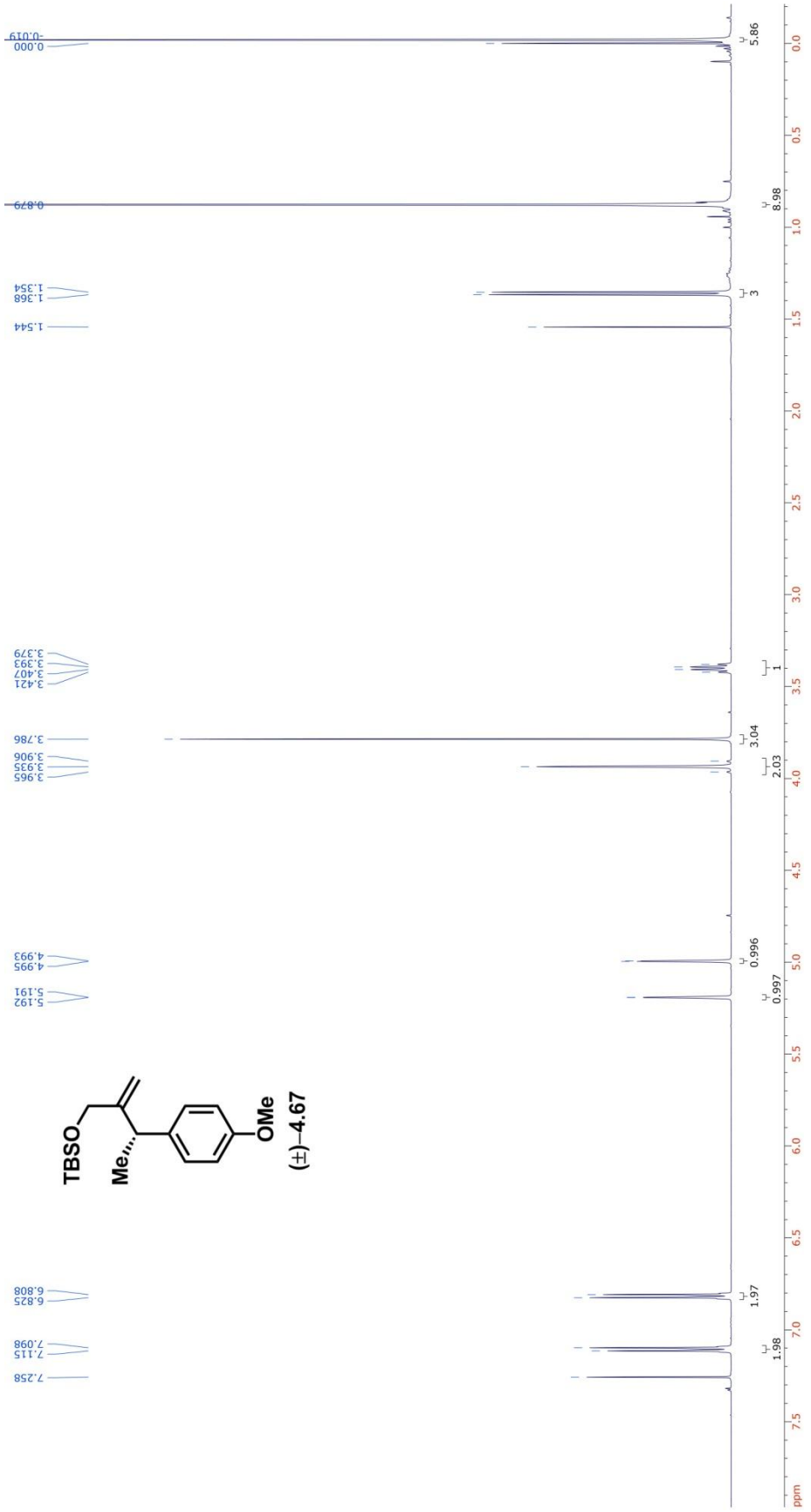
TBSO
Me
OMe
(±)–4.67

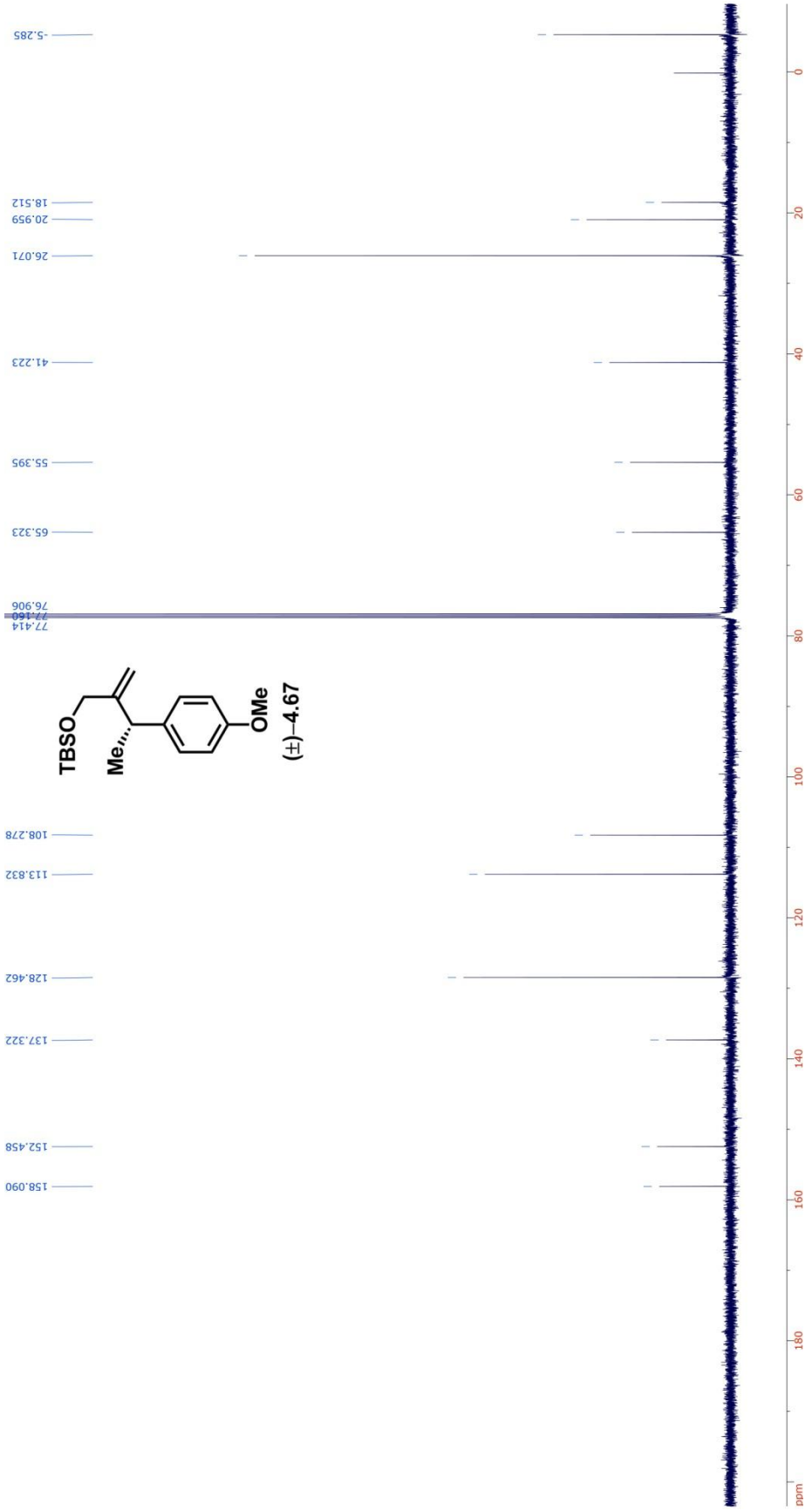
-5.285
18.512
20.959
26.071
41.223
55.395
65.323
76.906
77.160
77.414
108.278
113.832
128.462
137.322
152.458
158.090
TBSO
Me
OMe
(±)-4.67
0
20
40
60
80
100
120
140
160
180
ppm

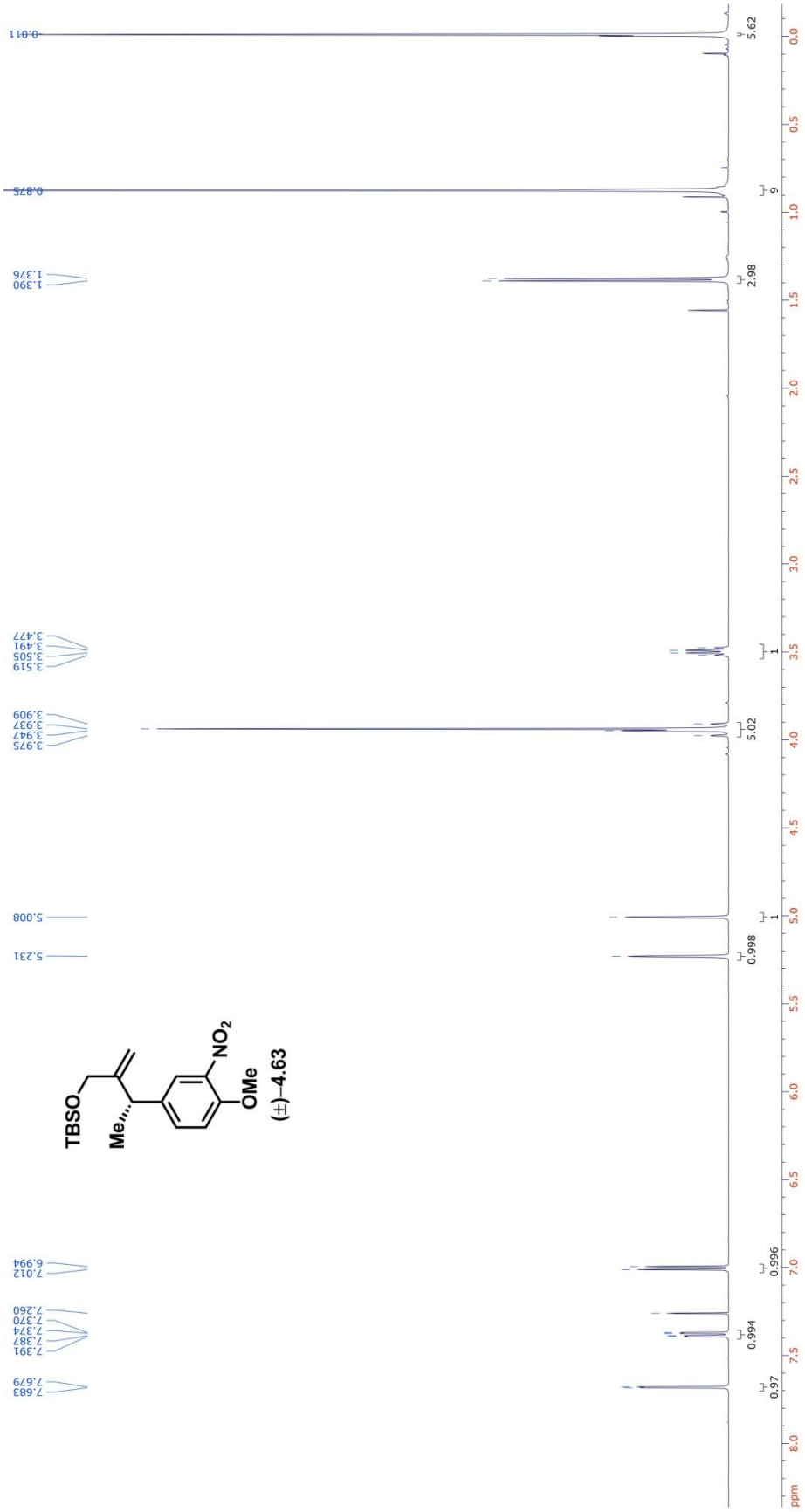
0.011
0.875
1.390
1.376
3.519
3.505
3.491
3.477
3.975
3.947
3.937
3.909
5.008
5.231
7.683
7.679
7.391
7.387
7.374
7.370
7.260
7.012
6.994
5.62
9
2.98
1
5.02
1
0.998
0.996
0.994
0.97
ppm
TBSO
Me
NO2
OMe
(±)-4.63

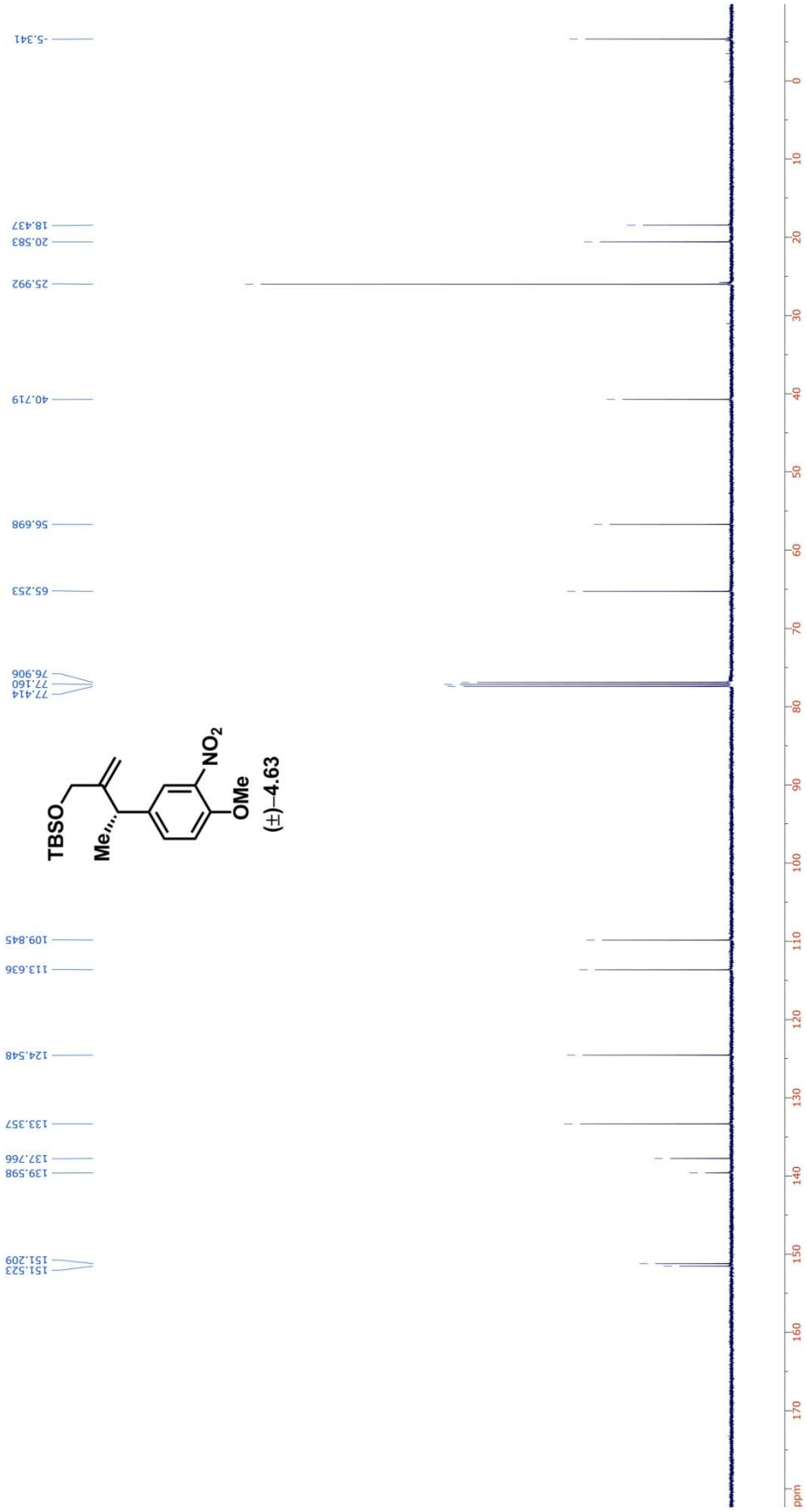
-5.341
18.437
20.583
25.992
40.719
56.698
65.253
76.906
77.160
77.414
109.845
113.636
124.548
133.357
137.766
139.598
151.209
151.523
TBSO
Me
OMe
NO2
(±)-4.63
0
10
20
30
40
50
60
70
80
90
100
110
120
130
140
150
160
170
ppm